ROSSBY WAVES AND TWO-DIMENSIONAL TURBULENCE IN THE PRESENCE OF A LARGE-SCALE ZONAL JET

by

THEODORE GORDON SHEPHERD
B.Sc., University of Toronto
(1979)

Submitted to the Department of Earth, Atmospheric and Planetary Sciences in Partial Fulfillment of the Requirements for the Degree of

DOCTOR OF PHILOSOPHY
in
METEOROLOGY

at the

MASSACHUSETTS INSTITUTE OF TECHNOLOGY
September 1984

© Massachusetts Institute of Technology, 1984

Signature of Author _____

Center for Meteorology and Physical Oceanography
Department of Earth, Atmospheric and Planetary Sciences
July 12, 1984

Certified by _____

Peter B. Rhines
Thesis Supervisor

Accepted by _____

Theodore R. Madden
Chairman, Departmental Committee on Graduate Students

WITHDRAWN
MASSACHUSETTS INSTITUTE OF TECHNOLOGY
AUG 31 1984
Lindgren

ROSSBY WAVES AND TWO-DIMENSIONAL TURBULENCE IN THE PRESENCE OF A LARGE-SCALE ZONAL JET

by

THEODORE GORDON SHEPHERD

Submitted to the Department of Earth, Atmospheric and Planetary Sciences on July 12, 1984, in Partial Fulfillment of the Requirements for the Degree of Doctor of Philosophy in Meteorology.

ABSTRACT

This dissertation represents a theoretical, numerical, and observational study of barotropic waves and turbulence in an inhomogeneous background flow environment. The theoretical aspects of the work are simplified by restricting attention to the two-dimensional doubly-periodic beta-plane, and in nearly every respect to large-scale zonal flows which are barotropically stable (in a normal-mode sense).

The role of the flow inhomogeneity is investigated by considering both nonlinear and linear theory of wave, mean-flow interaction; the key concept to emerge is that of induced spectral transfer of conserved wave quantities by the basic-state flow. Along the way, some new nonlinear conservation laws are derived. In the special case examined of a large-scale zonal jet, the wave enstrophy is approximately conserved in a fully nonlinear sense, and the wave, mean-flow interaction may be characterized as an induced spectral transfer of the wave enstrophy along lines of constant zonal wavenumber k. Because of the scale separation, the linear part of the interaction problem can be closed by applying WKB ray-tracing theory. The turbulent dynamics act to smooth the spectral gradients by irreversible mixing of wave enstrophy; their closure is less easily quantified.

The theoretical ideas are tested by performing numerical simulation experiments of both the spin-down and forced-dissipative equilibrium variety. In particular, the nature of the wave, mean-flow interaction can be identified by examining the interaction terms as functions of the meridional wavenumber ℓ for fixed k. In so doing one can determine the point at which irreversible nonlinear dynamics take over from reversible linear dynamics; while the latter are characterized by induced transfer of enstrophy <u>along</u> lines of constant k, the former operate by diffusing energy and enstrophy <u>across</u> such contours.

Finally the ideas of the thesis are applied to atmospheric data, and the results used to interpret the observed nonlinear spectral fluxes of kinetic energy and of enstrophy, as well as the interaction between the stationary (viz. one-month time-mean) and transient flow components.

Thesis Supervisor: Dr. Peter B. Rhines

Title: Senior Scientist,
Woods Hole Oceanographic Institution

Dedicated to

Professor Jule Gregory Charney

ACKNOWLEDGEMENTS

The completion of graduate study and of a doctoral dissertation is a lengthy, complex process; it is, consequently, not a simple matter to identify all of the varied elements which together contributed to the state of the final product.

The responsibility for my commitment to meteorology and geophysical fluid dynamics rests with George Boer, who was my mentor during three formative summers at the Canadian Climate Centre in Toronto, and whose measured skepticism has served to restrain my youthful enthusiasms at various stages of this work.

At M.I.T. I am indebted first of all to the late Jule Charney, my first advisor; his enormous energy and creativity, in the face of great physical suffering, provided a source of inspiration (as well as no small amount of trepidation) to me during my first two years of graduate study. Prof. Charney's enthusiasm towards the initial form of my research proposal was of immeasurable value, and I can only hope that the end result reflects a small measure of his greatness.

By far the greatest part of my doctoral research has been conducted under the supervision of Peter Rhines, who very kindly took me on following the death of Prof. Charney. I am indebted to Dr. Rhines for his persistent raising of uncomfortable questions which I was tempted to ignore, as well as for his original and imaginative understanding of fluid dynamics which provided both scientific and emotional inspiration, mingled with a healthy degree of provocation.

In addition I must express my gratitude to the other members of my supervising committee for their encouragement and guidance: Edward Lorenz and Joseph Pedlosky lasted the course, while Glenn Flierl generously took over from Mark Cane at a late stage of the work. In the case of Prof. Lorenz and Dr. Pedlosky, my appreciation extends to their considerable pedagogical abilities as expressed in influential and indeed formative lecture courses which I was fortunate to take.

The thesis research acquired a particular cohesion during the summer of 1983, while I was a visitor to the Oceanography section of the National Center for Atmospheric Research. I am grateful to NCAR for much hospitality during an especially fruitful period of my work.

I have been supported over the last three years by a variety of sources: NSF grants ATM-76-20070, ATM-81-15712, and OCE-82-19780; NASA grant NGR-22-009-727; and a Postgraduate Fellowship from the Natural Sciences and Engineering Research Council of Canada. The computer time was provided by the NCAR Computing Facility, which is itself sponsored by the National Science Foundation. Dale Haidvogel provided the code which formed the core of the numerical model, and I must acknowledge his kind help in many computational matters.

Finally, the preservation of my sanity has been due in large part to the stabilizing effects of marriage; my gratitude to my wife Jennifer is surpassed only by her relief at my having finished. I would also like to thank my parents for continuous encouragement and support.

BIOGRAPHICAL NOTE

Born 6 August 1958 in Saskatoon, Saskatchewan, Canada; moved to Toronto, Ontario, Canada, in 1970. Educated at the University of Toronto Schools (1971-1975); Trinity College, University of Toronto (1975-1979); and the Massachusetts Institute of Technology (1979-1984). Received the Honours B.Sc. (with Distinction) in Mathematics & Physics from the University of Toronto, 1979. Spent three summers (1978-1980) working under Dr. George Boer at the Canadian Climate Centre in Toronto. Held a Fellowship at the 1982 Summer School in Geophysical Fluid Dynamics (Theme: Lagrangian Motions) at the Woods Hole Oceanographic Institution. Received a Post-graduate Fellowship from the Natural Sciences and Engineering Research Council of Canada, 1982-1983, for study at M.I.T. under Dr. Peter Rhines. Visited the Oceanography Department of the National Center for Atmospheric Research in Boulder, Colorado, for ten weeks in the summer of 1983. Received a Postdoctoral Fellowship from the Natural Sciences and Engineering Research Council of Canada, 1984-1985, for study at the University of Cambridge under Dr. Michael McIntyre. Publications in refereed journals: "Large-Scale Two-Dimensional Turbulence in the Atmosphere", J.Atmos.Sci., 40, 164-184 (1983) [with G.J. Boer]; "Mean Motions Induced by Baroclinic Instability in a Jet", Geophys.Astrophys. Fluid Dynamics, 27, 35-72 (1983). Married in June 1981 to Jennifer Louise Glenesk of Toronto; father to one daughter, Ariel Glenesk Shepherd, who was born on 8 February 1983.

TABLE OF CONTENTS

Title Page 1
Abstract 3
Dedication 5
Acknowledgements 7
Biographical Note 9
Table of Contents 10

CHAPTER I - INTRODUCTION 12

CHAPTER II - TWO-DIMENSIONAL TURBULENCE 21
§2a. Introduction and Equations 21
§2b. Spectral Arguments 25
§2c. Physical-Space Arguments 28
§2d. Inviscid Equilibrium Theory 30
§2e. Viscous Equilibrium Theory 34
§2f. Similarity Theory for Evolving Turbulence 37
§2g. Closure Theory 40
§2h. Spherical Geometry 45
§2i. Discretization and Truncation 49

CHAPTER III - GEOSTROPHIC TURBULENCE 54
§3a. Introduction 54
§3b. Homogeneous Rotating Flow and the f-plane 56
§3c. Waves and Turbulence on the β-plane 59
§3d. Turbulence in a Rotating Stratified Fluid 68
§3e. Geostrophic Turbulence in the Two-Layer Model 75

CHAPTER IV - ATMOSPHERIC OBSERVATIONS 84
§4a. Introduction 84
§4b. Eddies and the General Circulation 87
§4c. Spectral Observations 98
§4d. Some Questions and a Simple Model 111

CHAPTER V - WAVES AND TURBULENCE ON A STATIONARY BACKGROUND FLOW . 116
§5a. Introduction 116
§5b. Equations for a Perturbed Flow 120
§5c. Scale Analysis 125
§5d. Spectral Dynamics 129

§5e. Nonlinear Conservation Laws: General 134
§5f. Nonlinear Conservation Laws: Specific 144
§5g. Linearized Conservation Laws 159

CHAPTER VI - LINEAR WAVE, MEAN-FLOW INTERACTION THEORY FOR A ZONAL JET 166
§6a. Introduction 166
§6b. General Arguments 168
§6c. Ray-Tracing Theory 174
§6d. Ray Tracing in a Cosine Jet 182
§6e. Quantization and Normal-Mode Theory 195

CHAPTER VII - NUMERICAL SIMULATIONS: SPIN-DOWN 204
§7a. Introduction 204
§7b. The Model and the Experimental Choices 207
§7c. Diagnostic Formulae 212
§7d. Discussion of the Linear Runs 220
§7e. Discussion of the Nonlinear Runs 252
§7f. Summary of Results 278

CHAPTER VIII - NUMERICAL SIMULATIONS: EQUILIBRIUM 281
§8a. Introduction 281
§8b. The Model and the Experimental Choices 283
§8c. Runs U and V: The Atmospheric Regime 291
§8d. Runs W and X: Effects of Stronger Beta 314
§8e. Run T: Effects of Increased Nonlinearity 326
§8f. Run S: Effects of Weaker Friction 337
§8g. Summary of Results 343

CHAPTER IX - ATMOSPHERIC OBSERVATIONS, RE-VISITED 350
§9a. Introduction 350
§9b. Stationary-Transient Interaction 351
§9c. Some Answers? 359

CHAPTER X - CONCLUDING REMARKS 362

REFERENCES 366

APPENDIX - NUMERICAL SIMULATIONS WITH HIGHER-MODE JETS 378

CHAPTER I - INTRODUCTION

When one observes the behaviour of atmospheric flow, one is immediately struck by the fact that activity seems to occur on all scales of motion, from the smallest boundary-layer eddy to waves that span an entire continent. It is then perhaps somewhat surprising that instantaneous fields of meteorological quantities such as geopotential height should be as smooth and coherent as they are - even allowing for the artificial smoothing associated with a discrete observational network. Yet it is certainly true that, at least away from the surface boundary layer, typical horizontal length scales of atmospheric phenomena tend to rather significantly exceed the resolution scale of the synoptic network (over land). This observation is reflected in the wavenumber spectrum of kinetic energy, which demonstrates that the greater part of the kinetic energy in the atmosphere may be associated with features involving wavelengths of 4000 km or greater.

In order to explain this predominance of activity on planetary scales of motion, one may first of all appeal to the fact that the direct forcing of the atmosphere from radiative effects is fundamentally a large-scale phenomenon; specifically, differential solar heating provides available potential energy primarily in the (n=2,m=0) spherical harmonic mode. Moreover, the forcing induced by land-sea thermal contrasts on the one hand, and by topography on the other, tends also to be of planetary scale (except perhaps in equatorial regions).

However, these remarks do not by themselves provide a satisfying explanation of the situation. In three-dimensional homogeneous turbulence, it is well known (Batchelor, 1953) that energy cascades rapidly

from large to small scales of motion, where it is finally dissipated by viscosity. If the atmosphere behaved in such a fashion, then in spite of large-scale forcing one would probably be unable to observe persistent large-scale motions. Of course the extreme shallowness of the atmosphere prohibits anything like three-dimensional homogeneous turbulence even for mesoscale phenomena, to say nothing of planetary-scale waves. Rather, the atmosphere tends to behave in a manner more consistent with two-dimensional turbulence theory. The most important ramification of this fact is that random eddies, instead of breaking down into smaller-scale motions, conspire to organize themselves in such a fashion as to feed energy into the largest scales.

One particular aspect of this process, namely eddy rectification of zonal-mean flows, was recognized first by Jeffreys (1926) and then championed by Starr (1953); Starr found the effect sufficiently startling to give it the defensible though somewhat contentious name of "negative viscosity" (Starr, 1968). However, the link between wave, mean-flow interaction theory, a subject which has been much studied (e.g. Charney & Drazin, 1961; Andrews & McIntyre, 1976; Dunkerton, 1980), and two-dimensional turbulence theory, a well-established field in its own right (dating back to Onsager, 1949; Lee, 1951; and Fjørtoft, 1953), has not been seriously developed. This is due in good measure to the fact that the intermediate regime, of inhomogeneous turbulence and strongly nonlinear wave, mean-flow interaction, has largely defied analytical treatment.

The key point to be made is that this "reverse energy cascade" is a mechanism by which forced planetary-scale motions can retain their integrity, avoiding the lethal down-scale cascade that would be their

lot in three-dimensional turbulence. The reason for this phenomenon is that disturbance energy excited at intermediate synoptic scales is channeled up-scale, where it must interact with the forced waves. Consequently, if one desires to investigate the question of how the planetary-scale waves and currents - which, it has been argued, are the dominant features of atmospheric motion - are maintained, then it seems that a two-pronged approach is necessary. On the one side, one must study the way in which these features can be forced at large scales; Held (1983) has recently reviewed some of the work in this area.

However, it is perhaps equally necessary to investigate the second side of the story, namely, the extent to which the "reverse energy cascade" both confines planetary-scale waves and currents to the largest scales, and feeds them with cascading energy from smaller scales. It is this latter question which will be explored in the present study. Of course this general topic has long been considered in relation to the zonally-averaged circulation (e.g. Lorenz, 1967; Green, 1970), and has recently attracted attention with regard to three-dimensional aspects of climate (e.g. Hoskins, 1983; Shutts, 1983a). But it has not as yet been addressed very carefully within the context of turbulence theory.

Briefly stated, the hypothesis which motivates this research has two components. The first part is that existing horizontally homogeneous versions of 2-D and geostrophic turbulence theory appear to explain certain fundamental dynamical aspects of the observed large-scale atmospheric circulation. While this is hardly a new insight, it is probably fair to say that it is not widely appreciated; consequently more space will be devoted to these matters than might otherwise be necessary. Moreover the point of view is somewhat controversial, which is why it is

properly regarded as a hypothesis. Yet there are definite discrepancies between the turbulence theories and atmospheric reality, as well as points of obscurity regarding the correct interpretation of some of the observed features. This is hardly surprising, given the fact that the assumptions of homogeneity and isotropy of flow statistics, required for the theoretical development, are not well satisfied in the atmosphere.

The second and more substantial part of my hypothesis is that by generalizing homogeneous turbulence theory to include a "background" flow consisting of a forced, stationary zonal jet, the remarkable success of the homogeneous theories can be accounted for, a number of the discrepancies resolved, and some of the ambiguities clarified. However it should be stated at the outset that due to various simplifications made to render the problem tractable, a quantitative comparison of theory with observations cannot be made. Nevertheless it is possible to apply some of the qualitative lessons and insights to the data in order to gain a better understanding of the atmospheric circulation dynamics.

The starting point of the discussion is a review of homogeneous and isotropic 2-D turbulence theory, in Chapter II. There the dual constraints of energy and enstrophy conservation are shown to lead to a spectral evolution involving up-scale transfer of energy and a simultaneous down-scale transfer of enstrophy. Since no single analytical approach can completely capture the dynamics a variety of theories are presented, each of which contributes differently to an elucidation of the phenomenology. It is felt that such thoroughness is justified because a solid understanding of the 2-D homogeneous theory is essential if one is to grasp the significance of the present work.

However no physical fluid is strictly two-dimensional, and Chapter III is devoted to a review of the theoretical rationale for the applicability of 2-D theory to geophysical fluids - in particular to the large-scale atmospheric dynamics. At a fundamental level, this connection is due to the influence of rotation. While the theory must be considerably generalized, horizontal (and to some extent vertical) homogeneity remains a necessary assumption and the anisotropy which is introduced has its influence localized to a single scale. The two most significant such generalizations involve the consideration of Rossby-wave dispersion on a beta-plane (Rhines, 1975), which effects an arrest of the reverse energy cascade at the so-called "Rhines radius"; and the incorporation of stratification within quasi-geostrophic dynamics (Rhines, 1977), which suggests that 2-D theory should describe the behaviour of the barotropic flow component except at the scale of the internal Rossby radius of deformation.

The next step is to establish the first part of the hypothesis by examining atmospheric observations in the light of the theories of Chapters II and III; this is done in Chapter IV. Consideration is given first to spatial diagnostics, an area in which there has been much recent effort, but to which the interpretative context of geostrophic turbulence is rarely applied. A more natural form of diagnostic for this purpose is that produced by spectral analysis; generally this has been performed in terms of a zonal-wavenumber decomposition, however as argued in §2h this format is inappropriate for spherical geometry. Observations from a spherical harmonic analysis by Boer & Shepherd (1983) are reviewed, and some new diagnostics from the same data presented. The chapter ends with a number of questions, and argues that

they may be fruitfully addressed within the context of barotropic beta-plane turbulence in the presence of an inhomogeneous large-scale forced stationary zonal flow.

At this point the stage is set for the original aspects of the thesis work to begin in earnest. However, the consideration of large-scale inhomogeneous turbulence places one parametrically in the intermediate regime between wave, mean-flow interaction theory and homogeneous turbulence theory: too nonlinear for the former, but not sufficiently nonlinear for the latter. While the fluid dynamical literature is replete with references to "shear-flow turbulence", this work does not appear to be useful in the present geophysical fluid dynamical context for at least two reasons. First, the turbulent motions envisaged are fully three-dimensional, which takes one into a completely different phenomenological regime; and secondly, the theory for fully-developed turbulence consists almost entirely of empirical laws of unclear dynamical origin, most of the theoretical effort having been directed at the important but distinct problem of instability and the transition to turbulence.

For flows which are nonlinear but not too turbulent, Lagrangian approaches such as those of Andrews & McIntyre (1978a) and of Rhines & Holland (1979) may be considered. But because of the dearth of work on fully nonlinear (by which I mean strongly turbulent and dynamically irreversible) wave, mean-flow interaction, it was decided to devote a chapter to analytical efforts along this line. In the event, with the exception of §§5a-c Chapter V is perhaps the least important in terms of the central flow of ideas in the thesis; quite frankly, I was unable to make enough progress for the theory to be of much prognostic value.

Nevertheless, the results are offered as an example of an attempt to make some headway in a very frustrating area. In order to place the original work of §5f in some context, it was necessary to review other related theory in §§5e,g.

If one restricts attention to the "linearized" interaction between a large-scale zonal flow and random disturbances, as is done in Chapter VI, then considerably more progress is possible; moreover this treatment turns out to be essential to an understanding of the fully nonlinear dynamics. General arguments are presented first, and then the scale separation in the problem is exploited using a combined spectral-spatial interpretation of ray-tracing theory to "close" the dynamics. This really represents the conceptual heart of the thesis, especially §6b. Obviously the theory of Chapter VI cannot describe the behaviour of inhomogeneous turbulence; the point is that it proves to be of prime importance in identifying the role of the flow inhomogeneity within the full problem.

With only a handful of partial theories and no over-arching formulation to provide a unification, one is led to experimentation as a means of testing the validity of the partial theories and of gaining further insight; this is a well-worn path in turbulence research, as emphasized by Batchelor (1953). For barotropic turbulence the optimal experimental approach seems to be that of direct numerical simulation. In the present case, two distinct dynamical regimes are investigated.

Chapter VII treats the case of "spin-down" - viz., unforced, weakly-damped - evolution, which although physically "unrealistic" is of great didactic value. For simplicity a single set of external conditions is explored through the consideration of a linear run with the

mean flow held fixed and wave-wave interactions suppressed; a beta-plane turbulence run with no imposed mean flow; and the full scenario with mean flow, waves and turbulence. The point is to determine the extent to which the linear theory of Chapter VI is useful, as well as when and how it fails. Without going into the results, it may be said here that when the linear theory breaks down it does so in a strongly turbulent manner, suggesting that weakly-nonlinear and "laminar" wave, mean-flow interaction theory are not of much relevance to the present problem - the latter being, however, admittedly more turbulent than most parts of the atmosphere or oceans.

The more geophysically relevant, but diagnostically less clear-cut, regime of forced-dissipative equilibrium is investigated in Chapter VIII. The forcing is principally at intermediate scale, to simulate the barotropic energy-enstrophy input due to baroclinic instability. While one can obtain reasonable atmospheric estimates for all external parameters except the high-order diffusion coefficient, an attempt is also made to explore parameter space to a limited extent in order to determine the robustness of the results; this latter issue is of course essential to face whenever one does numerical work.

The question of higher-mode basic-state jets is relegated to an Appendix, so as not to divert attention from the central train of development. Whenever the perturbations reach a scale larger than that of the mean flow, the theory of Chapter VI can no longer be applied and the flow dynamics are uncertain. Yet it is felt that some treatment of this problem is desirable, insofar as it explains why the beta-jets which develop internally in beta-plane turbulence are of fundamentally different dynamical significance than the large-scale inhomogeneous jets

considered in this study.

Finally, the second part of the original hypothesis is addressed in Chapter IX, by returning to the spectral observations in the light of the present work. I believe that the advances made within this context are indeed significant, but they are nonetheless severely limited in scope due to the simplicity of the model. For this reason one may be tempted to consider the work primarily within the more abstract context of the theories of nonlinear wave, mean-flow interaction and large-scale turbulence, in terms of which the present research has bridged in at least a small way a rather notable gap. This issue, as well as the most important results of the work, are discussed in a brief concluding chapter.

CHAPTER II - TWO-DIMENSIONAL TURBULENCE

§2a. Introduction and Equations

It is the purpose of this chapter to review the key aspects of 2-D homogeneous turbulence theory. This is important both in trying to determine the relevance of the theory to the atmospheric circulation, a matter addressed in Chapter IV, as well as in understanding the dynamics of the inhomogeneous turbulent flows studied in the central part of this thesis.

The striking and fundamental differences in behaviour between two-dimensional and three-dimensional homogeneous turbulent flows have been understood for some time, and have been discussed extensively in the literature (Lee, 1951; Fjørtoft, 1953; Kraichnan, 1967; Batchelor, 1969; Tennekes, 1978). While 3-D turbulence exhibits a rapid cascade of energy to small scales via the mechanism of vortex stretching (Batchelor, 1953), the twin constraints of kinetic energy and mean-squared vorticity (or enstrophy) conservation in an inviscid 2-D fluid effectively prevent such a phenomenon. There is instead a tendency for energy to be transferred from smaller eddies up to the largest scales of motion, and it is this "reverse energy cascade" effect that represents the most distinctive and unusual feature of 2-D turbulent flow.

For the sake of simplicity I shall assume a Cartesian geometry for the present discussion, leaving the question of spherical geometry until later. The Navier-Stokes equation for 2-D nondivergent plane turbulent flow leads to the vorticity equation

$$\nabla^2\psi_t + J(\psi,\nabla^2\psi) = \nu\nabla^4\psi - r\nabla^2\psi \quad , \tag{2.1}$$

where ν is kinematic viscosity, r is the Ekman drag at the bottom

surface, and ψ is the streamfunction. Here the convention $J(A,B)=A_xB_y - A_yB_x$ has been used. Multiplication of (2.1) by ψ or by $\nabla^2\psi$ and integration over the domain (assumed infinite or periodic) leads, respectively, to kinetic energy or enstrophy budget equations given by

$$\frac{d}{dt}\iint \frac{1}{2}\left|\nabla\psi\right|^2 dxdy = \iint \psi J(\psi,\nabla^2\psi)dxdy - \nu\iint(\nabla^2\psi)^2 dxdy - r\iint\left|\nabla\psi\right|^2 dxdy \quad (2.2a)$$

$$\frac{d}{dt}\iint\frac{1}{2}(\nabla^2\psi)^2 dxdy = -\iint\nabla^2\psi J(\psi,\nabla^2\psi)dxdy - \nu\iint\left|\nabla^3\psi\right|^2 dxdy - r\iint(\nabla^2\psi)^2 dxdy \quad (2.2b)$$

Note that the first term on the right-hand side of each equation (2.2a,b) vanishes; the terms are left in for reasons to become apparent below. For convenience, and without loss of generality, the integrals are assumed to be properly convergent. It is useful to perform a Fourier transform of ψ, namely

$$\hat{\psi}(\underline{k}) \equiv \iint \psi(x,y)\, e^{-i(k_x x+k_y y)}\, dxdy \equiv \{\psi\}(\underline{k}) \quad (2.3)$$

where $\underline{k} \equiv (k_x,k_y)$ is the 2-D wavenumber, and $k^2 = k_x^2 + k_y^2$. For realizability, the transform of any physical field A must satisfy $\hat{A}(-\underline{k}) = \hat{A}^*(\underline{k})$. It then follows that

$$E = \iint\frac{1}{2}\left|\nabla\psi\right|^2 dxdy = \iint\frac{1}{2}k^2\left|\hat{\psi}(\underline{k})\right|^2 dk_x dk_y \equiv \iint E(\underline{k})dk_x dk_y \quad (2.4)$$

using the Fourier transform identity $\iint AB dxdy = \iint \hat{A}^*\hat{B}dk_x dk_y$; then (2.4) suggests the identification of $E(\underline{k}) \equiv \frac{1}{2}k^2\left|\hat{\psi}(\underline{k})\right|^2$ as the spectral kinetic energy density. Making similar conversions, (2.2a,b) are transformed into

$$\frac{d}{dt}\iint E(\underline{k})dk_x dk_y = \iint\hat{\psi}^*(\underline{k})\{J(\psi,\nabla^2\psi)\}(\underline{k})dk_x dk_y - 2\nu\iint k^2 E(\underline{k})dk_x dk_y - 2r\iint E(\underline{k})dk_x dk_y \quad (2.5a)$$

$$\frac{d}{dt}\iint k^2 E(\underline{k})dk_x dk_y = \iint k^2\hat{\psi}^*(\underline{k})\{J(\psi,\nabla^2\psi)\}(\underline{k})dk_x dk_y - 2\nu\iint k^4 E(\underline{k})dk_x dk_y - 2r\iint k^2 E(\underline{k})dk_x dk_y \quad . \quad (2.5b)$$

Alternatively and more directly, to obtain (2.5a,b) one may transform

(2.1) and then multiply it by $\hat{\psi}^*(\underline{k})$ or by $-k^2\hat{\psi}^*(\underline{k})$. Now the interpretation of the first term on the right-hand side of (2.5a,b) is that of the sum of all nonlinear transfers between waves of different scales; the sums both vanish since what one wave gains, another must lose. Frequently the integrand $\hat{\psi}^*(\underline{k})\{J(\psi,\nabla^2\psi)\}(\underline{k})$ is interpreted as a convolution of triads $(\underline{k},\underline{p},\underline{q})$ in wavenumber space satisfying $\underline{k} + \underline{p} + \underline{q} = 0$ with none of $\underline{k}$, $\underline{p}$, $\underline{q}$ collinear; for each triad (2.5a,b) imply an exchange of both energy and enstrophy between the triad members (Lorenz, 1960; Pedlosky, 1962).

The horizontal velocities u and v are derived from the streamfunction via

$$v = \frac{\partial \psi}{\partial x} \quad ; \qquad u = -\frac{\partial \psi}{\partial y} \quad .$$

Therefore one may divide the energy into "zonal" and "meridional" components as follows:

$$E_U \equiv \iint E_U(\underline{k})dk_x dk_y = \iint \frac{1}{2}k_y^2\left|\hat{\psi}(\underline{k})\right|^2 dk_x dk_y = \iint \frac{1}{2}\left|\hat{u}(\underline{k})\right|^2 dk_x dk_y, \quad (2.6a)$$

$$E_V \equiv \iint E_V(\underline{k})dk_x dk_y = \iint \frac{1}{2}k_x^2\left|\hat{\psi}(\underline{k})\right|^2 dk_x dk_y = \iint \frac{1}{2}\left|\hat{v}(\underline{k})\right|^2 dk_x dk_y. \quad (2.6b)$$

It is now appropriate to introduce the concepts of statistical homogeneity and isotropy. Consider the covariance function

$$B(\underline{r}_1,\underline{r}_2) \equiv \langle\psi(\underline{r}_1)\psi(\underline{r}_2)\rangle \ ,$$

where the angle brackets denote an ensemble average. The concept of an ensemble average is treated in more detail in §2d; here the discussion is kept simple. Then the turbulence is considered homogeneous if B is a function of the separation only, that is if

$$B(\underline{r}_1,\underline{r}_2) = B(\underline{r}_1-\underline{r}_2) \ . \quad (2.7a)$$

Additionally, the turbulence is isotropic if B is a function only of the absolute separation,

$$B(\underline{r}_1,\underline{r}_2) = B(|\underline{r}_1-\underline{r}_2|) \ . \qquad (2.7b)$$

Condition (2.7a) is equivalent to the flow statistics being independent of position, (2.7b) to their being independent of orientation of the axes of reference. Clearly isotropy is impossible without homogeneity, for without homogeneity there would always be a preferred direction. Moreover, homogeneity requires either an infinite or a periodic domain, and it is evident that in the former case the integrals above cannot converge; there are, however, remedies (see Batchelor, 1953, Chapter 2) so that the formalism remains valid. Under conditions of homogeneity the spatial averages are equivalent to ensemble averages, and there is the simple identity $E = -\nabla^2 B(0)/2$.

Equations (2.5a,b) can be written in the form

$$\frac{d}{dt}\int_0^\infty \varepsilon(k)dk = \int_0^\infty I(k)dk - 2\nu\int_0^\infty k^2\varepsilon(k)dk - 2r\int_0^\infty \varepsilon(k)dk \ , \qquad (2.8a)$$

$$\frac{d}{dt}\int_0^\infty k^2\varepsilon(k)dk = \int_0^\infty k^2 I(k)dk - 2\nu\int_0^\infty k^4\varepsilon(k)dk - 2r\int_0^\infty k^2\varepsilon(k)dk \ , \qquad (2.8b)$$

where

$$\varepsilon(k) \equiv \int_0^{2\pi} E(\underline{k})kd\theta \quad \text{and} \quad I(k) \equiv \int_0^{2\pi} \hat{\psi}^*(\underline{k})\{J(\psi,\nabla^2\psi)\}(\underline{k})kd\theta \ . \qquad (2.9)$$

If, as is often assumed in turbulence theory, the motion is homogeneous and isotropic, then $E(\underline{k}) = E(k)$ and $\varepsilon(k) = 2\pi kE(k)$. The vector components u and v must nevertheless be anisotropic, of course, but $\varepsilon_U(k) = \varepsilon_V(k)$ for homogeneous, isotropic flow.

For inviscid flow $\nu = r = 0$, (2.8a,b) reduce to conservation of energy and enstrophy,

$$\frac{d}{dt}\int_0^\infty \varepsilon(k)dk = 0 = \frac{d}{dt}\int_0^\infty k^2\varepsilon(k)dk \ . \qquad (2.10)$$

Whether the inviscid limit $\nu,r \to 0$ is singular depends on how quickly

$\varepsilon(k)$ decays as $k \to \infty$. If $\int_0^\infty k^4\varepsilon(k)dk < \infty$ then the limit is nonsingular and the dissipation of energy and enstrophy approaches zero as $\nu,r \to 0$. But in any case the enstrophy is usually finite, so that $\int_0^\infty k^2\varepsilon(k)dk < \infty$ and the dissipation of energy vanishes in the limit $\nu,r \to 0$. It is important that weakly dissipative flow is qualitatively similar in its energetic behaviour to inviscid flow. This is in contrast to the situation in 3-D turbulence, where the inviscid limit is singular and where finite viscosity, no matter how small, will drain energy from the energy-containing scales in a finite length of time.

Then for each wavenumber k, there is the single budget equation

$$\frac{\partial}{\partial t}\varepsilon(k) = I(k) - 2\nu k^2\varepsilon(k) - 2r\varepsilon(k) \ , \qquad (2.11)$$

where $I(k)$ equals the transfer of energy into scale k from all other waves, and must satisfy the double constraint

$$\int_0^\infty I(k)dk = 0 = \int_0^\infty k^2 I(k)dk \ . \qquad (2.12)$$

From the transfer functions $I(k)$ and $k^2I(k)$ can be obtained nonlinear fluxes of energy and enstrophy, respectively, defined by

$$F(k) = -\int_0^k I(\kappa)d\kappa \quad \text{and} \quad H(k) = -\int_0^k \kappa^2 I(\kappa)d\kappa \ , \qquad (2.13)$$

so that $F(0) = F(\infty) = H(0) = H(\infty) = 0$. A positive flux corresponds to a down-scale cascade, namely to higher k. (2.11), or its enstrophy equivalent, together with (2.12), are the fundamental equations of 2-D turbulence.

§2b. Spectral Arguments

Consider now inviscid flow ($\nu = 0 = r$), in order to isolate the nonlinear processes. The double constraint (2.10), or equivalently

(2.12), places a severe restriction on the possible exchanges of energy and enstrophy between different scales. One can visualize the problem (e.g. Rhines, 1979) as one of redistributing a fixed mass of density $\varepsilon(k)$ along the rod $k > 0$, while conserving the mass's moment of inertia about $k = 0$. Clearly a cascade of energy to small scale or large k, as one finds in 3-D turbulence, is excluded by the "moment of inertia" enstrophy constraint. Specifically, assume an initial distribution of energy very sharply localized about $k = k_0$, a constant. Then the first moment of ε, $k_1 \equiv [\int k\varepsilon(k)dk]/[\int \varepsilon(k)dk]$, evolves in time according to

$$\frac{d}{dt} k_1^2 = - \frac{d}{dt} \left\{ \frac{\int (k-k_0)^2 \varepsilon(k)dk}{\int \varepsilon(k)dk} \right\} \quad , \tag{2.14}$$

which may be easily verified by considering the inviscid conservation relations (2.10). If one now assumes that the nonlinear interactions will act to spread out an initially concentrated distribution (e.g. Batchelor, 1953, pg. 186), then the dispersion of ε about its centre k_0 will increase in time, viz.

$$\frac{d}{dt} \left\{ \frac{\int (k-k_0)^2 \varepsilon(k)dk}{\int \varepsilon(k)dk} \right\} > 0 \quad . \tag{2.15}$$

Hence (2.14) implies that $dk_1/dt < 0$, or that energy moves in the main to smaller wavenumbers. The presence of viscosity, neglected in (2.14), tends to accelerate the process: taking the inequality (2.15), and including viscous effects from (2.8a,b), yields

$$\frac{d}{dt} k_1^2 < \frac{d}{dt} k_2^2 = -2\nu(k_4^4 - k_2^4) < 0 \quad , \tag{2.16}$$

provided that $k_2 > 1$; here $k_n^n \equiv [\int k^n \varepsilon(k)dk]/[\int \varepsilon(k)dk]$.

The crucial assumption of the preceding calculation was (2.15), which represents a statistical assumption of irreversibility akin to the Second Law of Thermodynamics. The inviscid equations are themselves

fully reversible, however: if some "deus ex machina" were to suddenly change the sign of the streamfunction field, the flow would run backwards until it reached its initial configuration (but with the opposite sign). There is nothing inconsistent about this. Conservation of energy and enstrophy, (2.10), is absolute, and is satisfied by the hypothetical flow in both its forward- and backward-running phases. In any particular flow realization, the principal direction of energy flow may be either up-scale or down-scale, as long as the enstrophy constraint is observed. But if one does not know the details of the flow, and only knows the constraints acting on it - which is the case for a turbulent flow, almost by definition - then the most likely outcome will involve dispersion of energy and enstrophy in wavenumber space, with a consequent shift of energy to larger scale and of enstrophy to smaller scale.

As a demonstration of the extent of this asymmetry, consider the total redistribution of energy ε_0 from an initial wavenumber k_0 to both $2k_0$ and $k_0/2$. Admittedly this is highly unlikely in a statistical sense, but it serves to illustrate the power of the enstrophy constraint. Let ε_1 end up at $k_0/2$, and ε_2 at $2k_0$. The energy constraint says only that $\varepsilon_0 = \varepsilon_1 + \varepsilon_2$, which is not too revealing. But with the enstrophy constraint, namely $\varepsilon_0 = \varepsilon_1/4 + 4\varepsilon_2$, it follows that $\varepsilon_1/\varepsilon_2 = 4$ while $(k^2\varepsilon)_1/(k^2\varepsilon)_2 = (\varepsilon_1/4)/4\varepsilon_2 = 1/4$. Thus there is four times the energy at $k_0/2$ as at $2k_0$, and four times the enstrophy at $2k_0$ as at $k_0/2$.

When considering nonlinear interactions involving triads of wavenumbers, for which the global constraints hold, it is important to emphasize that spectral dispersion of energy from the intermediate

wavenumber does not imply greater up-scale than down-scale transfer of energy for every triad, but only when averaged over all possible triads (Merilees & Warn, 1975). The effect is thus not systematic but rather stochastic in nature.

§2c. Physical-Space Arguments

In §2b the analysis proceeded by using only the integral constraints of constant total energy and enstrophy for inviscid flow; there is, however, another conserved quantity, namely the vorticity $\zeta \equiv \nabla^2\psi$ following fluid particles, as is evident from (2.1). The consideration of this constraint to deduce flow behaviour is most effective in physical space. Since the conclusions reinforce the spectral arguments, they may be regarded as possible physical-space visualizations of the spectral cascades of energy and enstrophy.

It is the nonlinear interaction term $J(\psi,\zeta)$ of (2.1) which gives the subject of 2-D turbulence its unique richness and flavour. The term represents the advection of vorticity by the velocity field, $\underline{V}\cdot\nabla\zeta$, and it is thus plausible that to a first approximation one might expect vorticity to behave like a passive tracer distorted by larger-scale eddies (Batchelor, 1953; Kraichnan, 1975). In that case, one would expect the enstrophy spectrum to obey the law $\Omega(k) \equiv k^2\varepsilon(k) \propto k^{-1}$ associated with the variance of a passively advected scalar quantity (Batchelor, 1959). The justification for this notion lies in the fact that the streamfunction field is dominated by large-scale eddies, while the vorticity field is dominated by small-scale features; this is a generic quality of 2-D turbulence (see for example Rhines, 1977). The weakness in the argument is of course that vorticity is not a passive

but rather an active tracer, and is thus intimately related to the advecting flow field.

Given the above warning, however, consider the following arguments for inviscid flow. Since contours of vorticity are material lines, one expects them on average to lengthen in time as they are sheared and distorted by larger-scale eddies (Cocke, 1969); here the Second Law of Thermodynamics has come in again. But conservation of vorticity requires that any stretching of ζ-contours be accompanied by a decrease in the distance between neighbouring contours, that is to say by an increase in the average gradient of ζ. This necessitates an increase in the fourth moment of ε, k_4, which implies a movement of enstrophy to large k. However, this "enstrophy cascade" is localized to thin and spatially-intermittent shear layers attached to the large eddies (Batchelor, 1953), which suggests that any assumptions of spatial homogeneity or spectral localness may be somewhat problematical (Kraichnan, 1967).

Alternatively, small eddies which are distorted by larger eddies in the advective sense of a passive tracer, lean along the shear rather than into it; consequently their Reynolds stress patterns are such as to feed energy into the larger scales of motion. The same eddies, as they are strained by the shear to increasingly larger k, must conserve their vorticity $k^2\varepsilon$; thus the eddy energy decreases, which by conservation of total energy implies a transfer of energy into the larger scales, in agreement with the above argument. A more detailed discussion of this process can be found in Kraichnan (1975).

§2d. Inviscid Equilibrium Theory

The qualitative conclusions of §2b and §2c regarding movement of energy and enstrophy in the spectral domain are also obtainable through a quite distinct approach, namely by a consideration of the classical statistical mechanical equilibrium solutions for an inviscid, truncated system. The connection between the behaviour of a system described by a finite-dimensional phase space, to which the classical theory is applicable, and the motion of a macroscopic, continuous fluid describable in principle only by an infinite number of degrees of freedom, is far from self-evident. But when carefully interpreted, the statistical equilibrium theory can suggest the tendency of nonlinear interactions in a real, forced-dissipative fluid, even when the flow is well away from equilibrium. It should be said that the problem of relying on a finite-dimensional phase space is in any case a general one in fluid dynamics: for example, any direct simulation via a numerical model must deal with a truncated system. The weakness of the inviscid equilibrium theory is of a quite different nature.

A classical treatment of statistical mechanical equilibrium theory can be found in many textbooks (e.g., Tolman, 1938); the application to 2-D turbulence has been made by Onsager (1949), Kraichnan (1967, 1975), and by Salmon, Holloway & Hendershott (1976). For that reason I will only sketch the procedure here.

One begins by considering a system whose state is described by an N-dimensional vector $\underline{y} = [y_1, y_2, \ldots, y_N]$, and which evolves according to a set of N first-order ordinary differential equations of the form

$$\frac{d}{dt} y_i \equiv \dot{y}_i = F_i(y_1, y_2, \ldots, y_N) \quad . \tag{2.17}$$

For the problem of barotropic turbulence (2.1), with $\nu=r=0$, a convenient choice for the y_i's is the Fourier transform

$$y_i = k_i\hat{\psi}(\underline{k}_i)/\sqrt{2} \tag{2.18}$$

where a finite, discrete set of wavenumbers $[\underline{k}_1,\underline{k}_2,\ldots,\underline{k}_N]$ has been chosen. This allows

$$E_i = \frac{1}{2}k_i^2(\hat{\psi}(\underline{k}_i))^2 = y_i^2 \ ; \tag{2.19}$$

note that for this closed system, the assumption has been made of a finite domain with boundary conditions allowing real $\hat{\psi}(\underline{k}_i)$. The generalization to complex $\hat{\psi}$ is trivial (e.g., Frederiksen & Sawford, 1980).

The vector $\underline{y}$ spans an N-dimensional phase space, and the joint-probability distribution of the y_i's over an ensemble of flow realizations is defined to be $P(y_1,y_2,\ldots,y_N,t)$. P represents the density of phase points, and must satisfy a "continuity equation" of the form

$$\frac{\partial P}{\partial t} + \sum_i \frac{\partial}{\partial y_i}(\dot{y}_i P) = 0 \quad . \tag{2.20}$$

For this system, and in fact for many systems,

$$\sum_i \partial\dot{y}_i/\partial y_i = 0 \tag{2.21}$$

whence

$$\frac{\partial P}{\partial t} + \sum_i \dot{y}_i \frac{\partial P}{\partial y_i} = 0 \quad . \tag{2.22}$$

The significance of P is that it provides statistical information on the expected values of functions $F(y_1,y_2,\ldots,y_N,t)$, when averaged over an ensemble of flow realizations:

$$\langle F\rangle \equiv \int\int\cdots\int F\ P \prod_i dy_i \quad . \tag{2.23}$$

Now, the critical assumption is introduced that the system represented by (2.17) is an ergodic or a "mixing" system; this means that P, if initially concentrated at a time t_0, will spread out in phase

space for $t>t_0$. In fact, the Second Law of Thermodynamics suggests that P will spread so as to maximize the entropy S, where

$$S \equiv - \int\int\cdots\int P \log P \prod_i dy_i \quad . \tag{2.24}$$

There are, however, constraints on this mixing, for the system has two constants of motion: the kinetic energy

$$E = \sum_i E_i \equiv \sum_i y_i^2 \ , \tag{2.25a}$$

and the enstrophy

$$\Omega = \sum_i \Omega_i \equiv \sum_i k_i^2 y_i^2 \ . \tag{2.25b}$$

Absolute equilibrium is defined to be the state in which only the integral constraints are known, all other information having been lost. The problem is then to maximize $S \equiv \langle \log P \rangle$ subject to the constraints $\langle E-E_0 \rangle = 0 = \langle \Omega - \Omega_0 \rangle$. Applying the method of Lagrange multipliers, one seeks $\frac{\partial}{\partial y_i} (\log P - \alpha E - \gamma \Omega) = 0$ for all i, which has a solution

$$P = \exp\{\lambda - \alpha E - \gamma \Omega\} \quad . \tag{2.26}$$

Alternatively, the assumption of equal <u>a priori</u> probability distributions in phase space for all accessible states leads to the microcanonical distribution at equilibrium:

$$P(y_1, y_2, \ldots, y_N) = C \ \delta(E-E_0) \ \delta(\Omega - \Omega_0) \quad . \tag{2.27}$$

From (2.27), an asymptotic analysis in the limit of large N (see Salmon <u>et al.</u>, 1976, Appendix A) leads to the Boltzmann distribution for a single coordinate y_i,

$$P_i(y_i) \approx \left[(\alpha + \gamma k_i^2)/\pi\right]^{1/2} \exp\{-\alpha E_i - \gamma \Omega_i\} \tag{2.28}$$

which is an equipartition distribution (see Tolman, 1938, pg.95) for the constant of motion

$$\sum_i (\alpha + \gamma k_i^2) \ y_i^2 .$$

In (2.26), λ is determined by the requirement that $\langle 1 \rangle = 1$. For (2.26) or (2.28), the other constants α, γ are determined by the constraints

$\langle E\rangle = E_0$, $\langle\Omega\rangle = \Omega_0$; for any realizable values of E_0 and Ω_0 (if $k_0<k_i<k_{00}$ then realizable means $k_0^2 < \Omega_0/E_0 < k_{00}^2$) it is possible to show (Fox & Orszag, 1973) that α,γ are determined uniquely and that they yield a positive energy spectrum.

Expectation values can be obtained from either (2.26) or (2.28). Using (2.26) together with (2.23) provides

$$\langle y_j^2\rangle = \int\int\cdots\int \left\{ \int y_j^2 \exp\left[-\alpha y_j^2-\gamma k_j^2 y_j^2\right]dy_j\right\} \exp\left[\lambda-\alpha(E-E_j)-\gamma(\Omega-\Omega_j)\right] \prod_{i\neq j} dy_i$$

$$= \int\int\cdots\int \left\{ \frac{1}{2(\alpha+\gamma k_j^2)} \int \exp\left[-\alpha y_j^2-\gamma k_j^2 y_j^2\right]dy_j\right\} \exp[\cdots] \prod_{i\neq j} dy_i$$

whence

$$\langle y_j^2\rangle = \frac{1}{2(\alpha+\gamma k_j^2)} \quad . \tag{2.29}$$

Equation (2.29) suggests an energy spectrum

$$\varepsilon(k) \approx \frac{\pi k}{\alpha+\gamma k^2} \tag{2.30}$$

which formally diverges as $k \to \infty$; this divergence serves as a reminder that absolute equilibrium is realizable only in a truncated system. However, the divergence is weak when compared to that of 3-D homogeneous turbulence, where equipartition of E_i leads to an absolute equilibrium spectrum $\varepsilon(k) \propto k^2$. In 3-D turbulence, the exercise of keeping E_0 fixed while increasing N yields a spectrum with ever-greater amounts of E at large k; this suggests that nonlinear interactions in a real fluid will act to move energy rapidly out to high k: hence the down-scale energy cascade. In 2-D turbulent flow, however, the absolute equilibrium spectra for large k are $\varepsilon(k) \approx 1/k$ and $k^2\varepsilon(k) \approx k$. The same mental exercise in this case supports the notion of a down-scale enstrophy cascade, which by the conservation laws (2.12) also implies an up-scale cascade of energy. Since most of the energy is found at small

k, the limit $k \to \infty$ does not provide any direct information on the energy transfers.

§2e. Viscous Equilibrium Theory

In both 2-D and 3-D homogeneous, isotropic turbulence one may consider the equilibrium theory of Kolmogorov (Kolmogorov, 1941; Batchelor, 1953) for forced-dissipative flow. The basic properties of randomness and nonlinearity are present in 2-D as in 3-D flow, despite their notable differences, and this serves as the basis for hoping that such theories, developed for 3-D turbulence, might prove useful in the 2-D situation (Batchelor, 1969). The idea proceeds by assuming that the forcing and dissipation are localized in a spectral sense; then scales of motion which are removed from the forced-dissipative scales are dominated by inertial effects, provided that nonlinear interactions are spectrally local. This latter "localness" assumption is certainly valid for 3-D turbulence, but is somewhat problematical in the 2-D case (Kraichnan, 1967).

At equilibrium $\partial\varepsilon(k)/\partial t = 0$, so (2.11) implies that $I(k) = 0$ and that the associated flux functions $F(k)$ and $H(k)$, defined by (2.13), are constant over this "inertial subrange". However it is clear that a constant cascade cannot exist over the same subrange for both energy and enstrophy, as argued by Kraichnan (1967): the process of moving a fixed amount of enstrophy from k_0 to ever-higher k will inevitably be associated with a decrease in energy proportional to $(k_0/k)^2$. Similarly, moving a fixed amount of energy up-scale from k_0 to ever-smaller k must involve a decrease in enstrophy proportional to $(k/k_0)^2$. It is evident that there are only two inertial subranges

possible in 2-D turbulent flow: one with a constant negative (that is, up-scale) flux of energy accompanied by an asymptotically vanishing flux of enstrophy; the other with a constant positive (or down-scale) flux of enstrophy together with a vanishing flux of energy. The hidden statistical assumption of spectral broadening, necessary to obtain cascade directions, is here contained in the supposition of the cascades themselves.

Again making the assumption of local-in-k triad interactions, it is plausible that the energy spectrum in an inertial subrange will depend only on k and on the appropriate cascade rate. Dimensional analysis then suggests the power-law dependencies

$$\varepsilon(k) \propto \xi^{2/3} k^{-5/3} \quad \text{corresponding to} \quad F \equiv -\xi \; ; \; H \equiv 0 \; ; \qquad (2.31a)$$

$$\varepsilon(k) \propto \eta^{2/3} k^{-3} \quad \text{corresponding to} \quad F \equiv 0 \; ; \; H \equiv \eta \; . \qquad (2.31b)$$

(2.31a) describes the energy-cascading subrange, (2.31b) the enstrophy-cascading subrange. It turns out that the k^{-3} power law in (2.31b) is not consistent with the localness assumption (Kraichnan, 1967) and must be corrected by a logarithmic factor (Kraichnan, 1971):

$$\varepsilon(k) \propto \eta^{2/3} k^{-3} (\log k)^{-1/3} . \qquad (2.31c)$$

Moreover the $k^{-5/3}$ range (2.31a) cannot exist as a steady state unless there is spectrally-localized dissipation at small k, which is unlikely on physical grounds. Note that the k^{-3} range of (2.31b) has the same slope that would be expected from applying Batchelor's (1959) theory regarding the variance of a passive tracer to the vorticity; however that theory is inherently nonlocal, while the present arguments are decidedly local. In fact, it is clear that <u>any</u> dimensional argument assuming $E = E(k,\sigma)$ with σ having the dimensions of time, will yield a k^{-3} energy spectrum.

A common turbulence model derived from the above notions posits an energy-enstrophy source localized in a particular wavenumber range, together with viscous removal of energy at large scales and of enstrophy at small scales. The source and sink regions are connected by two inertial subranges, one transporting energy and the other enstrophy towards their sink regions. Such behaviour has been produced in a numerical model first by Lilly (1969, 1972), and recently under more general conditions by Basdevant, Legras, Sadourny & Béland (1981). The spectral slopes (2.31a,b) are not too difficult to obtain in such studies (the modification (2.31c) being too small to detect), nor are the qualitative features of the energy and enstrophy cascades. However the constant fluxes in (2.31a,b) are notoriously difficult to achieve in numerical studies, and so the theoretical question of the existence of "true" inertial subranges must still be considered an open one. In any case it must be said that (2.31a,b,c) are not predictions, but are rather particularly simple solutions which may or may not obtain.

The phenomenological model presented by (2.31a,b) is consistent with the inviscid absolute equilibrium solution (2.30), provided that one interprets the latter as the state toward which nonlinear interactions would take the system in the absence of other effects. In the enstrophy-cascading inertial subrange, which represents the high-k portion of the flow, an energy spectrum with a spectral slope $\varepsilon(k) \propto k^{-3}$ is decaying much more rapidly as $k \to \infty$ than is the absolute equilibrium spectrum $\varepsilon(k) \propto k^{-1}$. Since the presumption of an inertial subrange involves spectral localness and the lack of an explicit dependence on forcing or dissipation, one expects the nonlinear interactions associated with the k^{-3} spectrum to transfer energy or enstrophy to

large k in an attempt to decrease the spectral slope; that is, a down-scale cascade is anticipated. The actual nature of the cascade must be determined from a consideration of the integral constraints, which suggests that a down-scale cascade must be primarily a cascade of enstrophy, and must be accompanied by an up-scale cascade (primarily of energy) at smaller k. Here the statistical assumption which yields the cascade directions is the presumption of a tendency towards inviscid equilibrium.

In addition, it can be noted that the log-modified energy spectrum (2.31c) taken as $k \to \infty$ gives $\int_0^\infty k^2\varepsilon(k)dk < \infty$ but leaves $\int_0^\infty k^4\varepsilon(k)dk$ divergent; thus, according to the discussion of §2a, the inviscid limit is singular insofar as even a small amount of viscosity will be sufficient to maintain the enstrophy cascade. In such a limit, however, the energy dissipation will vanish, and the energy-cascading subrange will be eaten away as energy piles up around the spectral boundary k=0.

§2f. Similarity Theory for Evolving Turbulence

The discussion of the previous sections has indicated that in high Reynolds number 2-D turbulence, that is to say in the limit $\nu, r \to 0$ of (2.1), the enstrophy cascade can be expected to persist and to drain enstrophy continuously, while the total energy remains constant. Under these conditions of unforced, weakly-dissipative "spin-down" flow, and assuming that the influence of initial conditions decreases in time, one might suppose that as $t \to \infty$ the turbulence approaches a similarity state. Following Batchelor (1969), the only quantities which are then relevant to the energy spectrum $\varepsilon(k)$ are U, k, and t, where $U^2/2 \equiv \int \varepsilon dk$. Dimensional considerations then suggest a similarity solution

$$\varepsilon(k,t) = \frac{1}{2}tU^3 g(Ukt) \tag{2.32}$$

where g is some universal function of unknown shape. Note that (2.32) is consistent with the definition of U and that the total energy is indeed constant, provided that

$$\int_0^\infty g(x)dx = 1 \quad . \tag{2.33}$$

The decrease of enstrophy goes as t^{-2}, viz.

$$\Omega(t) = \int_0^\infty k^2\varepsilon(k)dk = \int_0^\infty \frac{1}{2}tU^3k^2g(Ukt)dk = \frac{1}{2}t^{-2}\int_0^\infty x^2g(x)dx \tag{2.34}$$

where the integrals must be convergent if the initial enstrophy is finite.

If g(x) peaks at x_0, then at any given time the energy spectrum peaks at $k = x_0/(Ut)$, and the peak moves towards k = 0 with time. Thus the spectrum is being compressed laterally at a rate 1/t, but is magnifying at a rate t to conserve total energy. More precisely, the evolution of the first moment k_1 proceeds as follows:

$$k_1 \equiv \frac{1}{\frac{1}{2}U^2}\int_0^\infty \frac{1}{2}ktU^3g(Ukt)dk = \frac{1}{Ut}\int_0^\infty xg(x)dx \equiv \frac{C}{Ut} \tag{2.35a}$$

whence

$$\frac{dk_1}{dt} = -\frac{C}{Ut^2} \quad ; \tag{2.35b}$$

this is consistent with the heuristic argument above.

If τ_D is the time it takes for the dominant eddies to double in size, then

$$\frac{1}{k_1\tau_D} \approx \frac{d}{dt}\frac{1}{k_1} = -\frac{1}{k_1^2}\frac{dk_1}{dt} = \frac{U^2t^2}{C^2}\frac{C}{Ut^2} = \frac{U}{C} \quad . \tag{2.36}$$

But the inertial or "eddy turn-around" time τ_I, characterizing the turbulence, is defined by

$$\tau_I = \frac{1}{Uk_1} \quad , \tag{2.37}$$

which leads to the result

$$\tau_D = C\ \tau_I \quad . \tag{2.38}$$

Consequently the cascade is a fairly rapid process, occurring on a time-scale which is of the same order (asymptotically) as the inertial time.

Knowledge of $\varepsilon(k,t)$ enables one to obtain the energy and enstrophy flux functions F,H defined by (2.13): from (2.32),

$$\frac{\partial \varepsilon}{\partial t} = \tfrac{1}{2}U^3 g(x) + \tfrac{1}{2}ktU^4 g'(x) \ , \tag{2.39a}$$

$$\frac{\partial (k^2\varepsilon)}{\partial t} = \tfrac{1}{2}U^3 k^2 g(x) + \tfrac{1}{2}k^3 tU^4 g'(x) \ , \tag{2.39b}$$

where $x \equiv Ukt$ (see also Rhines, 1979). The choice

$$F(k,t) = -\tfrac{1}{2}kU^3 g(x) = -\frac{\varepsilon k}{t} \tag{2.40a}$$

satisfies

$$-\frac{\partial F}{\partial k} = \tfrac{1}{2}U^3 g(x) + \tfrac{1}{2}ktU^4 g'(x) = \frac{\partial \varepsilon}{\partial t} \quad ,$$

but the trial solution $H_1(k,t) = -\tfrac{1}{2}U^3 k^3 g(x) = -\varepsilon k^3/t$ leads only to

$$-\frac{\partial H_1}{\partial k} = \tfrac{3}{2}U^3 k^2 g(x) + \tfrac{1}{2}k^3 tU^4 g'(x)$$

and thus requires an additional term H_2 such that $\frac{\partial H_2}{\partial k} = U^3 k^2 g(x)$. The solution is then

$$H(k,t) = -\frac{\varepsilon k^3}{t} + \frac{2}{t}\int_0^k \kappa^2 \varepsilon(\kappa,t)\,d\kappa \quad . \tag{2.40b}$$

From (2.40a,b), it is seen that the energy flux is everywhere up-scale, while the enstrophy flux operates in both directions. In the limit $k \to \infty$ with t held fixed,

$$H(k,t) \to \frac{2}{t}\,\Omega(t) \quad , \tag{2.41}$$

which clearly cannot hold indefinitely; however it can be expected to hold over the enstrophy-cascading scales (Batchelor, 1969).

§2g. Closure Theory

The theories of the preceding two sections are incomplete, asymptotic, and involve ad hoc phenomenological assumptions. Inviscid equilibrium theory is more deductive, but clearly fails in a predictive sense for any turbulent flow that is far from absolute equilibrium - as geophysical flows are apt to be. Recognizing that detailed knowledge of a turbulent flow is inherently impossible, one semi-deductive approach is to attempt to solve for the behaviour of statistical moments of vorticity $\langle\hat{\zeta}_i\hat{\zeta}_j\rangle$, $\langle\hat{\zeta}_i\hat{\zeta}_j\hat{\zeta}_\ell\rangle$, etc.

The problem with the statistical moment method is that it leads to an unclosed coupled hierarchy of equations, in which the equation for the n-th moment contains a term involving the (n+1)-th; the origin of this difficulty is the nonlinear coupling term $J(\psi,\nabla^2\psi)$ of (2.1), which leads in the spectral second-order moment equation (2.11) to the triad interaction term I(k). The challenge posed by the unclosed hierarchy is known as the "closure problem"; methods of closing the hierarchy in order to solve for the low-order moments, which necessarily require additional assumptions of an undeductive, phenomenological nature, are closure theories. Unfortunately, perturbation methods based on a small-parameter expansion, successful elsewhere, are to no avail in turbulence theory (Orszag, 1970). To this point, closure theories represent the only analytical solutions of nonequilibrium turbulence that are even semi-deductive, yet they remain quite unsatisfactory in many respects.

To outline the closure methodology, it is easiest to solve for the moments of y_i, defined by (2.18), rather than those of $\hat{\zeta}_i$ or of $\hat{\psi}_i$. This follows the notation of Salmon (1982). To get anything that is computa-

tionally feasible out of closure theory, one usually assumes that

$$\langle y_i(t)\rangle = 0 \quad , \tag{2.42a}$$

$$\langle y_i(t)y_j(t)\rangle = Y_i(t)\delta_{ij} \quad , \tag{2.42b}$$

which amounts to an assumption of spatial statistical homogeneity. This turns out to be a major limitation of existing closure theories, and in particular excludes their application to the present study. Then formally one can write the second-order moment equation (2.11) as

$$\left\{ \frac{d}{dt} + 2\nu_i \right\} Y_i = 2 \sum_{j,\ell} P_{ij\ell}\langle y_i y_j y_\ell\rangle \quad , \tag{2.43}$$

where $\nu_i \equiv r + \nu k_i^2$ and the $P_{ij\ell}$'s are coupling coefficients for the triads which satisfy $P_{ij\ell} = P_{i\ell j}$ and $P_{ijj} = 0 = P_{iij}$, and which vanish unless $\underline{k}_i + \underline{k}_j + \underline{k}_\ell = 0$. Solving for the third-order moment yields the equation

$$\left\{ \frac{d}{dt} + \nu_i + \nu_j + \nu_\ell \right\} \langle y_i y_j y_\ell\rangle = \sum_{m,n} \left\{ P_{imn}\langle y_m y_n y_j y_\ell\rangle + P_{jmn}\langle y_m y_n y_i y_\ell\rangle + P_{\ell mn}\langle y_m y_n y_j y_i\rangle \right\} \quad . \tag{2.44}$$

The simplest of all closures is just to set $\langle y_i y_j y_\ell\rangle \equiv 0$, in which case (2.43) implies viscous decay of an initial spectral distribution without any nonlinear interaction. Such a scenario is naturally not of much interest here. The next simplest closure involves factoring the fourth-order moments into second-order moments, viz.

$$\langle y_m y_n y_j y_\ell\rangle = \langle y_m y_n\rangle\langle y_j y_\ell\rangle + \langle y_m y_j\rangle\langle y_n y_\ell\rangle + \langle y_m y_\ell\rangle\langle y_n y_j\rangle \quad , \tag{2.45}$$

then using (2.45) to solve (2.44) and substituting the result into (2.43). One obtains, instead of (2.43), the equation

$$\left\{ \frac{d}{dt} + 2\nu_i \right\} Y_i = \sum_{j,\ell} \int_0^\infty \exp\left[-(t-\tau)(\nu_i+\nu_j+\nu_\ell)\right] \left\{4(P_{ij\ell})^2 Y_j(\tau)Y_\ell(\tau) + 8P_{ij\ell}P_{ji\ell}Y_\ell(\tau)Y_i(\tau)\right\} d\tau \quad . \tag{2.46}$$

For a Gaussian or "normal" distribution of y_i, (2.45) is exact but $\langle y_i y_j y_\ell\rangle \equiv 0$ also; thus the above algorithm is known as the quasi-normal

approximation, since it allows non-zero third-order moments. However this closure leads to unphysical negative values of energy after a finite time, as was shown first by Ogura (1963). A good discussion of the failure of the quasi-normal approximation can be found in Orszag (1970), where it is argued that the principal weakness of the method is its inefficient memory cut-off due to a neglect of relaxation by nonlinear scrambling effects.

A modification of the quasi-normal approximation which apparently rectifies its most glaring faults, and which has acquired much popularity, is the "eddy-damped Markovian" (EDM) approximation. Essentially, the modification consists of allowing the fourth-order cumulants (a cumulant is the difference between a moment and its Gaussian value) to relax the third-order moments, by augmenting the viscosity ν_i with an "eddy" viscosity μ_i on the right-hand side of (2.46), in order to accelerate the memory loss (Orszag, 1970). In addition, to simplify the time integration, Markovization can be imposed by replacing the $Y_j(\tau)$'s in (2.46) with $Y_j(t)$'s, thus eliminating nonsimultaneous covariances (see Leith, 1971). Note that the augmented viscosity does not directly dissipate energy or enstrophy; its sole role is to control the third-order moments. The resulting algorithm is very simple, namely

$$\left\{ \frac{d}{dt} + 2\nu_i + 2\eta_i \right\} Y_i = \sum_{j,\ell} \Theta_{ij\ell}\left[4(P_{ij\ell})^2 Y_j Y_\ell\right] \quad , \tag{2.47a}$$

where

$$\eta_i \equiv -4 \sum_{j,\ell} \Theta_{ij\ell} P_{ij\ell} P_{ji\ell} Y_\ell \tag{2.47b}$$

and

$$\Theta_{ij\ell}(t) \equiv \int_0^t \exp\left[-(\nu_i+\nu_j+\nu_\ell+\mu_i+\mu_j+\mu_\ell)(t-\tau)\right] d\tau \tag{2.47c}$$

the μ_i's being the eddy viscosities. (2.47c) presumes strictly Gaussian initial conditions, namely $\Theta_{ij\ell}(0) = 0$. Θ represents the decorrelation

time for the higher moments, and it is evident that a specification of $\Theta_{ij\ell}$ (or of μ_i) is enough to determine the closure. Note that (2.47c) implies

$$\Theta_{ij\ell} \to (\nu_i + \nu_j + \nu_\ell + \mu_i + \mu_j + \mu_\ell)^{-1} \quad \text{as } t \to \infty \ . \qquad (2.48)$$

The greatest weakness of closure lies in its necessary resort to phenomenological assumptions: while in principle the methodology is deductive, in practice it can never be wholly so. Nevertheless, comparison between theory and direct numerical simulation shows that the theory works fairly well within its expected range of validity (Herring, Orszag, Kraichnan & Fox, 1974). When it is reliable, the advantage of closure over direct simulation is that the former can handle a much higher resolution and consequently higher Reynolds numbers than can the latter. The restriction to homogeneous flows is a major shortcoming, however. While formally one can write down a closure algorithm for inhomogeneous flows that appears compact, in practice it turns out to be intractable with present-day computers unless severe restrictions are made (see, for example, Lin's (1982) attempt to apply closure theory to weakly inhomogeneous turbulence).

It is worth mentioning briefly an exceedingly simple closure of another nature altogether, namely Leith's (1968) diffusion approximation. This theory assumes that the inertial transfer functions $I(k)$ and $k^2 I(k)$ of (2.11) act to diffuse energy and enstrophy in wave-number space, and hence may behave according to a second-order diffusion operator applied to the energy spectrum. The only relevant parameters being $\varepsilon(k)$ and k, dimensional considerations then suggest the following form for the energy flux function F of (2.13):

$$F(k) = - \alpha \, k^{(7/2)-m} \, \frac{\partial}{\partial k} \left\{ k^m \left[\varepsilon(k) \right]^{3/2} \right\} \ , \qquad (2.49)$$

with α a nondimensional positive constant coefficient. To fix α the constraints (2.12) may be applied. It seems to be necessary to assume that $F(0) = 0 = F(\infty)$ automatically, though this is not totally evident from (2.49). In any case the enstrophy constraint gives

$$0 = -\int_0^\infty k^2 I(k)dk = \int_0^\infty k^2 \frac{\partial F}{\partial k} dk = k^2 F(k)\Big|_0^\infty - 2\int_0^\infty kF(k)dk$$

$$= 2\alpha \int_0^\infty k^{(9/2)-m} \frac{\partial}{\partial k}\{k^m [\varepsilon(k)]^{3/2}\}\, dk$$

$$= 2\alpha k^{9/2}\varepsilon^{3/2}\Big|_0^\infty - 2\alpha \int_0^\infty [(9/2)-m]k^{7/2}\varepsilon(k)dk \quad ,$$

whence $m = 9/2$, and F,H can be written as

$$F(k) = -\alpha\, k^{-1} \frac{\partial}{\partial k} (k^{9/2}\varepsilon^{3/2}) \tag{2.50a}$$

$$H(k) = -\alpha\, k^3 \frac{\partial}{\partial k} (k^{5/2}\varepsilon^{3/2}) \quad , \tag{2.50b}$$

with (2.50b) following from the identity

$$\frac{\partial H}{\partial k} = k^2 \frac{\partial F}{\partial k} \quad . \tag{2.51}$$

A remarkable result is that (2.50a,b) predicts the inertial subranges of §2e: substituting $\varepsilon(k) = Ak^{-5/3}$ gives the energy-cascading range

$$F = -2\alpha A^{3/2} \equiv -\xi \quad ; \qquad H \equiv 0 \tag{2.52a}$$

while substituting $\varepsilon(k) = Bk^{-3}$ yields the enstrophy-cascading subrange

$$F \equiv 0 \quad ; \qquad H = 2\alpha B^{3/2} \equiv \eta \quad . \tag{2.52b}$$

However, in principle (2.50a,b) ought to apply equally well to spectral ranges which are not inertial subranges, in which both flux functions will be non-zero and non-constant. One problem with the diffusion approximation is that it is inconsistent with the inviscid absolute equilibrium distribution (2.30); this is clearly unavoidable since inviscid equilibrium requires $F \equiv 0 \equiv H$, but that condition can never obtain from the forms (2.50a,b).

§2h. Spherical Geometry

For large-scale turbulence in the atmosphere, the assumption of Cartesian geometry used in the previous sections is no longer appropriate. The analogy between Fourier decomposition on a plane and spherical harmonic decomposition on a spherical shell has been pointed out by Baer (1972) and by Tang & Orszag (1978). On the sphere the 2-D total wavenumber squared $k^2 \equiv k_x^2 + k_y^2$ is replaced by $s^2 \equiv n(n+1)/\rho^2$ where n is the degree of the Legendre polynomial and ρ equals the radius of the sphere. This factor not only is the spectral biharmonic diffusion coefficient, but also represents the link between $\hat{\zeta}$ and $\hat{\psi}$. For simplicity one usually takes the 2-D scale index to be n rather than s. Although spectral decomposition has traditionally been performed in terms of the zonal wavenumber m, this representation suffers from the fact that identical wavenumbers at different latitudes correspond to different wavelengths. The 2-D index n, on the other hand, is a truly isotropic index which has a well-defined correspondence to wavelength. For a more detailed treatment of these questions, as well as of spherical harmonic analysis in general, see Boer (1983).

An arbitrary scalar function $A(\lambda,\phi,t)$ on a unit sphere, where λ is the longitude, ϕ the latitude, and $\rho \equiv 1$, may be expanded in terms of a series of spherical harmonics in the form

$$A(\lambda,\phi,t) = \sum_{n=0}^{\infty} \sum_{m=-n}^{+n} \hat{A}_n^m(t) Y_n^m \equiv \sum_{\alpha} \hat{A}_\alpha Y_\alpha \ , \qquad (2.53a)$$

where the spectral coefficients $\hat{A}_n^m$ are obtained by

$$\hat{A}_n^m(t) \equiv \hat{A}_\alpha \equiv \{A\}_\alpha = \frac{1}{2\pi} \int_0^{2\pi} \int_{-1}^{1} A(\lambda,\phi,t) Y_\alpha^*(\lambda,\phi) \, d(\sin\phi) \, d\lambda \ . \qquad (2.53b)$$

Here the complex wavenumber $\alpha \equiv n_\alpha + im_\alpha$ has been introduced. Subscripts are used rather than functional forms because of the discrete spectral index. The spherical harmonics Y_α are defined as

$$Y_\alpha = P_\alpha(\mu)\ e^{im_\alpha\lambda} \ ,$$

where $\mu \equiv \sin\phi$ and

$$P_\alpha(\mu) \equiv P_n^m(\mu) = \left\{ \frac{(2n+1)(n-m)!}{2(n+m)!} \right\}^{1/2} \frac{(1-\mu^2)^{m/2}}{2^n\, n!} \frac{d^{(n+m)}}{d\mu^{(n+m)}}\left[(\mu^2-1)^n\right] \qquad (2.54)$$

is the associated Legendre polynomial of degree n. In this representation the basis functions are orthonormal; that is,

$$\frac{1}{2\pi}\int_0^{2\pi}\int_{-1}^{1} Y_\alpha Y_\gamma^* d\mu d\lambda = \delta_\alpha^\gamma \ . \qquad (2.55)$$

The most important property of the Y_α's is

$$\nabla^2 Y_\alpha = -\, n_\alpha(n_\alpha+1)\ Y_\alpha \qquad (2.56)$$

so that in particular

$$\hat{\zeta}_\alpha \equiv \{\nabla^2\psi\}_\alpha = -\, n_\alpha(n_\alpha+1)\ \hat{\psi}_\alpha \ . \qquad (2.57)$$

However, single derivatives are more complicated:

$$(1-\mu^2)\frac{dP_n^m}{d\mu} = (n+1)\mu\ P_n^m - (n+1)\left(\frac{2n+1}{2n+3}\right)^{1/2} P_{n+1}^m \ . \qquad (2.58)$$

It should be noted that permissible wavenumbers now form a discrete set, whereas in the 2-D infinite plane case the set was continuous. However, because n is the total 2-D index for spherical harmonics, it is a simple matter to obtain an isotropic spectral representation of A by summing over all m, in a manner equivalent to (2.9): specifically,

$$\hat{A}_n \equiv \sum_{m=-n}^{+n} \hat{A}_n^m \ . \qquad (2.59)$$

Similarly to the plane case, there are the quadratic identities representing global averages,

$$\frac{1}{2\pi}\int_0^{2\pi}\int_{-1}^{1} AB\,d\mu d\lambda \equiv \langle AB\rangle = \sum_\alpha \frac{1}{2}\hat{A}_\alpha \hat{B}_\alpha^* \qquad (2.60a)$$

and

$$\langle A^2 \rangle = \sum_{\alpha} \frac{1}{2} \left| \hat{A}_\alpha \right|^2 \quad , \tag{2.60b}$$

so that spectra are well-defined. $\langle \cdot \rangle$ is not strictly an ensemble average, unless the turbulence is homogeneous. In particular, the energy and enstrophy spectra are given by

$$E = \sum_{\alpha} E_\alpha = \sum_{n=0}^{\infty} E_n = \sum_{n=0}^{\infty} \{ \sum_{m=-n}^{+n} \frac{1}{4} n(n+1) \left| \hat{\psi}_\alpha \right|^2 \} \quad , \tag{2.61a}$$

$$\Omega = \sum_{\alpha} \Omega_\alpha = \sum_{n=0}^{\infty} \Omega_n = \sum_{n=0}^{\infty} \{ \sum_{m=-n}^{+n} \frac{1}{4} n^2 (n+1)^2 \left| \hat{\psi}_\alpha \right|^2 \} \quad , \tag{2.61b}$$

where again $\rho \equiv 1$. (2.61a) is the spherical equivalent of (2.4). A more detailed discussion of these formulae, including the corresponding energy and enstrophy budget equations and flux functions, is given in Boer & Shepherd (1983).

Despite the evident analogy between the formulae for spherical and infinite plane geometries, there are some important differences with dynamical implications. The first is that on a sphere there is, in addition to conservation of total energy and enstrophy, the constraint of conservation of angular momentum; the latter ensures the separate invariance of both $\hat{\psi}_1^0$ and $\left| \hat{\psi}_1^1 \right|$. The implications of these and other spherical effects with regard to the inviscid equilibrium spectral distributions have been considered by Frederiksen & Sawford (1980). Roughly speaking the results are very similar, and this is no surprise: by (2.61a,b) the energy and enstrophy are functions of n only (assuming equipartition), as they are functions of k only in the plane case; and the number of independent modes with $n=n_0$ is almost proportional to n_0, namely $(2n_0+1)$, as compared with $2\pi k_0$ in the plane case. Consequently the absolute equilibrium spectrum is given by

$$\varepsilon(n) = \frac{n + (1/2)}{\alpha + \gamma n(n+1)} \quad , \tag{2.62}$$

which is very similar to (2.30). Note that α in (2.62) is <u>not</u> the complex wavenumber, but is used for consistency with (2.30).

Another difference relates to the division of the energy spectrum into zonal and meridional components. Equation (2.6a,b) shows that for the plane geometry, the spectrum of energy equals the sum of the spectra of u and v (i.e. at each <u>k</u>) so that there is no ambiguity. In a spherical geometry, however, the situation is not so clear-cut. Baer's (1972) analysis proceeds by transforming u and v directly via (2.53a) to obtain

$$\langle \tfrac{1}{2}u^2 \rangle = E_U = \sum_\alpha E_{U,\alpha} \equiv \sum_\alpha \tfrac{1}{4}\left|\hat{u}_\alpha\right|^2 \quad , \tag{2.63a}$$

$$\langle \tfrac{1}{2}v^2 \rangle = E_V = \sum_\alpha E_{V,\alpha} \equiv \sum_\alpha \tfrac{1}{4}\left|\hat{v}_\alpha\right|^2 \quad . \tag{2.63b}$$

Unfortunately, $E_\alpha \neq E_{U,\alpha} + E_{V,\alpha}$ so the decomposition (2.63a,b) lacks a straightforward interpretation comparable to that of (2.6a,b). This is due to (2.58), and to the fact that u and v are vectors, not scalars.

To rectify this difficulty, Tang & Orszag (1978) propose transforming not (u,v) but rather $\cos\phi\cdot(u,v)$, which they argue is more appropriate for vectors; this leads to the simple relationship

$$\{\cos\phi\cdot v\}_\alpha = im_\alpha\hat{\psi}_\alpha \quad . \tag{2.64}$$

Considering now the <u>single wave</u> whose streamfunction is $\mathrm{Re}(\hat{\psi}_\alpha Y_\alpha)$, and using (2.64) to obtain v in terms of $\hat{\psi}_\alpha$, the energy in the velocity in the meridional direction for this single wave is given by

$$E_{\phi,\alpha} = \tfrac{1}{4}\left(n+\tfrac{1}{2}\right)\left|m\right|\left|\hat{\psi}_\alpha\right|^2 \quad . \tag{2.65a}$$

The difference between the total energy E_α and $E_{\phi,\alpha}$ is assigned to the zonal component $E_{\lambda,\alpha}$: thus (2.61a) and (2.65a) imply

$$E_{\lambda,\alpha} = \frac{1}{4}\left[n(n+1)-\left(n+\frac{1}{2}\right)\left|m\right|\right]\left|\hat{\psi}_\alpha\right|^2 \quad . \tag{2.65b}$$

It may be easily verified that for homogeneous, isotropic flow, where $\left|\hat{\psi}_n^m\right|$ is independent of m (Boer, 1983), there is an equal partition of E_n between its zonal and meridional components: $E_{\lambda,n} = E_{\phi,n}$. Note that Tang & Orszag (1978) have an error in their equations (24a,b), which leads them to conclude only an approximate equipartition. This single-wave calculation can be repeated with a full spectrum provided that the flow is homogeneous and isotropic, since then the cross-product terms are uncorrelated (Boer, 1983). Further characteristics of homogeneous and isotropic flow on the sphere are developed in the Boer paper.

A final difference between spherical and plane 2-D turbulence concerns the nonlinear interactions between different modes. On a plane, the coupling between two Fourier modes is additive in a vectorial sense; consequently one is naturally led to consider triads of waves. But the coupling between spherical harmonics is significantly more complicated and far less restrictive; Tang & Orszag (1978) describe this feature of multi-component transfer and show that it has two major ramifications: the first is that energy and enstrophy transfer between scales is more local in spherical than in Cartesian geometry; the second, which is related to the first, is that cascades can be expected to be slower. It is worth mentioning that the angular momentum constraint also forbids transfer into the n=1 modes.

§2i. Discretization and Truncation

In trying to deduce the characteristics of 2-D turbulent flow from the form of the governing equations, one realizes fairly quickly that it

is difficult to obtain results which are much more specific than those of the preceding sections. The difficulty is of course inherent in the very nature of turbulence, which is essentially random and unpredictable and which demands statistical methods. Indeed, even if one were clever enough to find a particular solution of the equations, it would very likely be of little significance with regard to the expected behaviour of actual turbulent flows, since the particular solution would be of zero measure in the space of all possible solutions.

The analytical possibilities being limited by the fundamental non-linearity of the dynamical equations, one is consequently led to consider more phenomenological approaches. In 3-D homogeneous turbulence, theoretical advances have largely proceeded hand in hand with experimental evidence (see Batchelor, 1953). With 2-D turbulence, the possibility of experimental verification is hampered by the difficulty of suppressing 3-D instabilities and keeping the fluid truly two-dimensional - unless the fluid is rotating. This latter qualification turns out to be the critical one which makes the field of 2-D turbulence relevant to geophysical fluid dynamics, as will be discussed in the next chapter. But with regard to non-rotating 2-D turbulence, the lack of experimental evidence is made up for by the possibility of direct numerical simulation, something which is still not feasible for 3-D homogeneous turbulence at high Reynolds numbers.

Direct numerical simulation of 2-D turbulence proceeds by solving the governing equation (2.1) from a given set of initial conditions. This numerical solution is of necessity approximate, in two distinct ways: the time-stepping algorithm cannot represent high-frequency evolution, while the spatial discretization cannot represent small-scale

motion. Though in practice the first difficulty tends to be the more serious, especially with regard to error growth, it is the second which is of concern at this time. With the exception of §2d, all of the theory of the preceding sections assumed a continuous distribution of wavenumbers, and it is clear that a numerical model cannot avoid dealing with not only a discrete but also a finite set of modes; this is the case regardless of whether the model is of the spectral or the finite-difference variety.

Discretization of the set of permissible wavenumbers is possible without approximation, of course, whenever the domain is restricted, for then the boundary conditions forbid all but a discrete set of modes. If there exist solid boundaries, then statistical homogeneity and isotropy are automatically excluded (except, perhaps, well within the interior of the fluid) and application of the various theories is certainly problematical. But there are two important situations where homogeneity and isotropy are possible within a restricted domain: when the domain is a closed surface in a higher-dimensional space (such as the surface of a sphere, e.g. §2h), and when the domain is periodic. Obviously the latter situation is not precisely physically realizable, but it does approximate an infinite domain provided that the size of the domain is sufficiently large to allow all realistic motions.

In situations where the spectra are discretized, there are no a priori reasons why the theories formulated for continuous spectra should not apply; after all, the theories themselves are not derived in any rigour. But more importantly, the qualitative arguments of §2b and §2c must still apply, since the spectral interactions are closed: that is, the interaction between one mode and another produces a resultant

which is exactly resolvable into another mode (or modes).

The difficulty with direct numerical simulation, and for that matter with most "analytical" closures, is that they demand a truncation of the countably infinite discretized spectrum. Now spectral interactions are no longer closed, and there is a lower limit to the scale of motions which can be resolved. On the face of it, this could be an enormous problem. For example, if the truncation were made within a reverse-energy-cascading inertial subrange (assuming it existed), then the model could not avoid catastrophic errors in the resolved motions.

Yet there is one situation in which 2-D turbulence has a chance of being accurately modelled with a finite set of modes, namely where the initial energy and any subsequently forced energy is separated in a spectral sense from the (smaller) truncation scale. There are, however, a few obvious requirements. The first is that the inertial interactions must be computed in such a way as to exactly conserve both the total energy and the total enstrophy, for those are the crucial constraints of 2-D turbulence; this must be done despite the inevitable loss of information through nonlinear interactions which have unresolved resultants. The other requirement is that the enstrophy cascade down to the truncation scale, which need not correspond to an inertial subrange, must be correctly simulated, in order to avoid a piling up of enstrophy at the truncation scale; this clearly demands a removal of enstrophy before it actually reaches that scale. While there is agreement on the necessity of such a removal mechanism, there have been no methods developed thus far which can claim to be either totally satisfactory or even universally accepted. Two of the most appealing on theoretical grounds are the proposals of Leith (1971) and of Sadourny & Basdevant

(1981); with regard to the latter, see also Basdevant & Sadourny (1983). However, in practice it is most common to simply use a high-order multi-harmonic (i.e. ∇^{2n}) operator (e.g. Haidvogel, 1983).

CHAPTER III - GEOSTROPHIC TURBULENCE

§3a. Introduction

Because of the large ratio of horizontal to vertical scale in the atmosphere and oceans, one is tempted to conclude that behaviour characteristic of 2-D turbulent flow may be expected simply as a consequence of the quasi-two-dimensional geometry. To some extent this may not be too far-fetched; certainly the possibility of 3-D homogeneous turbulence is eliminated. But even for shallow fluids, the vorticity equation (2.1) is not generally appropriate and the flow is not strictly two-dimensional, for there is the possibility of vertical motion and thus of vertical coupling between horizontal layers. On the face of it, this would seem to make the study of 2-D fluids a purely academic exercise.

However, the subject of 2-D turbulence is saved from irrelevance by the rather special character of shallow, rotating flows with low Rossby number $Ro = \frac{U}{2\Omega L}$, namely those flows for which the fluid velocities are only slight deviations from solid-body rotation. Here U and L are representative velocity and length scales, and Ω is the angular velocity of the body; clearly Ro will differ for different classes of motion. In the geophysical context, motions which are significantly affected by the earth's rotation will be called "large-scale"; the use of the term is justified a posteriori by the observational fact that the Rossby number generally increases with decreasing length scale.

The most important feature of shallow, weakly-dissipative, low-Rossby-number flows is their tendency to be in a state of geostrophic and hydrostatic balance. Geostrophic balance represents an approxima-

tion to the full horizontal momentum equation in which the horizontal pressure gradient balances the Coriolis acceleration associated with the horizontal velocity, and which results from the small Rossby number. Hydrostatic balance, on the other hand, is a consequence of the shallowness of the fluid, and represents an approximation to the full vertical momentum equation in which vertical pressure differences are due solely to the differential weight of the fluid at rest. These balances place severe constraints on permissible fluid motions, and are responsible for the relevance of 2-D fluid dynamical theory to large-scale geophysical flows.

It will be shown in §3b that there is indeed a physical system to which 2-D theory is strictly relevant, namely a shallow, rotating, homogeneous and incompressible quasi-geostrophic fluid. This identification is noteworthy in itself, although even without it the 2-D theory might be useful from an analogical point of view; but it is especially important because the same system is often used by geophysical fluid dynamicists to describe large-scale flow phenomena of relevance to the atmosphere and oceans. There are, however, two principal complications to the system which give rise to significant geophysical effects and which must be addressed within the context of 2-D turbulence theory. The first is that the geophysical geometry is spherical, and large-scale motions are likely to feel the effects of the surface curvature; this gives rise to a far more profound effect than any found in the non-rotating spherical case of §2h, namely the possibility of Rossby waves. Such a mixed case of waves and turbulence is treated in §3c.

The second complication is that the atmosphere and oceans are not

homogeneous, but are rather stratified with lighter fluid overlying heavier; moreover the atmosphere is not at all incompressible. These considerations lead to a generalization of 2-D turbulence known as "geostrophic turbulence", which is presented in §§3d,e; although, as in §3b, the quasi-geostrophic constraints keep the system two-dimensional in a mathematical sense, and thus preserve the character of 2-D turbulence, nevertheless the formalism of the 2-D theory must be substantially modified. However it turns out that some rather simple arguments, supported by evidence from both closure theory and numerical simulation, suggest that for many phenomena of interest, geostrophic turbulence reduces to a case of forced 2-D turbulence. Consequently the study of 2-D turbulence is once again justified, even for stratified flows, and not simply for analogical reasons.

§3b. Homogeneous Rotating Flow and the f-plane

It is simplest to begin by considering the case of a homogeneous (that is, uniform density), incompressible, inviscid fluid in a flat geometry, with a free upper surface $\eta(x,y,t)$. The angular velocity vector $\underline{\Omega}$ associated with the rotation is chosen to point upwards. Then the three-dimensional vorticity equation in this low-Rossby-number case implies that the horizontal velocities u,v are independent of height z (Pedlosky, 1979, §2.7):

$$\frac{\partial u}{\partial z} = \frac{\partial v}{\partial z} = 0 \quad . \tag{3.1}$$

Condition (3.1) is essentially the Taylor-Proudman theorem; it states that the fluid moves as a set of vertical columns. The assumption of a shallow fluid allows hydrostatic balance to be imposed, and one is then led to the "shallow-water equations" (Pedlosky, 1979, §3.3), which are a

set of three partial differential equations for u, v, and η.

However, the assumption $Ro \ll 1$ implies that, at least to a first approximation, geostrophic balance must hold:

$$u = -\frac{g}{f}\frac{\partial \eta}{\partial y} \quad ; \qquad v = \frac{g}{f}\frac{\partial \eta}{\partial x} \quad . \tag{3.2a,b}$$

In the above g is the gravitational acceleration, and $f \equiv 2\Omega$ is the Coriolis torque parameter; the latter is constant for this plane geometry, namely the "f-plane". Applying (3.2a,b) strictly would render the shallow-water equations degenerate; to determine the evolution of a unique solution one must consider instead the vorticity equation, which in this case can be written in the "potential-vorticity" form,

$$\frac{d}{dt}\left\{\frac{\zeta + f}{D + \eta}\right\} = 0 \quad , \tag{3.3}$$

D being the (constant) depth of the fluid at rest, $\zeta \equiv v_x - u_y = \frac{g}{f}\nabla^2\eta$ the relative vorticity. Here $\frac{d}{dt}$ is the material derivative $\frac{\partial}{\partial t} + u\frac{\partial}{\partial x} + v\frac{\partial}{\partial y}$. Formally, (3.2a,b) is the leading-order balance which applies to the lowest-order terms in an expansion of the variables in terms of the small parameter Ro. The higher-order ageostrophic corrections are only present implicitly, yet they are crucial in order to avoid the problem of geostrophic degeneracy and to determine the temporal evolution of the flow via (3.3). This procedure of imposing geostrophic balance at leading order whilst allowing small ageostrophic fluctuations to enter at higher order, is known as the "quasi-geostrophic approximation"; it is treated in great detail by Pedlosky (1979, §3.12, §6.3), who derives it rigorously through scaling arguments for the case of both homogeneous and stratified fluids.

Because of the leading-order geostrophic balance (3.2a,b), the horizontal velocities are nondivergent on horizontal planes and the free

surface displacement η serves as a streamfunction for the motion; this explains why the vorticity equation is sufficient to determine the evolution of the leading-order quantities. Moreover, condition (3.1) can be supplemented by the additional relations

$$\frac{\partial u}{\partial x} + \frac{\partial v}{\partial y} = 0 = \frac{\partial w}{\partial z} \quad ; \tag{3.4}$$

together, (3.1) and (3.4) provide a full statement of the consequences of the Taylor-Proudman theorem. Since the flow is inviscid at this order (equivalently, the Ekman number is small), the lower boundary condition of $w = 0$ applied with (3.4) implies that $w = 0$ at all levels (to leading order), and that the vertical columns are truly rigid. Hence the fluid is effectively two-dimensional.

To establish the mathematical connection with 2-D turbulence theory, it is necessary to consider the leading-order approximation to (3.3). Quasi-geostrophic scaling (see Pedlosky, 1979, §3.12) necessitates that

$$\eta = O\left(\frac{DL^2 Ro}{R^2} \right) \quad , \tag{3.5}$$

where R is the external Rossby radius of deformation, namely

$$R^2 \equiv \frac{gD}{f^2} \quad . \tag{3.6}$$

Obviously $\zeta = O(U/L)$, and an advective time scale is chosen without loss of generality. Introducing the parameter

$$F \equiv \frac{f^2 L^2}{gD} \equiv \left(\frac{L}{R}\right)^2 \quad , \tag{3.7}$$

allows the potential vorticity $\frac{\zeta+f}{D+\eta}$ to be expanded in terms of non-dimensional parameters (denoted by primes) as

$$\frac{\zeta+f}{D+\eta} = \frac{f}{D}\left(Ro\zeta' + 1\right)\left(1 - RoF\eta' + \ldots\right) = \frac{f}{D}\left\{1 + Ro(\zeta' - F\eta') + \ldots\right\}, \tag{3.8}$$

where the dots indicate higher-order terms in the Rossby-number expansion. The validity of (3.8) requires that $F \lesssim O(1)$. Dropping the

primes now, (3.8) implies that (3.3) may be approximated by

$$\frac{d}{dt}\left(\zeta - F\eta\right) \equiv \frac{\partial}{\partial t}\left(\zeta - F\eta\right) + J(\eta, \zeta - F\eta) = 0$$

$$\Leftrightarrow \qquad \nabla^2\eta_t - F\eta_t + J(\eta, \nabla^2\eta) = 0 \quad , \tag{3.9}$$

which is strictly two-dimensional and, moreover, is very close to the inviscid form of (2.1). For sufficiently small L, $F \ll 1$ and (3.9) merely describes 2-D turbulence. The up-scale energy cascade will be arrested at $L = O(R)$, however, since by (3.9), $\eta_t \to 0$ for $F \gg 1$.

To estimate the relative importance of F in the dynamics of the mid-latitude troposphere, for example, take $f = 10$ m/s, and $D = 10^4$ m; then $R \approx 3 \times 10^6$ m. The associated wavelength would be $\lambda_R = 2\pi R \approx 2 \times 10^7$ m, which certainly exceeds the wavelength of most synoptic-scale disturbances in the mid-latitude troposphere. Thus one might imagine that with the exception of the very largest waves, which in any case would be only weakly active in nonlinear interactions, one may take $F \ll 1$ in (3.9) so that the fluid is effectively bounded on top by a rigid lid; then the dynamics are entirely governed by the equation of 2-D turbulence, and all of the theory of chapter II must be considered relevant. The argument works just as well for oceanic parameter settings, but becomes questionable for tropical values of f. It is an easy matter to include the effects of weak friction in the shallow-water equations (see Pedlosky, 1979, chapter 4) in such a way as to arrive at (2.1) for this small-F situation.

§3c. Waves and Turbulence on the β-plane

When one employs a Cartesian model such as the f-plane of §3b to represent geophysical fluid phenomena, the presumption is that a portion of the earth's surface can be locally approximated by a tangent plane.

The only dynamically significant part of the earth's planetary vorticity, namely that part entering into the geostrophic balance, is the component normal to the earth's surface $f = 2\Omega\sin\phi$, where ϕ is the latitude and Ω the angular velocity. In §3b f was presumed constant. But insofar as the plane is supposed to locally approximate the surface of a sphere, where f is a function of ϕ, it is reasonable to suppose that, in order to model large-scale motions, one ought to consider the effects of a variable f. Indeed, it is evident from (3.8) that even small variations in f could enter into the leading-order potential-vorticity dynamics and could thus be quite significant.

An approximation of immense utility to geophysical fluid dynamics, due to Rossby (Rossby et al., 1939), is that of linearizing f about some mean latitude ϕ_0:

$$f \approx f_0 + \left.\frac{\partial f}{\partial y}\right|_{\phi_0} y \quad , \tag{3.10}$$

where y is the north-south coordinate on the plane surface. Here $f_0 \equiv 2\Omega\sin\phi_0$, and it is customary to write $\beta_0 \equiv \left.\frac{\partial f}{\partial y}\right|_{\phi_0}$; hence the appellation "β-plane" to describe the geometry. For $y = a\phi$ with a the radius of the earth,

$$\beta_0 \equiv \frac{2\Omega}{a}\cos\phi_0 = \left.\frac{\partial f}{\partial y}\right|_{\phi_0} . \tag{3.11}$$

It is evident that within a quasi-geostrophic context, (3.10) can only be a reasonable approximation for motions which are of a sufficiently limited meridional extent that

$$\Delta f \approx \beta_0 \Delta y \ll f_0 \quad ; \tag{3.12}$$

for mid-latitudes, (3.12) is equivalent to the condition $\Delta y \ll a$. For ϕ_0 near the equator, (3.12) is clearly impossible and quasi-geostrophy must be abandoned altogether, though the β-plane may still be useful. A rigorous derivation of the β-plane approximation is given by Pedlosky (1979, §6.2, §6.3).

While the β-plane is not a suitable framework in which to solve the momentum equations (Pedlosky, 1979, §6.3), it is generally valid for the vorticity equation which is, after all, the governing equation for a quasi-geostrophic system. Applying (3.10) to (3.3) via (3.8) and taking F to be small, one arrives at the (non-dimensional) equation for inviscid β-plane turbulence:

$$\nabla^2\psi_t + J(\psi,\nabla^2\psi) + \beta\psi_x = 0 \quad ; \tag{3.13}$$

in the above $\beta \equiv \beta_0 L^2/U$, and η has been replaced by the symbol ψ to emphasize its role as a streamfunction. For large-scale geophysical phenomena, β may be less than, equal to, or greater than order unity, depending on the appropriate values of L and U.

In the limit $\beta \to \infty$, the nonlinear Jacobian term of (3.13) becomes small so that the equation reduces to the linear Rossby-wave equation

$$\nabla^2\psi_t + \beta\psi_x = 0 \quad , \tag{3.14}$$

which allows solutions of the form

$$\psi = \exp\{i(kx+\ell y-\omega t)\} \quad , \quad \omega = -\beta k/(k^2+\ell^2) \quad . \tag{3.15}$$

One may introduce weak nonlinear effects to describe the coupling between waves by expanding ψ in terms of the small parameter β^{-1}, and by introducing a two-timing approximation, viz.

$$\psi(x,y,t) = \psi_0(x,y,t,\tau) + \frac{1}{\beta}\,\psi_1(x,y,t,\tau) + \ . \ . \ . \tag{3.16}$$

(see Pedlosky, 1979, §3.26), where $\tau \equiv \beta t$ is the "fast" time scale on which the waves oscillate, and t is the "slow" time scale on which they interact. Only resonant interactions will have an O(1) effect on the wave amplitudes (i.e. an effect on ψ_0), namely triad interactions between waves ψ_a, ψ_b, ψ_c for which not only

$$k_a + k_b + k_c = 0 \quad , \quad \ell_a + \ell_b + \ell_c = 0 \tag{3.17a}$$

(the definition of a triad), but also

$$\omega_a + \omega_b + \omega_c = 0 \quad ; \tag{3.17b}$$

(3.17a,b) provide a severe restriction on possible interactions.

It is easy to verify that (3.13) conserves both energy and enstrophy in an unbounded domain; moreover, the equations governing interactions between members of a resonant triad also conserve both quantities to leading order, as non-resonant interactions occur on a much slower time scale. This means that in any resonant triad interaction, a transfer of energy to smaller scale must be accompanied by a transfer to larger scale, which is again Fjørtoft's (1953) condition. The non-resonant result that spectral dispersion of energy leads, on average, to greater up-scale than down-scale transfer (Merilees & Warn, 1975), must be modified to incorporate the resonance "selection rule" (Yamagata & Kono, 1976). But for an isotropic distribution of energy, the conclusions turn out to be the same.

One might therefore anticipate the energy and enstrophy cascades of 2-D turbulence, provided that the appropriate statistical hypothesis could be made. Such a possibility is unlikely, however, since before two eddies could have an appreciable interaction on the slow time scale, the dispersive effects of wave propagation, acting on the fast time scale, would have separated them; stated otherwise, nonlinear interactions require physical coincidence, while dispersive wave propagation creates physical separation. Because a turbulent cascade requires many nonlinear interactions, it would seem an unlikely outcome of resonant interactions, the more especially since the condition of resonance is so restrictive.

Nevertheless, linear instability theory applied to such resonant

triad interactions (Rhines, 1975) does indicate that high-frequency Rossby waves will tend to be unstable to lower-frequency waves. It is most easy for energy to move in wavenumber space on curves of constant total wavenumber $(k^2+\ell^2)^{1/2}$, the enstrophy constraint then not entering, and on such curves (3.15) shows that the lowest-frequency waves are those with the smallest values of k. As k decreases, moreover, the favouring of up-scale over down-scale energy exchanges disappears (Yamagata & Kono, 1976), encouraging movement along those constant-wavenumber paths. Consequently the expected result of resonant interactions within a sea of Rossby waves will be a slow migration of wave energy and enstrophy along lines of constant $(k^2+\ell^2)$ towards the "zonal" axis $k = 0$, corresponding in physical space to an adjustment along geostrophic contours, f/D = constant, which in this case are simply east-west or "zonal" contours. This tendency has been verified in a calculation by Kenyon (1967). Energy cannot enter $k = 0$ modes by pure resonance involving discrete wavenumber triads, but the frequency condition (3.17b) is broadened by finite-amplitude effects so that only near-resonance is needed (Gill, 1974).

The opposite limit, $\beta \to 0$, yields merely the 2-D vorticity equation considered in chapter II, namely

$$\nabla^2\psi_t + J(\psi,\nabla^2\psi) = 0 \ , \qquad (3.18)$$

and no more need be said about the dynamics of this regime. The interesting aspects of β-plane turbulence come from considering, as Rhines (1975) originally did, the fact that 2-D turbulence on a β-plane has an inherent tendency to evolve into a field of Rossby waves: a set of disturbances with small β will tend, through nonlinear interactions, to increase the length scale of its energetic eddies, thus increasing L

while conserving U and thereby increasing β. Unless constrained by geometrical factors, β will inevitably reach a value of order unity; at that point Rossby-wave dispersion will take over, and the only further spectral evolution will be the slow resonant triad focussing of energy into zonal jets.

The most striking predictions of β-plane turbulence are the cut-off of the reverse energy cascade at a 2-D wavenumber k_β such that $k_\beta^2 = O(\beta_0/U)$, and the ensuing development of zonal anisotropy: first at the large scales where $\beta = O(1)$, and then at the smaller scales as the vorticity field is strained by the anisotropic large-scale motions (Herring, 1975). For "spin-down" scenarios involving the slow decay of a spectrally-localized initial disturbance, these predictions have been verified by direct numerical simulation (Rhines, 1975). Additionally, Holloway & Hendershott (1977) have found corroborative evidence using a closure scheme which includes the effects of wave propagation in such a way that in the limit $t \to \infty$, one obtains in place of (2.48)

$$\Theta_{ij\ell} \to \frac{\mu_i + \mu_j + \mu_\ell}{(\mu_i + \mu_j + \mu_\ell)^2 + (\omega_i + \omega_j + \omega_\ell)^2} \quad \text{as } t \to \infty , \tag{3.19}$$

for the triad relaxation or decorrelation time; here the ν_i's have been dropped for convenience, and the ω_i's are the Rossby-wave frequencies defined by (3.15). Note that in the "strong-wave" limit $\beta \to 0$ or $\mu \gg \omega$, (3.19) reduces to (2.48); while in the "weak-wave" limit $\beta \to \infty$ or $\omega \gg \mu$, (3.19) leads to the resonance condition

$$\Theta_{ij\ell} \to \pi \cdot \delta(\omega_i + \omega_j + \omega_\ell) \quad \text{as } t \to \infty . \tag{3.20}$$

The predicted end state for evolving turbulence of zonal anisotropy seems somewhat paradoxical, however, in light of the fact that since, in the absence of boundaries, the $\beta\psi_x$ term of (3.13) leaves

the global balance of both energy and enstrophy unaltered, the isotropic inviscid equilibrium solution (2.30) of 2-D turbulence must still apply. Although no numerical experiments have been run for a sufficiently long time to absolutely rule out the appropriateness of (2.30) for β-plane turbulence, it does seem on the basis of the present evidence that the ergodic hypothesis of stochastic mixing, necessary for an approach to statistical equilibrium, is no longer valid in the wave regime.

It should also be mentioned that the end state of zonal anisotropy requires a fairly homogeneous spatial distribution of disturbance energy. If the turbulence is initially confined to a "patch", then wave dispersion will tear apart the patch before any weak-wave interaction can take place. Rhines (1975, 1977) discusses this matter, which seems to be particularly relevant to the oceans, in more detail.

The above remarks concerning β-plane turbulence have dealt specifically with a hypothetical situation of spin-down or freely-evolving flow, but a more geophysically relevant scenario is that where the wave and turbulence regimes exist simultaneously in a forced, dissipated flow. In that case the parameter β may be somewhat difficult to define. A presumption of localness in triad interactions would indicate that, for a given scale k, the appropriate U should represent the energy of all scales within some width Δk of k; similarly, long-wave advection of small-scale eddies can be easily incorporated into the wave solution (3.15), so that U should not include such effects. A reasonable approach is to assume that all waves within an octave of k contribute to U, so that

$$(U(k))^2 = 2 \int_{k/2}^{2k} E(\kappa) d\kappa \quad . \tag{3.21}$$

If the energy spectrum of the flow at equilibrium is of the form $E(k) \propto$

k^{-m}, then $U(k) \propto k^{(m-1)/2}$ and hence $\beta(k) \propto k^{(m-5)/2}$. It is thus evident that the predictions of β-plane turbulence cannot be valid in an equilibrium situation unless the energy spectrum decays less quickly than k^{-5} as $k \to \infty$. On the other hand, if E(k) is less steep than k^{-5}, it follows that one can divide the flow into two regimes: one being turbulent and unpredictable, corresponding to smaller length scales for which $\beta < O(1)$; the other being wave-like, coherent, and relatively predictable, valid for scales with $\beta > O(1)$. The regimes are, however, connected by the fact that the characteristics of 2-D turbulence tend to drive turbulent disturbances into the wave-like scales. Numerical simulations (e.g. Williams, 1978; Basdevant et al., 1981) have confirmed this picture.

While there is a clear separation between waves and turbulence in the spectral domain, the picture in physical space is rather that of the two regimes co-existing. If one traces particle trajectories, they tend to demonstrate both wave-like and turbulent behaviour (Rhines, 1979). But the physical-space signature of 2-D turbulence described in §2c, namely large vortices encircled by thin shear layers of enstrophy which are being continually peeled off and broken up, requires more spatial coherence than would seem likely in the presence of Rossby-wave dispersion. Indeed, the peculiar ability of 2-D turbulence to generate long-lived coherent vortices of high kurtosis (McWilliams, 1984) is entirely absent from β-plane turbulence.

In part because of the difficulty of fixing β, observational confirmation of the predictions of β-plane turbulence in the atmosphere or oceans tends to be ambiguous: Rhines (1975) has suggested wave-turbulence boundary scales of $k_\beta^{-1} \approx 1000$ km and $k_\beta^{-1} \approx 70$ km for the mid-latitude atmosphere and oceans, respectively, but these estimates

are subject to considerable uncertainty; in any case the numerical experiments indicate that the wave-turbulence boundary is fairly "soft". However the atmospheric reverse energy cascade does have a sharp cut-off for $n < 6$ (Boer & Shepherd, 1983), which is at least consistent with Rhines's estimate of mid-latitude zonal wavenumber 4; the significance of this coincidence will be explored in some detail in later chapters of this study. For the oceans, the data is far too sparse to enable calculation of nonlinear fluxes, but away from the strongest currents there does seem to be evidence of an energy maximum at about the transition scale of 70 km (Simmons et al., 1978). Because of the spatial inhomogeneity of oceanic large-scale turbulence, wave radiation of the disturbance energy away from its turbulent "patches" would probably preclude any development of zonal anisotropy there.

A more likely demonstration of pure β-plane turbulence might be found in the less viscous atmosphere of Jupiter, where k_β^{-1} is small enough that the ambiguity of the terrestrial situation is less of a problem. Williams (1978) has performed numerical experiments of β-plane turbulence using Jovian parameter settings, and has found that the results are in reasonable agreement with what is so far known of that planet's atmosphere. However the subject is far from closed: recent Voyager observations (Ingersoll et al., 1981) indicate the jets to be both barotropically unstable and a sink for eddy kinetic energy, apparently contradictory findings, though the sampling errors are still a matter of some concern. Moreover there are competitive "deep circulation" theories to explain the zonal bandedness (e.g. Busse, 1983), although the validity of these at mid-latitudes is questionable.

§3d. Turbulence in a Rotating Stratified Fluid

Although the homogeneous model of §§3b,c is able to exhibit a great many geophysical phenomena, in fact the atmosphere and oceans have a stable density stratification and are decidedly baroclinic. The possible tilting of constant-density or isopycnal surfaces, so that they do not coincide with isobaric surfaces, introduces baroclinicity which violates the conditions for the Taylor-Proudman theorem. Consequently the flow is no longer constrained to be two-dimensional in any real sense.

However geostrophy still provides the leading-order balance in the horizontal momentum equation, and thus the flow is approximately non-divergent on horizontal surfaces and a streamfunction may be defined. The vertical motion is small, indeed it vanishes to leading order in a Rossby-number expansion, yet it is dynamically significant due to the stratification: (3.13) must be modified, in this inviscid, unforced case, to

$$\nabla^2\psi_t + J(\psi,\nabla^2\psi) + \beta\psi_x = \frac{1}{\rho_s}\frac{\partial}{\partial z}\left(\rho_s \frac{w}{Ro}\right) \quad , \tag{3.22}$$

a non-dimensional equation, where again the quasi-geostrophic scaling of Pedlosky (1979) has been used; (3.22) holds for each z, and $\rho_s(z)$ is the stable density profile in the absence of motion. It is clear that the vortex-stretching mechanism of 3-D turbulence is now present, though its potency is limited by the geostrophic scaling; hence the enstrophy will not be a conserved quantity.

For this quasi-geostrophic system, however, the small vertical motion is related to the streamfunction according to the (adiabatic) heat equation

$$\frac{d\theta}{dt} + S\frac{w}{Ro} = 0 \quad , \tag{3.23}$$

where $S \equiv \frac{N^2 D^2}{f_0^2 L^2} \equiv \frac{L_R^2}{L^2}$ is the Burger number; L and D the horizontal and vertical length scales; N(z) the Brunt-Väisälä frequency; L_R the internal Rossby radius of deformation; and θ the perturbation potential temperature. In fact (3.23) is the leading-order approximation to the equation for conservation of total potential temperature, which is the key additional constraint for this 3-D fluid. For the mid-latitude atmosphere and oceans, $L_R \approx 1000$ km and $L_R \approx 100$ km respectively, so that $S = O(1)$ roughly corresponds to $\beta = O(1)$: an important coincidence! The hydrostatic relation still holds, and is simply written as

$$\frac{\partial \psi}{\partial z} = \theta \quad . \tag{3.24}$$

Then (3.22), (3.23), and (3.24) can be combined into a single equation for ψ, namely

$$\frac{d}{dt} \left\{ \nabla^2 \psi + \frac{1}{\rho_s} \frac{\partial}{\partial z} \left(\frac{\rho_s}{S} \frac{\partial \psi}{\partial z} \right) + \beta y \right\} \equiv q_t + J(\psi, q) = 0 \quad , \tag{3.25a}$$

which expresses conservation of "pseudo-potential vorticity" q (Charney, 1971); the distinction "pseudo" is made by Charney to emphasize that the conservation holds along the horizontal projection of the particle motion, whereas the Ertel potential vorticity is exactly conserved following a particle. Here the phrase "potential vorticity" will be used for either quantity, unless ambiguity is possible.

For the atmosphere and oceans $L_R \ll R$, and thus for motions with $S = O(1)$, free surfaces will behave like rigid lids; then the vertical boundary condition on flat inviscid surfaces will be

$$\frac{d}{dt} \left(\frac{\partial \psi}{\partial z} \right) = 0 \qquad \text{at } z = z_{\text{surface}} \, , \tag{3.25b}$$

using (3.23) and (3.24). Pedlosky (1979, chapter 6) discusses oceanic and atmospheric boundary conditions in more depth; here I shall be content to assume "rigid lids" at top and bottom, z = 0,1, and an

infinite horizontal domain.

Charney (1971) pioneered the subject of geostrophic turbulence by arguing that conservation of potential vorticity for 3-D quasi-geostrophic flow is analogous to conservation of "kinetic" vorticity in a 2-D fluid, and that that constraint, together with the conservation of total geostrophic (i.e. 2-D kinetic plus available potential) energy, place the same strong limitations on geostrophic turbulence as conservation of kinetic energy and enstrophy do for 2-D turbulence. The energy equation is simply obtained by multiplying (3.25a) by $\rho_s\psi$ and integrating over the domain:

$$\frac{d}{dt}\iiint \frac{1}{2}\rho_s\left\{\left|\nabla\psi\right|^2 + \frac{1}{S}\left|\psi_z\right|^2\right\} dxdydz = \iint \left[\frac{\rho_s}{S}\psi\frac{d}{dt}\psi_z\right]\Big|_{z=0}^{z=1} dxdy = 0 \ . \qquad (3.26)$$

It is evident from (3.25a) that the mean-squared potential vorticity, and in fact the mean of any power of q, will be conserved; however q^2 is not a very useful quantity to consider, as the βy term presents difficulties in the spectral analysis. Instead, Charney chose to re-write (3.25a) as

$$\xi_t + J(\psi,\xi) + \beta\psi_x = 0 \ , \qquad (3.27)$$

where $\xi \equiv \nabla^2\psi + \frac{1}{\rho_s}\left(\frac{\rho_s}{S}\psi_z\right)_z = q - \beta y$. Then multiplying (3.27) by $\rho_s\xi$ and integrating yields

$$\frac{d}{dt}\iiint \frac{1}{2}\rho_s\xi^2\, dxdydz = -\beta \iint \left[\frac{\rho_s}{S}\psi_x\psi_z\right]\Big|_{z=0}^{z=1} dxdy \ . \qquad (3.28)$$

The quantity ξ^2 will be called the "potential enstrophy". The right-hand side of (3.28) will not vanish in general, but can be made to do so if one of the following conditions is met: either $\beta \to 0$ (how small β has to be depends on $\psi_x\psi_z$); or $\psi_z \equiv 0$ at $z = 0,1$. Charney argued that for motions deep in the interior of the fluid, well away from boundary effects, the latter is not an unreasonable assumption. Defining a spectrum from the vertical structure equation

$$\frac{1}{\rho_s}\frac{\partial}{\partial z}\left(\frac{\rho_s}{S}\frac{\partial\psi}{\partial z}\right) = -m^2\,\psi \quad , \tag{3.29}$$

(this is always possible for a finite depth (Pedlosky, 1979, §6.12)), and transforming in three dimensions using the eigenfunctions of (3.29) to define the vertical representation, it may be easily verified that the spectral coefficients satisfy

$$\hat{\xi}_{k\ell m} = -(k^2+\ell^2+m^2)\,\hat{\psi}_{k\ell m} \equiv -\kappa^2\,\hat{\psi}_{k\ell m} \quad , \tag{3.30}$$

which is completely analogous to the 2-D relation for the vorticity spectrum; here $\underline{\kappa} = (k,\ell,m)$ is the 3-D wavenumber. In particular, it is evident that all of the predictions of the 2-D theory can be easily generalized to this 3-D quasi-geostrophic situation: Fjørtoft's rule, by example, becomes a statement that any movement of energy to larger κ must be accompanied by a transfer to smaller κ.

To establish a formal correspondence with the 2-D theory, it is necessary to make a few additional assumptions. Noting that

$$\frac{1}{\rho_s}\left(\frac{\rho_s}{S}\psi_z\right)_z = \frac{1}{S}\left\{\psi_{zz} + \frac{1}{\rho_s}\left(\frac{\partial\rho_s}{\partial z}\right)\psi_z - \frac{1}{S}\left(\frac{\partial S}{\partial z}\right)\psi_z\right\} \quad , \tag{3.31}$$

the last two terms of (3.31) may be neglected provided that one's interest is restricted to motions with a small enough vertical scale that ρ_s and S can be considered constant. In the case of ρ_s, this means that the vertical scale D must be less than the scale height, not a severe restriction. Under these conditions (3.29) is much simplified: the vertical eigenmodes are cosines, and there is a clear connection between m and the vertical scale. Defining the geostrophic energy by

$$E = \iiint \frac{1}{2}\rho_s\left\{\left|\nabla\psi\right|^2 + \frac{1}{S}\left|\psi_z\right|^2\right\}\,dxdydz = \iint \sum_m \frac{1}{2}\rho_s(k^2+\ell^2+m^2)\left|\hat{\psi}(\underline{\kappa})\right|^2\,dkd\ell$$

$$\equiv \iint \sum_m E(\underline{\kappa})\,dkd\ell \quad , \tag{3.32}$$

then conservation of geostrophic energy and potential enstrophy can be written as

$$\frac{d}{dt} \iint \sum_{m} E(\underline{\kappa})\, dk d\ell = 0 = \frac{d}{dt} \iint \sum_{m} \kappa^2\, E(\underline{\kappa})\, dk d\ell \quad , \qquad (3.33)$$

a form very similar to the 2-D conservation relations (2.10).

For horizontal scales smaller than the deformation radius L_R, where the turbulence will be locally homogeneous and isotropic in horizontal planes, and will be relatively unaffected by Rossby-wave dispersion, Charney argued that one can also expect 3-D homogeneity and isotropy in the re-scaled coordinates $(x,y,\sqrt{S}z)$; this implies that at a given isotropic scale κ, the energy will be partitioned equally between available potential energy (APE) and the two horizontal components of kinetic energy. Such a prediction is fairly easy to check against data, and appears to be valid for the atmosphere (Boer & Shepherd, 1983).

One may also employ arguments similar to those of §2e, under the assumption of being in a potential-enstrophy cascading inertial subrange (appropriate to this high-κ limit), to obtain a power-law relationship

$$\varepsilon(\kappa) \propto \kappa^{-3} \quad , \qquad (3.34)$$

where $\varepsilon(\kappa)$ is now the "isotropic" geostrophic energy, and κ is the 3-D wavenumber corresponding to the 3-D Laplacian operator in the re-scaled coordinates. Provided that the 3-D isotropy described above holds, it follows that each of the three "components" of energy will also follow a κ^{-3} spectrum, and that the κ^{-3} power law can be observed by integrating over two of the coordinates and computing spectra in one direction alone (Charney, 1971). However if the spectra are calculated in a model with a limited vertical resolution, such as a two-layer model, Merilees & Warn (1972) have shown that for sufficiently large κ the APE will follow a κ^{-5} rather than a κ^{-3} power law. Of course these predictions cannot

hold for arbitrarily large κ, as the validity of the quasi-geostrophic approximation must eventually break down; however they might be expected to hold over the resolution of the standard atmospheric observational network.

A problem with the theory as applied to the real atmosphere or oceans concerns the vertical structure equation (3.29). In general, ρ_s and S may be functions of x, y, and t, as well as of z; additionally, the eigenfunctions will not necessarily be clearly associated with a single vertical scale. Moreover the nature of the solutions depends heavily on the boundary conditions: while one obtains an infinite but discrete spectrum of m for a finite depth of fluid, considered here, treatment of the unbounded atmosphere may yield no baroclinic modes for realistic profiles of ρ_s and S (see Pedlosky, 1979, §6.12). Of course the purely barotropic mode ($\psi_z \equiv 0, m=0$) is always a solution of (3.29).

In decomposing atmospheric energy, however, Baer (1981) does find that for large horizontal scales, by far the dominant part of the energy is contained in the barotropic or nearly barotropic "external mode". This is consistent with a theoretical study of decaying geostrophic turbulence by Herring (1980) using a statistical closure: assuming 3-D homogeneity in the re-scaled coordinates, the flow evolves into 3-D isotropy for $\kappa \gg \kappa_0$, where κ_0 is the energy peak, and into barotropy for $\kappa \ll \kappa_0$. The first result agrees with Charney's high-κ prediction; the second, which is just the consequence of a reverse energy cascade to large vertical scale, is rather striking and in fact provides a key justification for the relevance of the present study. This important "barotropization" effect will be discussed further in the next section.

As Herring (1980) points out, an assumption of vertical statis-

tical homogeneity, necessary for application of closure theory, is somewhat restrictive for quasi-geostrophic flow since there is nothing in the quasi-geostrophic equations which by itself enforces vertical homogeneity; on the contrary, the dynamics of (3.25a,b) are clearly anisotropic. This is quite different from the situation in (infinite) 3-D Navier-Stokes turbulence, where homogeneity will be approached regardless of the initial conditions. Horizontal homogeneity can be expected in geostrophic turbulence, however, provided that β is sufficiently small.

Blumen (1978) has considered the complementary problem to Charney's, in which (3.25a,b) is simplified by setting $q \equiv 0$ in the interior of the fluid, but with ψ_z permitted to be non-zero at the top and bottom plane horizontal boundaries. The dynamics are then those of Eady's (1949) model of baroclinic instability. Blumen demonstrates that the principle of conservation of potential enstrophy is replaced by conservation of available potential energy on the boundaries, and that this together with conservation of total energy places a restriction on energy exchanges which is analogous to that of the Charney theory. However the inertial subranges of Blumen's theory are rather different: in particular, the APE on the horizontal boundaries is expected to follow a $k^{-5/3}$ power law in terms of the horizontal wavenumbers, in its down-scale cascading subrange.

Hoyer & Sadourny (1982) have discussed both the Charney (1971) and the Blumen (1978) models of geostrophic turbulence under a unified formalism, and have shown that the two become asymptotically equivalent as $\kappa \to 0$. By applying very simple phenomenological arguments, they are able to demonstrate that stationary large-scale baroclinic forcing

(appropriate to the atmosphere) leads very naturally both to baroclinic instability and, in the Blumen case, to quasi-geostrophic frontogenesis.

§3e. Geostrophic Turbulence in the Two-Layer Model

The discussion of §3d revealed a number of characteristics of geostrophic turbulence, in particular its analogical relationship to 2-D turbulence, and its tendency for energy to "barotropize" as part of the cascade to gravest total wavenumber κ. To explore the manner in which barotropization occurs, it is helpful to focus on a model of quasi-geostrophic flow which has proved to be of immense utility to geophysical fluid dynamicists: namely the two-layer model, in which the fluid is represented by two layers of homogeneous fluid with uniform but distinct densities, and the Taylor-Proudman theorem holds within each layer.

As Pedlosky (1979) has emphasized, the two-layer model provides an accurate description of the dynamics of a physically realizable system; moreover this system, though idealized, is appropriate for much of the oceans. The atmosphere is clearly not similar to a two layer fluid, but the equations of the two-layer model are equivalent, in this quasi-geostrophic context, to those obtained by making either a two-level finite-difference approximation to the continuous equations (3.25a,b), or equivalently a two-mode truncation of the spectral form of (3.25a,b) which resolves only the gravest two vertical modes. The connection between "layer" and "level" models is treated in detail by Pedlosky (1979, §6.18).

Dynamical meteorologists are in any case very familiar with the two-level or two-mode model, which seems to be capable of resolving small Rossby number motions in at least a qualitatively correct

fashion. Insofar as the theory of §3d is valid for high vertical modes, the latter motions ought to cascade into the two gravest modes; thus the two-mode model is justifiable a priori for describing geostrophic turbulence. Nevertheless it is comforting that the observations confirm this: the barotropic and first baroclinic modes appear to contain most of the non-equatorial oceanic energy (Simmons et al., 1978); in the atmosphere, although identification of vertical modes is less clear-cut, one can reach a similar conclusion (Baer, 1981).

From a dynamical standpoint, however, the two-layer model is justifiable in that it is the simplest possible system which demonstrates the phenomena of interest (a common pedagogical argument!). Consistent with this philosophy, attention will be focussed on the nonlinear interactions by considering an inviscid, unforced system on a flat f-plane; furthermore, the analysis is much simplified if the assumption is made of equal layer depths (not bad for the atmosphere, not so good for the oceans). Then the (non-dimensional) equations are (see Pedlosky, 1979, §6.16 for a derivation),

$$q_{i_t} + J(\psi_i, q_i) = 0 \qquad [i=1,2] \,, \tag{3.35}$$

where $q = \nabla^2\psi_i + (-1)^i\hat{F}(\psi_1-\psi_2)$ and $\hat{F} \equiv \frac{f_0^2L^2}{gD}\frac{\rho_0}{\Delta\rho} = F\frac{\rho_0}{\Delta\rho}$. Let i=1 and i=2 denote respectively the upper and lower layers. Following Salmon (1978), it is convenient to transform (3.35) into a two-mode representation. Set

$$\psi \equiv \frac{1}{2}(\psi_1+\psi_2) \,, \quad \tau \equiv \frac{1}{2}(\psi_1-\psi_2) \,, \tag{3.36a,b}$$

to define "barotropic" and "baroclinic" streamfunctions; τ is equivalent to the temperature at the fluid interface. Introducing

$$k_R \equiv (2\hat{F})^{1/2} = \sqrt{2}\,\frac{L}{L_R} \tag{3.36c}$$

as the relevant non-dimensional Rossby deformation scale, (3.35) can be

re-written as

$$\nabla^2\psi_t + J(\psi,\nabla^2\psi) + J(\tau,\nabla^2\tau) = 0 \quad , \tag{3.37a}$$

$$(\nabla^2-k_R^2)\tau_t + J(\psi,(\nabla^2-k_R^2)\tau) + J(\tau,\nabla^2\psi) = 0 \quad . \tag{3.37b}$$

It is evident from (3.37a,b) that a state of pure baroclinicity will produce barotropic energy, but that purely barotropic flow will forever remain so; hence the system has an inherent asymmetry which favours barotropy.

(3.37a,b) allow three conservation relations: conservation of total energy,

$$\frac{d}{dt}\iint \frac{1}{2}\left\{\left|\nabla\psi\right|^2 + \left|\nabla\tau\right|^2 + k_R^2\tau^2\right\} dxdy$$

$$= \frac{d}{dt}\iint \frac{1}{2}\left\{\left|\nabla\psi_1\right|^2 + \left|\nabla\psi_2\right|^2 + \frac{1}{4}k_R^2(\psi_1-\psi_2)^2\right\} dxdy = 0 \ , \tag{3.38a}$$

of the sum potential enstrophy,

$$\frac{d}{dt}\iint \frac{1}{2}\{(\nabla^2\psi)^2 + (\nabla^2\tau-k_R^2\tau)^2\}\, dxdy = \frac{d}{dt}\iint \frac{1}{2}\{q_1^2+q_2^2\}\, dxdy = 0 \ , \tag{3.38b}$$

and of the difference potential enstrophy,

$$\frac{d}{dt}\iint \frac{1}{4}\{\nabla^2\psi\cdot(\nabla^2-k_R^2)\tau\}\, dxdy = \frac{d}{dt}\iint \frac{1}{2}\{q_1^2-q_2^2\}\, dxdy = 0 \ . \tag{3.38c}$$

(3.38b,c) are, naturally, equivalent to conservation of q within each layer, a result immediately obvious from (3.35). In (3.38a), the three "components" of energy are given the following interpretation: on the left they are, in order, the barotropic KE, baroclinic KE, and APE; on the right, they are the upper layer KE, lower layer KE, and APE.

Now expanding ψ and τ in Fourier series according to (2.3), one obtains energy spectra as follows:

$$U(\underline{k}) = \frac{1}{2}k^2\left|\hat{\psi}(\underline{k})\right|^2 = \text{barotropic energy in wave } \underline{k} \ , \tag{3.39a}$$

$$E(\underline{k}) = \frac{1}{2}(k^2 + k_R^2)\left|\hat{\tau}(\underline{k})\right|^2 = \text{baroclinic energy in wave } \underline{k} \ , \tag{3.39b}$$

where in the latter the KE and APE are related by the ratio $\frac{KE}{APE} = \frac{k^2}{k_R^2}$.

Now the conservation relations (3.38a,b) become

$$\frac{d}{dt}\int\int_{\underline{k}} [U(\underline{k}) + E(\underline{k})]dk = 0 = \frac{d}{dt}\int\int_{\underline{k}} [k^2U(\underline{k}) + (k^2+k_R^2)E(\underline{k})]dk, \quad (3.40)$$

which is the two-layer equivalent of (3.33). The constraint (3.38c) limits the energy transfer between layers, but it is unclear how to apply it, and whether it can in fact yield any useful information in the present case; consequently (3.38c) will not be considered in what follows. There is nothing wrong with this: the point of the exercise is to see whether any conclusions can be obtained on the basis of (3.40) alone, and including (3.38c) could not allow any new possibilities. Under an assumption of vertical statistical symmetry, used by Salmon (1978) and by Herring (1980), the constraint (3.38c) disappears anyway.

Considering single triads $(\underline{k},\underline{p},\underline{q})$ of (3.40) with $\underline{k} + \underline{p} + \underline{q} = 0$, it is clear that they fall into two distinct classes: barotropic (UUU) triads, satisfying

$$\dot{U}(\underline{k}) + \dot{U}(\underline{p}) + \dot{U}(\underline{q}) = 0 = k^2\dot{U}(\underline{k}) + p^2\dot{U}(\underline{p}) + q^2\dot{U}(\underline{q}) , \quad (3.41a)$$

(the dot signifying a time derivative, as is standard), and mixed baroclinic-barotropic (UEE) triads, satisfying

$$\dot{U}(\underline{k}) + \dot{E}(\underline{p}) + \dot{E}(\underline{q}) = 0 = k^2\dot{U}(\underline{k}) + (p^2+k_R^2)\dot{E}(\underline{p}) + (q^2+k_R^2)\dot{E}(\underline{q}) . \quad (3.41b)$$

The UUU triads are of course the triads of 2-D turbulence; they have a proclivity to transfer energy up-scale and (potential) enstrophy down-scale (Merilees & Warn, 1975), and nonlocal triads are disfavoured because of their inefficiency in exchanging energy. With the UEE triads, however, the conclusions depend strongly on the position of the triad wavenumbers relative to k_R.

In the limit $k,p,q \gg k_R$, (3.41b) is indistinguishable from (3.41a)

and the dynamics are therefore those of two uncoupled layers of 2-D turbulence; this is sensible because at small horizontal scale, the interface is effectively rigid and vortex stretching is insignificant. For $k,p,q \ll k_R$, on the other hand, it is easily seen that $\dot{U}(\underline{k}) \approx 0$ and that (3.41b) reduces to a description of the "pairwise" interactions of 3-D turbulence (see Kraichnan, 1967),

$$\dot{E}(\underline{p}) + \dot{E}(\underline{q}) = 0 \quad . \tag{3.42}$$

In this limit there are no restrictions on down-scale transfer of baroclinic energy; note, moreover, that if energy does cascade down-scale, it will imply a conversion of APE to KE, that is to say baroclinic instability. With the enstrophy constraint gone, baroclinic energy can move freely in the spectral domain, and nonlocal interactions are no longer precluded. Interaction with the barotropic mode $U(\underline{k})$ is only possible for $k \approx k_R$; in Rhines's (1977) terminology, the scale k_R is an "aperture" through which barotropic-baroclinic energy exchange can take place. The aperture is one-way, however, in the sense that barotropic energy can never by itself give rise to baroclinicity.

These notions are quantified by Marshall & Chen (1982), who extend the analysis of Merilees & Warn (1975) to a two-layer quasi-geostrophic fluid. By calculating the percentage of triad interactions which involve a net energy exchange with larger scales, Marshall & Chen demonstrate a great sensitivity of this quantity to the relative positions of the wavenumbers, and verify the qualitative results obtained above. Except in very rare instances, potential enstrophy exchanges are overwhelmingly with smaller scales. Fu & Flierl (1980) have made similar calculations using a realistic oceanic stratification, and considering higher-order baroclinic modes. They verify the "attractor"

status of the first baroclinic and, even more, of the barotropic modes, and show the connection with Rossby-wave instability theory.

It is worth mentioning that classical linear baroclinic instability theory considers the special triads $k \approx q \gg p \to 0$, with the initial energy entirely located in $\underline{p}$. The instability results (e.g. Phillips, 1954) are consistent with the geostrophic turbulence arguments, as indeed they must be since baroclinic instability is really just a special, albeit important, kind of triad interaction: there is a short-wave cut-off in the two-layer model at $k = k_R$, demonstrating the inability of energy to move into the region $k > k_R$; and the wavelength of maximum instability is at $k = k_R/\sqrt{2} = O(k_R)$, demonstrating the efficiency of nonlocal interactions.

As in the case of the 2-D theory of chapter II, to obtain cascade directions one must make a statistical assumption equivalent to the Second Law of Thermodynamics. One way of doing this is to presume that nonlinear interactions will attempt to drive the system into statistical mechanical equilibrium. Salmon *et al.* (1976) have computed the equilibrium states for two-layer flow, and find a two-fold result: for $k \gg k_R$, the two layers are uncorrelated and each obeys the 2-D result of §2d; while for $k \ll k_R$, the layers are locked together and behave like a single barotropic fluid.

In "spin-down" experiments with the energy initially spectrally localized, the statistical hypothesis is simply that of spectral broadening. Then the arguments given above imply that energy will always move into large-scale barotropic modes, regardless of its initial spectral location, while the potential enstrophy will always move down-scale. The various tendencies are shown in Figure 3.1, with solid

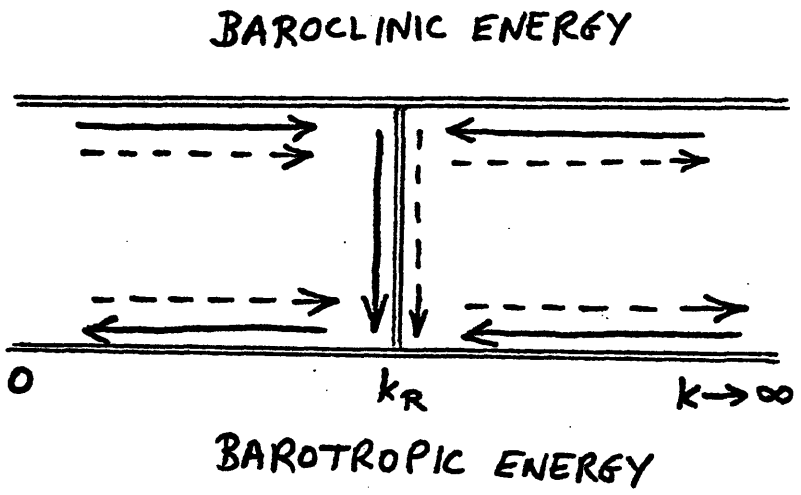


Fig. 3.1: Cascade tendencies of two-layer quasi-geostrophic turbulence for a spin-down experiment with spectrally-localized initial energy; as a function of wavenumber. Solid arrows represent energy, dashed the potential enstrophy.

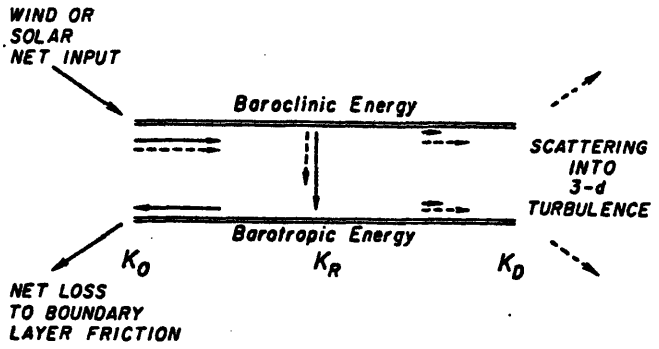


Fig. 3.2: A spectral representation of the energy and potential enstrophy cycles of a baroclinically forced two-layer model representative of the mid-latitude atmosphere. Solid arrows denote energy, dashed potential enstrophy. Taken from Salmon (1978).

arrows representing energy and dashed arrows potential enstrophy. Rhines (1977) has classified these cases in some detail, including the effects of Rossby-wave propagation, and has verified the cascades through numerical "spin-down" experiments. The ubiquity and completeness of the barotropization in these experiments is remarkable.

To a first approximation, the mid-latitude atmosphere is driven by large-scale baroclinic forcing in the guise of an imposed meridional temperature gradient (or equivalently, a vertical wind shear). Dissipation of potential enstrophy will presumably occur at small scales $k \gtrsim O(k_D)$, where the quasi-geostrophic approximation breaks down, but no energy can be dissipated there. The discussion above suggests that in forced-dissipative equilibrium the needed potential enstrophy cascade will ensure an energy cascade involving barotropization; dissipation of barotropic energy at large scales completes the balance. The picture is that of Figure 3.2. Salmon (1980) has examined this situation in detail, paying particular attention to the effects of the mean vertical shear and β on the cascades: the arrest of the reverse barotropic energy cascade has already been discussed in §3c, but β will affect the down-scale baroclinic energy cascade insofar as it affects baroclinic instability results.

The scenario of Figure 3.2 has been investigated by direct numerical simulation (Williams, 1979; Salmon, 1980; Haidvogel & Held, 1980) and by statistical closure (Salmon, 1980; Hoyer & Sadourny, 1982). All of the studies have emphasized the utility of geostrophic turbulence theory as a way of anticipating the behaviour of finite-amplitude, fully-developed baroclinic instability. In addition to the general correspondence between the down-scale baroclinic energy cascade

and the APE → KE conversion of baroclinic instability, there are other parallels: the secondary instability of ($k \approx k_R, \ell \approx 0$) modes to ($k \approx \ell \approx k_R$) structures obtainable from weakly-nonlinear theory (Pedlosky, 1975) corresponds to turbulent isotropization; and the occlusion of baroclinic waves deducible from initial-value calculations (Farrell, 1982) may be an example of barotropization.

The idealized model described in this section is not as generally appropriate to the oceans as it is to the atmosphere, due to the presence of lateral boundaries in the former. One exception may be the apparent barotropization associated with the Gulf Stream after it separates from the coast (Rhines, 1977). Another is the Antarctic Circumpolar Current, the one "closed" oceanic feature not blocked by coasts; McWilliams & Chow (1981) have studied this flow numerically using a three-layer model, and have found results consistent with geostrophic turbulence theory.

CHAPTER IV - ATMOSPHERIC OBSERVATIONS

§4a. Introduction

It has been argued that the phenomena of two-dimensional and geostrophic turbulence described in the two previous chapters arise in systems of equations (or "models") commonly used to describe certain aspects of atmospheric flow behaviour. While such a conclusion is inescapable it can, however, only be considered as inconclusive evidence of the relevance of the theory to the atmosphere itself, as the models are extreme simplifications of the actual dynamics and are difficult to defend a priori.

Yet it is the nature of geophysical fluid dynamics that very little can be derived in such a manner as to be deductively correct, due to the overwhelming complexity and uncertainty of the system; rather, the normal procedure of research is to make questionable though (one hopes) defensible approximations which yield results in agreement with observed phenomena. The acceptance of barotropic models, for example, is due in large measure to the demonstrated success of early barotropic numerical weather forecasts (Charney, Fjørtoft & von Neumann, 1950).

One can argue that it is precisely this apparent difficulty, necessitating an intuitive and creative approach, which makes the field so exciting. On the other hand it means that conclusive results are very difficult to obtain: often there may exist many "explanations" of a certain phenomenon, with none of them being formulated in such a way as to positively disprove the competing hypotheses.

It is the purpose of the present chapter to consider the observational evidence for relevance of two-dimensional and geostrophic turbu-

lence theory to the circulation of the mid-latitude atmosphere. A very brief treatment of this question of relevance within the broader scope of geophysical fluid dynamics has been given recently by McWilliams (1983), but here the discussion will be considerably more thorough. The aim is not only to identify points of correspondence, but also to indicate discrepancies which might be rectified through the consideration of a suitably generalized theory of turbulence. In fact this latter point provides the atmospheric motivation for the scenario of inhomogeneous large-scale turbulence that is the focus of the present thesis research.

In §4b an attempt is made to interpret the vast body of observational analyses concerning the role of eddies in the general circulation. This task is made difficult by a number of factors. One is that different analyses generally measure different periods and regions, and hence, due to the low-frequency atmospheric variability, different flow regimes; one cannot assume that the same dynamical processes will be operative during substantially different flow configurations. A second difficulty is that certain conclusions, in particular those describing the eddy, mean-flow interaction, depend very much on the diagnostic formulation as well as on the quantity (e.g. momentum, heat, vorticity) under consideration. In principle these differences should be reconcilable, and indeed a great deal of effort is currently being directed towards obtaining such a unified picture.

A final difficulty, somewhat linked with the last one, concerns the fact that the observational diagnostics are not always geared very carefully to theoretical considerations. To be sure, mechanical interpretations can usually be found for mathematical expressions; but the physical content of the various diagnostic terms is a matter which must

incorporate dynamical insight, particularly when there is some indeterminacy with regard to the mathematical formulation - as is usually the case. It is not uncommon to attempt to establish links between partial dynamical theories (e.g. linear normal-mode baroclinic instability) and certain aspects of the observations, but because the full dynamical context is neglected these links can rarely be conclusive.

Geostrophic turbulence theory, which is in many ways the most complete conceptual framework in which to view the transient part of the atmospheric circulation, appears to offer a way out of this dilemma. However it is not at all clear how to decompose the atmospheric energy into barotropic and baroclinic components in order to properly test the theory (Baer, 1981); generally the decomposition made is into kinetic and available potential energy, which is quite another matter. The other necessary breakdown, namely in terms of a total horizontal spectral index, is feasible but rarely performed, the zonal-wavenumber spectral analysis being preferred among investigators.

A spectral observational analysis in terms of the 2-D spherical harmonic index has recently been presented by Boer & Shepherd (1983); the essential results are reviewed in §4c, along with some related analyses not shown in the paper. Not too surprisingly, the evidence in favour of large-scale turbulence theory is more clearly visible in the spectral than in the spatial diagnostics, but it is important to establish that the two are at least consistent. In general, whenever a flow is turbulent but not homogeneous and isotropic, both spectral and spatial analyses are necessary and complementary to an understanding of the problem.

Finally in §4d, some questions are raised with regard to the

spectral observations, and a simple model of barotropic turbulence in an inhomogeneous zonal jet is proposed as a means of investigating them. It is this model which is studied in the remainder of the thesis; although the motivation as presented here is essentially atmospheric, the subject is of much broader interest within the contexts of nonlinear geophysical fluid dynamics and inhomogeneous turbulence theory.

§4b. Eddies and the General Circulation

Following the demonstration by Jeffreys (1926) that deviations from axisymmetric flow were required to account for the observed surface winds, the importance of eddies in the general circulation has been consistently recognized. Due in large part to the impetus of Starr (1953), the 1950's and 1960's saw systematic attempts to study the zonally-averaged atmospheric circulation by evaluating "eddy fluxes" of such quantities as heat and momentum. Generally the diagnostics were interpreted via the "Lorenz energy cycle" (see Lorenz, 1967), which describes a flow of energy in the following sense: Zonal-Mean Available Potential Energy (ZAPE) → Eddy APE (EAPE) → Eddy Kinetic Energy (EKE) → Zonal-Mean KE (ZKE).

The last conversion of the energy cycle, describing the rectification of zonal currents by eddy Reynolds stresses, attracted the particular attention of Starr who was led to dub it "negative viscosity" (Starr, 1968) in light of the implied up-gradient momentum transfer. One may view the process more simply as an example of the tendency to focus kinetic energy into large-scale zonal motions that characterizes geostrophic turbulence (see Chapter III). The identification is not clear-cut, however, as it is only the barotropic KE which should exhibit

the reverse cascade; yet despite the difficulty of defining that component, work such as that of Baer (1981) suggests most of the atmospheric kinetic energy to be barotropic or equivalent-barotropic (viz., exhibiting no phase tilt with height). Therefore the Lorenz energy cycle appears to agree in large measure with the picture represented in Fig. 3.2: ZAPE → EAPE → EKE corresponding to a cascade from large-scale baroclinic energy to $\kappa \approx \kappa_R$ barotropic energy, and EKE → ZKE corresponding to the up-scale barotropic energy cascade and, possibly, to the evolution into zonal jets of beta-plane turbulence theory.

The conventional Eulerian-mean analysis employed by, e.g., Lorenz (1967) and Starr, Peixoto & Gaut (1970), has come under recent criticism on several counts. In the first place, to say that the mean flow is driven by the eddies is perhaps to suggest that, in the absence of eddy activity, the mean flow would be weaker. Yet that is far from being evident. Rather, conservation of angular momentum would lead to zonal velocities on the upper branch of the Hadley cell which were far in excess of those observed, as verified in the eddy-free circulation model of Schneider (1977). Of course such an axisymmetric flow would be highly unstable, so the argument is rather hypothetical; nevertheless the point is well taken: one should avoid using ambiguous language.

A more substantial criticism is that the observed eddy fluxes do not represent the total effect of the eddies, as the latter also induce secondary mean circulations with their own fluxes. For example, it is well known (Pedlosky, 1979, §6.14) that under conservative conditions, quasi-geostrophic waves induce a zonal-mean ageostrophic circulation which precisely cancels the effects of the eddy fluxes; this is the Charney-Drazin (1961) "non-interaction" theorem, and is treated in more

detail in §5f(ii) of the next chapter.

One method advanced to account for the secondary circulation is that of examining the "Eliassen-Palm flux" (Edmon, Hoskins & McIntyre, 1980); the related concepts have recently been applied to the energy cycle by Plumb (1983) and Kanzawa (1984). While the motivation behind the E-P flux is certainly well-founded, its advantage is more clear in nearly conservative situations such as often prevail in the stratosphere, than in the mid-latitude troposphere. Moreover the theory is usually framed in terms of quasi-geostrophic dynamics, and fails to include eddy-induced changes in physical processes such as friction and diabatic heating. As such it is only a partial solution.

Opposition to the zonal-mean, eddy picture of the traditional diagnostics has grown as more complete sets of observations and larger computing resources have permitted diagnostic studies which investigate zonal asymmetries. Blackmon, Wallace, Lau & Mullen (1977) and Lau (1978) find that while the zonally-averaged mid-latitude meridional circulation is a weak Ferrel cell, the local meridional circulations tend to be an order of magnitude larger, with Hadley cells over the continents and Ferrel cells over the oceans. Thus zonally-averaged statistics tend to hide the importance of stationary meridional motions, thereby over-emphasizing the role of the transient eddies.

The Hadley cells correspond to the regions where the mid-latitude jet is accelerating as one moves downstream, while the Ferrel cells are found in the deceleration regions. Acting against the Coriolis torque associated with the upper branches of these cells are the transient eddy fluxes of momentum, which in the studies cited are filtered to allow only disturbances with periods between 2.5 and 6 days. The eddy

activity is found to be at a maximum slightly poleward and downstream of the jet cores, in the conventional baroclinic storm track regions over the western part of the oceans. What is most striking is that the jet acceleration regions are correlated strongly with Coriolis torque acceleration and moderately with eddy flux torque deceleration, and vice-versa, from which Blackmon et al. (1977) and Lau (1978) conclude that it is in fact the stationary circulations associated with thermal and topographic forcing, and not the transient eddies, which "drive" the upper-level mean flow.

Of course, downstream acceleration and deceleration of the jet say nothing about what maintains its mean energy level. Since the net effect of the meridional cells is decelerating, it would still appear that the eddies play a crucial role in this balance. Moreover, the conclusions of Blackmon et al. and Lau refer to conversion processes appropriate to a zonal-mean picture, though they are applied over longitudinally restricted regions; furthermore they completely ignore the deeper question of eddy-induced mean circulations, which are of even greater importance in 3-D diagnostics. More sophisticated analyses by Holopainen & Oort (1981), Hoskins, James & White (1983), and Lau & Holopainen (1984), each using a different diagnostic approach, have agreed that transient eddy fluxes act to accelerate the axisymmetric part of the westerly jet.

Most of the diagnostic efforts of the past six or seven years have turned from the zonal-mean, eddy interaction question to that of the interaction between the stationary and transient flow components. In this context "stationary" generally means a monthly or a seasonal mean, but usage varies and this naturally complicates matters. Attention has

been focussed on transient eddy fluxes of heat, vorticity, and potential vorticity. One of the important distinctions to emerge early was that between "low-pass" (i.e. low frequency) eddies, whose vertical structure is largely equivalent barotropic, and "band-pass" (i.e. medium frequency with periods generally between 2.5 and 6 days) eddies, which are more characteristic of developing baroclinic waves (Lau, 1978); the role of the two classes of transients in relation to stationary features turns out to be quite distinct.

The primary effect of the transient eddies is clearly that of down-gradient heat transfer, destroying both ZAPE and stationary-wave EAPE (Lau, 1979; Lau & Wallace, 1979; Holopainen, Rontu & Lau, 1982; Lau & Holopainen, 1984), which is not surprising considering the dominance of baroclinic instability within the transient dynamics, and is certainly consistent with geostrophic turbulence theory. However, most of this transfer appears to come from the large-scale, low-pass transients, except in the storm-track regions (Holopainen et al., 1982); this is somewhat more of a surprise. Perhaps connected with this latter point is the fact that while the heat transfer is down-gradient, it is not diffusive in the sense of greater mean gradients being correlated with greater transfers (Lau & Wallace, 1979; Lorenz, 1979; Sasamori & Chen, 1982). This suggests that the eddy flux parameterization problem is not nearly as simple as advocated by Green (1970) among others, a matter discussed succinctly by Hoskins (1983).

Secondary but important effects of the transients that have emerged from the recent studies are those of barotropic enhancement of the axisymmetric flow, discussed above, and the maintenance of extra-tropical stationary surface vorticity extrema or "centres-of-action"

(Holopainen, 1978; Lau & Wallace, 1979; Holopainen & Oort, 1981); both effects are evident in vorticity analyses. Combining the vorticity and heat transfers into a potential-vorticity analysis, the transients are seen to be dissipative of potential vorticity (Youngblut & Sasamori, 1980; Holopainen et al., 1982) and of potential enstrophy (Holopainen, 1983), which again is what one would expect from geostrophic turbulence theory: a down-scale potential enstrophy cascade followed by small-scale diffusion. However localized regions can exhibit up-gradient transfer, particularly at the end of the storm tracks, which provides further evidence against diffusive parameterizations such as that of Green (1970) (see Hoskins, 1983).

Apart from observational diagnostics, another way of assessing the effect of the transients on the time-mean flow is to calculate the linear response of a stationary-wave model to observed eddy-flux forcing; such an approach has been followed by Youngblut & Sasamori (1980) and by Opsteegh & Vernekar (1982). In the former case the month studied had an anomalously energetic stationary-wave field, and the transients yielded a dissipative effect on the potential-vorticity response. Opsteegh & Vernekar, on the other hand, focussed on the geopotential height response under more typical conditions; they found the transient eddy contribution to be as important in magnitude as topographic effects (thermal effects being small), and essential in getting the correct phase structure of the stationary waves.

It is generally felt that a leading-order explanation of the observed stationary-wave field can be obtained from linear models incorporating topographic and thermal forcing (Held, 1983); however such models can never be self-consistent, as certain aspects of the flow must

be specified that really ought to arise out of the internal dynamics, moreover they are infamous for their ability to be "tuned". The evidence discussed so far in this section suggests that eddy effects are critical to an understanding of the detailed stationary-wave response of the atmosphere. Beyond this, the question of the transition between different stationary flow "equilibria", a matter of prime importance to medium-range weather forecasting, can only be investigated by a consideration of the eddies (Reinhold & Pierrehumbert, 1982; Källén, 1984).

In view of the evident role that transient eddies play in the maintenance of stationary (or more properly, seasonal climatological) waves, attention has quite naturally been directed recently towards their possible role with regard to anomalous flow configurations such as "blocking". A starting point was Green's (1977) argument that the anomalous warm ridge that lodged over the British Isles in July 1976 could not be explained by a steady circulation, but had to be forced by eddy processes. Observational analyses of blocking by Savijärvi (1978) and Illari & Marshall (1983) have shown that potential vorticity extraction by eddy fluxes is essential to the maintenance of the vorticity minimum against friction, much as it is with the "centres-of-action" as described previously. Theoretical arguments by Shutts (1983b) identify this process with an enhanced enstrophy cascade involving straining of the eddies by the stationary flow, a theme that will emerge very strongly in the remainder of this study. Indeed, Hansen & Chen (1982) and Hansen & Sutera (1984) both find evidence of an enhanced energy cycle and intensified spectral fluxes in two out of three blocking cases examined.

While blocking is a loosely-defined set of phenomena of apparently

no single dynamical origin, it is now clear that in at least some cases - particularly the split-jet configuration over western Europe - its existence is closely linked with anomalous geostrophic-turbulence cascades. One might speculate that an important diagnostic quantity is the ratio of up-scale to down-scale fluxes following injection at L_R (presumably by baroclinic instability upstream), for this determines in part the extent of irreversibility in the dynamics (see McIntyre & Palmer, 1984). While this ratio is fixed for a pulse of energy in a fluid at rest (see §2b) it is generally dependent on the spectral shape, as well as on flow inhomogeneities (as shall be seen); moreover the injection is not strictly confined to L_R and its scale dependence may vary.

Another area in which synoptic-scale transients have received recent attention concerns their possible interaction with transient ultra-long waves. Early studies by Tsay & Kao (1978) and by Kao & Chi (1978) argued that zonal waves k = 1 and k = 3 grow and decay in amplitude according to the sense of nonlinear KE interactions with the synoptic-scale transients k = 4-8, with direct conversions from APE playing a relatively minor role; on the other hand k = 2 exhibits the opposite behaviour, which the authors attribute to the particular k = 2 thermal forcing associated with land-sea contrasts. Itoh (1983) has confirmed these findings, and shown further that in the case of the k = 1 and k = 3 waves, the reverse KE cascade occurs after synoptic-scale baroclinic wave development; this must be considered as rather strong evidence for the validity of the geostrophic turbulence arguments.

It should however be mentioned that Hayashi & Golder (1983) have challenged this interpretation to a certain extent, presenting evidence from a General Circulation Model indicating direct large-scale APE → KE

conversion to be more important than the KE cascade. The numerical simulations of Gall, Blakeslee & Somerville (1979a) suggest both processes to be important, with the relevant dynamics being fundamentally nonlinear. The issue is still open.

A word of caution also comes from Madden (1983), who argues that much of the observed variation in ultra-long wave amplitude may come from a simple process of interference with stationary long waves; Madden's analysis considers only $k = 1$, but the effect is certainly a generic one. However the interference mechanism seems to be more relevant to stratospheric dynamics and to zonal-mean, eddy interaction: Madden does not address the studies cited above. On a somewhat different note, an interesting paper by Gambo (1982) finds support for the hypothesis that the vorticity of ultra-long waves obeys a Langevin equation for Brownian motion. The stochastic nature of the forcing thus implied seems more consistent with turbulent processes than with the comparatively deterministic dynamics of direct large-scale baroclinic instability or wave interference.

Up to this point, the discussion of this section has addressed the role of the eddies in the general circulation as seen through interaction and conversion terms. But there is another way in which the presence of turbulent cascades may be seen, though more indirectly, namely in the failure of linear baroclinic instability theory to account for the observed spectrum of KE. Following the striking success of the first models (Charney, 1947; Eady, 1949) in obtaining the approximate scale of the synoptic eddies, more detailed investigations have generally agreed that the peak of transient KE is at larger scales and greater altitudes than those predicted by linear theory (Gall, 1976).

To be sure, studies along this line are constrained to employ simplified models of atmospheric flow; it is thus quite possible that with more complicated initial conditions, the linear models would yield more realistic results. An example of such an attempt is that of Lin (1980), who proposed the possibility of finite-amplitude planetary-scale Green modes becoming unstable to baroclinic eddies of a scale lying between the deformation radius and the planetary wave scale. A different explanation allowing for "quasi-linear" stabilization has been advocated by Gall et al. (1979b), and is related to finite-amplitude equilibration effects (e.g. Pedlosky, 1970; Hart, 1979). And a recent re-awakening of interest in the initial-value as opposed to the normal-mode problem (e.g. Farrell, 1982) may help to clarify the issues. Nevertheless the question must still be considered unanswered, with the reverse energy cascade remaining a plausible mechanism for moving the synoptic-scale eddy energy from its generation scale up to its larger observed scale.

Further support for the cascade in the linear versus nonlinear debate comes from the study of Simmons & Hoskins (1978), in which an unstable baroclinic wave is allowed to develop in a nonlinear model. It is found that for realistic mean flows, there is a clearly-defined life cycle in which linear baroclinic growth of the wave is followed by occlusion, transformation to the barotropic mode, and a subsequent rectification of the mean flow through a barotropic eddy decay which is as dramatic as the initial growth. This process seems to be a clear manifestation of the barotropization predicted by geostrophic turbulence theory (Rhines, 1977; Salmon, 1980; and Chapter III). Simmons & Hoskins find that a barotropic model suffices to describe the development of the wave following occlusion; interestingly, they also discover that signi-

ficant horizontal resolution is required to model the decay, though not the growth, of the wave. The latter finding implies the existence of strong nonlinearity involving many different scales, even subsynoptic ones - and thus of turbulent cascades.

The importance of the barotropic decay phase to the net eddy transports is seen in an analysis of the Eliassen-Palm flux in Edmon et al. (1980). There it is shown that the observed E-P flux divergence at the surface and convergence throughout the mid-latitude atmosphere is well-represented by nonlinear life cycles such as those of Simmons & Hoskins, but not by linear models which tend to concentrate their activity near the surface. Observational support for the life-cycle picture comes from the fact that the momentum flux largely occurs downstream of the heat flux over the storm-track regions (Lau, 1978).

Although the evidence on this point is as yet inconclusive, there are strong indications from instantaneous potential vorticity maps that the potential enstrophy cascade, in the guise of planetary-scale Rossby-wave breaking, may be of prime importance to the dynamics of the wintertime stratosphere (McIntyre & Palmer, 1983, 1984). The crucial dynamical point concerns the irreversibility associated with the down-scale cascade; the precise details of the mixing, such as the role of instabilities or nonlinear critical layers, is a secondary issue (McIntyre, 1982; McIntyre & Palmer, 1984). McIntyre (1982) has discussed the relevance of such fully nonlinear dynamics to stratospheric sudden warmings, and there is strong evidence that similar "wave-breaking" potential enstrophy cascades in the vicinity of the subtropical jet may be the dominant mechanism in the decay phase of synoptic-scale baroclinic waves (Edmon et al., 1980; Hoskins, 1983;

McIntyre & Palmer, 1984). Indeed, Boer & Shepherd (1983) have shown the observed nonlinear spectral cascades of energy and enstrophy to be maximized on the underside of the jet stream level.

§4c. Spectral Observations

The present section is not intended to be a review of spectral observational analyses, which in any case tend to be in terms of the zonal wavenumber k; that area has been summarized very thoroughly by Tomatsu (1979), and more recently as well as succinctly in Holopainen's (1983) review of transient eddies. Rather, the intention here is to focus on a particular spectral analysis, that of Boer & Shepherd (1983), although a few projections of the data will be presented which are not included in the paper.

The defence for such parochialism is two-fold. First, the observational data used in the Boer & Shepherd study are very special, coming from the intensive high-resolution global FGGE 1979 observing periods. Secondly and perhaps more importantly, the diagnostics are specifically designed to address the predictions of geostrophic turbulence theory, by computing spectra and nonlinear fluxes as functions of the 2-D spherical harmonic index n. It was shown in §2h that n is the appropriate index for turbulence theory on a sphere, whereas the zonal-wavenumber representation lumps together waves of different scales (i.e. the same k, but at different latitudes) and compresses all axisymmetric motions into the k = 0 mode.

The details of the data set are given in Boer & Shepherd; it suffices to say that the diagnostics to be shown here are all integrated vertically over 12 pressure levels from 1000 to 50 mb, and are obtained

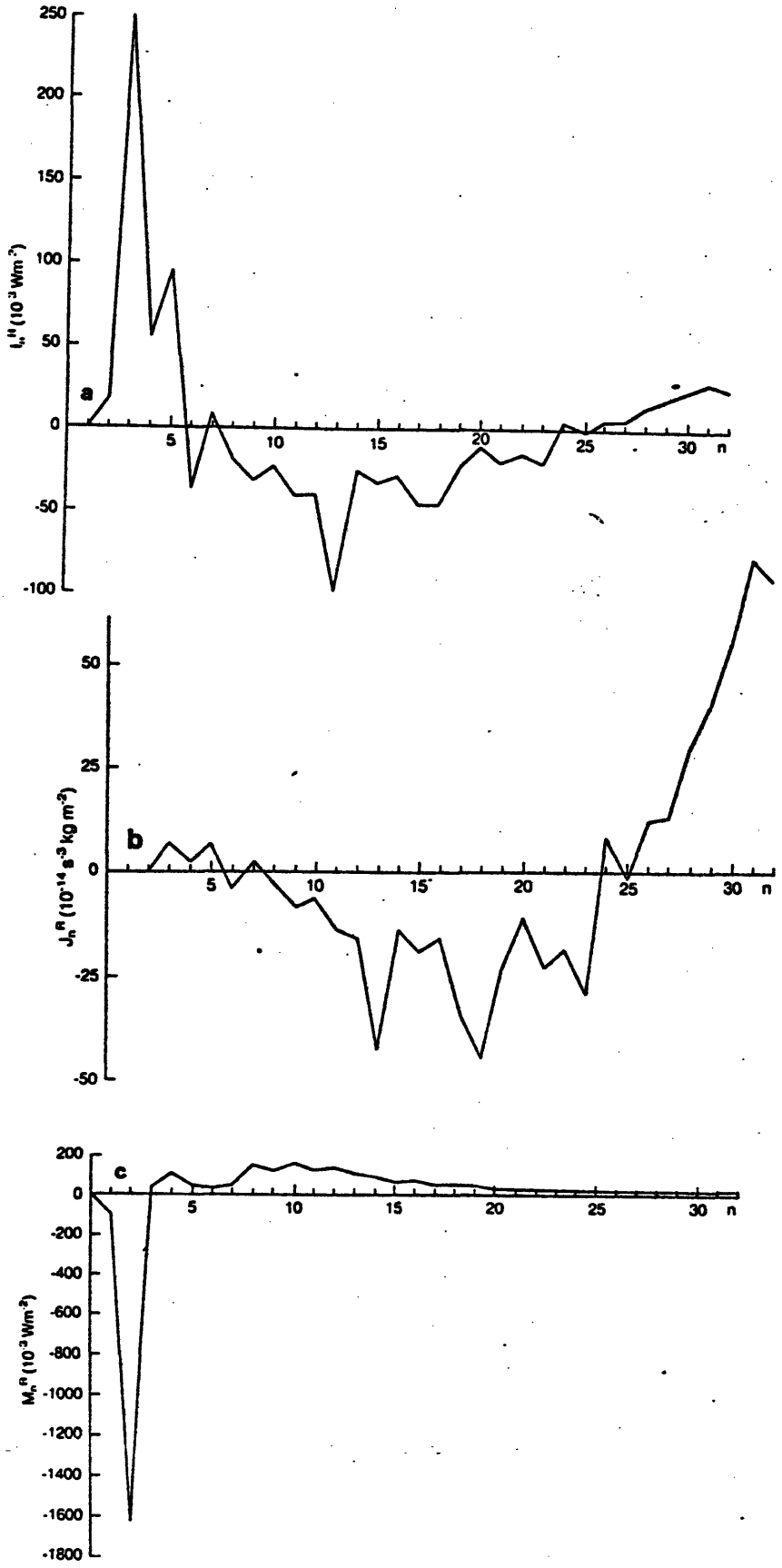


Fig. 4.1: The resolved part of the nonlinear interaction term for N=32 for (a) KE, (b) enstrophy, and (c) APE. Positive values indicate that the quantity is being transferred to that wavenumber from other scales. From Boer & Shepherd (1983).

from the single month of January 1979 with samples taken twice daily. The available potential energy is computed directly from the temperature data, rather than according to the quasi-geostrophic formulation, as the latter involves vertical derivatives and would not be reliable. Zonal and meridional KE components are obtained according to the formulae of §2h, while the stationary and transient flow components represent respectively monthly means and fluctuations with periods between 24 hours and one month.

In order to make a complete comparison with geostrophic turbulence theory, one would like to have the energy decomposed into barotropic and baroclinic parts, and projected onto a vertical spectral representation. The difficulties inherent in applying such a procedure to the atmosphere have already been discussed in §3d, and as yet have not been overcome. Consequently the present arrangement seems to be optimal, imperfect though it may be.

Fig. 4.1 shows the nonlinear interaction terms for KE, enstrophy, and APE, for a truncation of N = 32. The formulae are given in Boer & Shepherd, and will not be duplicated here; the energy and enstrophy interaction terms at each level are as defined in §2a, however, suitably modified for the spherical domain (see §2h). The physical interpretation to be given to Fig. 4.1 is that the terms represent a net source (if positive) or sink (if negative) of the appropriate quantity for a given scale index n, due to nonlinear interactions with all other resolved scales. The sum over all n must vanish. Thus Fig. 4.1a indicates a transfer of KE out of a band of wavenumbers $7 < n < 24$, primarily to larger scales and secondarily to smaller ones; this is much as one would expect for 2-D turbulence driven by an energy input in

intermediate wavenumbers. In fact, since the budgets must approximately balance over a month, the interaction spectra may be used to get an idea of the forcing distribution (allowing of course for frictional damping); the implied intermediate-scale energy source may plausibly be attributed to conversion from APE via baroclinic instability.

The enstrophy interaction term, shown in Fig. 4.1b, indicates a net down-scale transfer from the forced intermediate-scale band, with maximum transfer into scales at the truncation limit. Obviously this distribution is truncation-dependent, but its general character, which agrees again with 2-D turbulence theory, is presumably robust. Fig. 4.1c depicts the APE conversion, and this is fairly clearly characterized by a transfer from $n = 2$ (the principal component of baroclinic solar forcing) down-scale, mainly into $7 < n < 15$.

Taken together, the consistency of the observed fluxes together with the simplified picture offered in Fig. 3.2 of §3e is indeed striking. The implied APE → KE conversion is apparently from $7 < n < 15$ into $7 < n < 24$, which is an acceptable range since part of that conversion occurs within the down-scale baroclinic energy cascade itself (see §3e). But it should be noted that the magnitude of the cascade of APE greatly exceeds that of KE, a feature which is also seen in energy cycles insofar as the ZAPE → EAPE conversion is much greater than the EKE → ZKE one (Lorenz, 1967). This fact is also consistent with the spatial diagnostic studies reviewed in §4b, which find down-gradient heat transfer to overwhelm up-gradient vorticity or momentum transfer, resulting in a net down-gradient "diffusion" of potential vorticity. The leakage of potential enstrophy to small scales and thence to dissipation is of course easily understandable within the context of

geostrophic turbulence theory.

The apparent "arrest" of the up-scale KE cascade at n = 3-5 might be due to the arrest predicted by beta-plane turbulence theory (§3c). On the other hand it could also be a result of blocking at F = 1 (§3b), or of frictional drag; all three processes are plausible based on rough scale estimates (Williams, 1978; McWilliams, 1983). Then again it might be totally unconnected with existing versions of geostrophic turbulence theory. This is clearly an area demanding future clarification.

Fig. 4.1 naturally shows only the interactions within a finite set of modes, and it is consequently of interest to investigate the extent to which the results depend on the truncation wavenumber. To that end, Fig. 4.2 displays KE and enstrophy flux functions (the negative integrals of the interaction terms, as in (2.13)) for truncations of N = 20, 32, and 40, the latter coming from the recently available higher-resolution FGGE-3B data set covering the same period. It is evident from Fig. 4.1c that the APE flux will be essentially insensitive to these differences, as is indeed the case. Now, the maximum up-scale KE flux (Fig. 4.2a) is only moderately affected by the truncation changes, and occurs in each case at n = 5 . On the other hand the maximum down-scale enstrophy flux (Fig. 4.2b) increases by a factor of three between N = 20 and N = 40 . If the truncation were being imposed within a true enstrophy-cascading inertial subrange, then an increase in N would not alter the maximum flux; however this is not the case, and there is no evidence of the flux function itself flattening out in Fig. 4.2b.

One of the most interesting results of Boer & Shepherd came from a decomposition of the KE into stationary and transient, as well as into zonal and meridional, components; this is shown here in Fig. 4.3. What

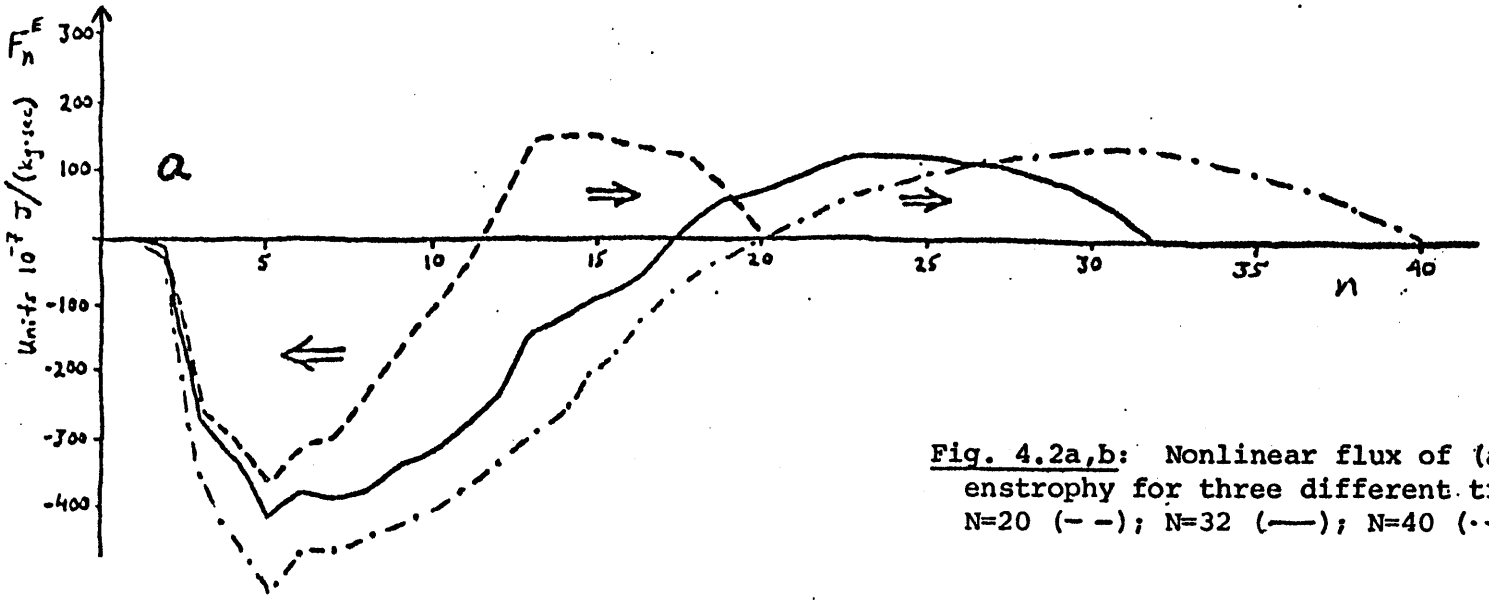
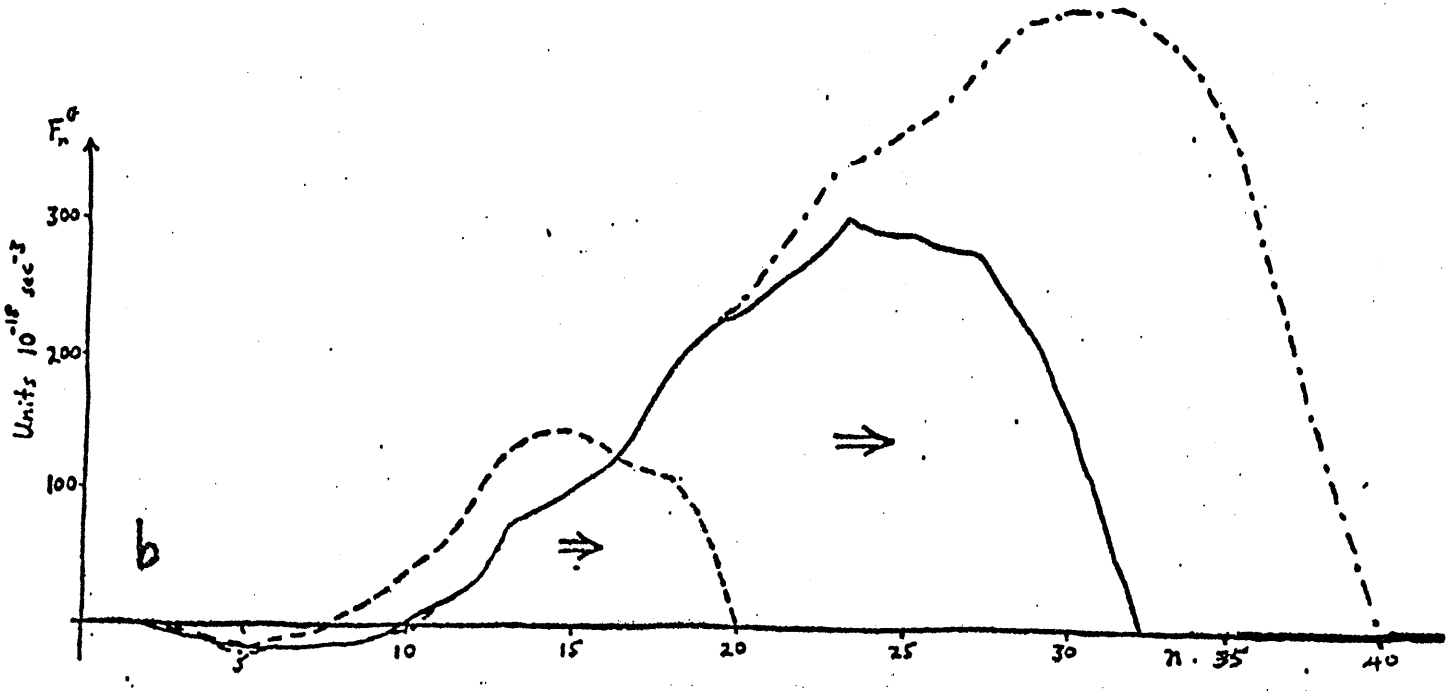


Fig. 4.2a,b: Nonlinear flux of (a) KE and (b) enstrophy for three different truncations: N=20 (– –); N=32 (——); N=40 (·—·).



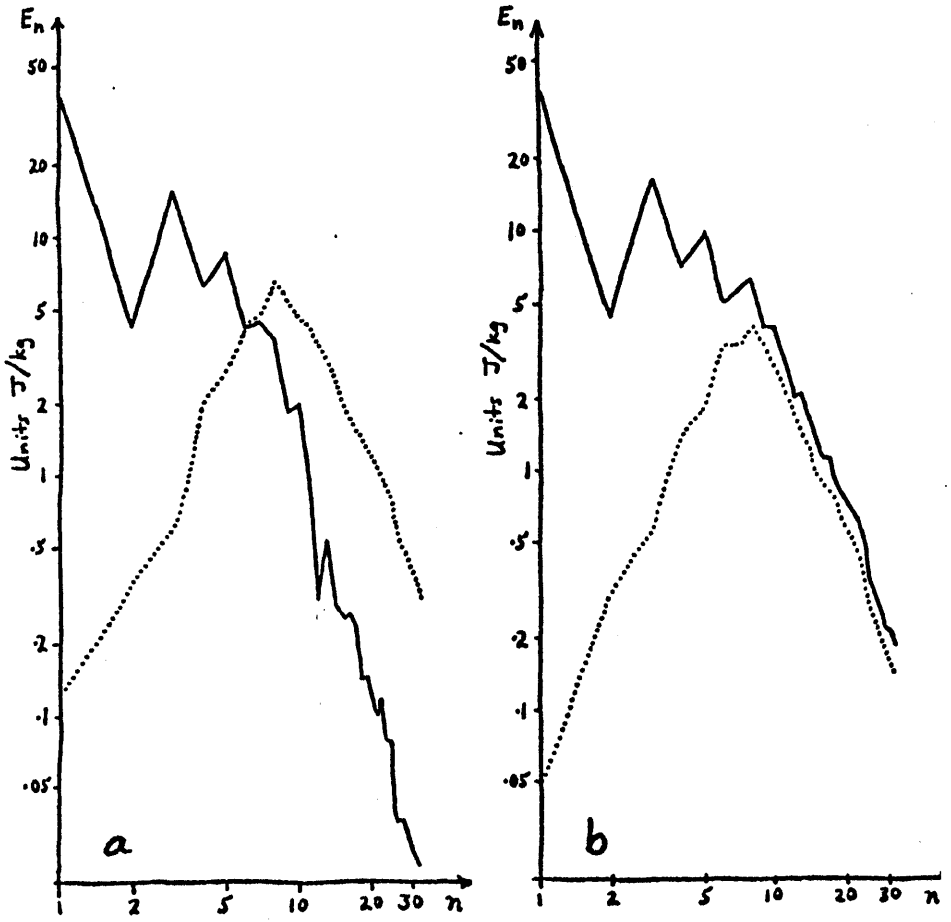


Fig. 4.3a,b: Spectra of (a) stationary (——) and transient (·····) KE; (b) zonal (——) and meridional (·····) KE.

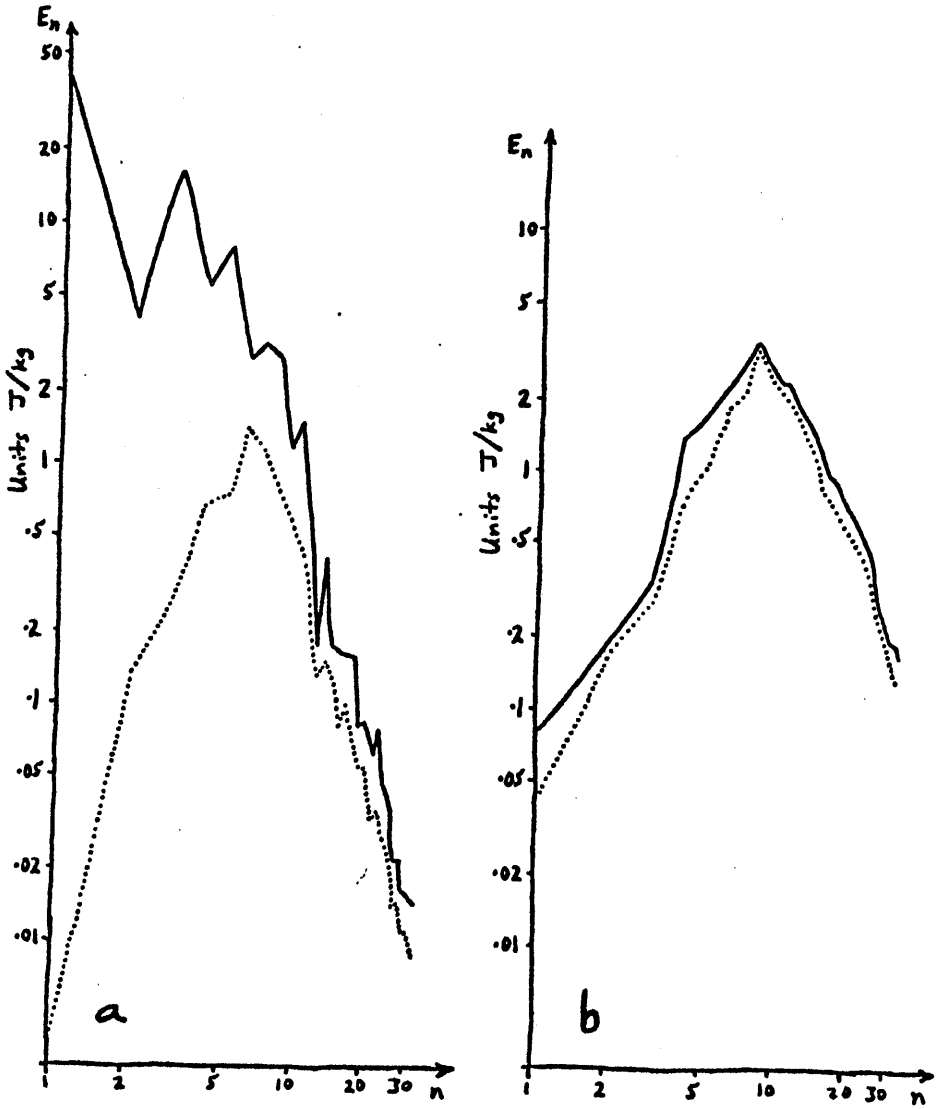


Fig. 4.4a,b: Spectra of zonal (——) and meridional (·····) components of (a) stationary and (b) transient KE.

one finds is a separation in scale between two rather different flow regimes. At large scale, $n < 6$, the KE is predominantly zonal and stationary, and although there is an evident up-scale KE cascade, the spectrum bears no resemblance to the -5/3 power law that would characterize an energy-cascading inertial subrange (§2e).

For small scales, $n > 7$, the situation is completely different. Here the KE is predominantly transient and approximately isotropic, and obeys a power law close to the -3 log slope appropriate to an enstrophy-cascading inertial subrange (§2e). Indeed, there is a rough equipartitioning of zonal and meridional KE and APE in this range (see Fig. 8 of Boer & Shepherd), as predicted by Charney's (1971) theory for scales smaller than the deformation radius. While the enstrophy flux itself is never really constant, it may be concluded that the data are at least not inconsistent with the existence of an enstrophy-cascading inertial subrange in the atmosphere; moreover, it is evident that a description of the dynamical behaviour of these scales must take 2-D and geostrophic turbulence theory into account.

To explore matters further, Figs. 4.4a,b show a decomposition of, respectively, stationary and transient KE into their zonal and meridional components. The description offered above is made more vivid, but something else is apparent: the transient KE is approximately isotropic on <u>all</u> scales. This is certainly not in accord with beta-plane turbulence theory, which would predict zonal anisotropy at large scales. A 2-D spectral representation of the transient KE in terms of meridional (n-m) and zonal (m) wavenumber, given in Fig. 4.5, shows that the conditions for local homogeneity and isotropy, namely that KE(n,m) be a function of n alone, can only be said to hold for $n >$

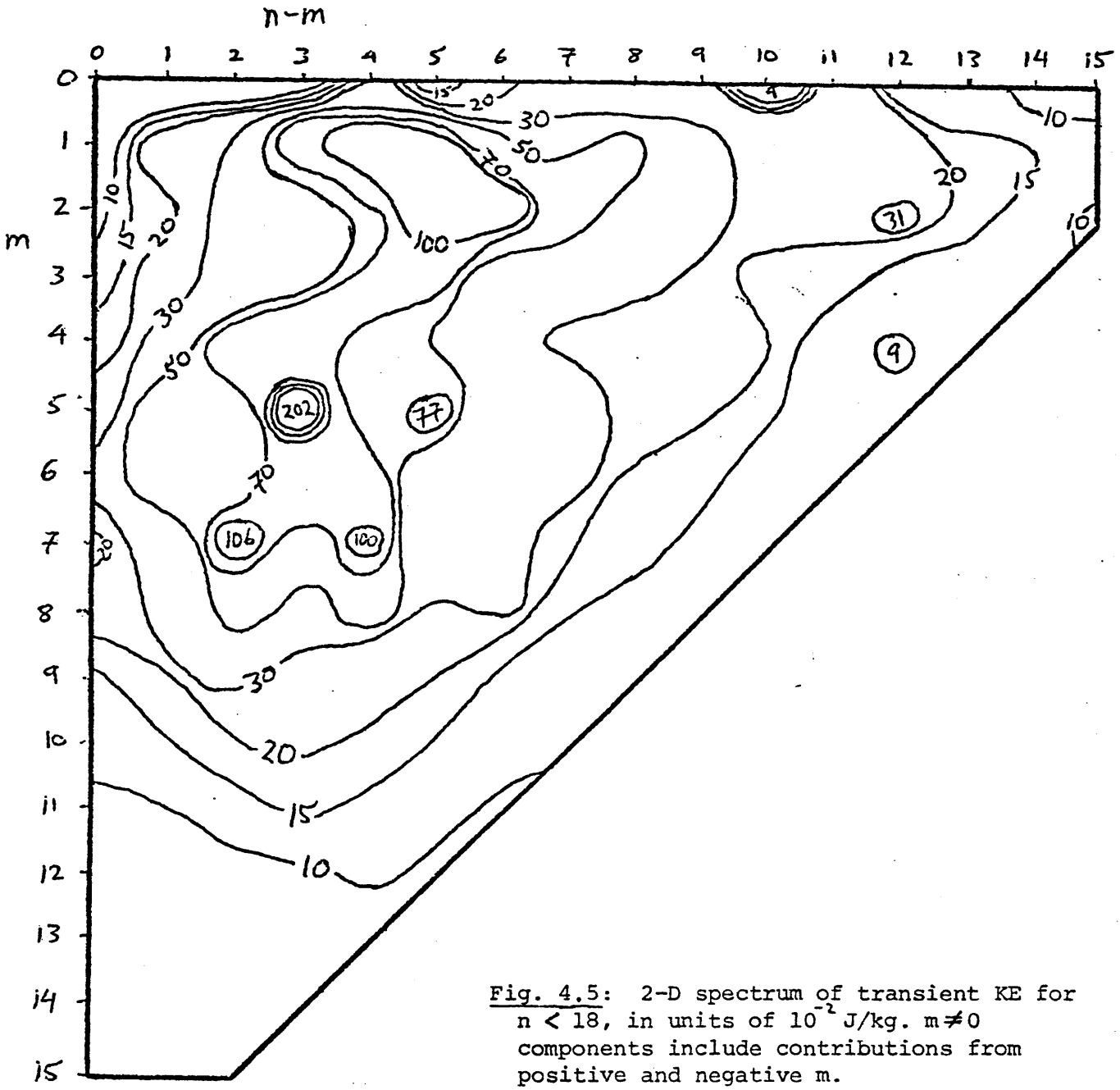


Fig. 4.5: 2-D spectrum of transient KE for $n < 18$, in units of 10^{-2} J/kg. $m \neq 0$ components include contributions from positive and negative m.

12 (see also Fig. 5 of Boer & Shepherd). Nevertheless the picture is not in agreement with beta-plane turbulence theory: there is indeed a pool of zonally-anisotropic transient KE at n ≈ 6-7 and m ≈ 1-2, but this is balanced off by meridionally-anisotropic KE at n ≈ 8 and m ≈ 5.

As a final diagnostic, consider the following decomposition. Spectral fluxes and interaction terms arise out of triple correlations as in (2.9). If the flow field is divided into stationary and transient components, denoted by an overbar and a prime, then triple correlations can be generally broken down as follows:

$$\overline{abc} = \bar{a}\bar{b}\bar{c} + \overline{a'b'c'} + \{\bar{a}\overline{b'c'} + \bar{b}\overline{c'a'} + \bar{c}\overline{a'b'}\} . \qquad (4.1)$$

Now, in the case of KE and enstrophy interaction terms, the first quantity on the rhs of (4.1) would represent nonlinear interactions between different scales of the stationary flow; both KE and enstrophy versions would integrate to zero over all n, but since the stationary flow is largely zonal the contribution at each n would presumably be small in any case (since $J(\psi,\nabla^2\psi)$ vanishes for a strictly zonal flow). The second term of (4.1), representing interactions between different components of the transient flow, would likewise integrate to zero for both KE and enstrophy; however the contribution at each n should be significant, in fact if turbulence theory is to apply to any part of the dynamics it should describe the sense of these interactions.

As far as the third, composite term of (4.1) is concerned, consisting of three separate parts, this describes the interaction between the stationary and transient flows. This is not the place to develop the theory of wave, mean-flow interaction; such discussion will emerge through the remainder of the thesis. Suffice it to say that if the stationary flow is neither homogeneous nor isotropic, and it most

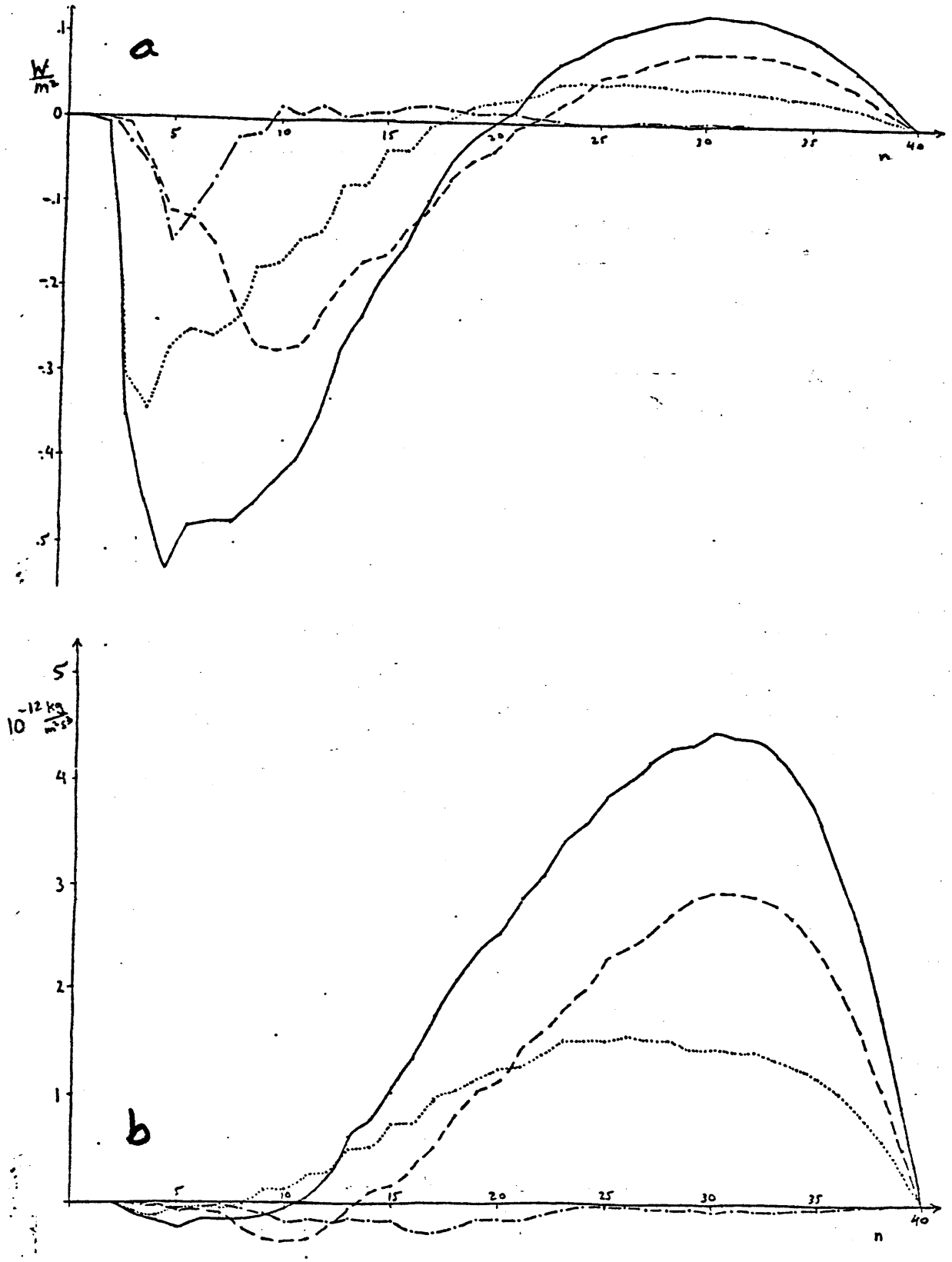


Fig. 4.6a,b: Nonlinear flux of (a) KE and (b) enstrophy for N=40 (—), broken down into pure stationary (—·—), pure transient (– – –), and mixed stationary-transient (·····) components.

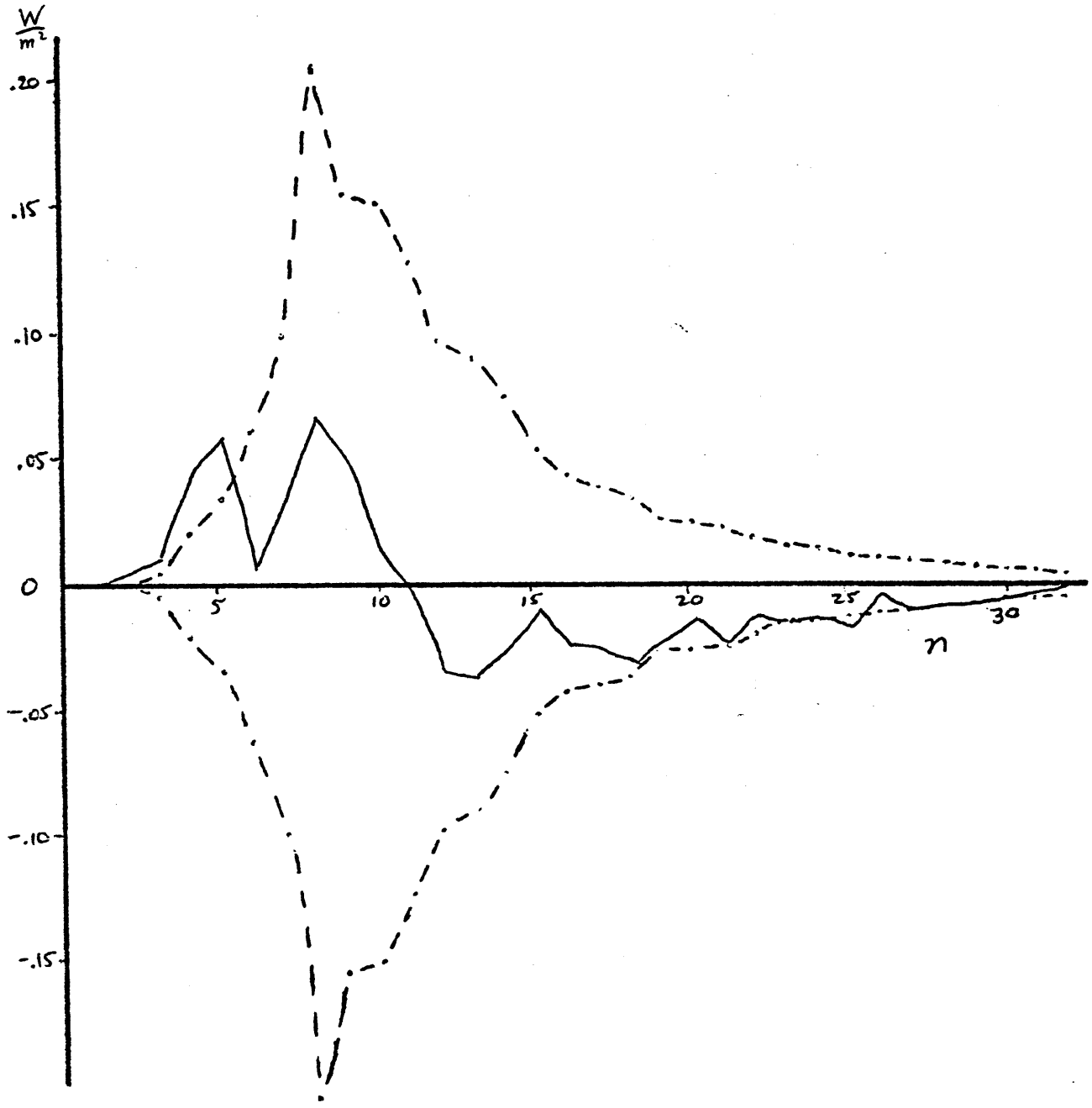


Fig. 4.7: Transient KE self-interaction term $L_T(n)$ (——) and "local" scale estimate (–·–) computed via $(2E_T(n))^{3/2} \times \frac{n}{a} \times \frac{\rho_o}{g}$.

definitely is not in the atmosphere, then this feature of the dynamics can evidently not be described by (horizontally) homogeneous and isotropic turbulence theory such as that of Chapters II and III.

The KE and enstrophy fluxes are broken down into these three components according to (4.1), and shown in Fig. 4.6. While the stationary flux is generally small, the other two are of roughly equal importance; moreover although they appear to act in the same overall sense, their distribution is rather different. In particular, the "turbulent" transient flux seems to play only a minor role at large scales.

If the flux arising out of the transient self-interactions does describe the turbulent character of the atmospheric flow, then it is of interest to see how the terms compare with a "local" scale analysis using the energy at each n to estimate a velocity. The rationale behind this is that turbulent interactions are expected to be spectrally local. The result is given in Fig. 4.7. Now the scale analysis gives an absolute estimate, while the actual interaction can be of either sign. Near the "wings" of the distribution the scale analysis seems to be reasonable; in between, however, there is obviously strong cancellation between positive and negative interactions. Indeed, an inertial subrange would exhibit zero net interaction at each n though the scale estimate would still be non-zero, so it is not entirely clear how one should interpret Fig. 4.7. Moreover the interaction terms are truncation-dependent. At least the local scale analysis appears to yield a reliable upper bound, with the exception of $n = 4$ and $n = 5$, and this may give some support to the hypothesis that the turbulence is dominated by local triad interactions.

§4d. Some Questions and a Simple Model

The results of the last section, particularly the nonlinear fluxes of kinetic energy and enstrophy depicted in Figs. 4.2a,b, demonstrate that the notions of 2-D and geostrophic turbulence theory are an appropriate framework in which to view at least some aspects of the atmospheric circulation. An important example of this is the reverse energy cascade, which acts to confine atmospheric energy to the largest scales of motion. It is noteworthy that a theory which hypothesizes isotropic and homogeneous turbulence should be qualitatively so much in accord with the behaviour of a fluid as anisotropic and inhomogeneous as is the atmosphere, in which disturbances at intermediate scales are often so distinct from one another that one would be hard pressed to describe them as comprising a field of turbulence. This in itself suggests that it might be fruitful to investigate 2-D or geostrophic turbulence in an environment that is decidedly non-ideal, to determine the extent to which the theoretical predictions are altered. It would seem that the effects could well be less profound than one might expect.

As a starting point, it is worth making a simple calculation. It was seen that most of the cascading energy flowed into waves n = 3, 4, and 5. In the absence of all other effects, the doubling time τ for these waves due to nonlinear transfers is then given by

$$\tau = \frac{E_3+E_4+E_5}{I_3+I_4+I_5} = \frac{35\ \text{J/kg}}{4\times10^{-5}\ \text{J/(kg}\cdot\text{s)}} = 8.8\times10^5\ \text{s} \approx 10\ \text{days} . \quad (4.2)$$

Considering the transient energy alone, the effect is far more dramatic:

$$\tau^T = \frac{E_3^T+E_4^T+E_5^T}{I_3+I_4+I_5} = 1.4\times10^5\ \text{s} \approx 1.5\ \text{days} . \quad (4.3)$$

Now, 1.5 days is a rather fast doubling time for transient waves of that scale, and is certainly not observed; consequently, it seems that ultra-long transients either do not play a major role in the cascade process, or else they give up their energy to the stationary waves very shortly after receiving it. As for the growth timescale of 10 days for the total KE of those waves, this would seem to roughly balance the spin-down due to friction. The calculation is only of the "order-of-magnitude" sort; nevertheless, it does suggest that the nonlinear eddy flux into the large-scale stationary waves is far from negligible.

The spectral observations presented in §4c raise a number of interesting questions. In rather general form, these include:

a. Baroclinic excitation produces isotropic, transient KE. Yet the reverse energy cascade seems to take this energy through and into anisotropic, stationary energy. How does this transformation occur?

b. What role do the stationary waves play in the turbulent cascade?

c. Is there really a wave-turbulence "boundary" at n=3, as suggested by the cascade cut-off? How can this be reconciled with the other "boundary" at n=8?

d. Why are the transient long waves isotropic, when they should be strongly affected by the zonally anisotropic beta geometry?

e. What is the significance of the various terms in Figs. 4.6a,b? In particular, to what extent can the combined stationary-transient interaction terms be understood theoretically?

f. Why does 2-D homogeneous turbulence theory appear to work so well given the inhomogeneous, anisotropic nature of the stationary flow?

These questions should all be considered within the broader context of:

g. What is the role of the transient eddies, and of the reverse energy cascade, in the general circulation of the atmosphere?

As stated, the last question is rather vague and ill-defined; in fact it is also very difficult, and must be broken up into simpler pieces (the scientific method!) for progress to be made. Questions a through f represent some of those pieces.

Fortunately, the results of §4c not only raise questions, but also provide some clues as to how they might be resolved. The most important such clue is the picture offered of a field of transient, turbulent, intermediate-scale eddies evolving within a larger-scale stationary-wave environment. This suggests that a useful idealization might involve the consideration of geostrophic turbulence in the presence of an inhomogeneous "background" flow. To pose a meteorologically meaningful wave, mean-flow interaction problem, one would have to choose an appropriate background flow: not the observed stationary flow, for example. Presumably the choice would represent the response to planetary-scale forcing, both axially symmetric (such as differential solar heating) and zonally inhomogeneous (such as topography and land-sea contrast). This would not be a straightforward procedure, and would very possibly lead one down the slippery slope to a full-blown General Circulation Model (not a bad thing in itself, but hardly recommended for thesis work!).

As a simpler starting point, questions a through f might be considered within the context of a far more restricted model, namely that of the barotropic beta-plane with forcing introduced at intermediate scales to simulate baroclinic instability. In fact this would represent a barotropic truncation of the circulation model of Fig. 3.2. Clearly such a simplification would preclude a quantitative study of the atmospheric cascade, by eliminating the baroclinic part of the feedback between the stationary and transient flows. However, this is not the

immediate goal in any case; rather, the intention is to explore the nature of the reverse cascade under inhomogeneous conditions which are relevant to the atmosphere, and both theoretical and observational evidence suggest that this problem can be meaningfully addressed within the barotropic context.

As regards the beta-plane approximation, this would be clearly inappropriate for a study of planetary-scale waves, and thus also for a quantitative investigation of stationary-transient interaction. However the beta-plane is certainly adequate for representing most of the energy-cascading range, and it does allow for the cascade cut-off by Rossby-wave dispersion. Moreover, most of the eddy flux activity and kinetic energy is located at mid-latitudes, where the approximation is most secure.

A final restriction is to large-scale, and, in Chapters VI through VIII, to zonal basic-state flows. The defence for this is two-fold: first, it is the crudest representation of the atmospheric stationary flow, and thus of the "correct" eddy-free basic state (which is presumably no more complicated than the former); secondly, it is a situation which can be treated theoretically to a certain extent.

It should be evident that in proceeding through these simplifications, the study has moved from one of atmospheric dynamics into the realm of geophysical fluid dynamics. Any relevance to the atmosphere can no longer be direct; instead, the proposed model is properly viewed as a "process model" which considers the interaction of various dynamical processes which are themselves part of the atmospheric dynamics. While this may seem lamentable from a strictly meteorological point of view, the truth of the matter is that a compromise between

reality and tractability (and thereby comprehension) must always be made. In the present case, the problem of inhomogeneous 2-D turbulence and nonlinear wave, mean-flow interaction is in fact of general fluid dynamical interest; indeed this latter motivation might well have provided a safer foundation than the atmospheric one discussed in such detail, but it would at the same time have considerably limited the scope and importance of the conclusions.

CHAPTER V - WAVES AND TURBULENCE ON A STATIONARY BACKGROUND FLOW

§5a. Introduction

The preceding chapter of this study has demonstrated that while the atmosphere exhibits some of the characteristics of 2-D and geostrophic turbulence, there are nevertheless some major discrepancies between observations and idealized homogeneous theory at the largest scales of motion. The discrepancies are hardly surprising, of course, given the fundamental anisotropy and inhomogeneity of the orographic and thermal large-scale atmospheric forcing; this is especially the case in the Northern Hemisphere. Indeed, what should perhaps be considered surprising is rather the fact that 2-D turbulence theory is of <u>any</u> relevance to the synoptic-scale dynamics of the atmosphere.

As was emphasized in the discussion of §4b, there can be little question that linearized theory of forced waves, of both the normal-mode and the wave-train variety, goes a long way in explaining the existence of observed low-frequency large-scale motions (see, for example, the recent review article by Held (1983)). However, if one is interested in questions of equilibration or maintenance of the forced waves, or of the rapid transition between quasi-stationary states, then it is becoming increasingly clear that one must consider nonlinear interactions involving waves over a significant range of scales: the study of Reinhold & Pierrehumbert (1982) is particularly suggestive in this regard.

Consequently, it would seem that in order to deal with the questions which it has recently begun to consider, dynamical meteorology is going to have to come to grips with the interaction between the

large-scale, low-frequency regime and the intermediate-scale, high-frequency one. This is not a new insight, of course; certainly it was ever-present in the work of Victor Starr and his collaborators. However the theoretical understanding of this problem is still very much in its infancy. In part this is due to the recent over-reaction against the zonally-averaged view of the atmosphere considered by Starr (who had little choice, given the existing quality of the data), which has been accompanied, I believe, by an over-reaction against the role of the eddies in the general circulation.

All this has been discussed in some detail in Chapter IV: suffice it to say here that the subject of stationary-transient interactions is far from closed; and that there is a substantial body of recent evidence of various types indicating that questions such as those mentioned above concerning quasi-stationary flows cannot be addressed in a self-consistent manner unless attention is paid to the transient eddies. Beyond this remains the consideration that the transients are worthy of investigation in their own right, regardless of their role in the general circulation; not only are such motions responsible for "weather", but they play a crucial role in limiting the predictability of the atmosphere (Lorenz, 1969).

Because of the apparent utility of turbulence theory in describing the statistical behaviour of intermediate-scale (that is, $L \lesssim L_R$) quasi-geostrophic phenomena, one would not want to abandon such theory altogether. Indeed, Fjørtoft's (1953) spectral blocking theorem suggests that the (undeniable) down-scale enstrophy cascade must be associated with at least part of the observed up-scale kinetic energy cascade. Rather it would seem desirable to consider the extent to which the idealized

homogeneous theory might be modified by the presence of a stationary or quasi-stationary background flow. An immediate goal of such an investigation would be to answer the questions regarding the spectral observations posed at the end of the previous chapter. A more ambitious aim would be that of putting the theories of stationary and transient eddies - to this point quite separate disciplines - under a unified framework.

Obviously the latter programme is extremely challenging from a theoretical point of view. So far nonlinear fluid dynamical theory has been limited to a number of special, though important, cases: examples are homogenous turbulence, considered in chapters II and III; isolated coherent structures such as solitons (e.g. Redekopp, 1977); weakly-nonlinear instability (e.g. Pedlosky, 1970); and "laminar" wave, mean-flow interaction (e.g. Andrews & McIntyre, 1978a). The problem suggested by the spectral observations of the last chapter - namely that of a transient, turbulent, intermediate-scale regime interacting with a quasi-stationary, forced, large-scale one - unfortunately lies outside the domain of existing nonlinear theory.

In the absence of a unified, over-arching theory of waves and turbulence - an absence which will regrettably not be rectified by this thesis - a reasonable procedure is to investigate the relative importance of various partial theories, and to determine their regimes of validity. Such in fact is the spirit of the present work. To a limited extent one may make progress analytically, and such attempts will be described in this and the subsequent chapters. However, it seems clear that reliable advances can only be made by considering the behaviour of actual flows, whether physical or numerical. In this

respect there is a considerable parallel with the evolution of 3-D homogeneous turbulence theory (see Batchelor, 1953).

While the atmosphere is decidedly baroclinic, it is the hypothesis of this study that a barotropic approach may nevertheless yield significant insight into stationary-transient interactions, and particularly into the way in which the transient self-interactions are modified by a stationary flow environment. Certainly a barotropic fluid is sufficiently dynamically rich to include the kinds of phenomena under consideration; hence the investigation can be justified on a purely mathematical level as a treatment of a generic scenario of inhomogeneous turbulence. Since barotropic motion is always a possible atmospheric response, quasi-geostrophic or not, one can argue that barotropic wave-turbulence phenomena are at least possible features of atmospheric flow; certainly barotropic theory seems to explain many qualitative features of observed geostrophic dynamics, as has been already discussed in the context of 2-D or barotropic turbulence. But perhaps the strongest argument for geophysical relevance comes from considering geostrophic turbulence theory (Chapter III), which predicts that the reverse energy cascade should occur in the barotropic mode. The simplified model of §3e suggests that a barotropic model can address stationary-transient interaction questions in a limited way, provided that the kinetic energy input from baroclinic instability is adequately simulated.

In the remainder of this chapter, the subject of fully-nonlinear waves on a stationary background flow is considered. In §5b the relevant equations are introduced; a scale analysis is performed in §5c, with some attention paid to limiting cases. The scale analysis gives insight into the spectral dynamics of a perturbed flow, as described in

§5d. The subject of conservation laws is then addressed: first for nonlinear waves in §§5e,f, and then in §5g for linearized or small-amplitude waves. §5f is entirely new. Nearly all previous work on conservation laws has neglected nonlinear effects, since they impede progress so effectively. This parallels the situation in stability theory, which is natural since stability conditions are so intimately linked to conservation relations. Attention is focussed on barotropic flows, even though most of the results are easily generalized to the baroclinic quasi-geostrophic case (given suitable, if somewhat worrisome, restrictions).

§5b. Equations for a Perturbed Flow

The simplest system which is able to treat a mixed problem of waves and turbulence, and which can still be expected to yield useful insight into understanding large-scale atmospheric dynamics, is the barotropic beta-plane: the equation for the streamfunction ψ is then

$$\nabla^2\psi_t + J(\psi,\nabla^2\psi) + \beta_0\psi_x = S(\psi;x,y,t) \ , \tag{5.1}$$

where S represents all source and sink terms. In the discussion of Chapter II, for example, the dissipative part of S was $(\nu\nabla^4\psi - r\nabla^2\psi)$. It is convenient to consider (5.1) over a doubly-periodic domain.

Now introduce a fixed stationary wave field $\Psi(x,y)$ which itself is a solution of (5.1); i.e.,

$$J(\Psi,\nabla^2\Psi) + \beta_0\Psi_x = S(\Psi;x,y) \ . \tag{5.2}$$

This is only possible if S has no explicit dependence on t, although in (5.1) S might vary temporally through its dependence on ψ. In practice one could choose Ψ first and then determine the required forcing S; or one could choose S first and then solve (5.2) for Ψ. The latter

procedure is clearly the more difficult, and raises the question of the uniqueness of Ψ. Then writing the full streamfunction as

$$\psi = \Psi + \phi \ , \tag{5.3}$$

the "perturbation" ϕ must satisfy

$$\nabla^2\phi_t + J(\phi,\nabla^2\phi) + J(\Psi,\nabla^2\phi) + J(\phi,\nabla^2\Psi) + \beta_0\phi_x = S(\psi) - S(\Psi) \equiv S' . \tag{5.4}$$

Note that (5.2) and (5.4) differ from the equations governing the stationary and transient components of ψ; this is reflected in the fact that, in general, the stationary part of ϕ does not vanish. Also, S' does not equal $S(\phi)$ unless S is a linear functional.

It must be emphasized that consideration of (5.4) is totally equivalent to consideration of (5.1); no approximation has been made whatsoever. However, for a judicious choice of Ψ, (5.4) may turn out to be more amenable to analysis than (5.1). This is particularly the case when one wishes to examine the small-amplitude stability of the forced stationary flow Ψ with $S' = 0$, for then (5.4) may be linearized. In the present context, the aim is rather to choose a Ψ that represents the "basic-state" forced flow, that is to say the flow that would exist in the absence of waves, and that serves as a kind of "first approximation" to the actual time-mean flow $\bar{\psi}$. It must not be forgotten that any given Ψ implies a forcing $S(\Psi)$ which in turn affects S'; to the extent that one makes assumptions regarding S' and the initial conditions for ϕ, the choice of Ψ can be expected to affect the flow statistics.

For now it shall be assumed that $S' = 0$, so that the perturbation source-sink term vanishes. To determine the energetics, multiply (5.4) by ϕ. Treating each term separately,

$$\phi\nabla^2\phi_t = \nabla\cdot(\phi\nabla\phi_t) - (\tfrac{1}{2}\,|\nabla\phi|^2)_t \ , \tag{5.5a}$$

$$\phi J(\phi,\nabla^2\phi) = J(\phi,\phi\nabla^2\phi) = \nabla\cdot(\phi\nabla^2\phi\underline{v}) \ , \tag{5.5b}$$

$$\phi J(\phi,\nabla^2\Psi) = J(\phi,\phi\nabla^2\Psi) = \nabla\cdot(\phi\nabla^2\Psi\underline{v}) \ , \tag{5.5c}$$

$$\beta_0\phi\phi_x = \beta_0(\tfrac{1}{2}\phi^2)_x \ , \tag{5.5d}$$

$$\phi J(\Psi,\nabla^2\phi) = J(\Psi\phi,\nabla^2\phi) - \Psi J(\phi,\nabla^2\phi) \tag{5.5e}$$

$$= J(\Psi,\phi\nabla^2\phi) - \nabla^2\phi J(\Psi,\phi) \ . \tag{5.5f}$$

Here $\underline{v}$ denotes the velocity field determined by ϕ and $\underline{V}$ the field determined by Ψ. Integration of a divergence over a doubly-periodic domain makes that term vanish; hence in the global energy balance (5.5b-d) do not contribute and one is left with

$$\frac{d}{dt}\iint \frac{1}{2}\,|\nabla\phi|^2\,dxdy = -\iint \Psi\, J(\phi,\nabla^2\phi)\,dxdy \tag{5.6a}$$

$$= \iint \nabla^2\phi\, J(\phi,\Psi)\,dxdy \ . \tag{5.6b}$$

For the special case of a zonal mean flow $\Psi(y) = -\int U(y)dy$, one can re-write the right-hand side (rhs) of (5.6b) in more traditional forms,

$$\frac{d}{dt}\iint \frac{1}{2}\,|\nabla\phi|^2\,dxdy = \iint U(y)\,\frac{\partial(uv)}{\partial y}\,dxdy \tag{5.7a}$$

$$= -\iint (uv)\,\frac{dU}{dy}(y)\,dxdy \ . \tag{5.7b}$$

It is conventional to give physical interpretations to (5.7a,b) of, respectively, eddy stresses acting on a mean flow, and of diffusion of momentum relative to a mean gradient. This is all very well, but the indeterminateness of the integrand on the rhs of (5.6) and (5.7) (one can add any term of the form $\nabla\cdot[\ ]$) should caution against one's adhering to any single interpretation too narrowly.

It is often useful to write down a "local" form of (5.6), and again there is some liberty in how this may best be done. Adopting (5.5a-d) as written and taking (5.5f) yields

$$\frac{\partial}{\partial t}\left(\frac{1}{2}\left|\nabla\phi\right|^2\right) - \nabla\cdot\left(\phi\nabla\phi_t + \phi\underline{v}\nabla^2(\phi+\Psi) + \phi\underline{V}\nabla^2\phi + \frac{1}{2}\beta_0\phi^2\underline{i}\right) = -\nabla^2\phi\nabla\cdot\left(\phi\underline{V}\right) . \quad (5.8)$$

Perhaps the most important point to be made at this stage is that while the total energy of the flow,

$$E(\psi) = \iint \frac{1}{2}\left|\nabla\psi\right|^2 dxdy ,$$

is conserved in the absence of sources or sinks, the "perturbation" energy,

$$E(\phi) = \iint \frac{1}{2}\left|\nabla\phi\right|^2 dxdy = \iint \frac{1}{2}\left(u^2+v^2\right) dxdy ,$$

is not, and it is the $J(\Psi,\nabla^2\phi)$ term in (5.4) which violates energy conservation. This term represents straining of the perturbation vorticity by the shear in the basic-state flow. Since the energy of the basic-state flow, $E(\Psi)$, is obviously a constant, this can only mean that the energies are not additive. In fact, one easily verifies that

$$E(\psi) = E(\Psi) + E(\phi) + (Uu + Vv) . \quad (5.9)$$

Note that if $\psi = \bar{\psi} + \psi'$, the overbar denoting a time average, then

$$\bar{E}(\psi) = E(\bar{\psi}) + \bar{E}(\psi') ; \quad (5.10)$$

then applying a time average to (5.9) and using (5.10) yields

$$E(\bar{\psi}) = E(\Psi) + E(\bar{\phi}) + (U\bar{u} + V\bar{v}) . \quad (5.11)$$

It is clear from (5.9) that to call $E(\phi)$ the perturbation energy, as is traditional, may be somewhat misleading in view of the fact that the correlation factor (Uu+Vv) is also due to the perturbation. Nevertheless the terminology will be adhered to in what follows, with the above considerations kept carefully in mind.

Although $E(\phi)$ is not generally conserved, it is evidently bounded when the flow is conservative (i.e. when $S \equiv 0$). Clearly $E(\phi) = 0$ cannot be ruled out, so there is no positive lower bound. To determine the upper bound, let $\nabla\Psi$ be assumed anti-parallel to $\nabla\psi$ as this will

maximize $E(\phi)$. Specifically, define $\nabla\Psi \equiv -a\nabla\psi$ with $a \geq 0$; then $\nabla\phi = (1+a)\nabla\psi$. Using the fact that $E(\Psi) = a^2E(\psi)$, one can write

$$\begin{aligned} E(\phi) &= (1+a)^2E(\psi) \\ &= 2E(\psi) + 2a^2E(\psi) + (2a-a^2-1)E(\psi) \\ &= 2\left[E(\psi)+E(\Psi)\right] - (a-1)^2E(\psi) \end{aligned}$$

which gives the bound

$$E(\phi) \leq 2\left[E(\psi)+E(\Psi)\right] . \tag{5.12}$$

Note, however, that for a given $E(\psi)$ one can make $E(\phi)$ arbitrarily large simply by choosing a Ψ which gives a ludicrously large $E(\Psi)$.

One can also place an upper bound on the growth rate of $E(\phi)$ by using (5.6); such calculations have been exploited to great effect in linear stability theory (e.g. Pedlosky, 1979, §7.5). Their success in a finite-amplitude case depends on the fact that the rhs of (5.6) is a quadratic in the disturbance quantities, or, stated otherwise, that the nonlinear triplet interactions have no effect on the global balance of perturbation energy. Using (5.6b) as a starting point,

$$\begin{aligned} \frac{\partial E(\phi)}{\partial t} &= \iint \left(u_y - v_x\right)(Uv - Vu)\, dxdy \\ &= \iint \left\{U\left[(uv)_y - (v^2/2)_x - uv_y\right] + V\left[(uv)_x - (u^2/2)_y - vu_x\right]\right\} dxdy \\ &= \iint \left\{U(uv)_y + V(uv)_x + U\left[(u^2-v^2)/2\right]_x + V\left[(v^2-u^2)/2\right]_y\right\} dxdy \\ &= -\iint \left(U_y + V_x\right)(uv)\, dxdy + 2\iint V_y\left[(u^2-v^2)/2\right] dxdy \quad . \end{aligned} \tag{5.13}$$

In the above, the equations of continuity,

$$u_x + v_y = 0 = U_x + V_y \quad , \tag{5.14}$$

have been used freely. For a zonal basic-state flow, (5.13) reduces to (5.7b). Using the inequalities

$$u^2 - 2uv + v^2 = (u-v)^2 \geq 0 \qquad \Leftrightarrow \qquad uv \leq (u^2+v^2)/2 \tag{5.15a}$$

and

$$(u^2-v^2)/2 \leq (u^2+v^2)/2 \quad , \tag{5.15b}$$

one may use (5.13) to write

$$\left|\frac{\partial}{\partial t}\log[E(\phi)]\right| \leq \sup|U_y| + \sup|V_x| + 2\sup|V_y| , \qquad (5.16)$$

the supremum being taken over the flow domain. For a periodic or a bounded domain, where $\iint(\nabla^2\phi)^2/\iint|\nabla\phi|^2$ has a lower bound, alternatives to (5.16) can be obtained which may, in the event, prove to be tighter.

To obtain the perturbation enstrophy equation, multiply (5.4) by $\nabla^2\phi$. Then integrating the expression over the domain yields the equivalent to (5.6a,b), namely

$$\frac{d}{dt}\iint \frac{1}{2}(\nabla^2\phi)^2\,dxdy = \iint \nabla^2\Psi\, J(\phi,\nabla^2\phi)\,dxdy \qquad (5.17a)$$

$$= -\iint \nabla^2\phi\, J(\phi,\nabla^2\Psi)\,dxdy , \qquad (5.17b)$$

but here it is the $J(\phi,\nabla^2\Psi)$ term in (5.4) which violates enstrophy conservation. For a barotropic fluid, this term is similar to enstrophy generation by topography. Similar manipulations to those performed for the energy can be done for the enstrophy, but that seems unnecessary at this point; however it might be instructive to write down at least one local form of the perturbation enstrophy relation:

$$\frac{\partial}{\partial t}\left(\frac{1}{2}(\nabla^2\phi)^2\right) + \nabla\cdot\left(\frac{1}{2}(\nabla^2\phi)^2(\underline{v}+\underline{V}) + \beta_0\left[\frac{1}{2}(v^2-u^2)\underline{i} - (uv)\underline{j}\right]\right)$$

$$= -\nabla^2\phi\nabla\cdot(\nabla^2\Psi\underline{v}) . \qquad (5.18)$$

§5c. Scale Analysis

Considering now (5.4) with $S' \equiv 0$, non-dimensionalize by scaling the terms with $\Psi = U_0L_0\Psi'$ for the basic-state flow, and $\phi = UL\phi'$ for the perturbation, where the single length and velocity scales for each streamfunction are based on an assumption of either isotropy or else dependence on a single spatial component. The primed quantities are taken to be order unity. Let $t = Tt'$, with T to be determined. Then

$$\beta_0\phi_x = O(\beta_0 U) \quad ; \qquad J(\Psi,\nabla^2\phi) = O(U_0 U/L^2) \quad ;$$
$$J(\phi,\nabla^2\phi) = O(U^2/L^2) \quad ; \quad J(\phi,\nabla^2\Psi) = O(U_0 U/{L_0}^2) \quad .$$

The non-dimensional equation, after dropping the primes, is

$$\left(\frac{L}{UT}\right)\nabla^2\phi_t + J(\phi,\nabla^2\phi) + \left(\frac{U_0}{U}\right)J(\Psi,\nabla^2\phi) + \left(\frac{U_0 L^2}{U{L_0}^2}\right)J(\phi,\nabla^2\Psi) + \left(\frac{\beta_0 L^2}{U}\right)\phi_x = 0 \; ; \tag{5.19a}$$

this may be written more succinctly as

$$\left(\frac{L}{UT}\right)\nabla^2\phi_t + J(\phi,\nabla^2\phi) + \alpha J(\Psi,\nabla^2\phi) + \alpha\gamma J(\phi,\nabla^2\Psi) + \beta\phi_x = 0 \; , \tag{5.19b}$$

where the following non-dimensional parameters have been introduced:

$$\alpha \equiv U_0/U \quad ; \qquad \gamma \equiv L^2/{L_0}^2 \quad ; \qquad \beta \equiv \beta_0 L^2/U \quad . \tag{5.20}$$

Note in particular that for the geophysically important case of a scale separation between the basic-state flow and the perturbation, one may take $\gamma \ll 1$; in that case the perturbation enstrophy is approximately conserved. Even when this simplification does not obtain, one can normally expect that $\gamma \lesssim 1$ unless the basic-state flow has been peculiarly ill-chosen.

If either β, α, or $\alpha\gamma$ exceeds order unity, then (5.19) is "linear" in ϕ to leading order, and may be solvable analytically. For example, the no-mean-flow beta-plane Rossby wave is recovered by considering $\beta \gg (\alpha,\alpha\gamma,1)$, in which case $T = 1/(\beta_0 L)$ is the appropriate timescale of the problem. The inclusion of a constant mean flow is trivial, merely adding a Doppler shift to the phase speed. Normal-mode solutions are sometimes obtainable for weak mean-flow shear, even when $\gamma \approx 1$; an example of an approximate solution for small $\alpha\gamma/\beta$ for a zonal cosine jet, employing a WKB analysis, is presented in §6e of the next chapter. For stronger non-constant mean shear, the global approach breaks down and wave solutions are only valid locally.

The opposite "linear" limit of $\alpha \gg (\beta,\alpha\gamma,1)$, where the $J(\Psi,\nabla^2\phi)$ term dominates (5.19), also allows closed-form solutions. The equation becomes

$$\left(\frac{\partial}{\partial t} + \underline{V}\cdot\nabla\right) \nabla^2\phi = 0 \quad , \tag{5.21}$$

which is easily solved, at least in principle, by the method of characteristics. Here the perturbation vorticity behaves as a passive tracer. In the simpler case of a zonal flow, for example, one may write

$$\nabla^2\phi = F\left(x-U(y)t\right) \tag{5.22a}$$

for some differentiable function F; alternatively

$$\nabla^2\phi(x,y,t) = \nabla^2\phi(x-U(y)t,y,0) \equiv \nabla^2\phi_0(x-U(y)t,y) \tag{5.22b}$$

in terms of the initial conditions. However solutions such as (5.22) are easily destroyed by even weak viscous effects (e.g. Rhines & Young, 1983), and may be expected to be equally sensitive to nonlinear mixing.

The case of $\alpha \approx \beta \gg 1$ can be treated in the special case of a unidirectional mean flow with constant shear in an unbounded domain, by using the "convected coordinates" formulation (Phillips, 1966, §5.5; Yamagata, 1976); with constant shear, $\gamma = 0$ identically so there is infinite scale separation. For small but finite γ, one may employ ray-tracing techniques (Lighthill, 1978, §§4.5,4.6). This problem is treated in greater detail in the subsequent chapter for the important case of a zonal basic-state flow, but it is important to note here that a wave disturbance propagating in an inhomogeneous large-scale flow generally conserves neither its wave energy, its wave enstrophy, nor its local wavenumber. This clearly has profound implications for the spectral dynamics of a perturbed flow.

Under certain conditions, what <u>is</u> conserved in the linearized case is the "wave action" $A \equiv E/\hat{\omega}$ (Bretherton & Garrett, 1968) , where $\hat{\omega}$ is

the intrinsic frequency and E the local or intrinsic wave energy $\frac{1}{2}|\nabla\phi|^2$. For Rossby waves $A = -(k^2+\ell^2)E/(\beta_0 k)$, so evolution to larger scale would involve an increase in wave energy. However the conditions on the mean state required for this result appear to be quite restrictive for Rossby waves: in particular, they seem to require a zonal flow with $\alpha\gamma \ll 1$ (Bretherton & Garrett, 1968, §3.5). A general discussion of conservation laws is presented in §§5e,f,g, in an attempt to at least partially clarify a portion of the literature that strikes me (and, no doubt, others as well) as more than a little confusing. For an arbitrary mean flow such as the one considered here, not much can be said with confidence.

In (5.19), the ratio of linear to nonlinear effects is somewhat more complicated than the "wave steepness" β discussed in §3c; here it is given by

$$M \equiv \frac{\beta_0 L^2 + U_0(L/L_0)^2 + U_0}{U} = \beta + \alpha(\gamma+1) \quad . \qquad (5.23)$$

While it is true that $M \ll 1$ still represents a turbulent regime where the results of Chapter II may be expected to hold, it is evident that the dynamics of the "linear" regime $M \gg 1$ are a good deal richer and much less tractable than are those of the pure Rossby-wave regime of beta-plane turbulence. In particular, if $\alpha \gg 1$ then $M \gg 1$ over <u>all</u> scales. It is, consequently, reasonable to anticipate that the wave-turbulence "boundary" or "transition" regimes, $M \approx 1$, will be correspondingly less clear-cut.

§5d. Spectral Dynamics

For the case of pure beta-plane turbulence considered in §3c, the evolution dynamics of a disturbance in wavenumber space, or the "spectral dynamics" of conservative flow, were found to be quite straightforward. Since the wave energy is conserved, U is a constant; then given β_0, the transition wavenumber κ_β is fixed. One has $\beta \ll 1$ for $\kappa \gg \kappa_\beta$ (here κ represents the "isotropic" 2-D wavenumber $|\underline{k}|$), and $\beta \gg 1$ for $\kappa \ll \kappa_\beta$. Moreover, one can define trajectories in wavenumber space representing the principal evolution of a disturbance ("principal" referring to the first moment of $\varepsilon(\underline{k})$, in the sense of §2b), and these trajectories will generally not cross since they are reasonably well-defined by $\underline{k}$ alone (there is perhaps a weak dependence on higher moments of ε). The spectral dynamics are represented by Figure 5.1: for $\beta \ll 1$ the trajectories point in the direction of lower κ (isotropy being assumed, since it is so rapidly established); for $\beta \gg 1$ the trajectories are fixed points, representing propagation of Rossby waves; and for $\beta \approx 1$ the trajectories lie along lines of constant κ and point toward the "zonal" axis $k = 0$. This picture is true for <u>any</u> parameter setting, although with a truncated spectrum κ_β might lie outside the range of κ.

When one considers the more general case of this chapter, however, it is readily apparent that the spectral dynamics are not so easily characterized. Most importantly, the wave energy and enstrophy are not generally conserved. Not only does this render Fjørtoft's condition inapplicable when $M \gtrsim 1$, but it also means that the non-dimensional parameters vary with U as well as with L. Trajectories in wavenumber space

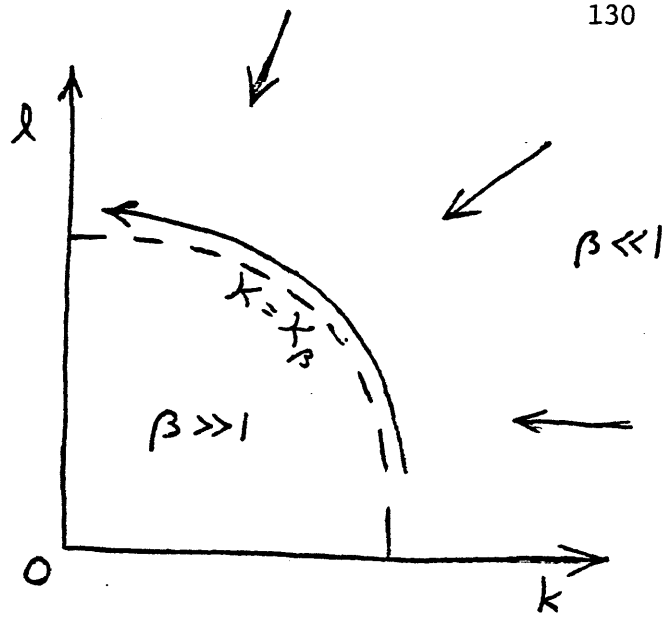


Fig. 5.1: Spectral dynamics of beta-plane turbulence. Arrows denote trajectories of disturbance evolution in wavenumber space.

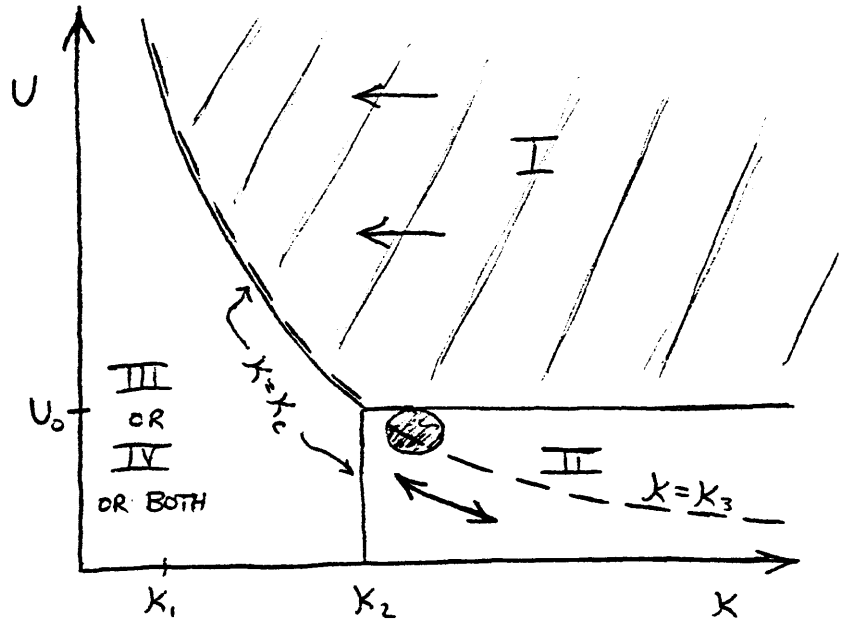


Fig. 5.2: Spectral dynamics of (5.19). Solid lines delineate regions dominated by one of two terms, indicated by Roman numerals after (5.27). Hatched lines indicate the nonlinear regime. Arrows denote approximate trajectories of disturbance evolution, where known. The shaded circle represents the parametric location of mid-latitude transient eddies, as described in the text. For $\mu \gg 1$, $K_1 = K_0$; $K_2 = K_\alpha$; $K_3 = K_\beta$. For $\mu \ll 1$, $K_1 = K_\alpha$; $K_2 = K_0$; $K_3 = K_\gamma$. For $\mu \approx 1$, $K_2 \approx K_0 \approx K_\alpha$; $K_3 \approx K_\beta \approx K_\gamma$; and K_1 is irrelevant.

are no longer well-defined: in fact there is a family of trajectories emanating from each $\underline{k}$, corresponding to different values of U. One should rather imagine trajectories in the 3-D space defined by $(\underline{k},U)$. Moreover the picture depends on the external parameters, unlike in Figure 5.1.

In order to carry the scale analysis any further, it is necessary to assume that the scale estimates of the Jacobian terms leading to (5.19) are reasonably accurate. This is not a trivial matter, as Jacobians can easily yield resultants well short of their "optimal" value if the gradients of the two fields are nearly parallel. To ensure significant interaction, it is necessary to assume either that Ψ is fairly isotropic (i.e. has both zonal and meridional components), or that ϕ is. The latter assumption is generally a fairly safe one for a fully-developed turbulent flow. For non-turbulent flows, that is for $M \gg 1$, the former assumption may be required. The case of a zonal flow is considered in the next chapter. Any special case requires a more delicate treatment, but at this point only rather crude results are desired.

The only fixed non-dimensional parameter of the problem is

$$\mu \equiv \frac{\beta_0 L_0^2}{U_0} = \frac{\beta}{\alpha\gamma} \quad ; \tag{5.24}$$

then for a given value of μ, one must consider various values of U, or equivalently of α. It is helpful to introduce the following scale parameters, representing transition scales between various regimes:

$$\kappa_0^2 \equiv \frac{1}{L_0^2} = \frac{\gamma}{L^2} \quad ; \qquad \kappa_\beta^2 \equiv \frac{\beta_0}{U} = \frac{\beta}{L^2} = \alpha\mu\kappa_0^2 \quad ;$$

$$\kappa_\alpha^2 \equiv \frac{\beta_0}{U_0} = \frac{\beta}{\alpha L^2} = \mu\kappa_0^2 \quad ; \qquad \kappa_\gamma^2 \equiv \frac{U_0}{UL_0^2} = \frac{\alpha\gamma}{L^2} = \alpha\kappa_0^2 \, . \tag{5.25}$$

Note that factors of 2π have been neglected. These scale parameters delineate the following orderings:

$$(1) \quad \kappa \approx \kappa_0 \iff \gamma \approx 1 \; ; \quad \kappa \gg \kappa_0 \iff \gamma \ll 1 \; ; \tag{5.26a}$$

$$(2) \quad \kappa \approx \kappa_\beta \iff \beta \approx 1 \; ; \quad \kappa \gg \kappa_\beta \iff \beta \ll 1 \; ; \tag{5.26b}$$

$$(3) \quad \kappa \approx \kappa_\alpha \iff \beta \approx \alpha \; ; \quad \kappa \gg \kappa_\alpha \iff \beta \ll \alpha \; ; \tag{5.26c}$$

$$(4) \quad \kappa \approx \kappa_\gamma \iff \alpha\gamma \approx 1 \; ; \quad \kappa \gg \kappa_\gamma \iff \alpha\gamma \ll 1 \; . \tag{5.26d}$$

Finally, for economy of notation the four possibly dominant terms of (5.19) will be identified according to

$$\text{I} \to J(\phi,\nabla^2\phi) \; ; \quad \text{II} \to J(\Psi,\nabla^2\phi) \; ; \quad \text{III} \to J(\phi,\nabla^2\Psi) \; ; \quad \text{IV} \to \phi_x \; . \tag{5.27}$$

It is now possible to consider the cases corresponding to various values of μ and of α.

CASE 1: $\mu \gg 1$ (hence III is never dominant).

1.1: $\alpha \gg 1$. Then $\kappa_\beta \gg \kappa_\alpha \gg \kappa_0$ by (5.25). $M \gg 1$ for all κ.
$\kappa \gg \kappa_\alpha \Rightarrow$ II ; $\kappa \ll \kappa_\alpha \Rightarrow$ IV.

1.2: $\alpha \approx 1$. Then $\kappa_\beta \approx \kappa_\alpha \gg \kappa_0$. $M \approx 1$ for $\kappa \gg \kappa_\alpha$.
$\kappa \gg \kappa_\alpha \Rightarrow$ I,II ; $\kappa \ll \kappa_\alpha \Rightarrow$ IV.

1.3: $\alpha \ll 1$. Then $\kappa_\alpha \gg \kappa_\beta, \kappa_0$. $M \ll 1$ for $\kappa \gg \kappa_\beta$.
$\kappa \gg \kappa_\beta \Rightarrow$ I ; $\kappa \ll \kappa_\beta \Rightarrow$ IV.

CASE 2: $\mu \ll 1$ (hence IV is never dominant).

2.1: $\alpha \gg 1$. Then $\kappa_\gamma \gg \kappa_0 \gg \kappa_\alpha$. $M \gg 1$ for all κ.
$\kappa \gg \kappa_0 \Rightarrow$ II ; $\kappa \ll \kappa_0 \Rightarrow$ III.

2.2: $\alpha \approx 1$. Then $\kappa_\gamma \approx \kappa_0 \gg \kappa_\alpha$. $M \approx 1$ for $\kappa \gg \kappa_0$.
$\kappa \gg \kappa_0 \Rightarrow$ I,II ; $\kappa \ll \kappa_0 \Rightarrow$ III.

2.3: $\alpha \ll 1$. Then $\kappa_0 \gg \kappa_\gamma, \kappa_\alpha$. $M \ll 1$ for $\kappa \gg \kappa_\gamma$.
$\kappa \gg \kappa_\gamma \Rightarrow$ I ; $\kappa \ll \kappa_\gamma \Rightarrow$ III.

CASE 3: $\mu \approx 1$ (all terms potentially dominant; $\beta \approx \alpha\gamma$, $\kappa_\beta \approx \kappa_\gamma$, $\kappa_\alpha \approx \kappa_0$)

3.1: $\alpha \gg 1$. Then $\kappa_\beta \gg \kappa_0$. $M \gg 1$ for all κ.
$\kappa \gg \kappa_0 \Rightarrow$ II ; $\kappa \ll \kappa_0 \Rightarrow$ III,IV.

3.2: $\alpha \approx 1$. Then $\kappa_\beta \approx \kappa_0$. $M \approx 1$ for $\kappa \gg \kappa_0$.
$\kappa \gg \kappa_0 \Rightarrow$ I,II ; $\kappa \ll \kappa_0 \Rightarrow$ III,IV.

3.3: $\alpha \ll 1$. Then $\kappa_0 \gg \kappa_\beta$. $M \ll 1$ for $\kappa \gg \kappa_\beta$.
$\kappa \gg \kappa_\beta \Rightarrow$ I ; $\kappa \ll \kappa_\beta \Rightarrow$ III,IV.

In every case described above, there is a critical wavenumber κ_c which divides the wavenumber domain into two distinct regimes: for $\kappa \gg \kappa_c$ the flow is dominated by I or II or both, depending on α; for $\kappa \ll \kappa_c$ the flow is dominated by III or IV or both, depending on μ. The situation is portrayed in Figure 5.2, with an explanation of the parameters given in the caption. Trajectories have been sketched for $\kappa \gg \kappa_c$, under the assumption that U increases with decreasing κ for a disturbance dominated by II; this assumption may well not be generally correct, but it is at least approximately correct for $\kappa \gg \kappa_0$ (i.e. for $\gamma \ll 1$) since then the perturbation enstrophy is approximately conserved. Two trajectories from each point must be given for $\alpha \gg 1$, as the evolution depends critically on $\underline{k}$.

Pure beta-plane turbulence corresponds to Case 1.3. Passive advection of the perturbation vorticity corresponds to Cases 1.1, 2.1, and 3.1, for $\kappa \gg \max\{\kappa_0, \kappa_\alpha\}$. 2-D turbulence is described by Cases 1.3, 2.3, and 3.3, for $\kappa \gg \max\{\kappa_\gamma, \kappa_\beta\}$. Ray tracing is appropriate for Case 1.1, in the range $\kappa_0 \ll \kappa \approx \kappa_\alpha \ll \kappa_\beta$. These special cases unfortunately do not cover all of parameter space.

To determine where the tropospheric synoptic-scale transient eddies fit into this scheme, one can make a rough estimate based on the spectral observations presented in Chapter IV. Taking $U \approx 10$ m/s, $U_0 \approx 20$ m/s, $L \approx 10^6$ m (at $n = 8$), and $L_0 \approx 3 \times 10^6$ m, one arrives at $\alpha \approx 2$, $\gamma \approx 0.1$, $\beta \approx 1$, and thus $\mu \approx 5$. This pretty much corresponds to somewhere between Cases 1.2 and 3.2, and is represented in Figure 5.2 by a shaded circle. Not only does it fail to fall under any of the special

cases described above, but this setting is also located uncomfortably close to the region in parameter space where none of the terms in (5.19) may be safely ignored. This analysis illustrates the extreme difficulty of the problem under consideration.

§5e. Nonlinear Conservation Laws: General

There is a deep and fundamental connection between symmetries or invariance properties of a dynamical system, and the existence of conservation laws governing the behaviour of the system. If the physical problem itself, described by the equations of motion, is invariant under a translation of the temporal coordinate, it follows that the energy of the whole system is conserved. Similarly, invariance of the physical problem under spatial translations is associated with conservation of the appropriate component of momentum.

It turns out that these concepts have analogues in the case of a perturbed system. Provided that a mean state and a perturbation can be defined, invariances of the mean state are connected to conservation laws governing the perturbation. In theoretical physics, where this was apparently first understood, it has become customary to refer to the conserved perturbation quantities associated with temporal and spatial translational invariance of the mean state as, respectively, "pseudo-energy" and "pseudomomentum".

For the sake of completeness it should be mentioned that conservation of potential vorticity following a fluid particle, a key property for systems such as the barotropic vorticity equation, is related to invariance of the equations under particle "relabelling" (Salmon, 1983). This is a rather subtle and often problematical

symmetry; however it rarely applies to the perturbation equations, and so need not be addressed here.

The distinction between momentum and pseudomomentum is discussed in the context of solid-state physics by Peierls (1979, §4.2). It seems that an equivalent appreciation of the distinction has been slower to reach the discipline of fluid dynamics, despite the fact that the concepts are fundamental to the whole subject of wave, mean-flow interaction (McIntyre, 1981). However a substantial body of recent theoretical work concerning finite-amplitude waves on mean flows, especially Andrews & McIntyre (1978a,b), has begun to make the relevant points quite forcefully. An important by-product of this work has been a rationalization of the various linearized or small-amplitude conservation laws that have been obtained in the past (e.g. Taylor, 1915; Fjørtoft, 1950; Bretherton & Garrett, 1968; Pedlosky, 1979, §7.3; Young & Rhines, 1980; Zeng, 1982), and the establishment of a systematic framework in which to obtain new ones (e.g. Andrews, 1983a; Ripa, 1983; Plumb, 1984a,b); more will be said on this matter in §5g below.

In principle one of the greatest potential benefits of the finite-amplitude wave, mean-flow interaction theory would appear to lie in the acquisition of conservation laws for truly nonlinear perturbations, given the dearth of such results at the present time. Unfortunately, the theory requires that the perturbations be defined as particle displacements from a Lagrangian-mean flow, and these particle displacements, while mathematically well-defined given certain assumptions, are in practice quite difficult to obtain except in the case of a small-amplitude disturbance. For a turbulent flow, definition of the particle displacements becomes very problematical indeed.

Consequently, one may face the rather peculiar situation of knowing that a mean flow has one or more invariance properties, and that these guarantee the existence of nonlinear conservation laws, without being able to find expressions for those laws in terms of tractable quantities. This would not be a problem if one were interested in stability criteria; but for other applications it remains true that useful nonlinear conservation laws are, because of their rarity, extremely precious.

The reason that conservation laws are so valuable is not so much that their conditions are commonly satisfied, but rather that they define a reasonable measure of "wave activity" that would be conserved if those conditions were satisfied. In wave, mean-flow interaction problems this enables one to isolate the dynamically significant interactions; indeed, there is a fundamental connection between conservation relations for perturbation quantities and mean-flow "non-acceleration" theorems (Andrews & McIntyre, 1978a). For turbulent flows, any constraint on the perturbation is desirable insofar as it limits the range of possible flow configurations and yields information on the expected statistics.

In order to understand the theoretical connection between symmetries or invariances, and conservation laws, it is instructive to consider a system governed by a variational principle. The question of how to choose the precise form of the variational principle can be a thorny one (see Bretherton, 1970; Mobbs, 1982), whose discussion lies beyond the scope of this study. It is therefore reassuring that the existence of the conservation laws does not depend on the variational derivation (Andrews & McIntyre, 1978b); however the <u>origin</u> of the laws

seems most evident when viewed from this perspective, and this connection can represent a distinct advantage when formulating rational approximations to the governing equations (Salmon, 1983).

Assume, therefore, that the physical system obeys a variational principle

$$\delta \int L(q,q_{,\mu};\mu)\, d\mu = 0 \tag{5.28}$$

for finite variations δq, where L is a Lagrangian density. In (5.28) μ represents the independent variables, e.g. $\underline{x}$ and t, $q(\mu)$ the dependent variables, and $q_{,\mu} \equiv \partial q/\partial\mu$ their derivatives. Formally μ and q ought to have subscripts, but these will be omitted to simplify the notation. It should be realized that L can easily incorporate dissipative effects (Mobbs, 1982). From (5.28) the Euler equations, or equations of motion, are obtained:

$$0 = \delta \int L\, d\mu = \int \left(\frac{\partial L}{\partial q}\delta q + \frac{\partial L}{\partial q_{,\nu}}\delta q_{,\nu}\right) d\mu = \int \left(\frac{\partial L}{\partial q} - \frac{\partial}{\partial \nu}\frac{\partial L}{\partial q_{,\nu}}\right) \delta q\, d\mu$$

$$\Rightarrow \qquad \frac{\partial}{\partial \nu}\frac{\partial L}{\partial q_{,\nu}} - \frac{\partial L}{\partial q} = 0 \qquad \text{for each } q. \tag{5.29}$$

The Einstein double-index summation notation will be used throughout this section. It is important to distinguish partial derivatives of L in the <u>physical</u> space $\{\mu\}$ from those in the <u>argument</u> space $\{q,q_{,\mu},\mu\}$: $\partial L/\partial\mu$ shall represent the former, and $L_{,\mu}$ the latter. For $\partial L/\partial q$ there is no ambiguity, of course.

Now, (5.29) proves useful in establishing the identity:

$$\frac{\partial L}{\partial \mu} = \frac{\partial L}{\partial q} q_{,\mu} + \frac{\partial L}{\partial q_{,\nu}} q_{,\nu\mu} + L_{,\mu} = q_{,\mu}\frac{\partial}{\partial \nu}\frac{\partial L}{\partial q_{,\nu}} + \frac{\partial L}{\partial q_{,\nu}}\frac{\partial}{\partial \nu}\left(q_{,\mu}\right) + L_{,\mu}$$

$$\Rightarrow \qquad \frac{\partial L}{\partial \mu} = \frac{\partial}{\partial \nu}\left(q_{,\mu}\frac{\partial L}{\partial q_{,\nu}}\right) + L_{,\mu}\ . \tag{5.30}$$

Introducing the canonical energy-momentum tensor (Landau & Lifshitz,

1971, §32)

$$T_{\mu\nu} \equiv q_{,\mu} \frac{\partial L}{\partial q_{,\nu}} - L\,\delta_{\mu\nu} \quad , \tag{5.31}$$

it follows easily from (5.30) and (5.31) that

$$T_{\mu\nu,\nu} = - L_{,\mu} \quad . \tag{5.32}$$

Hence if L has no explicit dependence on a particular physical coordinate μ, a condition which is equivalent to the problem being invariant under translations along that coordinate, then $T_{\mu\nu,\nu} = 0$. That this represents a conservation law is clear when the choice $\mu \to (\underline{x},t)$ is made, for then

$$T_{\mu\nu,\nu} = \frac{\partial}{\partial t} T_{\mu t} + \nabla \cdot T_{\mu \underline{x}} = 0 \quad . \tag{5.33}$$

In classical physics, $T_{tt} = \dot{q}(\partial L/\partial \dot{q}) - L$ is the Hamiltonian or energy density, which obeys a global conservation law when $L_{,t} = 0$; its flux is $\dot{q}(\partial L/\partial(\nabla q))$. Similarly, T_{xt} is the x-momentum, and $T_{x\underline{x}}$ its flux.

Following Hayes (1970), consider a one-parameter differentiable family of disturbed-flow solutions $q(\mu;\alpha)$ to (5.29), where α is some ensemble label, and an ensemble average $\langle\ \rangle$ is obtained by integrating over α. To represent a consistent definition of disturbance and mean, it is necessary to assume that

$$\langle q \rangle_{,\alpha} = \langle q_{,\alpha} \rangle = 0 \quad ; \tag{5.34}$$

Hayes ensures (5.34) by insisting that q be periodic in α, but the condition need not be that restrictive. Then the mean and perturbation are given by

$$q \equiv \langle q \rangle + q' \quad , \tag{5.35}$$

which defines q'. If one permits a generalization of $T_{\mu\nu}$, replacing μ with α, namely

$$T_{\alpha\nu} \equiv \left\langle q_{,\alpha} \frac{\partial L}{\partial q_{,\nu}} \right\rangle \quad , \tag{5.36}$$

then it is immediately apparent that, since (5.30) still applies with $\mu = \alpha$, $T_{\alpha\nu}$ satisfies

$$T_{\alpha\nu,\nu} = \langle L_{,\alpha} \rangle = 0 . \tag{5.37}$$

(5.37) is referred to as the wave-action conservation law. It may be written in the form

$$\frac{\partial A}{\partial t} + \nabla \cdot \underline{B} = 0 , \tag{5.38}$$

where

$$A \equiv T_{\alpha t} = \langle q_{,\alpha} \, \partial L/\partial \dot{q} \rangle \tag{5.39a}$$

is the wave-action density, and

$$\underline{B} \equiv T_{\alpha \underline{x}} = \langle q_{,\alpha} \, \partial L/\partial(\nabla q) \rangle \tag{5.39b}$$

its flux. That A and $\underline{B}$ are disturbance quantities is evident from the fact that $\langle q_{,\alpha} \rangle = \langle q'_{,\alpha} \rangle$. As Hayes (1970) emphasizes, (5.37) and (5.38) represent an absolute conservation law, whose application depends on the choice of the family $q(\mu;\alpha)$; for example, if L is independent both of the "longitudinal" coordinate x and of t in a wave propagation problem, then α may be interpreted as a phase shift parameter: $q(\mu;\alpha) = f(y) \exp\{i(kx-\omega t-\alpha)\}$. For general wave motion, however, the identification of $q(\mu;\alpha)$ is far from trivial, and Hayes was forced to employ a multiple-scale approximation (assuming slow modulation) in order to apply the method.

The difficulties associated with the general wave-action conservation law are rooted in the difficulty of defining a "mean flow" and a "disturbance" in a completely general fashion. It has been known for some time that the resolution of the dilemma lies in the use of a Lagrangian-mean formulation, considering a disturbance particle-displacement field $\underline{\xi}(\underline{x},t)$; indeed, Hayes (1970) and Bretherton (1971) discuss this matter in some detail, tracing it back to Eckart (1963),

but they cannot avoid a small-amplitude assumption. The fully nonlinear formulation of a wave, mean-flow interaction theory was finally achieved in terms of the "generalized Lagrangian mean" (GLM) by Andrews & McIntyre (1978a,b).

Without going into too many details, the GLM theory defines the disturbance mapping $I: \underline{x} \to \underline{x} + \underline{\xi}(\underline{x},t)$, in terms of which the GLM itself is given by

$$\bar{\phi}^L(\underline{x},t) \equiv \langle \phi(\underline{x}+\underline{\xi}(\underline{x},t),t) \rangle , \qquad (5.40)$$

the angle brackets representing any "Eulerian-mean" operator such as a temporal, spatial, or ensemble average. By definition,

$$\langle \underline{\xi} \rangle = 0 \qquad (5.41a)$$

and

$$(\frac{\partial}{\partial t} + \bar{\underline{u}}^L \cdot \nabla)\underline{\xi} \equiv \bar{D}^L \underline{\xi} = \underline{u}(\underline{x}+\underline{\xi},t) - \bar{\underline{u}}^L(\underline{x},t) \equiv \underline{u}^\ell(\underline{x},t) , \qquad (5.41b)$$

$\underline{u}$ representing the full velocity field.

Following Andrews & McIntyre (1978b), the aim is to find an analogue of the energy-momentum tensor $T_{\mu\nu}$ for the "disturbance problem", the latter defined by holding the mean fields fixed and varying $\underline{\xi}$. The variational principle (5.28), after all, must hold for all variations. Choose $\underline{\xi}(\underline{x},t)$ as some of the $q(\mu)$'s, and the mean fields as the others, call them $\bar{q}$; then $L = L(\xi,\xi_{,\mu};\bar{q},\bar{q}_{,\mu};\mu)$. Define L_0 to be the "undisturbed" Lagrangian evaluated with $\xi = 0 = \xi_{,\mu}$: i.e. $L_0(\bar{q},\bar{q}_{,\mu};\mu) \equiv L(0,0;\bar{q},\bar{q}_{,\mu};\mu)$. Then the "perturbation Lagrangian" which governs the disturbance, L_1, may be defined as (Hayes, 1970)

$$L_1(\xi,\xi_{,\mu};\mu) \equiv L(\xi,\xi_{,\mu};\bar{q},\bar{q}_{,\mu};\mu) - L_0(\bar{q},\bar{q}_{,\mu};\mu) - \frac{\partial L_0}{\partial \bar{q}}\,\xi - \frac{\partial L_0}{\partial \bar{q}_{,\nu}}\,\xi_{,\nu}. \qquad (5.42)$$

L_1 does depend on the mean fields, but only through its explicit dependence on μ; this is because as far as L_1 is concerned, the mean fields are considered to be fixed. Note that $\langle L_1 \rangle = \langle L - L_0 \rangle$. The

disturbance problem then consists of applying (5.28) with L replaced by L_1. In place of (5.29), one obtains

$$\frac{\partial}{\partial \nu} \frac{\partial L_1}{\partial \xi_{i,\nu}} - \frac{\partial L_1}{\partial \xi_i} = 0 \quad , \tag{5.43}$$

where subscripts have been explicitly introduced. Since all the dependence of L_1 on the mean fields is contained in μ, (5.30) can be immediately applied in the form

$$\frac{\partial L_1}{\partial \mu} = \frac{\partial}{\partial \nu}\left(\xi_{i,\mu} \frac{\partial L_1}{\partial \xi_{i,\nu}}\right) + L_{1,\mu} \quad . \tag{5.44}$$

Then introducing

$$S_{\mu\nu} \equiv \left\langle \xi_{i,\mu} \frac{\partial L}{\partial \xi_{i,\nu}} \right\rangle - \langle L_1 \rangle \delta_{\mu\nu} \quad , \tag{5.45}$$

it follows from (5.42), (5.44), and (5.45) that

$$S_{\mu\nu,\nu} = \frac{\partial}{\partial \nu} \left\langle \xi_{i,\mu} \frac{\partial L_0}{\partial \bar{q}_{i,\nu}} \right\rangle - \langle L_1 \rangle_{,\mu} = - \langle L_1 \rangle_{,\mu} \quad . \tag{5.46}$$

Thus the condition for $S_{\mu\nu,\nu}$ to vanish is that $\langle L_1 \rangle = \langle L - L_0 \rangle$ have no explicit dependence on μ; this requires in turn that the <u>mean flow</u> have no explicit dependence on μ, in addition to the condition $L_{,\mu} = 0$ that is required for (5.33).

By analogy with the energy-momentum tensor $T_{\mu\nu}$, it seems sensible to call $S_{\mu\nu}$ the pseudo-energy-momentum tensor. Whereas spatial or temporal translational invariances of the physical problem lead to conservation laws for momentum or energy, spatial or temporal translational invariances of the mean flow in a perturbed situation lead to conservation laws for the disturbance quantities pseudomomentum or pseudoenergy.

If L is quadratic in ξ and $\xi_{,\mu}$, then $S_{\mu\nu}$ is quadratic also. For a linearized system this is always the case. But it is still true for a

wide class of fluid dynamical systems, including the one under discussion in this thesis. Taking the definition of L provided by Andrews & McIntyre (1978b,eq.(5.5)), and choosing the sign by historical precedent (op.cit.), one obtains

$$S_{it} = -\hat{\rho}\, p_i \equiv \hat{\rho} < \underline{\xi}_{,i} \cdot (\underline{u}^{\ell} + \underline{\Omega}\times\underline{\xi}) > \quad [i=1,2,3] , \tag{5.47a}$$

where p_i is the i-th component of pseudomomentum, $\hat{\rho}$ is the "mean-flow density" (Andrews & McIntyre, 1978a, §4.1), and $\underline{u}^{\ell}$ is given by (5.41b). $\underline{\Omega}$ is the angular velocity of the rotating coordinate system. On the other hand

$$S_{tt} = \hat{\rho}\, e - <L-L_0> \equiv \hat{\rho} < \underline{\xi}_{,t} \cdot (\underline{u}^{\ell} + \underline{\Omega}\times\underline{\xi}) > - <L-L_0> , \tag{5.47b}$$

where e is the pseudoenergy. The $<L-L_0>$ term in (5.47b) is not advected by the mean flow $\underline{u}^{L}$ (Andrews & McIntyre, 1978b), and is usually time-invariant if the mean flow is; consequently it may often be ignored. Dunkerton (1983) has recently discussed the subject of pseudoenergy conservation in the GLM context, developing these ideas further.

As before, to obtain the wave-action conservation law one merely generalizes $S_{\mu\nu}$, replacing μ with α where α is an ensemble label, and letting $< >$ represent an ensemble average. Thus

$$S_{\alpha\nu} \equiv < \xi_{i,\alpha} \frac{\partial L}{\partial \xi_{i,\nu}} > , \tag{5.48}$$

the extra term of (5.45) not entering, whence

$$S_{\alpha\nu,\nu} = - <L_1>_{,\alpha} = 0 ; \tag{5.49}$$

(5.49) may be written alternatively as

$$\frac{\partial(\hat{\rho}\hat{A})}{\partial t} + \nabla\cdot\underline{\hat{B}} = 0 = \left(\frac{\partial}{\partial t} + \underline{u}^{L}\cdot\nabla\right)\hat{A} + \frac{1}{\hat{\rho}}\nabla\cdot\underline{\hat{B}}^{*} , \tag{5.50a,b}$$

where

$$\hat{A} = \frac{1}{\hat{\rho}} S_{\alpha t} \equiv \langle \underline{\xi}_{,\alpha} \cdot (\underline{u}^{\ell} + \underline{\Omega} \times \underline{\xi}) \rangle \tag{5.51a}$$

is the wave-action density, and

$$\underline{\hat{B}} = (\hat{\rho}\hat{A})\underline{\bar{u}}^{L} + \underline{\hat{B}}^{*} = S_{\alpha \underline{x}} \tag{5.51b}$$

its flux. $\underline{\hat{B}}^{*}$ is a somewhat complicated quantity, representing the non-advective flux of wave-action; see Andrews & McIntyre (1978b) for details. Aside from the factor of $\hat{\rho}$, $\hat{A}$ is identical to Hayes's (1970) A of (5.39a); the difference is that the GLM provides a reliable way of identifying the family $q(\mu;\alpha)$.

As mentioned earlier, the wave-action conservation law (5.50) and its relatives, conservation of pseudomomentum and of pseudoenergy, can be derived directly from the equations of motion, without recourse to a variational formulation (Andrews & McIntyre, 1978b). However the present approach emphasizes the connection with the energy-momentum tensor formalism of theoretical physics. The difficulty remains that even if one is able to identify invariance properties of the mean flow, the particle displacements $\underline{\xi}(\underline{x},t)$ may be intractable for finite-amplitude disturbances; thus the GLM conservation laws described above may be difficult to apply in a diagnostic situation. On the other hand they do lead to stability criteria: Craik (1982), for example, has recently rederived the inflection-point and semicircle theorems for parallel shear flows very concisely in the GLM format. One would nevertheless prefer to have nonlinear conservation laws expressed in terms of "Eulerian" quantities such as the velocity, but this is not generally possible. There are, however, a few special cases when such laws can be obtained.

§5f. Nonlinear Conservation Laws: Specific

The aim of this section is to develop, as far as is possible, nonlinear conservation laws for disturbances in an Eulerian framework, as these tend to be more useful than the Lagrangian relations derived in §5e. Because it appears, barring any new discoveries, that Eulerian laws are not generally obtainable, the task becomes one of identifying the special cases when they can be found.

(i) Conservation of Pseudoenergy

Consider then the perturbed system of §5b, for which the basic-state or "mean" flow is time-invariant. If an Eulerian conservation law can be found for the perturbation, then it may be identified with conservation of pseudoenergy. Assume that the basic-state flow is not only stationary but unforced; this is the first restriction. Then $S(\Psi;x,y) = 0$ in (5.2), and the latter may be written as

$$J(\Psi,Q) = 0 \quad , \tag{5.52}$$

where $Q \equiv \nabla^2\Psi + \beta_0 y$. (Topography could easily be introduced, however, as could baroclinicity.) (5.52) implies that Q is a function of Ψ, i.e. $Q = Q(\Psi)$, whence

$$J(f,Q) = \frac{\partial Q}{\partial \Psi} J(f,\Psi) \equiv \Lambda(\Psi)\, J(f,\Psi) \quad \text{for all } f. \tag{5.53}$$

Since $\Lambda = \Lambda(\Psi)$, any function of Λ commutes with Jacobians involving Ψ or Q:

$$g(\Lambda)\, J(\Psi,f) = J(\Psi,fg(\Lambda)) \quad \text{for all } f. \tag{5.54}$$

It is useful to note the identities

$$\Lambda \equiv \frac{\partial Q}{\partial \Psi} = \frac{Q_y}{\Psi_y} = \frac{Q_x}{\Psi_x} = -\frac{Q_y}{U} = \frac{Q_x}{V} \quad , \tag{5.55}$$

the comma notation for differentiation having been dropped.

Now, the perturbation energy obeys the relation (5.8), which is written below in a slightly different form:

$$\frac{\partial}{\partial t}\left(\frac{1}{2}\left|\nabla\phi\right|^2\right) - \nabla\cdot\left(\phi\nabla\phi_t + \underline{v}\phi(q+Q) + \underline{V}\phi q\right) = -qJ(\Psi,\phi)\ ; \qquad (5.56)$$

here $q \equiv \nabla^2\phi$. To obtain a pseudoenergy conservation law, the idea is to combine (5.56) with a relation involving the vorticity in such a way that the right-hand sides cancel each other out.

The enstrophy relation (5.18) is found after multiplying (5.4) by q. For greater generality, multiply (5.4) with $S' = 0$ by the quantity $f'(q)/\Lambda$, where f is an arbitrary function of q, and $f'(q) \equiv \partial f/\partial q$; $\partial\Lambda/\partial t = 0$ by hypothesis. This yields

$$\frac{\partial}{\partial t}\left(\frac{f(q)}{\Lambda}\right) + J\left(\Psi+\phi,\frac{f(q)}{\Lambda}\right) - f(q)J\left(\phi,\frac{1}{\Lambda}\right) + \frac{f'(q)}{\Lambda}J(\phi,Q) = 0\ , \qquad (5.57)$$

noting that $J(\Psi,1/\Lambda) = 0$ by (5.54). Now,

$$J(\phi,1/\Lambda) = -\frac{1}{\Lambda^2}J(\phi,\Lambda) = \frac{\partial\Lambda/\partial\Psi}{\Lambda^2}J(\Psi,\phi)\ . \qquad (5.58)$$

Using (5.53) to deal with the last term of (5.57), and (5.58) to handle the second last, one obtains

$$\frac{\partial}{\partial t}\left(\frac{f(q)}{\Lambda}\right) + \nabla\cdot\left((\underline{V}+\underline{v})\frac{f(q)}{\Lambda}\right) = \left(f'(q) + f(q)\frac{\partial\Lambda/\partial\Psi}{\Lambda^2}\right)J(\Psi,\phi)\ . \qquad (5.59)$$

Then (5.56) and (5.59) can be combined to yield

$$\frac{\partial}{\partial t}\left(\frac{1}{2}\left|\nabla\phi\right|^2 + \frac{f(q)}{\Lambda}\right) + \nabla\cdot\left((\underline{V}+\underline{v})\frac{f(q)}{\Lambda} - \phi\nabla\phi_t - \underline{v}\phi(q+Q) - \underline{V}\phi q\right)$$

$$= \left(f'(q) - q + f(q)\frac{\partial\Lambda/\partial\Psi}{\Lambda^2}\right)J(\Psi,\phi)\ . \qquad (5.60)$$

In order for (5.60) to represent a conservation law the rhs must vanish, and this can only happen for arbitrary ϕ if

$$\frac{\partial\Lambda/\partial\Psi}{\Lambda^2} = \text{constant} \equiv \lambda\ . \qquad (5.61)$$

But

$$\frac{\partial\Lambda}{\partial\Psi} = \lambda\Lambda^2 \quad\Rightarrow\quad \Lambda(\Psi) = \frac{-1}{\lambda\Psi+c_1}\ , \qquad (5.62)$$

and

$$\frac{\partial Q}{\partial \Psi} = \Lambda(\Psi) \quad \Rightarrow \quad Q(\Psi) = -\frac{1}{\lambda}\log(\lambda\Psi + c_1) + c_2 \ . \tag{5.63}$$

Of course any constant in Q is dynamically meaningless, so c_2 can be set equal to zero. If $\lambda = 0$ then (5.61) permits the simple solution

$$Q(\Psi) = \frac{-1}{c_1}\Psi \ . \tag{5.64}$$

For $\lambda \neq 0$, (5.63) is appropriate. The limit $\lambda \to 0$ appears to be singular, but in fact is not so troublesome: applying it to (5.63) gives

$$\begin{aligned} Q(\Psi) &= -\frac{1}{\lambda}\left\{\log c_1 + \log\left(1+\frac{\lambda\Psi}{c_1}\right)\right\} \\ &= -\frac{\log c_1}{\lambda} - \frac{1}{c_1}\Psi + \ . \ . \ . \qquad \text{as } \frac{\lambda\Psi}{c_1} \to 0 \ , \end{aligned} \tag{5.65}$$

the dots representing higher-order terms in $\lambda\Psi/c_1$; from (5.62) it is evident that the limit $\lambda \to 0$ must be accompanied by $\lambda\Psi/c_1 \to 0$. Now, although (5.65) is strictly singular as $\lambda \to 0$, the divergent term $-(\log c_1)/\lambda$ is a constant for any finite λ and can be ignored; one is thus left with (5.64) as the limiting functional dependence.

Taking (5.61), the rhs of (5.60) will vanish provided that

$$f'(q) + \lambda f(q) = q \ . \tag{5.66}$$

For $\lambda = 0$, (5.66) implies

$$f(q) = \frac{1}{2}q^2 + c_3 \ ; \tag{5.67a}$$

however c_3 is dynamically meaningless if Λ is constant, and may be set to zero. For $\lambda \neq 0$, on the other hand, the general solution is

$$f(q) = \frac{q}{\lambda} - \frac{1}{\lambda^2} + c_4\, e^{-\lambda q} \ , \tag{5.67b}$$

the constant multiplying the homogeneous solution to (5.66). If q is bounded, then (5.67b) approaches (5.67a) uniformly as $\lambda \to 0$ with $c_4 = \lambda^{-2}$. These results can be summarized in the following theorem:

THEOREM I: An unforced stationary basic-state flow (Ψ,Q) allows a conservation relation for the perturbation pseudoenergy given by

$$\frac{\partial}{\partial t}\left(\frac{1}{2}|\nabla\phi|^2 + \frac{f(q)}{\Lambda}\right) + \nabla\cdot\left((\underline{V}+\underline{v})\frac{f(q)}{\Lambda} - \phi\nabla\phi_t - \underline{v}\phi(q+Q) - \underline{V}\phi q\right) = 0 , \quad (5.68)$$

if $Q(\Psi)$ takes one of the two following forms (neglecting additive constants):

(i) $Q(\Psi) = c_1\Psi$, in which case $f(q) = q^2/2$ and $\Lambda = c_1$;

(ii) $Q(\Psi) = -\frac{1}{\lambda}\log(\lambda\Psi+c_2)$, in which case $f(q) = \frac{q}{\lambda} - \frac{1}{\lambda^2} + c_3 e^{-\lambda q}$ and $\Lambda = \frac{-1}{\lambda\Psi+c_2}$.

It must be mentioned that the establishment of Theorem I is equally valid for baroclinic quasi-geostrophic flow, and for variable topography. In the former case, (5.68) holds at each z, and the constants c_i may be functions of z. At no point in the derivation was an assumption of barotropy used.

Case (i) of Theorem I, with Λ a constant, allows the manipulation $-\nabla\cdot(\underline{v}\phi Q) = -J(\phi,\phi Q) = -\phi J(\phi,Q) = \Lambda J(\Psi,\phi^2/2) = \nabla\cdot(\underline{V}\Lambda\phi^2/2)$; then noting that

$$\nabla\cdot(\underline{v}\Lambda\phi^2/2) = (\Lambda/2)J(\phi,\phi^2) = 0$$

for this case, the pseudoenergy conservation law can be written in the form

$$\frac{\partial}{\partial t}\left(\frac{1}{2}|\nabla\phi|^2 + \frac{q^2}{2\Lambda}\right) + \nabla\cdot\left(\frac{1}{2\Lambda}(\underline{V}+\underline{v})(q-\Lambda\phi)^2 - \phi\nabla\phi_t\right) = 0 . \quad (5.69)$$

Note that the pseudoenergy is a linear combination of the energy and the enstrophy. The global conservation law corresponding to (5.69), namely

$$\frac{d}{dt}\iint\left(\frac{1}{2}|\nabla\phi|^2 + \frac{q^2}{2\Lambda}\right)dxdy = 0 , \quad (5.70)$$

was implicit in the work of Fjørtoft (1950), Arnol'd (1965), and Blumen (1968), though it was obtained there by a different method and given a

different emphasis. Their results rather concerned the fact that if the constant Λ were positive, then the integrand of (5.70) would be positive definite and the basic-state flow would be stable to disturbance perturbations. The stability criteria were derived for general stationary unforced flows, in which case the disturbance must be assumed to be of small amplitude (Blumen, 1968). But it is clear from the present discussion that the stability criterion is an absolute one, valid for any disturbance, for basic-state flows satisfying $Q(\Psi) = c_1\Psi$.

What class of flows does $Q(\Psi) = c_1\Psi$ allow? To determine this for the barotropic beta-plane, without topography,

$$\nabla^2\Psi + \beta_0 y = c_1\Psi \quad <=> \quad (\nabla^2 - c_1)\Psi = -\beta_0 y \tag{5.71}$$

allows a particular solution

$$\Psi^{(p)} = \frac{\beta_0}{c_1} y \equiv \hat{U}\, y \,. \tag{5.72}$$

This represents a constant zonal flow, which is without dynamical significance for flat topography; yet it must be included in the solution if (5.71) is to hold. The point to be made is that when $\nabla^2\Psi = c_1\Psi$, then (5.69) and (5.70) hold with $\Lambda = c_1$; this can also be seen immediately from the energy and enstrophy relations (5.6a) and (5.17a). But case (i) of Theorem I requires that $Q = c_1\Psi$. However, any flow satisfying $\nabla^2\Psi = c_1\Psi$ can be made to satisfy $Q = c_1\Psi$ merely by adding on a constant (i.e. vorticity-free) zonal flow given by (5.72), which changes nothing in the problem; this resolves the apparent discrepancy. For variable topography h(x,y), though, $\Psi^{(p)} = [\beta_0 y + h(x,y)]/c_1$, and the situation is a good deal more complicated.

The homogeneous solution of (5.71) depends on the sign of c_1. For negative c_1 ,

$$\Psi^{(h)} = \iint_{(k^2+\ell^2=-c_1)} \{A_{k\ell}\sin(kx+\ell y) + B_{k\ell}\cos(kx+\ell y)\}\, dk d\ell \ , \qquad (5.73)$$

the integration running over the perimeter of a circle in wavenumber space; (5.73) is especially appropriate for periodic or bounded domains. In particular, any basic-state flow consisting of a single Fourier component will belong to the class $Q(\Psi) = c_1\Psi$ (by adding a meaningless Doppler shift term (5.72)), and Theorem I will then apply. This includes, significantly, the flows considered by Lorenz (1972) and Gill (1974) in their Rossby-wave barotropic instability calculations.

Turning now to positive c_1,

$$\Psi^{(h)} = \iint_{(k^2+\ell^2=c_1)} \{C_{k\ell}e^{kx+\ell y} + D_{k\ell}e^{-(kx+\ell y)}\}\, dk d\ell \ , \qquad (5.74)$$

a solution which is particularly appropriate for infinite domains. The combination of (5.72) and (5.74) as a solution of (5.71) is common in the theory of solitary waves, for which Theorem I would again be relevant.

To explore the implications of (5.70), consider an initial distribution of perturbation energy E spectrally localized at wavenumber κ, and let it all move to wavenumber $\kappa+\delta\kappa$; E is not generally conserved, and will take the new value $E+\delta E$. The perturbation enstrophy, initially $\Omega = \kappa^2 E$, will become $\Omega+\delta\Omega$, but $\delta\Omega$ must satisfy both

$$\delta\Omega = -\Lambda\, \delta E \qquad (5.75)$$

and

$$\delta\Omega = (E+\delta E)(\kappa+\delta\kappa)^2 - E\kappa^2 = \kappa^2(\delta E) + 2\kappa E(\delta\kappa) + \ldots \qquad (5.76)$$

Taken together, (5.75) and (5.76) give

$$\frac{\delta E}{\delta\kappa} = -\frac{2\kappa E}{\Lambda+\kappa^2} \ , \qquad (5.77)$$

for small variations $\delta\kappa$. One also has

$$\frac{\delta\Omega}{\Omega} = -\frac{\Lambda}{\kappa^2}\frac{\delta E}{E} \quad . \tag{5.78}$$

For sufficiently large κ, (5.78) implies approximate conservation of enstrophy, a result mentioned in §5c; in that case (5.77) becomes $\delta E/\delta\kappa \approx -2E/\kappa$. But as long as $\Lambda > -\kappa^2$, then (5.77) shows that E increases with decreasing κ.

Of course the 2-D turbulence behaviour $\delta E = 0 = \delta\Omega$ is always a possible solution of (5.70) and (5.75); the hypothetical movement of all the energy in one spectral direction, represented by (5.77), would then not be allowed.

In the case $\Lambda = c_1 > 0$, the perturbation is obviously constrained insofar as the basic-state flow is absolutely stable. However (5.77) does indicate that the energy can grow, though only at the expense of the enstrophy. Consider now an arbitrary initial condition with energy E_0 and enstrophy Ω_0; then (5.70) can be expressed as

$$\Lambda\, E(t) + \Omega(t) = \Lambda\, E_0 + \Omega_0 \quad . \tag{5.79}$$

Assume that the perturbation is spectrally confined to the wavenumber range $\kappa_1 \leq \kappa \leq \kappa_2$, where $\kappa^2 \equiv k^2 + \ell^2$; it then follows that

$$\kappa_1^2\, E(t) \leq \Omega(t) \leq \kappa_2^2\, E(t) \quad . \tag{5.80}$$

Combining (5.80) with (5.79) yields the bounds

$$0 < \frac{\Lambda E_0+\Omega_0}{\Lambda+\kappa_2^2} \leq E(t) \leq \frac{\Lambda E_0+\Omega_0}{\Lambda+\kappa_1^2} < \frac{\Lambda E_0+\Omega_0}{\Lambda} \tag{5.81a}$$

and

$$0 < \kappa_1^2\,\frac{\Lambda E_0+\Omega_0}{\Lambda+\kappa_1^2} \leq \Omega(t) \leq \kappa_2^2\,\frac{\Lambda E_0+\Omega_0}{\Lambda+\kappa_2^2} < \Lambda E_0+\Omega_0 \quad , \tag{5.81b}$$

the outermost bounds representing the limits $\kappa_1 \to 0$, $\kappa_2 \to \infty$, corresponding to an infinite domain.

The case $\Lambda = c_1 < 0$, on the other hand, clearly has the

possibility of being unstable as both E(t) and $\Omega(t)$ could conceivably grow. Nevertheless the flow may be constrained if the perturbation is spectrally confined. Assume $\kappa_1 \leq \kappa \leq \kappa_2$ as before; one may also write $\Lambda = -\kappa_0^2$, where κ_0 is the basic-state wavenumber as expressed in (5.73). Then (5.70) takes the form

$$\Omega(t) - \kappa_0^2 E(t) = \Omega_0 - \kappa_0^2 E_0 \equiv P_0 . \tag{5.82}$$

Application of (5.80) with (5.82) leads to the inequalities

$$\begin{aligned}(\kappa_1^2-\kappa_0^2)E(t) \leq \frac{(\kappa_1^2-\kappa_0^2)}{\kappa_1^2}\Omega(t) \leq P_0 \leq \frac{(\kappa_2^2-\kappa_0^2)}{\kappa_2^2}\Omega(t) \\ \leq (\kappa_2^2-\kappa_0^2)E(t) .\end{aligned} \tag{5.83}$$

Whether (5.83) represent bounds on E(t) depends on the case:

$$\kappa_0 < \kappa_1 \Rightarrow \left| \begin{aligned} 0 < \frac{P_0}{\kappa_2^2-\kappa_0^2} \leq E(t) \leq \frac{P_0}{\kappa_1^2-\kappa_0^2} , \qquad (5.84a) \\ P_0 < \frac{\kappa_2^2 P_0}{\kappa_2^2-\kappa_0^2} \leq \Omega(t) \leq \frac{\kappa_1^2 P_0}{\kappa_1^2-\kappa_0^2} , \qquad (5.84b) \end{aligned} \right.$$

with $P_0 > 0$ and the lowest bounds being approached as $\kappa_2 \to \infty$;

$$\kappa_0 > \kappa_2 \Rightarrow \left| \begin{aligned} \frac{-P_0}{\kappa_0^2} < \frac{-P_0}{\kappa_0^2-\kappa_1^2} \leq E(t) \leq \frac{-P_0}{\kappa_0^2-\kappa_2^2} , \qquad (5.85a) \\ 0 < \frac{-\kappa_1^2 P_0}{\kappa_0^2-\kappa_1^2} \leq \Omega(t) \leq \frac{-\kappa_2^2 P_0}{\kappa_0^2-\kappa_2^2} , \qquad (5.85b) \end{aligned} \right.$$

with $P_0 < 0$ and the lowest bounds being approached as $\kappa_1 \to 0$. In both (5.84) and (5.85) the upper bound diverges as κ_0 approaches, respectively, κ_1 and κ_2. For $\kappa_1 \leq \kappa_0 \leq \kappa_2$, only lower bounds can be found:

$$\kappa_1 < \kappa_0 < \kappa_2 \Rightarrow \left| \begin{aligned} E(t) \geq \max\left\{ \frac{P_0}{\kappa_2^2-\kappa_0^2} , \frac{-P_0}{\kappa_0^2-\kappa_1^2} \right\} \geq \max\left\{ 0 , \frac{-P_0}{\kappa_0^2} \right\} , \\ \Omega(t) \geq \max\left\{ \frac{\kappa_2^2 P_0}{\kappa_2^2-\kappa_0^2} , \frac{-\kappa_1^2 P_0}{\kappa_0^2-\kappa_1^2} \right\} \geq \max\left\{ 0 , P_0 \right\} , \end{aligned} \right. \tag{5.86a,b}$$

the lowest bounds being approached in the limit $\kappa_1 \to 0$, $\kappa_2 \to \infty$; and

$$\kappa_0 = \kappa_1 \quad \Rightarrow \quad E(t) \geq \frac{\Omega(t)}{\kappa_2^2} \geq \frac{P_0}{\kappa_2^2-\kappa_1^2} , \tag{5.87}$$

$$\kappa_0 = \kappa_2 \quad \Rightarrow \quad \frac{\Omega(t)}{\kappa_1^2} \geq E(t) \geq \frac{-P_0}{\kappa_2^2-\kappa_1^2} . \tag{5.88}$$

The explanation for the lack of an upper bound when $\kappa_1 \leq \kappa_0 \leq \kappa_2$ lies in the fact that energy and enstrophy can then be gained at modes with $\kappa = \kappa_0$ in the ratio $\delta\Omega = \kappa_0^2\delta E$, exactly satisfying (5.82) without any effect on the rest of the spectrum; there is no apparent limit to the growth obtainable by such a process. This is also reflected in the fact that for $\kappa = \kappa_0$ and $\Lambda = -\kappa_0^2$, $\delta E/\delta\kappa$ diverges according to (5.77). $E(t)$ is ultimately bounded by conservation of total energy, as expressed in (5.12), and $\Omega(t)$ is similarly bounded; however this would not prevent a rapid initial growth of energy and enstrophy at $\kappa = \kappa_0$. Indeed, the linear barotropic instability calculations of Lorenz (1972) and Gill (1974) show that instability is to be expected for $\kappa_1 < \kappa_0 < \kappa_2$, unless β is very large.

(ii) Conservation of Pseudomomentum

Consider now the case when the basic-state flow is invariant in the zonal component x; any Eulerian conservation law connected with this invariance property may then be identified with conservation of pseudomomentum. If topography were present it would have to be zonally invariant as well, which would be a severe restriction. By the equation of continuity $\partial V/\partial y = 0$, so $U = U(y,t)$ and $V = V(t)$ for the basic-state flow. The unforced perturbation vorticity equation (5.4) takes the form

$$q_t + J(\Psi,q) + \phi_x Q_y + J(\phi,q) = 0 . \tag{5.89}$$

Multiplying (5.89) through by $f'(q)/Q_y$, where f is an arbitrary

function of q and $\partial(Q_y)/\partial x = 0$, yields

$$\frac{\partial}{\partial t}\left(\frac{f(q)}{Q_y}\right) + \nabla\cdot\left((\underline{V}+\underline{v})\frac{f(q)}{Q_y}\right) = - f'(q)\phi_x - f(q)\left(\frac{Q_{yt}+(\phi_x+V)Q_{yy}}{Q_y^2}\right) . \qquad (5.90)$$

In order for (5.90) to represent a conservation law the rhs must vanish for arbitrary ϕ, and this can only happen if

$$\frac{Q_{yy}}{Q_y^2} = \text{constant} \equiv \lambda_1 \quad \text{and} \quad \frac{Q_{yt}}{Q_y^2} = \text{constant} \equiv \lambda_2 . \qquad (5.91a,b)$$

Now,

$$Q_{yy} = \lambda_1 Q_y^2 \quad \Rightarrow \quad Q_y = \frac{-1}{\lambda_1 y + c_1(t)} \qquad (5.92a)$$

but

$$Q_{yt} = \lambda_2 Q_y^2 \quad \Rightarrow \quad Q_y = \frac{-1}{\lambda_2 t + c_2(y)} \ ; \qquad (5.92b)$$

both (5.92a) and (5.92b) will hold simultaneously if

$$Q_y = \frac{-1}{\lambda_1 y + \lambda_2 t + c_3} . \qquad (5.93)$$

Taking (5.93), the rhs of (5.90) will vanish provided that

$$\left(\lambda_1\phi_x + \lambda_1 V + \lambda_2\right) f(q) + \phi_x f'(q) = 0 \ ; \qquad (5.94)$$

unfortunately (5.94) is quite nonlinear, and will not readily yield a general solution. However if $\lambda_1 V + \lambda_2 = 0$ then the nonlinearity disappears, leaving

$$f'(q) + \lambda_1 f(q) = 0 \quad \Rightarrow \quad f(q) = c_4 e^{-\lambda_1 q} . \qquad (5.95)$$

The following theorem is thus apparent:

THEOREM II: A zonally-invariant basic-state flow $(\underline{V},Q)$ with a constant meridional velocity V allows a conservation relation for the perturbation pseudomomentum $f(q)/Q_y$ given by

$$\frac{\partial}{\partial t}\left(\frac{f(q)}{Q_y}\right) + \nabla\cdot\left((\underline{V}+\underline{v})\frac{f(q)}{Q_y}\right) = 0 , \qquad (5.96)$$

if Q_y is of the form $Q_y = \frac{-1}{\lambda(y-Vt)+c_1}$; then $f(q) = c_2 e^{-\lambda q}$.

To this point the property $q = \nabla^2\phi$ has not been used. Choosing the quadratic form $f(q) = q^2/2$, it follows that

$$\phi_x f'(q) = \phi_x(\phi_{xx} + \phi_{yy}) = \frac{\partial}{\partial x}(\tfrac{1}{2}\phi_x^2) + \frac{\partial}{\partial y}(\phi_x\phi_y) - \frac{\partial}{\partial x}(\tfrac{1}{2}\phi_y^2) . \quad (5.97)$$

In this special case, then, (5.90) may be re-written as

$$\frac{\partial}{\partial t}\left(\frac{q^2}{2Q_y}\right) + \nabla\cdot\left(\tfrac{1}{2}(v^2-u^2)\underline{i} - (uv)\underline{j} + \frac{q^2}{2Q_y}(\underline{V}+\underline{v})\right) = -\frac{q^2}{2Q_y^2}\left((V+v)Q_{yy} + Q_{yt}\right) . \quad (5.98)$$

Obviously the rhs of (5.98) will only vanish exactly if $Q_{yy} = Q_{yt} = 0$, namely for a constant shear flow. In that case Q_y is a constant, and (5.98) represents a conservation law for the perturbation enstrophy. This result could have been anticipated from (5.17) of §5b.

A geophysically relevant situation involves the case when the mean state is slowly varying in y, so that Q_{yy} and Q_{yt} are small. Taking $Q_y \approx \beta_0$, $Q_{yy} \approx -U_{yyy}$, and $Q_{yt} \approx -U_{yyt}$, one can make the estimates

$$\frac{vQ_{yy}}{Q_y} = O\left(\frac{U'U_0}{\beta_0 L_0^3}\right) \approx \frac{U_0}{L_0}\frac{\gamma}{\beta} , \quad \frac{Q_{yt}}{Q_y} = O\left(\frac{U_0}{\beta_0 L_0^2\tau}\right) \approx \frac{\alpha\gamma}{\beta}\frac{1}{\tau} , \quad (5.99a,b)$$

$$\text{and} \quad \frac{VQ_{yy}}{Q_y} = O\left(\frac{V_0U_0}{\beta_0 L_0^3}\right) \approx \frac{V_0}{L_0}\frac{\alpha\gamma}{\beta} , \quad (5.99c)$$

where the non-dimensional parameters α, β, and γ are defined by (5.20) of §5c (though here the primes have been introduced to denote perturbation quantities), and τ is the evolution timescale of the basic-state zonal velocity. This leads to the following:

THEOREM III: A zonally-invariant basic-state flow $(\underline{V},Q)$ on a flat beta-plane, with a zonal velocity U whose vorticity varies slowly in y, allows the approximate conservation relation for the perturbation pseudomomentum $q^2/(2Q_y)$ given by

$$\frac{\partial}{\partial t}\left(\frac{q^2}{2Q_y}\right) + \nabla\cdot\left(\frac{1}{2}(v^2-u^2)\underline{i} - (uv)\underline{j} + \frac{q^2}{2Q_y}(\underline{V}+\underline{v})\right)$$

$$= \left(\frac{q^2}{2Q_y}\right) O\left(\frac{\gamma}{\beta}\left[\frac{U_0}{L_0} + \frac{V_0\alpha}{L_0} + \frac{\alpha}{\tau}\right]\right) , \qquad (5.100)$$

where $\gamma \equiv L'^2/L_0^2$, $\beta \equiv \beta_0 L'^2/U'$, $\alpha \equiv U_0/U'$, the U's and L's representing velocity and length scales for the vorticity of the basic-state zonal (subscript $_0$) and perturbation (superscript ') flows; V_0 is the basic-state meridional velocity scale; and τ is the evolution timescale of U. The slow variation assumption implies $\gamma \ll 1$. In the limiting case $\gamma = 0$, (5.100) reduces to conservation of perturbation enstrophy.

It will be clear that the slowly-varying situation can also be treated by considering the perturbation enstrophy equation alone; in that case the rhs of (5.18) may be estimated by

$$-q\,(\underline{v}\cdot\nabla)\nabla^2\psi = \frac{q^2}{2} O\left(\frac{2U'L'(U_0+V_0)}{U'L_0^2}\right) \approx \frac{q^2}{2}\frac{2(U_0+V_0)\gamma}{L'} , \qquad (5.101)$$

with no need for an assumption of zonal invariance, and (5.18) then suggests:

•

THEOREM IV: A basic-state flow $(\underline{V},Q)$ whose relative vorticity varies slowly in x and y allows the approximate conservation relation for the perturbation enstrophy given by

$$\frac{\partial}{\partial t}\left(\frac{q^2}{2}\right) + \nabla\cdot\left(\frac{1}{2}\beta_0(v^2-u^2)\underline{i} - \beta_0(uv)\underline{j} + \frac{q^2}{2}(\underline{V}+\underline{v})\right) = \frac{q^2}{2} O\left(\frac{U_0\gamma}{L'}\right) ,$$

where $\gamma \equiv L'^2/L_0^2 \ll 1$ by hypothesis. (5.102)

Theorem IV is still a pseudomomentum relation insofar as it relies on the fact that $Q_x = 0$ to leading order.

To this point of §5f attention has been focussed on finding nonlinear disturbance conservation laws of the form $\partial A/\partial t + \nabla\cdot\underline{B} = 0$,

with A and $\underline{B}$ expressed entirely in terms of "Eulerian" variables (i.e. not in terms of particle displacements). It would appear that such laws are almost non-existent in the geophysical fluid dynamics literature. There is, however, an important class of nonlinear pseudomomentum conservation relations for zonal flows with the non-advective part of the flux, $\underline{B}^*$, being a purely Eulerian quantity; these are known as "Eliassen-Palm" (E-P) relations, following the initial (albeit linear) work of Eliassen & Palm (1961). Under what are generally known as "non-acceleration" conditions - namely inviscid, unforced dynamics; constant perturbation amplitudes; and a steady mean flow (see Edmon et al., 1980, §2c) - so that the time derivatives vanish, an E-P relation states that $\nabla\cdot\underline{F} = 0$ where $\underline{F}$ is some zonally-averaged perturbation quantity known as the E-P flux.

For quasi-geostrophic disturbances on the beta-plane, where

$$\underline{F} = \{F_{(y)}, F_{(z)}\} \equiv \left\{-\overline{uv}, \frac{\overline{fv\theta}}{\bar{\theta}_z}\right\} , \tag{5.103}$$

with the overbar denoting a zonal average and θ representing the potential temperature, it is easily shown that

$$\nabla \cdot \underline{F} \equiv \frac{\partial}{\partial y} F_{(y)} + \frac{\partial}{\partial z} F_{(z)} = \overline{vq} \tag{5.104}$$

for $q = \nabla^2\phi + f\left(\frac{\theta'}{\bar{\theta}_z}\right)_z$. Edmon et al. (1980) give a short proof to demonstrate that under nonacceleration conditions,

$$\nabla \cdot \underline{F} = \overline{vq} = 0 \tag{5.105}$$

for finite-amplitude disturbances, which is a nonlinear extension of Eliassen & Palm's (1961) result. Andrews (1983b) has recently shown that (5.105), with $\underline{F}$ and q appropriately defined, holds to finite amplitude for the primitive equations as well. Both results are really

special cases of the pseudomomentum relation (5.46) with $\mu = x$, with the crucial advantage that $\underline{F}$ is a purely Eulerian quantity. One practical difficulty is that the nonlinear nonacceleration hypotheses represent conditions on Lagrangian quantities, so that it may often be difficult to verify whether they are truly satisfied. Nevertheless the E-P flux has proven to be an illuminating diagnostic of wave activity in atmospheric applications (e.g. Edmon et al., 1980; Palmer, 1981).

In any finite-amplitude wave, mean-flow interaction problem there are really two coupled sub-problems to be considered: the effect of the mean flow on the development of the waves, and the effect of the waves on the evolution of the mean flow. A complete solution to the problem must address both sub-problems. The conservation laws and E-P relations discussed in this section fall under the first category. But wave quantities such as the E-P flux and the pseudomomentum also enter the second sub-problem, where they describe mean-flow acceleration and rectification effects due to wave activity. For a detailed discussion of this connection, see the recent review article by Grimshaw (1984).

"Nonacceleration" theorems, describing conditions under which wave activity causes no net mean-flow driving, are sometimes called "Charney-Drazin" (C-D) theorems, following the pioneering (linear) work of Charney & Drazin (1961). The GLM expression for nonlinear C-D theorems was presented by Andrews & McIntyre (1978a, §5.3), and a thorough discussion of nonacceleration and its breakdown has been given by Dunkerton (1980). For a zonal basic-state flow, the mean zonal momentum equation may be written under conservative (i.e. inviscid, unforced) conditions as (Andrews & McIntyre, loc.cit.)

$$\bar{D}^L(\bar{u}^L - p_1 - 2\Omega\bar{y}) \equiv \left(\frac{\partial}{\partial t} + \underline{\bar{u}}^L\cdot\nabla\right)(\bar{u}^L - p_1 - 2\Omega\bar{y}) = 0 , \qquad (5.106)$$

with $\underline{u}$ the full velocity field and p_1 the x-component of pseudomomentum. (5.106) clearly shows how wave activity, expressed by p_1, can lead to mean flow acceleration; however if p_1 obeys a conservation relation, then (5.106) describes a nonacceleration theorem.

A classical nonacceleration theorem of a slightly different sort, itself fully nonlinear, is Kelvin's circulation theorem (see e.g. Bretherton, 1971, §6.8; Pedlosky, 1979, §2.3). It can be obtained concisely in the GLM theory, and is intimately linked to the C-D theorems. The following derivation was suggested by Andrews & McIntyre (1978a) and Dunkerton (1980), but was not presented there explicitly; consequently it seems worthwhile to elucidate the steps here.

The circulation of absolute velocity around a closed quasi-zonal material contour $\Gamma = \{\underline{x}+\underline{\xi}\}$ is given by

$$C \equiv \oint_\Gamma \underline{u}_{abs}\cdot d\underline{s} \equiv \oint_\Gamma \left[\underline{u}(\underline{x}+\underline{\xi},t) + \underline{\Omega}\times(\underline{x}+\underline{\xi})\right]\cdot d(\underline{x}+\underline{\xi})$$

$$= \bar{u}^L \oint_\Gamma dx + \oint_\Gamma \left(\underline{u}^\ell + \underline{\Omega}\times\underline{\xi}\right)\cdot\left(\frac{\partial\underline{\xi}}{\partial x}\,dx + \frac{\partial\underline{\xi}}{\partial y}\,dy\right) + \oint_\Gamma \left(\underline{\Omega}\times\underline{x}\right)\cdot d\underline{x} \quad ,$$

noting that linear disturbance terms vanish under the integration. Using the definition of p_i, (5.47a), in the case where the Eulerian mean $\langle\ \rangle$ is a zonal average, corresponding to this quasi-zonal contour, one can write

$$C = \left(\bar{u}^L - p_1\right)\oint_\Gamma dx - p_2\oint_\Gamma dy - 2\Omega\oint_\Gamma y\,dx + 2\Omega\oint_\Gamma d(xy)$$

$$\Rightarrow \quad C = \left(\bar{u}^L - p_1 - 2\Omega\bar{y}\right)\oint_\Gamma dx \quad , \qquad (5.107)$$

since $\oint_\Gamma dy = 0$. According to the GLM formulation, Γ moves, by definition, with velocity $\underline{\bar{u}}^L$. Therefore under conservative conditions, where (5.106) applies,

$$\frac{dC}{dt} = \left(\frac{\partial}{\partial t} + \underline{\bar{u}}^L\cdot\nabla\right) C = 0 \quad , \qquad (5.108)$$

since $\oint_\Gamma dx$ is constant; this is Kelvin's circulation theorem.

§5g. Linearized Conservation Laws

When the perturbation can be assumed to be of small amplitude so that the governing equation (5.4) may be linearized, conservation laws are much easier to obtain.

(i) Conservation of Pseudoenergy

Following the approach of §5f(i), consider an unforced stationary basic-state flow with $Q = Q(\Psi)$ and $\Lambda(\Psi) \equiv \partial Q/\partial\Psi$. The linearized version of the perturbation energy equation (5.56) is

$$\frac{\partial}{\partial t}\left(\frac{1}{2}|\nabla\phi|^2\right) - \nabla\cdot\left(\phi\nabla\phi_t + \underline{v}\phi Q + \underline{V}\phi q\right) = -q\,J(\Psi,\phi)\,, \qquad (5.109a)$$

while the linearized version of (5.59) is

$$\frac{\partial}{\partial t}\left(\frac{f(q)}{\Lambda}\right) + \nabla\cdot\left(\underline{V}\frac{f(q)}{\Lambda}\right) = f'(q)\,J(\Psi,\phi)\,. \qquad (5.109b)$$

It is evident that upon combining (5.109a,b), the rhs will vanish for arbitrary ϕ if and only if $f'(q) = q$, or $f(q) = q^2/2$, which is the perturbation enstrophy. One then has

$$\frac{\partial}{\partial t}\left(\frac{1}{2}|\nabla\phi|^2 + \frac{q^2}{2\Lambda}\right) + \nabla\cdot\left(\frac{1}{2\Lambda}(q-\Lambda\phi)^2\underline{V} - \phi\nabla\phi_t\right) = 0\,, \qquad (5.110)$$

using the identity $-\nabla\cdot(\underline{v}\phi Q) = -\phi J(\phi,Q) = \Lambda J(\Psi,\phi^2/2) = \nabla\cdot(\underline{V}\Lambda\phi^2/2)$. (5.110) was obtained by Andrews (1983a), and an equivalent relation has also been found by Plumb (1984a). Integrating (5.110) over a volume containing the disturbance yields

$$\frac{d}{dt}\iint\left(\frac{1}{2}|\nabla\phi|^2 + \frac{q^2}{2\Lambda}\right)dxdy = 0 = \frac{d}{dt}\iint\left(\frac{1}{2}|\nabla\phi|^2 - \frac{Uq^2}{2Q_y}\right)dxdy\,, \qquad (5.111)$$

using (5.55) to re-write Λ. These or similar expressions have been used to obtain stability criteria in various fluid dynamical contexts: Fjørtoft, 1950; Arnol'd, 1965; Blumen, 1968; Tung, 1981; Pierrehumbert,

1983; Ripa, 1983. Arnol'd claimed his result to be a nonlinear one, but it was pointed out by Blumen that the restriction to small variations in Arnol'd's derivation was effectively a small-amplitude assumption (though the disturbance need not be strictly infinitessimal: Pierrehumbert, private communication).

(5.111) is always appropriate for zonal basic-state flows, since they automatically satisfy $J(\Psi,Q) = 0$ and are thus unforced; a derivation of (5.111) for such flows not relying on $\Lambda(\Psi)$ is given in Pedlosky (1979, §7.3). Often the rhs of (5.111) is written in terms of the meridional particle displacement η: for stationary zonal flows $U(y)$, η satisfies the linearized version of (5.41b),

$$\left(\frac{\partial}{\partial t} + U \frac{\partial}{\partial x}\right) \eta = v \quad , \tag{5.112}$$

whence the linearized potential vorticity equation may be written

$$\left(\frac{\partial}{\partial t} + U \frac{\partial}{\partial x}\right) q = - vQ_y = - \left(\frac{\partial}{\partial t} + U \frac{\partial}{\partial x}\right) (\eta Q_y) \quad , \tag{5.113}$$

with the particular solution

$$q = - \eta Q_y \quad . \tag{5.114}$$

One may then replace q^2 by $\eta^2 Q_y{}^2$ in (5.111).

(ii) Conservation of Pseudomomentum

Now consider a zonally-invariant basic-state flow, as in §5f(ii), with $U(y,t)$ and $V(t)$. The linearized version of (5.90) is

$$\frac{\partial}{\partial t}\left(\frac{f(q)}{Q_y}\right) + \nabla \cdot \left(\underline{V} \frac{f(q)}{Q_y}\right) = - f'(q)v - f(q)\left(\frac{Q_{yt}+VQ_{yy}}{Q_y{}^2}\right) \quad , \tag{5.115}$$

which does not look any more promising than (5.90). As before, make the choice of the quadratic form $f(q) = q^2/2$. Then $f'(q)v$ may be incorporated into the flux divergence, viz.

$$\frac{\partial}{\partial t}\left(\frac{q^2}{2Q_y}\right) + \nabla \cdot \left(\frac{1}{2}(v^2-u^2)\underline{i} - (uv)\underline{j} + \frac{q^2}{2Q_y}\underline{V}\right) = \frac{-q^2}{2Q_y{}^2}(VQ_{yy}+Q_{yt}) \quad . \tag{5.116}$$

The rhs of (5.116) will vanish if either $V = 0 = \partial U/\partial t$, describing a stationary zonal flow, or $\partial^2 U/\partial y^2 = 0$, corresponding to a constant meridional shear in the zonal flow component. A purely meridional flow would fall under the latter category.

Because of its geophysical relevance, the case of a stationary zonal basic-state flow has attracted a good deal of attention; then a zonal average of (5.116) gives

$$\frac{\partial}{\partial t}\left(\frac{\overline{q^2}}{2Q_y}\right) = \frac{\partial}{\partial y}\left(\overline{uv}\right) , \tag{5.117}$$

while an integration over the whole domain yields

$$\frac{d}{dt}\iint \frac{q^2}{2Q_y}\,dxdy = 0 = \frac{d}{dt}\iint \frac{1}{2}\eta^2 Q_y\,dxdy , \tag{5.118}$$

using the meridional particle displacement parameter η. "E-P relations" corresponding to (5.116) or, more commonly, to (5.117), have been obtained in various contexts by Taylor (1915), Eliassen & Palm (1961), Andrews & McIntyre (1976), Ripa (1983), and Plumb (1984a,b). Under nonacceleration conditions the rhs of (5.117), which is the barotropic E-P flux, vanishes. The so-called "Rayleigh-Kuo" stability criterion, that Q_y must change sign if a disturbance is to grow globally, is an obvious consequence of (5.118), and is explained in detail by Pedlosky (1979, §7.3).

(iii) Slowly-Modulated Waves

For small-amplitude perturbations the GLM formulation of §5e becomes quite tractable: the particle displacement field $\underline{\xi}$ satisfies the leading-order linearized approximation to (5.41b),

$$\bar{D}\,\underline{\xi} \equiv \left(\frac{\partial}{\partial t} + \underline{V}\cdot\nabla\right)\underline{\xi} \approx \left(\frac{\partial}{\partial t} + \underline{\bar{u}}^{L}\cdot\nabla\right)\underline{\xi} = \underline{u}^{\ell} \approx \underline{v} + (\underline{\xi}\cdot\nabla)\underline{V} \tag{5.119}$$

(Andrews & McIntyre, 1978b), with $\langle\underline{\xi}\rangle = 0$ as before. If the mean flow

is varying slowly relative to the perturbation then the last term of (5.119) must be neglected; also the WKB approximation

$$\underline{v} = \hat{\underline{v}}(X,Y,T)\ \exp\{\tfrac{i}{\varepsilon}\theta(X,Y,T)\} \quad , \quad \underline{\xi} = \hat{\underline{\xi}}(X,Y,T)\ \exp\{\tfrac{i}{\varepsilon}\theta(X,Y,T)\} \ , \tag{5.120}$$

can be made, where $[X,Y,T] = \varepsilon[x,y,t]$ and $\varepsilon \ll 1$ by hypothesis. To leading order in ε, then,

$$\frac{1}{\omega}\frac{\partial \underline{\xi}}{\partial t} = -\frac{1}{k}\frac{\partial \underline{\xi}}{\partial x} = -\frac{1}{\ell}\frac{\partial \underline{\xi}}{\partial y} = \frac{\partial \underline{\xi}}{\partial \alpha} \ , \tag{5.121}$$

where

$$\theta_X \equiv k \ , \quad \theta_Y \equiv \ell \ , \quad \theta_T \equiv -\omega \ , \quad \theta_\alpha \equiv -\varepsilon \ , \tag{5.122}$$

and the phase shift parameter α has been explicitly introduced. It follows from (5.119) that

$$\underline{v} \approx \left(\frac{\partial}{\partial t} + \underline{V}\cdot\nabla\right)\underline{\xi} \approx \left(\omega - \underline{V}\cdot\underline{k}\right)\frac{\partial \underline{\xi}}{\partial \alpha} \equiv \hat{\omega}\frac{\partial \underline{\xi}}{\partial \alpha} \ , \tag{5.123}$$

which defines the "intrinsic frequency" $\hat{\omega}$ (namely the frequency observed in a frame of reference moving with the mean flow). The parameters k, ℓ, ω and $\hat{\omega}$ vary on the "slow" scales (X,Y,T): the waves are slowly modulated. Consistent with this scenario, it is necessary to assume that the medium is stable and non-dissipative so that the wavenumber and frequency parameters are real. (5.123) may then be used to simplify the expressions for wave action, pseudoenergy, and pseudomomentum.

In the slowly-varying approximation, time, space, and phase-shift averages <u>all</u> represent ensemble averages which can be used to define the local value of the perturbation or wave energy E; this is the crux of the whole procedure, which can make the definition of "slowly varying" both subtle and stringent (Bretherton & Garrett, 1968).

To approximate (5.51a) to leading order in ε, (5.123) implies that

$$\hat{A} \approx \left\langle \frac{1}{\hat{\omega}}\left(\underline{v}\cdot\underline{v}\right) + \frac{1}{\hat{\omega}}\,\underline{v}\cdot(\underline{\Omega}\times\underline{\xi}) \right\rangle \ . \tag{5.124}$$

Calculation of the second quantity in (5.124) requires what Andrews & McIntyre (1978b) refer to as the "virial theorem", but which in the barotropic linearized case is not so complicated as it appears there. The perturbation momentum equation

$$\bar{D}\,\underline{v} + 2\,\underline{\Omega}\times\underline{v} + \nabla p' = 0 , \tag{5.125}$$

when multiplied by $\underline{\xi}$, yields

$$0 = \underline{\xi}\cdot\bar{D}\underline{v} + 2\,\underline{\xi}\cdot(\underline{\Omega}\times\underline{v}) + (\underline{\xi}\cdot\nabla)p' = \underline{\xi}\cdot\bar{D}^2\underline{\xi} - 2\,\underline{v}\cdot(\underline{\Omega}\times\underline{\xi}) + \nabla\cdot(p'\underline{\xi})$$

$$= \frac{1}{2}\bar{D}^2(\underline{\xi}\cdot\underline{\xi}) - (\underline{v}\cdot\underline{v}) - 2\,\underline{v}\cdot(\underline{\Omega}\times\underline{\xi}) + \nabla\cdot(p'\underline{\xi}) . \tag{5.126}$$

Taking an ensemble average of (5.126), the first and last terms become derivatives of mean quantities and must be neglected under the slowly-varying hypothesis. Consequently

$$\langle\, \underline{v}\cdot(\underline{\Omega}\times\underline{\xi}) \,\rangle = -\frac{1}{2}\langle\, \underline{v}\cdot\underline{v} \,\rangle \equiv -E . \tag{5.127}$$

Then (5.127) applied to (5.124) yields

$$\hat{A} \approx \frac{E}{\hat{\omega}} , \tag{5.128a}$$

which is Bretherton & Garrett's (1968) definition of wave action; similarly, from (5.47a,b),

$$p_1 \approx \frac{Ek}{\hat{\omega}} \approx k\hat{A} ; \quad p_2 \approx \frac{E\ell}{\hat{\omega}} \approx \ell\hat{A} ; \quad e \approx \frac{E\omega}{\hat{\omega}} \approx \omega\hat{A} \approx E + \underline{V}\cdot\underline{p} . \tag{5.128b,c,d}$$

Note that for Rossby waves, where

$$\hat{\omega} = -\beta_0 k/(k^2+\ell^2) , \tag{5.129}$$

p_1 is proportional to the wave enstrophy:

$$p_1 \approx \frac{-1}{\beta_0}(k^2+\ell^2)E . \tag{5.130}$$

When the basic-state flow is stationary the pseudoenergy e obeys a conservation relation, the linearized version of (5.46). To see the connection with (5.110), note that an unforced, slowly-varying flow on the beta-plane must be zonal to leading order, as $Q_y \approx \beta_0 y$:

$$J(\Psi,\beta_0 y) \approx 0 \quad \Rightarrow \quad V = \Psi_x \approx 0 . \tag{5.131}$$

In that case (5.128d) and (5.130) yield

$$e = E - \frac{U}{\beta_0}(k^2+\ell^2)E , \tag{5.132}$$

which is the slowly-varying version of $\frac{1}{2}\left|\nabla\phi\right|^2 + \frac{q^2}{2\Lambda}$. This WKB form of the pseudoenergy conservation law has been discussed by Zeng (1982). It is a tedious but trivial task to verify that for the dispersion relation (5.129), the flux in (5.110) approximates to

$$\frac{1}{2\Lambda}(q-\Lambda\phi)^2 U\underline{i} - \phi\nabla\phi_t = \underline{c}_g e \equiv \left(\frac{\partial\omega}{\partial k} e, \frac{\partial\omega}{\partial\ell} e\right) , \tag{5.133}$$

where $\underline{c}_g$ is the local group velocity which is well-defined for this WKB situation; then (5.110) becomes

$$\frac{\partial e}{\partial t} + \nabla\cdot\left(\underline{c}_g e\right) = 0 . \tag{5.134}$$

For a zonally-invariant basic-state flow the conserved quantity is p_1, which by (5.130) is proportional to the wave enstrophy; it is also the slowly-varying approximation to $-q^2/(2Q_y)$. This establishes the connection with (5.116), noting that a slowly-varying mean flow represents, to leading order, the second class of flows for which (5.116) is a conservation law. Also the flux of (5.116) approximates to

$$\frac{1}{2}(v^2-u^2)\underline{i} - (uv)\underline{j} + \frac{q^2}{2\beta_0}\underline{V} = \underline{c}_g \frac{q^2}{2\beta_0} = -\underline{c}_g p_1 , \tag{5.135}$$

so that the equation becomes

$$\frac{\partial p_1}{\partial t} + \nabla\cdot\left(\underline{c}_g p_1\right) = 0 . \tag{5.136}$$

This is a linearized application of Theorem IV. Young & Rhines's (1980) discussion of wave enstrophy conservation in a meridional flow is clearly an example of pseudomomentum conservation, as is Zeng's (1982) wave enstrophy relation for a zonal flow.

Although conservation of wave action is in some sense the most fundamental of the conservation relations, in practice it often fails to obtain because the required conditions concerning slow modulation are violated. On the beta-plane this is particularly the case: slow variation of the basic state in both time and space requires a zonal flow, since large-scale Rossby waves propagate faster than small-scale ones. This restriction seems also to be connected with the fact that the wave energy E is not defined unambiguously unless the mean flow is unforced (Bretherton & Garrett, 1968) and thus, on the beta-plane, zonal; indeed, Young & Rhines (1980) show clearly how nonconservation of wave action is linked to forcing of the mean state and flow across mean geostrophic contours.

When the basic-state flow is in fact zonal and not simply zonally-invariant, then conservation of both p_1 and $\hat{A}$ implies by (5.128b) conservation of the zonal wavenumber k. If the mean flow is furthermore stationary, then conservation of both e and $\hat{A}$ implies, by (5.128d), conservation of the absolute frequency ω. These results are in agreement with ray-tracing theory (e.g. Lighthill, 1978, §4.6).

For a medium that is strongly inhomogeneous in one direction, one must integrate over that spatial component and consider conservation laws within the orthogonal subspace (Hayes, 1970). McWilliams (1976), for example, has derived a vertically integrated wave action conservation relation for a two-layer ocean.

CHAPTER VI - LINEAR WAVE, MEAN-FLOW INTERACTION THEORY FOR A ZONAL JET

§6a. Introduction

As was explained in §5a, the problem of strongly inhomogeneous turbulence considered in this thesis lies outside the domain of any existing analytical framework. Until a comprehensive theory can be established, the best that one can do is to examine partial theories which explain processes governed by some of the terms in the equation. The aim is then to determine which aspects of these partial theories survive in the full problem, in what fashion and to what extent they are modified, and what their regimes of validity are. Since the theories themselves cannot reliably predict when they will succeed or fail under broader circumstances, the test must therefore come from experiment, and this experimental verification in the form of direct numerical simulation is the subject of the two subsequent chapters.

The only analytical approach capable of treating strongly nonlinear (i.e. irreversible) flows seems to be that of homogeneous turbulence theory, described in Chapter II. Fully nonlinear wave, mean-flow interaction theory was discussed in Chapter V, and some new results presented, but on the whole the theory falls far short of what one would call a "solution" to the problem. In the present chapter the opposite regime to that of Chapter II is considered, namely the linear interaction between waves and a zonal mean flow.

By "linear" is meant here, for simplicity, a fixed mean flow. There are certainly ways of treating the "quasi-linear" (or "quasi-nonlinear", depending on one's point of reference) problem where the mean flow is allowed to vary, while wave-wave interactions are suppressed (e.g. Pedlosky, 1970). However such approaches are rather

complicated and technical, and are really only appropriate for weakly nonlinear systems. The supposition made here is that while linear theory may in certain cases describe behaviour occurring on a fast timescale, the slower nonlinear evolution will involve a significant range of the spectrum and will be turbulent. Consequently there seems little point in considering quasi-linear interaction theory.

Similarly the linearized problem itself will not be treated in great detail, but rather with an eye to identifying more qualitative "signatures" of linear dynamics which can then be used to interpret the experiments. There are at present many hotly-debated questions concerning linearized systems, for example the behaviour around critical layers (e.g. Hartman, 1975; Tung, 1983); however such sensitive issues, though they may be essential in understanding certain phenomena, are presumably easily upset by turbulent processes. The aim is not to understand completely the linearized problem which is, indeed, often subtle and full of pitfalls (see the warnings by Bretherton & Garrett, 1968); instead it is to understand and identify linear processes which may be operative in the fully nonlinear system.

In §6b some general arguments are presented which use constraints on the perturbation dynamics to anticipate possible behaviour in terms of spectral dispersion. To actually determine the direction of evolution one must close the problem, which is done here through ray-tracing theory: the general theory is reviewed in §6c, and then applied in §6d to the problem at hand. However ray tracing breaks down at large scale, where effects of the periodic domain can be felt. Consequently §6e examines normal-mode theory, and includes a new calculation of Rossby waves modified by weak shear.

§6b. General Arguments

The following arguments rely heavily on the triad representation of nonlinear interactions proposed by Lorenz (1960), which has already been utilized in the discussion of Chapters II and III. The essential point is that in the energy and enstrophy budgets, the nonlinear triple correlation terms due to advection can be represented as a sum of interactions within triads of wavevectors ($\underline{k},\underline{p},\underline{q}$) where $\underline{k} + \underline{p} + \underline{q} = 0$. It is also possible to consider tetrads consisting of four wavevectors, and so on, but these higher-order combinations are generally important only when the triads are not: an example being the resonant interaction of surface gravity waves, for which there are no non-trivial triads (Phillips, 1977, §3.8).

If one then characterizes the wave, mean-flow interaction problem through a consideration of the possible triads that may be formed between a large-scale zonal jet and a wave (k,ℓ), it is immediately apparent that the interaction must only involve other waves with the same zonal wavenumber k. In the particular case where the mean flow is characterized by a single wavenumber $(0,\ell_0)$, for example, triads formed between it and (k,ℓ) can involve only $(k,\ell+\ell_0)$ and $(k,\ell-\ell_0)$; this simple geometrical constraint is shown in Fig. 6.1. But even when the mean flow consists of a spectrum of meridional modes, the same restriction applies; the localness of the wave-wave part of the triad would then depend on how quickly the spectrum of Ψ fell off with increasing ℓ.

This argument can obviously be generalized to include certain special classes of non-zonal basic-state flows, in particular those consisting of collinear wave vectors, although the book-keeping then becomes more tricky. However such extensions do not work in spherical

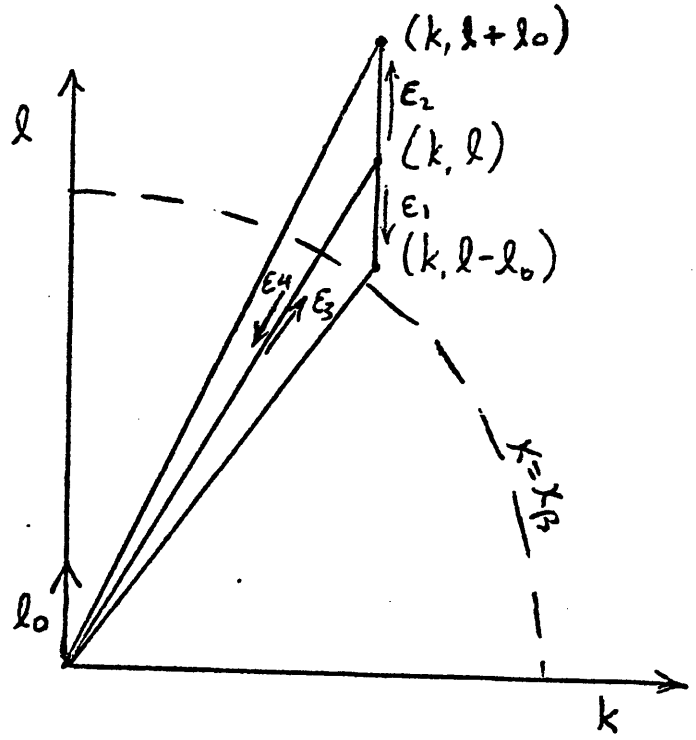


Fig. 6.1: Schematic of induced spectral transfer by zonal jet. Comments in text.

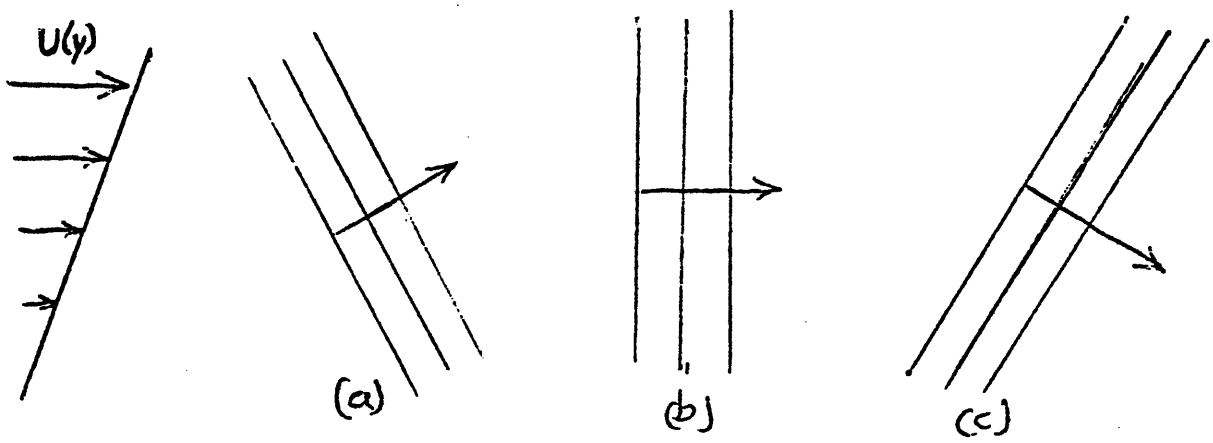


Fig. 6.2: Wave crest tilting in Couette flow, at progressive times (a), (b) and (c); arrows show wave vectors.

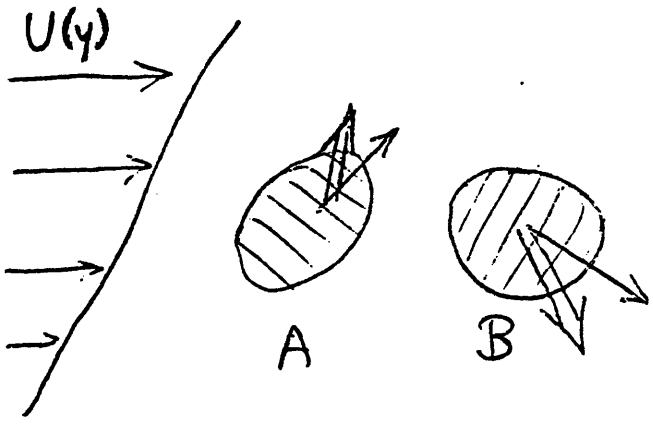


Fig. 6.3: Propagation of two wave packets A and B in a shear flow. Lines show wave crests, single arrows wave vectors, and double arrows the group velocity.

geometry, and the zonal homogeneity is diagnostically advantageous. Consequently only zonal flows are considered here; in any case the atmosphere's stationary flow component is predominantly zonal (Fig. 4.4a).

It has been shown in Chapter V that given an invariance property of the mean flow, an associated perturbation quantity can always be defined which is conserved in the absence of direct forcing or dissipation. For a zonal mean flow, such a quantity is termed the pseudomomentum p_1. In general it seems to be impossible to find an Eulerian expression of the appropriate conservation law, although some exceptions were presented in §5f. But if one does not insist that the perturbation quantity be conserved in wave-wave interactions - in other words, if one considers only the linearized problem - then, as was demonstrated in §5g, a conservation law can always be found in terms of Eulerian quantities.

Consequently it is useful to visualize the interaction between a zonal mean flow and a field of eddies as consisting of the spectral transfer of some conservative eddy quantity, such as p_1 or the pseudoenergy e, along lines of constant zonal wavenumber k. In this transfer process the mean flow plays an essential catalytic role, in that it forms the third member of the triad, but it is passive in terms of p_1- or e-"energetics". This concept is a familiar one to the oceanic internal wave community, where the notion of "induced diffusion" of wave action through highly nonlocal resonant triads is well-established (Phillips, 1977, §5.5). However in the present case there is no restriction to resonant interactions, which broadens the scope of the problem considerably; and the formalism is exact rather than approximate, at least in principle, because the mean flow is fixed.

Knowledge of flow constraints does not provide a solution to the evolution problem, unfortunately; there is a parallel here with 2-D turbulence, where the constraints provided by conservation of energy and enstrophy need to be combined with some statistical hypothesis in order to provide a closure. But whereas the hypothesis of isotropic spectral broadening utilized in Chapter II is appropriate for the ergodic dynamics of turbulence, the relatively deterministic nature of the linear problem would seem to demand some other approach. This concern is addressed in the subsequent sections.

Connected with the closure issue is another matter, namely that the linear conservation constraints may not be expressible in a form which makes their spectral implications very evident. In fact this is generally the case for both pseudoenergy and pseudomomentum: the integrands of (5.111) and (5.118) contain inhomogeneous factors $\Lambda(y)$ and $Q_y(y)$ which preclude a simple spectral interpretation of either e or p_1. Of course one could presumably choose a different spectral representation than the Fourier one, which might be more illuminating in this regard; however one would then be faced with the problem of interpreting nonlinear (i.e. wave-wave) interactions in this space. This is a reflection of the fact that e and p_1, as defined from (5.111) and (5.118), are generally not conserved in a nonlinear sense.

Nevertheless there are two cases where the linearized conservation laws have clear spectral interpretations, and not accidentally these correspond to the two cases of §5f where the conservation laws are fully nonlinear. The first concerns when the basic-state flow is not only zonal but consists of a single Fourier component ℓ_0: then $e = E-(\Omega/\ell_0^2)$ is conserved (see (5.68)). The other case obtains when there is a

separation in scale between the basic-state flow and the eddies, for which $p_1 = -\Omega/\beta_0$ is approximately conserved (see (5.102) and (5.130)). When both circumstances occur, the two laws are in agreement.

The basic-state flow to be considered in the numerical simulations of the two succeeding chapters is a cosine jet, consisting of a single Fourier component ℓ_0. This choice is made for convenience, on the presumption that it does not give pathological results. On the basis of the present discussion such a presumption might seem rather optimistic, in view of the fact that the pseudoenergy conservation law can only be applied in that special case. However the critical conservation law is not so much the one governing e (which is convenient, but inessential), but rather the one governing p_1 for a scale separation; and in fact it is only under the latter assumption that the spectral transfer problem can be closed, as shall be seen in the sections to follow.

Given such a single-wave zonal basic-state flow, then, consider this scenario of induced spectral transfer along lines of constant k: an initial disturbance is located in wave vector (k,ℓ), and interacts with the basic-state flow $(0,\ell_0)$ to form triads as in Fig. 6.1, coupling with waves $(k,\ell+\ell_0)$ and $(k,\ell-\ell_0)$. Assume positive k, ℓ, and ℓ_0 for definiteness. Now consider the implications of the two following assumptions. The first case presumes symmetric transfer of e, that is to say equal amounts moving from (k,ℓ) to both $(k,\ell+\ell_0)$ and $(k,\ell-\ell_0)$. Referring to Fig. 6.1 for definitions, this implies that

$$\varepsilon_2\left(1 - \frac{k^2+(\ell+\ell_0)^2}{\ell_0^2}\right) = e(k,\ell+\ell_0) = e(k,\ell-\ell_0) = \varepsilon_1\left(1 - \frac{k^2+(\ell-\ell_0)^2}{\ell_0^2}\right)$$

$$\Leftrightarrow \qquad \frac{\varepsilon_1}{\varepsilon_2} = \frac{k^2+\ell^2+2\ell\ell_0}{k^2+\ell^2-2\ell\ell_0} > 1 \quad ; \tag{6.1}$$

consequently more energy moves up-scale than down-scale. Of course the

perturbation energy and enstrophy are not themselves conserved: conservation of total energy and enstrophy within each triad leads, after some algebra, to

$$\frac{\varepsilon_4}{\varepsilon_3} = \frac{(k^2+\ell^2-2\ell\ell_0)(2\ell\ell_0+\ell_0^2)}{(k^2+\ell^2+2\ell\ell_0)(2\ell\ell_0-\ell_0^2)} = \frac{2\ell\ell_0(k^2+\ell^2-\ell_0^2) - \ell_0^2(3\ell^2-k^2)}{2\ell\ell_0(k^2+\ell^2-\ell_0^2) + \ell_0^2(3\ell^2-k^2)} \; ; \quad (6.2)$$

hence $\varepsilon_4 < \varepsilon_3$ indicating net perturbation gain for $\ell^2 > k^2/3$, while $\varepsilon_4 > \varepsilon_3$ for $\ell^2 < k^2/3$. However with a scale separation the net energy exchange is slight, indeed it vanishes to leading order in (ℓ_0/ℓ).

The other case recognizes that it is in fact quite possible to configure the interaction in such a way that not only e, but also E and Ω separately, are conserved for the perturbation. Under this assumption $\varepsilon_3 = \varepsilon_4$; then conservation of total energy and enstrophy within each triad, together with a little algebra, leads to

$$\frac{\varepsilon_1}{\varepsilon_2} = \frac{2\ell\ell_0+\ell_0^2}{2\ell\ell_0-\ell_0^2} > 1 \; ; \quad (6.3)$$

as in (6.1), once again the net perturbation energy transfer is up-scale. However the net perturbation enstrophy transfer is generally down-scale:

$$\frac{\Omega(k,\ell+\ell_0)}{\Omega(k,\ell-\ell_0)} = \frac{[k^2+(\ell+\ell_0)^2]\varepsilon_2}{[k^2+(\ell-\ell_0)^2]\varepsilon_1} = \frac{2\ell\ell_0(k^2+\ell^2) + \ell_0^2(3\ell^2-k^2-\ell_0^2)}{2\ell\ell_0(k^2+\ell^2) - \ell_0^2(3\ell^2-k^2-\ell_0^2)} \; , \quad (6.4)$$

which exceeds unity unless $\ell^2 < (k^2+\ell_0^2)/3$.

An important point to be made is that under either of the above assumptions, the consequent spectral dispersion looks remarkably like that of 2-D turbulence: energy transfer primarily up-scale, enstrophy transfer primarily down-scale. The difference is that the dispersion occurs along lines of constant zonal wavenumber k, not isotropically. This rather fortuitous circumstance will be a constantly-recurring theme of this study.

The second crucial point is that this mechanism of induced transfer provides a path in spectral space whereby perturbation energy (or strictly, the pseudoenergy) may be transferred up-scale past the cascade cut-off scale κ_β of beta-plane turbulence (see §3c), into the largest scales of motion: as suggested in Fig. 6.1, this allows for the possibility of large-scale meridional anisotropy (namely $k > \ell$, or $\langle v^2 \rangle > \langle u^2 \rangle$), in striking contrast to the zonal anisotropy of beta-plane turbulence. Whether these possible developments in fact obtain depends on the closure employed, which is the subject of the next sections.

§6c. Ray-Tracing Theory

The constraints on the linear perturbation dynamics discussed in §6b, while suggestive, nonetheless fall short of providing a solution to the linear problem. What is required is some form of closure: in the best of circumstances this might consist of a complete exact solution, which would make the constraints redundant; more generally, however, the solution will only be approximate, and the closure incomplete. Since it is not necessary to understand the linearized problem in its entirety, this last situation would not be considered unacceptable in the context of the present study.

Nevertheless, the initial-value problem concerned with the evolution of a disturbance in the presence of a zonal shear flow does have an exact analytical solution in the special case of constant-shear, or Couette, flow. Although the solution can be traced back as far as Orr (1907), the number of recent treatments (e.g. Phillips, 1966, §5.5; Hartman, 1975; Yamagata, 1976; Farrell, 1982; Boyd, 1983; Tung, 1983) suggests that the significance of Orr's work is still not fully appre-

ciated. Solutions to the problem being so plentiful, there is no point in providing yet another; however the essential physical mechanism is so ubiquitous that it bears repeating.

In the special linearized case of Couette flow $U(y) \propto y$ on an f-plane, the barotropic perturbation vorticity equation (5.4) reduces, for a suitably chosen timescale, to

$$\left(\frac{\partial}{\partial t} + y \frac{\partial}{\partial x}\right) \nabla^2 \phi = 0 \quad ; \tag{6.5}$$

as suggested in §5c, this allows a straightforward application of the method of characteristics. Avoiding the question of boundary conditions (treatment of which can be found in Orr's and Farrell's papers), each "wavecrest" of a single Fourier mode governed by (6.5) is simply tilted in a clockwise direction about $y = 0$; Fig. 6.2 depicts this process. Since Fourier modes provide a complete representation of any initial condition, the problem is thus solved. The key point to be noted from Fig. 6.2 is that the zonal wavenumber k is fixed, while the meridional wavenumber ℓ is continuously varying. If the wavecrests initially lean into the mean shear (Fig. 6.2a) then $|\ell|$ decreases, passes through zero, and then increases without limit; however if the wavecrests are initially vertical (Fig. 6.2b) or lean along the mean shear (Fig. 6.2c), then $|\ell|$ simply increases according to $|\ell| = |\ell_0| + |k_0|t$ (e.g., Boyd, 1983). In both cases the end state is $|\ell| \to \infty$, or a zonal orientation of the crests. An energetic argument based on a consideration of the Reynolds stresses would indicate that the disturbance energy is then completely absorbed by the mean flow.

It is to be noted that the process just described conforms to the

spectral constraints discussed in §6b; also, at any given time the disturbance can be characterized by a single meridional wavenumber ℓ. Boyd (1983) has recently argued that the inclusion of β makes no difference to the result, which seems self-evident for an infinite domain since a propagating wave would encounter the same shear everywhere; Boyd's argument that boundary effects are negligible is, on the other hand, somewhat less than convincing.

In any event the case of interest is not Couette flow but rather a mean flow with variable shear, in particular a jet. The problem is that then the convected coordinates manipulation cannot get rid of the inhomogeneity in the equation, and a clean analytical solution cannot be obtained. One might also expect that Boyd's result concerning the irrelevance of β would itself become irrelevant, since now a propagating wave would encounter different mean shears; the effects of this could well be non-trivial.

Fortunately there is a way of treating such inhomogeneous problems, provided that the inhomogeneity is sufficiently weak. Strictly, the required condition is that the mean state (basic-state flow as well as other factors such as the potential vorticity gradient) vary sufficiently slowly over a wavelength of the disturbance that a local frame of reference can be defined at each point, in which the waves are effectively propagating through fluid at rest (see, e.g., Lighthill, 1978, §4.6). This condition is crucial, as it enables an unambiguous measure of wave energy to be defined (Bretherton & Garrett, 1968); locally this wave energy must obey a conservation relation. Additionally the medium must be stable and inviscid, so that the local frequency and wavenumber associated with a wave are real numbers. For

Rossby waves this can be ensured by a sufficiently large value of β_0, or by sufficiently weak mean-flow variation. The case of an unstable medium is by comparison far more complicated, and is fraught with technical difficulties (e.g. Merkine, 1977; Craik, 1981).

The condition of slow mean-flow variation means that solutions may be sought in the form of "wave packets": namely, localized disturbance envelopes modulating a dominant wavenumber $\underline{k}$. The scale of the envelope must be intermediate between the scale of the mean-flow variation and the wavelength corresponding to $\underline{k}$. In a frame of reference moving with the local value of the mean flow, the wave packet has a central frequency given by the Rossby-wave dispersion relation

$$\hat{\omega}(k,\ell,x,y) = -\frac{\beta_0 k}{k^2+\ell^2} \quad , \tag{6.6}$$

called the "intrinsic frequency"; and it propagates with the well-defined intrinsic group velocity

$$\underline{\hat{c}}_g = \left(\frac{\partial\hat{\omega}}{\partial k} , \frac{\partial\hat{\omega}}{\partial\ell}\right) = \left(\frac{\beta_0(k^2-\ell^2)}{(k^2+\ell^2)^2} , \frac{2\beta_0 k\ell}{(k^2+\ell^2)^2}\right) . \tag{6.7}$$

Because of the slowly-varying assumption, the "absolute" frequency and group velocity, defined relative to an observer at rest, are obtained from a Doppler shift as in a constant zonal flow:

$$\omega = \hat{\omega} + Uk \quad ; \qquad \underline{c}_g = \underline{\hat{c}}_g + U\underline{i} \quad . \tag{6.8a,b}$$

However everything is in principle a slowly-varying function of the spatial (and possibly temporal) coordinates.

Viewed from the perspective of the mean flow, the wave packet appears as a point $\underline{x}(t)$ with a given wavenumber $\underline{k}(t)$. The point moves with the group velocity according to the "ray-tracing" equations

$$\frac{dx}{dt} = \frac{\partial\omega}{\partial k} = U + \frac{\partial\hat{\omega}}{\partial k} \quad ; \qquad \frac{dy}{dt} = \frac{\partial\omega}{\partial\ell} = \frac{\partial\hat{\omega}}{\partial\ell} \quad ; \tag{6.9a,b}$$

while the wavenumber itself evolves according to the generalized Snell's law

$$\frac{dk}{dt} = -\frac{\partial\omega}{\partial x} = 0 \quad ; \qquad \frac{d\ell}{dt} = -\frac{\partial\omega}{\partial y} = -k\frac{dU}{dy} \qquad (6.10a,b)$$

(Lighthill, loc. cit.). The parallel between (6.9,6.10) and Hamilton's equations is not purely coincidental; in fact it points to a macroscopic version of the "correspondence principle", with $\underline{x}$ representing the generalized coordinates and $\underline{k}$ the generalized momenta of the dynamical system. Similarly the frequency ω corresponds to the energy. And just as invariance properties lead to energy and momenta conservation laws in Hamilton's equations, here the zonal homogeneity implies conservation of k, while the time invariance of the mean flow incorporated implicitly in (6.10) implies conservation of ω (along the ray path):

$$\frac{d\omega}{dt} = \frac{\partial\omega}{\partial k_i}\frac{dk_i}{dt} + \frac{\partial\omega}{\partial x_i}\frac{dx_i}{dt} \equiv 0 \; . \qquad (6.11)$$

In (6.11), as in (6.10), d/dt refers to the Lagrangian derivative $d/dt \equiv \partial/\partial t + \underline{c}_g\cdot\nabla$ evaluated along the rays (6.9).

For this two-dimensional fluid, (6.9a,b), (6.10a,b), and (6.11) represent a system of five equations; however they are not independent, as shown by (6.11) itself. The "wave-particle duality" of ray-tracing theory has an obvious parallel with its more famous cousin in quantum mechanics: on the scale of the mean flow the particle interpretation is more intuitively satisfying, while the wave interpretation seems more appropriate on the scale of the disturbance; however both representations are equally correct.

There are two sources of error in the theory. The first comes from the slowly-varying approximation, and is proportional to the scale separation factor

$$\delta = \frac{\text{length scale of perturbation}}{\text{length scale of mean flow}} \; ; \qquad (6.12)$$

indeed the ray-tracing equations correspond to the "geometrical optics" approximation to the vorticity equation under a WKB expansion in the small parameter δ (e.g. Zeng, 1982). It is worth noting that, just as a single Rossby wave in a constant mean flow is an exact solution of the full nonlinear equation (the Jacobian term $J(\phi,\nabla^2\phi)$ vanishing), so a single wave packet in a slowly-varying mean flow is a leading-order solution to the full equation: i.e.,

$$J(\phi,\nabla^2\phi) = O\left(\delta\left|\underline{k}\right|^2\phi\nabla^2\phi\right) . \tag{6.13}$$

Consequently the errors due to nonlinearities for a <u>single</u> wave packet are of the same order as those due to the slowly-varying approximation. This may help account for the apparent success of ray-tracing theory in describing many features of stationary wave propagation in the atmosphere (Hoskins & Karoly, 1981; Held, 1983).

If more than one wave packet is present, then the situation is not so straightforward. However this second source of error is manageable again provided that the waves are weak: that is to say if the non-dimensional parameter β of (5.20) is large. Physically the explanation for this is that the packets disperse before they suffer appreciable interaction. In fact the leading-order interaction is due solely to resonant triads for which both the frequencies and wavenumbers match, and these are naturally rather rare. Hasselmann (1967) has developed a very powerful application of Feynman diagram techniques to analyze such resonant triad interactions, and the method has been utilized with regard to the oceanic internal wave field (e.g. Müller, 1978), although Holloway (1980) suggests the weak-wave assumption to be incorrect there. For Rossby waves the weak-wave assumption is quite problematical, since the smaller one makes δ, the smaller β becomes. Certainly in the model

problem of this thesis the application of ray-tracing theory cannot be justified a priori, but must be tested by numerical simulation.

The ray-tracing equations (6.9) and (6.10) do not themselves describe the change in disturbance energy along the ray, a change which is inevitable over the scale of the mean-flow variation since the packet is moving in an accelerating frame of reference (see Lighthill, loc. cit.). A general though somewhat nuanced derivation of the linearized wave action conservation law has been given by Bretherton & Garrett (1968); the restrictions required to achieve the result are considerable, however, most notably the necessity of a zonal mean flow for Rossby-wave disturbances. A much quicker derivation is usually obtainable by a WKB analysis of the specific case, in which the energy and action equations come out at the level of "physical optics". This latter procedure was employed by Young & Rhines (1980) and by Zeng (1982), and was sketched in §5g.

Since the flow studied in this chapter is indeed zonal, one may proceed directly from conservation of wave action

$$\frac{d}{dt}\left(\frac{E}{\hat{\omega}}\right) + (\nabla\cdot\underline{c}_g)\left(\frac{E}{\hat{\omega}}\right) = \frac{\partial}{\partial t}\left(\frac{E}{\hat{\omega}}\right) + \nabla\cdot\left(\underline{c}_g\,\frac{E}{\hat{\omega}}\right) = 0 \qquad (6.14)$$

(Bretherton & Garrett, 1968), where E is the wave energy density measured in the frame of reference moving with the local value of the mean flow, and d/dt is evaluated moving with the packet along the ray. Note that (6.14) describes conservation of the integrated wave action density, integrated, that is, over the extent of the packet whose size will in general vary. The wave action density $\hat{A} \equiv E/\hat{\omega}$ itself decreases as the rays diverge, and vice-versa. But since $\hat{\omega}$ can vary from point to point within the medium, neither the wave energy density E nor the integrated energy is generally conserved, and this is the main point to

be made.

If one views the wave packet from the perspective of the mean flow, as a single point, then the integration over the disturbance is already accomplished; this is the approach employed in this study. For practical applications one is often more interested in the energy density or "intensity", but the evaluation of $\nabla \cdot \underline{c}_g$ is usually non-trivial (e.g. Buckley, 1982).

The connection between the approximate theory of ray tracing and the exact solution for Couette flow is made clear by a consideration of the wave packet dynamics. Choosing a positive shear and $k > 0$ for definiteness, imagine two wave packets as shown in Fig. 6.3: packet A has $k/\ell > 0$, or crests leaning into the mean shear; while packet B has $k/\ell < 0$, or crests leaning along the shear. Consider first packet A. By (6.7) and (6.9b), it has a northward or positive meridional group velocity; as it propagates, however, its crests are tilted by the mean shear as in Fig. 6.2, and this is reflected in the decreasing value of ℓ predicted by (6.10b). As in the constant-shear case, k is fixed (see (6.10a)). The orientation of the crests is such that the associated Reynolds stresses extract energy from the mean flow, and this is again consistent with the ray-tracing picture: (6.6) implies that if the total wavenumber decreases, then $\hat{\omega}$ increases; thus conservation of wave action implies an increase in wave energy, an increase which will be especially pronounced for small k.

Similar reasoning applied to packet B, which has $\ell < 0$, demonstrates that it propagates southward, ℓ becomes more negative, hence $\hat{\omega}$ and the wave energy decrease. The general result is that packets propagating into increasingly westerly flow increase both their wave energy and

their meridional wavelength, while packets propagating into increasingly easterly flow decrease both quantities.

§6d. Ray Tracing in a Cosine Jet

In this section the ray-tracing theory described in §6c above is applied to the specific case of a cosine mean-flow jet structure. The jet is given by

$$U(y) = -U_0 \cos y \quad [0 \leq y < 2\pi] \tag{6.15}$$

in a doubly-periodic domain, which conforms to the situation examined in the spin-down simulations of Chapter VII. A ray is defined by its initial location (x_0,y_0) and wavenumber (k_0,ℓ_0); k_0 is assumed positive for definiteness, while x_0 is irrelevant because of the zonal homogeneity in the problem. A ray-tracing calculation begins with these initial values and iterates forward in time according to (6.9) and (6.10), which defines the ray path followed by the wave packet (treated as a point).

Now, as the ray propagates two things can happen of a rather singular nature. One is that ℓ may pass through zero and change sign, so that the ray reflects (by (6.9b)) off this so-called "turning line". Without a mean flow the ray would form a cusp, but with it the path is smooth (Lighthill, 1978, §4.6). Turning lines occur when

$$\omega = Uk - \frac{\beta_0}{k} \iff U(y_T) = \frac{\omega}{k} + \frac{\beta_0}{k^2} = U(y_0) + \frac{\beta_0 \ell_0^2}{k^2(k^2+\ell_0^2)} \tag{6.16}$$

in terms of the initial parameters defining the ray. Obviously $U(y_T)$ will not always be in the range of U, hence not every ray will have a turning line within the flow. At the turning line itself the WKB solution is invalid, since the scale separation parameter δ diverges; however the ray can still be continued (Lighthill, loc. cit.).

Certainly the physical process is simple enough, as it corresponds to Fig. 6.2b in the Couette flow problem.

The other thing that can happen is that the ray can approach a "critical line" defined by $\omega = kU$ or $\hat{\omega} = 0$; in that case (6.6) implies that ℓ^2 goes rapidly to infinity, and the ray-tracing arguments must break down since they rely on slow variations in ℓ. Near the critical line, (6.9) suggests that the ray flattens out and parallels the x-axis, and never quite reaches it. What actually happens is still an open question: there are viscous continuation vs. nonlinear continuation schemes, and absorption vs. reflection arguments (see e.g. Tung, 1983). But since ℓ^2 grows fairly large even before the WKB methodology is invalid, in any model (such as the one in this study) with high-wavenumber enstrophy diffusion one would expect the wave packet to be diffused near the critical line. The location is at

$$U(y_c) = \frac{\omega}{k} = U(y_0) - \frac{\beta_0}{k^2+\ell_0^2} \tag{6.17}$$

in terms of the initial parameters. Again, critical lines will not exist for every wave packet.

Unless stated otherwise, this section assumes the choice $U_0 = 2\sqrt{2}$ and $\beta_0 = 25$ appropriate to the spin-down runs. It is evident from (6.16) that turning lines will exist unless $(k^2+\ell_0^2)$ is too small, or y_0 is too close to the centre of the westerly jet, $y = \pi$. Similarly, from (6.17) critical lines will exist unless $(k^2+\ell_0^2)$ is too small or y_0 is too close to the centre of the easterly jet, $y = 0$. This is connected to the fact that, provided they exist, turning lines always lie between the initial point and the centre of the westerly jet, critical lines between the initial point and the centre of the easterly jet.

It was shown in §6c that wave packets moving into the region of increasingly westerly flow, with decreasing ℓ^2, will experience an increase in wave energy E (referring now to the integrated quantity). According to ray-tracing theory, however, any growth in E can only be temporary, as the ray will either reflect off a turning line or else pass through the westerly jet centre; in both cases ℓ^2 will begin to increase again and the energy will be given back to the mean flow. If a critical line is approached, then the wave energy is lost irretrievably (assuming absorption): however, it can be shown that most of the energy is fed into the mean flow before the wave packet gets close to the critical line, so that dissipation only represents a small part of the loss (Tung, 1983) - though it may prevent a reflection and subsequent growth. Even without a critical line, a ray moving into easterly flow may slow down (by (6.9)) so much as to effectively stagnate relative to U.

For a given mean flow U(y) and fixed β_0, there are four possible environments for a wave packet defined by its initial parameters (x_0, y_0, k_0, ℓ_0): no CL or TL (I); CL on the "easterly" side of y_0 (II); TL on the "westerly" side of y_0 (III); both CL and TL (IV). By the symmetry of the jet, TL's and CL's must always come in pairs. These possible scenarios are sketched in Fig. 6.4, along with representative ray paths calculated by a simple numerical integration.

To determine what fraction of parameter space is occupied by the four regimes, consider the case of $k^2 + \ell_0^2 = 100$, which is appropriate to the spin-down runs. Then (6.17) implies that

$$U(y_c) = U(y_0) - 0.25 \iff y_c = \arccos\left[(U_0 \cos y_0 + 0.25)/U_0\right] \qquad (6.18)$$

which is defined provided that

$$\cos y_0 \leq 1 - \frac{.25}{2\sqrt{2}} \Rightarrow y_0 \geq .42 \approx .13\pi \text{ and } y_0 \leq 2\pi - .13\pi . \qquad (6.19)$$

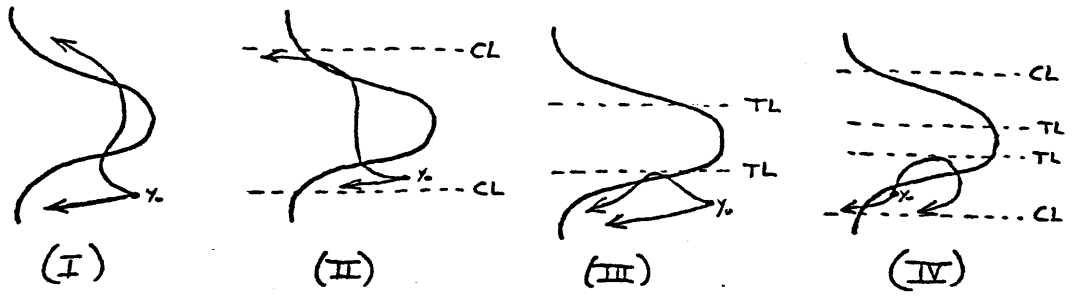


Fig. 6.4: The four ray-tracing regimes described in the text, together with representative ray paths. The thick line shows the mean flow speed for reference.

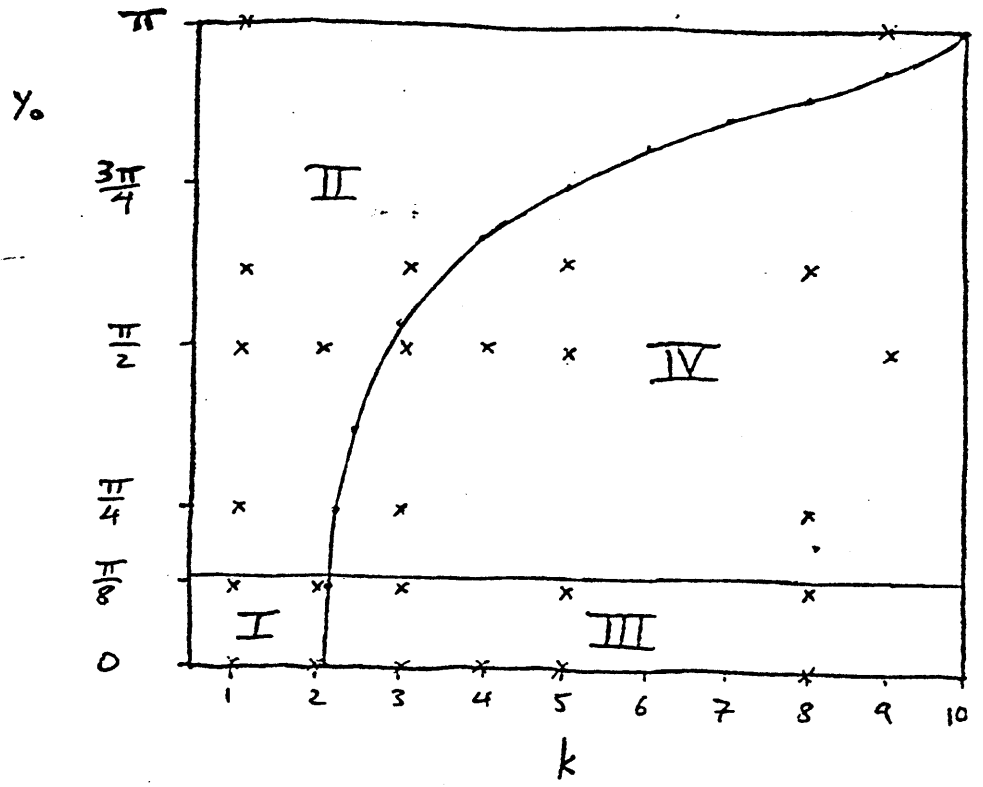


Fig. 6.5: Extent of ray-tracing regimes in terms of k and y_0, for $k^2 + \ell_0^2 = 100$. The range $\pi \leq y \leq 2\pi$ is completely symmetric. Crosses mark points for which ray-tracing integrations have been carried out.

Hence 87% of wavepackets, given homogeneous initial conditions, have CL's, and would be absorbed by the mean flow in a spin-down situation (assuming high wavenumber enstrophy diffusion). Note that y_c is always quite close to y_0 for these parameters. With regard to turning lines, the verdict depends on both y_0 and k: (6.16) implies that

$$\begin{aligned} U(y_T) &= U(y_0) + \frac{25(100-k^2)}{100k^2} = U(y_0) + \frac{25}{k^2} - 0.25 \\ \Leftrightarrow \quad y_T &= \arccos\left[(U_0\cos y_0 + 0.25 - 25/k^2)/U_0\right] , \end{aligned} \tag{6.20}$$

which is defined provided that

$$\cos y_0 \geq \frac{25}{2\sqrt{2}k^2} - \frac{.25}{2\sqrt{2}} - 1 \approx \frac{8.84}{k^2} - 1.0884 . \tag{6.21}$$

Note that $0 \leq k^2 \leq 10$ so $25/k^2 \geq 0.25$. Therefore unless $k \approx 10$, y_T may be some distance from y_0. Now, (6.21) is impossible to fulfil unless

$$k^2 \geq 4.23 \quad \Leftrightarrow \quad k \geq 2.06 . \tag{6.22}$$

At the lower limit of this range, turning lines exist for y_0 very close to 0; as k increases, the range of y_0 broadens, but it only includes $y_0 = \pi$ if $k = 10$: for given k, turning lines exist provided that

$$\left|y_0 - \pi\right| \geq \arccos\left(1.0884 - \frac{8.84}{k^2}\right) . \tag{6.23}$$

When $k = 10$ then $\ell_0 = 0$ and $y_T = y_0$ for all wavepackets; ℓ^2 can only increase since it is initially zero. A sketch of the various regimes in (k,y_0)-space is provided in Fig. 6.5; arc cos varies quickly with its argument when cosine varies slowly, namely for the argument of (6.23) near $\pm$ 1, which corresponds to k near 2.06 or 10. But the argument of (6.23) itself is more sensitive to changes in k when k is near the smaller value.

Fig. 6.5 indicates that for $k \geq 2.06$, there will be a "waveguide"

around $y = 0$ in which initial disturbances will be trapped by turning lines, but where there will be no critical lines to dissipate the wave energy; the trapping region becomes increasingly narrow for large k, reaching $y_T = y_0$ for $k = 10$.

For future reference, the effects of higher β_0 should be discussed at this point. Examining (6.16) and (6.17), it is evident that for given k and ℓ_0, an increase in β_0 has the effect of expanding the ranges of y_0 for which turning lines or critical lines do not exist. In the specific case $k^2 + \ell_0^2 = 100$, (6.16) and (6.17) imply that the horizontal line above regions I and III of Fig. 6.5 will move up, while the curved line on the right of regions I and II will move further right. Consequently a smaller percentage of wave packets are ultimately absorbed by the mean flow: assuming homogeneous initial conditions, increasing β_0 from 25 to 65, for example (of relevance to §8d), decreases this fraction from 87% to 78%.

This effect of stronger β_0 may be understood as an acceleration of the meridional group velocity (6.7) while leaving the refraction rate (6.10b) unchanged: hence $\Delta\ell/\Delta y$ decreases, and more packets pass through the westerly jet maximum before encountering $\ell = 0$ and a turning line. Additionally, the minimum (non-zero) ℓ achieved by such packets is increased when β_0 is increased. Fig. 6.6 shows this effect: imagining an ensemble of wave packets to be released uniformly in y, with $k = 2$ and $k^2 + \ell_0^2 = 100$, the minimum ℓ_{min} for $\beta_0 = 25$ is at $\ell = 0.5$ and most values are bunched around $\ell = 1$ and $\ell = 2$. When β_0 is increased to 65, however, the minimum ℓ_{min} increases to $\ell = 2.5$ and most of the values are concentrated around $\ell = 3$.

With respect to the temporary growth in wave energy E, the

greatest potential growth is found for small k: indeed, conservation of wave action would suggest a maximum possible amplification factor of

$$A \equiv \frac{E(\ell=0)}{E(\ell=\ell_0)} = \frac{k^2+\ell_0^2}{k^2} = 1 + \frac{\ell_0^2}{k^2} , \qquad (6.24)$$

which is clearly a sensitive function of k when k is small. However (6.22) and Fig. 6.5 show that for $k < 2.06$, the potential of $\ell = 0$ is never realized as the ray passes through the maximum westerly flow before it reaches its turning line. Moreover the factor $d\ell/dt$, which determines the rate of energy growth, is, according to (6.10b), a linear function of k, and is particularly weak for small k. Since high-k modes have little potential growth and their rays reflect quickly, this suggests that energy growth should be optimized for some intermediate range of k.

Thinking for a moment in terms of the nonlinear problem, it is not unreasonable to suppose that when turbulent effects are present, there will be a tendency towards isotropy that may mitigate the large-scale meridional anisotropization involved in the purely linear dynamics. At sufficiently large scale, Rossby-wave dispersion will assert itself over nonlinear interaction; but now, rather than the slow spectral evolution via resonant interactions that characterizes beta-plane turbulence, the mean-flow straining and wave propagation will act as described here and in §6b.

This suggests that the more appropriate initial conditions for the ray-tracing calculations might not be so much the circle $k^2 + \ell^2 = 100$, but rather the isotropic line $k^2 = \ell^2$, presuming some turbulent mixing to have already taken place. Spectral symmetry would then be assured by the randomness of the turbulent mixing, rather than by some <u>ad hoc</u>

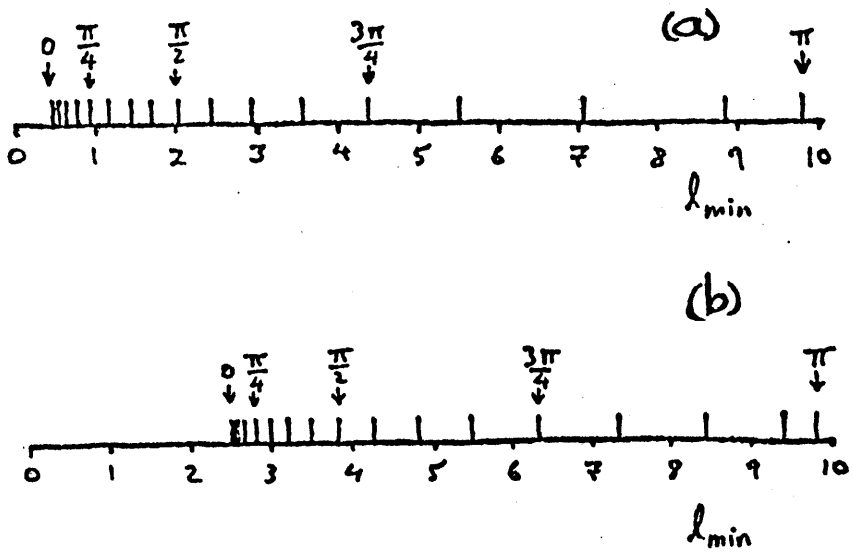


Fig. 6.6a,b: Minimum ℓ obtained by k=2 wavepacket with no turning line, as a function of y_o, for U(y) given by (6.15) and (a) β_o=25, (b) β_o=65.

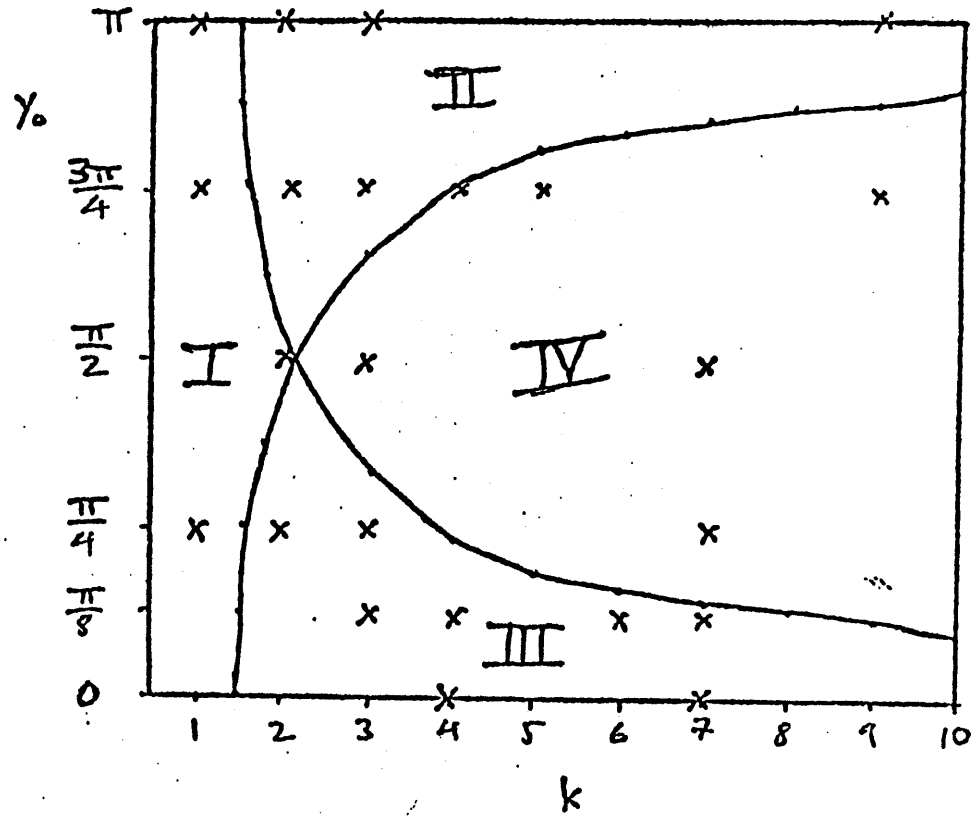


Fig. 6.7: Same as Fig. 6.5, but for $k^2 = \ell_o^2$.

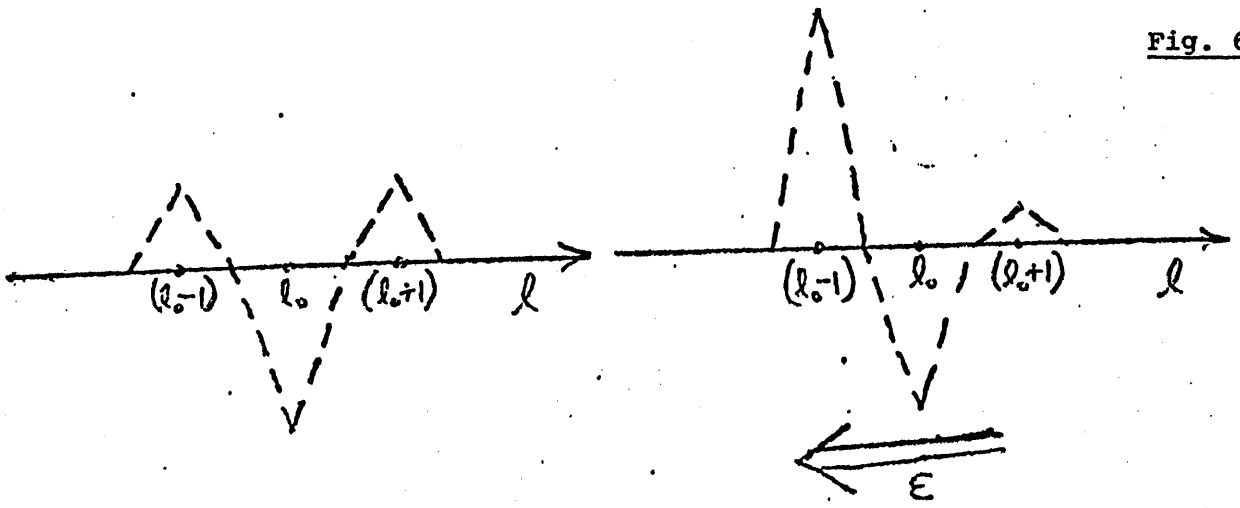


Fig. 6.8: Enstrophy (left) and energy (right) transfer terms for interaction with zonal jet, assuming spectral symmetry. Arrow indicates implied energy "cascade".

assumption. Consequently, it is interesting to re-do the calculations leading up to Fig. 6.5, but taking $k^2 = \ell_0^2$ rather than $k^2 + \ell_0^2 = 100$. From (6.17),

$$U(y_c) = U(y_0) - \frac{\beta_0}{2k^2} \quad <=> \quad y_c = \arccos\left[(U_0 \cos y_0 + 12.5/k^2)/U_0\right] \tag{6.25}$$

which is defined provided that

$$\cos y_0 \leq 1 - \frac{12.5}{2\sqrt{2}k^2} \approx 1 - \frac{4.42}{k^2} \; ; \tag{6.26}$$

but this is impossible to fulfil unless

$$k^2 \geq 2.21 \quad <=> \quad k \geq 1.49 \; . \tag{6.27}$$

Therefore critical lines exist provided that

$$\left|y - \pi\right| \leq \pi - \arccos\left(1.0 - \frac{4.42}{k^2}\right) \; , \tag{6.28}$$

which defines a curve rather similar in form to that defined by (6.23), but inverted. Here when $k = 1.49$, the range of y_0 allowing critical lines is simply $y_0 = \pi$; as k increases the range broadens, and by $k = 10$ only a strip 0.09π wide on either side of $y = 0$ is excluded. This is quite different from the situation of Fig. 6.5.

As for turning lines, (6.16) gives $U(y_T) = U(y_0) + \beta_0/2k^2$, which is defined provided that

$$\cos y_0 \geq \frac{12.5}{2\sqrt{2}k^2} - 1 \approx \frac{4.42}{k^2} - 1 \; ; \tag{6.29}$$

as with (6.26), this is impossible to fulfil unless (6.27) holds. Rather than (6.23), the condition for existence of turning lines is instead

$$\left|y_0 - \pi\right| \geq \arccos\left(1.0 - \frac{4.42}{k^2}\right) \; . \tag{6.30}$$

A sketch of the various regimes in (k,y_0)-space is provided in Fig. 6.7. Comparing this with Fig. 6.5, the principal difference is that in the present case a much larger fraction of parameter space represents wave

packets with no critical lines - this is especially true for the smaller values of k, for which this calculation is most appropriately applied.

It has been established that the wave energy of packets evolving to larger scale will increase. But what are the expected values of the zonal and meridional energies $\langle u^2\rangle/2$ and $\langle v^2\rangle/2$ according to ray-tracing theory? In terms of the conserved enstrophy Ω,

$$\frac{\langle u^2\rangle}{2} = \frac{\ell^2 E}{k^2+\ell^2} = \frac{\ell^2\Omega}{(k^2+\ell^2)^2} \to \frac{\ell^2\Omega}{k^4} \quad \text{as} \quad \ell \to 0 \; ; \tag{6.31a}$$

$$\frac{\langle v^2\rangle}{2} = \frac{k^2 E}{k^2+\ell^2} = \frac{k^2\Omega}{(k^2+\ell^2)^2} \to \frac{\Omega}{k^2} \quad \text{as} \quad \ell \to 0 \; ; \tag{6.31b}$$

$$\frac{\partial}{\partial \ell}\frac{\langle u^2\rangle}{2} = \Omega\left\{\frac{2\ell(k^2+\ell^2) - 4\ell^3}{(k^2+\ell^2)^3}\right\} = 0 \quad \langle = \rangle \quad \ell^2 = k^2 \; ; \tag{6.32a}$$

$$\frac{\partial}{\partial \ell}\frac{\langle v^2\rangle}{2} = -\frac{4k^2\ell\Omega}{(k^2+\ell^2)^3} < 0 \quad \text{for} \quad \ell > 0 \; . \tag{6.32b}$$

Therefore a wave packet with $\ell_0^2 > k_0^2$ will initially increase both $\langle u^2\rangle$ and $\langle v^2\rangle$ as it moves to smaller ℓ^2, though the latter much more quickly than the former, until $\ell^2 = k^2$; from then on, $\langle v^2\rangle$ will continue to increase but $\langle u^2\rangle$ will decrease. This suggests that $\langle v^2\rangle$ is a much more sensitive field than is $\langle u^2\rangle$ for diagnosing the activity of ray-tracing dynamics.

It would be wise at this point to recapitulate what has been learned from the discussion of this and the previous sections. One may recall that the original justification for examining ray-tracing theory was that it offered a way of closing the spectral transfer problem outlined in §6b. In fact the theory does offer a fairly detailed prescription, as follows. Given spectrally symmetric initial conditions, namely a packet with $k/\ell_0 < 0$ matching each with $k/\ell_0 > 0$, with equal amplitude and the same y_0, then each pair of packets will propagate initially in opposite meridional directions with equal speeds,

as in Fig. 6.3; in the spectral domain this will appear as a pair of enstrophy "pulses" of equal amplitude, moving one to larger and one to smaller ℓ^2 but at the same rate, along a line of constant k. As a consequence of the relation between enstrophy and energy, this latter picture will be represented in energetic terms as a pulse moving to larger ℓ^2 while losing energy, together with one moving to smaller ℓ^2 while gaining energy. Fig. 6.8 shows a slightly exaggerated form of this rather canonical situation.

The symmetry of the above picture holds as long as the packets feel only the (weak) shear in the mean flow, but not the (even weaker) variation of mean shear. It should be noted, however, that assuming this symmetric transfer of enstrophy, to leading order the gain of energy by the amplifying packet is exactly equal to the loss by the decaying packet, which also agrees with the more exact calculation leading to (6.1) in §6b. In that case a calculation of energy and enstrophy fluxes is justified, especially since the transfer is clearly local in wavenumber space: one would find a symmetric flux of enstrophy both up- and down-scale, but a net up-scale flux of energy.

If one now considers an ensemble of wave packets (k,ℓ_0) and $(k,-\ell_0)$ distributed homogeneously in space, rather than just a single pair, then this scenario is unchanged except that spectral dispersion about each composite "pulse" enters immediately. The reason is that different pulses evolve at different rates $d\ell/dt$, since they operate under the influence of different mean shear strengths. In the still more general case of a double ensemble, with homogeneous distributions of packets with different k and ℓ but a single value of κ, one can easily see that the same picture will again emerge - as long as one is

careful to look along "cuts" defined by lines of constant k.

Although Fig. 6.8 depicts the initial spectral evolution of all disturbances which have spectral symmetry, it cannot hold indefinitely. To the up-scale moving pulse one of two things must happen: either it will reach $\ell = 0$ and then turn back, corresponding to a wave packet reflection off a turning line; or it will reverse direction before it reaches $\ell = 0$, indicating that the packet has passed through the westerly jet maximum and that no turning lines exist. In both cases the pulse returns to $\ell = \ell_0$, and is then identical to the initial down-scale moving pulse (neglecting any frictional loss). As far as the latter is concerned, there are again two possibilities: either the pulse will head off to very high ℓ^2, corresponding to absorption near a critical line; or it will reverse its tendency and move back up-scale, indicating that the packet has passed through the easterly jet maximum and that no critical lines exist.

The essential point to be made, however, is that according to ray-tracing theory any energy gain by pulses moving up-scale must be temporary, and is indeed reversed. In a few cases the decay phase is also reversible, and the pulses undergo oscillations in ℓ with no net wave, mean-flow interaction. But in the great majority of cases critical lines exist, and the decay and absorption process is the end of the story.

Because of the periodicity in the problem packets without critical lines can traverse the domain many times, which suggests that the "inital-value problem" approach emphasized thus far is not so appropriate for these disturbances. There is also the concern about the ability of ray-tracing theory to describe behaviour at very large meridional

scale. Both issues lead to the alternative methodology of normal-mode theory, which is the subject of the next section. But before proceeding it is worthwhile to make one more calculation, this one concerning the question of timescales.

Recall that the energy and enstrophy cascades resulting from turbulent interactions are due to a random process of turbulent straining, and involve a sum over triads not all of which have a net up-scale energy transfer (Merilees & Warn, 1975). In striking contrast, the induced cascades of linear dynamics are systematic and result from continuous mean-flow straining; in each pair of triads as in Fig. 6.1 there is <u>always</u> a net up-scale energy flux (see (6.1)). A scale doubling time τ_1 due to the linear dynamics might be estimated by

$$\frac{1}{\kappa\tau_1} \approx \frac{d}{dt}\frac{1}{\kappa} = -\frac{1}{\kappa^2}\frac{\ell}{\kappa}\frac{d\ell}{dt} = \frac{k\ell}{\kappa^3}U'(y_0) \quad <=> \quad \tau_1 \approx \frac{k^2+\ell^2}{k\ell U'(y_0)}, \qquad (6.33)$$

using (6.10b) and the geometrical relation $d\kappa/d\ell = \ell/\kappa$, where $\kappa^2 \equiv k^2 + \ell^2$. Note that for fixed κ and y_0, τ_1 is minimized for $k = \ell = \kappa/\sqrt{2}$. This estimate may be compared with the nonlinear doubling time τ_2 obtained from turbulent similarity theory in §2f:

$$\tau_2 \approx C\,\tau_I = \frac{C}{u\kappa}, \qquad (6.34)$$

where u is the perturbation velocity scale, and C is a constant typically of order 20 or greater. For initial conditions $k^2 + \ell_0^2 = 100$, $U_0 = 2\sqrt{2}$, and $u \approx 1$, the minimum τ_1 (for packets located in the maximum shear) would be about 0.7; while τ_2 would be around 2.

These estimates are naturally very rough. However they do suggest that scale analysis of the terms in the full equation is an extremely problematical business, since the ratio of linear to nonlinear effects is apparently a rather sensitive function of both physical and spectral

location. This sensitivity to the angular dependence of the spectrum is reminiscent of Pedlosky (1962), though the approach employed there was rather different. Obviously the analysis of §5c must thus be seen as rather naive, as it is not the mean-flow strength but instead the shear which is dynamically significant; whether it could be substantially improved without in fact solving the problem is quite another matter.

§6e. Quantization and Normal-Mode Theory

The imposition of doubly-periodic boundary conditions requires disturbances to be quantized according to a discrete set of integral wavenumbers (for a domain size of $2\pi \times 2\pi$), given a spectral representation in terms of Fourier modes. While the (infinite) set of basis functions is in principle complete, in practice a truncation must be performed if one is to arrive at a solution.

It is immediately evident that for a discrete, finite set of wavenumbers, ray-tracing theory may be questioned on two accounts: first, a wave packet cannot be represented exactly as a Gaussian (for instance) distribution in the spectral and physical domains, but only as an approximation to it; and secondly, while ray-tracing presumes the packet centroid wavenumber to vary continuously as the ray propagates, in a periodic domain it must jump in integral steps. Both problems are presumably less of a concern for high wavenumbers, but at large scale they could well be significant. This is accentuated by the fact that, by (6.7), small-scale packets propagate with a relatively slow group velocity relative to U, and thus do not move far from their initial points (in the mean-flow frame of reference); while large-scale disturbances propagate relatively quickly, are more prone to cross the

domain several times, and are thus less appropriately treated by the ray-tracing approach.

One way of investigating the properties of the linearized version of (5.4) is to search for "normal-mode" solutions: that is, functions $\Phi(y)$ satisfying the Sturm-Liouville equation

$$\Phi''(y) + \left\{\frac{\beta_0 - U''(y)}{U(y)-c} - k^2\right\}\Phi(y) = 0 \qquad (6.35)$$

subject to periodicity over $[0,2\pi)$. (6.35) is obtained from (5.4) by substituting the normal-mode form $\phi(x,y,t) = \mathrm{Re}\{\Phi(y)\exp[ik(x-ct)]\}$, taking advantage of the homogeneity in x and t; k is taken to be positive and real, but $c = c_r + ic_i$ is in general complex. For a given k, (6.35) represents an eigenvalue problem for c. This was the approach followed by Kuo (1949) in his pioneering work on barotropic instability: each normal mode or eigenfunction is said to be unstable if and only if its associated eigenvalue c has $c_i > 0$.

Eigenvalue/eigenfunction solutions of (6.35) fall into one of four classes, any of which may be empty. The first consists of complex conjugate pairs of unstable and stable modes, with $c_i \neq 0$ and c_r in the range, for this geometry,

$$U_{min} - \frac{2\beta_0}{4k^2+1} < c_r < U_{max} \equiv U_0 \; ; \qquad (6.36)$$

this expression is a slight modification of a similar relation in Pedlosky (1979, §7.14). When unstable modes exist they tend to capture most of the attention, which is certainly understandable. Kuo (1949) focussed on the instability problem, and showed that a necessary (though not sufficient) criterion for instability of a zonal jet is that $\beta_0 - U''$ change sign; clearly then a sufficiently large value of β_0, or a sufficiently weak mean-flow variation, can always ensure stability. For an unstable cosine jet modes of this class are restricted to those with k

less than the mean-flow wavenumber, a result which is a simple consequence of Fjørtoft's (1953) "blocking theorem".

The second class of solutions includes neutral modes with c_r in the range of U, but with $\beta_0 = U''(y_c)$ where $U(y_c) = c$ to avoid a singularity in (6.35). These are discussed by Pedlosky (loc. cit.), and take the form of plane waves; for a mean jet $U(y) \propto \cos(\ell_0 y)$ only ℓ_0 such modes exist at specific values of k, and these k's rarely take integral values.

A third class consists of a continuous spectrum of singular neutral modes with c_r in the range of U, whose eigenfunctions have discontinuous derivatives at the critical lines y_c. An arbitrary initial condition will generally include a contribution from many such modes. While it is true that asymptotically this contribution seems to decay as $1/t^2$, which was Orr's (1907) result, nevertheless a temporary algebraic growth can occur and may be quite substantial (Farrell, 1982; Boyd, 1983; Tung, 1983). The ray-tracing theory of §§6c,d implicitly dealt with the continuous spectrum; the results obtained there concur with what is generally known on this subject, although it must be said that, apart from the specific calculations referred to above, this knowledge cannot be considered very great at the present time.

The fourth and final class is the one of most interest in the context of the present section, for it includes those neutral modes with c_r outside the range of U; in the limit of large β_0 these can be interpreted as Rossby waves modified by the large-scale shear. As the stability is decreased and thus $c_r \to U_{min}$ (since in fact $c_r < U_{min}$ for this class), the modes become less identifiable as Rossby waves and more like the unstable modes of the first class, but the transition is a

smooth one. This process has been recently investigated by Drazin, Beaumont & Coaker (1982), using a combination of asymptotic analysis and numerical computation.

Drazin et al.'s (1982) formalism is however rather technical, and they do not provide the details for the shear-induced Rossby-wave modification in the case of large stability; consequently it seems worthwhile to present a simple calculation of such modes that might bridge the gap with ray-tracing theory. Considering (6.35) for the class of cosine jets $U(y) = - U_0 \cos(\ell_0 y)$, a WKB approach is employed which takes $\varepsilon \equiv U_0 \ell_0^2/\beta_0$ as the small parameter (the inverse of the non-dimensional parameter μ of (5.24)); the goal is to obtain the leading-order amplitude and phase modifications to the $U \equiv 0$ Rossby wave solutions. The method cannot predict the shift in phase speed due to the mean flow, but an application of Drazin et al.'s (1982) eqn. (19) demonstrates that, for the cosine jet, the leading-order correction to c vanishes in any case.

First non-dimensionalize (6.35), taking $y = y'/\ell_0$, $k = k'\ell_0$, and $c = c'\beta_0/\ell_0^2$; the last choice is made with the expectation of obtaining the usual Rossby wave phase speed. Next transform the meridional coordinate from y' to $Y = \varepsilon y'$, and drop all primes. (6.35) may then be written as

$$\big(\varepsilon \cos(Y/\varepsilon) + c\big)\big(\varepsilon^2 \Phi''(Y) - k^2 \Phi(Y)\big) - \big(1 - \varepsilon \cos(Y/\varepsilon)\big)\Phi(Y) = 0 \ . \quad (6.37)$$

Choosing the WKB ansatz $\Phi(Y) = \exp\{\frac{1}{\varepsilon}[S_0(Y) + \varepsilon S_1(Y) + \varepsilon^2 S_2(Y) + \ldots]\}$, it follows that

$$\Phi''(Y) = \{\frac{1}{\varepsilon^2}[(S_0')^2 + 2\varepsilon S_0' S_1' + \varepsilon^2((S_1')^2 + 2S_0' S_2') + \ldots] + \frac{1}{\varepsilon}[S_0'' + \varepsilon S_1'' + \ldots]\}\, \Phi(Y) \ . \quad (6.38)$$

Now solve (6.37) at each order in ε.

$$\underline{O(1)}: \qquad c\left[(S_0')^2 - k^2\right] - 1 = 0 \quad \Rightarrow \quad S_0'(Y) = \left(\frac{1}{c} + k^2\right)^{1/2} \equiv i\ell$$

$$\Rightarrow \quad S_0(Y) = i\ell Y \tag{6.39}$$

(ignoring the constant). To satisfy periodicity in $2\pi\ell_0$ of Φ and Φ', $\exp\{S_0(Y)/\varepsilon\} = \exp\{i\ell y\}$ implies that $\ell\ell_0$ must be an integer. These are the pure Rossby modes $\ell\ell_0 = 0,1,2,\ldots$, for each of which $c = -(k^2+\ell^2)^{-1}$ by definition.

$$\underline{O(\varepsilon)}: \qquad c\left[2S_0'S_1' + S_0''\right] + \cos(Y/\varepsilon)\left[(S_0')^2 - k^2 + 1\right] = 0$$

$$\Rightarrow \quad 2i\ell S_1' = -(k^2+\ell^2)(k^2+\ell^2-1)\cos(Y/\varepsilon)$$

$$\Rightarrow \quad S_1(Y) = \frac{i\varepsilon}{2\ell}(k^2+\ell^2)(k^2+\ell^2-1)\sin(Y/\varepsilon)\ . \tag{6.40}$$

This accounts for the phase variation; the amplitude variation is obtained at the next order calculation.

$$\underline{O(\varepsilon^2)}: \qquad c\left[(S_1')^2 + 2S_0'S_2' + S_1''\right] + \cos(Y/\varepsilon)\left[2S_0'S_1' + S_0''\right] = 0$$

$$\Rightarrow \quad 2i\ell S_2' = (k^2+\ell^2)^2(k^2+\ell^2-1)\left(\frac{k^2+\ell^2-1}{4\ell^2} - 1\right)\cos^2(Y/\varepsilon)$$

$$+ \frac{i}{2\varepsilon\ell}(k^2+\ell^2)(k^2+\ell^2-1)\sin(Y/\varepsilon)$$

$$\Rightarrow \quad S_2(Y) = -\frac{i}{16\ell^3}(k^2+\ell^2)^2(k^2+\ell^2-1)(k^2-3\ell^2-1)\left\{Y + \frac{\varepsilon}{2}\sin(2Y/\varepsilon)\right\}$$

$$- \frac{1}{4\ell^2}(k^2+\ell^2)(k^2+\ell^2-1)\cos(Y/\varepsilon)\ . \tag{6.41}$$

Now consider $\log\Phi(Y) = \frac{1}{\varepsilon}\left(S_0(Y) + \varepsilon S_1(Y) + \varepsilon^2 S_2(Y) + \ldots\right)$, keeping only terms to $O(\varepsilon)$:

$$\begin{aligned} S_0(Y) &= O(Y) = O(\varepsilon)\ ; \\ S_1(Y) &= O(\varepsilon)\ ; \\ S_2(Y) &= \left[O(Y) + O(\varepsilon)\right] + O(1)\ ; \end{aligned} \tag{6.42}$$

Therefore

$$\log\Phi(y) = -\left\{\frac{\varepsilon}{4\ell^2}(k^2+\ell^2)(k^2+\ell^2-1)\cos y\right\}$$

$$+ i\left\{\ell y + \frac{\varepsilon}{2\ell}(k^2+\ell^2)(k^2+\ell^2-1)\sin y\right\} + O(\varepsilon^2)\ , \tag{6.43}$$

returning to the independent variable y. The real part of (6.43) gives the amplitude, the imaginary part the phase, of Φ. Since constants have been disregarded, there is an arbitrary constant amplitude not included

in this expression. But the amplitude modification is provided by the factor

$$\mathrm{AMP}(\Phi) \propto 1 - \frac{\varepsilon}{4\ell^2}(k^2+\ell^2)(k^2+\ell^2-1)\cos y + O(\varepsilon^2) , \quad (6.44)$$

while the phase behaves as

$$\frac{d}{dy}\mathrm{PHASE}(\Phi) = \ell\left\{1 + \frac{\varepsilon}{2\ell^2}(k^2+\ell^2)(k^2+\ell^2-1)\cos y\right\} . \quad (6.45)$$

Note that the net phase variation across the domain is still $2\pi\ell\ell_0$, the same as for pure Rossby waves.

These results have been checked by employing a different and somewhat more cumbersome solution technique, namely a Poincaré perturbation expansion of (6.35) where both Φ and c are expanded in powers of ε. The first correction to c was indeed found to vanish, and considering $\Phi_0 + \varepsilon\Phi_1$ one obtains a slightly modified version of (6.43), where the coefficients of cos y and sin y are multiplied by $4\ell^2/(4\ell^2-1)$. But this factor differs from unity only by a term which is of the same order as the error. Since the perturbation series is regular, such agreement is of course to be expected.

A numerical computation of eigenmodes of (6.35) has been performed using a matrix method with a 29-wave truncation. For values of $\varepsilon = 0.1$ and $\ell_0 = 1$ appropriate to the numerical simulations of Chapter VII (see §7b), Figs. 6.9 show the first five propagating neutral modes for $k = 1$; they are obviously modified Rossby waves, whose leading-order modification is well explained by (6.44) and (6.45). Note in particular that the phase variation is slowest in the centre of the westerly jet, hence the mode has largest meridional scale there, while the phase variation is most rapid in the centre of the easterly jet. Additionally the amplitude is greatest at the former latitude, and weakest at the latter.

The phase-speed errors, given in the captions to Figs. 6.9,

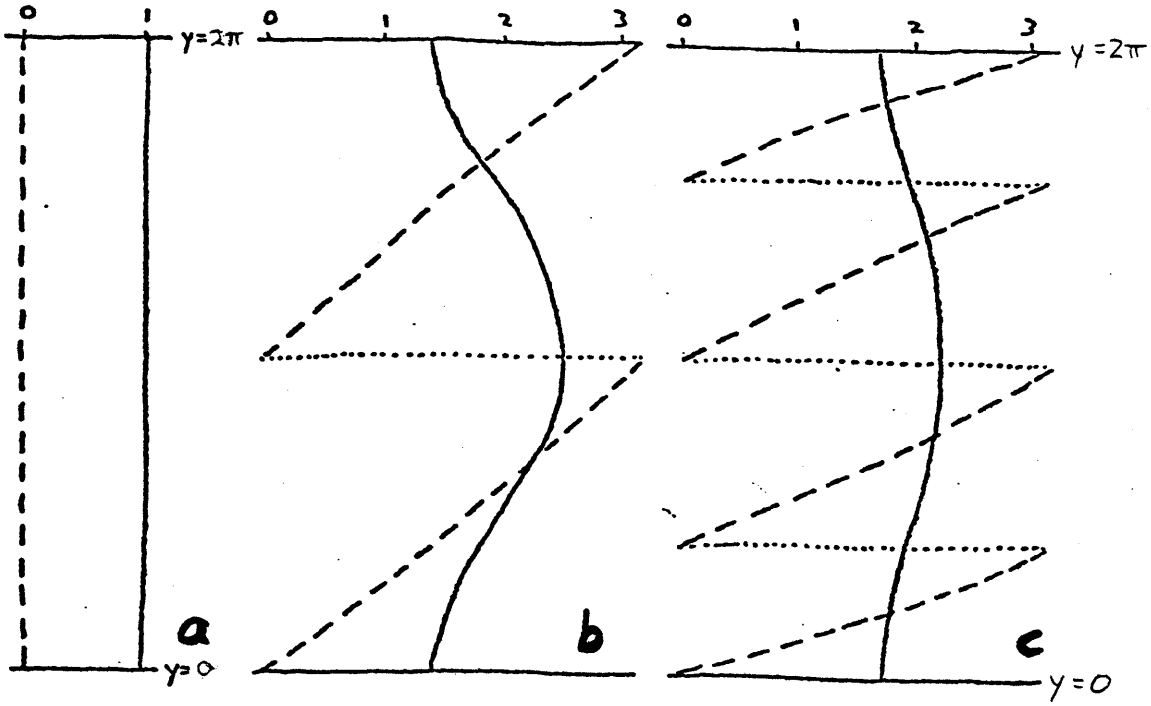


Fig. 6.9a-c: Propagating neutral modes for cosine jet with k = 1, β_o = 1, and U_o = 0.1, showing amplitude (——) and phase (– –) as a function of y. (a) ℓ = 0 mode; c = -1.0 ; c(U=0) = -1.0. (b) ℓ = 1 mode; c = -.50335 ; c(U=0) = -.50000 ; (amplitude - 6.0) is plotted. (c) ℓ = 2 mode; c = -.21456 ; c(U=0) = -.20000 .

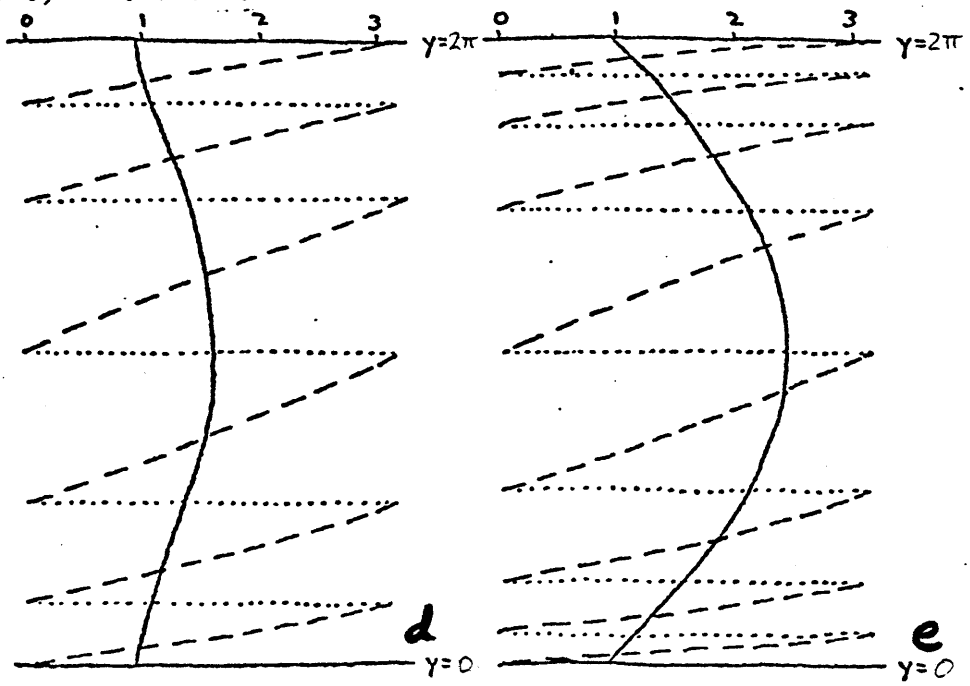


Fig. 6.9d,e: As above, (d) ℓ = 3 mode; c = -.13134 ; c(U=0) = -.10000 .
(e) ℓ = 4 mode; c = -.10762 ; c(U=0) = -.0588 .

indicate increasing error for higher ℓ. Other computations performed with higher k, moreover, do not show a recognizable Rossby-wave structure for k greater than unity. Both of these findings are compatible with the fact that, from (6.44) and (6.45), the magnitude of the modification increases as $\max(k^4/\ell^2, k^2, \ell^2)$: hence especially rapidly with k.

The connection between these modified Rossby waves and the ray tracing calculations is apparent when one recalls that a ray which managed to propagate meridionally through the domain several times, would be observed to have maximum amplitude and scale in the centre of the westerly jet, and corresponding minima in the easterly jet; it would thus appear in a time average as the normal mode found above. Indeed, it is precisely when rays are able to propagate unscathed across the domain that the normal-mode interpretation becomes the more appropriate one. It is then perhaps no coincidence that, from §6d, the only rays which have no critical lines for any y_0 are those with k = 1 and small ℓ_0 (see also Fig. 6.7): these correspond to the parameters required for a non-singular neutral normal mode as in Figs. 6.9 and (6.44), (6.45).

Farrell (1982) has studied the emergence of normal modes numerically in the context of baroclinic instability, arguing that large-scale modes not present to any significant extent in the initial conditions may be "excited" by the development of the continuous spectrum. This latter phenomenon is made possible by the fact that the discrete and the continuum modes are not energetically orthogonal. When the long waves are unstable, this excitation can be particularly significant. In the present context of a stable flow, the implication is rather that the reversibility of the ray-tracing picture of §§6c,d may not entirely obtain, even when critical lines are present: neutral normal modes of

the type derived above may be excited at small k and ℓ_0.

Boyd (1983) has argued, rather loosely, that for Farrell's problem the rigid boundaries produce boundary layers that are insignificant except for small k, in which case they overlap and prevent disturbances from reaching the $\ell = 0$ mode. The present situation is of course rather different, in that there are no boundaries as such but only a quantization condition. In any event §6d has shown that, for $\beta_0 = 25$, $k = 1$ disturbances never have turning lines, and consequently never reach $\ell = 0$ even according to ray-tracing theory.

In summary one can say that, with the exception of rays without critical lines and "excited" neutral normal modes (which may not be distinct phenomena), linear theory predicts eventual absorption of disturbances by the mean zonal flow. This process has been called "rotational adaptation" by Zeng (1982). The extent of the large-scale trapping, expected to be negligible except for small k, can be determined numerically without excessive spectral resolution since the process is indeed a large-scale one; this is in fact done in §7d, where it is found to be fairly small for the chosen parameters. However an important temporary feature of the linear dynamics is the initial amplification, up-scale "cascade", and large-scale meridional anisotropy of favourably orientated disturbances; while this development is largely temporary according to linear theory, its significance within the fully nonlinear problem is far-reaching - as shall be seen in the numerical simulations of the two succeeding chapters.

CHAPTER VII - NUMERICAL SIMULATIONS: SPIN-DOWN

§7a. Introduction

The dynamical scenario under investigation in this study is that of barotropic turbulence in the presence of a large-scale zonal shear flow. The Introduction to Chapter V has discussed the rationale for such an undertaking in light of questions concerning the general circulation of the atmosphere that were raised in §4d of Chapter IV, while indicating the limitations inherent in any barotropic model. Yet the subject is also of some intrinsic interest within fluid dynamics in general, insofar as it ventures into the largely unexplored territory of inhomogeneous turbulence theory, and provides a next step beyond the beta-plane turbulence theory of §3c.

Unfortunately it would seem that there is as yet no nonlinear analytical framework which can encompass the problem; while a closure methodology may be formally established, in practice it is impossibly cumbersome for strongly inhomogeneous flows (see Lin, 1982). Chapter V described some nonlinear approaches, with the principal results coming from conservation laws, but not much progress was possible. In Chapter VI the more popular and certainly far easier methodology of linear theory was explored, in order to identify processes of wave, mean-flow interaction that are presumably operative to at least a limited extent in the fully nonlinear problem.

The difficulty with applying linear theory to linearized systems, of course, is that the results are formally invalid for any realizable disturbance. It is true that for very weak nonlinearities one can sometimes establish an asymptotic ordering which is deductively correct

for a finite time (e.g. Pedlosky, 1970), but such a method is not generally applicable and certainly fails to describe turbulent behaviour. Consequently the only way of knowing whether, and to what extent, the predictions of linear theory hold true, is to test them by experiment: the most convenient experimental procedure for barotropic turbulence being direct numerical simulation. The results of such testing, while presumably secure for the case at hand are, however, open to question with regard to their general validity. This is an old and intractable issue. Since one cannot perform any sort of experiment over the full range of parameter space, one must normally be content with findings of a more qualitative nature; similarly one must pay particular attention to the robustness of the conclusions, relying to some degree on a combination of faith and of intuition gleaned from experiments of the same general nature.

In this chapter the notions of mean-flow straining and large-scale meridional anisotropy, as developed from the linear theory of the previous chapter, are tested in some numerical simulations of the "spin-down" variety: that is to say unforced, nearly-inviscid evolution from spectrally-localized initial conditions. Attention is focussed on identifying which features of the linear dynamics survive the nonlinear, wave-wave interactions; and on how the latter modify the former. The work of Rhines (1975, 1977) has amply demonstrated the pedagogical utility of spin-down runs in other contexts of geostrophic turbulence, and it is in that spirit that they are performed here.

One of the principal attractions of spin-down runs is that, because of their spectrally-localized initial conditions and corresponding spectral gaps, the concept of a turbulent cascade takes on a very

concrete meaning which can be carefully observed in the time evolution of the experiment. Of course the natural systems which motivate the study have a full spectrum, and one does not see a cascade but can only infer it from the nonlinear interaction terms; moreover the basic-state flow is unknown, only the stationary and transient fields being available. All this suggests that spin-down runs should not be analyzed in excessive quantitative detail, but rather with an eye to discerning dynamical phenomena and processes. A description of forced-dissipative simulations run to statistical (turbulent) equilibrium, which are the closest analogues to natural systems that will be considered, and which form the most rigorous test of the concepts discussed thus far, will be presented in the next chapter. However the detailed analysis of those experiments is made much easier by the clear isolation of the relevant dynamical processes in the spin-down runs.

§7b is devoted to a description of the numerical model, and to a discussion of the experimental choices behind the various spin-down simulations. The diagnostic formulae used for evaluating spectra and nonlinear interaction terms are presented in §7c. Then in §7d the linear runs are shown, with wave-wave interactions suppressed and a fixed zonal flow; the aim is to determine the extent to which the linear theory of Chapter VI describes the flow evolution, especially with regard to the spectral dynamics. This is not a trivial matter, since the theory is all approximate. The simulations are not adequate to resolve the fine points of linear theory such as the behaviour around critical layers, but are rather meant to demonstrate the more robust phenomena which might be expected to persist in the fully nonlinear model. Finally the nonlinear simulations themselves are presented in

§7e. While various conclusions are described along the way, a summary is given in §7f.

§7b. The Model and the Experimental Choices

This study has already been restricted to the barotropic beta-plane with a zonal basic-state flow; here a further restriction is made to a doubly-periodic domain (as opposed to a channel - a box is clearly impossible) and to a specific basic-state jet. The first choice is made in order to ensure that any spatial inhomogeneity of the turbulence can be attributed to the basic-state flow alone, rather than to walls; the latter represents a quite distinct sort of inhomogeneity which is not relevant to the present situation. The relation between such a "process" model and any physical system is of course a problematical one, as it is for all but general circulation models: there is an implicit assumption that all remote influences are expressed through the basic-state flow. Haidvogel (1983) has recently discussed the role of similar "process" models in the oceanic context. As regards the restriction to a specific jet, there is no doubt that in an ideal world, with unlimited computer resources and personal time, one would like to consider many different kinds of jets. However in this finite world, it seems better to focus on a single flow so that inter-experimental comparisons can be usefully made; in any case the purpose of the spin-down runs is primarily pedagogical and illustrative.

The linear theory of Chapter VI suggests that the basic-state flow ought to have variable shear and an inflection point in order to be considered in any way representative, and that interesting phenomena may be associated with easterly and westerly flow maxima. The doubly-periodic

domain in fact ensures these features. The simplest large-scale flow would seem to be the cosine jet, and it is also easily handled by a spectral model so that resolution problems ought to be minimized. Since the conceptual model concerns a flow which is barotropically stable in a normal-mode sense, one need only choose a value of β_0 sufficiently large to guarantee this. Finally, for the spin-down runs the cosine jet will have the gravest possible meridional structure, that is to say wave-number one. This is clearly not the most general situation, but it allows the maximum scale separation between the basic-state flow and the perturbation. Some higher-mode jets are treated in the Appendix.

The governing equation for the barotropic beta-plane is the vorticity equation (5.1), written here in the form

$$\nabla^2\psi_t + J(\psi,\nabla^2\psi) + \beta_0\psi_x = -\nu\nabla^6\psi + F_0 \quad ; \tag{7.1}$$

doubly-periodic boundary conditions are applied on a square domain of width 2π, and the disturbance is arranged to have an rms velocity $u \approx 1$. These are the units appropriate to the model; in any application one would choose geophysical length and velocity scales in order to determine the other parameters and interpret the results. Note that the highly scale-selective biharmonic diffusion represents the only form of friction, so that the large-scale dynamics are nearly inviscid (see Haidvogel, 1983). Introducing the basic-state zonal cosine jet

$$\Psi(y) = U_0 \sin y \quad ; \quad U(y) = -U_0 \cos y \quad [0 \leq y < 2\pi] \, , \tag{7.2}$$

and substituting into (7.1), the lhs vanishes and one requires

$$F_0 = \nu\nabla^6\Psi = -\nu U_0 \sin y \, . \tag{7.3}$$

Given this balance, the perturbation $\phi \equiv \psi - \Psi$ must satisfy

$$\nabla^2\phi_t + J(\phi,\nabla^2\phi) + J(\Psi,\nabla^2\phi) + J(\phi,\nabla^2\Psi) + \beta_0\phi_x = -\nu\nabla^6\phi \, . \tag{7.4}$$

To determine scales relevant to the atmosphere, summing up the stationary and transient components of energy from the FGGE-3A data (Boer & Shepherd, 1983; and Chapter IV) leads to

$$E_{stat} \approx 100 \text{ J/kg} \quad \Rightarrow \quad U_* \approx 17 \text{ m/s} \; ; \tag{7.5a}$$

$$E_{trans} \approx 50 \text{ J/kg} \quad \Rightarrow \quad u_* \approx 10 \text{ m/s} \; . \tag{7.5b}$$

Given $u_{rms} \approx 1$ in the model, this suggests choosing $U_0 = 2\sqrt{2}$ so that $\langle U^2(y) \rangle \approx 4$ and thus the non-dimensional parameter α of §5c takes the value 2 - as argued in §5d. To find a length scale, choose the mid-latitude domain scale $L_* = 24{,}000$ km ; then

$$L = \frac{L_*}{2\pi} \approx 4 \times 10^6 \text{ m} \; , \quad T = \frac{L}{U} \approx 4 \times 10^5 \text{ s} \approx 5 \text{ days} \; , \tag{7.5c,d}$$

$$\text{and} \quad \beta_0 = \frac{\beta_{0*} L^2}{U} \approx 25 \; . \tag{7.5e}$$

One implication of the turbulent enstrophy cascade is that it prevents the large- and intermediate-scale waves from approaching the inviscid statistical equilibrium solution. For this model, inviscid statistical equilibrium is thwarted by simulating the off-scale enstrophy cascade with biharmonic diffusion, which also minimizes nonlinear aliasing. To achieve this, ν must be chosen so that the "grid Reynolds number" $\frac{u_{rms}}{\nu N^3} \leq 10$ (Haidvogel, private communication). Here N is the truncation wavenumber, where most of the dissipation should be concentrated. For $N = 32$ and $u_{rms} = 1$, for example, this suggests the value $\nu = 3 \times 10^{-6}$. It should be said that while the choice of a high-order diffusion operator is still a matter of some debate within the turbulence community (e.g. Basdevant & Sadourny, 1983), nevertheless for proper simulation of the large scales it seems necessary only to remove enstrophy at small scales - which all such operators do, in their own different ways.

The initial conditions that are utilized in the spin-down runs are classical in this sort of simulation: namely a narrow isotropic ring, spectrally localized to

$$E(k,\ell)\Big|_{t=0} = \begin{cases} 0.01 & \text{for } 9 \leq \sqrt{(k^2+\ell^2)} < 12 \\ 0.0 & \text{otherwise} \end{cases} \tag{7.6}$$

Phases are assigned randomly. The choice of the central wavenumber is meant to roughly correspond to the barotropic energy input scale of the atmosphere, but it is not too crucial as long as it lies safely outside of the "cascade cut-off" scale κ_β , which in this case is 5. The value of this kind of initial condition, as will be seen, is that it highlights the nonlinear cascades of energy and enstrophy in a way that is not possible with either "equilibrium" simulation or observational data.

It has been found that a truncation wavenumber of N = 32 , corresponding to a 64×64 set of gridpoints, is sufficient to handle the enstrophy cascade and to resolve the essential dynamics. It is not high enough to give much of a hint of an enstrophy-cascading inertial subrange, but that is not the object of this study. For a more strongly inhomogeneous jet with smaller-scale structure, a higher resolution might well be required.

The numerical procedure employed is to solve the Fourier transform of either (7.1) or (7.4), advancing in time through a leapfrog algorithm with a leapfrog-trapezoidal step being taken every 23 timesteps to damp the computational mode. For these runs the timestep is $\Delta t = .0015$. The nonlinear coupling arising from the advection terms is handled using the "transform method", namely by performing the multiplication in physical space in a manner that conserves both energy and enstrophy, then trans-

forming back to the spectral domain. Although the procedure is not alias-free, with high-order diffusion this should not present a problem. The evaluation of derivatives is exact, as is the quadrature used for the Fourier transforms.

Three principal spin-down runs are described in this chapter, using the parameter settings outlined above. Run P is pure beta-plane turbulence, that is with $U_0 = 0$ so there is no basic-state flow; it represents the "control". Run R is a linear calculation, in the sense that the zonal basic-state component is held fixed and wave-wave interactions are suppressed; to achieve this (7.4) is solved without the $J(\phi,\nabla^2\phi)$ term. Finally Run O is the full nonlinear simulation, with all terms included; for computational expediency (7.1) is solved, although (7.4) would have done just as well.

The rationale behind these choices is that described in §7a. The linear run is made in order to evaluate the success of the approximate linear theory of Chapter VI, and to isolate the purely linear wave, mean-flow interaction processes. While the numerical model is easily seen to be inadequate in describing fine-scale phenomena such as the behaviour around critical lines, one may argue that the high-order diffusion and enstrophy cascade would make the study of such features questionable in any event. The aim is not to understand the linearized problem perfectly, but rather to examine the role of linear dynamics in the fully nonlinear problem; many of the subtle and sensitive questions of linear theory then become moot. Indeed, it will be seen that the resolution problems of Run R are completely absent from Run O. All three runs begin from identical initial conditions, and are carried out to $t = 15$.

To further elucidate the linear dynamics, a set of "single-wave" linear runs is also performed. These are entitled Runs R2, R4, and R6, and begin with disturbance energy in, respectively, modes $(k,\ell) = (2,10)$ and $(2,-10)$; $(4,9)$ and $(4,-9)$; and $(6,8)$ and $(6,-8)$. In principle each of these runs is contained within Run R, but there is a particular clarity obtained by examining each wave's evolution on its own. These runs are only extended to $t = 3$.

§7c. Diagnostic Formulae

At this point it is necessary to work out the diagnostic equations for spectral energy and enstrophy budgets, in order to define the terms which are used to interpret the behaviour of the model. The procedure is analogous to that of §2a. Beginning with the perturbation equation (7.4), take a Fourier transform, multiply the result by $\hat{\phi}^*(\underline{k})$, and add the complex conjugate; this yields the energy equation for each $\underline{k}$,

$$\frac{\partial}{\partial t}\frac{1}{2}k^2\left|\hat{\phi}(\underline{k})\right|^2 = \frac{1}{2}\left(\hat{\phi}^*(\underline{k})\{J(\phi,\nabla^2\phi)\}(\underline{k}) + \hat{\phi}^*(\underline{k})\{J(\Psi,\nabla^2\phi)\}(\underline{k}) + \hat{\phi}^*(\underline{k})\{J(\phi,\nabla^2\Psi)\}(\underline{k})\right) + \text{c.c.} - \nu k^6\left|\hat{\phi}(\underline{k})\right|^2 . \tag{7.7}$$

Here the curly brackets as well as the cap indicate a Fourier transform; $k^2 \equiv \left|\underline{k}\right|^2$; and the term arising from β has not been included as it does not affect the energetics. Making the following definitions:

$$E(\underline{k}) \equiv \frac{1}{2}k^2\left|\hat{\phi}(\underline{k})\right|^2 ; \quad PSI(\underline{k}) \equiv \frac{1}{2}\hat{\phi}^*(\underline{k})\{J(\phi,\nabla^2\phi)\}(\underline{k}) + \text{c.c.} ; \tag{7.8a,b}$$

$$EMI(\underline{k}) \equiv \frac{1}{2}\hat{\phi}^*(\underline{k})\left(\{J(\Psi,\nabla^2\phi)\}(\underline{k}) + \{J(\phi,\nabla^2\Psi)\}(\underline{k})\right) + \text{c.c.} ; \tag{7.8c}$$

(7.7) can be re-written in the more compact form

$$\frac{\partial}{\partial t}E(\underline{k}) = PSI(\underline{k}) + EMI(\underline{k}) - 2\nu k^4 E(\underline{k}) , \tag{7.9}$$

and this is similar to (2.11). Note that $PSI(\underline{k})$ is a true nonlinear interaction term, the analogue of $I(k)$ in (2.11), in the sense that it

only moves energy between different wavenumbers; hence

$$\sum_{\underline{k}} \mathrm{PSI}(\underline{k}) = \iint \phi J(\phi,\nabla^2\phi)\, dxdy = 0 . \tag{7.10}$$

On the other hand the sum of EMI($\underline{k}$) does not vanish, so it represents a net source or sink for the perturbation; some of the physical-space expressions for this conversion have been considered in §5b.

The enstrophy budget equation is obtained through multiplying the Fourier transform of (7.4) by $\{\nabla^2\phi\}^* \equiv -k^2\hat{\phi}^*(\underline{k})$, and adding the complex conjugate, which yields

$$\begin{aligned}\frac{\partial}{\partial t}\frac{1}{2}k^4\left|\hat{\phi}(\underline{k})\right|^2 = \frac{1}{2}\big(& k^2\hat{\phi}^*(\underline{k})\{J(\phi,\nabla^2\phi)\}(\underline{k}) + k^2\hat{\phi}^*(\underline{k})\{J(\Psi,\nabla^2\phi)\}(\underline{k}) \\ & + k^2\hat{\phi}^*(\underline{k})\{J(\phi,\nabla^2\Psi)\}(\underline{k})\big) + \text{c.c.} - \nu k^8\left|\hat{\phi}(\underline{k})\right|^2.\end{aligned} \tag{7.11}$$

Then using the definitions (7.8), one may write (7.11) as

$$\frac{\partial}{\partial t}\Omega(\underline{k}) \equiv \frac{\partial}{\partial t}k^2E(\underline{k}) = k^2\mathrm{PSI}(\underline{k}) + k^2\mathrm{EMI}(\underline{k}) - 2\nu k^6E(\underline{k}) . \tag{7.12}$$

Once again, $k^2\mathrm{PSI}(\underline{k})$ can be interpreted as a true interaction term since

$$\sum_{\underline{k}} k^2\mathrm{PSI}(\underline{k}) = -\iint \nabla^2\phi J(\phi,\nabla^2\phi)\, dxdy = 0 , \tag{7.13}$$

while $\sum k^2\mathrm{EMI}(\underline{k})$ represents a net enstrophy conversion which may be expressed as in (5.17). Of course, both EMI($\underline{k}$) and k^2EMI($\underline{k}$) in fact represent a combination of nonlinear perturbation interaction and basic-state perturbation conversion, with the partition between these two processes being ambiguous at any given wavenumber. There are, however, two cases when one may safely choose one interpretation over the other: if EMI($\underline{k}$) is of one sign for all $\underline{k}$, then it may perhaps be viewed as a pure conversion term at each $\underline{k}$; while if $\sum \mathrm{EMI}(\underline{k})$ or $\sum k^2\mathrm{EMI}(\underline{k})$ is very small, then it may be seen as an interaction term for that quantity (either energy or enstrophy, but not generally both). Indeed, in the case of a separation in scale between the basic-state flow and the

perturbation, it has been shown in Chapters V and VI that the perturbation enstrophy is approximately conserved. In such a situation $k^2 EMI(\underline{k})$ has the interpretation of an interaction term between different perturbation waves, with the basic-state flow playing a catalytic but otherwise passive role.

In the diagnostics to be presented, the energy and enstrophy spectra and interaction terms are generally summed over one index to give a more compact representation. Then flux terms can be defined as in Chapter II, as the negative running integral of the interaction terms. The three methods used correspond to zonal or k-spectra; meridional or ℓ-spectra; and "isotropic" or n-spectra, summing over an annulus of unit width. The last case is analogous to the integration of (2.9), and is the appropriate index for homogeneous turbulence; its utility in an inhomogeneous situation remains to be demonstrated, although the spectral observations of Chapter IV show promise in this regard. There is a minor nuisance which arises when forming such sums for a Cartesian domain with a discrete spectrum, which does not occur for spherical harmonics: the number of waves in a given annular band is not precisely proportional to $\sqrt{(k^2+\ell^2)}$, but only approximately so. This means that spectra, for example, appear rougher than they might otherwise, especially at large scale. The formula used is

$$E(n) = \sum_{\substack{\underline{k} \\ (n^2 \leq k^2+\ell^2 < (n+1)^2)}} E(\underline{k}) \ . \tag{7.14}$$

The above formulae are for the "perturbation" energy and enstrophy. In many cases it is more appropriate, and easier, to compute the stationary and transient budgets instead. Rather than (7.4), one must consider the pair

$$J(\bar{\psi},\nabla^2\bar{\psi}) + \beta_0\bar{\psi}_x = -\nu\nabla^6\bar{\psi} + F_0 - \overline{J(\psi',\nabla^2\psi')} \quad , \tag{7.15a}$$

$$J(\psi',\nabla^2\psi') + J(\bar{\psi},\nabla^2\psi') + J(\psi',\nabla^2\bar{\psi}) + \beta_0\psi'_x = -\nu\nabla^6\psi' + \overline{J(\psi',\nabla^2\psi')}, \tag{7.15b}$$

where $\psi \equiv \bar{\psi} + \psi'$, the overbar denoting a time average over some interval. The transient budgets are obtained by multiplying the Fourier transform of (7.15b) by $\hat{\psi}'^*(\underline{k})$ or by $-k^2\hat{\psi}'^*(\underline{k})$, adding the c.c., and then taking a time average; the result is completely analogous to (7.9) and (7.12), namely

$$\frac{\partial}{\partial t} E_T(\underline{k}) = 0 = TSI(\underline{k}) + EMI_T(\underline{k}) - 2\nu k^4 E_T(\underline{k}) \quad , \tag{7.16a}$$

$$\frac{\partial}{\partial t} \Omega_T(\underline{k}) = 0 = k^2 TSI(\underline{k}) + k^2 EMI_T(\underline{k}) - 2\nu k^6 E_T(\underline{k}) \quad , \tag{7.16b}$$

where

$$E_T(\underline{k}) \equiv \tfrac{1}{2}k^2\overline{\left|\hat{\psi}'(\underline{k})\right|^2} \; ; \quad TSI(\underline{k}) \equiv \overline{\tfrac{1}{2}\hat{\psi}'^*(\underline{k})\{J(\psi',\nabla^2\psi')\}(\underline{k})} + c.c. \tag{7.17a,b}$$

$$EMI_T(\underline{k}) \equiv \overline{\tfrac{1}{2}\hat{\psi}'^*(\underline{k})\left(\{J(\bar{\psi},\nabla^2\psi')\}(\underline{k}) + \{J(\psi',\nabla^2\bar{\psi})\}(\underline{k})\right)} + c.c. \tag{7.17c}$$

However the stationary flow now no longer satisfies the governing equation (7.1), but rather the balance equation (7.15a). To obtain stationary budgets, multiply the Fourier transform of (7.15a) by $\hat{\bar{\psi}}^*(\underline{k})$ or $-k^2\hat{\bar{\psi}}^*(\underline{k})$ and add the c.c.; in the first case this yields the energy budget

$$\begin{aligned} 0 = \tfrac{1}{2}\Big(&\hat{\bar{\psi}}^*(\underline{k})\{J(\bar{\psi},\nabla^2\bar{\psi})\}(\underline{k}) + \hat{\bar{\psi}}^*(\underline{k})\overline{\{J(\psi',\nabla^2\psi')\}}(\underline{k}) \Big) + c.c. \\ &- \nu k^6\left|\hat{\bar{\psi}}(\underline{k})\right|^2 + \tfrac{1}{2}\nu k^6\left(\hat{\bar{\psi}}^*(\underline{k})\hat{\Psi}(\underline{k}) + c.c.\right) , \end{aligned} \tag{7.18}$$

where the β term has again been omitted and (7.3) has been used to re-write F_0. (7.18) as well as its enstrophy equivalent can be put into the more compact form

$$\frac{\partial}{\partial t} E_S(\underline{k}) = 0 = MSI(\underline{k}) + C(\underline{k}) + F_1(\underline{k}) \quad , \tag{7.19a}$$

$$\frac{\partial}{\partial t} \Omega_S(\underline{k}) = 0 = k^2 MSI(\underline{k}) + k^2 C(\underline{k}) + k^2 F_1(\underline{k}) \quad , \tag{7.19b}$$

where

$$E_S(\underline{k}) \equiv \tfrac{1}{2}k^2\left|\hat{\bar{\psi}}(\underline{k})\right|^2 \; ; \quad MSI(\underline{k}) \equiv \tfrac{1}{2}\hat{\bar{\psi}}^*(\underline{k})\{J(\bar{\psi},\nabla^2\bar{\psi})\}(\underline{k}) + * \; ; \qquad (7.20a,b)$$

$$C(\underline{k}) \equiv \tfrac{1}{2}\hat{\bar{\psi}}^*(\underline{k})\{\overline{J(\psi',\nabla^2\psi')}\}(\underline{k}) + * \; ; \; F_1(\underline{k}) \equiv -\tfrac{1}{2}\nu k^6\left(\hat{\bar{\psi}}^*(\underline{k})\hat{\bar{\phi}}(\underline{k})+*\right). \qquad (7.20c,d)$$

It is easily seen that $TSI(\underline{k})$ and $MSI(\underline{k})$ represent true interaction terms for both energy and enstrophy, the first effecting transfers between transient waves, the second between stationary waves; thus

$$\sum_{\underline{k}} TSI(\underline{k}) = \sum_{\underline{k}} k^2 TSI(\underline{k}) = \sum_{\underline{k}} MSI(\underline{k}) = \sum_{\underline{k}} k^2 MSI(\underline{k}) = 0 \; . \qquad (7.21)$$

Note that the stationary-transient conversion terms seen by the stationary flow, $C(\underline{k})$ and $k^2C(\underline{k})$, are not the same at each wavenumber as the conversion terms seen by the transient flow, $EMI_T(\underline{k})$ and $k^2EMI_T(\underline{k})$. However they are consistent in an integrated sense:

$$\sum_{\underline{k}} C(\underline{k}) = -\sum_{\underline{k}} EMI_T(\underline{k}) \quad \text{and} \quad \sum_{\underline{k}} k^2C(\underline{k}) = -\sum_{\underline{k}} k^2EMI_T(\underline{k}) \; . \qquad (7.22a,b)$$

(7.22) may be verified in physical space using integration by parts, or in the following direct fashion. Define

$$MITI(\underline{k}) \equiv EMI_T(\underline{k}) + C(\underline{k}) = \bar{I}(\underline{k}) - MSI(\underline{k}) - TSI(\underline{k}) \; , \qquad (7.23)$$

where $I(\underline{k})$ is the interaction term computed for the full streamfunction ψ. But the rhs of (7.23) consists entirely of interaction terms, which vanish when integrated as in (7.21); hence

$$\sum_{\underline{k}} MITI(\underline{k}) = 0 \quad \text{and similarly} \quad \sum_{\underline{k}} k^2MITI(\underline{k}) = 0 \; . \qquad (7.24)$$

The point of this formalism is that one may reconcile (7.16) and (7.19) by re-writing (7.16) as

$$0 = TSI(\underline{k}) + MITI(\underline{k}) - C(\underline{k}) - 2\nu k^4E_T(\underline{k}) \; , \qquad (7.25)$$

with $MITI(\underline{k})$ representing an interaction between transient waves induced by the catalytic though passive presence of the stationary flow. The

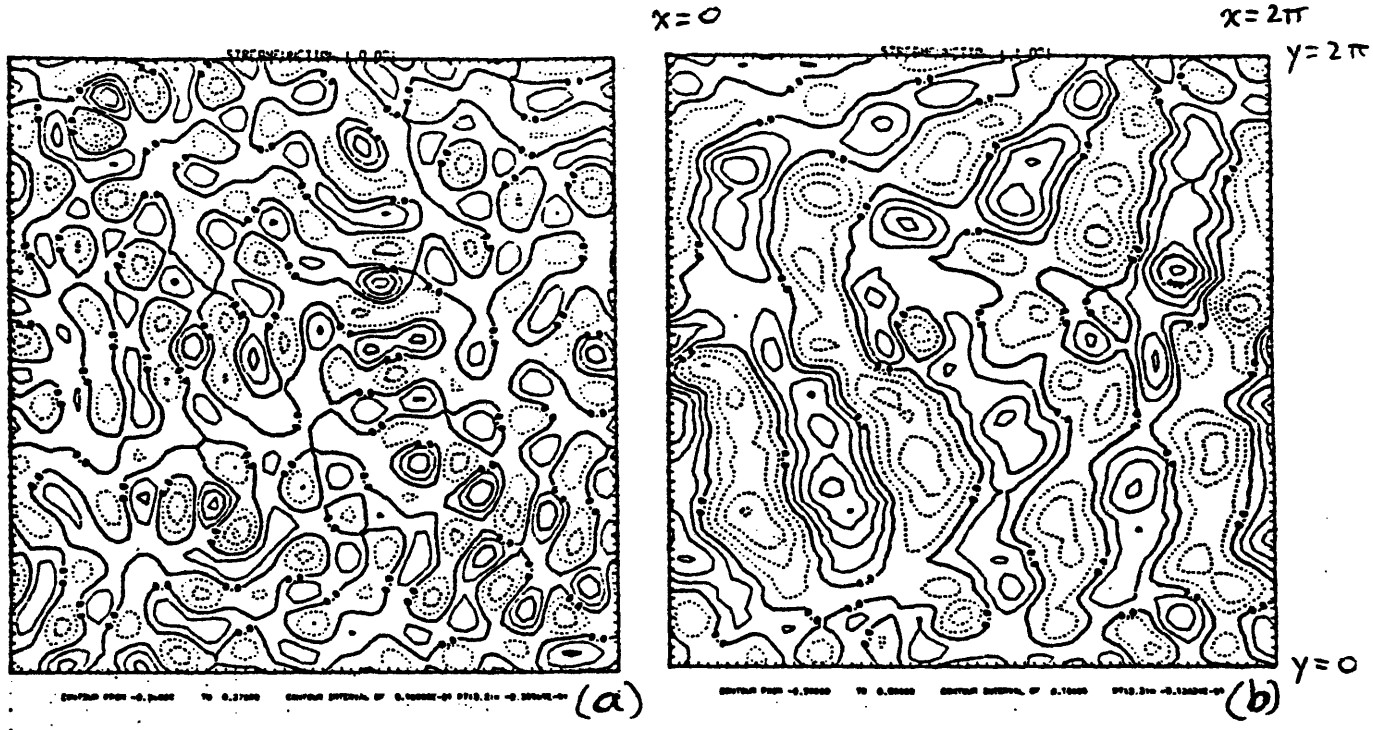


Fig. 7.1: Streamfunction field $\phi(x,y)$ for Run R at (a) t = 0 ; (b) t = 1 ; y runs up from 0 to 2π ; x runs across from 0 to 2π .

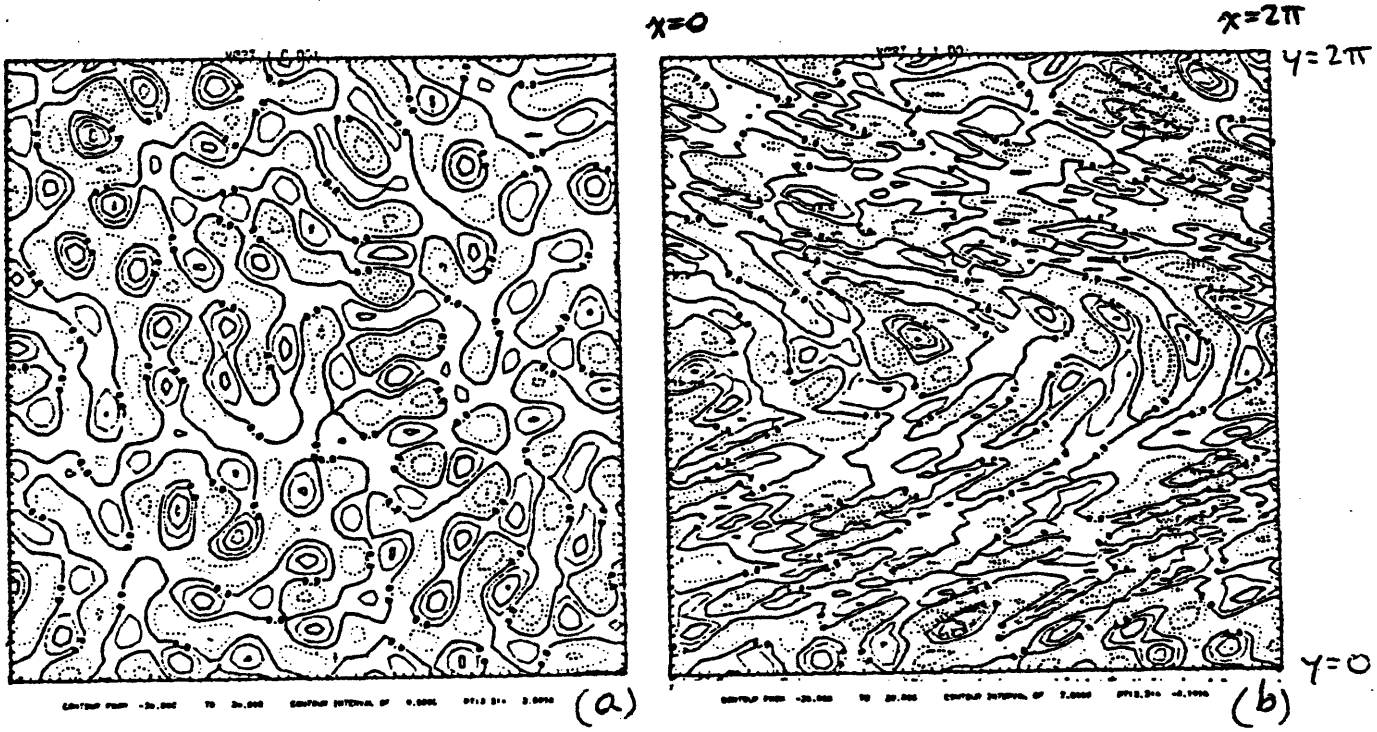


Fig. 7.2: Vorticity field $\nabla^2\phi(x,y)$ for Run R at (a) t = 0 and (b) t = 1 .

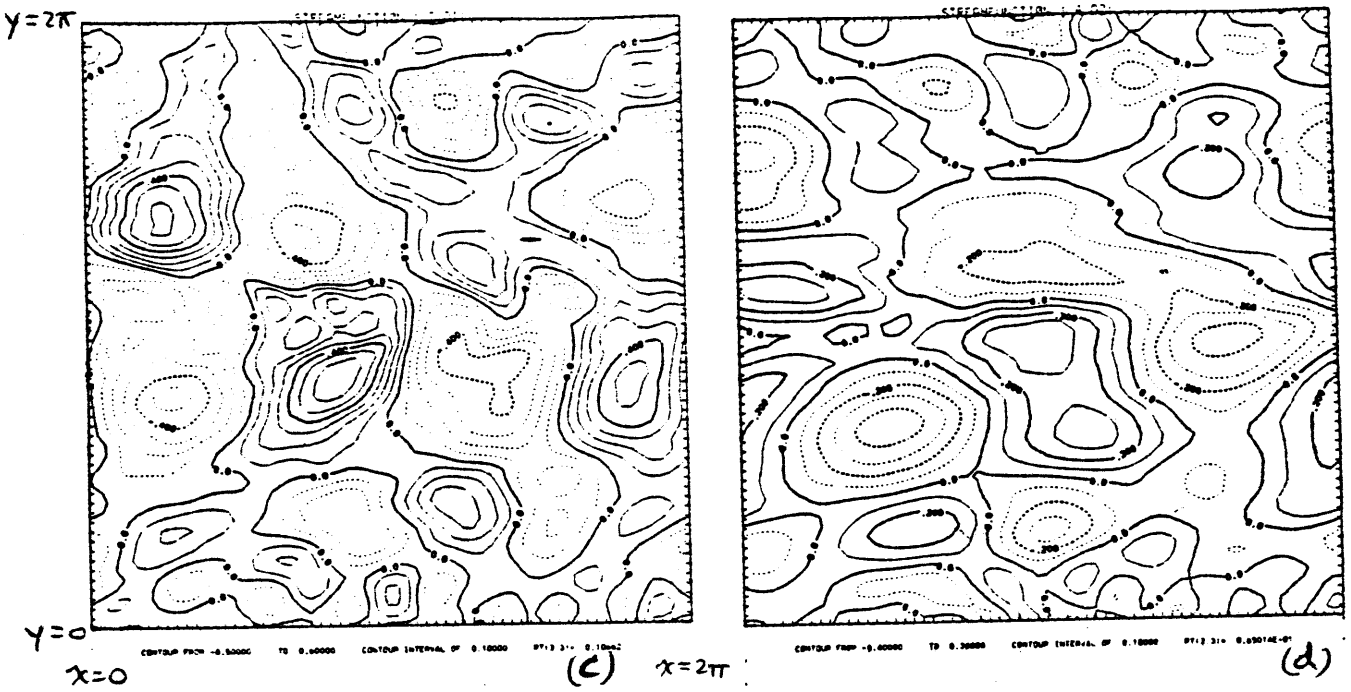


Fig. 7.1: Φ at (c) t = 2 and (d) t = 4 .

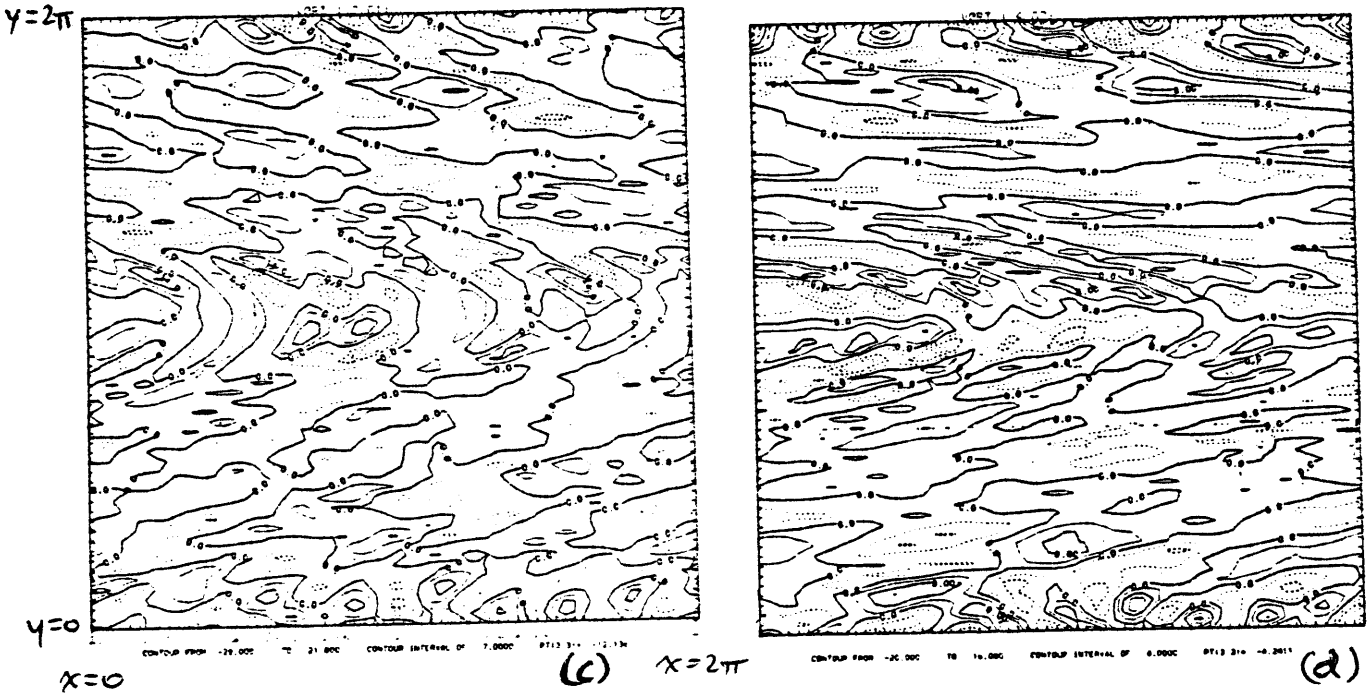


Fig. 7.2: $\nabla^2\Phi$ at (c) t = 2 and (d) t = 4 .

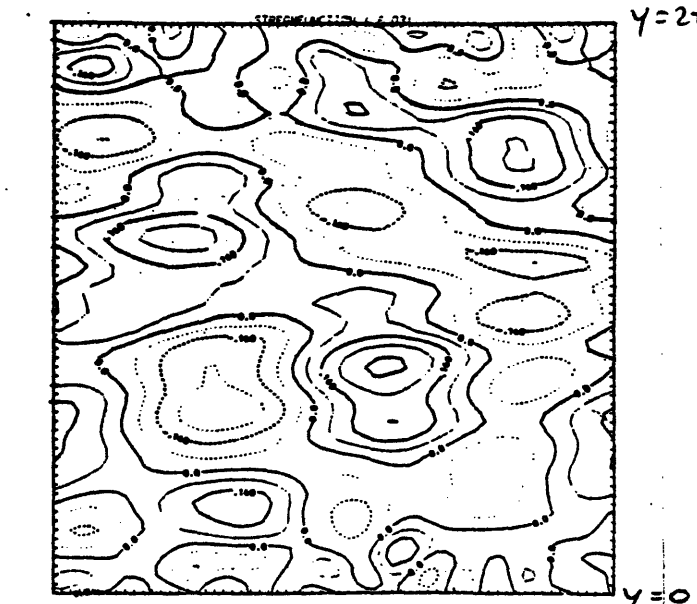


Fig. 7.1e: ϕ at t = 6 .

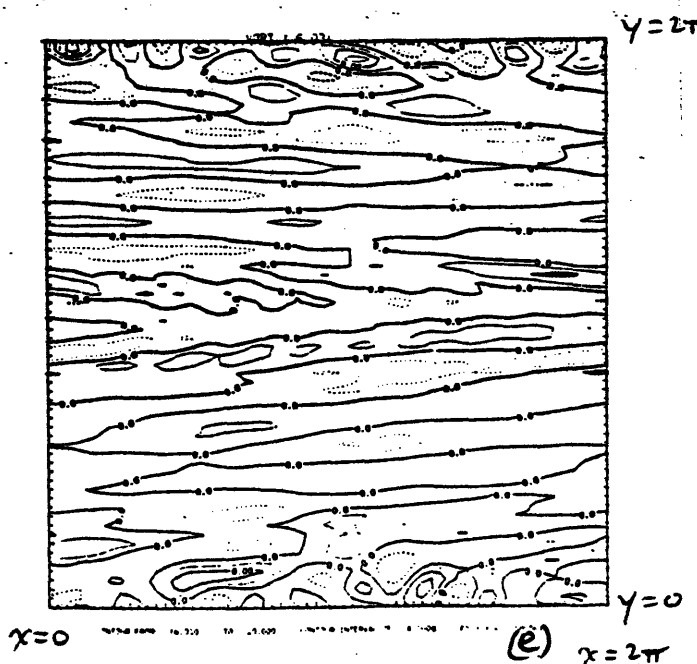


Fig. 7.2e: $\nabla^2\phi$ at t = 6 .

physical content of such a term must be considered carefully, however, as the definition is not free from ambiguity. This matter also arose in the previous discussion of this section concerning the interpretation of $EMI(\underline{k})$; all that has been done here is that a particular partitioning of $EMI_T(\underline{k})$ into interaction and conversion effects has been chosen.

§7d. Discussion of the Linear Runs

In the instantaneous streamfunction and vorticity maps to be shown presently, the upper and lower edges of the figures correspond to the centre of the easterly jet maximum at $y = 2\pi$ and $y = 0$, while the westerly jet is centred at $y = \pi$ across the middle of the domain. The maximum mean-flow shear naturally obtains at $y = \pi/2$ and $y = 3\pi/2$, being positive in the former case and negative in the latter.

Run R begins with isotropic homogeneous initial conditions (Figs. 7.1a,7.2a), but within one "day" there is a remarkable meridional anisotropy in the (relatively long-wave) instantaneous perturbation streamfunction field, combined with an expected zonal (advective) anisotropy in the (relatively short-wave) vorticity field (Figs. 7.1b,7.2b). The contrast between these last two figures is so great that it is difficult to believe that they represent the same dynamical situation. In a way, they don't: it can be argued that ϕ shows the ensemble of wave packets which are propagating into the westerly jet with decreasing ℓ^2 and increasing E, while $\nabla^2\phi$ shows the ensemble of packets which are propagating into the easterly jet with increasing ℓ^2. The argument is a little weak insofar as the wave enstrophy is approximately conserved in the wave, mean-flow interaction and hence $\nabla^2\phi$ should show all wave packets equally; however with isotropic initial conditions most packets have ℓ^2

increasing by t = 1.

As time advances, the streamfunction maps (Figs. 7.1c-e) show maximum scale and intensity in the centre of the domain, where the westerly jet is located, and a "trapped" high-k structure in the easterly jet; both features are consistent with the ray-tracing arguments of §6d, the latter in particular corresponding to regime III of Fig. 6.5. The strength of the large-scale eddies weakens with time, but significant structure persists; this may be due in part to continued propagation of wave packets with no critical layers (regime I of Fig. 6.5), in part to a failure of ray-tracing theory at large scales. The last point would include excitation of normal modes due to the quantization of the periodic domain; these normal modes do indeed have greater meridional scales in the westerly part of the jet, as shown in §6e.

The vorticity maps (Figs. 7.2c-e), on the other hand, depict a complete diffusion of enstrophy throughout the domain except in the "channel" or "waveguide" around y = 0. Disturbances are first removed from the regions of maximum shear, $y = \pi/2$ and $3\pi/2$, where the mean-flow straining is strongest; and subsequently from the westerly jet, as the disturbances radiate away and surrender their energy to the mean flow. But the disturbances around y = 0 are only weakly damped even at t = 15, presumably by the biharmonic diffusion.

The physical processes described by the ray-tracing theory of §6d and evidenced in Run R, are much clarified by an examination of the evolution of "single-wave" disturbances in Runs R2, R4, and R6. In fact these are all "double-wave" disturbances, since both positive and negative ℓ_0 are initialized. For example, the initial condition of Run R2 (Figs. 7.3a,7.4a) consists of $(k_0,\ell_0) = (2,10),(2,-10)$, and if one

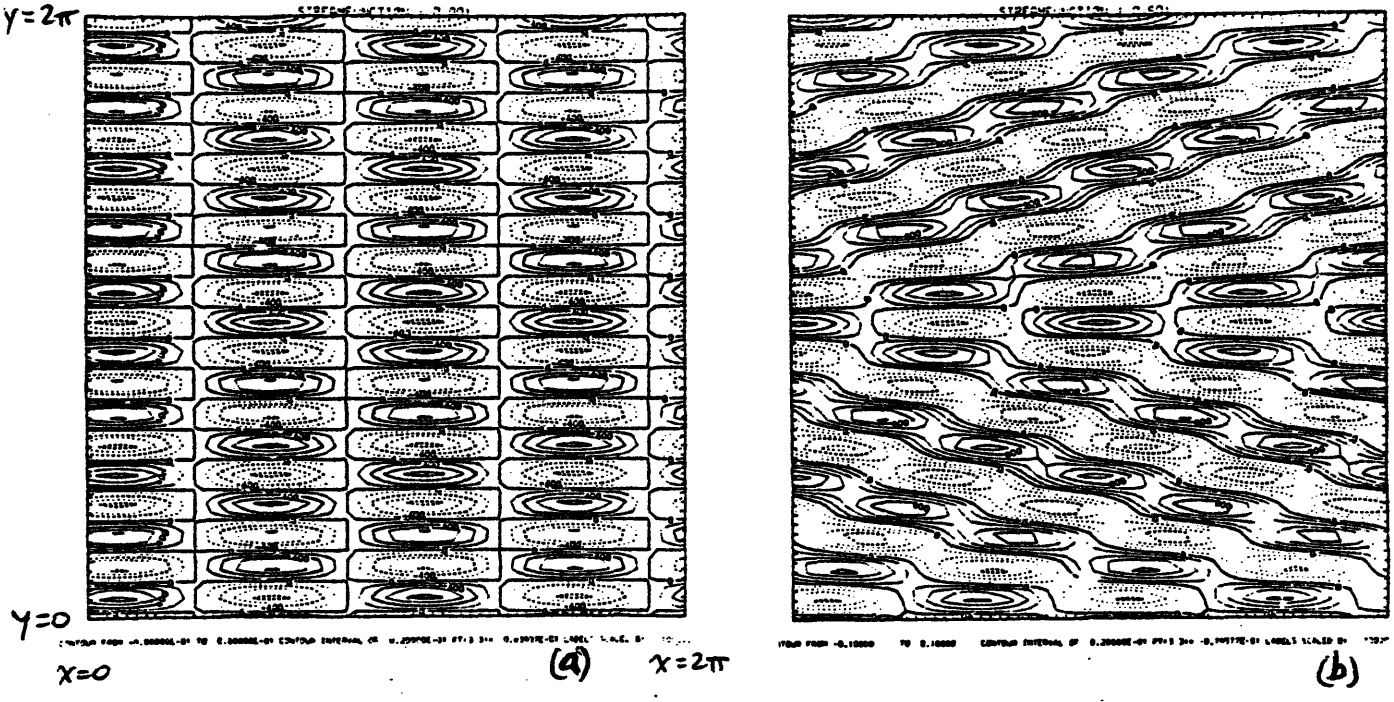


Fig. 7.3: $\phi(x,y)$ for Run R2 at (a) t = 0 and (b) t = 0.5 .

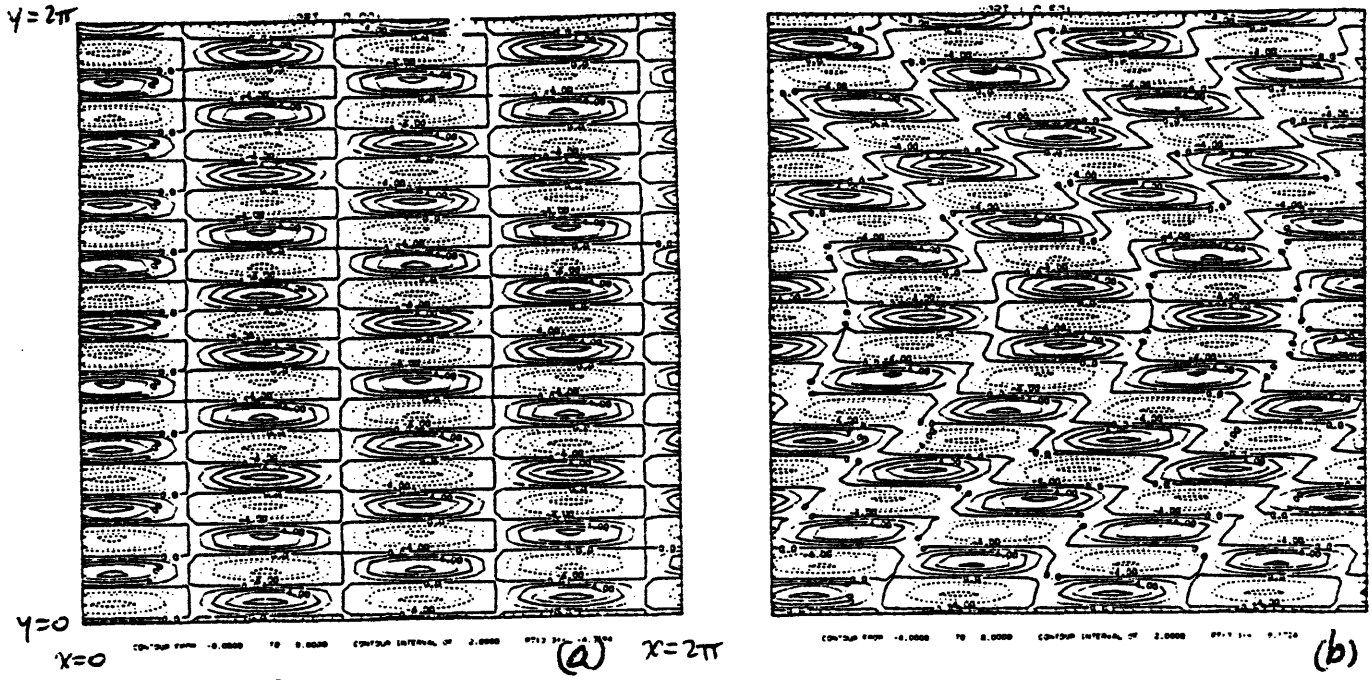


Fig. 7.4: $\nabla^2\phi(x,y)$ for Run R2 at (a) t = 0 and (b) t = 0.5 .

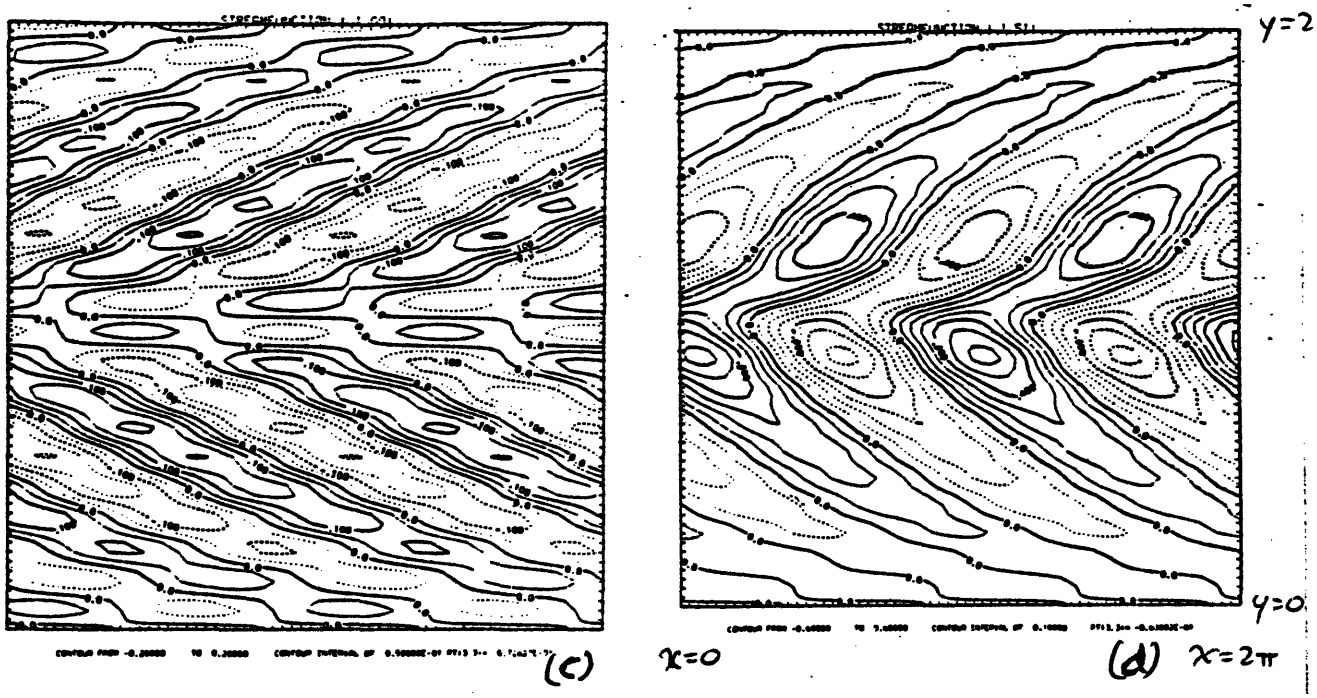


Fig. 7.3: ϕ at (c) t = 1.0 and (d) t = 1.5.

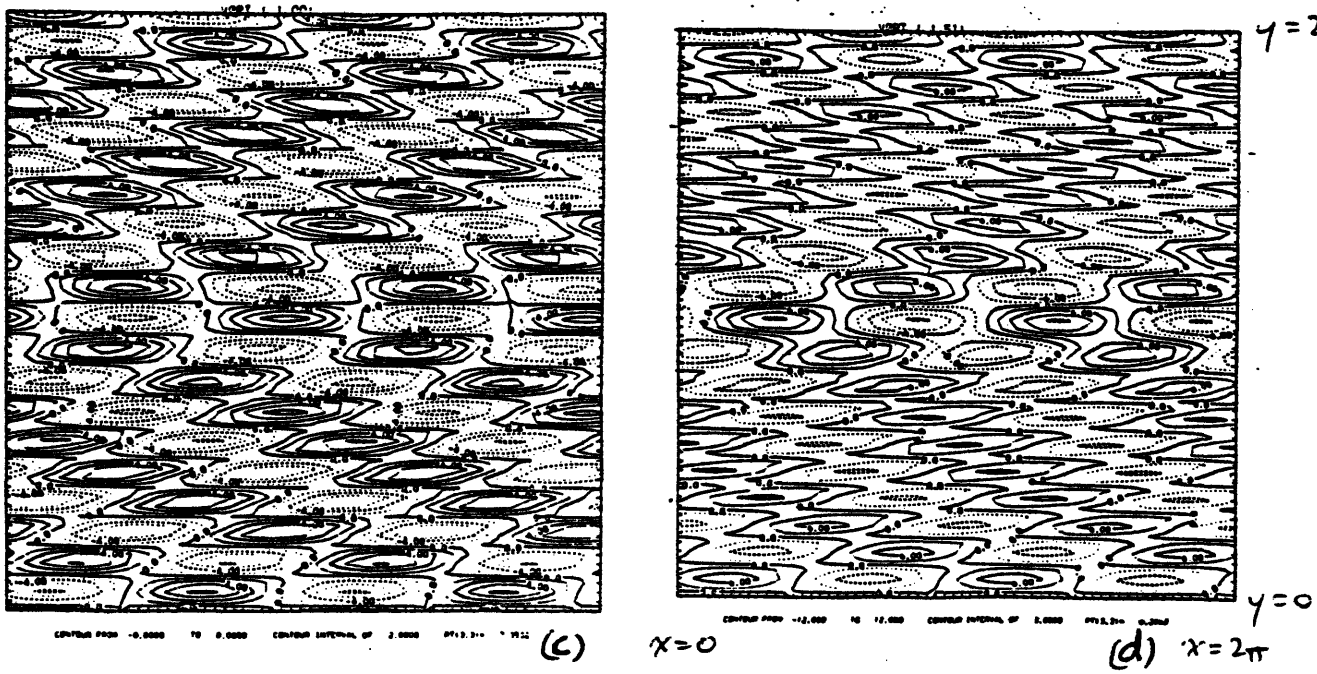


Fig. 7.4: $\nabla^2\phi$ at (c) t = 1.0 and (d) t = 1.5 .

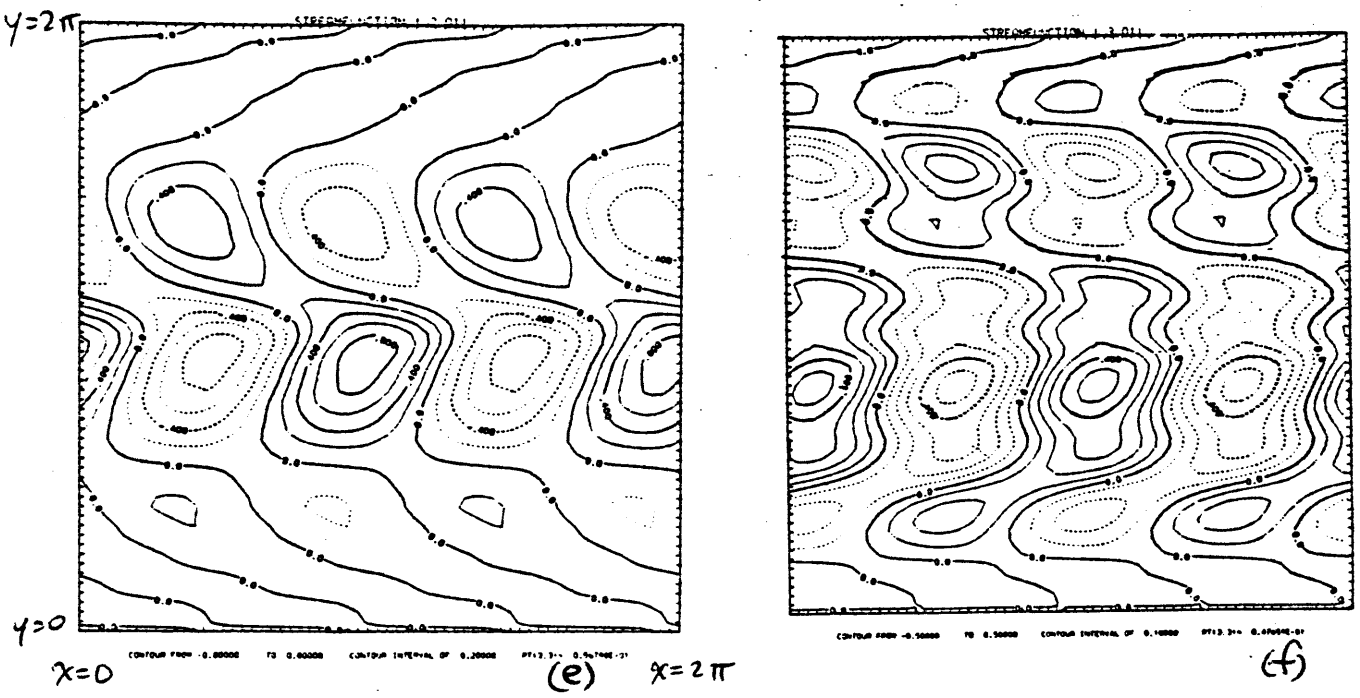


Fig. 7.3: ϕ at (e) t = 2.0 and (f) t = 2.5 .

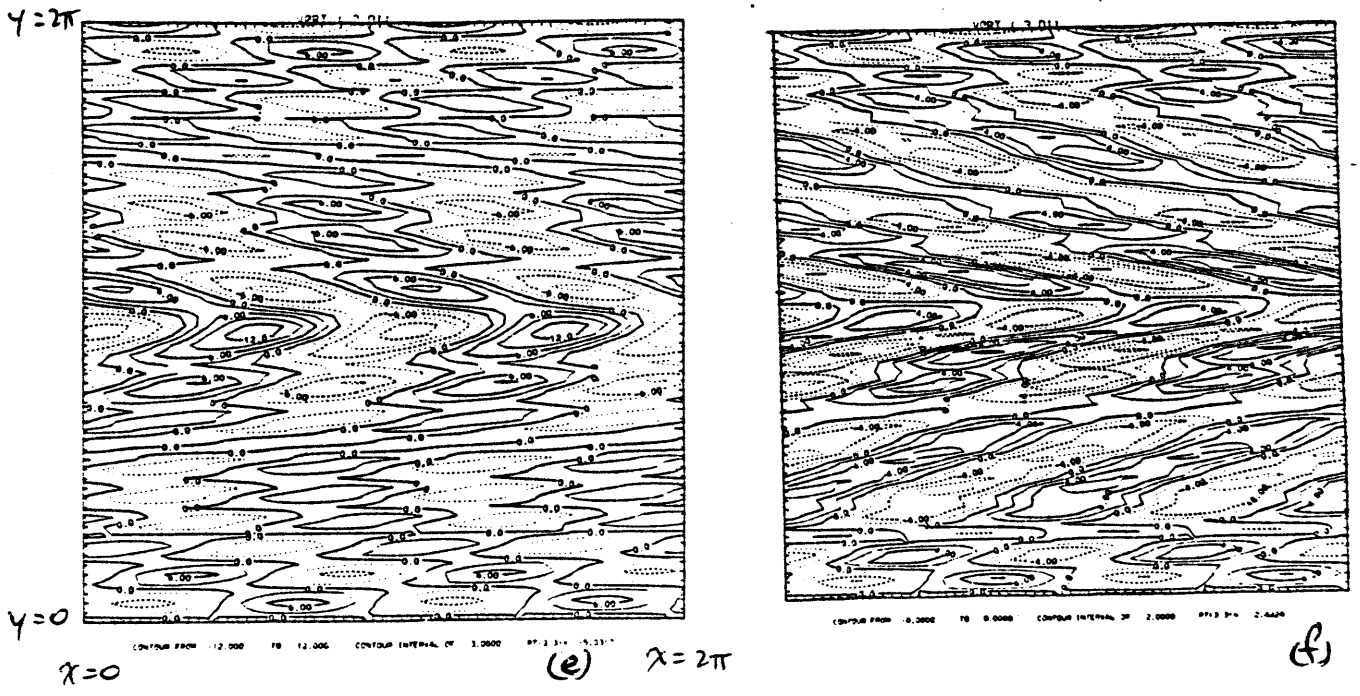


Fig. 7.4: $\nabla^2\phi$ at (e) t = 2.0 and (f) t = 2.5 .

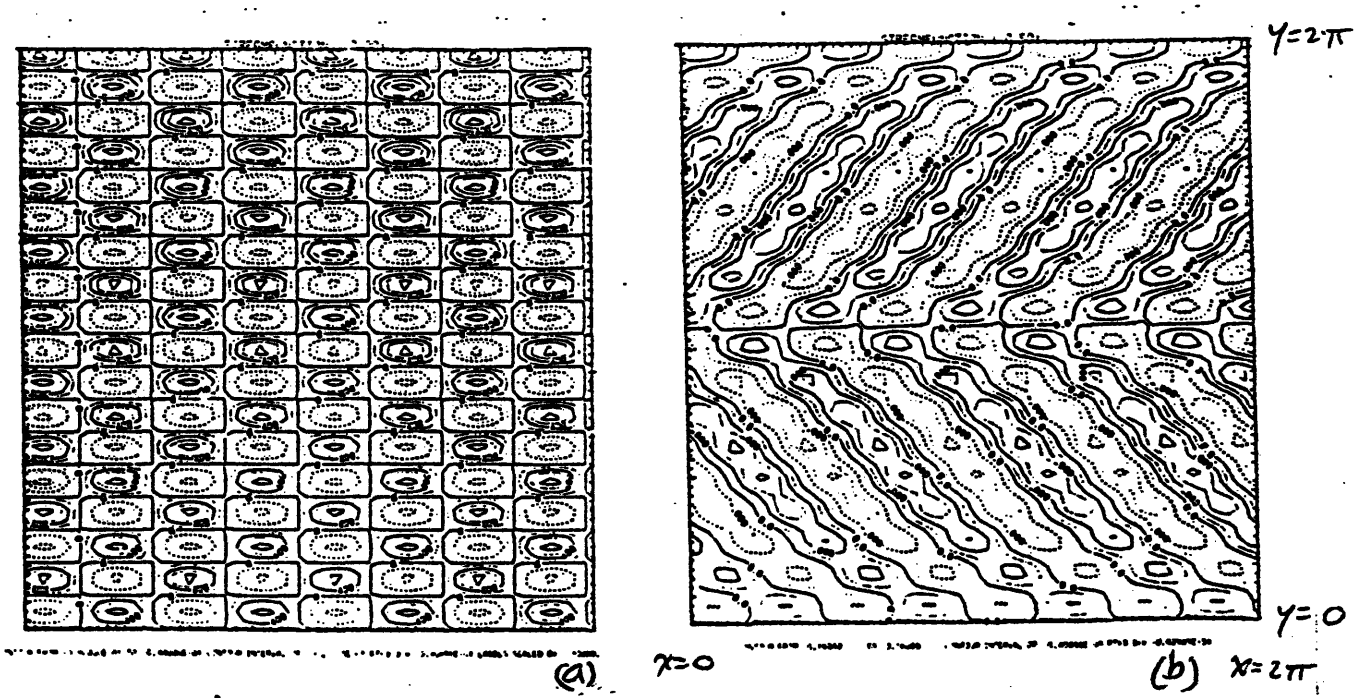


Fig. 7.5: $\phi(x,y)$ for Run R4 at (a) t = 0 and (b) t = 0.5 .

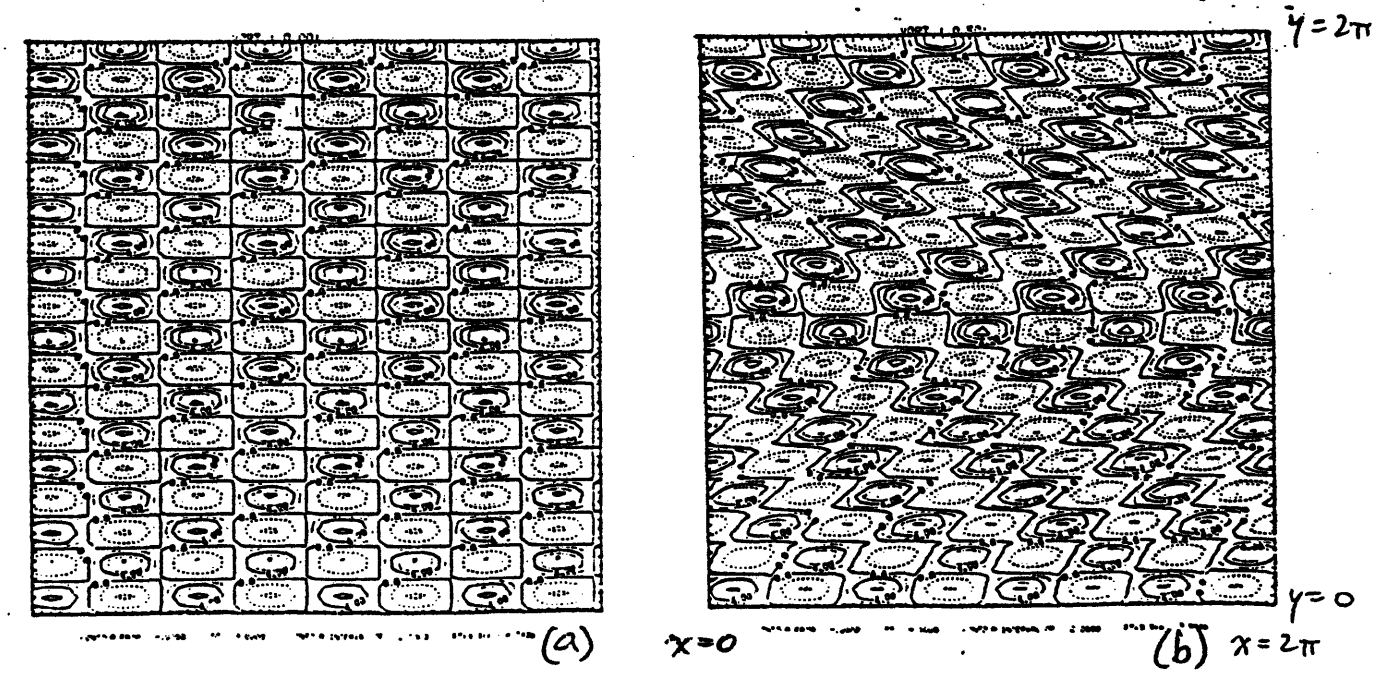


Fig. 7.6: $\nabla^2\phi(x,y)$ for Run R4 at (a) t = 0 and (b) t = 0.5 .

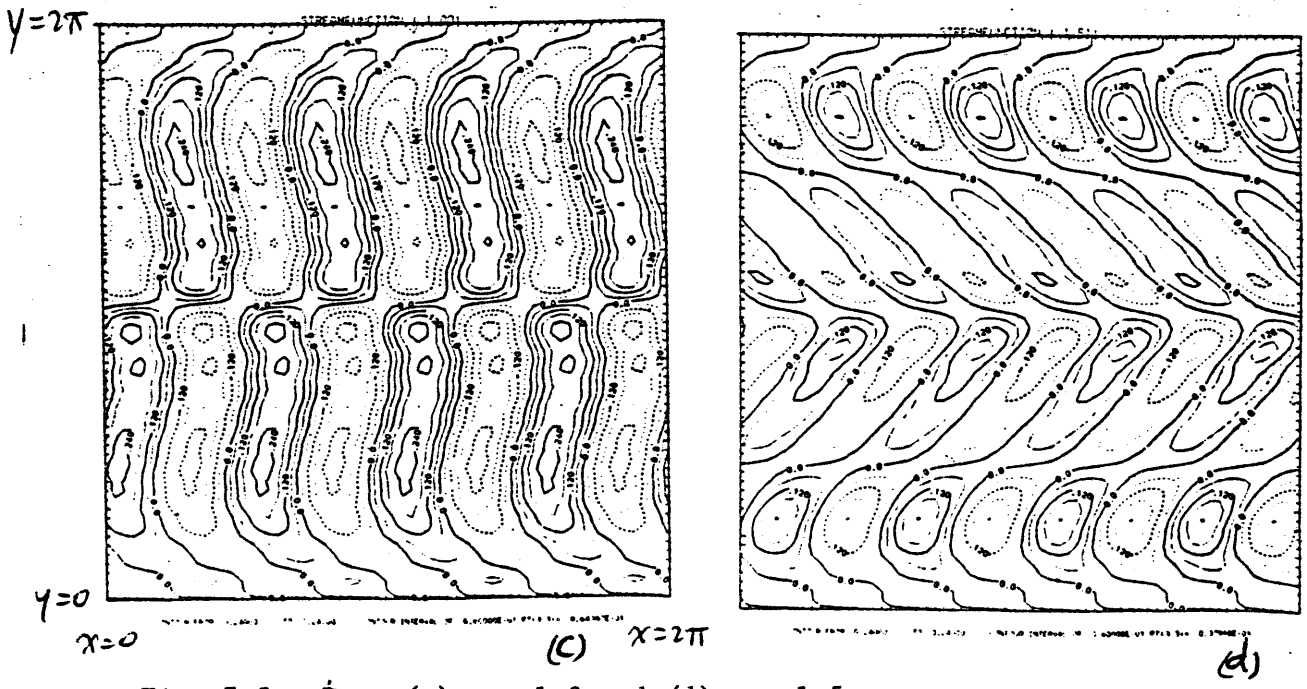


Fig. 7.5: $\dot{\phi}$ at (c) t = 1.0 and (d) t = 1.5 .

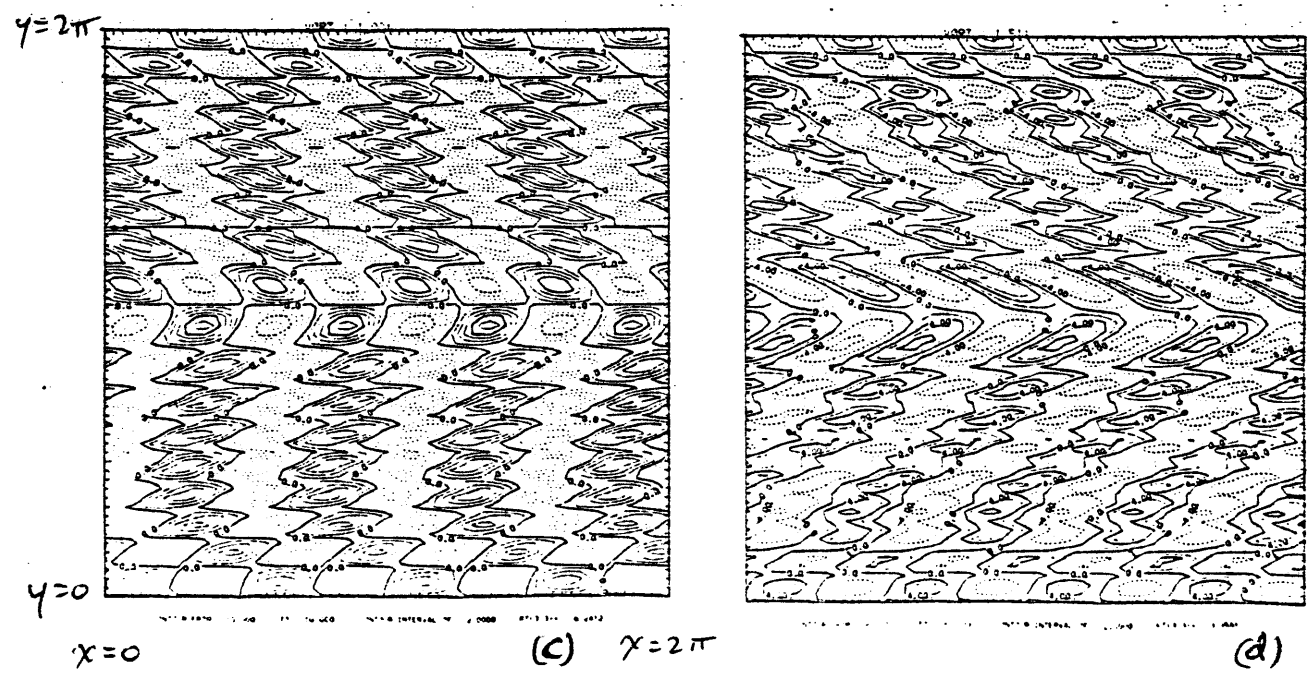


Fig. 7.6: $\nabla^2\phi$ at (c) t = 1.0 and (d) t = 1.5 .

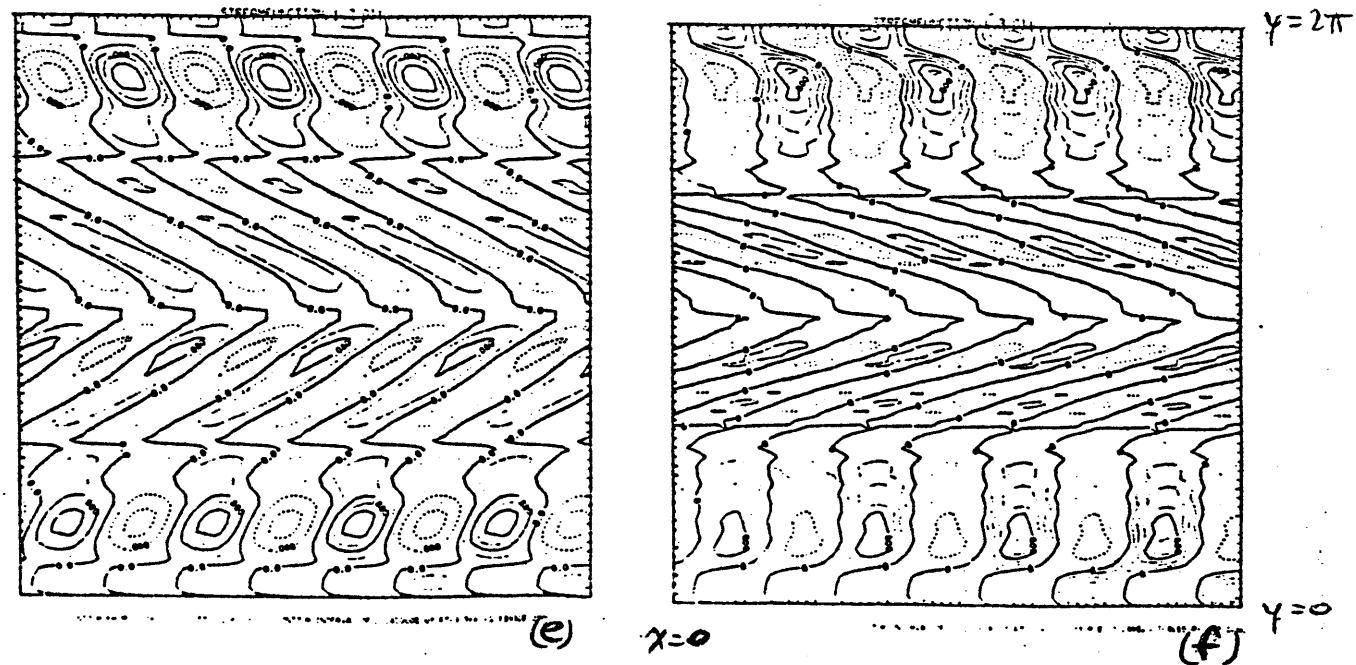


Fig. 7.5: ϕ at (e) t = 2.0 and (f) t = 2.5 .

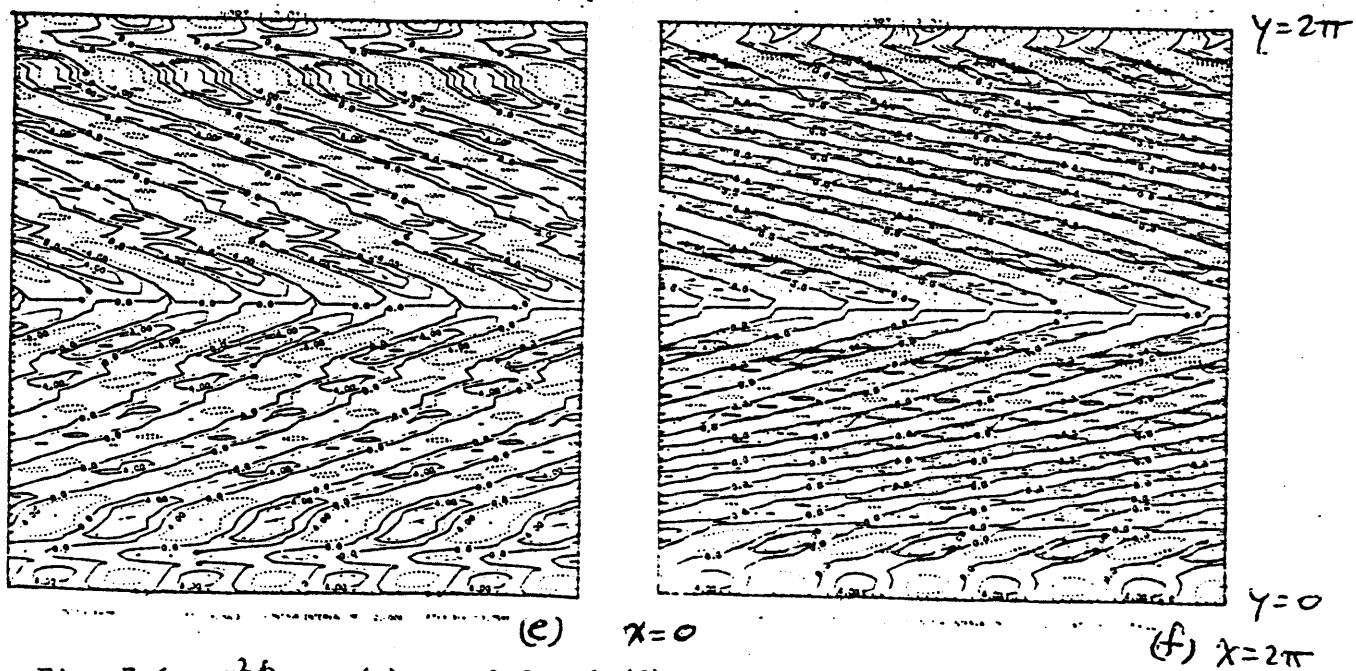


Fig. 7.6: $\nabla^2\phi$ at (e) t = 2.0 and (f) t = 2.5 .

imagines the homogeneous spatial distribution as an ensemble of wave packets centred at various (x_0,y_0) and the specified (k_0,ℓ_0), then the subsequent development is a convolution of the individual wave packet evolution. Each wave packet would consist of a few periods of the fundamental wave, at least in the y direction; since the problem is zonally homogeneous, the WKB problem is posed in the meridional coordinate for each zonal wavenumber k.

Looking at the next maps for t = 0.5 in Run R2 (Figs. 7.3b,7.4b), the dominant effect seems to be advection of the disturbances by the mean flow; the shear in the latter causes the highs and lows to overlap at the edges. The vorticity map shows this advective process clearly. But due to dispersion ϕ and $\nabla^2\phi$ no longer coincide, and the stream-function betrays a larger-scale structure which is actually evident in the vorticity if one squints at the latter (a crude low-pass filter!). The pattern of ϕ is actually opposite to the advective one, unless one looks in detail.

The development at t = 0.5 can also be explained in terms of ray tracing theory, which - it should be noted - is a generalization of rather than an alternative to the advective picture. The "wave packets" with wave crests leaning <u>into</u> the mean shear (i.e. NW-SE in the lower half of the domain, NE-SW in the upper) have those crests tipped towards the vertical by the mean shear, which keeps the zonal scale constant while increasing the meridional scale and decreasing ℓ^2; the latter being the prediction of ray tracing. Similarly the packets with wave crests leaning <u>along</u> the mean shear have those crests tipped towards the horizontal, thus increasing ℓ^2. The first case increases its energy while the second decreases it, so the first is what dominates the ϕ

field: wave crests leaning into the shear, hence anti-advective. However the next shot of ϕ at t = 1.0 (Fig. 7.3c) shows the advective development of this feature, namely towards the vertical, which may also be called meridional anisotropization since $\ell \to 0$.

But the effects of wave propagation are already apparent by t = 1, and become increasingly so thereafter (Figs. 7.3c-f,7.4c-f): energetic large-scale eddies are focussed into the westerly jet, and then slowly begin to radiate away. Since k = 2 disturbances have no turning lines (Fig. 6.5), there is no sign of a trapped waveguide region around y = 0. There may be some evidence however of critical lines at the edges of the easterly jet.

Much the same behaviour is observed in Run R4 (Figs. 7.5,7.6), except that the process is more rapid: ϕ at t = 0.5 (Fig. 7.5b) seems roughly equivalent to ϕ at t = 1.0 in R2 (Fig. 7.3c). There is also less concentration of energy in the westerly jet than before: Fig. 7.5c shows the features extend meridionally across nearly half the domain (the anti-symmetry about $y = \pi$ due to the combination of the anti-symmetry of the mean shear with the initial conditions), whereas Fig. 7.3e shows more concentration near the centre. This may be explained in part by the fact that whereas most disturbances in R4 have turning lines, in R2 the absence of such features prevents much energy from getting into the gravest meridional modes.

Development in run R4 after t = 1 shows radiation away from the westerly jet, with a trapping of disturbances in the easterly jet. In between there presumably lie critical lines. In fact the resolution of the model is inadequate for the rapidly advected structure in this region by t = 2, a point which will be seen again later in the spectral

figures.

The evolution of Run R6 (not shown) is even more rapid than R4, and is already in the radiating and "absorption" phase by t = 1. The resolution looks questionable by t = 1.5 in the regions of strongest shear, though dissipation is clearly doing its job. The disturbances in the westerly jet are slowly eaten away by the shear, until by t = 3.0 there is virtually nothing left; note that for these short waves, unlike the long waves of R2, the group velocities are slower and mean-flow advection is the dominant effect.

The details of what would be "critical-line absorption" are obviously not well represented by these linear simulations; however induced - diffusion (both spectrally and physically) by mean-flow straining clearly takes place, and the overall picture is probably not unrealistic. Note the disturbances trapped near y = 0 by the turning lines, which seem to resist shearing effects quite successfully; they are only weakly dissipated by the friction.

All these remarks are much quantified by looking at the spectral diagnostics. The conversion term seen by the eddies, namely EMI of (7.8c), is shown for Run R as a function of k in Figs. 7.7. There it is clear that in the first day, eddies with $k < 5$ are gaining energy (and enstrophy, since EMI(ENS) = EMI(KE) for each k when integrated over ℓ; but the relative gain of enstrophy is $O(L^2/L_0^2)$ as large as that of energy, which is the WKB error), and those with $k > 5$ losing; during day 2 the cross-over is at k = 3; by day 3 between k = 1 and k = 2; and over the whole run, there is a net loss at all scales (Fig. 7.7d). Note, however, that for these linear runs there is no interaction between waves with different k's.

A projection of the spectral statistics in terms of the "isotropic" 2-D wavenumber n is not particularly well justified for this inhomogeneous, non-turbulent situation, but it serves to illustrate how a linear process manages to masquerade as a nonlinear cascade when represented in this fashion. The KE spectra (Figs. 7.8) show an evolution of the initial peak around n = 10 both up-scale and down-scale, but with most energy moving up-scale; in fact the up-scale-moving disturbances are gaining energy from the mean flow, the down-scale-moving ones losing it, but that is not clear from these figures alone. However the non-turbulent nature of the process should be recognized in the anisotropy of the energy: meridional at large scales (i.e. MKE>ZKE) and zonal at small scales, in agreement with the ray-tracing arguments. The transition moves up-scale from n = 10 with time, as "packets" that had moved up-scale are reflected and proceed down-scale.

A significant amount of eddy energy winds up in n = 2 by t = 1-2 (Fig. 7.8b), which looks like a very rapid "cascade" indeed; however most of it is then lost, as reflected in the relatively smaller time-averaged amplitudes at that and other large scales (Fig. 7.8d).

The spectral interaction terms (Figs. 7.9,7.10) appear, for the first two days, very much like an up-scale cascade of energy and a down-scale cascade of enstrophy, but the interaction consists entirely of triads involving the basic-state flow. The enstrophy is approximately conserved, so this flux interpretation is not unsound as applied to it; however the energy is not, and it is in some sense accidental that the energy gain at large scales appears to largely cancel the loss at intermediate scales, allowing the flux interpretation. By t = 2-3 there is energy loss at almost all scales, but it is clearly related to a

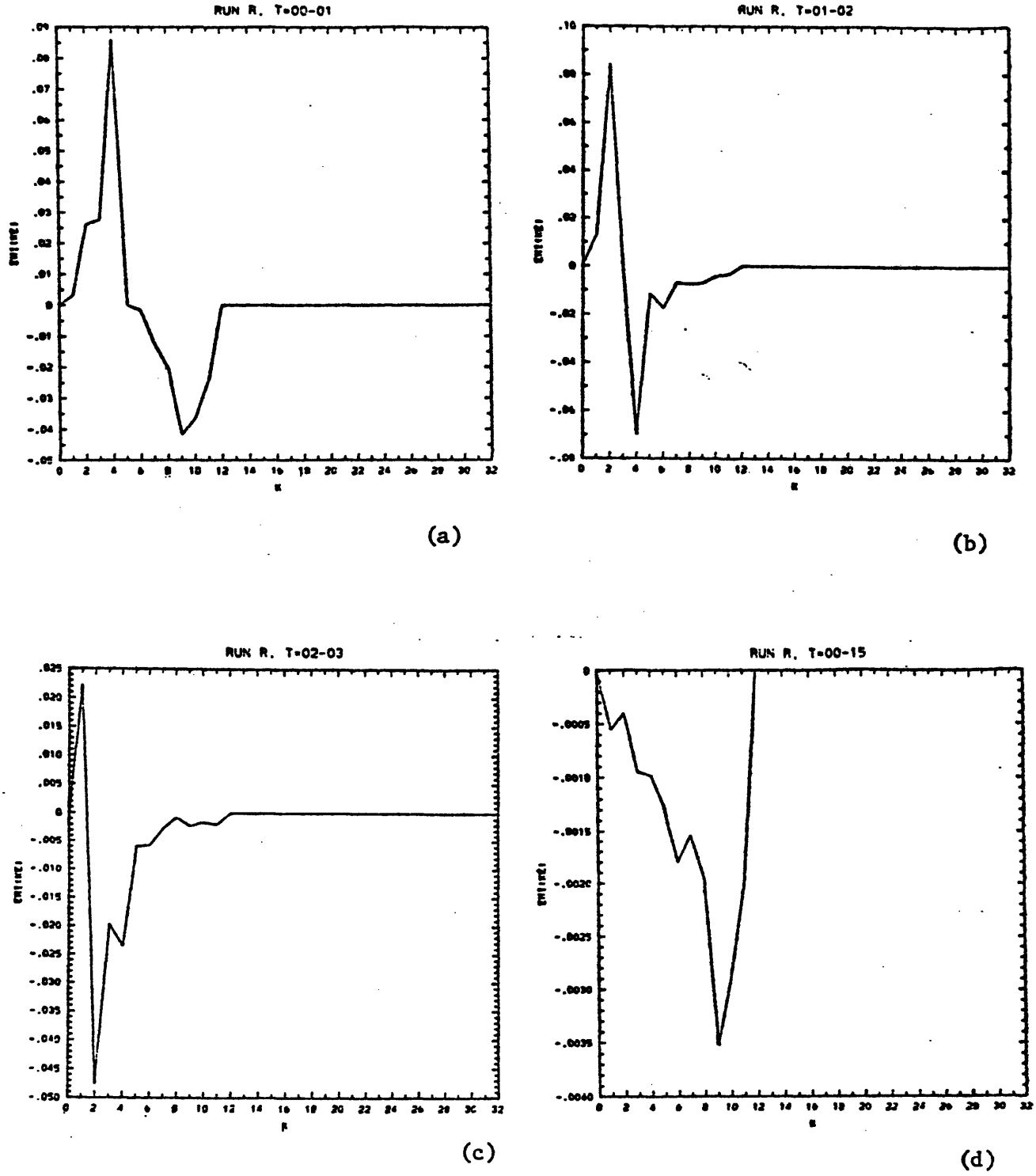


Fig. 7.7: Mean-to-eddy interaction term EMI as a function of zonal wavenumber k, averaged over (a) t = 0-1 , (b) t = 1-2 , (c) t = 2-3 , and (d) t = 0-15 ; for Run R. For this jet, these represent both energy and enstrophy interactions.

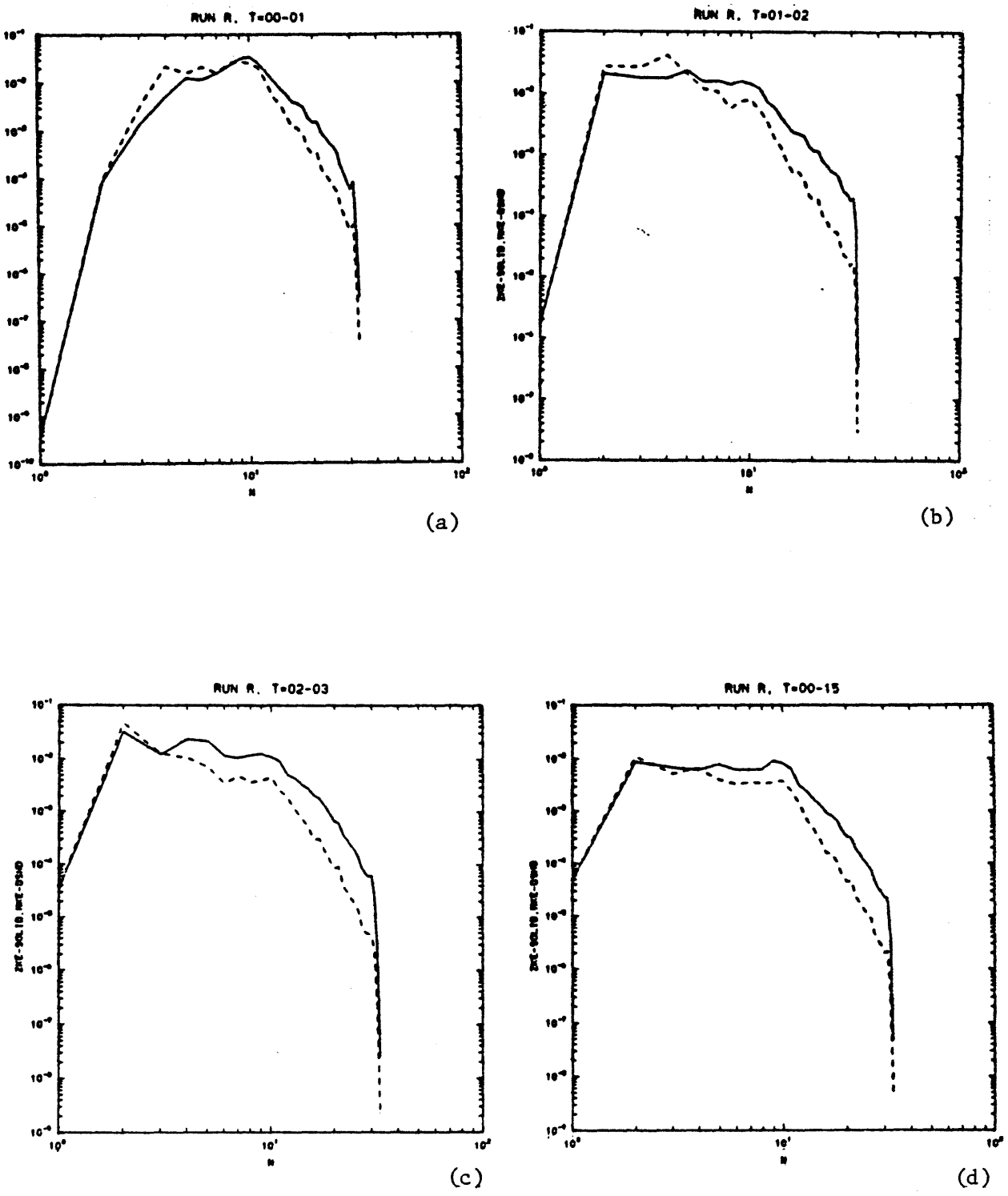


Fig. 7.8: Perturbation energy spectra for Run R, divided into $\langle u^2 \rangle$ = ZKE (——) and $\langle v^2 \rangle$ = MKE (– –) ; averaged over (a) t = 0–1 , (b) t = 1–2 , (c) t = 2–3 , and (d) t = 0–15 .

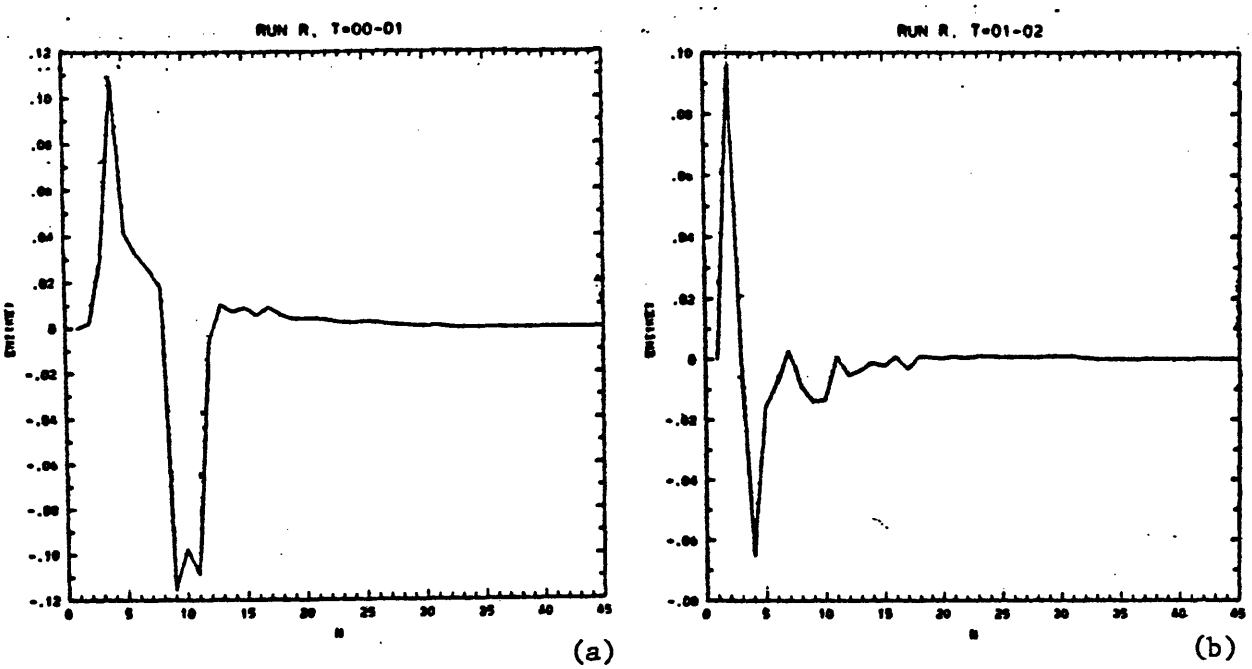


Fig. 7.9: Energy mean-to-eddy interaction term EMI for Run R, as a function of $n = \sqrt{k^2+\ell^2}$, averaged over (a) t = 0–1, (b) t = 1–2.

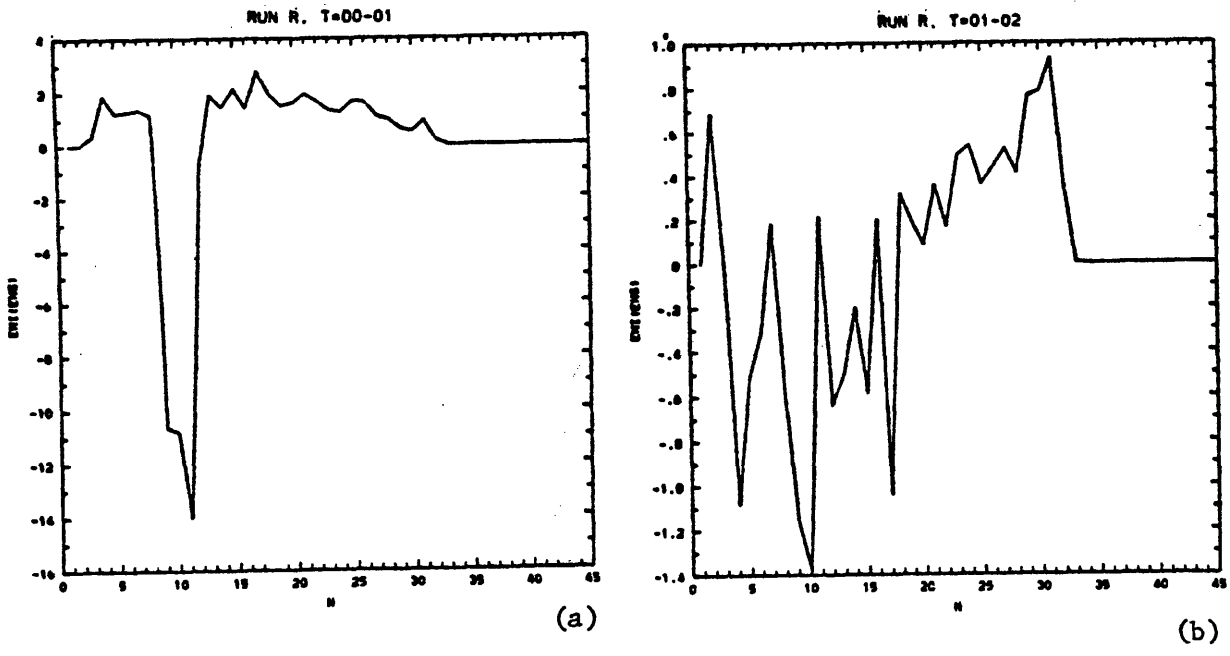


Fig. 7.10: Enstrophy mean-to-eddy interaction term, otherwise as in Fig. 7.9.

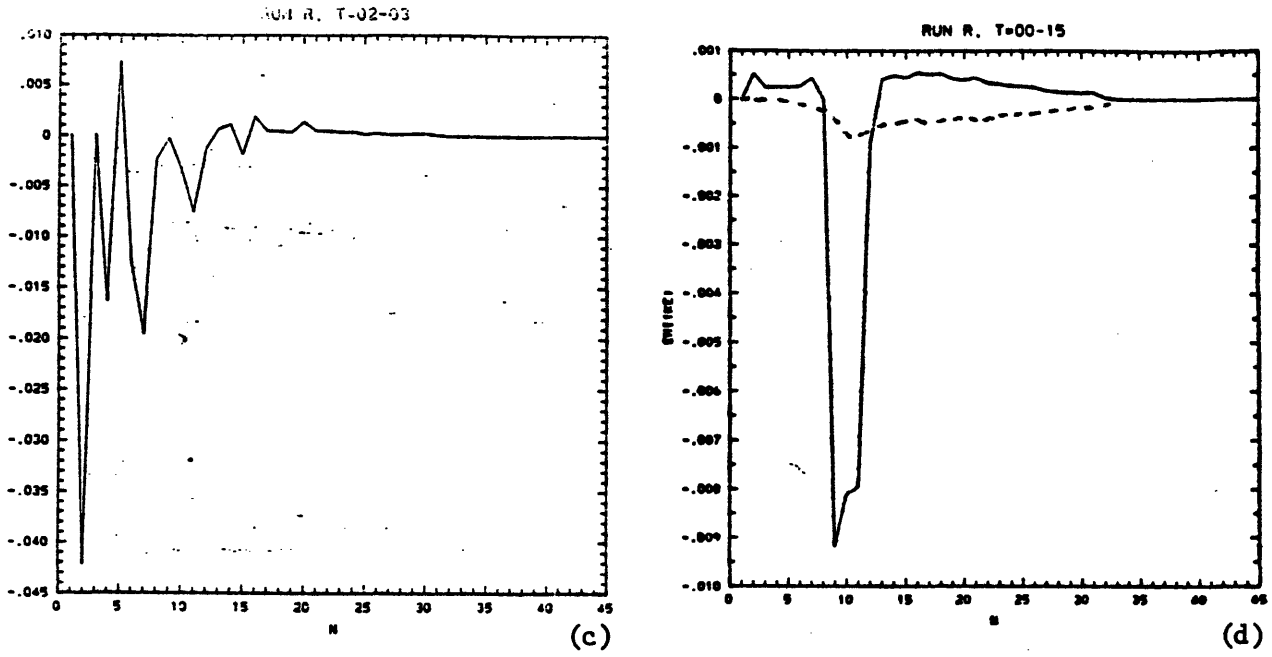


Fig. 7.9: For (c) t = 2-3 and (d) t = 0-15 . In (d), the dashed line indicates the frictional loss.

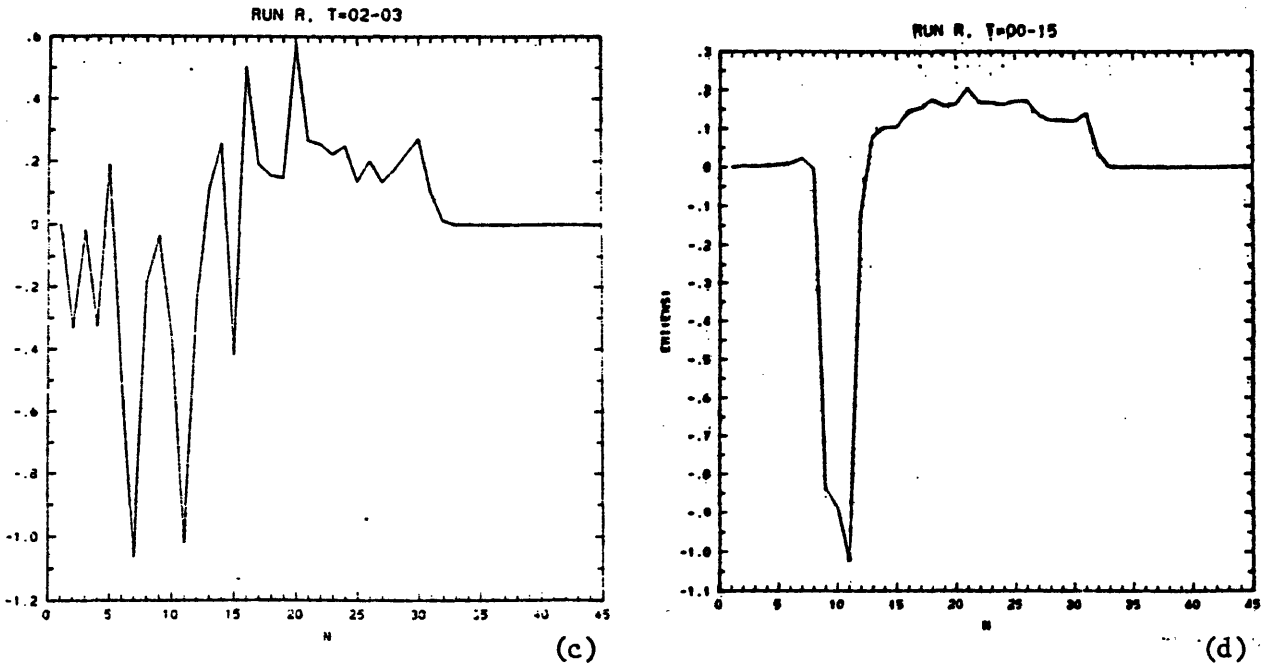


Fig. 7.10: For (c) t = 2-3 and (d) t = 0-15 .

purely down-scale "flux" of enstrophy (Figs. 7.9c,7.10c), something that would be impossible in pure 2-D turbulence. In the average over the run (Figs. 7.9d,7.10d), there is to leading order a net loss of energy at the initial scales, and a net transfer of enstrophy from those scales to smaller ones. Frictional effects are included in Fig. 7.9d, and are seen to closely balance the interaction terms for $n > 15$; however their influence is small for $n < 12$. These features are all sensible, and indicate that the model is representing the key dynamical behaviour despite some aliasing problems at small scales (note the blocking at $n = 32$ in Figs. 7.10b-d).

The 2-D KE spectra show the evolution in more detail (Figs. 7.11), revealing how $k = 4$ to $k = 7$ modes move up-scale first, along lines of constant k, with $k = 4$ dominant; then $k = 2$ and $k = 3$ move up, more slowly but gaining more energy in the process, with $k = 2$ the clear winner over all. $k = 1$ barely moves, even in the $t = 0$-15 average, and $k = 0$ of course moves not at all. The fact that dispersion occurs only along lines of constant k is clearly reflected in the predominantly vertical nature of the contours.

The next sets of figures depict the spectral conversion terms for given k as functions of ℓ, and therein lies the heart of the spectral implications of ray-tracing theory. In each figure two terms are shown which together add up to EMI: VS.ZP represents $V_0 \cdot \nabla \zeta'$, advection of perturbation vorticity by the mean flow; VP.ZS represents $V' \cdot \nabla \zeta_0$, advection of mean vorticity by the perturbation flow; both advection terms are multiplied by the perturbation ϕ to get EMI, of course. The former, VS.ZP, is clearly dominant, as it must be if ray-tracing theory is to have any validity, but less so at the largest scales.

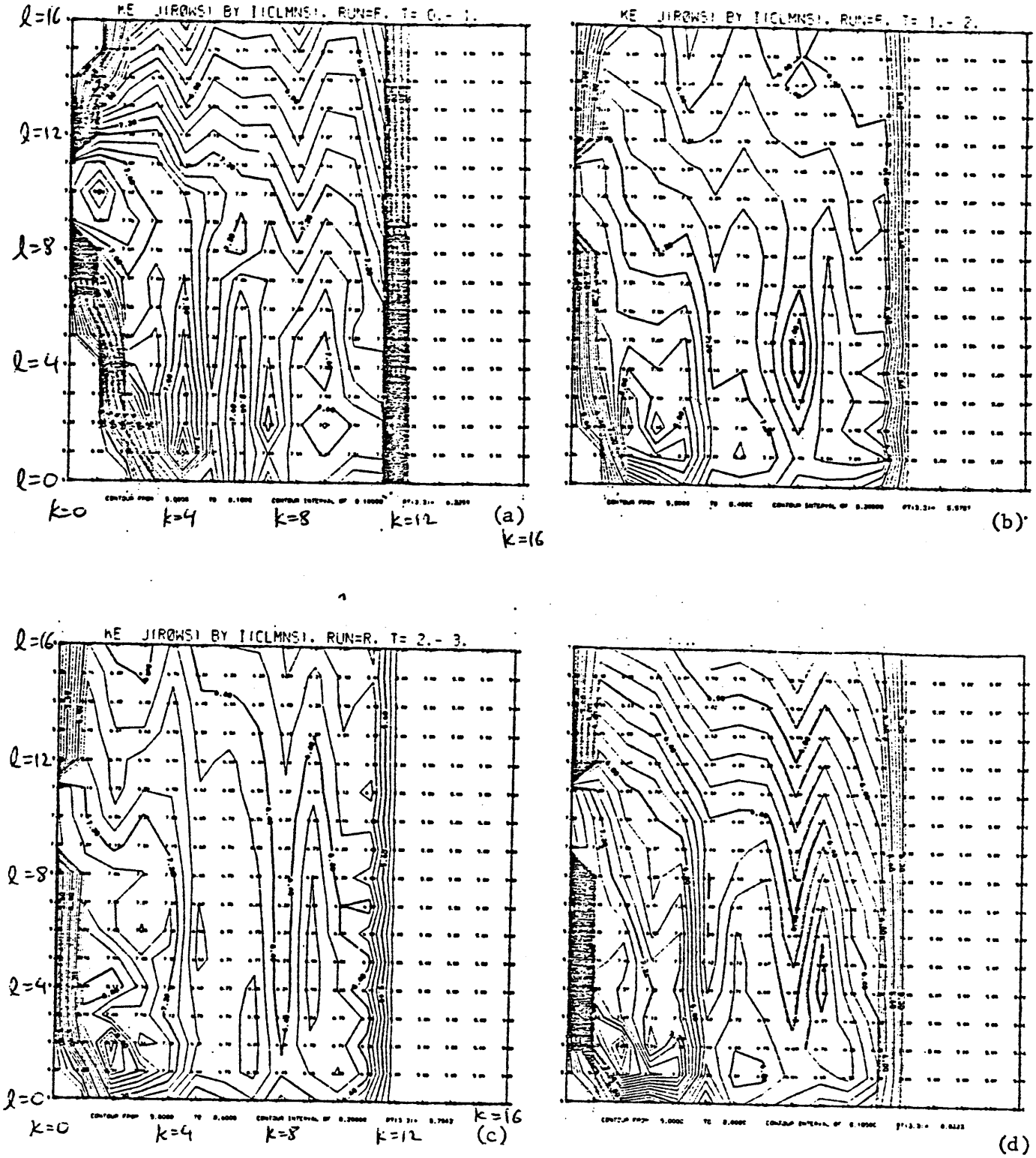


Fig. 7.11: Perturbation energy spectrum $E(k,\ell)$ for Run R, averaged over (a) t = 0–1 , (b) t = 1–2 , (c) t = 2–3 , and (d) t = 0–15. ℓ runs upwards from 0 to 16 ; k runs across from 0 to 16.

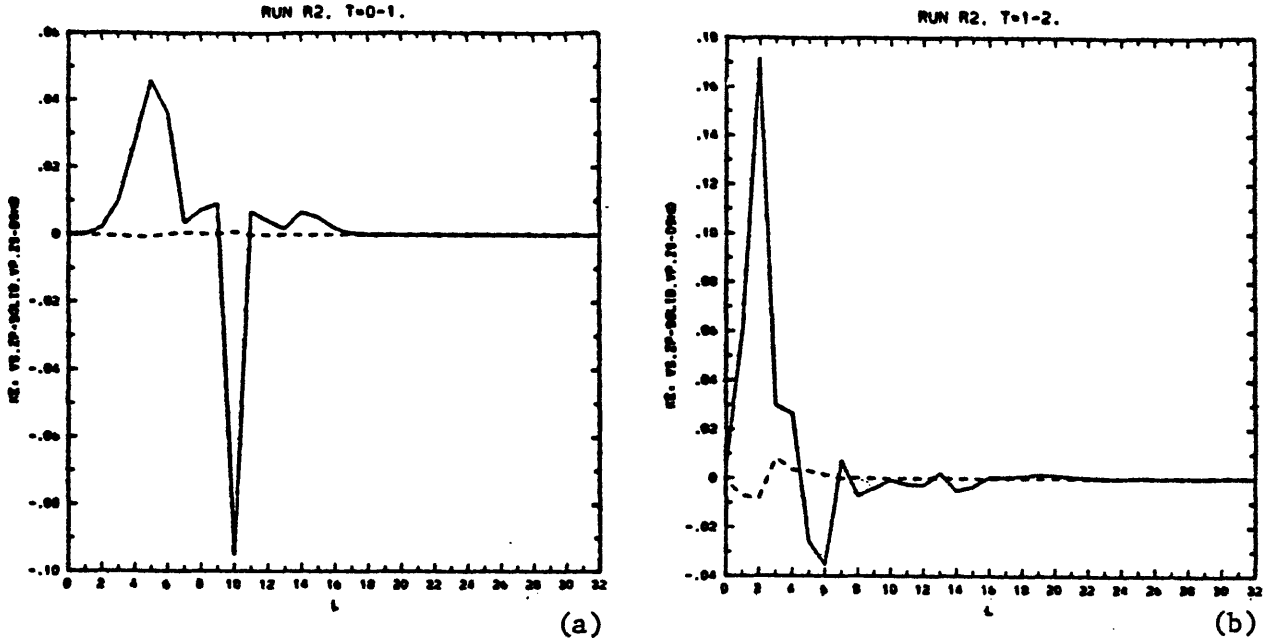


Fig. 7.12: Mean-to-eddy energy interaction term EMI for Run R2, as a function of the meridional wavenumber ℓ. The solid line indicates the part due to $J(\overline{\Psi}, \nabla^2\phi)$, the dashed line that due to $J(\phi, \nabla^2\overline{\Psi})$. Averaged over (a) t = 0–1 , (b) t = 1–2.

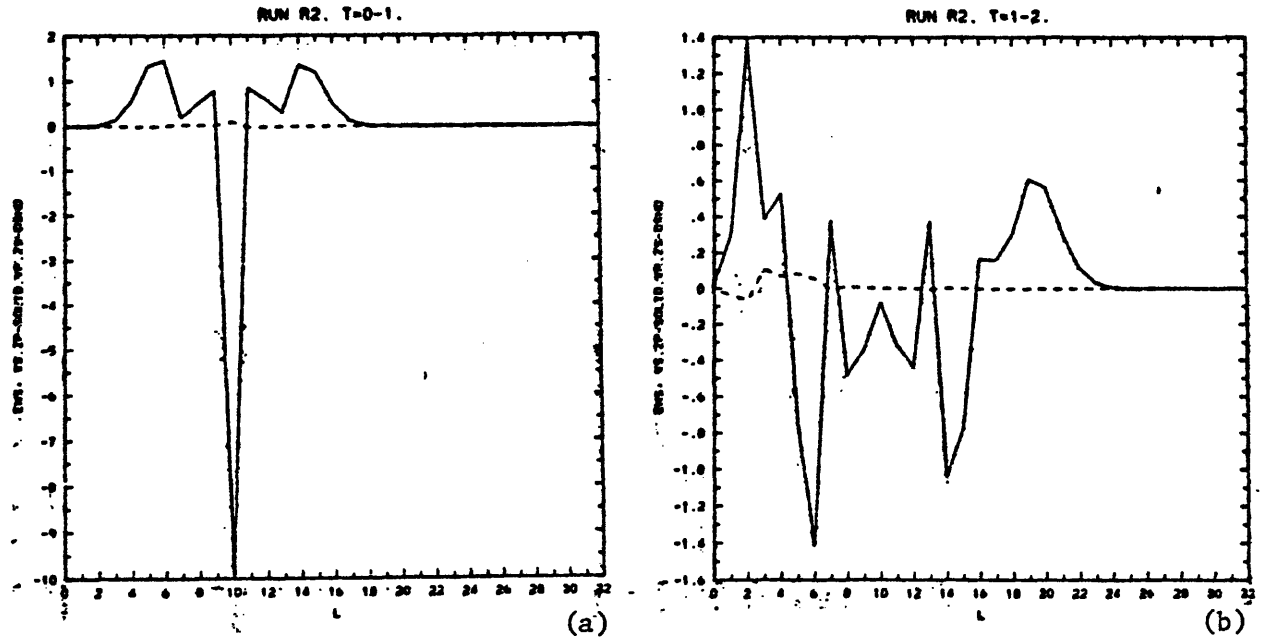
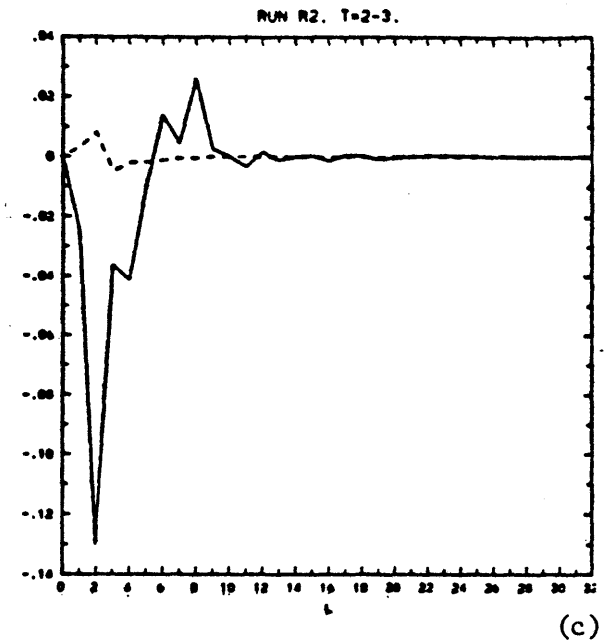
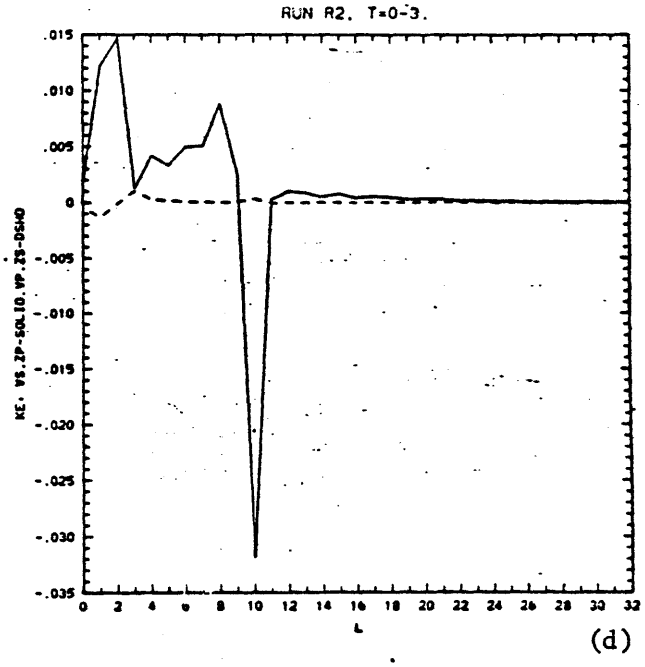


Fig. 7.13: Enstrophy interaction term, otherwise as in Fig. 7.12.

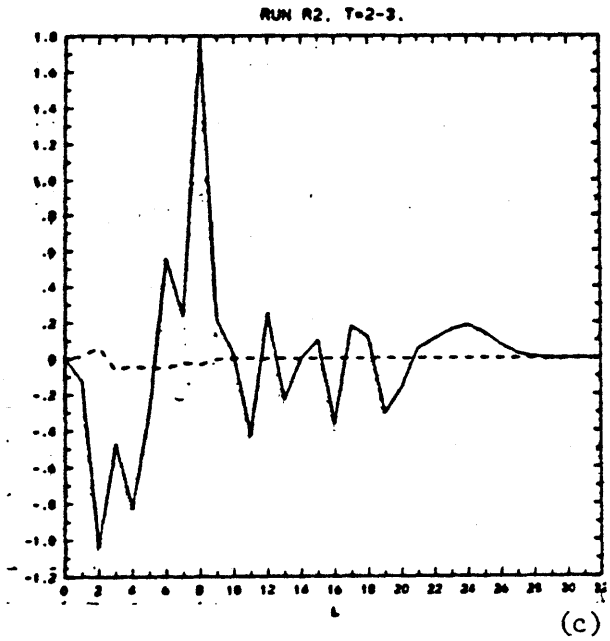


(c)

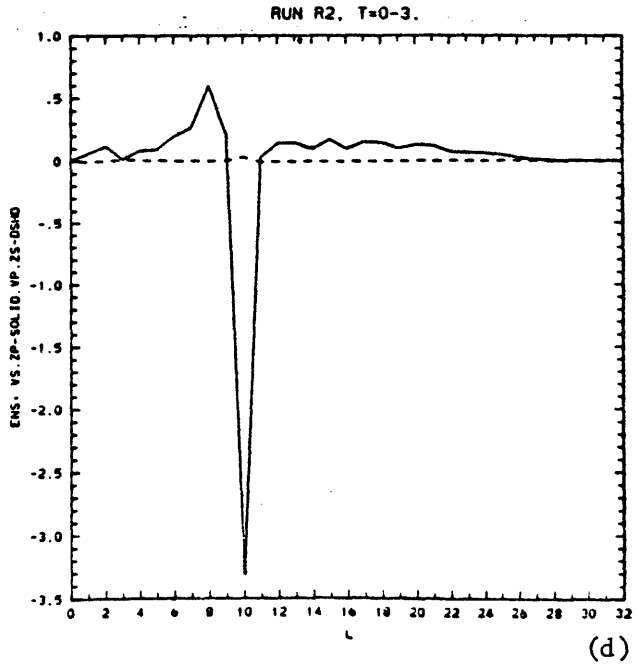


(d)

Fig. 7.12: (c) t = 2-3 and (d) t = 0-3 .



(c)



(d)

Fig. 7.13: (c) t = 2-3 and (d) t = 0-3 .

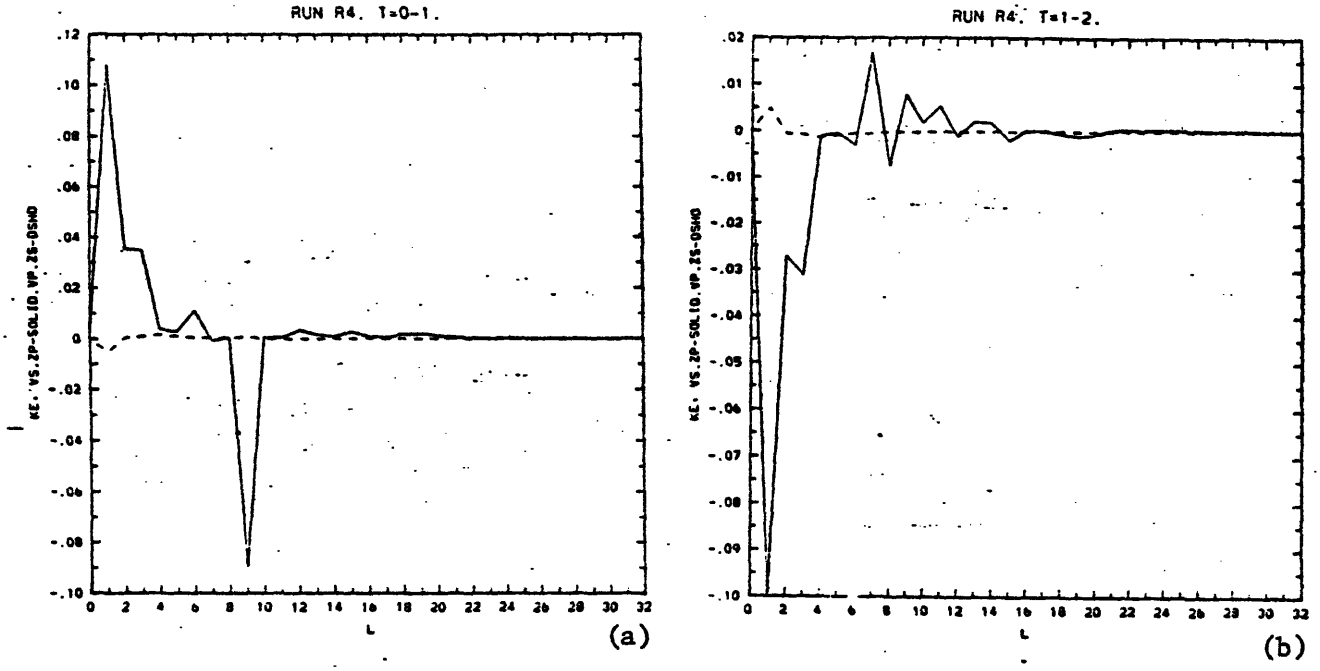


Fig. 7.14: Energy interaction term, as in Fig. 7.12 but for Run R4.

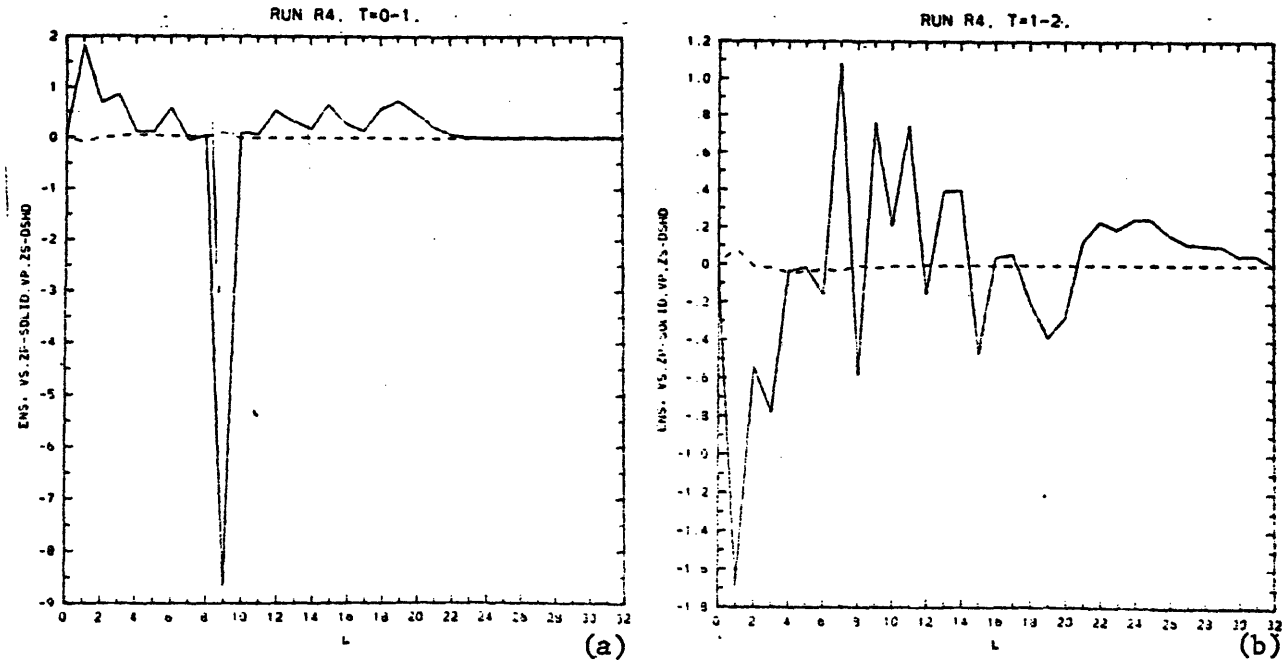
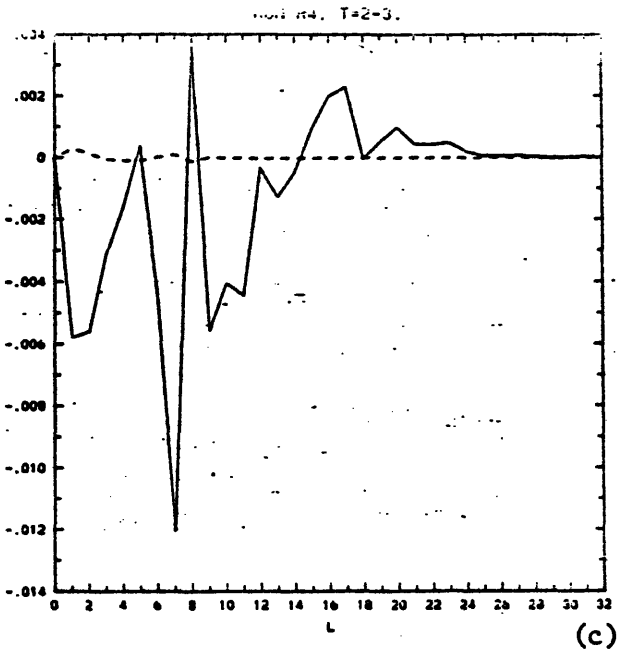
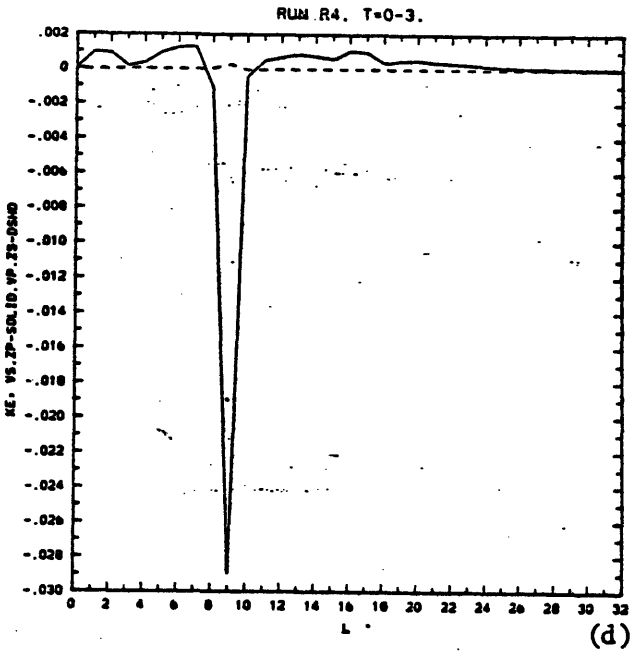


Fig. 7.15: Enstrophy interaction term, as in Fig. 7.13 but for Run R4.

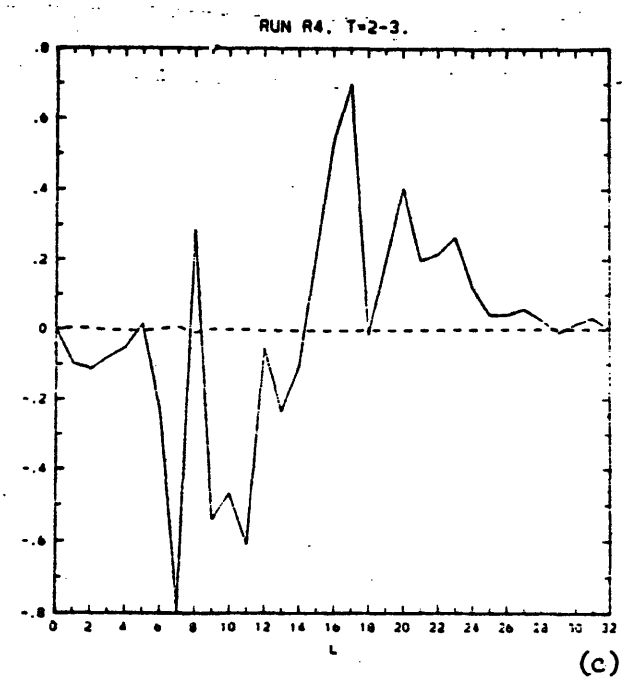


(c)

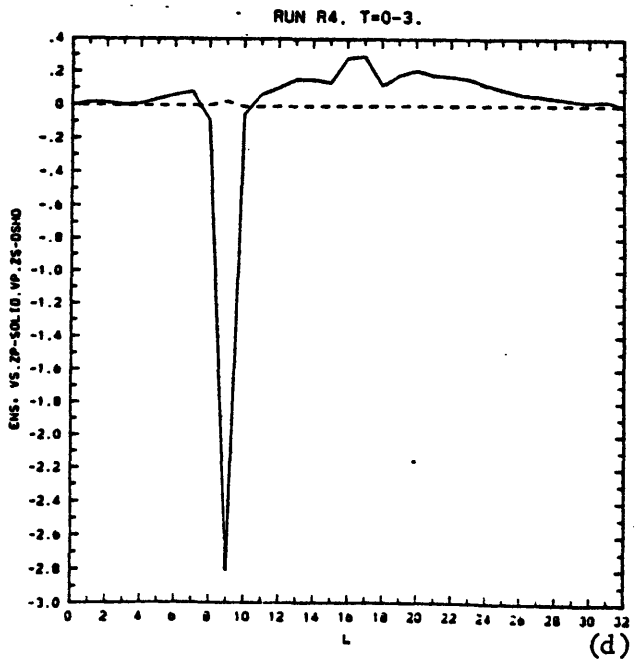


(d)

Fig. 7.14: (c); (d).



(c)



(d)

Fig. 7.15: (c), (d).

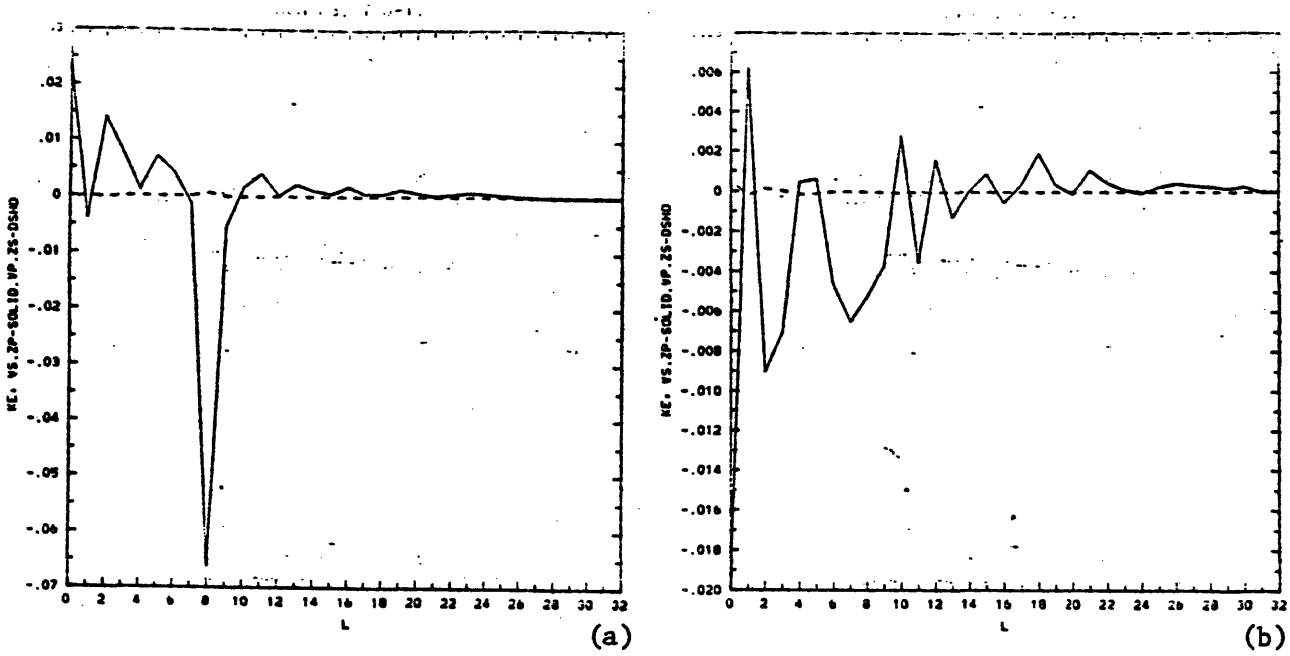


Fig. 7.16: As in Figs. 7.12, 7.14, but for Run R6.

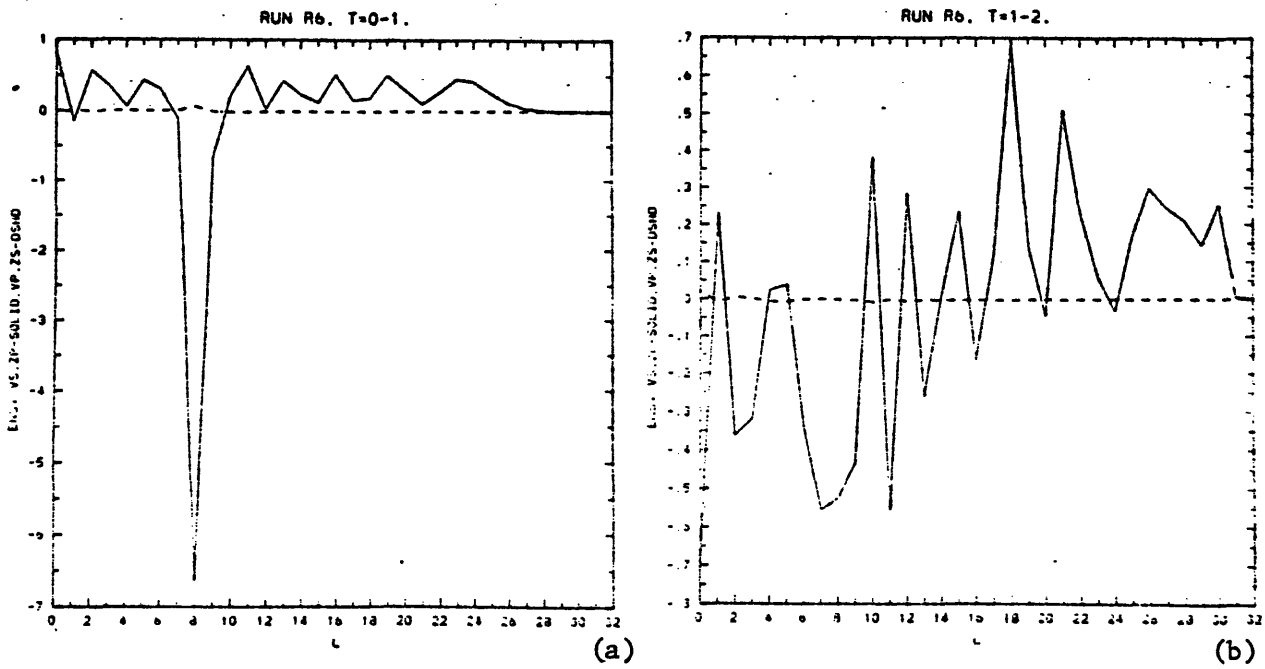
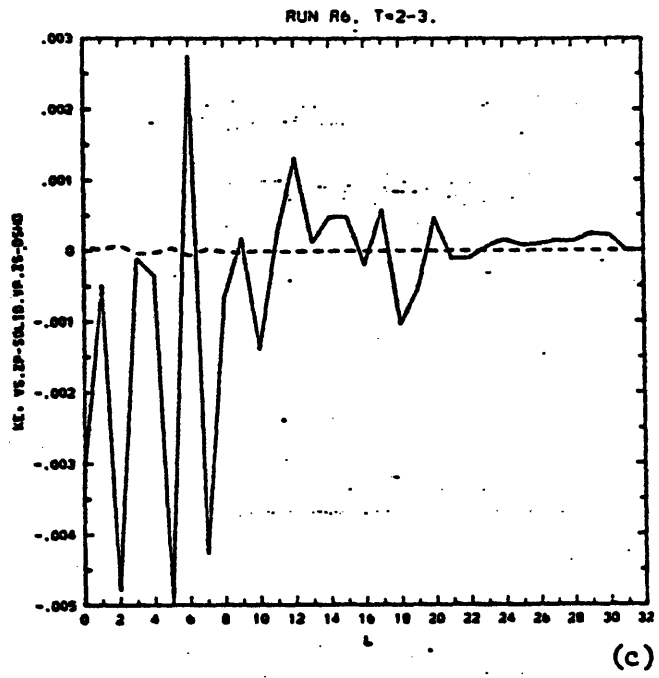


Fig. 7.17: As in Figs. 7.13, 7.15, but for Run R6.



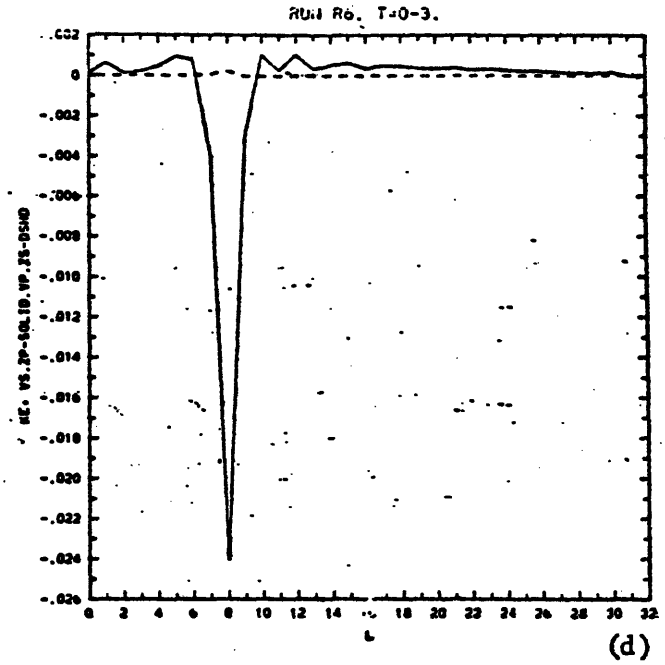
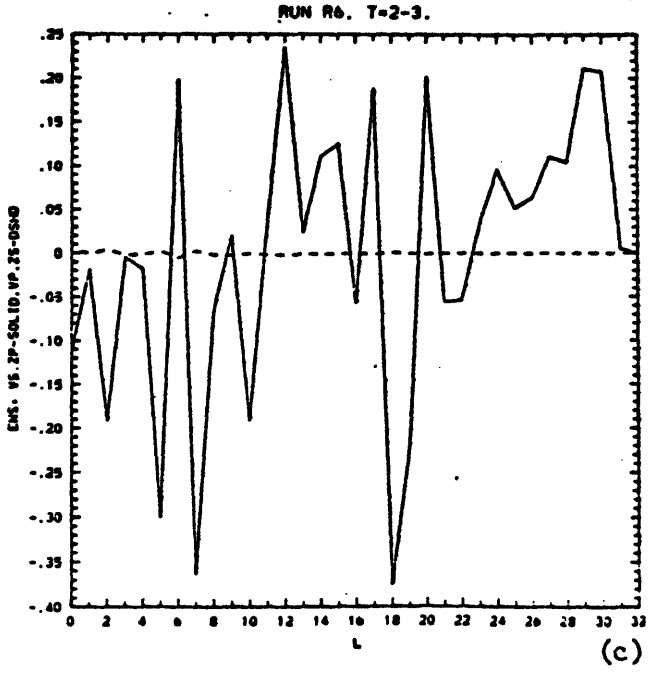


Fig. 7.16: (c), (d).



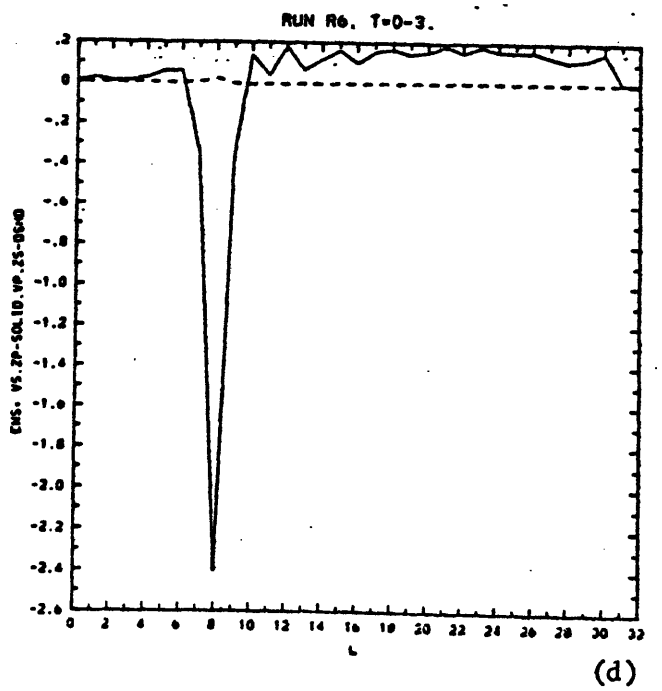


Fig. 7.17: (c), (d).

Figs. 7.12a and 7.13a, showing Run R2 for t = 0-1, apparently represent the initial energy and enstrophy conversion patterns for all disturbances except those with k = 0 or ℓ = 0. These patterns are convolutions of the ensemble of wave packets beginning at the initial wavenumbers, distributed over various y_0, and the clarity of the signal is a vindication of the arguments employed in Chapter VI. Note the close resemblance to the heuristic picture of Fig. 6.8. Since the initial conditions are spectrally symmetric in that both positive and negative ℓ are excited, there are two equal pulses (actually ensembles of pulses) of enstrophy moving to larger and smaller ℓ (Fig. 7.13a). Because of the wavenumber dependence, this translates to a gain of energy for the up-scale pulse and a loss for the down-scale one (Fig. 7.12a). This pair of figures is perhaps the most important in the entire set.

The up-scale pulse in R2 gets as far as ℓ = 2 in day 2, and the enstrophy pattern is still fairly symmetric (Figs. 7.12b,7.13b); but then in day 3 the movement is down-scale everywhere (Figs. 7.12c, 7.13c). Nevertheless the average over the first three days shows a significant energy gain at large scales, and enstrophy transfer in both directions - though the up-scale pulse is evidently returning (Figs. 7.12d,7.13d).

In Run R4 the pattern is repeated, but is more rapid, as the up-scale pulse reaches ℓ = 1 by the first day and is reflected back down-scale thereafter (Figs. 7.14a-c,7.15a-c); consequently the average over t = 0-3 shows a definite asymmetry in favour of down-scale enstrophy transfer, and little net energy gain by the long waves (Figs. 7.14d,7.15d). In Run R6 the up-scale pulse is reflected in the first

day (Figs. 7.16a,7.17a); the subsequent pictures (Figs. 7.16b-d, 7.17b-d) show that the truncation at $\ell = 32$ is playing a role, something that was totally absent for R2 and just hinted at for R4.

These conclusions are presented in a more quantitative fashion in Table 7.1. Note in particular the temporary gain in energy, most quickly in Run R4 but most effectively in Run R2; and the frictional loss of enstrophy, especially in Run R6. The high-order diffusion is clearly mopping up the cascaded enstrophy very effectively.

As far as the spectral truncation and aliasing effects are concerned, ray-tracing integrations can be used to estimate when wave packets obtain median ℓ's greater than 32; Table 7.2 shows approximate times for this as a function of k and y_0. These estimates are consistent with the numbers that have been mentioned for Runs R2, R4, and R6, and show that high-k disturbances are particularly susceptible to this problem - as has been seen in many different ways.

Physical-space diagnostics are also of some interest, although the "signal" contained in them is much less clearly evident than it is for the spectral diagnostics described thus far. This dichotomy is explained by the choice of the initial conditions, which are designed through their spectral compactness and spatial homogeneity for maximal spectral clarity. By a macroscopic version of the famed "uncertainty principle", this necessitates correspondingly unclear physical-space results. Heuristically the difficulty is that eddies seen at a given y and t represent a convolution of wave packets of different k's and y_0's, and it is hard to predict which will dominate. Consequently, less emphasis will be placed on these diagnostics.

Nevertheless certain conclusions can be obtained, provided that

		t=0.0	t=0.5	t=1.0	t=1.5	t=2.0	t=2.5	t=3.0
RUN R2:	KE:	.10	.10	.13	.22	.37	.33	.23
	EMI:	-	.02	.11	.30	.18	-.24	-.16
	EMI/KE:	-	.24	.81	1.36	.48	-.72	-.70
	ℓ_{med}:	10.	9.5	6.5	4.0	2.5	2.0	(1.5,6.)
	ENS:	10.4	10.4	9.8	9.4	8.8	7.9	7.0
	EMI/ENS:	-	.002	.011	.032	.020	-.030	-.023
RUN R4:	KE:	.10	.11	.20	.18	.10	.06	.04
	EMI:	-	.09	.17	-.17	-.11	-.05	-.03
	EMI/KE:	-	.85	.85	-.94	-1.11	-.87	-.64
	ℓ_{med}:	9.0	8.5	2.0	2.5	(2.,6.)	(2.,6.)	(2.,7.)
	ENS:	9.7	9.6	9.1	8.0	6.7	5.7	4.7
	EMI/ENS:	-	.010	.019	-.021	-.017	-.009	-.005
RUN R6:	KE:	.10	.11	.12	.07	.05	.03	.02
	EMI:	-	.07	-.07	-.06	-.03	-.02	-.01
	EMI/KE:	-	.66	-.58	-.80	-.67	-.65	-.52
	ℓ_{med}:	8.0	6.5	(.5,4.)	(1.,5.)	(1.,6.)	(1.,6.5)	7.0
	ENS:	10.0	9.8	9.0	7.2	5.5	3.8	2.7
	EMI/ENS:	-	.007	-.007	-.008	-.006	-.005	-.004

Table 7.1: Time sequence of numerical values of various diagnostic quantities for Runs R2, R4, and R6, integrated over all ℓ; in each case except t=0, the number represents an average over the previous half day. Symbols defined in §7c, except ℓ_{med} which is an estimate of the "median" meridional wavenumber ℓ of the energy distribution: where two values are given, the distribution is bimodal.

	k = 2	k = 4	k = 6
$y_0 = \pi/4$:	6	3	2
$\pi/2$:	4	2	1.5
$5\pi/8$:	4	2	1.5
$3\pi/4$:	5	2.5	2
π:	-	7	5

Table 7.2: Estimated time when the median ℓ of a wave packet exceeds the truncation ℓ=32, based on numerical integration of the ray-tracing equations; as a function of initial position y_0 and zonal wavenumber k. In all cases, $k^2 + \ell_0^2 = 100$.

one is prepared to filter out the "noise". For example, consider the time sequence of Reynolds stresses $\langle\overline{uv}\rangle$, where $u = -\phi_y$ and $v = \phi_x$, the overbar represents a time mean, and the angle brackets a zonal mean. Recall that $-U(y)d\langle\overline{uv}\rangle/dy$ is the eddy-to-mean conversion term for the zonal-mean energy, while $-\langle\overline{uv}\rangle dU(y)/dy$ is the mean-to-eddy conversion term for the eddy zonal energy. The figures that follow are calculated from a coarser grid spacing than is used for the integration itself.

Figs. 7.18 show this sequence for Run R6: in the first day (Fig. 7.18a) one can see a loss of eddy energy in the regions of maximum mean shear, $y = \pi/2$ and $y = 3\pi/2$; and a loss of mean energy in the centres of the mean jets, $y = 0$ and $y = \pi$. In fact, as can be verified from Table 7.1, over $t = 0$-1 there is almost no net energetic mean-eddy conversion for Run R6. The spatial inhomogeneity of the conversion, however, as with the spectral inhomogeneity, can be explained through the ray-tracing and mean-flow straining arguments. Note that for higher k such as $k = 6$ the turning lines occur very close to the initial wave packet locations, as do the critical lines for all k, so no packet travels very far. In the regions of strongest shear, the induced cascade is fastest, and thus already most disturbances are losing energy back to the mean flow; on the other hand where the shear is weakest, namely in the centres of the jets, the induced cascade is still in its early stages, and the net conversion favours the eddies.

In the next two days of Run R6, however (Figs. 7.18b,c), there is eddy energy loss everywhere, accompanied by mean gain, but especially in the jets; in the regions of strongest shear there is evidently no disturbance energy remaining. These conclusions are of course consistent with the corresponding spectral terms, seen in Figs. 7.16b,c and

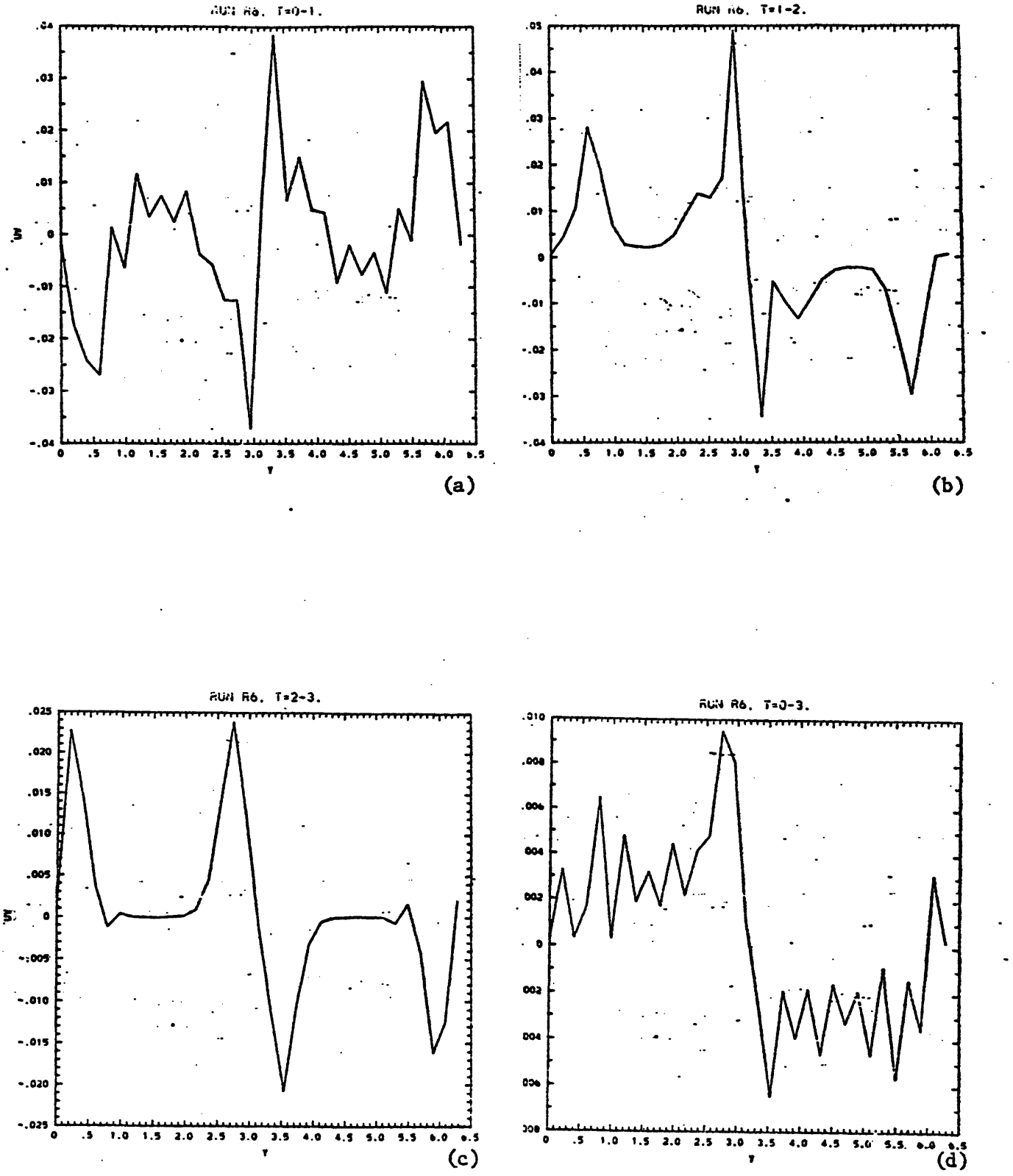


Fig. 7.18: Reynolds stress $\langle \overline{uv} \rangle$ for Run R6, shown as a function of y, averaged over (a) t = 0-1 , (b) t = 1-2 , (c) t = 2-3 , and (d) t = 0-3 .

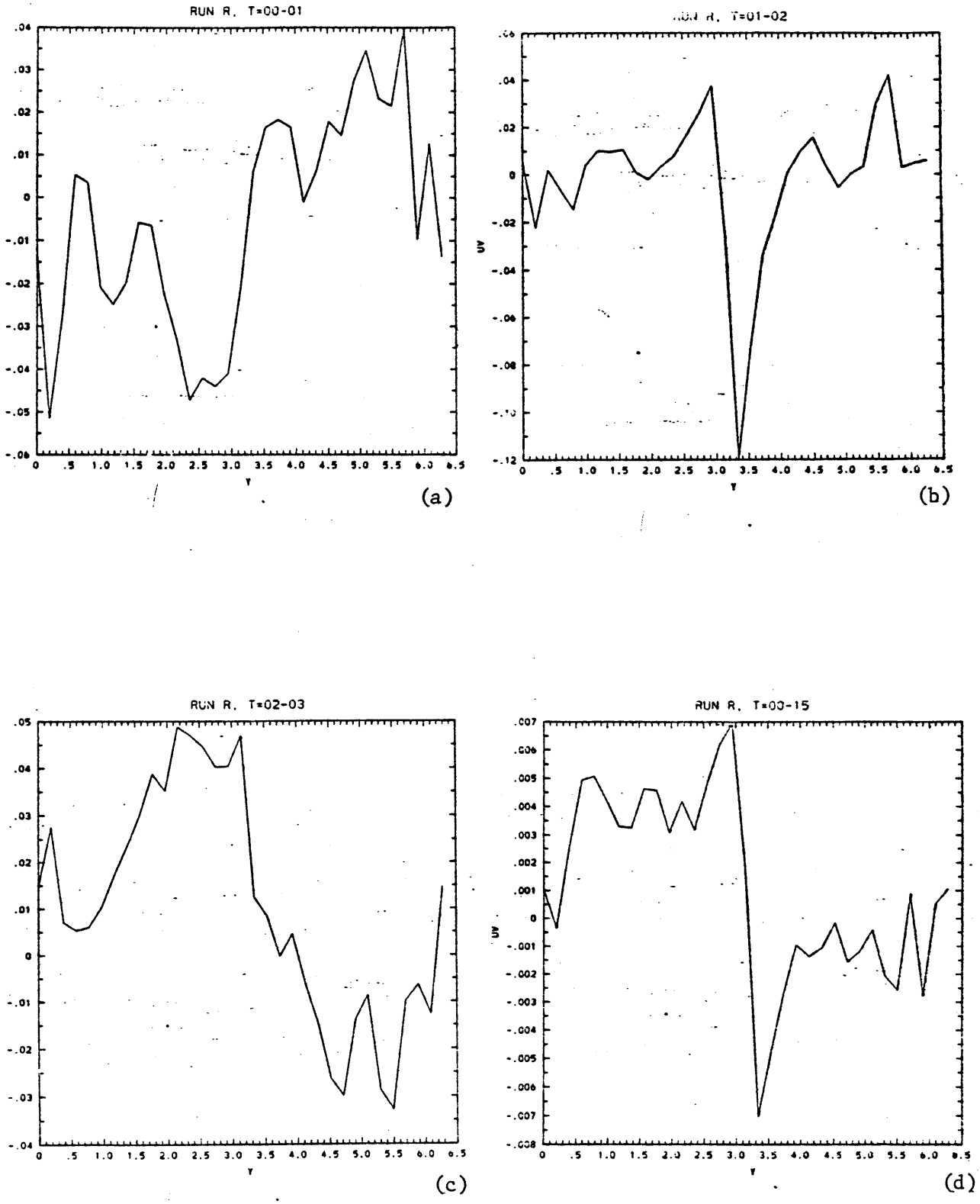


Fig. 7.19: As in Fig. 7.18, but for Run R, and (d) shows t = 0-15 .

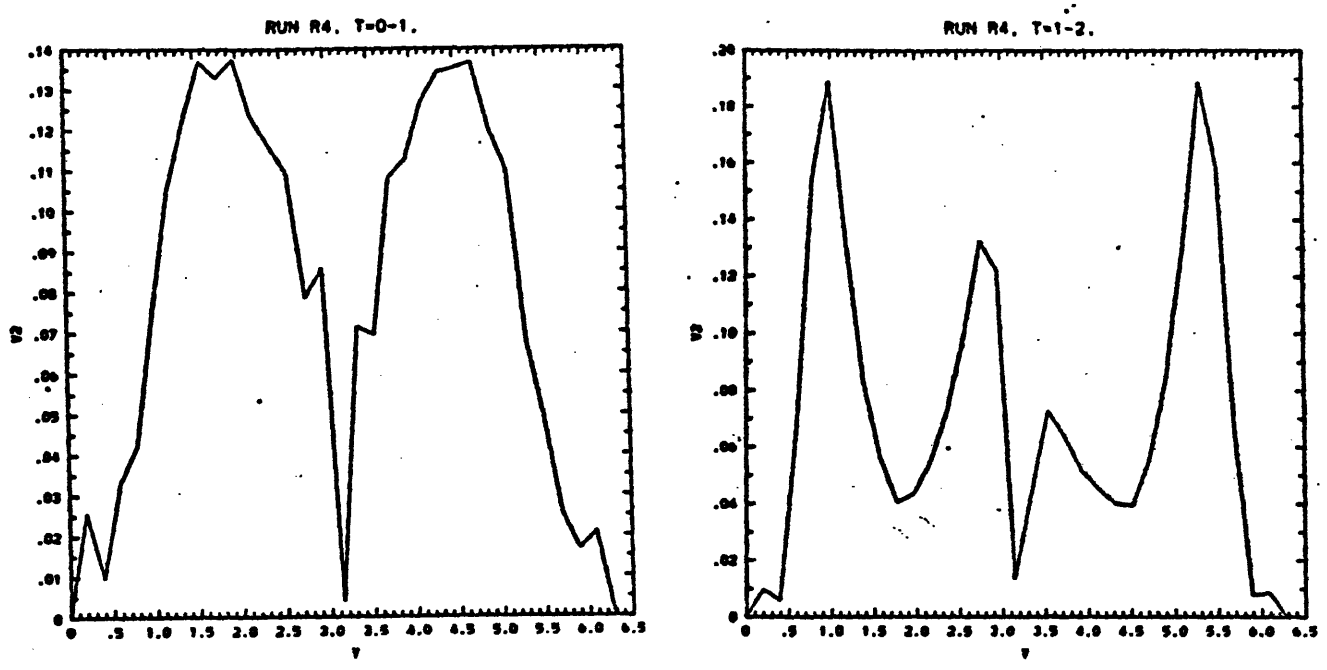


Fig. 7.20a,b: Meridional eddy velocity variance $\overline{\langle v'^2 \rangle}$ for Run R4, as a function of y, averaged over (a) t=0-1 and (b) t=1-2.

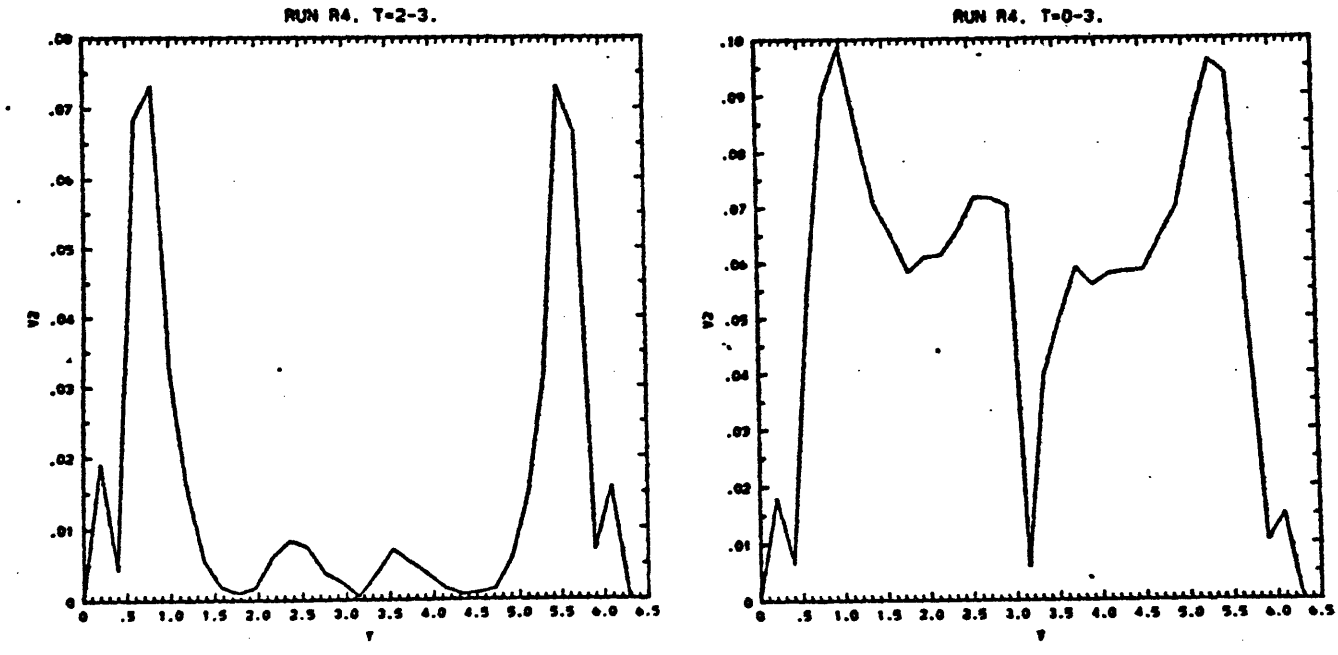


Fig. 7.20c,d: Same as above, for (c) t=2-3 and (d) t=0-3.

Table 7.1. Averaged over the first three days (Fig. 7.18d) one sees $\langle\overline{uv}\rangle dU/dy > 0$ for all y, indicating eddy energy loss, with maximum loss in the strong shear regions; and mean energy gain concentrated in the westerly jet with a much weaker gain spread over the easterly jet. Even this last finding can be understood in terms of the absence of critical lines for k = 6 disturbances originating close to y = 0 (see Fig. 6.5).

All of these conclusions can be seen, though developing on a slower timescale, in Runs R2 and R4; however the patterns are much less easily interpretable since packets move further from their original locations. When one examines Run R itself (Figs. 7.19) the picture is of a double ensemble of wave packets, if one sticks to the ray-tracing interpretation, so it is not too surprising that the findings are less clear-cut. In the first day (Fig. 7.19a) there is a gain of eddy energy in the strong-shear regions, which can presumably be attributed to the fast up-scale cascade of low-k disturbances, and a corresponding loss of mean energy. The situation is rather mixed for t = 1-2 (Fig. 7.19b), and by the third day (Fig. 7.19c) is the opposite of the first. Averaged over the entire 15-day run (Fig. 7.19d), the picture is not unlike Fig. 7.18d for t = 0-3 in Run R6, except that there is significant eddy energy loss in the entire southern half of the domain. The lack of symmetry about $y = \pi$ in Fig. 7.19d can only be attributed to the initial conditions; it is, however, not all that surprising when one remembers that a large portion of the initial energy is in low-ℓ modes around k = 10: a slight phase shift in y could thus strongly affect the physical-space eddy energy budget. However the mean energy conversion term is unaffected by the addition of a constant to the Reynolds stress, which could render Fig. 7.19 anti-symmetric about $y = \pi$.

As a final diagnostic, Figs. 7.20 show the meridional eddy velocity variance $\langle\overline{v'^2}\rangle$ for Run R4. This quantity was found in the calculations of §6d to be far more sensitive than was $\langle\overline{u'^2}\rangle$ to ℓ-space dispersion, hence only the former is shown here. Fig. 7.20a depicts the maximum amplification near turning lines (see Fig. 7.14a), then in the next day disturbances are beginning to radiate away from the westerly jet (Fig. 7.20b). The pattern of Fig. 7.20c is indicative of absorption near critical lines in the easterly jet as the rays slow down, and all these features are evident in the instantaneous vorticity maps (Figs. 7.6). In the time average of the run (Fig. 7.20d) there is a broad distribution of variance except in the jet core regions, but since this figure combines the behaviour of many different wave packets its interpretation is difficult.

§7e. Discussion of the Nonlinear Runs

The emphasis of this section is on the fully nonlinear Run 0, to see how it compares with the linear Run R, discussed above, and with pure beta-plane turbulence, Run P. To compare the instantaneous streamfunction and vorticity maps, it is helpful to filter the basic-state flow component out of the fields in Run 0 and simply show the "perturbation" maps. The initial conditions for all three runs are, apart from the basic-state, identical, and are those of Figs. 7.1a and 7.2a.

The development of Run P, shown in Figs. 7.21, exhibits the up-scale energy and down-scale enstrophy transfers of 2-D turbulence in the early part of the run; by t = 4 it has acquired large-scale zonal anisotropy with a fairly well-defined meridional scale ℓ_β, as predicted by the beta-plane turbulence theory of §3c (Fig. 7.21c). While

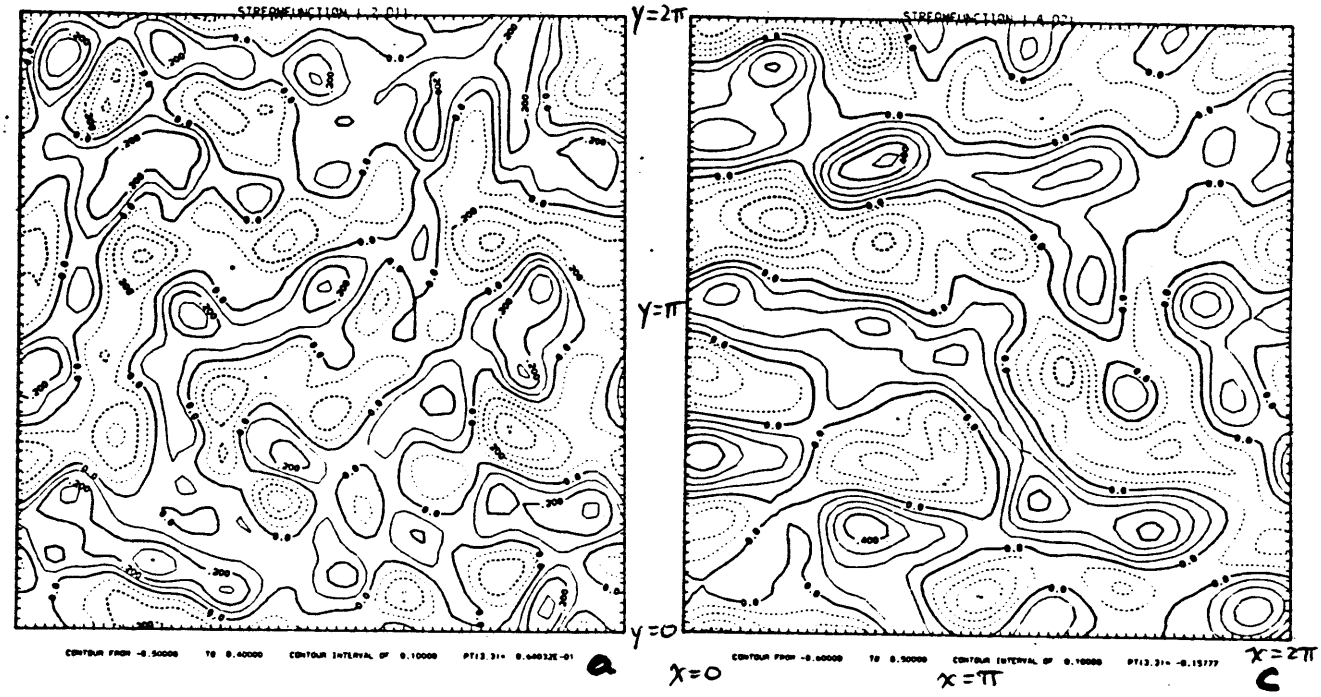


Fig. 7.21a,c: Instantaneous spatial map of the streamfunction field ψ for Run P at (a) t=2 and (c) t=4.

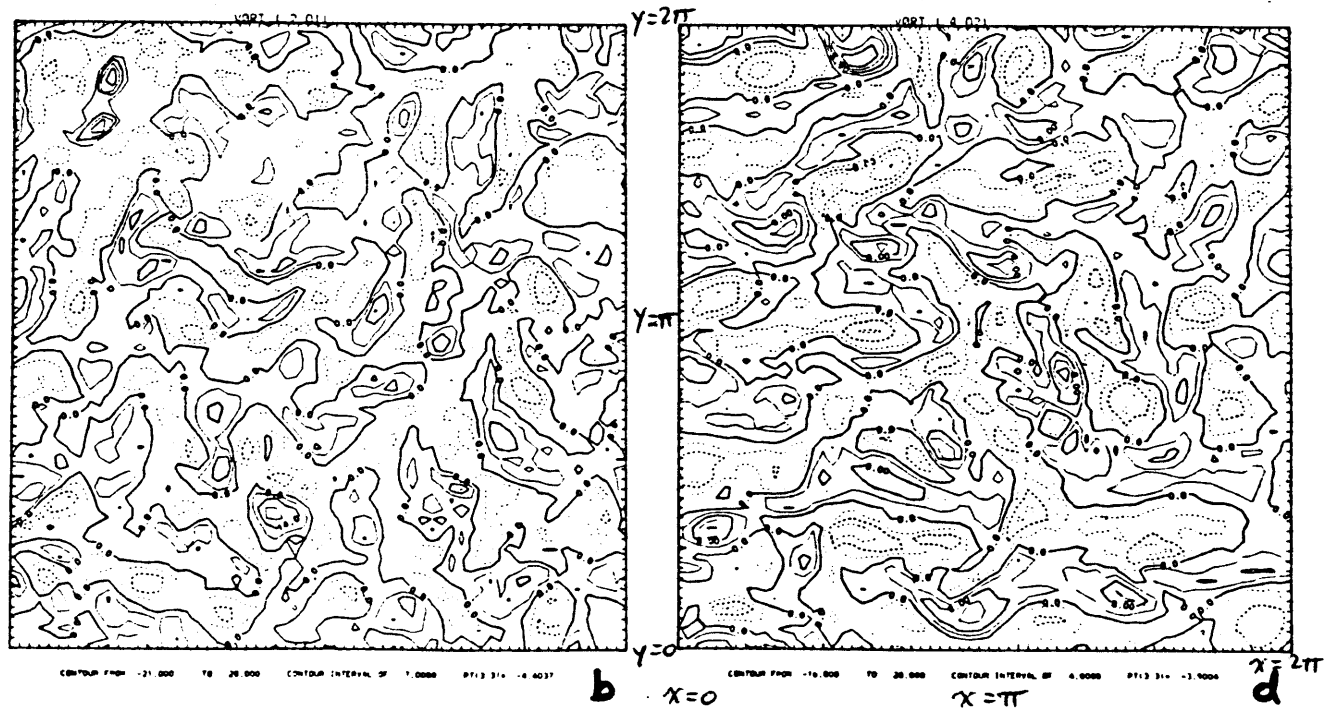


Fig. 7.21b,d: Instantaneous spatial map of the vorticity field $\nabla^2\psi$ for Run P at (b) t=2 and (d) t=4.

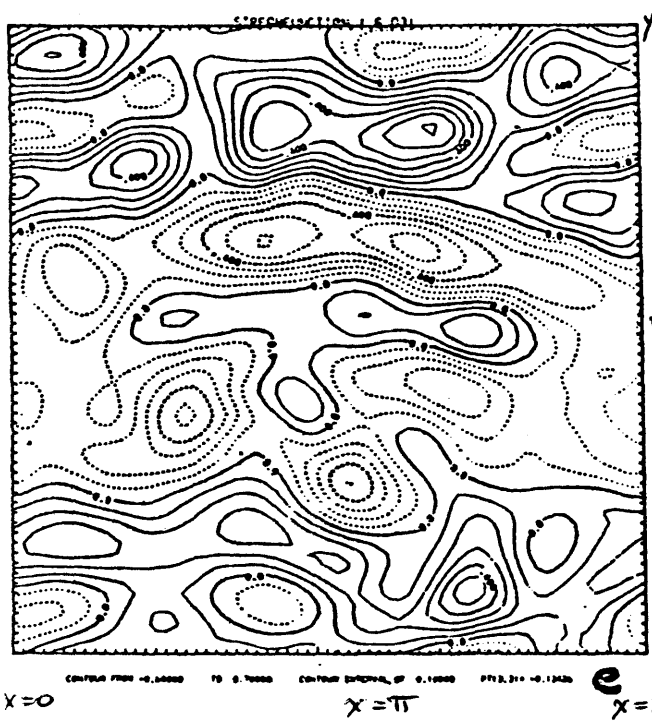


Fig. 7.21e: Streamfunction map for Run P at t=6.

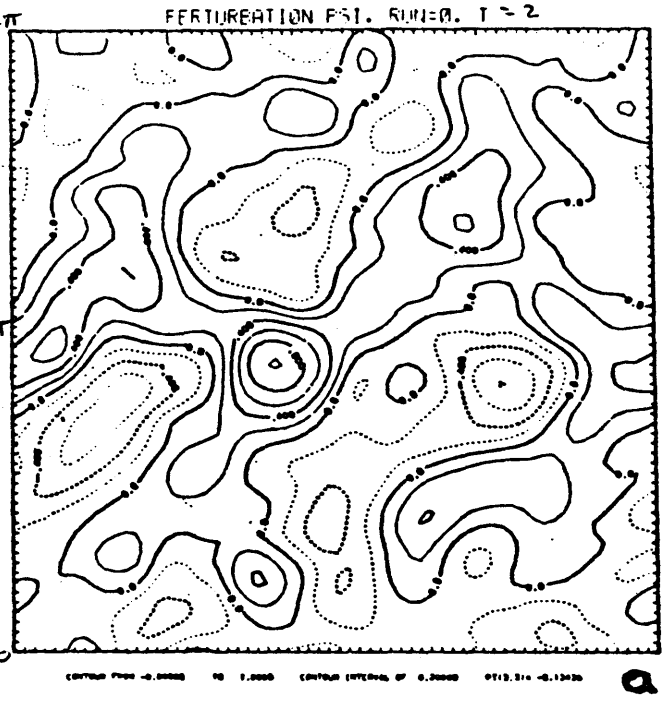


Fig. 7.22a: Instantaneous map of the perturbation streamfunction field ϕ for Run 0 at t=2.

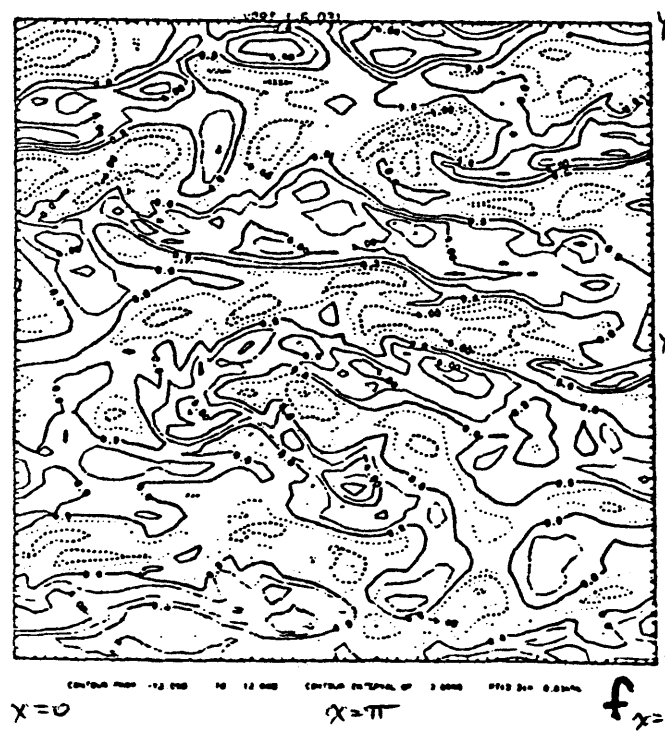


Fig. 7.21f: Vorticity map for Run P at t=6.



Fig. 7.23a: Instantaneous map of the perturbation vorticity field $\nabla^2\phi$ for Run 0 at t=2.

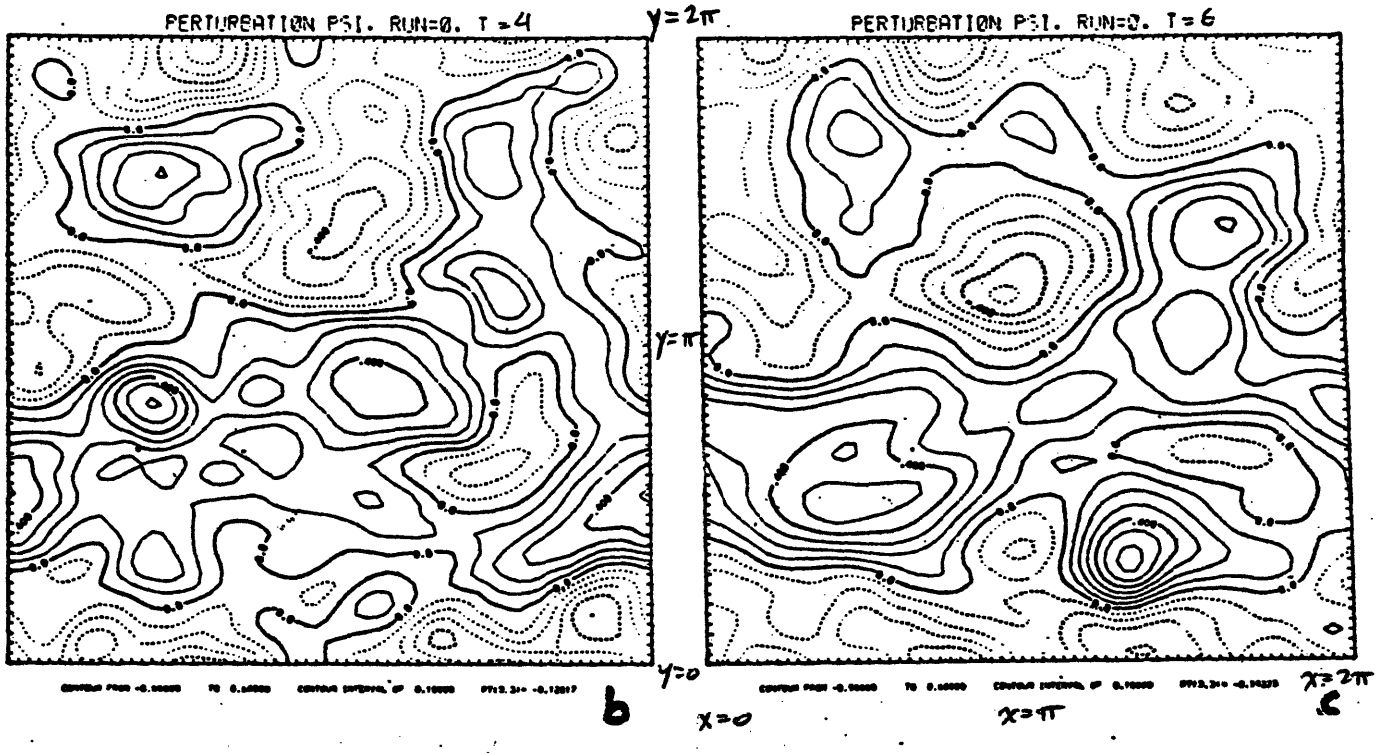


Fig. 7.22b,c: Perturbation streamfunction map for Run 0 at (b) t=4 and (c) t=6.

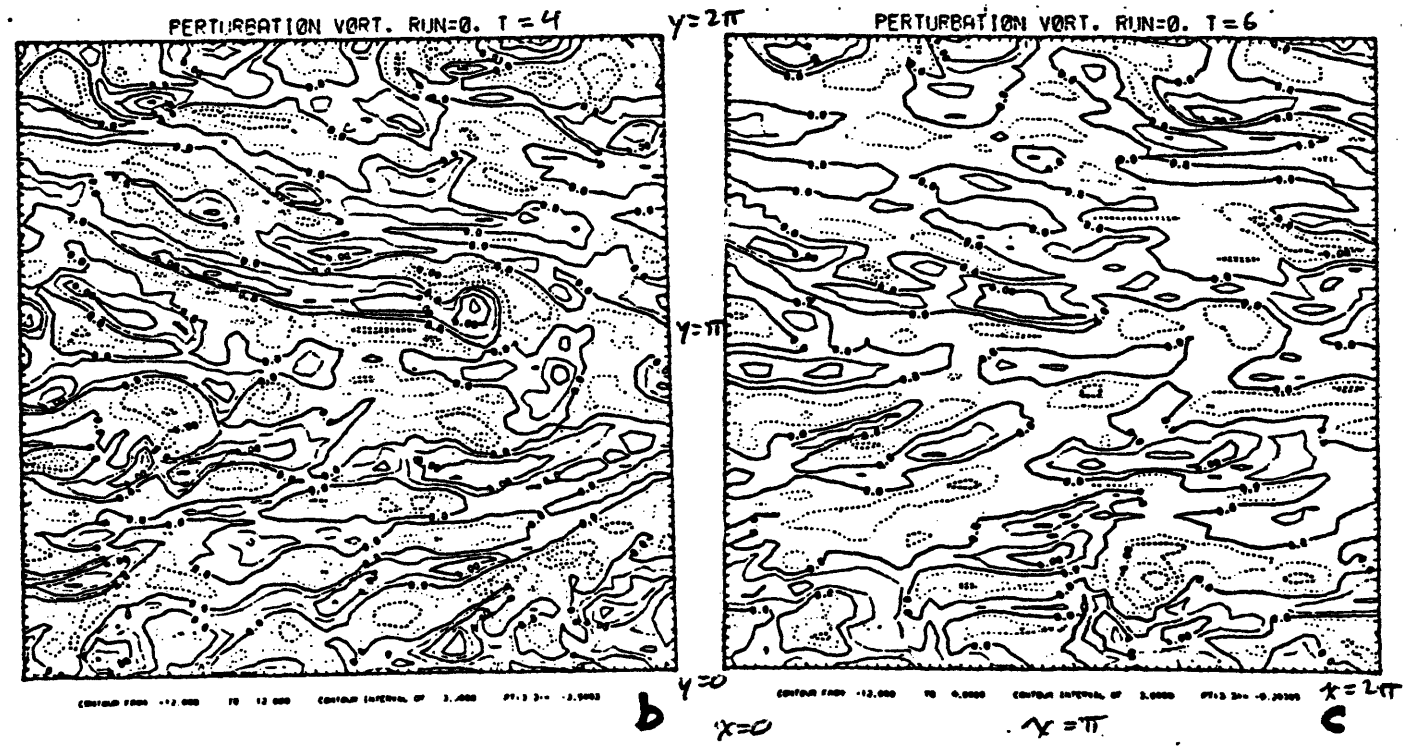


Fig. 7.23b,c: Perturbation vorticity map for Run 0 at (b) t=4 and (c) t=6.

the vorticity continues to display the vortex shearing associated with the enstrophy cascade, large-scale organization is beginning to appear by t = 6 (Fig. 7.21f).

The perturbation streamfunction field of Run 0 certainly evolves to large scale, but there is not much evidence of zonal anisotropy, nor of any cascade arrest (Figs. 7.22). But there is not a great deal of resemblance to Run R either: for example the strong spatial inhomogeneity of the latter (Figs. 7.1) is not particularly visible in Run 0.

Comparing the vorticity fields at t = 2 for Runs 0, P, and R, (Figs. 7.23a; 7.21b; 7.2c), one is struck by the strong spatial inhomogeneity of Run R and the clear stamp of mean-flow advection; the systematic straining which induces the enstrophy "cascade" is so effective in the regions of strong shear that already most of the enstrophy has been removed from there. But in Run 0, though there is certainly some evidence of advective effects (e.g. the teasing out of vortices in the strong shear regions), the spatial inhomogeneity is far less prevalent than in Run R. Indeed Run 0 appears in these pictures to be something of a cross between Runs P and R, exhibiting aspects of both.

By t = 4 the vorticity patterns of Run 0 (Fig. 7.23b) are beginning to bear more of a resemblance to Fig. 7.2d of Run R, and show none of the $\ell \approx \ell_\beta$ organization that is starting to appear in Run P (Figs. 7.21d,f). Nevertheless the spatial inhomogeneity is still weak; it is not until around t = 6 (Fig. 7.23c) that evidence of wave absorption and vorticity "homogenization" begins to show up. In Run R, in contrast, the vorticity has almost totally vanished by t = 6 - except around y = 0 (Fig. 7.2e). This trapping of disturbances around y = 0, so ubiquitous in Run R, is finally apparent in the later stages of Run 0

though the zonal eddy scale seems larger. This would seem to suggest that the onset of the linear dynamics follows an initial nonlinear cascade.

A rather different look at these observations is provided by an examination of the energy spectra in n-space (Figs. 7.8, 7.24, 7.25). There the dominance of the nonlinear enstrophy cascade over the "linear" induced down-scale enstrophy cascade in Run 0 is revealed through the near isotropy of the spectra at small scales, with a weak zonal tendency developing only after t = 2.0 ; in contrast, Run R shows strongly zonal small-scale energy right from the start. (Note that the basic-state flow at n = 1 is not explicitly shown in the spectra for Run R; also the persistent "hump" around n = 10 for the linear run reflects the initial energy at k = 0,1 that barely moves in a spectral sense, and that is dynamically inert.) At large scale the two runs appear more similar, except that there is less meridional anisotropy in Run 0 during the first two days (Figs. 7.24a,b); this is due perhaps to the fact that the mean-flow straining begins at smaller n than in Run R, perhaps to nonlinear mixing acting on a slightly slower timescale. At any rate there is no evidence in Run 0 of the cascade cut-off and large-scale zonal anisotropy that characterizes Run P; moreover the up-scale cascade itself is clearly a good deal quicker.

As far as this first-moment measure of anisotropy is concerned, the crudest description of Run 0 is that it lies between Runs P and R: Run P is zonally anisotropic at large scale and isotropic elsewhere; Run R is first meridionally anisotropic and then isotropic at large scale, and zonally anisotropic elsewhere; but Run 0 is at first fairly isotropic, and then weakly zonally anisotropic at all scales. Yet there

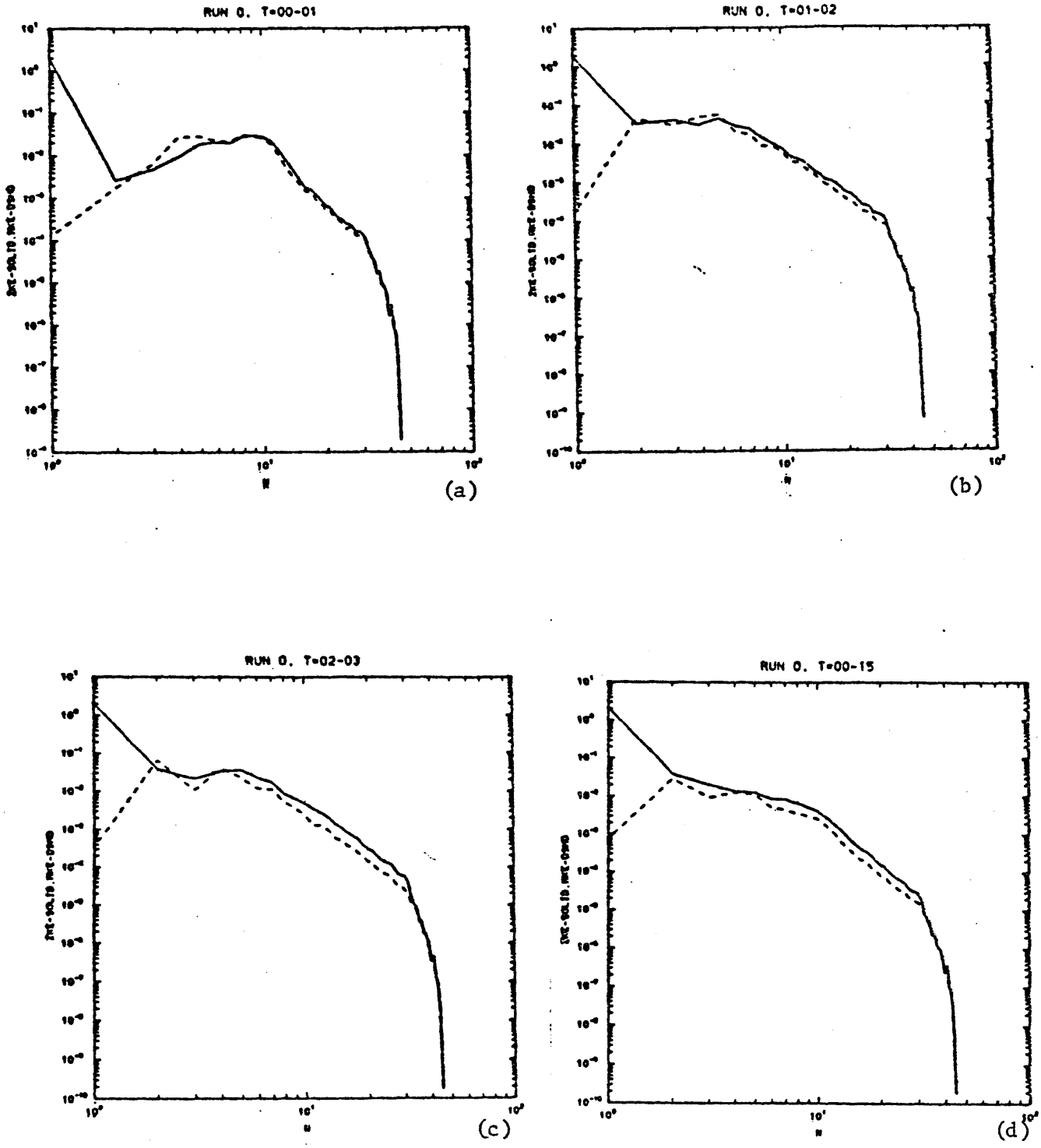


Fig. 7.24: Energy spectrum for Run 0, divided into $\langle u^2 \rangle$ = ZKE (——) and $\langle v^2 \rangle$ = MKE (– –), averaged over (a) t = 0–1 , (b) t = 1–2 , (c) t = 2–3 , and (d) t = 0–15 ; shown as a function of n.

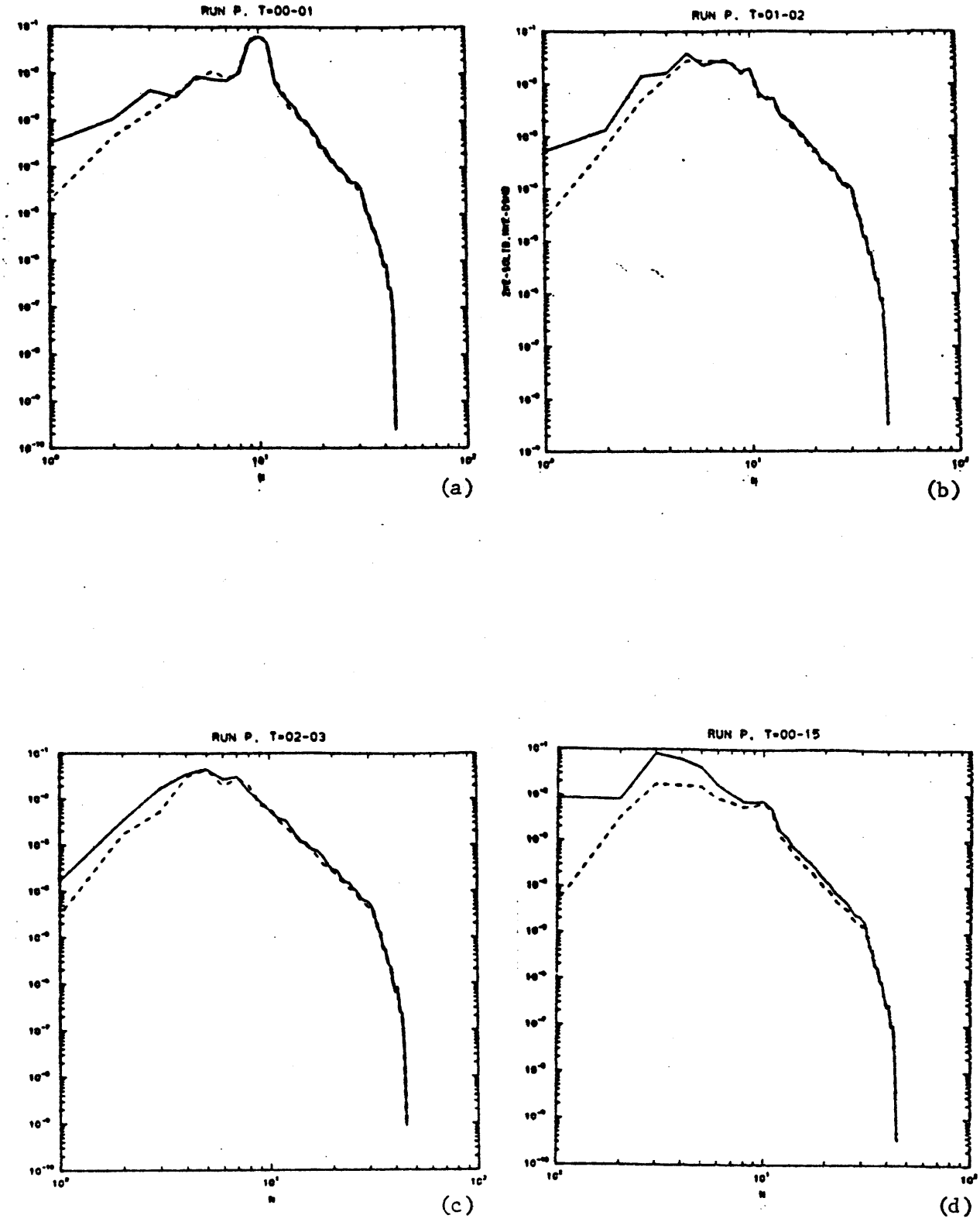


Fig. 7.25: As in Fig. 7.24, but for Run P.

is a significant way in which Run 0 reveals behaviour anticipated in neither Run P nor Run R, and that is in a "trapping" of energy at the largest scales $n < 3$.

Since quantitative comparison from the figures is difficult, the spectral amplitudes of energy up to $n = 8$ are given in tabular form for the three runs, averaged over the entire 15-day period in Table 7.3, and over the final day alone in Table 7.4. The temporary nature of the up-scale cascade and amplification in Run R is strikingly apparent, as it is also from, for example, Fig. 7.9d: the amount of energy left in $n < 9$ during $t = 14$–15 represents only 4% of the initial perturbation energy level of 0.47. In Run P, by contrast, where there can be no loss to conversion but only to high-order diffusion, 70% is left in $n < 9$ and indeed overall. Run 0 is found somewhere between these two: though it loses some energy to the basic-state flow (as reflected in the 12% increase in the $n = 1$ component by the last day), it does not lose as much as Run R. But unlike both P and R, in Run 0 there is a substantial amount of energy left at the largest scales of motion.

When one computes spectral conversion terms for Run 0, one may use the basic-state, perturbation formula (7.8c) to obtain $EMI(\underline{k})$, or the stationary, transient formulae (7.17c) and (7.20c) to obtain $EMI_T(\underline{k})$ and $C(\underline{k})$. Generally speaking, the former approach is most illuminating for one-day averages early in the run, the latter for averages over the entire run. When considering the interaction terms, it is useful to separate the "turbulent" $TSI(\underline{k})$ of (7.17b) from $MSI(\underline{k})$ of (7.20b), whereas $PSI(\underline{k})$ of (7.8b) is not so easily interpretable and so is not displayed. For Run P, of course, there is no choice.

	RUN P	RUN R	RUN O
n=1:	.87	.01	214.7
2:	1.13	1.98	6.75
3:	9.91	1.22	2.95
4:	7.83	1.28	2.63
5:	5.72	1.20	2.39
6:	2.60	.97	1.39
7:	1.73	.99	1.28
8:	1.23	.98	1.02
$2 \leq n \leq 8$:	30.15	8.62	18.41

Table 7.3: Energy spectra represented in n-space for the three spin-down runs, averaged over the entire run t = 0-15, and multiplied by 100. The n = 1 component for Run R shows the perturbation energy only.

	RUN P	RUN R	RUN O
n=1:	1.46	.00	223.0
2:	1.70	.53	6.78
3:	13.65	.27	2.11
4:	12.07	.18	.67
5:	2.48	.21	.32
6:	.77	.27	.29
7:	.32	.29	.26
8:	.16	.33	.24
$2 \leq n \leq 8$:	31.15	2.08	10.67

Table 7.4: As in Table 7.3, but over the final day t = 14-15.

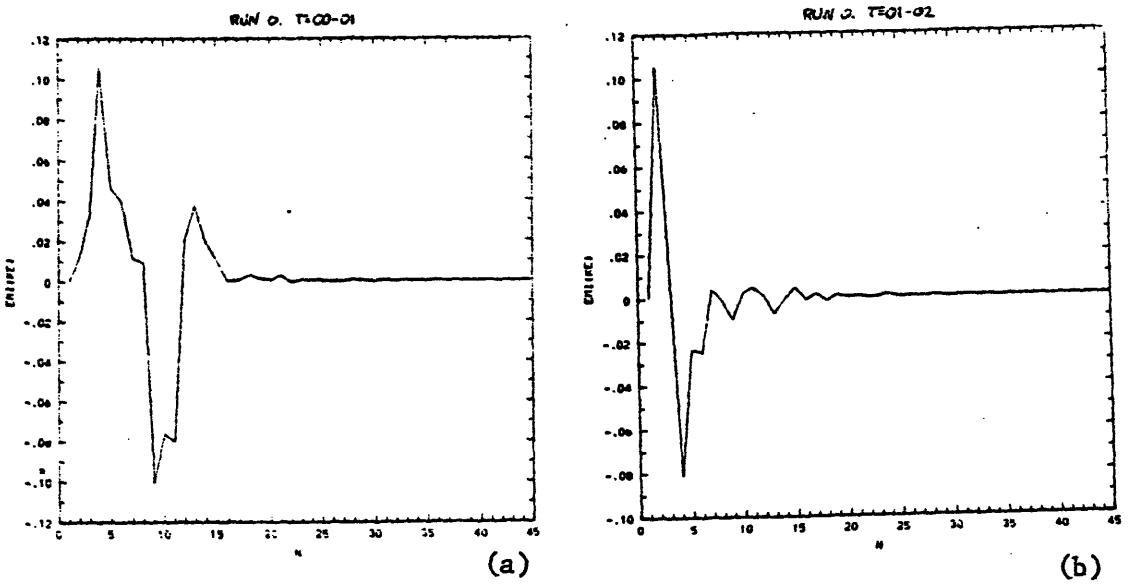


Fig. 7.26: Mean-to-eddy energy interaction term EMI for Run 0, as a function of n, averaged over (a) t = 0-1 , (b) t = 1-2, and (c) t = 2-3 .

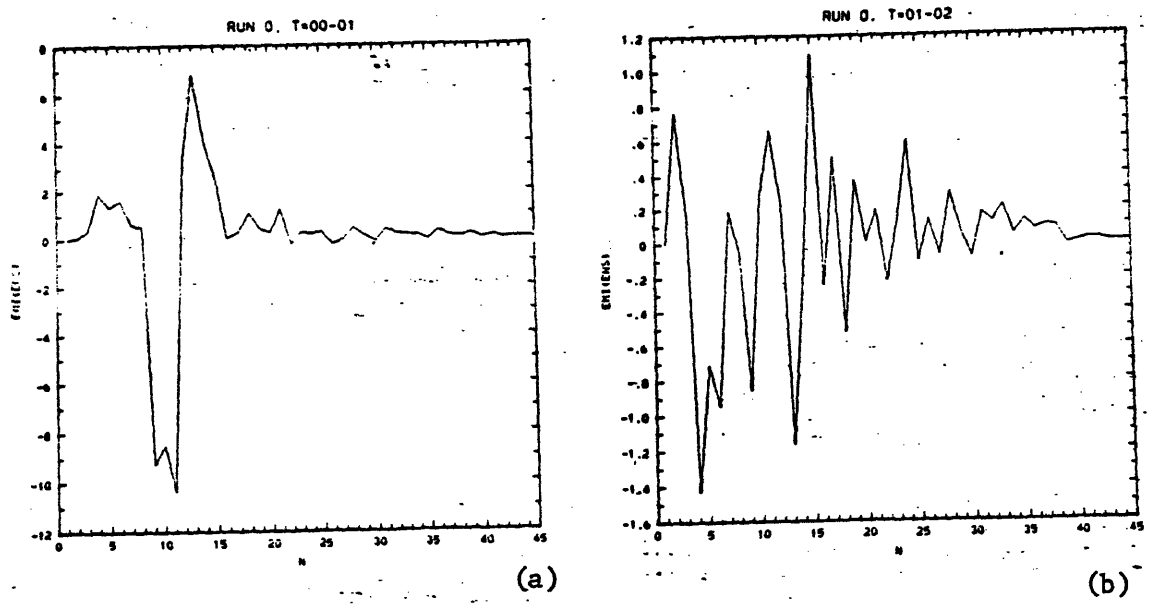


Fig. 7.27: As in Fig. 7.26, but for enstrophy.

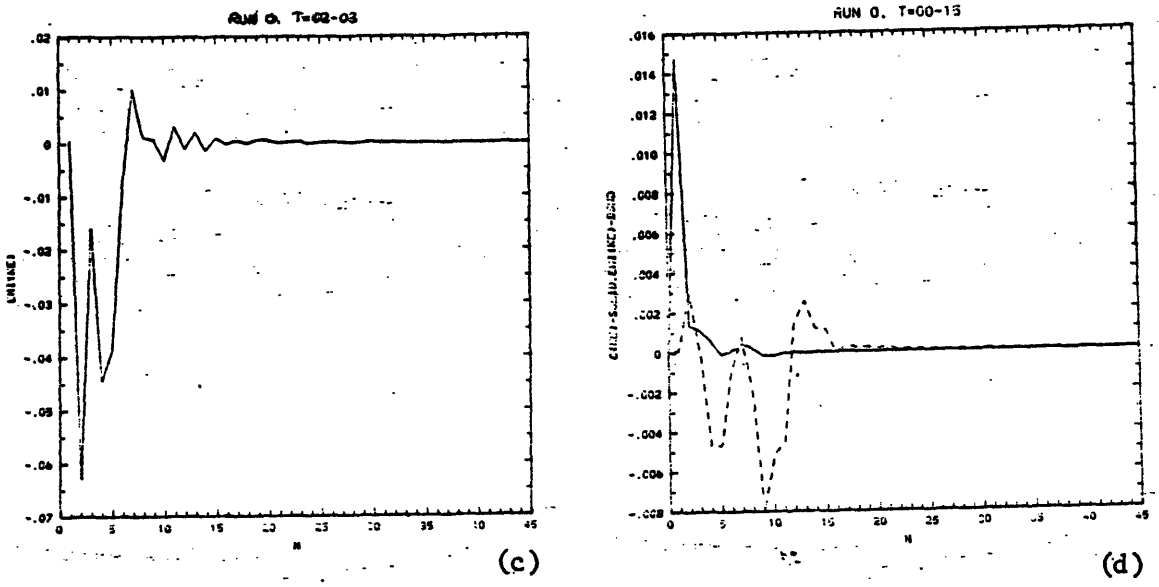


Fig. 7.26d: Stationary-to-transient interaction term EMI_T over t = 0-15 (- -) ; transient-to-stationary interaction C (——) ; for Run 0.

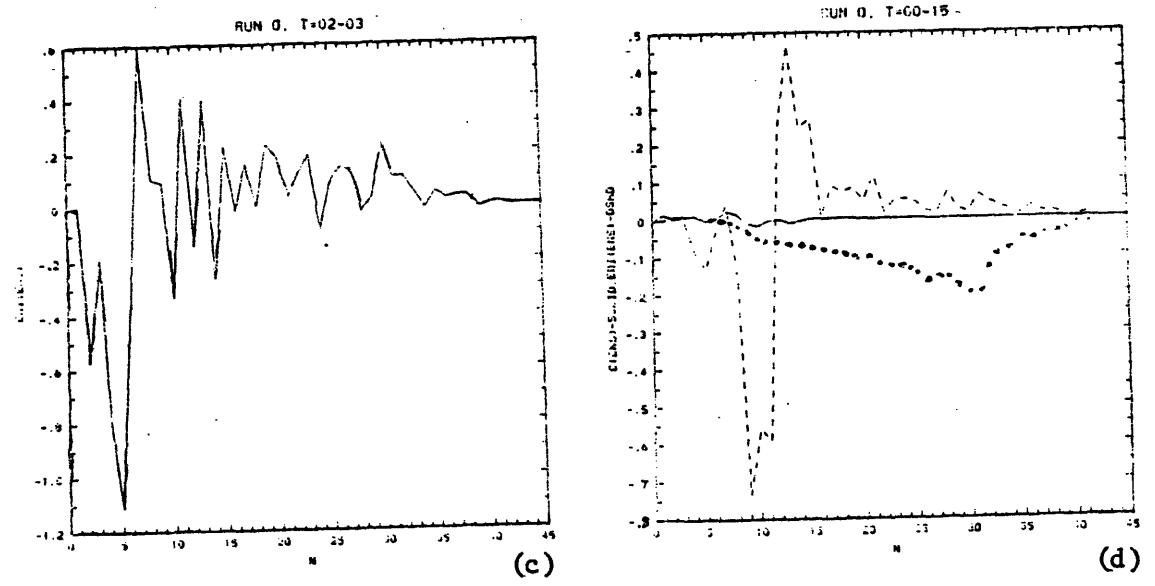


Fig. 7.27d: As in Fig. 7.26d, but for enstrophy; also the dotted line shows the frictional loss.

Examining the conversion term EMI as a function of the "isotropic" wavenumber n, there are no particularly noticeable differences between Runs O and R in the early days for the energy (Figs. 7.26a-c,7.9a-c), but in the average over the run there is a distinction (Figs. 7.26d vs. 7.9d): the nonlinear interactions apparently spread the transient energy loss from its initial location over a broader range of n, with an obvious peak around n = 4,5. In addition, Fig. 7.26d shows a net transfer into n = 2 that exceeds anything found in Fig. 7.9d. That the transient self-interactions do indeed move energy from the initial distribution up to n = 4,5 is confirmed by the transient energy flux term for Run O (Fig. 7.28b).

However n = 4,5 is just the point at which the reverse energy cascade of Run P begins to be arrested by Rossby-wave dispersion (e.g. Figs. 7.25a-c); though the energy there eventually winds up in the ℓ = 3,4 zonal modes, or n = 3,4. This again suggests that the nonlinear turbulent energy cascade is cut off by dispersion as in beta-plane turbulence, but with the important difference that with the mean flow the "cascade" can be carried further by the linear dynamics; and indeed it is, as shown by the flux obtained from MITI(n) in Fig. 7.28a. The sharpness of the arrest is perhaps a bit of a surprise; and it should be appreciated that the mean-flow straining does not wait until n = 4,5 to act, but is obviously also active at the initial scales around n = 10 (Figs. 7.26d,7.28a).

While the energy interaction terms highlight the larger scales, the enstrophy terms emphasize the smaller ones and the down-scale cascade. Examination of t = 0-1 (Figs. 7.27a,7.10a) shows that nonlinear effects severely slow down the induced enstrophy cascade; indeed,

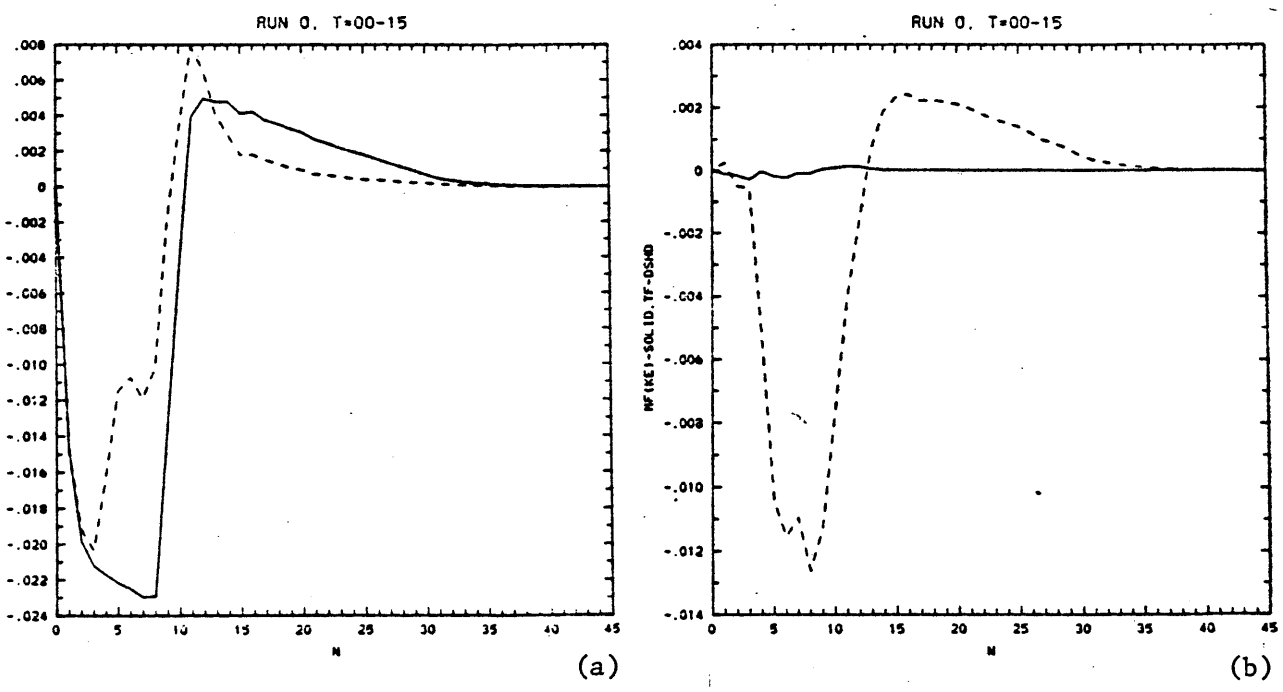


Fig. 7.28: (a) Total flux of energy, Run 0, t = 0-15 (——); flux from MITI (– –) ; (b) flux from TSI (– –) , and from MSI (——) . Note that I = MITI + TSI + MSI . Shown as a function of n. Positive values denote a down-scale flux.

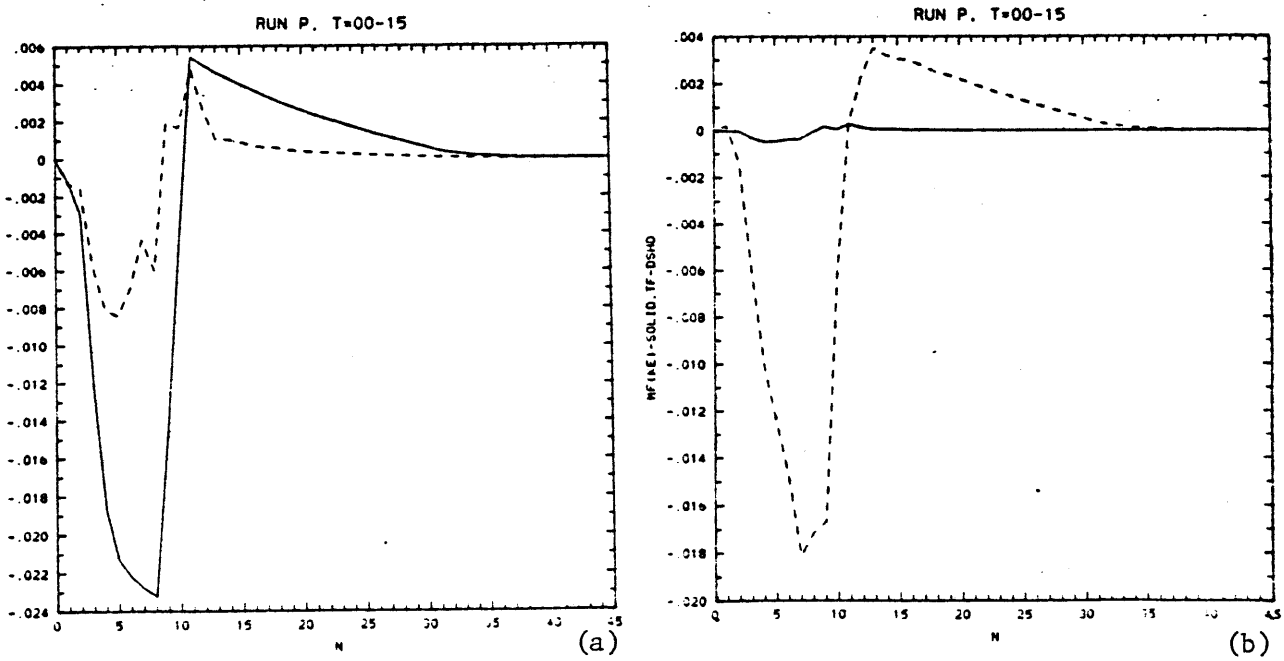


Fig. 7.29: As in Fig. 7.28, but for Run P.

in this respect Run O looks almost closer to Run P than it does to Run R. This feature was mentioned before with reference to the spatial vorticity maps. Whereas by t = 1-2 the truncation is obviously having a marked influence on Run R (Figs. 7.10b,c), in Run O the effect is relatively minor (Figs. 7.27b,c) though the terms are still characteristically noisy as is normal for turbulent enstrophy cascades. Over the course of Run O the induced enstrophy cascade is largely restricted to $n < 16$ (Fig. 7.27d), with the turbulent cascade taking over thereafter. This is also clear from the frictional loss, which is included in Fig. 7.27d: the loss is peaked at high wavenumber, and there is a clear deficit with the induced interaction term which can only be made up for by the turbulent cascade.

The role of the linear dynamics in Run O can be concisely seen through a comparison of run-averaged spectral interaction quantities with Run P. Nonlinear fluxes from I(n), MITI(n), TSI(n), and MSI(n) are shown for Run O in Figs. 7.28a,b and for Run P in Figs. 7.29a,b; recall that $I(n) = MITI(n) + TSI(n) + MSI(n)$. In both cases MSI(n) is negligible, while TSI(n) is similar in the two runs and acts to move energy from the initial scales around n = 10 up to n = 4,5 (Figs. 7.28b, 7.29b). The difference comes in MITI(n): for Run O it gives a strong transfer from the initial scales, and again from n = 4,5, up to n = 1,2, with a weaker transfer down-scale (Fig. 7.28a). It is interesting to note that Run P, which develops weaker zonal jets of its own at $\ell = 3,4$, shows a similar "induced cascade" mechanism though of less strength, which however cannot move energy to scales larger than the jets' own (Fig. 7.29a). This suggests that a higher-ℓ basic-state jet might not have succeeded in getting energy past its own scale, a hypothesis which

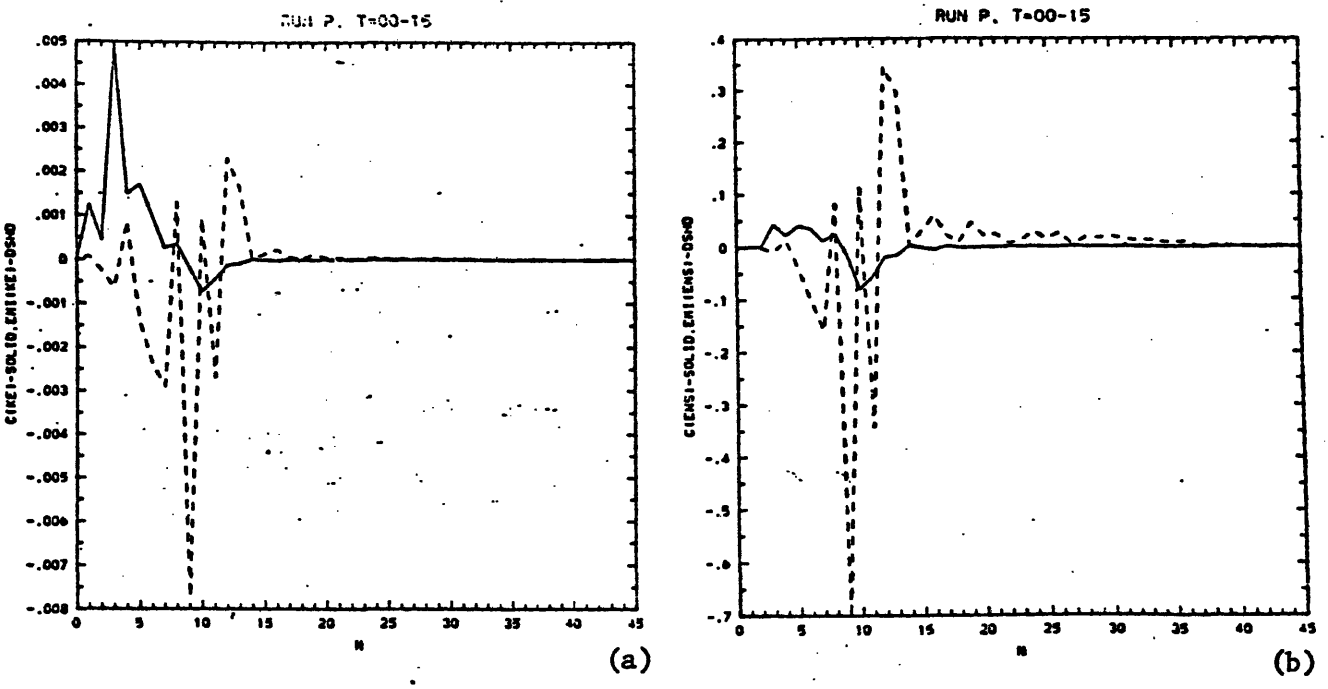


Fig. 7.30: EMI_T (- -) and C (——) for (a) energy and (b) enstrophy, Run P, t = 0-15, as a function of n.

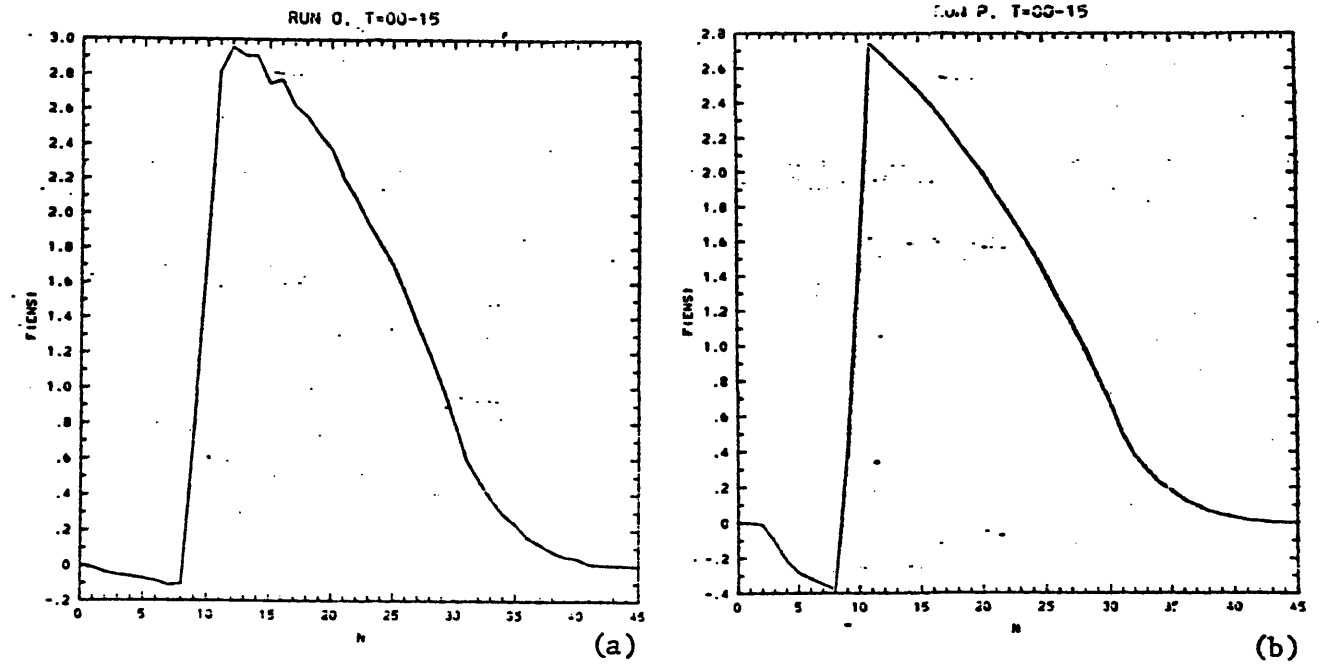


Fig. 7.31: Nonlinear flux of enstrophy for (a) Run O and (b) Run P, averaged over t = 0-15.

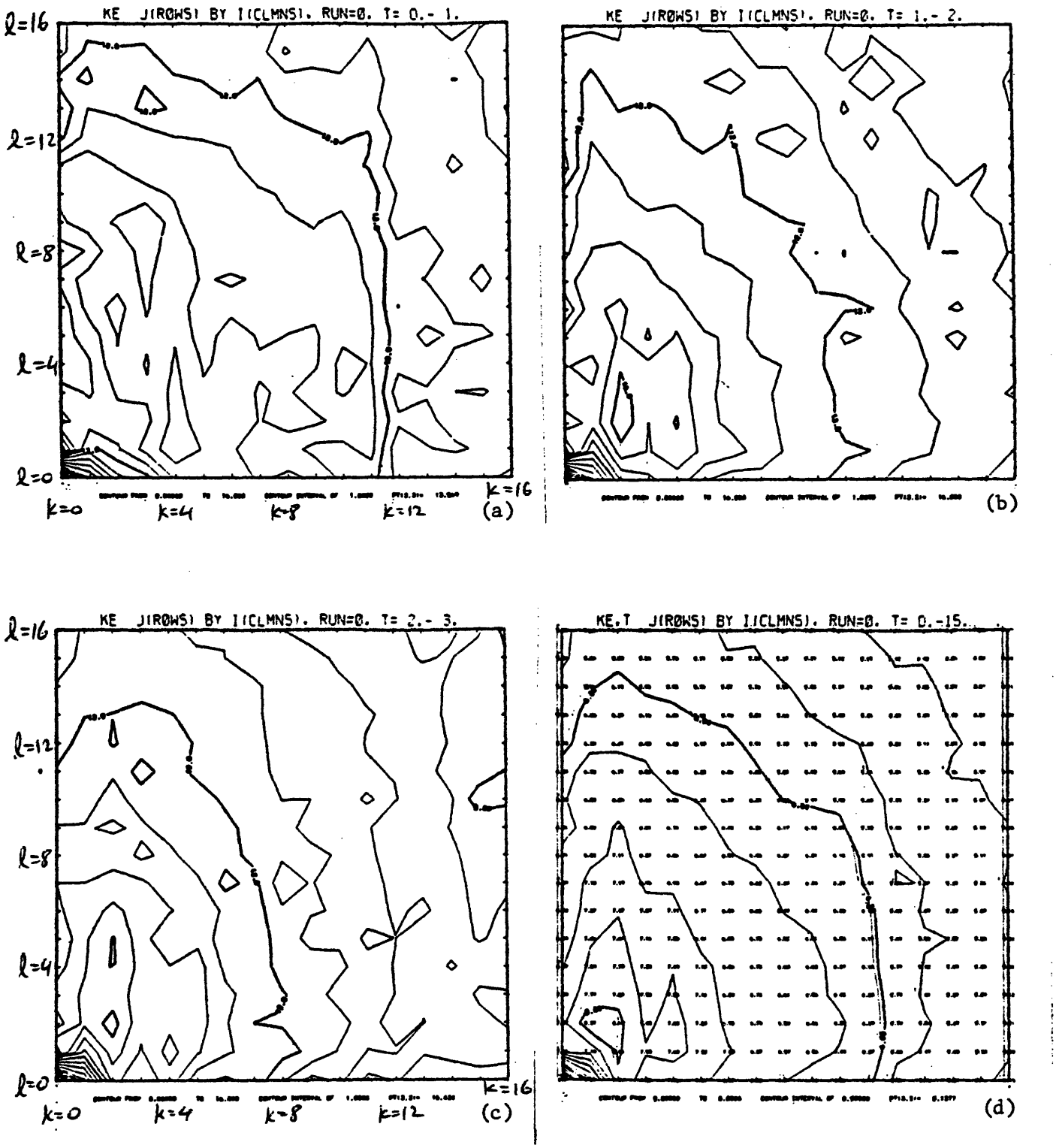


Fig. 7.32: 2-D spectrum of energy E(k,ℓ) for Run 0, averaged over (a) t = 0-1 , (b) t = 1-2 , (c) t = 2-3 ; transient energy only shown for t = 0-15 (d) . k runs across from 0 to 16, ℓ runs up from 0 to 16.

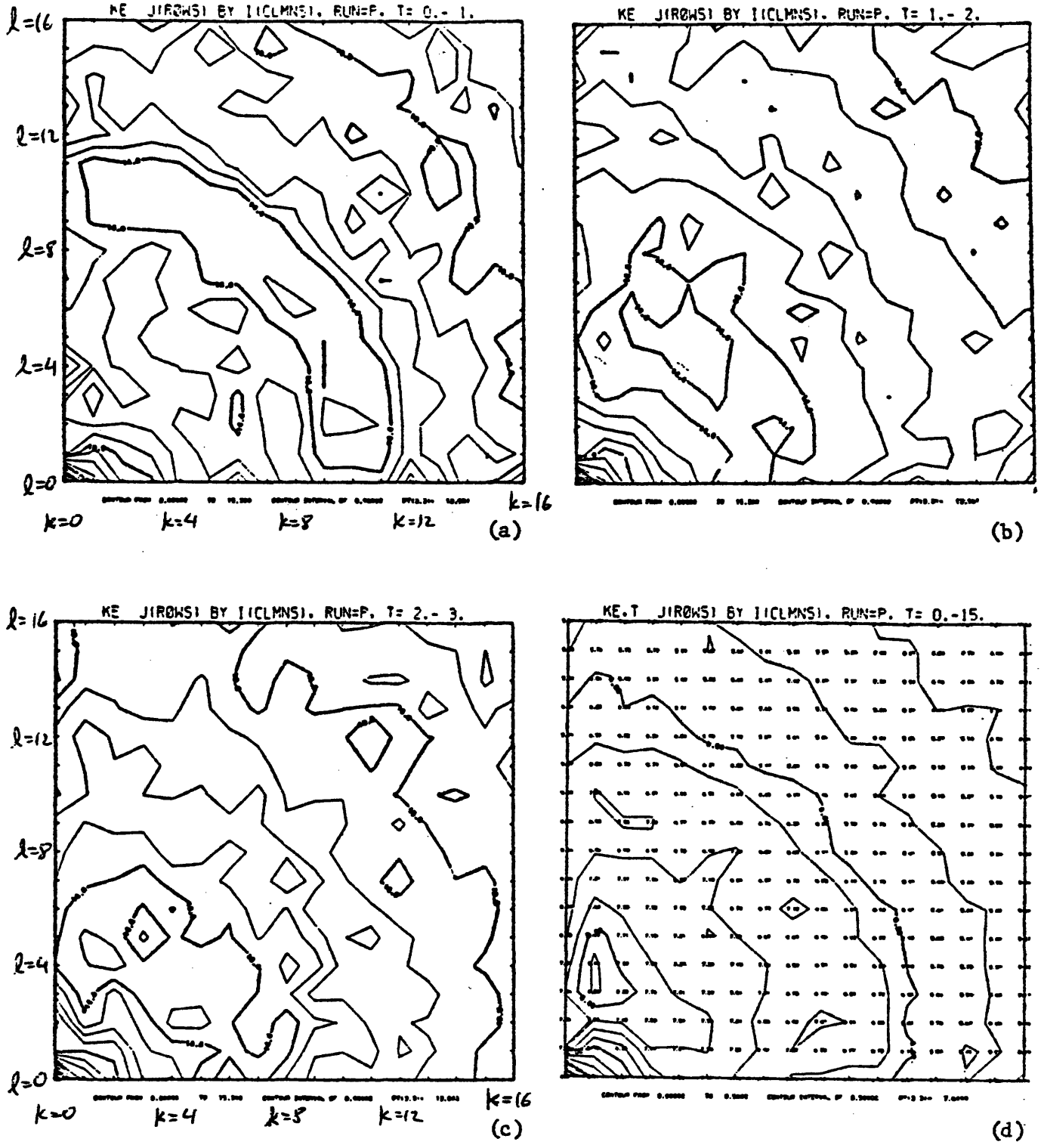


Fig. 7.33: As in Fig. 7.32, but for Run P.

is verified in the Appendix.

EMI(n) and C(n) are shown for both energy and enstrophy from Run P in Figs. 7.30a,b, and are to be compared with Figs. 7.26d and 7.27d. It is evident that the beta-plane turbulence jets of Run P do indeed manage to induce a significant transient cascade once they form, but this cascade cannot penetrate the cut-off scale; the mean conversion terms show the rectification of the stationary jets at n = 3,4,5.

Finally the total enstrophy fluxes are shown in Figs. 7.31a,b for Runs 0 and P; the strong down-scale enstrophy cascade induced by the linear processes in Run 0 shows up in the near cancellation of the small up-scale enstrophy cascade of Run P, and in an extension of a constant-flux plateau just past n = 10. Otherwise the figures are very similar.

On the basis of these remarks, the linear dynamics are seen to be important precisely where the turbulent dynamics are weak: at the very beginning of the run, before the narrow spectral line has had a chance to broaden sufficiently to let the nonlinear cascades begin in earnest; and for $n < 5$, where Rossby-wave dispersion dominates over nonlinear interaction. Elsewhere, the intuition from barotropic turbulence seems relevant.

The nonlinear effects are also clearly visible in the 2-D spectra (Figs. 7.11, 7.32, 7.33). The most prominent developments of t = 0-1 in Run R for small k, especially the rapid pulse of energy along k = 4 to small ℓ, are found in Run 0 (no surprise, since they are so rapid); but in a wide band around n = 10 isotropy is the rule (Fig. 7.32a). Even the initial high-n zonal anisotropy due to the rapid induced enstrophy cascade, evident in the first day, is subsequently smoothed out though not eliminated (Figs. 7.32b,c). At large scales, while the nonlinear

energy cascade initially penetrates to n = 4,5, the inevitable process of mean-flow straining dominates over a region which grows as the eddy energy is reduced (Figs. 7.32b,c). On the other hand the relatively slow isotropic turbulent enstrophy cascade of Run P, and the development of zonal anisotropy following the cascade cut-off, are very evident in Figs. 7.33a-c.

Over t = 0-15 nonlinear processes smooth the rough spectra of Run R considerably (compare Figs. 7.32d and 7.11d), and mitigate the zonal anisotropy at small scales; however the effects of the mean-flow straining break through the cascade cut-off of beta-plane turbulence, establishing large-scale isotropy and moderate zonal anisotropy everywhere else (compare Figs. 7.32d and 7.33d) - which is the exact opposite of Run P. Nevertheless the regime of slightly anisotropic barotropic turbulence surrounding the large-scale linear dynamical regime is apparently effective in keeping reflected "rays" from travelling very far and giving up much energy to the mean flow. Figs. 7.32d and 7.33d show the transient energy; the stationary energy is however much smaller outside of the zonal component.

The next set of figures to be studied concerns the spectral conversion terms EMI for fixed k as functions of ℓ; in §7d these proved to be the key to verifying the spectral implications of ray-tracing theory. The comparison to be made is qualitative rather than exact: for the fully nonlinear Run O a slice along constant k only tells part of the story, while for the linear runs it is a complete diagnostic for all waves with that value of k. Also Figs. 7.12-7.17 show the "single-wave" runs, but Run O includes the full initial conditions.

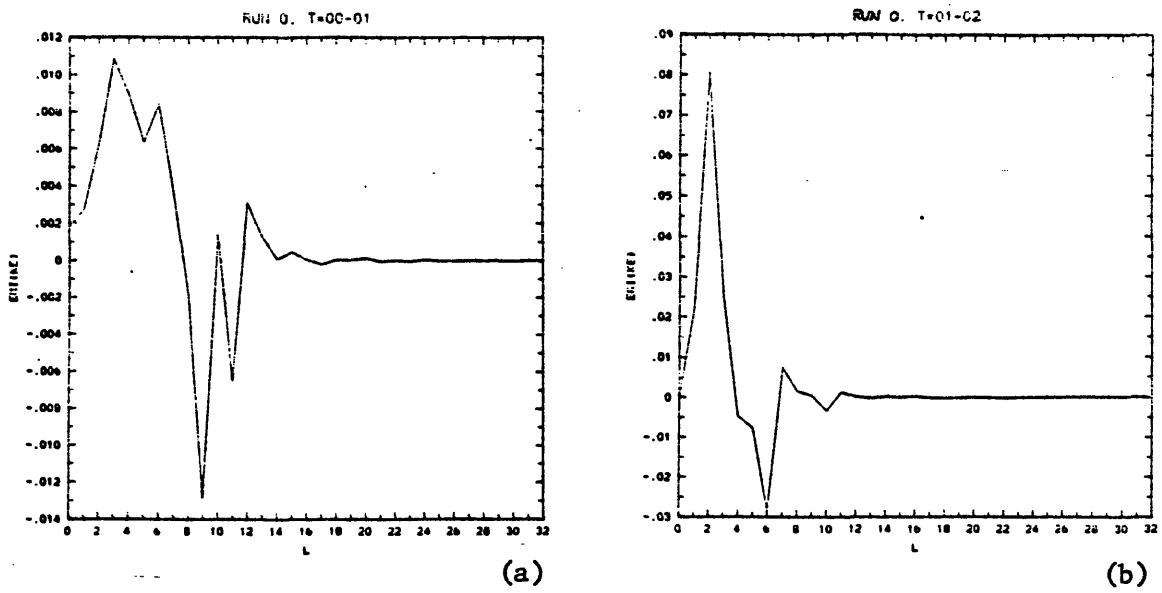


Fig. 7.34: Energy mean-to-eddy interaction term EMI for the slice $k = 2$, as a function of ℓ, Run 0. (a) $t = 0-1$, (b) $t = 1-2$, and (c) $t = 2-3$.

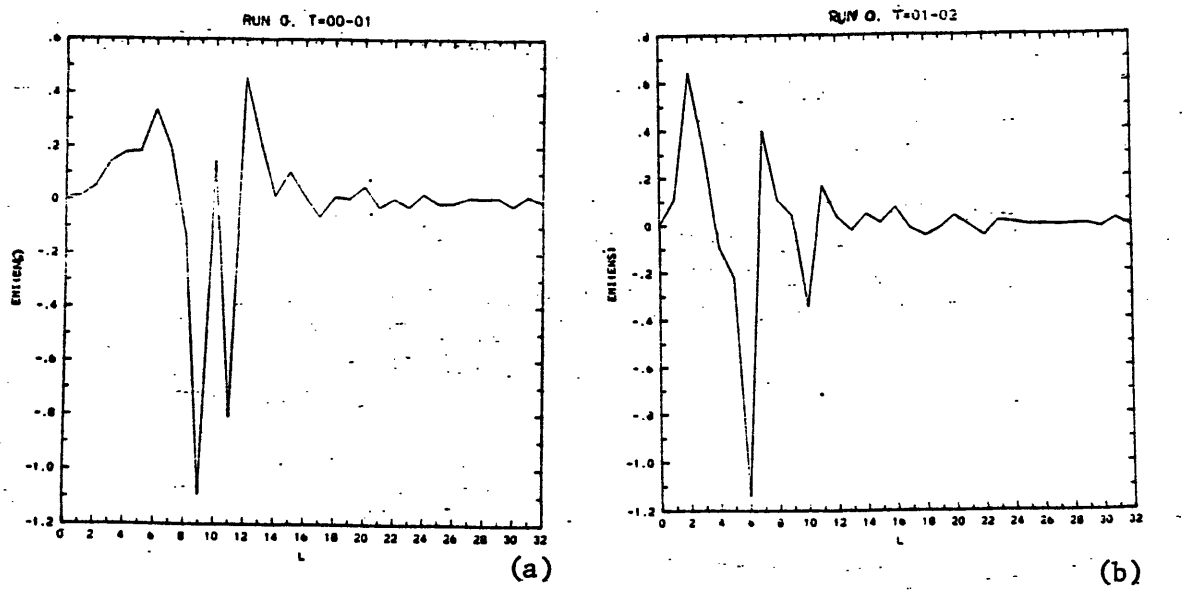
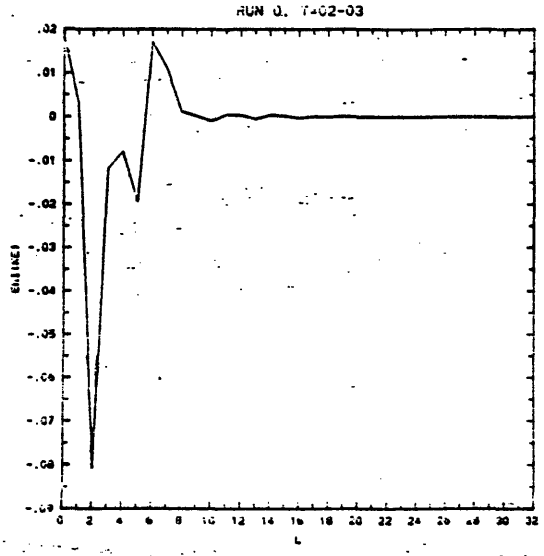
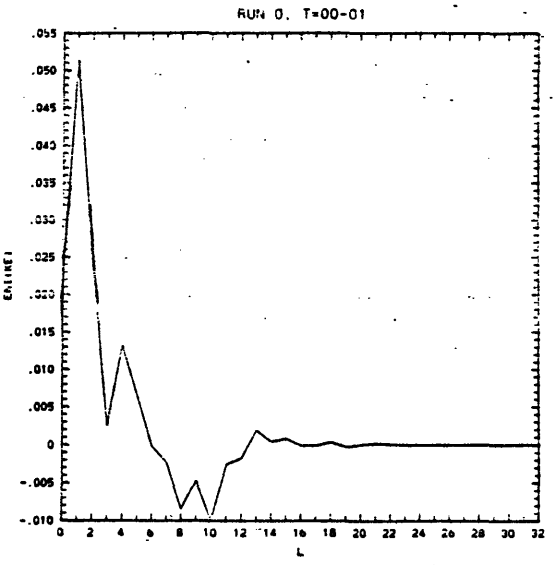


Fig. 7.35: As in Fig. 7.34, but for enstrophy.



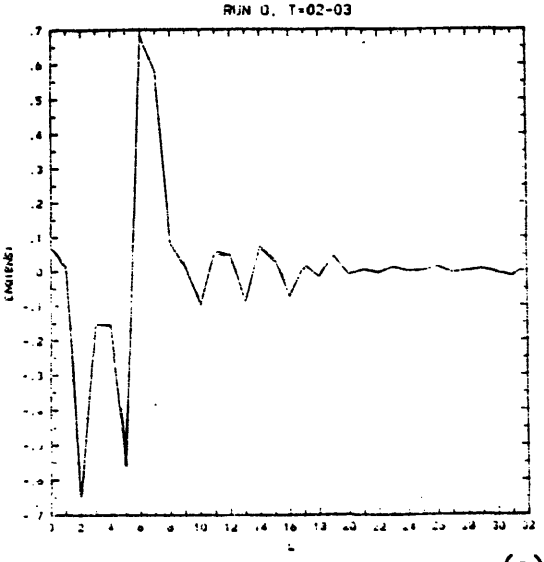
(c)

Fig. 7.34: (c)



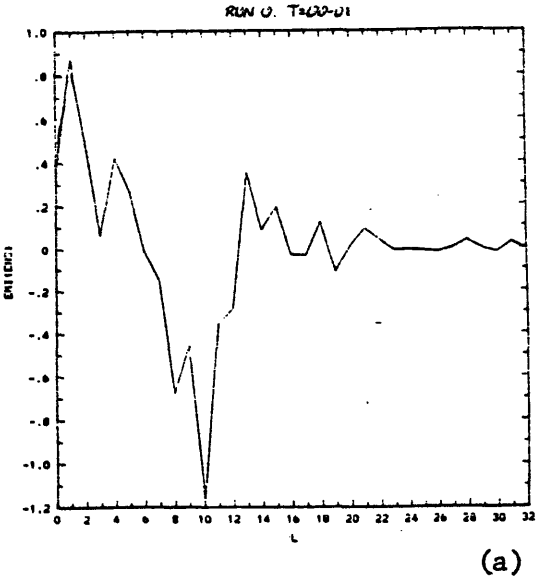
(a)

Fig. 7.36: As in Fig. 7.34, but for k = 4 .



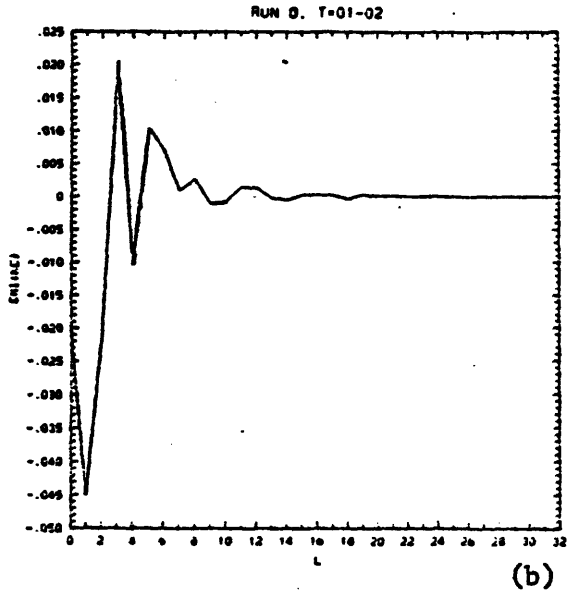
(c)

Fig. 7.35: (c)

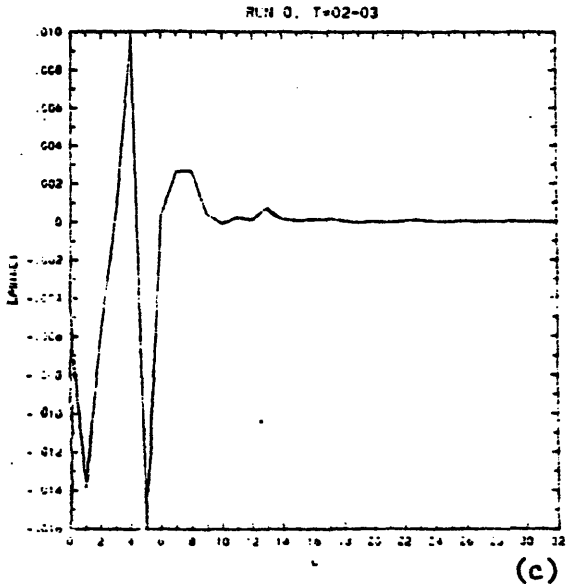


(a)

Fig. 7.37: As in Fig. 7.35, but for k = 4 .

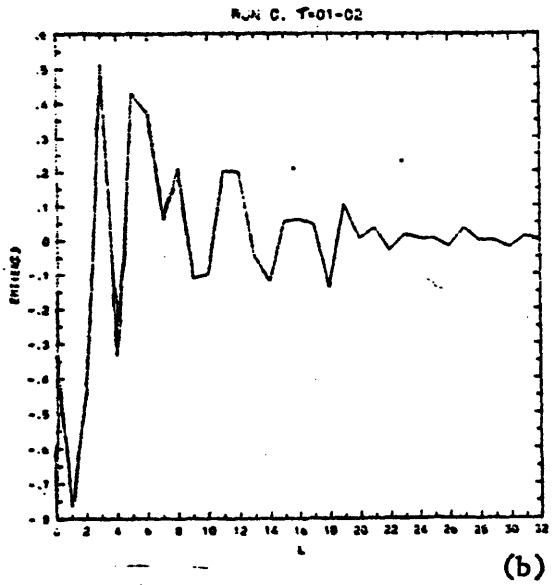


(b)

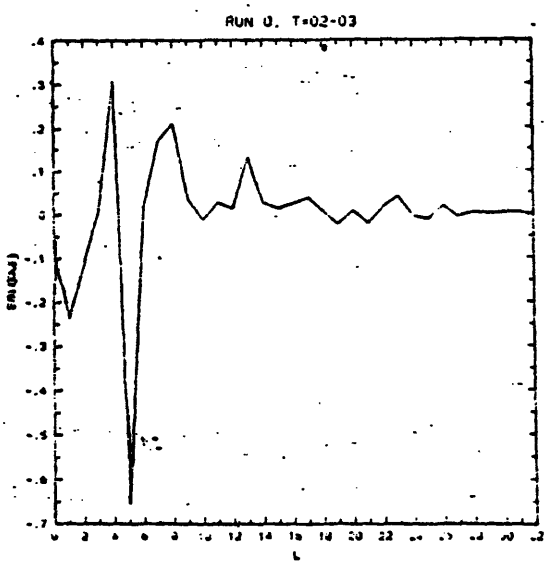


(c)

Fig. 7.36: (b), (c).



(b)



(c)

Fig. 7.37: (b), (c).

Looking first at k = 2, Figs. 7.34 and 7.35 show the principal characteristics exhibited in Run R2 (Figs. 7.12,7.13): initially a symmetric spreading of enstrophy with the consequent up-scale "transfer" of energy; a continuation of this process for t = 1-2, with greatest energy gain at ℓ = 2; and then a loss of energy from the largest scales. The differences for Run 0 are primarily the weaker transfers, and the confinement of the down-scale enstrophy transfer - both initially and during the decay of the large-scale waves.

Generally the same conclusions can be drawn from k = 4 (Figs. 7.36,7.37 vs. 7.14,7.15), with the "trapping" of the down-scale enstrophy transfers perhaps even more obvious. For k = 6 (not shown) there is a bias towards down-scale transfer even during t = 0-1, since many of the up-scale moving "rays" have already been reflected. But the catastrophic behaviour of Run R6 connected with its truncation problems seems entirely absent from Run 0.

Of course the resemblance between these particular diagnostics from Run 0 and their linear-run equivalents is due to the fact that the latter consist of precisely those features which propagate and evolve most rapidly, and are therefore most likely to survive nonlinear interference.

At the end of §7d above it was explained that, because of the nature of the spin-down experiments, the physical-space diagnostics are necessarily noisy in comparison with their spectral counterparts. This is even more of a problem in Run 0 than in the linear runs, which makes sense: the more turbulent the dynamics, the more homogeneous and isotropic are the eddies; and hence the less sharply defined are the physical-space fields. The spectral diagnostics have shown that Run 0

is indeed quite turbulent, and the instantaneous spatial vorticity maps have indicated weaker inhomogeneity than in the linear runs; consequently one cannot expect a strong signal from the spatial diagnostics.

Therefore the Reynolds stress and velocity variance fields to be shown below are obtained from an "ensemble average" of three spin-down runs, entitled 0, 0A, and 0B, with a different phase mixture in their initial conditions. Insofar as each run itself represents an ensemble of disturbance evolution, this merely increases the number of degrees of freedom. For the spectral diagnostics, Run 0 alone provides a strong signal; it is nevertheless reassuring that Runs 0A and 0B exhibit essentially the same spectral behaviour as does Run 0, with some differences of timing to be sure, but a similar ultimate development. For the spatial diagnostics, however, the additional averaging is necessary.

The Reynolds stress terms are shown in Fig. 7.38a: in the first day they act to extract energy from the zonal flow, but specifically from the westerly jet, which is consistent with the ray-tracing arguments. By the second day the pattern is reversed and the absorption phase has begun, and this latter effect dominates in the average over the run. The same pattern of initial eddy gain and ultimate loss was also seen in Run R (Figs. 7.19), and is reflected clearly in the spectral diagnostics; it is a vindication of the relevance of the linear theory of Chapter VI to the nonlinear regime.

Examining the time sequence of eddy velocity variances (Figs. 7.38b,c), the initial concentration of eddy energy in the westerly jet is in agreement with ray-tracing theory, especially so as the meridional energy $\langle\overline{v'^2}\rangle$ (MKE) greatly exceeds the zonal energy $\langle\overline{u'^2}\rangle$ (ZKE). In the run average this feature decays considerably; when the zonal-mean (k =

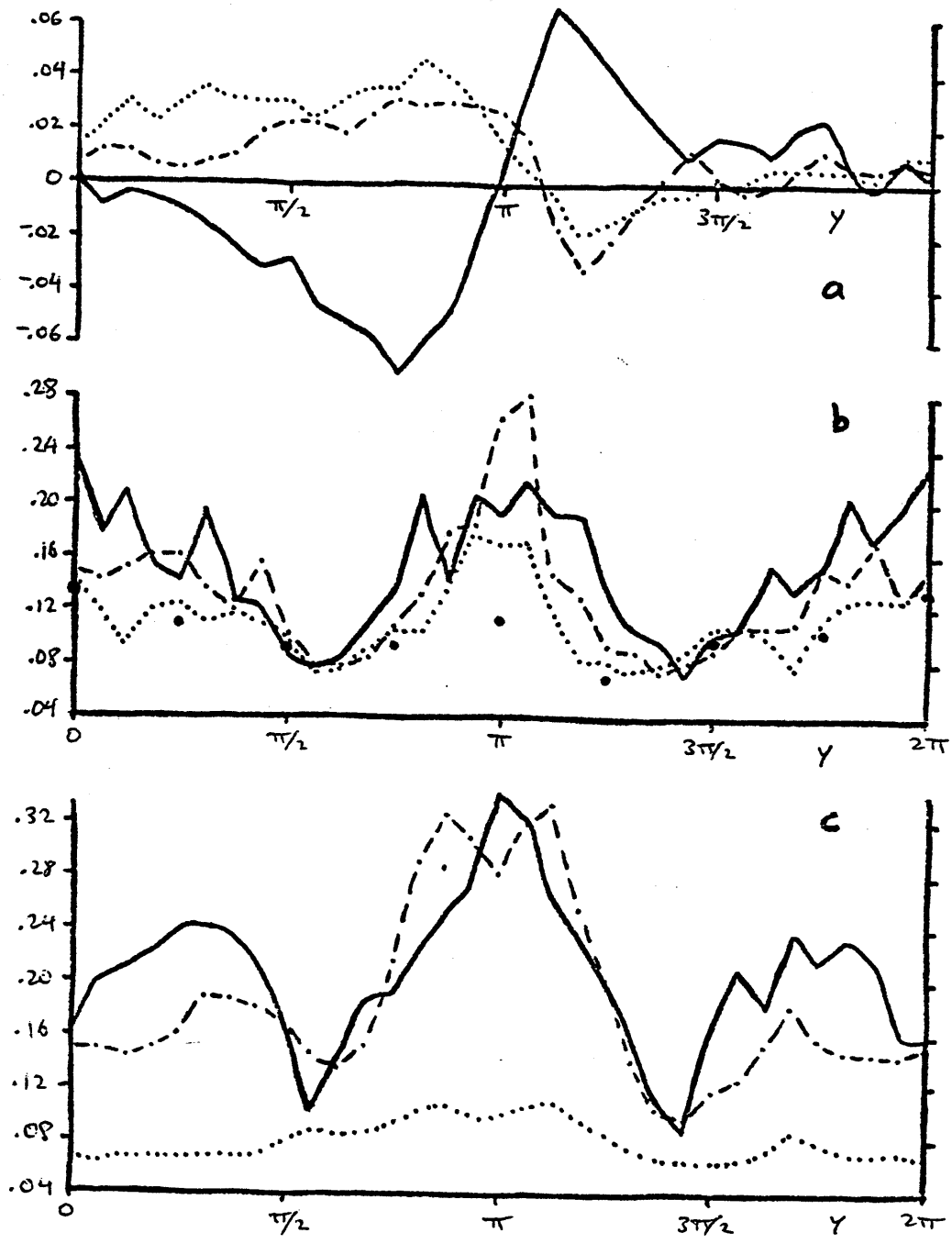


Fig. 7.38: Ensemble average of Runs 0, 0A, and 0B, for (a) $\langle \overline{uv} \rangle$, (b) $\langle \overline{u'^2} \rangle$, and (c) $\langle \overline{v'^2} \rangle$, for t = 0-1 (——), t = 1-2 (—·—), and t = 0-15 (····). The t = 0-15 values in (a) have been multiplied by 5 to be visible. Dots in (b) show the $k > 0$ component for t = 0-15.

0) component of ZKE is removed the remnant energy is roughly isotropic, which might be attributed to nonlinear mixing. On the other hand there is also a concentration of variance in the easterly jet, suggesting trapping by turning lines; however MKE is much weaker than ZKE there for Run O, which indicates larger zonal scales than in Run R. This agrees with similar remarks made previously, and gives further support to the notion that the linear dynamics only take over after the conventional reverse energy cascade has had some effect.

It might be added that the smoothness of these fields is present for each run of the ensemble, and indicates that the "spectral blocking" problem associated with the truncation is not entering; this is presumably due to the isotropization tendency at small scales which spreads the enstrophy over a broader range of k and slows down the induced cascade.

§7f. Summary of Results

Perhaps the broadest conclusion to be drawn from the spin-down runs discussed in this chapter is the following: the dynamical characteristics of beta-plane turbulence in the presence of a large-scale shear flow resemble neither pure beta-plane turbulence, nor pure wave, mean-flow interaction. In some respects the full problem represented by Run O is intermediate to the other two, in that it exhibits aspects of both; but there are also significant ways in which it displays behaviour unanticipated by either of the simpler dynamical pictures.

First it must be said that Run R seems to confirm the validity of applying ray-tracing theory to close the spectral transfer problem for the linear dynamics, as was done in §§6c,d; this success was not,

however, inevitable since the theory is approximate. There are indeed normal-mode effects at small k and ℓ for which ray-tracing theory cannot account, but these are adequately described by the linear simulation itself and are found to be small.

The features of the linear dynamics which persist in the nonlinear run are these: First, there is a penetration of perturbation energy past the cascade cut-off scale n_β into the largest scales of motion. Initially this large-scale energy exhibits meridional anisotropy, though it later relaxes to near isotropy. Secondly there is clear zonal anisotropy at small scales, indicating the importance of extremely non-local triad interactions involving the basic-state flow component. Both of these phenomena are connected with the third feature, namely pronounced transfer of enstrophy along lines of constant zonal wavenumber k, induced by the zonal jet. Finally one sees a maximum of meridional eddy energy variance $\langle\overline{v^2}\rangle$ in the westerly jet, as is predicted by ray-tracing theory; as well as a trapping of disturbance energy by turning lines in a "waveguide" around the centre of the easterly jet, $y = 0$.

The most important nonlinear modification of the linear dynamics concerns the fact that the up-scale cascade of wave enstrophy to small ℓ with corresponding energy growth, temporary and largely reversible according to linear theory, is <u>not</u> reversed to anywhere near so great an extent in the nonlinear run. This allows a "trapping" of energy at the largest scales, a phenomenon which may be understood in several ways. First, there is a turbulent energy cascade from the initial scales up to $n = 4,5$, so that in most cases the linear dynamics begin at smaller n than they would otherwise; this implies fewer critical lines, which itself would lead to more trapping. Secondly the down-scale induced

enstrophy cascade, which is essential to the wave, mean-flow interaction, is truncated by turbulent isotropization for $n > 5$. Even at large scale, but most prominently elsewhere, the nonlinear interactions act to smooth the spectra by diffusion of enstrophy across lines of constant k.

In fact the linear dynamics, though they are systematic, are apparently quite sensitive to nonlinear mixing and are easily defeated. Linear processes dominate at the beginning of the run, before the spectral peak broadens (though they themselves hasten the broadening); and at large scale, for $n < n_\beta$. Unlike the situation in beta-plane turbulence, however, the linear dynamics cannot describe the behaviour of a particular large-scale wave for very long: the disturbance can easily be refracted into a higher wavenumber as it propagates in the mean shear flow, and can thus enter the more turbulent regime.

To sum up briefly, the spin-down runs demonstrate that beta-plane turbulence in a sheared zonal jet consists of two regimes, separated rather sharply in wavenumber space: at smaller scales, the dynamics are those of barotropic turbulence modified by a weak zonal anisotropy; at large scales, linear dynamics dominate. Unfortunately it is at large scales that ray-tracing theory is most suspect, so these linear dynamics may be difficult to analyse. The transition scale, at least for the chosen energetic levels, is indistinguishable from the transition scale of pure beta-plane turbulence. Since the linear dynamics can change the scale of disturbances, the cascade arrest through Rossby-wave dispersion does not occur, and the slow focussing into zonal jets through resonant interactions is likewise defeated. Instead, energy penetrates to the largest scales, and is effectively trapped there by the turbulent regime lying just outside.

CHAPTER VIII - NUMERICAL SIMULATIONS: EQUILIBRIUM

§8a. Introduction

The present chapter is devoted to a discussion of a variety of forced-dissipative numerical simulations run to a state of turbulent statistical equilibrium. Examination of such experiments is essential if one wishes to make any meaningful evaluation of the role played in actual geophysical flows by the processes considered in this study, insofar as those flows - particularly the mid-latitude atmosphere - are strongly forced and dissipated, and have a full spectrum of active eddy motion.

Whether one chooses to view the dynamical scenario of this thesis as one of turbulence modified by systematic "linear" processes, or alternatively as one of wave, mean-flow interaction modified by strongly turbulent mixing, in both cases an understanding of the equilibrium problem demands an incremental approach. This has been accomplished by first, in Chapter VI, outlining an approximate linear theory to describe the spectral characteristics of the interaction between waves and a zonal basic-state flow. Then in §7d, some linear numerical simulations of a spin-down nature were presented in order to quantify and test the theoretical concepts. The next step was then to examine nonlinear simulations, using the insights gained from the previous stages to isolate the "linear" and "nonlinear" dynamical processes, and to examine the way in which each modifies the other. As described in §7e, the various diagnostics each tell a part of the story; the most useful were, however, the projection of the wave, mean-flow interaction terms on lines of constant zonal wavenumber k, and the 2-D energy spectra.

Obviously the applicability of the linear theory of Chapter VI becomes progressively more questionable with each step toward the equilibrium problem. The utility of the spin-down runs consists primarily in their clarity: fundamental turbulent processes such as nonlinear cascades and isotropization can be followed unambiguously as the spectrum fills out, while the anisotropization associated with the mean-flow straining and induced transfer can also be clearly identified. The problem with the spin-down runs is that they tend to underestimate the importance of the turbulent processes that would be operative in an equilibrated system with a filled-out spectrum.

Consequently it is necessary in this chapter to investigate forced-dissipative equilibrium regimes. The usual obstacle to understanding the dynamics of such situations is that budgets can only give inferred transfers, based on discrepancies between forcing and dissipation in regions of physical or spectral space, and these transfers are usually ambiguous unless dynamical assumptions can be invoked; the difficulty is often compounded by an uncertainty with regard to which budgets are the most dynamically significant. For example in the atmosphere, which is inhomogeneous in all three spatial dimensions and also in time, these problems have led to a considerable confusion over the nature of stationary-transient interaction which is just now beginning to be unravelled (see e.g. Hoskins, James & White, 1983; Holopainen, 1983).

Fortunately the present model is inhomogeneous in only a single dimension, which although sufficient to make the analytical problem intractable nevertheless reduces (but does not eliminate!) the interpretative quandaries. The two previous chapters have provided a number of

diagnostic criteria for identifying the dynamical behaviour of the system, and these will be seen to be invaluable - though some ambiguity cannot be avoided.

The numerical model employed is simply a forced-dissipative version of the one used in Chapter VII. The rationale behind the choice of the forcing mechanism is described in §8b, along with an outline of the various runs. §8c is devoted to the central run, whose parameters are chosen to correspond as closely as possible to the mid-latitude atmosphere. Subsequent sections examine the consequences of altering some of the external parameters, and a summary of the conclusions obtained is given in §8g.

§8b. The Model and the Experimental Choices

Some of the issues involved in the consideration of a doubly-periodic domain with a cosine zonal jet structure have already been discussed in §7b, to which the reader is referred. The numerical model used here is identical to the one described there, with the addition of intermediate-scale forcing and Ekman-type friction to dissipate energy: rather than (7.1), the governing equation is given by

$$\nabla^2\psi_t + J(\psi,\nabla^2\psi) + \beta_0\psi_x = -r\nabla^2\psi + \nu\nabla^8\psi + F_0 + F_1 . \quad (8.1)$$

F_1 represents the intermediate-scale energy/enstrophy source, designed to simulate the injection due to baroclinic instability at the scale of the deformation radius; see §3e and Fig. 3.2 for the atmospheric rationalization behind such a forcing. Note that now a triharmonic rather than a biharmonic diffusion operator has been introduced, in order to confine the enstrophy dissipation even more to high wavenumbers; this has been done because the biharmonic operator was seen in the spin-down

runs to play a stronger role than desired in the vicinity of the initial (and in the present case, the forced) scales. It may be observed that this is still a good deal less drastic than, for example, the octoharmonic operator used in the homogeneous turbulence study of Basdevant, Legras, Sadourny & Béland (1981). As in §7b, ν is made as weak as possible subject to the constraint on the "grid Reynolds number", which here is $\frac{u_{rms}}{\nu N^5}$: this suggests $\nu = 3\times10^{-9}$.

The initial conditions imposed are those of (7.6), namely a narrow isotropic band defined by $9 \leq \sqrt{(k^2+\ell^2)} < 12$. Similarly the forcing is imposed over this band, which given the scaling of (7.5c) corresponds roughly to the deformation scale κ_R of the mid-latitude atmosphere. Energetically the balance is between the input and the scale-independent Ekman friction; however the enstrophy balance is principally between the input and the high-order diffusion. This of course reflects the role of the down-scale enstrophy cascade and the up-scale energy cascade away from the forced scales. Yet the choice of the frictional operators does not induce the cascades, since they occur even in inviscid flow; rather it enables a steady state to be achieved.

There is no question that the choice of a forcing mechanism is a very troublesome matter. A few methods have been tried, and one has been settled upon, but it cannot be claimed that the scheme is entirely satisfactory. The simulations to be shown in this chapter all use the forcing

$$F_1\big(\hat{\psi}(k,\ell)\big) = \begin{cases} \gamma \dfrac{\hat{\psi}(k,\ell)}{\left|\hat{\psi}(k,\ell)\right|^2} & \text{for } 9 \leq \sqrt{(k^2+\ell^2)} < 12 \ , \\ 0.0 & \text{otherwise} \ , \end{cases} \tag{8.2}$$

which is easy to apply since (8.1) is solved in the spectral domain. The attractive aspect of (8.2) is that it provides a constant energy/enstrophy input at each mode in the forcing band:

$$\frac{\partial}{\partial t} E(k,\ell)\Big|_{F_1} = \gamma \quad ; \quad \frac{\partial}{\partial t} \Omega(k,\ell)\Big|_{F_1} = \gamma(k^2+\ell^2) \ . \tag{8.3}$$

While the enstrophy dissipation cannot be anticipated since it depends on the spectral distribution, the energy dissipation is scale independent and can be anticipated; consequently stationarity can be imposed with the initial energy level maintained. Moreover the energy-enstrophy input is always isotropic, which means that any anisotropy in the flow can only be attributable to internal processes; this is critical since anisotropy is one of the most important diagnostics examined.

Another forcing scheme considered is often called "instability" forcing, and consists of negative Ekman friction applied in the same wavenumber band. The attraction of such an approach lies in its appeal to notions of baroclinic instability, and indeed the coefficient is often chosen (e.g. Basdevant et al., 1981) to depend on wavenumber according to growth rate formulae from simple linear instability models. The negative viscosity in itself is not so troublesome, even though it would seem to be highly unstable, as the nonlinear cascades act to move energy and enstrophy away fairly efficiently. However after much experimentation with this approach it has been rejected, for two reasons. First, it is uncontrollable and causes a strong oscillation in energy input, making the approach to turbulent equilibrium unacceptably slow. Secondly the energy input cannot be guaranteed to be isotropic, in fact it tends to enter through nearly-zonal modes because the mean-flow straining is weakest there; those modes are consequently artificially energetic.

A problem which affects both of the forcing schemes described above, though the first to a lesser extent than the second, is that they

tend to reinforce the phase structure of the existing waves at the forced scales. This leads to a not inconsiderable roughness in the physical-space diagnostics on a scale of n ≈ 10, as shall be seen. While Basdevant et al. (1981) performed some experiments with the instability forcing, they were sufficiently dissatisfied with it that they also showed some runs made with a white-noise scheme, where the phases of the forcing were randomly scrambled each timestep. Clearly such a procedure would avoid the problem of phase locking, but it is difficult to get energy into the system this way without hitting it very hard. Moreover the impulse has to be monitored very carefully in order to ensure a stationary input. A reasonable compromise might involve some sort of a red-noise frequency filter: random forcing with a memory. However this would introduce non-trivial computational problems, as well as more external parameters.

It is felt that the phase locking of the first scheme is not a significant difficulty, because the turbulent mixing quickly confuses the phases for scales adjacent to the forced ones. Spectrally the problem is thus well confined, and the physical-space diagnostics simply have to be examined with a large-scale filter in mind. The method has the virtues of simplicity of application and transparency of interpretation, and it maintains an isotropic input. Since any barotropic study is necessarily limited by this problem of baroclinic-instability parameterization, there would seem to be little point in trying to perfect what is an inherently imperfect, essentially ad hoc mechanism.

It has been shown in §7b that it is possible to choose values of U, u, and β_0 based on scales appropriate to the mid-latitude atmosphere. With regard to the forcing and dissipation, there are no very good

estimates for r: in fact the use of Ekman friction itself relies on dynamical arguments (see Pedlosky, 1979, Ch.4) which may, in the case of the atmosphere, be open to some question. For the present "process" model of a shallow homogeneous fluid over a flat lower surface, the Ekman damping is supposed to represent the barotropic effects of a lower frictional boundary layer, and its use is well precedented in the literature (e.g. Lilly, 1972; Basdevant et al., 1981; Haidvogel, 1983).

While it is difficult to obtain an independent geophysical estimate of r, the (constant) energy injection rate can be determined to a certain extent. Perhaps the simplest way is to take the maximum observed up-scale kinetic energy cascade rate, which from Chapter IV and Boer & Shepherd (1983) is 4×10^{-5} J/(kg•sec). Assuming that this cascade originates from intermediate-scale baroclinic-to-barotropic conversion, one may take the same value as an estimate of the forcing parameter appropriate for a barotropic model; in fact it is probably a lower bound, but at least it gives an order-of-magnitude estimate. Putting this quantity in model units, using the scaling of (7.5), yields a total energy injection rate of 0.5, which corresponds to $\gamma = 0.0025$ for each of the approximately 200 modes in the forced wavenumber band. Since the Ekman damping rate is, from (2.5a), given by $-2rE$, this suggests taking $r = 0.5$ if the "damped" part of the spectrum, $(E-E_0)$, is to maintain an energy level of 0.5.

It is interesting that $r = 0.5$ implies a dimensional spin-down timescale of 5 terrestrial days, which happens to be the value which generally gives the best results for simple mid-latitude forced linear stationary-wave models (see e.g. Held, 1983). Without claiming the latter evidence to provide a reliable value for r, the fact that the two

quite independent estimates do not disagree is at least reassuring.

The central simulation is Run U, which takes parameter values given above as determined from the mid-latitude atmosphere; it uses the single cosine jet basic-state flow (7.2). For comparison an extended beta-plane turbulence run with the same parameters but no basic-state flow has been performed, and is entitled Run V. Then a pair of runs is considered with a higher value of β_0, almost doubling κ_β, to allow a greater scale separation between the basic-state flow and κ_β: Run W includes the jet, Run X does not. Two more single-jet runs were made with different parameter settings. In Run S, the injection rate was reduced by a factor of 20; and in Run T, the eddy energy level was doubled. It would be clearly impossible to cover all of parameter space for such extended equilibrium runs, but this set gives a fair sampling of some of the possibilities. Finally, the behaviour of higher-mode jets has been considered in two runs: Run Z has a quadruple-jet, while Run ZA has a jet with components in $\ell = 1$, 3, and 5. This leads to a whole new set of questions, and the discussion of Runs Z and ZA has therefore been relegated to an Appendix in order not to distract attention from the central dynamical regime being studied.

The runs are typically extended to $t = 50$, and averages are performed over the last 30 model days once the statistics have settled down. It is essential that this average represent a significant sampling, so one must verify that 30 days is in fact long enough to contain many "eddy turn-around periods" - the latter being an estimate of a turbulent mixing timescale. Unfortunately there is no unique way in which to define such a timescale; moreover it should presumably be scale-dependent, reflecting the different turbulent regimes of the flow.

If, however, the energy-containing eddies are localized primarily within a single octave of wavenumbers, then a crude integral measure may be considered; two possibilities are

$$\tau_1 \equiv \frac{L}{(2E)^{1/2}} = \frac{2\pi}{\kappa(2E)^{1/2}} \qquad \text{and} \qquad \tau_2 \equiv \frac{1}{(2\Omega)^{1/2}} , \qquad (8.4a,b)$$

with E and Ω representing respectively the transient (i.e. turbulent) energy and enstrophy of the flow, and L the length scale of the most energetic eddies. Obviously τ_1 characterizes the larger-scale flow component, and τ_2 the smaller-scale one; typically $\tau_1 \approx 1.$ and $\tau_2 \approx .1$ in the runs to be described, for both of which an averaging period of 30 days would thus seem adequate.

The ensemble average is generated by constructing an average of samples taken every $\Delta t = 0.2$, which is every 134 or 200 timesteps depending on the run; this corresponds to twice the enstrophy eddy turn-around timescale τ_2. The samples are not independent for the large scales, which have a mixing timescale closer to τ_1, but since the average normally consists of 150 samples this is not a problem. To verify the robustness of the statistics Run U was in fact extended to $t = 80$, and the two periods $t = 20$-50 and $t = 50$-80 were compared and found to be very similar; the matter is discussed in some detail in §8c below. There is nevertheless a sampling error involved in such a procedure: budgets for each n fail to balance by 2-3% for $n < 10$, and by as much as 10% for $n > 15$. Since the latter range covers the temporally intermittent enstrophy cascade, the imbalance there is not too surprising.

A summary of the various equilibrium runs is given in Table 8.1, indicating the external parameters, the basic-state jet structure, the two estimates τ_1 and τ_2 of (8.4) for the eddy turn-around times, and the wave-turbulence transition scale n_β.

RUN	E_0	$E-E_0$	γ	r	β_0	n_β	τ_1	τ_2	κ_e	COMMENTS
S	2.	.35	.000124	.03	25	5.5	4.8	.25	2	Reduced Ekman drag
T	2.	.94	.0025	.25	25	4	1.0	.10	5	Doubled eddy energy
U	2.	.47	.0025	.5	25	5	1.1	.11	6	Atmospheric regime
UA	2.	.47	.0025	.5	25	5	1.1	.11	6	Same parameters as U
V	0.	.47	.0025	.5	25	5	0.8	.11	8.5	β-plane turbulence
W	2.	.47	.0025	.5	65	8	0.9	.11	7.5	Higher value of β_0
X	0.	.47	.0025	.5	65	8	0.7	.11	9	β-plane turbulence
Z	2.	.47	.0025	.5	65	8	1.1	.12	6	Quadruple-jet
ZA	2.	.47	.0025	.5	65	8	0.9	.12	8	Jet with ℓ=1,3,5

Table 8.1: External and internal parameters of the various forced-dissipative equilibrium runs. E_0 is the energy of the basic-state flow, E the total energy, and κ_e the central scale of the energy-containing eddies used to obtain τ_1. All other symbols are explained in the text. Runs Z and ZA are discussed in the Appendix.

§8c. Runs U and V: The Atmospheric Regime

This section is devoted to an analysis of the central simulation of this chapter, namely Run U, for which parameter settings have been chosen to correspond as closely as possible to those of the atmosphere. The jet itself is of course only "realistic" insofar as it is zonal and of large scale relative to the disturbances. For purposes of comparison a companion beta-plane turbulence simulation entitled Run V is also examined, which is externally similar to Run U in all respects excepting the presence of the large-scale jet.

The time evolution of Run U is shown in Fig. 8.1 in terms of a few of the energetic quantities. While the intermediate-scale forcing provides a constant energy-enstrophy input to the system, there is a smaller source/sink of variable intensity at the basic-state wavenumber (0,1) which introduces a temporal fluctuation in the total energy. When $\hat{\psi}(0,1)$ falls below its initial (basic-state) amplitude, then the quantity $F_0 + (r+\nu)\hat{\psi}(0,1)$ on the rhs of (8.1) acts as a source of energy and to a lesser extent of enstrophy; this is in fact always the case in Run U, as Fig. 8.1 demonstrates. The energy input is approximately given by, for small perturbations,

$$r\nabla\hat{\psi}^*\cdot(\nabla\hat{\Psi}-\nabla\hat{\psi}) \approx r\nabla\hat{\Psi}^*\cdot(\nabla\hat{\Psi}-\nabla\hat{\psi}) \approx \frac{r}{2}\left(\left|\nabla\hat{\Psi}\right|^2-\left|\nabla\hat{\psi}\right|^2\right) = r\,\Delta E(0,1)\ ; \quad (8.5)$$

it is balanced over a time average by the interaction term in Fig. 8.1, which shows a net transfer from the basic-state scale to other smaller-scale waves. There is, however, no <u>a priori</u> constraint demanding that the equilibrium level of the basic-state jet lie below its initial value; in principle it could equally well have been above it, indicating a net transfer into the mode in order to maintain the excess.

It is nevertheless significant that the net effect of the eddies is to weaken the basic-state flow, as linear theory would predict eventual absorption and mean-flow rectification; indeed, the spin-down runs of Chapter VII all indicated net eddy-to-mean conversion. Of course a forced-dissipative simulation with a full spectrum is expected to be more turbulent than a spin-down one. The reliability of this characteristic of Run U has been verified in two different ways. First, a perturbation was made at t = 20 in which the basic-state flow component was "kicked" by a factor of 1.08 and then allowed to re-equilibrate. Despite an energy level well in excess of its initial (t=0) value, it rapidly fell back below this; the development from t = 25 to t = 40 clearly belongs to the same statistical ensemble as Run U (Fig. 8.1).

As a second test, another simulation with different initial conditions has been performed, Run UA; with white-noise forcing this would presumably be redundant, but the phase locking associated with the present forcing mechanism means that the initial conditions are not totally forgotten, and consequently such verification is necessary. The time evolution of both the total energy and that of the (0,1) component vary within the same range as they do in Run U, and with a similar (by eye) frequency spectrum; their time-mean values, moreover, are as close to the t = 50-80 values of Run U as the latter are to the t = 20-50 values of the same run. Indeed for all the diagnostics, t = 20-50 of Run UA is indistinguishable from t = 20-80 of Run U, any differences lying within the range represented by the two 30-day periods of the latter. Consequently both experiments appear to generate equivalent statistics.

The assumption made in this chapter is that the averages performed over 30 model days in each run represent an ensemble average of reason-

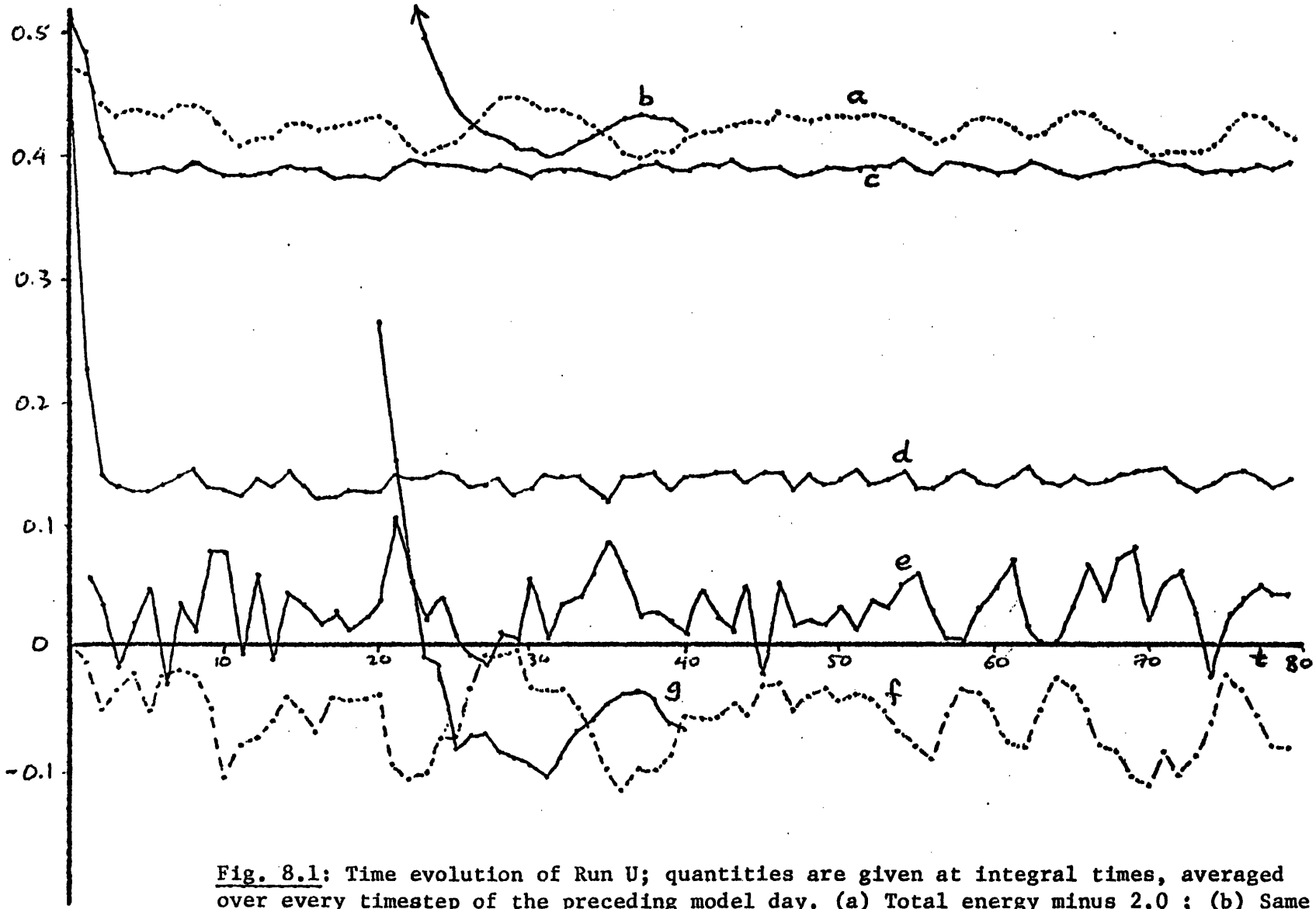


Fig. 8.1: Time evolution of Run U; quantities are given at integral times, averaged over every timestep of the preceding model day. (a) Total energy minus 2.0 ; (b) Same as (a), but for "perturbed" run from t = 20-40 ; (c) Perturbation enstrophy times 10^{-2}; (d) Energy for modes $9 \leq n < 12$; (e) Interaction from n = 1 mode; (f) Energy in (k,ℓ)= (0,1) mode minus 2.0; (g) same as (f), but for "perturbed" run from t = 20-40 (see text).

ably independent samples, which could be reproduced by a different experiment with the same external parameters. The testing of this assumption has been confined to Run U, which is thus taken to represent all such experiments; while the beta-plane turbulence Runs V and X are perhaps more problematical from this point of view, their ergodic properties being open to some question (e.g. Salmon, 1982), the emphasis of this thesis is rather on the problem of inhomogeneous waves and turbulence which characterizes Run U.

To investigate this question of statistical robustness, three 30-day periods have been defined: two are within Run U itself, t = 20-50 and t = 50-80, and the other is from t = 20-50 of the companion Run UA which has the same external parameters but a different phase mixture in the initial conditions. It has been claimed above that the three periods represent the same statistical ensemble. Examined qualitatively, for example by eyeing the figures, one is hard pressed to identify any differences at all. Since the conclusions from the numerical experiments can in any case only be interpreted qualitatively, this result would seem satisfactory.

Nevertheless, one can estimate the accuracy of the means by computing standard deviations from the means of the three periods, assuming them to be obtained from independent samples. In the case of the periods from Run U this is not completely correct, since the last samples of t = 20-50 are not totally independent at large scales from the first samples of t = 50-80 ; however this only represents a small error for such long averaging periods. The 95% confidence interval is given by $\bar{x} \pm t\sigma/\sqrt{3}$, where $2\sigma^2 \equiv \sum_{i=1}^{3} (\bar{x}-x_i)^2$ for two degrees of freedom, and t = 4.3 for this two-sided distribution. Confidence intervals for

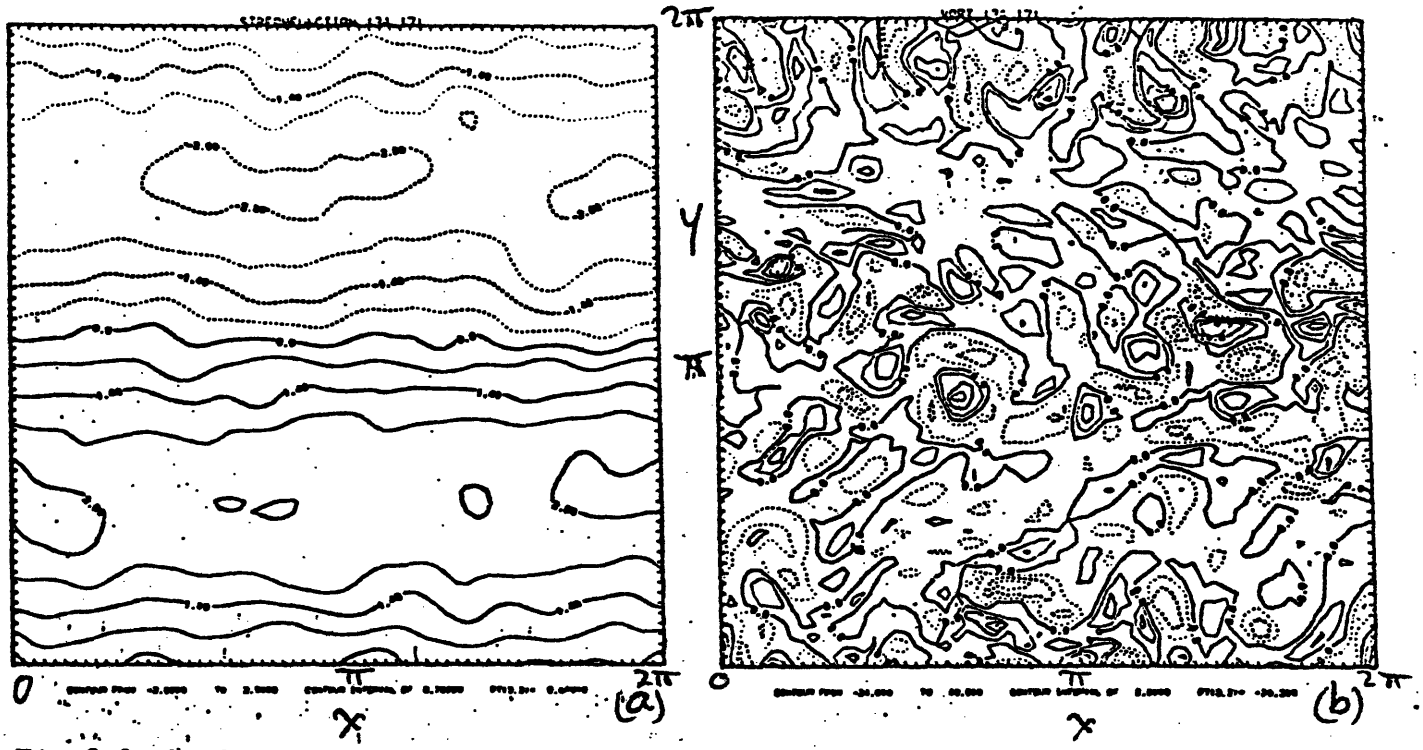


Fig.8.2a,b: Instantaneous spatial maps of total (a) streamfunction and (b) vorticity, Run U.

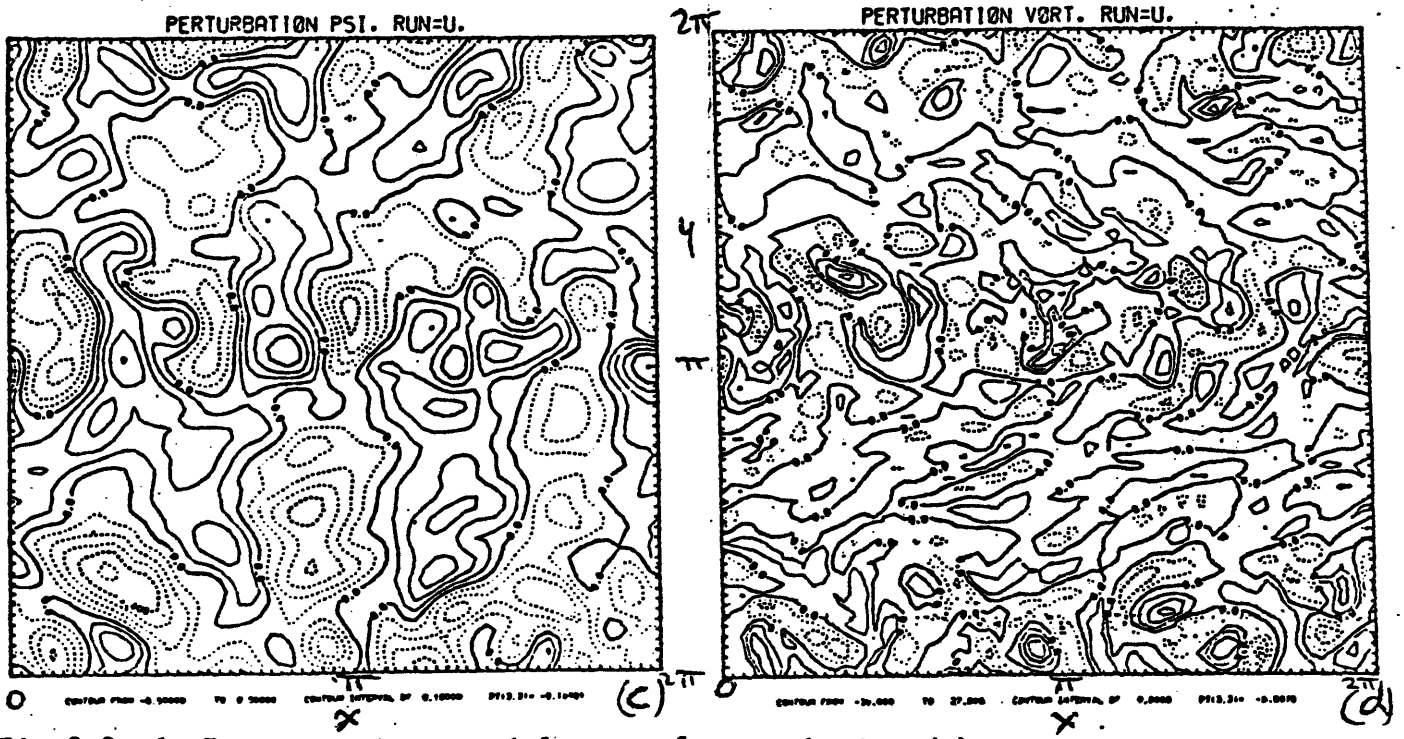


Fig.8.2c,d: Instantaneous spatial maps of perturbation (c) streamfunction and (d) vorticity, Run U.

some diagnostic quantities will be provided in the following discussion. It is felt that such intervals are probably overestimates, as one might be able to break down the entire 90-day period into more than 3 independent samples and obtain tighter estimates.

Returning to Fig. 8.1, there is considerable vacillation in the plotted quantities: for example the energy in the basic-state flow component varies aperiodically within approximately 2% of its mean value. The mean itself is 1.937 ± .010 , the 95% confidence interval lying well within the vacillation range. This vacillation cannot be attributed entirely to wave, mean-flow interaction, as the total energy varies in phase; however the total vacillation is less than half that of the (0,1) component, so most of the latter does arise out of interaction with other waves. The energy in the forced band around n = 10 also exhibits an aperiodic variation, though on a shorter timescale than that of the large-scale quantities. The perturbation enstrophy, being approximately conserved in its interaction with the mean flow, fluctuates mainly because of differing dissipation rates as the tail of the spectrum changes shape. Obviously such vacillatory behaviour is to be expected in a turbulence model; statistical equilibrium can only be defined over an ensemble of samples.

To give a sense of the flow, typical instantaneous spatial maps of streamfunction and vorticity fields for Run U are shown in Figs. 8.2: Figs. 8.2a,b represent the total fields, Figs. 8.2c,d the "perturbation" fields obtained by removing the cosine jet basic-state flow component (the two sets are not taken at the same time). The mean-flow vorticity straining is very much in evidence, as is the tendency for the perturbation streamfunction to exhibit a greater meridional scale in the

westerly ($y = \pi$) than in the easterly ($y = 0$ and $y = 2\pi$) jet.

The energy spectra for Runs U and V are shown in Figs. 8.3 through 8.6, in a 1-D representation in terms of the total wavenumber n, as well as a 2-D distribution over (k,ℓ). Both runs are clearly dominated by transient activity, with the exception of the basic-state component in Run U (Figs. 8.3a,8.4a). However the nature of the transient flows is clearly quite distinct. Run V shows the classical characteristics of beta-plane turbulence: an arrest of the up-scale transient cascade at the "Rhines radius" $n_\beta \approx 5$, though there is some leakage; zonal anisotropy for $n < n_\beta$, as the energy slowly migrates to $k = 0$ through resonant triad interactions; and an isotropic homogeneous 2-D turbulence regime elsewhere (Figs. 8.4b,8.6b). The beta-jets, though present (Fig. 8.6a), are clearly too weak to introduce any significant inhomogeneity into the flow; since they are not locked in phase, they tend to migrate around to a certain extent.

On the other hand in Run U the transient energy clearly penetrates up to the largest scales of motion, and is effectively isotropic (Figs. 8.3b,8.5b). There is a slight meridional anisotropy at large scale and zonal anisotropy at small, suggesting the influence of the "linear" mean-flow straining dynamics. However the absence of zonal anisotropy for $n < n_\beta$ in Run U itself testifies to the efficacy of this process. In both runs the stationary flow is, not surprisingly, overwhelmingly zonal (Figs. 8.5a,8.6a).

The zonal-meridional breakdown for Run U is given quantitatively in Table 8.2, where it is seen that the large-scale meridional anisotropy is statistically significant to 95% confidence for $n = 3$ and $n = 5$, and to 90% confidence for $n = 3$-5 ; while the small-scale zonal aniso-

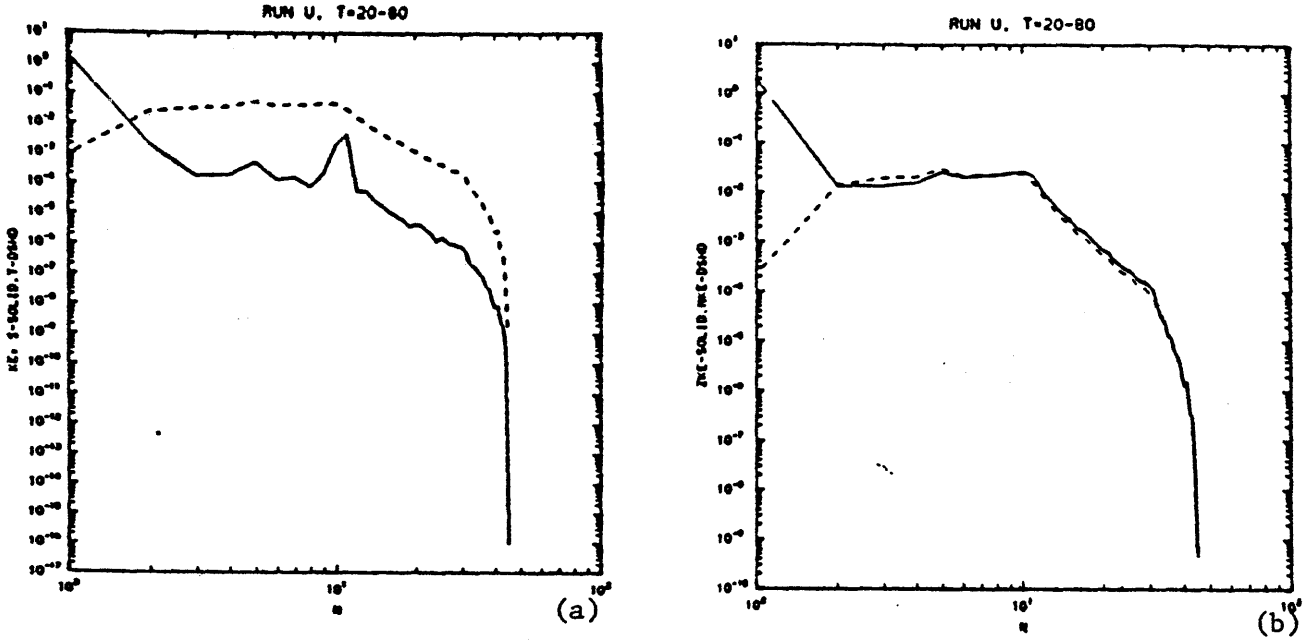


Fig. 8.3: (a) Stationary (——) and transient (- -) , and (b) zonal (——) and meridional (— —), energy n-spectra, Run U, t = 20-80.

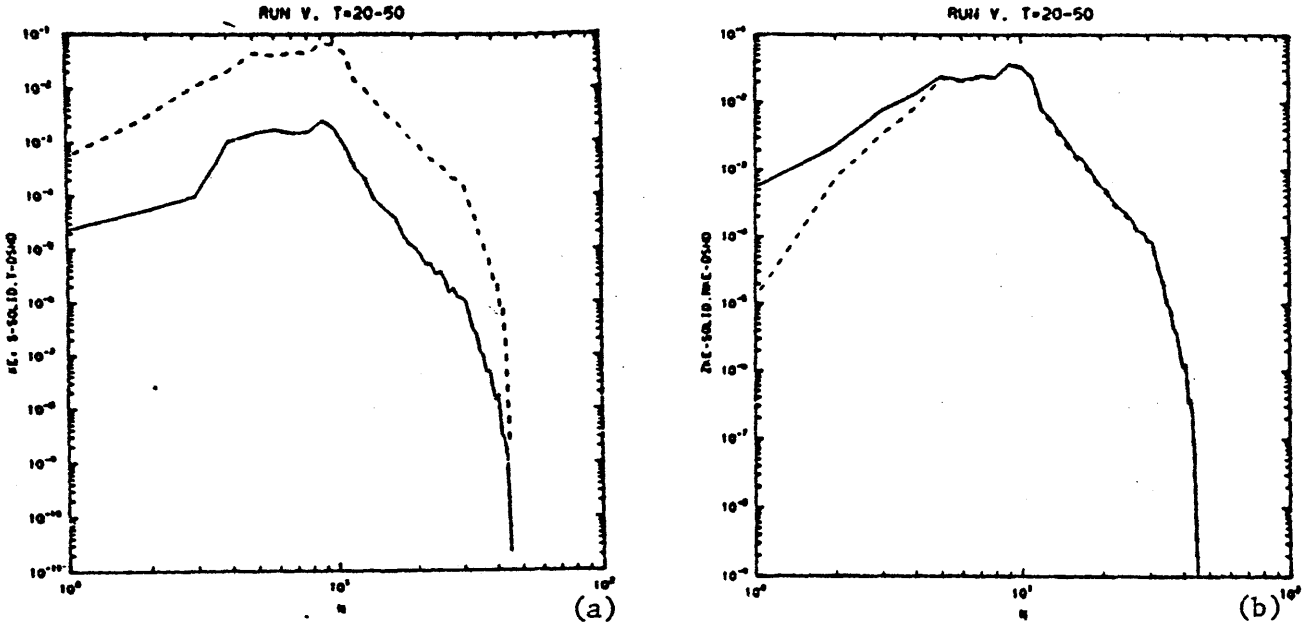


Fig. 8.4: Same as Fig. 8.3, but for Run V, t = 20-50.

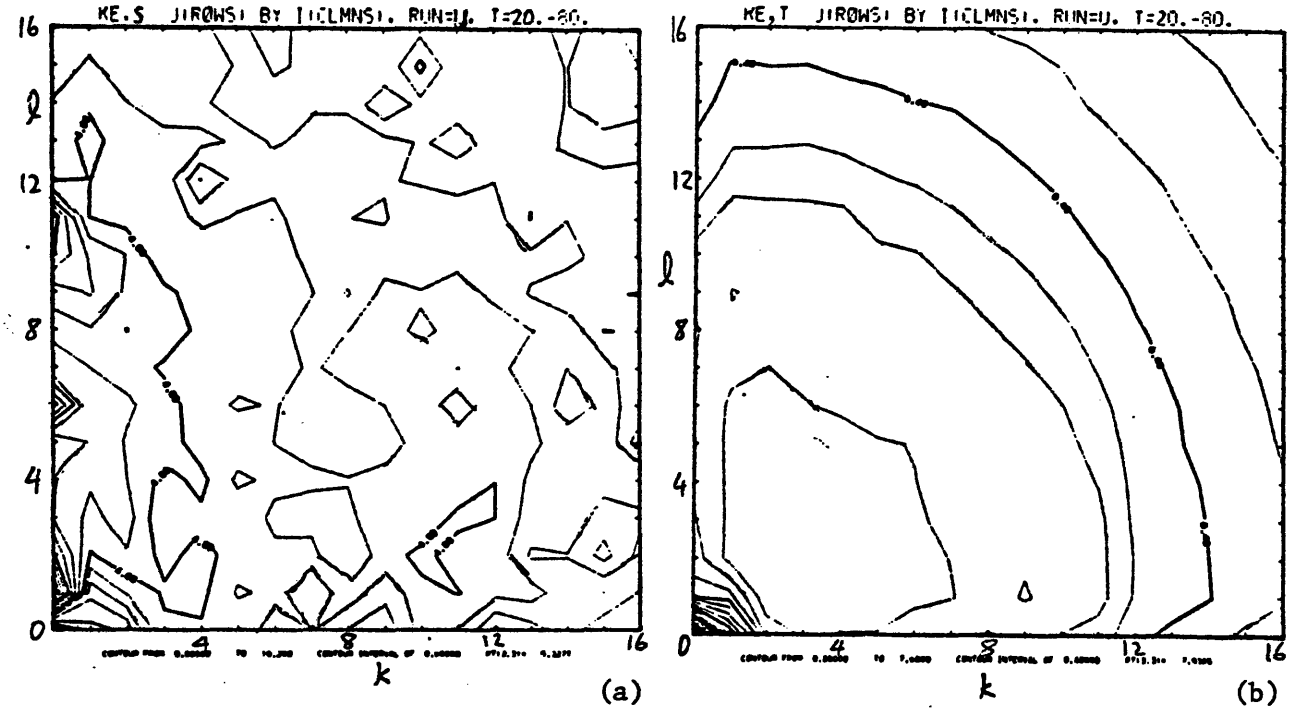


Fig. 8.5: 2-D (k,ℓ)-spectra of (a) stationary and (b) transient energy, Run U, t = 20-80 . k runs across from 0 to 16, ℓ runs up from 0 to 16.

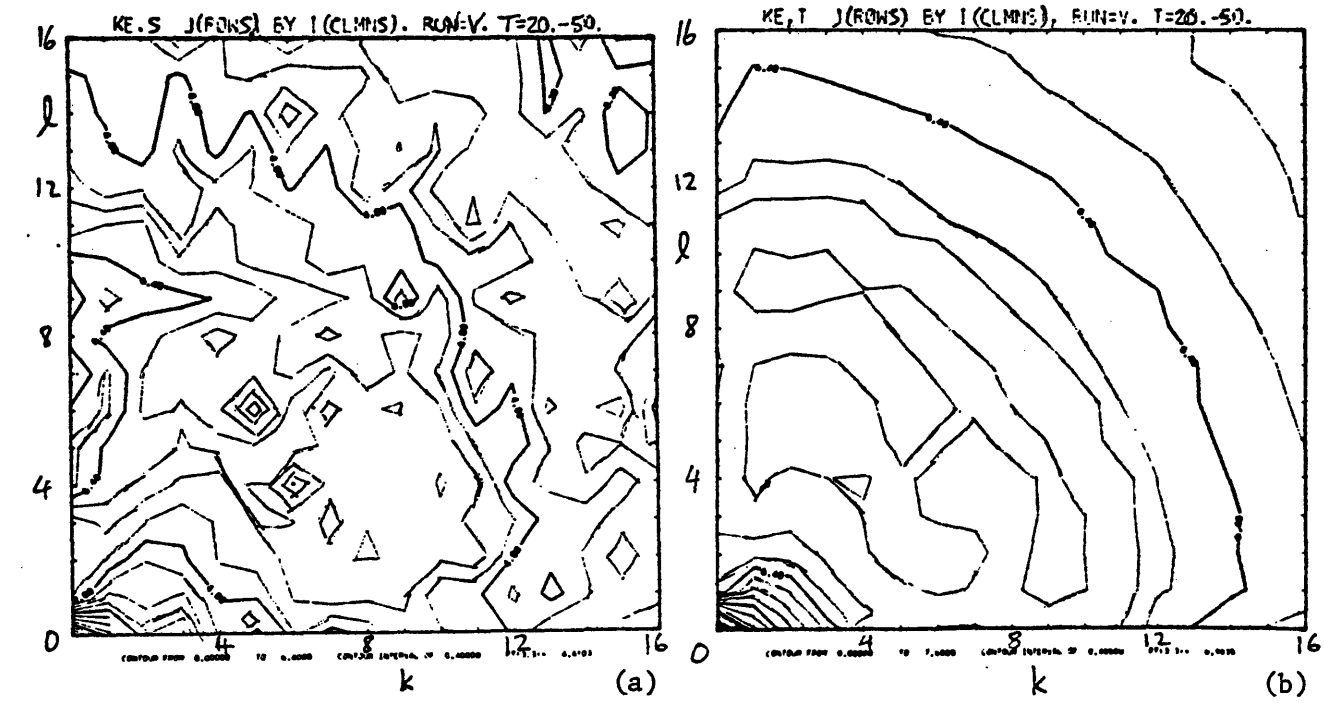


Fig. 8.6: Same as Fig. 8.5, but for Run V, t = 20-50 .

n	ZKE(n)×10²	MKE(n)×10²	$\frac{ZKE(n)-MKE(n)}{(\Delta Z+\Delta M)}$
1	193.7 ± 1.0	.0218 ± .0025	-
2	1.38 ± .24	1.46 ± .31	-.15
3	1.32 ± .24	1.97 ± .28	-1.3
4	1.62 ± .07	2.01 ± .49	-.70
5	2.63 ± .09	3.09 ± .27	-1.3
6	2.02 ± .07	2.16 ± .30	-.38
7	2.28 ± .27	2.37 ± .23	-.18
8	2.26 ± .08	2.16 ± .15	.44
9	2.45 ± .10	2.46 ± .17	.04
10	2.67 ± .34	2.35 ± .05	.82
11	2.03 ± .33	1.55 ± .03	1.3
12	.966 ± .010	.791 ± .003	13.5
13	.626 ± .018	.493 ± .012	4.4
14	.383 ± .012	.303 ± .021	2.4
15	.279 ± .015	.220 ± .007	2.7
16	.191 ± .012	.150 ± .008	2.1
17	.163 ± .004	.130 ± .012	2.1
18	.120 ± .003	.0934 ± .0011	6.7
19	.0882 ± .0031	.0693 ± .0012	4.4
20	.0697 ± .0023	.0542 ± .0023	3.4
21	.0607 ± .0025	.0473 ± .0010	3.8
22	.0447 ± .0010	.0342 ± .0011	5.0
23	.0363 ± .0007	.0277 ± .0016	3.7
24	.0309 ± .0020	.0240 ± .0009	2.4
25	.0275 ± .0018	.0209 ± .0007	2.6
26	.0231 ± .0010	.0178 ± .0009	2.8
27	.0183 ± .0000	.0138 ± .0002	22.5
28	.0160 ± .0002	.0120 ± .0002	10.0
29	.0154 ± .0006	.0117 ± .0002	4.6
30	.0133 ± .0007	.00966 ± .00020	4.0
31	.0107 ± .0003	.00904 ± .00009	4.2
32	.00525 ± .00004	.00467 ± .00012	3.6

Table 8.2: Zonal and meridional energy n-spectra for Run U, shown with 95% confidence interval as determined according to description in text. Last column shows the difference divided by the sum of the confidence intervals, to give an indication of the significance of the anisotropy. Note that n = 4 is significantly anisotropic to 90% confidence.

tropy is significant to 95% confidence for $n > 10$.

Whereas it was argued in the spin-down runs that irreversibility of the induced up-scale "linear" cascade and consequent trapping of energy at large scale demanded nonlinear mixing, one might object that in the present case, the strong frictional damping due to the Ekman drag of $r = 0.5$ could well introduce such irreversibility even with purely linear dynamics. However it would not lead to trapping: disturbances would simply experience a form-preserving decay as they followed their reversible paths out to large ℓ (Tung, 1983). In any case it is not hard to identify the importance of turbulent processes in Run U. A direct approach is to examine the actual spectral transfer functions, and this shall be done shortly. But one can also see the evidence in the spectra: Fig. 8.5b clearly demonstrates the isotropization which arises from the efficiency of nonlinear interactions in diffusing energy along lines of constant total wavenumber n.

To unravel the dynamics that give rise to the spectra it is necessary to look at several different projections of the spectral transfer terms for energy and enstrophy. First consider Figs. 8.7a,b, which show the two different stationary-transient conversion terms C and EMI as functions of the zonal wavenumber k. Note that for a zonal stationary flow of wavenumber one, the energy and enstrophy conversions are identical in this representation. Run U (Fig. 8.7a) indicates a net loss of energy by the stationary flow from the zonal $k = 0$ component, which is consistent with what was concluded from Fig. 8.1; the present figure demonstrates further that this transfer goes into transient waves with $k < 6$, and primarily into $k = 2,3$, while transients with $k > 6$ lose energy to the stationary flow. Such behaviour is characteristic of

the early development of the linear dynamics, and suggests that the latter are effective in the vicinity of the forced band. While the higher-k modes have small initial ℓ and are consequently in the absorption phase of their straining very quickly, their loss is more than offset by the gain from k = 2-5.

The conversion terms for Run V show a not dissimilar pattern (Fig. 8.7b), but the magnitudes are about a tenth of those for Run U, and the stationary term C(k) is not so cleanly confined to the zonal mode. Consequently the notion of mean-flow straining is somewhat less applicable: unlike the case for a zonal flow, stationary-transient triads can couple transient waves with different values of k.

Now consider the spectral transfers as a function of the total wavenumber n. The conversion terms C and EMI are given in Figs. 8.8 and 8.9 for the two runs; note that now the energy and enstrophy forms are quite different. Run U demonstrates a net energy conversion that is of the same order as most of the transfer terms (Fig. 8.8a): consequently the mean-flow straining must be considered to be partly induced transfer and partly mean-flow weakening, but neither one nor the other alone. The transfer away from the forced wavenumber band was seen in the spin-down runs, but here it leads to a strong net transfer into transients with $n < n_\beta$. 95% confidence intervals are included in Fig. 8.8a, and show the character of the picture to be quite robust.

On the other hand the enstrophy interaction (Fig. 8.8b) involves little net conversion, and can be accurately characterized as induced transfer within the immediate vicinity of the forced band. Obviously the nonlinear "scrambling" acts very quickly to truncate the induced enstrophy cascade; in contrast the strong up-scale energy transfer is

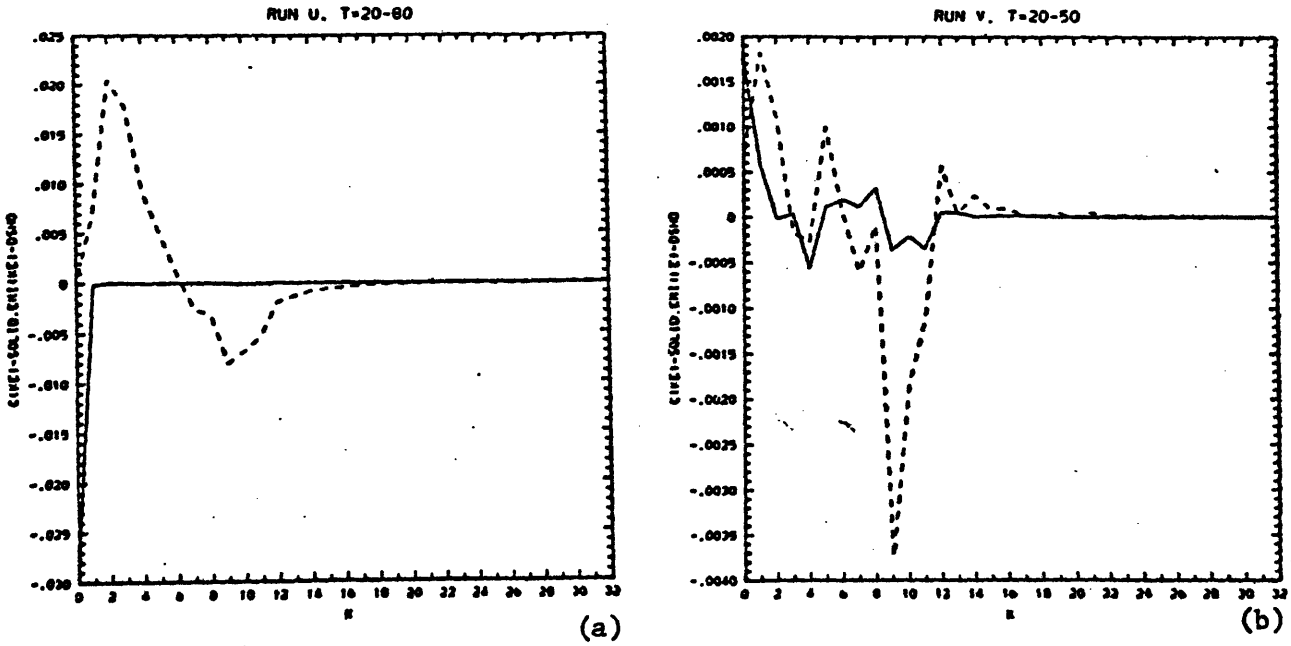


Fig. 8.7: k-space conversion terms C(k) (——) and EMI(k) (– –), for (a) Run U, t = 20–80 , and (b) Run V, t = 20–50 .

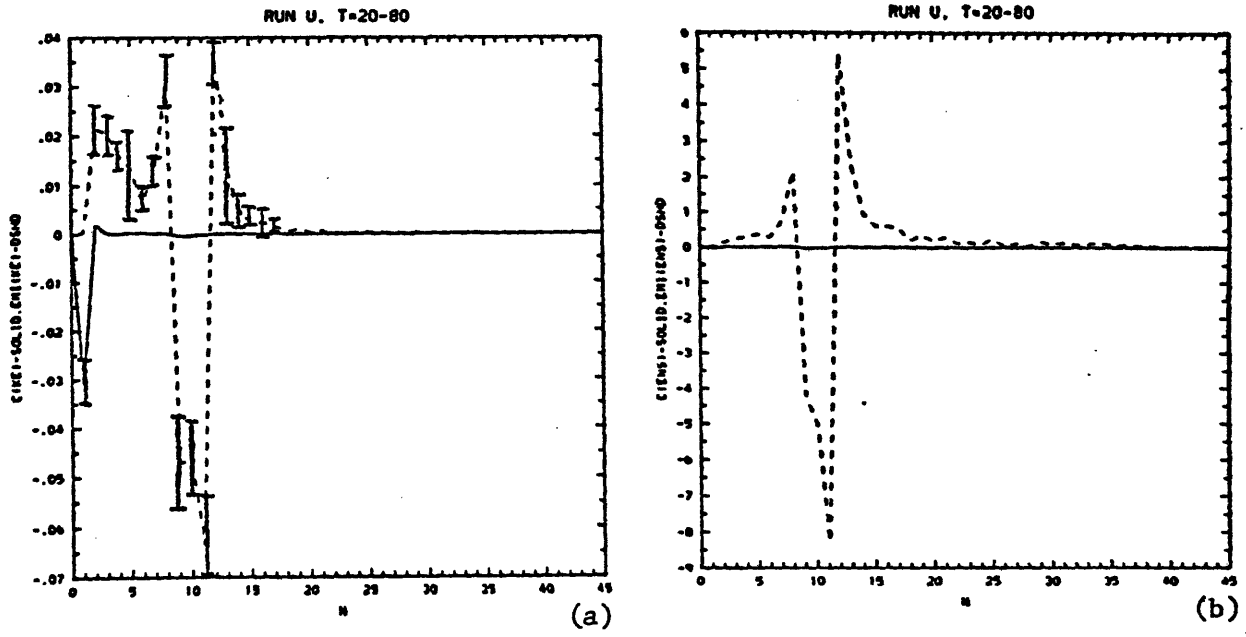


Fig. 8.8: n-space conversion terms: (a) for energy, C(n) (——) and EMI(n) (– –) , with error bars indicating 95% confidence interval (see text); (b) for enstrophy, $n^2C(n)$ (——) and $n^2EMI(n)$ (– –); both for Run U, t = 20–80 .

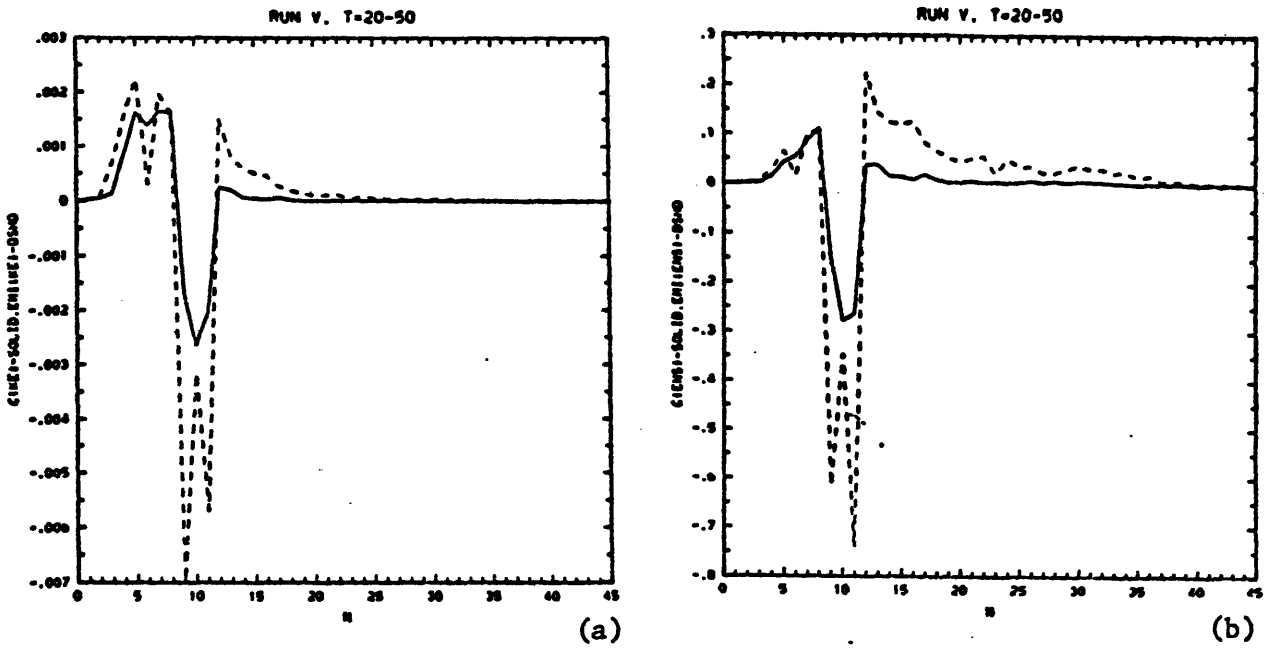


Fig. 8.9: Same as Fig. 8.8, but for Run V, t = 20–50.

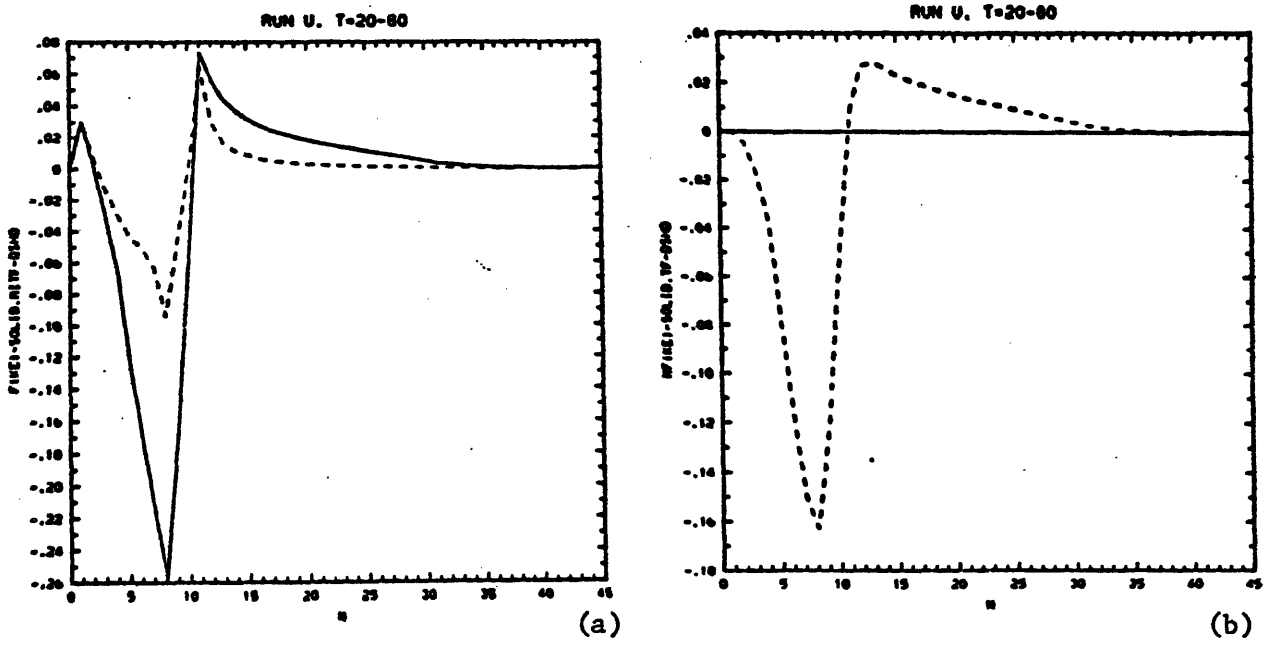


Fig. 8.10: (a) Total flux of energy F(n) (——) and induced flux MITF(n) (– –) ; (b) stationary flux MF(n) (——) and transient flux TF(n) (– –); Run U, t = 20–80. Note that F = MITF + MF + TF .

due to the amplification factor involved in that process. However the net effect of the linear dynamics, when viewed in this representation, is not easily distinguishable from the cascades of 2-D turbulence; this is a major theme of the present study.

As far as frictional effects are concerned, away from direct forcing at $n = 1$ or $n = 9$-11 the balance is strictly between nonlinear transfer and friction, and in Run U the Ekman drag dominates the triharmonic diffusion for $n < 23$. This intrinsic budgetary constraint notwithstanding, the nonlinear transfer functions show the effectiveness of the cascades inasmuch as a forced-dissipative equilibrium could in principle be achieved without any nonlinear transfer whatsoever; however such a dull outcome is happily not the case, the dynamics being manifestly more intriguing as a result.

It is evident from Figs. 8.9a,b that a similar mean-flow straining and induced transient cascade process occurs due to the beta-jets in Run V. However the strength is comparatively small, and furthermore the stationary flow is active at all scales; indeed the enstrophy terms show a net conversion, reflecting the lack of a scale separation between the stationary and transient flows.

Defining flux terms as in §7c, the total nonlinear flux of energy F can be divided into three parts: TF due to transient self-interactions TSI of (7.17b); MF due to stationary self-interactions MSI of (7.20b); and MITF due to stationary-transient interactions MITI of (7.23); recall that $F = TF + MF + MITF$. Now, Fig. 8.10a indicates a strong transfer from the forced intermediate-scale band to larger scales, with a much smaller transfer from $n = 1$. The total flux is dominated by TF, but MITF is clearly active and is especially important at the largest

scales; MF is effectively zero (Fig. 8.10b). In Run V the only significant component is TF (Figs. 8.11a,b), and it is arrested fairly effectively at n = 4,5 - as indeed is TF in Run U.

The maximum total up-scale energy flux in Run U, attained at n = 8, is 0.2583 ± .0065 ; the maximum down-scale enstrophy flux, attained at n = 11, is 26.53 ± .40 ; both are with 95% confidence. Admittedly these values are rather strongly controlled by the constant forcing. Yet because of this they show the sampling error to be acceptably small.

As a final way of investigating the spectral transfer functions of Run U, consider the conversion terms represented in terms of the meridional wavenumber ℓ along slices at fixed k; these were found in the spin-down runs to be very illuminating diagnostics. Figs. 8.12 to 8.14 show these statistics for energy and enstrophy for k = 2, 4, and 6; note that now the sum of C and EMI need not vanish, in fact for these $k \neq 0$ components $C(\ell)$ is nearly zero. The enstrophy conversions show approximate conservation along each slice, suggesting the appropriateness of the induced transfer concept for this quantity. In all three cases the transfer is fairly symmetric in amplitude, though the penetration is greater on the up-scale side; this is presumably due to the increasingly less turbulent nature of the dynamics at large scale. While for k = 2 and k = 4 there is a significant truncation of the induced cascade outside of scales immediately adjacent to the forced band, with k = 6 the faster rays manage to smooth the truncation somewhat.

In terms of energy transfers, the strong amplification factor found for k = 2-4 in the spin-down runs (and in agreement with the linear theory of Chapter VI) persists here (Figs. 8.12a,8.13a), and the non-conserved nature of the transient energy is evident. By comparing

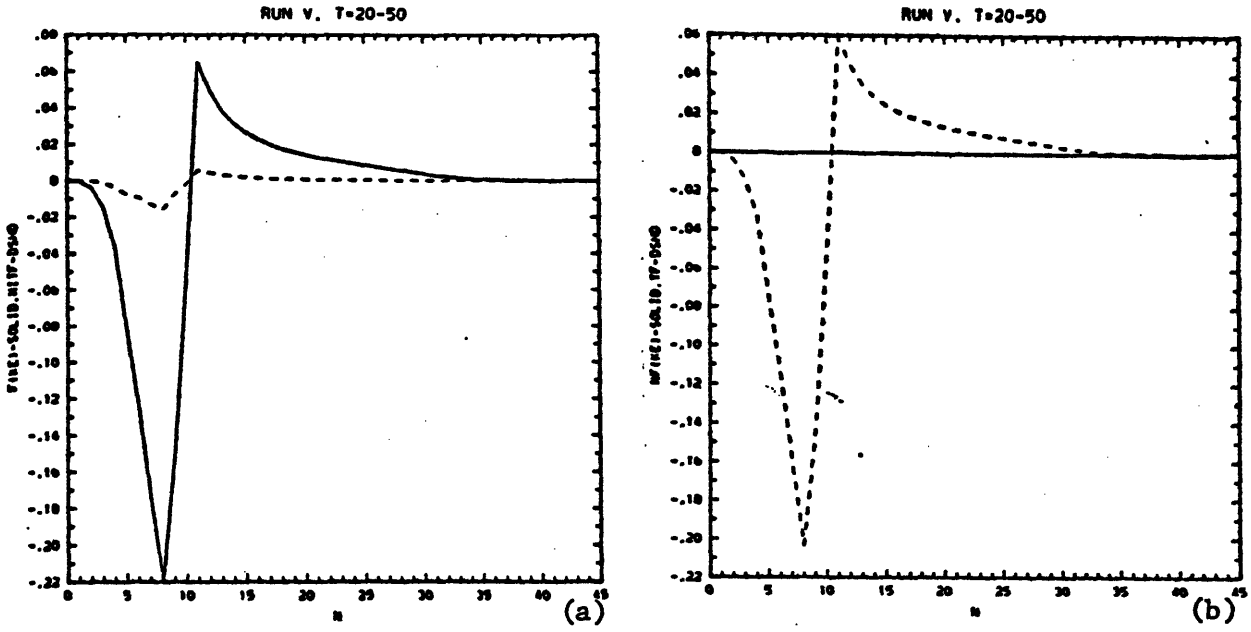


Fig. 8.11: Same as Fig. 8.10, but for Run V, t = 20-50 .

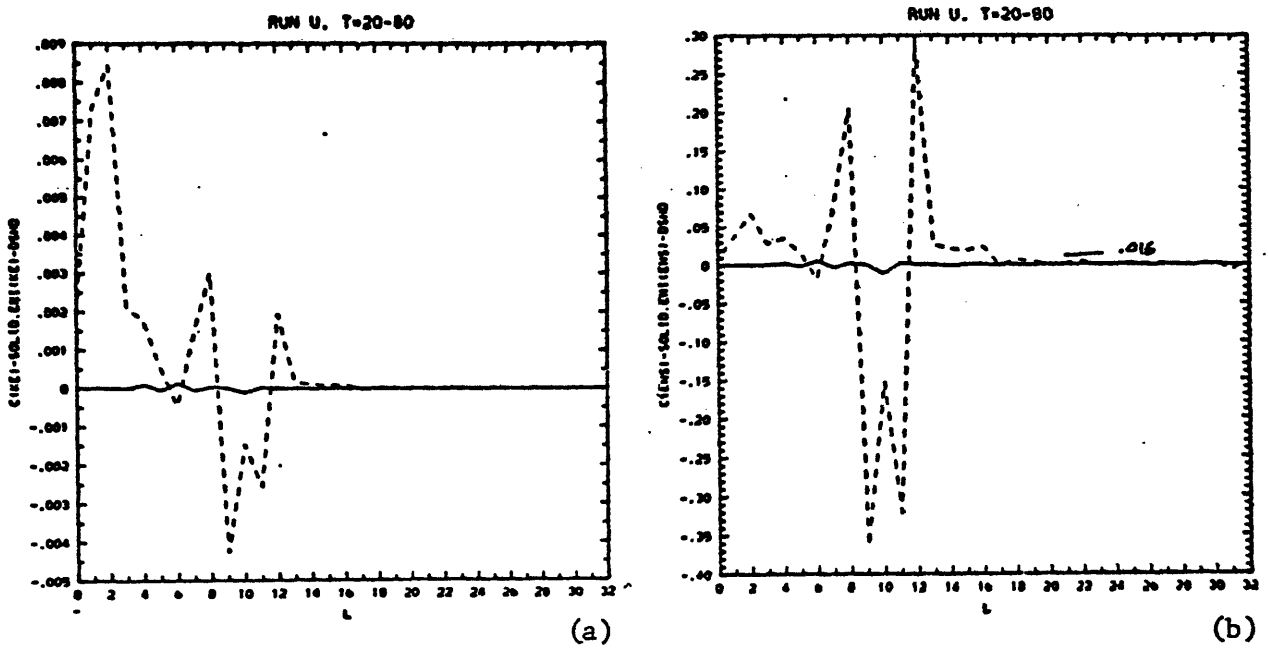


Fig. 8.12: ℓ-space conversion terms for the slice k = 2: (a) for energy, $C(\ell)$ (——) and $EMI(\ell)$ (– –); (b) for enstrophy, $n^2C(\ell)$ (——) and $n^2EMI(\ell)$ (– –); Run U, t = 20-80 . Mark on (b) shows the magnitude of the sum $\sum_{\ell=0}^{n} EMI(\ell)$, or the extent of non-conservation.

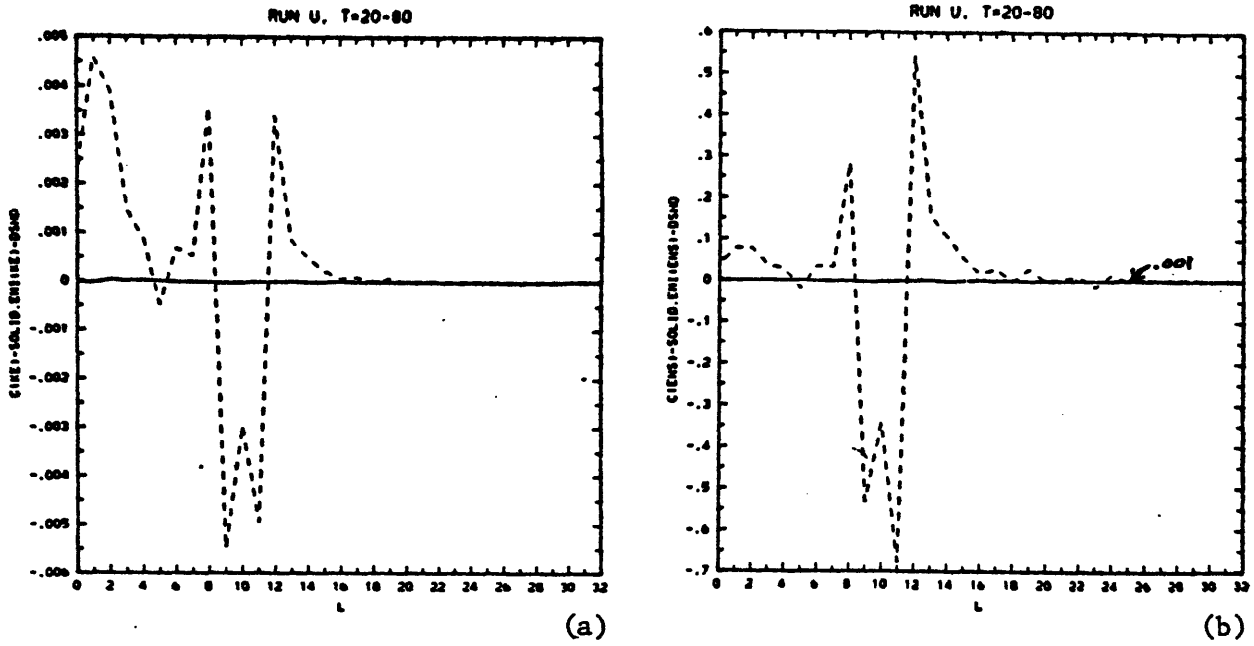


Fig. 8.13: Same as Fig. 8.12, but for k = 4 .

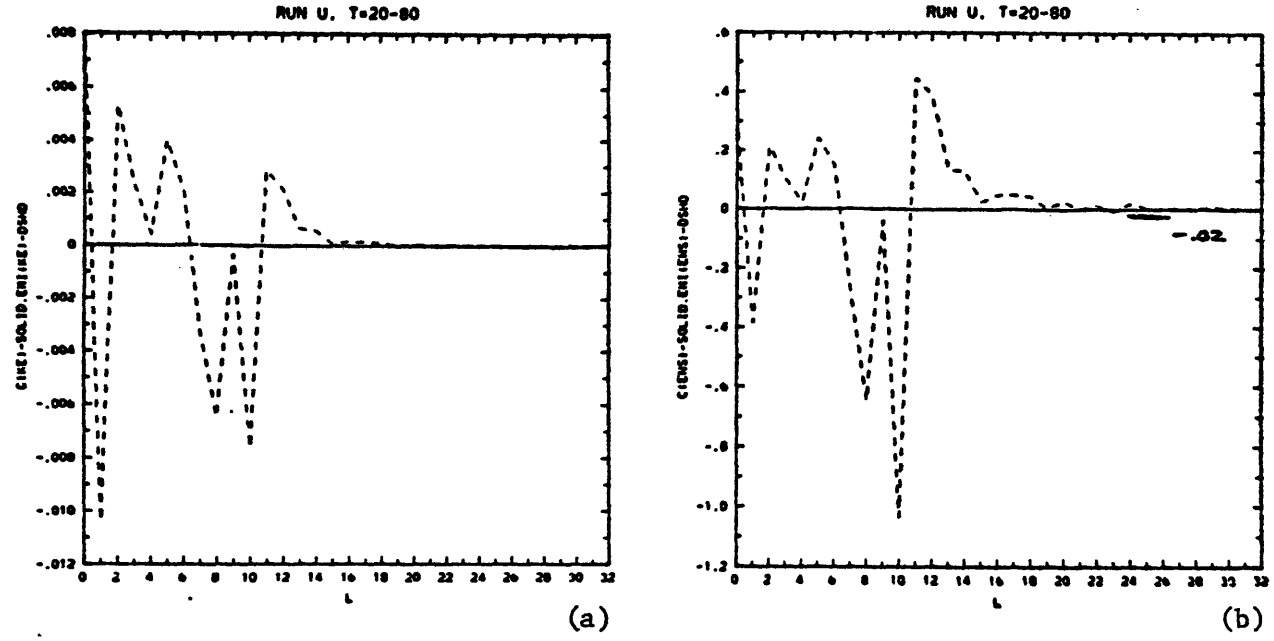


Fig. 8.14: Same as Fig. 8.12, but for k = 6 .

these figures with Figs. 7.34 through 7.37 of the nonlinear spin-down Run O, and even more with Figs. 7.12 through 7.17 of the linear spin-down Run R, it is very clear that the linear dynamical processes described so extensively in this thesis are important in the initial development of the forced intermediate-scale waves, but not after their maximum amplification; irreversibility introduced by the turbulent dynamics strongly alters the nature of the wave, mean-flow interaction. This may explain why the equilibrated zonal flow is weakened by the eddies: the latter extract energy in their initial linear development, but fail to give it back as their decay phase is aborted by the turbulent mixing.

While the spectral diagnostics are invaluable in deciphering the dynamics of Run U, much can also be derived from the physical-space statistics - provided that one looks on the large scale of the flow inhomogeneity rather than on the $\ell \approx 10$ scale which dominates the forced waves. In Chapter VII it was seen that terms such as the Reynolds stress were rather rough, and various attempts were made to explain this; one would however expect forced-dissipative equilibrium runs to be rather less sensitive to their initial conditions, though with the particular forcing mechanism used this is not as true as it might be.

The time-mean zonal flow is depicted in Fig. 8.15a, along with the basic-state jet. Although the (0,1) component of the equilibrated jet has been shown to be weaker than that of the basic-state flow, the small value of the difference is obvious here: the "kinks" associated with the phase-locked intermediate-scale forcing in fact overwhelm any difference in the large-scale pattern. The weakness of the net wave, mean-flow interaction was also seen in Fig. 8.8a, for example: the primary role of

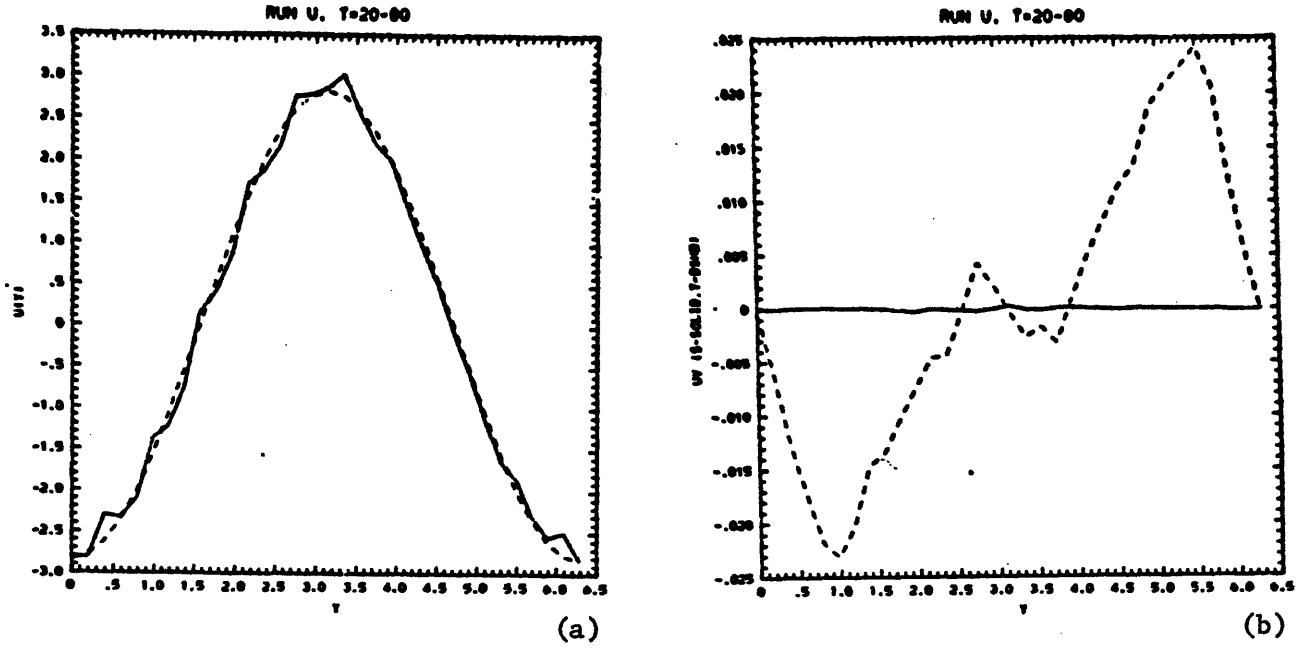


Fig. 8.15: (a) Time-averaged zonal flow $\bar{U}(y)$ (——), basic-state flow (- -); (b) Stationary (——) and transient (- -) Reynolds stress terms $\langle\overline{uv}\rangle(y)$; Run U, t = 20-80 .

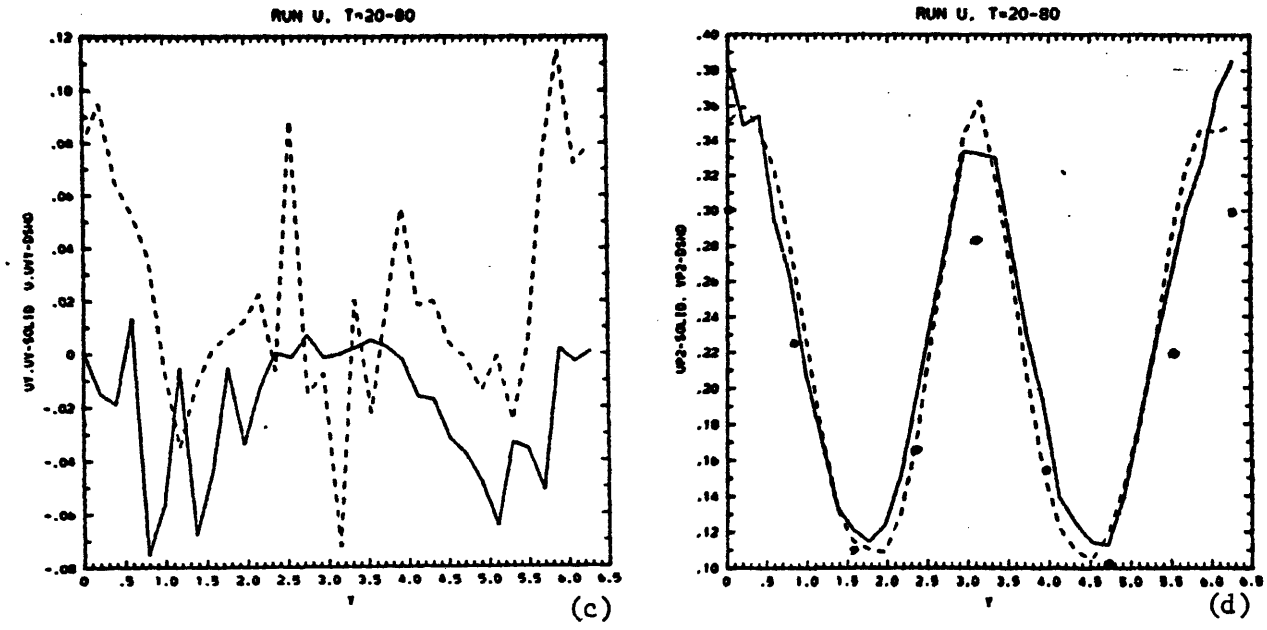


Fig. 8.15: (c) Conversion terms $\bar{U}\,\overline{uv}_y$ (——) and $\bar{U}(\overline{uv})_y$ (- -); (d) Transient variances $\langle\overline{u'^2}\rangle$ (——) and $\langle\overline{v'^2}\rangle$ (- -), dots indicate the former with the k = 0 component removed, at selected y. Run U.

the mean flow is a catalytic one of induced spectral transfer. More will be said about this somewhat negative result later, after some of the other equilibrium runs have been considered. It may be added that the northward gradient of mean potential vorticity is often close to zero, but is always positive.

Figs. 8.15b,c show respectively the averaged Reynolds stress term $\langle\overline{uv}\rangle$, and the zonal-wave conversion terms $\bar{u}(y)d\langle\overline{uv}\rangle/dy$ and $\langle\overline{uv}\rangle d\bar{u}(y)/dy$. The pattern indicates eddy energy gain in the strongly sheared regions $y = \pi/2$ and $y = 3\pi/2$, as the eddies extract energy from the mean-flow straining most efficiently there, and this shows up in the loss of mean zonal energy from the easterly jet. At the same time there is a sharpening of the westerly jet. These features can be seen in the zonal jet itself (Fig. 8.15a), but the effect is weak and one must look very closely indeed. The sharpening of the westerly jet core may be explained by the fact that the eddies forced there can only propagate into increasingly easterly flow, and can consequently only give up their energy to the zonal flow: no extraction is possible.

Finally the transient eddy variances $\langle\overline{u'^2}\rangle$ and $\langle\overline{v'^2}\rangle$ are presented in Fig. 8.15d. The near isotropy of the transients is evident but their distribution is far from being homogeneous, as maxima occur in both jet cores. Recall that the homogeneous nature of the forcing puts in energy evenly over y. One might choose to explain the minima in the strong-shear regions as being due to the rapid "induced transfer" that acts there. At the same time the maxima may have their own significance. In the spin-down runs a similar concentration of variance was observed in the jets, but was attributed to two quite distinct processes: the westerly jet maximum being due to amplification of disturbances as they

passed through it; the easterly jet maximum reflecting a trapping of energy by turning lines in the vicinity of $y = 0$.

For the equilibrium runs of this chapter, however, the interpretation of the variance maxima must be somewhat more cautious. The strength of the linear dynamical "signature" of induced transfer in ℓ-space (e.g. Figs. 8.12-8.14) suggests that it is responsible for the westerly jet maximum; and the near isotropy of the eddies there can be attributed to the rapidity of the turbulent mixing observed also in the 2-D energy spectrum (Fig. 8.5b). On the other hand, if the $k = 0$ component of $\overline{\langle u'^2 \rangle}$ is removed to obtain the traditional transient eddy variance, then one sees definite meridional anisotropy. It can be argued that since it is only the non-zonal (i.e. $k \neq 0$) eddies that participate in the mean-flow straining, the latter filtered field is the one that should be used to investigate those dynamics. However the validity of such an approach is not so clear for a flow as turbulent as that of Run U: in the extreme case of homogeneous isotropic turbulence, for example, removal of the $k = 0$ component would also produce meridional anisotropy, but this would have no dynamical significance.

Zonal-wavenumber spectra of $\overline{\langle u'^2 \rangle}$ and $\overline{\langle v'^2 \rangle}$ are displayed in Table 8.3 for certain key values of y. The fact that the former peak at lower k than do the latter is of course a geometrical constraint. A consistent pattern emerges from the $\overline{\langle v'^2 \rangle}$ field, namely that the maximum variance is obtained at lower k in the strong-shear regions $y = \pi/2$ and $y = 3\pi/2$ than in the jet regions $y = 0$ and $y = \pi$. An explanation for this, consistent with what has already been seen, might be that since higher-k modes are the most rapidly strained, the latitudes which are dominated by such straining have little energy in those zonal scales. Coincident-

k	y=0	y=π/4	y=π/2	y=3π/4	y=π	y=5π/4	y=3π/2	y=7π/4
0	.087	.038	.010	.025	.048	.038	.012	.037
1	.056	.043	.029	.042	.061	.037	.027	.042
2	.060	.049	.029	.034	.056	.035	.026	.045
3	.040	.035	.020	.026	.043	.024	.016	.042
4	.039	.027	.012	.019	.033	.018	.011	.031
5	.028	.021	.007	.015	.029	.012	.007	.023
6	.024	.017	.006	.010	.021	.010	.005	.013
7	.019	.012	.003	.009	.018	.007	.003	.010
8	.014	.008	.002	.005	.009	.004	.002	.007
9	.010	.005	.001	.004	.007	.004	.002	.006
10	.006	.003	.001	.003	.004	.002	.001	.003
11	.002	.002	.001	.002	.002	.001	.001	.002
12	.001	.001	.000	.001	.001	.000	.000	.001

Table 8.3(a): Transient eddy zonal energy spectrum of variance $\langle u'^2 \rangle(k)$ for k = 0-12 at selected values of y.

k	y=0	y=π/4	y=π/2	y=3π/4	y=π	y=5π/4	y=3π/2	y=7π/4
0	.000	.000	.000	.000	.000	.000	.000	.000
1	.002	.002	.002	.004	.004	.003	.002	.002
2	.006	.009	.020	.025	.028	.027	.020	.009
3	.019	.032	.032	.020	.029	.017	.034	.032
4	.034	.043	.019	.016	.036	.017	.021	.044
5	.042	.041	.012	.019	.046	.016	.013	.037
6	.047	.039	.010	.021	.044	.014	.010	.032
7	.041	.028	.005	.018	.045	.013	.006	.031
8	.036	.023	.004	.012	.039	.011	.004	.025
9	.046	.022	.003	.013	.040	.017	.004	.033
10	.041	.021	.003	.010	.031	.010	.003	.020
11	.028	.015	.002	.009	.016	.007	.002	.013
12	.008	.005	.001	.003	.005	.003	.001	.005

Table 8.3(b): Transient eddy meridional energy spectrum of variance $\langle v'^2 \rangle(k)$ for k = 0-12 at selected values of y.

ally the lower-k modes, which have the greatest potential amplification, achieve their maximum amplitude in the westerly jet; this effect cannot however explain the maximum in the easterly jet, whose existence must be tentatively attributed to trapping of locally-forced low-k waves by turning lines in the mean zonal flow.

§8d. Runs W and X: Effects of Stronger Beta

One of the principal arguments of this study is that the process of mean-flow straining, which characterizes the interaction between waves and a sheared zonal flow, is capable of transferring disturbance energy and, more properly, enstrophy past the cascade arrest scale n_β of beta-plane turbulence. The correctness of this hypothesis, as well as of the complementary hypothesis concerning the irreversible effects of nonlinear, turbulent mixing, has been demonstrated in the numerical simulation experiments of this and the previous chapters. However, the scale separation between the basic-state flow $n = 1$ and the observed cascade arrest scale of the beta-plane turbulence runs with $\beta_0 = 25$ is not particularly great: in the spin-down Run P the latter is $n = 3$, in the forced-dissipative Run V it is $n = 5$ (the difference arising because the evolution past $n = 5$ is very slow and thus easily damped by the Ekman drag), while the theoretical estimate based on $u_{rms} = 1$ is $n_\beta = 5$.

Consequently a set of runs similar to U and V but with higher beta has been performed: $\beta_0 = 65$ so $n_\beta \approx 8$. Because the generic issues involved in all of the equilibrium runs, as well as the principal results, have already been discussed in §8c, here the emphasis will be placed on the differences with Runs U and V. The experiment with the single-jet basic-state flow is entitled Run W, that of pure beta-plane

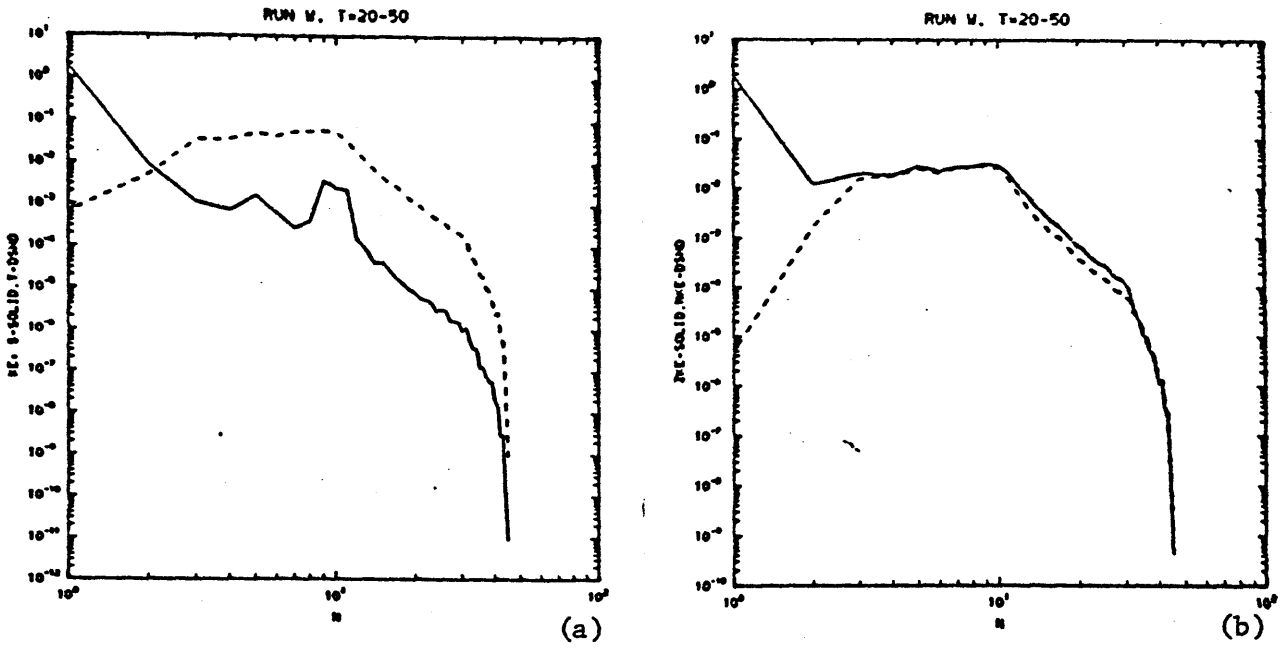


Fig. 8.16: (a) Stationary (——) and transient (– –) , and (b) zonal (——) and meridional (– –) , energy n-spectra, Run W, t = 20-50 .

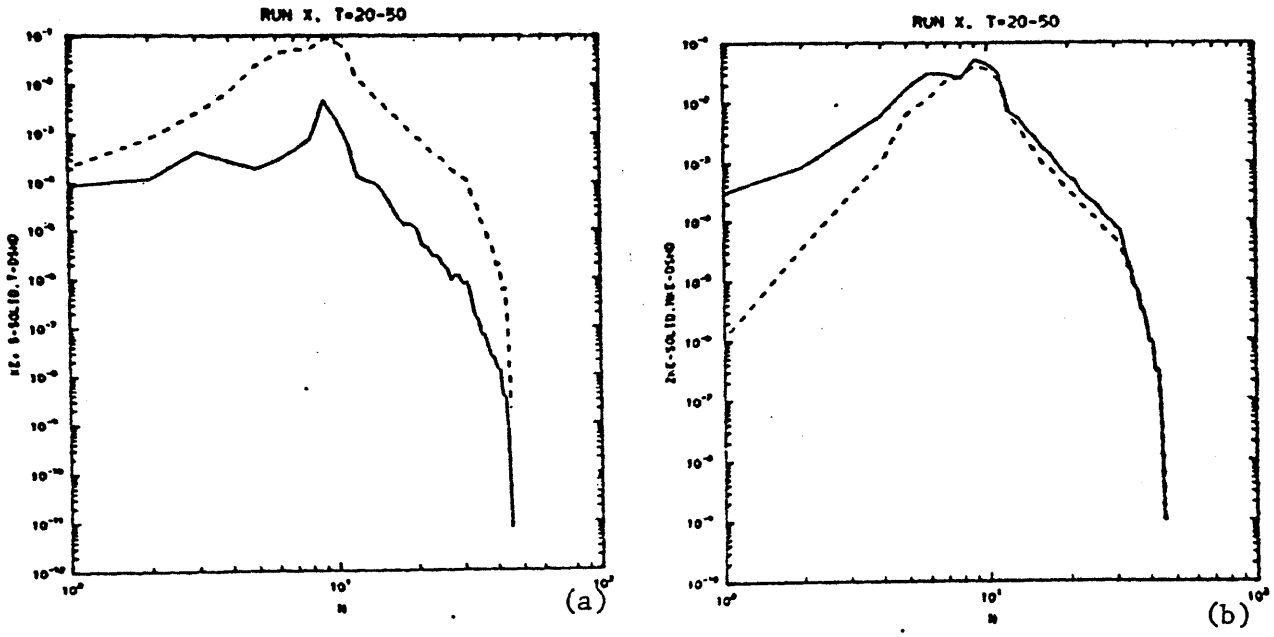


Fig. 8.17: Same as Fig. 8.16, but for Run X, t = 20-50 .

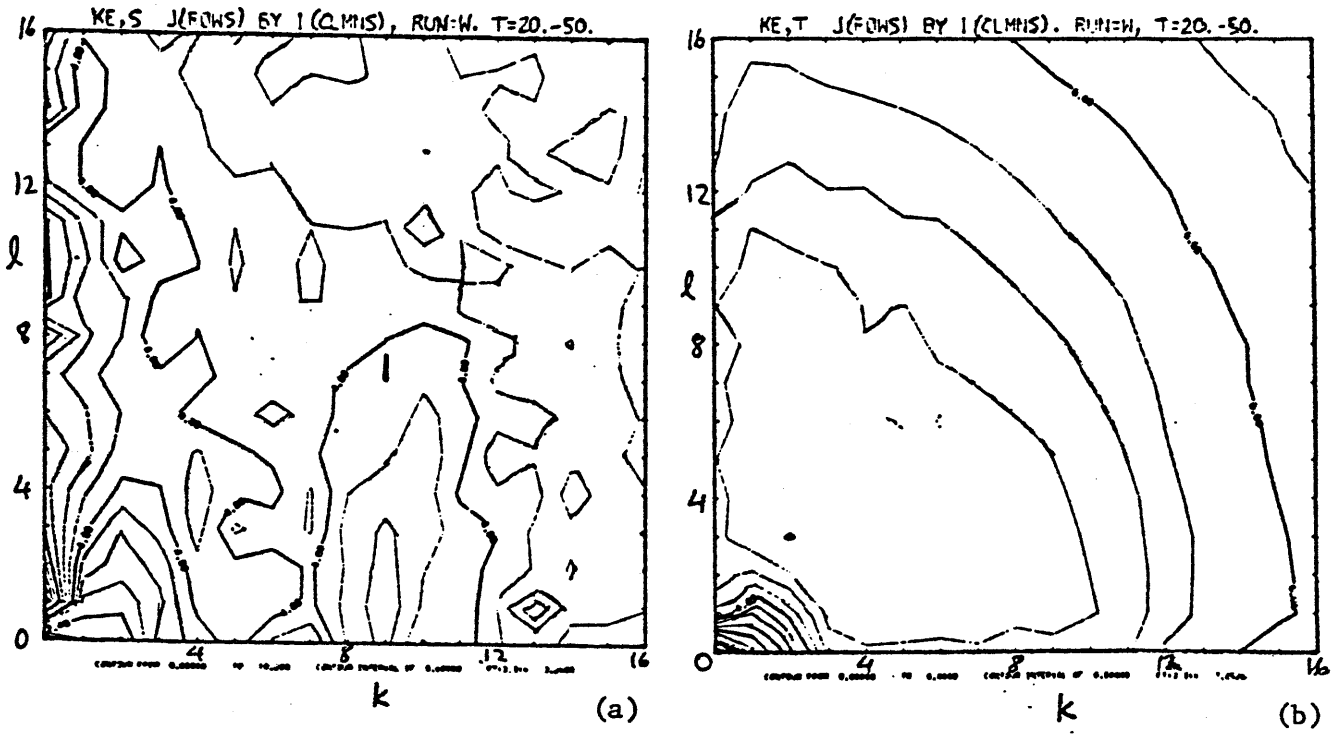


Fig. 8.18: 2-D (k,ℓ)-spectra of (a) stationary and (b) transient energy, Run W, t = 20-50 .

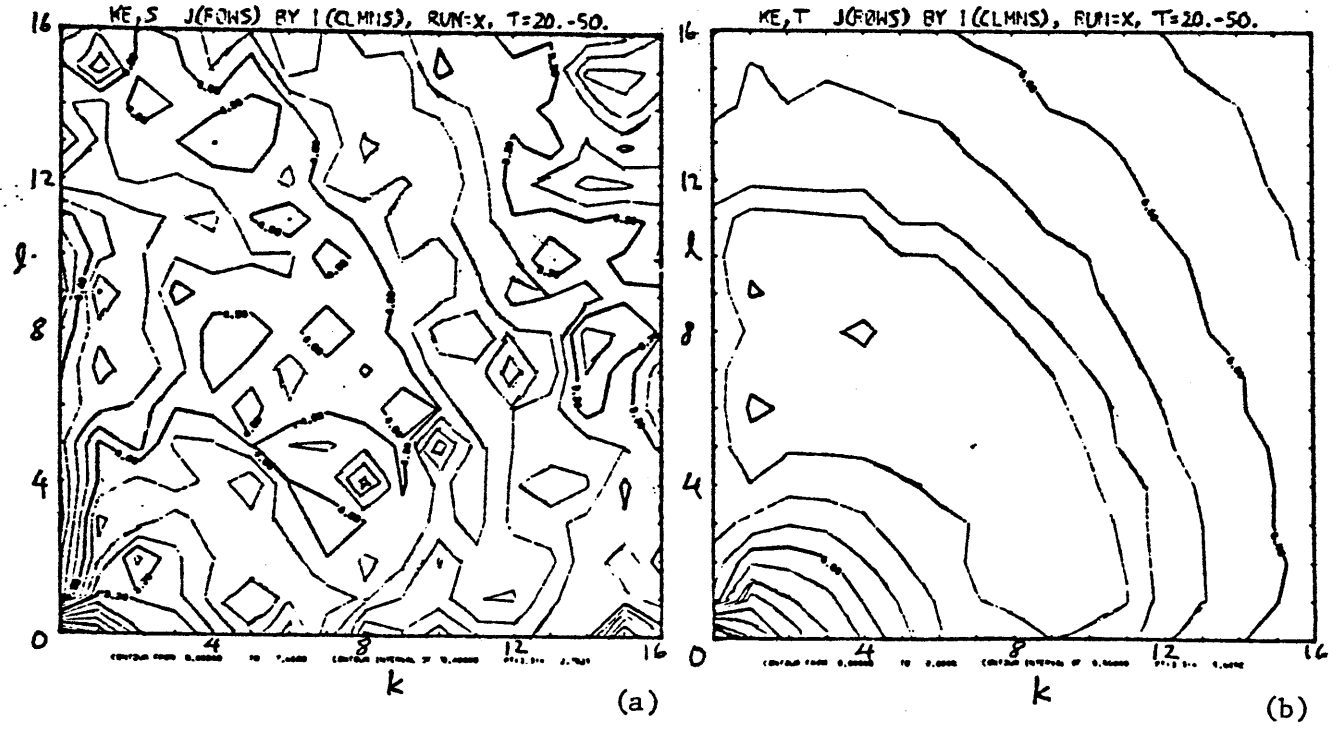


Fig. 8.19: Same as Fig. 8.18, but for Run X, t = 20-50 .

turbulence Run X. It should be noted that n_β is now very close to the forced wavenumber band; whether this in fact constrains the dynamics to be much less turbulent in the vicinity of the forced scales is a question that will be investigated in what follows.

As in §8c, the energy spectra shall be described first. Figs. 8.16 and 8.17 show the spectra for Runs W and X as a function of n, separated into stationary and transient, and into zonal and meridional, components. The stationary-transient breakdown is similar to that of Figs. 8.3a and 8.4a, namely strong transient dominance nearly everywhere; the only exceptions occur in Run W at $n = 1$, which is naturally nearly totally stationary, and at $n = 2$, where the two components are comparable in magnitude. It may be noted, however, that Run X demonstrates a much sharper stationary peak at $n = 9$ in the forced band (Fig. 8.17a) than is seen anywhere in Run V (Fig. 8.4a). One might plausibly argue that since $n = 9$ is so close to $n_\beta = 8$, the former scale is not as turbulent in Run X as in Run V, and consequently allows a stronger jet-like feature to develop <u>in situ</u> (spectrally speaking).

By comparing Figs. 8.16b and 8.17b with Figs. 8.3b and 8.4b, a few comments can be made. First, while the cascade arrest of the beta-plane turbulence Run X is fairly evident, it occurs at around $n = 6$ rather than the "predicted" $n = 8$; this "leakage" is reminiscent of that seen in the spin-down Run P. Secondly it can be seen that except in the immediate vicinity of the forced band, Run X is zonally anisotropic. This is in contrast to Run V, where the zonal anisotropy was confined to $n < n_\beta$. A possible explanation for this difference might be that the enhanced beta-jets of Run X, whose strength is presumably due to their proximity to the forced band, demonstrate a visible mean-flow straining on the higher wavenumbers.

The differences between Runs U and W are not as great in the n-space representation; perhaps the only perceptible change is an absence of the slight large-scale meridional anisotropy seen in Run U. However more details may be observed in the 2-D spectra, shown in Figs. 8.18 and 8.19. The stationary fields in both runs (Figs. 8.5a, 8.18a) exhibit strong zonal flow components at the basic-state scale $\ell = 1$; at the forced scales $\ell = 9$ through $\ell = 11$; and near n_β: specifically $\ell = 6$ for Run U, and $\ell = 8$ for Run W. As far as the transient spectra are concerned (Figs. 8.5b, 8.18b), there is an isotropic "plateau" of energy from $n = 2$ to just beyond n_β: $n = 7$ in Run U, $n = 10$ in Run W; this can also be checked quantitatively via Figs. 8.3 and 8.16, though one must take the factor of n into account. The 2-D spectra also demonstrate the zonal anisotropy that prevails in Run X (Fig. 8.19b), moreover the cascade arrest is more apparent there than it is in Fig. 8.6b from Run V.

Turning now to the spectral conversion and transfer terms, and focussing on Runs U and W, the energy and enstrophy conversion terms C(k) and EMI(k) are both quite similar in form and strength in the two runs; consequently the equivalent of Fig. 8.7a for Run W is not shown. A slight difference is that in Run W, the maximum transient gain occurs not at $k = 2$ but at $k = 3$; and the gain-loss crossover occurs at $k = 7$ rather than at $k = 6$. This gives a greater loss at $k = 0$ in C(k), but the qualitative effect is still the same.

Fig. 8.20 shows the same conversion terms for Run W represented as functions of n, but now separated into energy and enstrophy. The enstrophy terms (Fig. 8.20b) look very similar to those in Fig. 8.8b for Run U, and show that the induced transfer of enstrophy due to the mean-flow

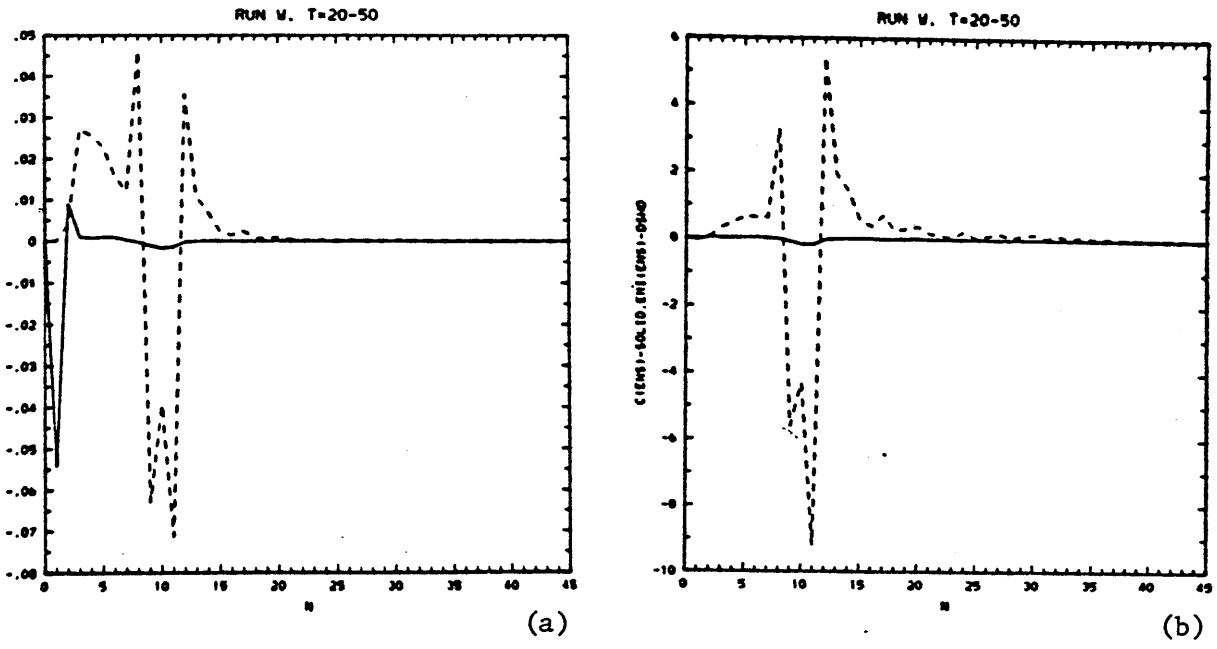


Fig. 8.20: n-space conversion terms: (a) for energy, C(n) (——) and EMI(n) (– –); (b) for enstrophy, n^2C(n) (——) and n^2EMI(n) (– –); both for Run W, t = 20-50 .

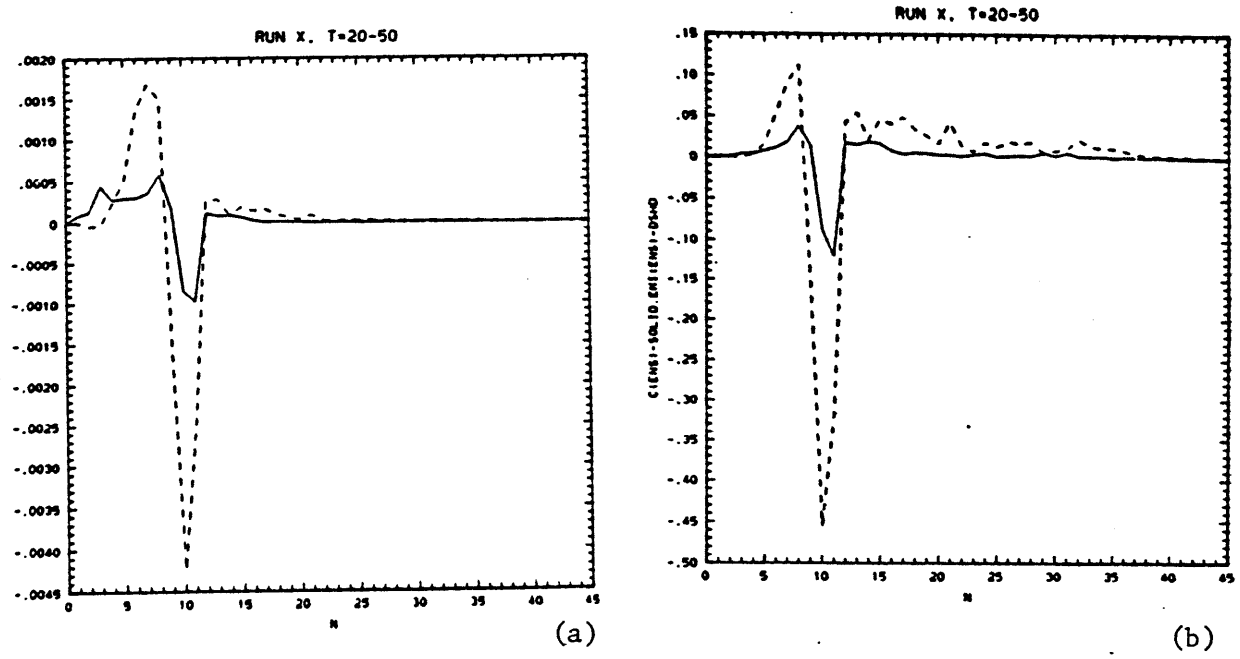


Fig. 8.21: Same as Fig. 8.20, but for Run X, t = 20-50 .

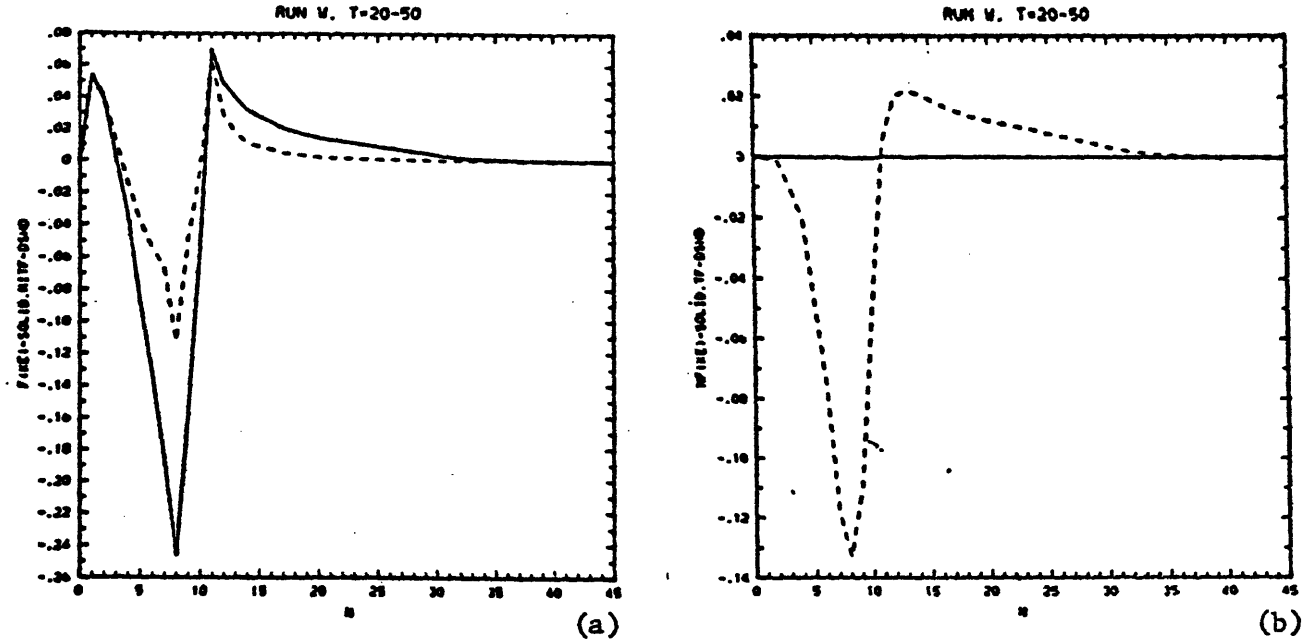


Fig. 8.22: (a) Total flux of energy F(n) (——) and induced flux MITF(n) (— —) ; (b) Stationary flux MF(n) (——) and transient flux TF(n) (– –); Run W, t = 20–50 .

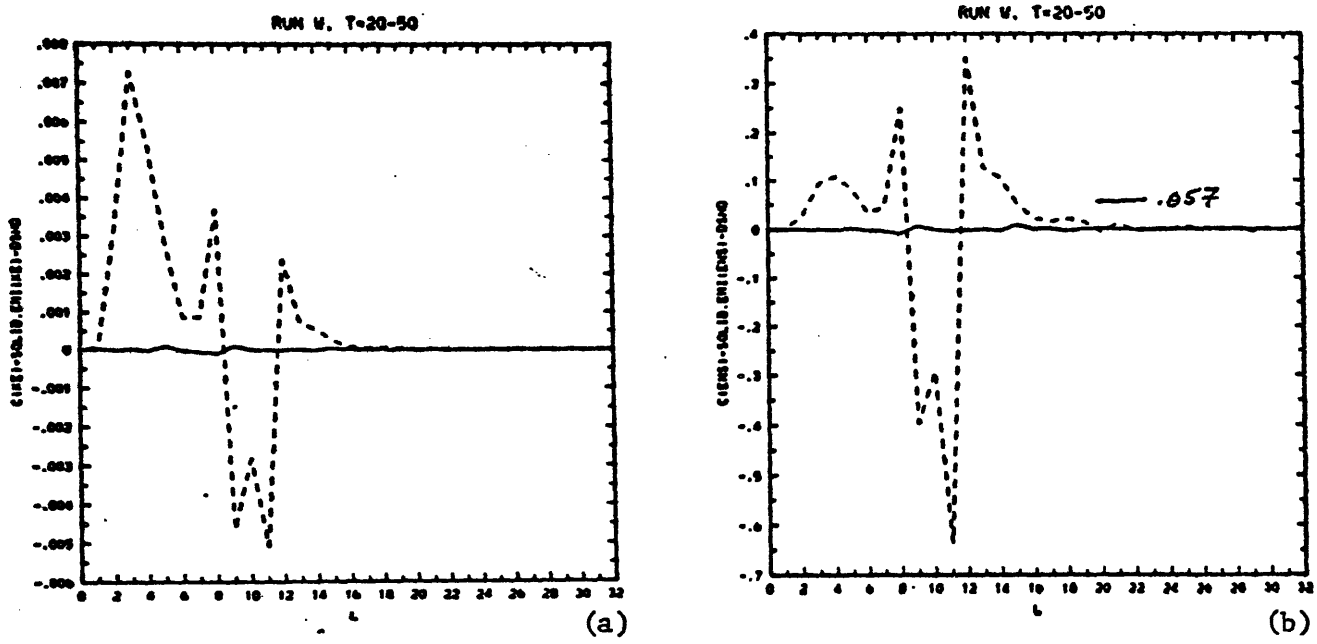


Fig. 8.23: ℓ-space conversion terms for the slice k = 2: (a) for energy, C(ℓ) (——) and EMI(ℓ) (– –); (b) enstrophy, n^2C(ℓ) (——) and n^2EMI(ℓ) (— —); Run W, t = 20–50. Mark on (b) shows the magnitude of the sum.

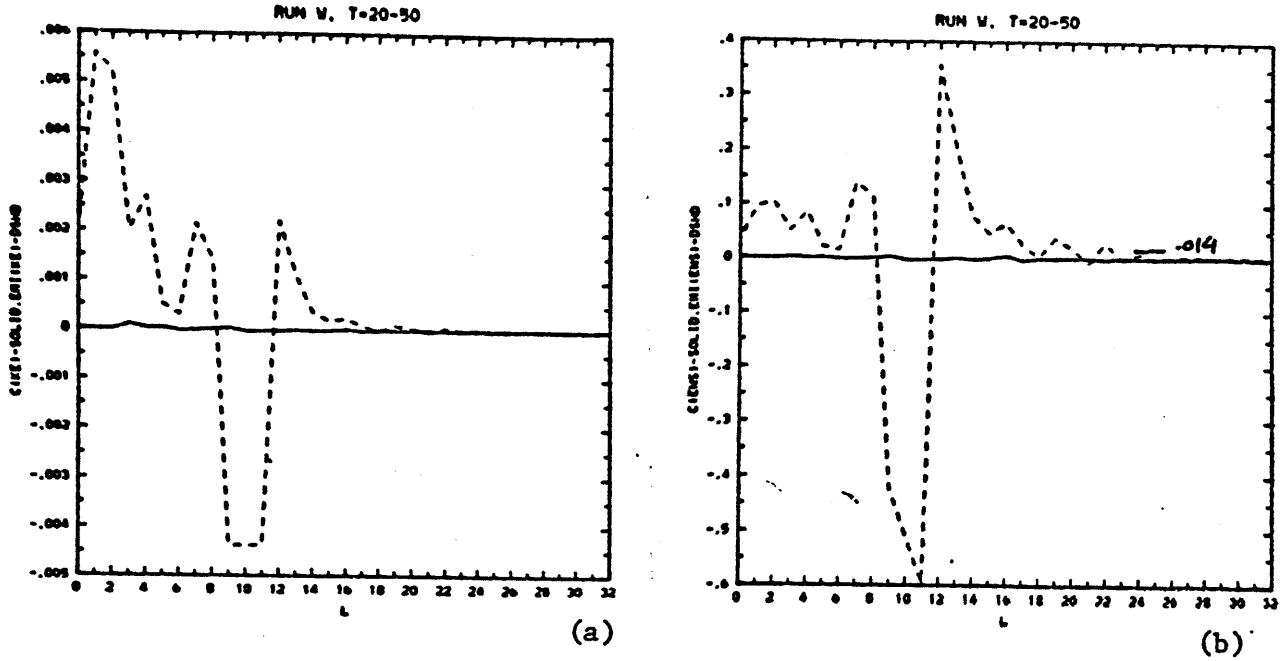


Fig. 8.24: Same as Fig. 8.23, but for k = 4 .

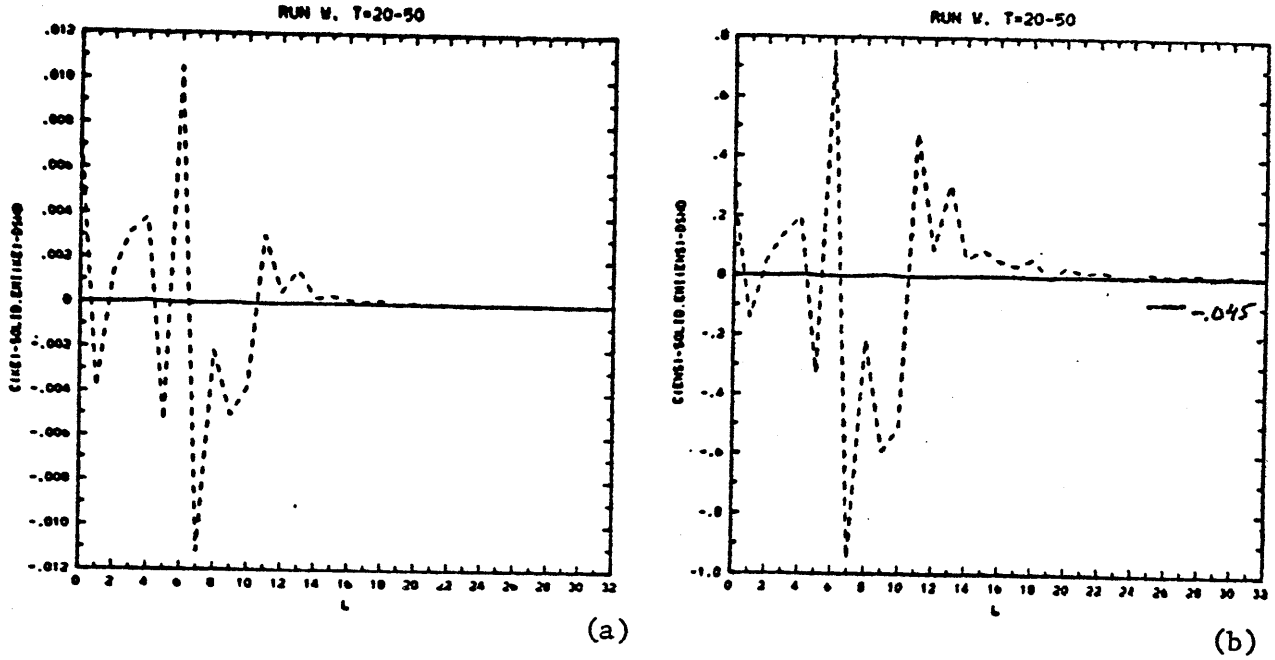


Fig. 8.25: Same as Fig. 8.23, but for k = 6 .

straining is a ubiquitous phenomenon. The up-scale energy "cascade" seen in EMI(n) (Fig. 8.20a) is equally ubiquitous, but here in Run W it is cut off at n = 3 rather than n = 2 ; an explanation for this will emerge when the transfer terms are examined in ℓ-space for fixed k. But note from (6.24) that the maximum possible amplification of a wave packet is independent of β_0. As mentioned above, n = 1 shows a greater stationary-to-transient conversion C in Run W, by about 70%; this is however partially offset by the conversion needed to maintain the significant stationary component at n = 2 (see also Fig. 8.16a).

It is also interesting to examine the same conversions for Run X, though as in Run V they represent only a small part of the spectral dynamics. Since the beta-jets of Run X are mixed up with the forced wavenumber band, the energy conversion term C(n) (Fig. 8.21a) does not exhibit the same scale separation as in Fig. 8.9a of Run V; however the induced cascade as seen in EMI(n) is evidently truncated at n = 7 rather than n = 5, and is of comparable magnitude. In terms of enstrophy (Fig. 8.21b), again the lack of a stationary-transient scale separation means that the notion of induced transfer is problematical at best; it is difficult to assign any more meaning to these figures.

Looking at the nonlinear flux functions for Run W (Figs. 8.22) the similarity with Run U (Figs. 8.10) is once again evident, despite the increased flow of energy out of the n = 1 component. Perhaps reflecting the "leakage" past $n_\beta = 8$ up to n = 6 observed in the beta-plane turbulence Run X for this higher value of β_0, the turbulent transient self-interaction gives a flux up to about n = 6 (Fig. 8.22b). It will be recalled that in §8c, the transient (i.e. turbulent) flux TF agreed between Runs U and V; the same result appears to hold between Runs W and

X. Once inside this spectral radius, the straining from the stationary-transient interaction dominates (Fig. 8.22a).

Throughout this study it has been claimed that the best way of diagnosing the stationary-transient interaction and the associated process of induced transfer comes from examining the meridional spectral transfers at fixed zonal wavenumber: this is done for Run W in Figs. 8.23 through 8.25. It is readily verified that the comments made in §8c with regard to Figs. 8.12 through 8.14 of Run U carry over to Run W, though with some modification. The approximate conservation of enstrophy again validates the concept of induced transfer, although the error is somewhat larger than in Run U; and the large net energy gain and up-scale transfer for $k = 2$ and $k = 4$ indicates the importance of the nonlinear mixing in providing irreversibility. Some differences may be noted: for example the up-scale penetration for $k = 2$ only gets to $\ell = 3$ in Run W (Figs. 8.23a,b), as compared to $\ell = 1$ in Run U (Figs. 8.12a,b). This is explained by the fact that, according to the linear ray-tracing theory of Chapter VI, higher β_0 implies smaller $\Delta\ell/\Delta y$; hence the low-k disturbances, which have no turning lines, fail to achieve as small a value of ℓ when their rays pass through the westerly jet maximum. A calculation presented in Chapter VI showed that while the minimum ℓ for $k = 2$ wave packets tended to be around $\ell = 1$ for $\beta_0 = 25$, that value increased to $\ell = 3$ for $\beta_0 = 65$ (and $U_0 = 2\sqrt{2}$, of course); these estimates seem to be verified by Figs. 8.12 and 8.23, demonstrating the rather remarkable success of ray-tracing theory in describing the up-scale part of the disturbance evolution for small scale separation and significant nonlinearity.

Finally some physical-space diagnostics are presented in Figs.

8.26, and are to be compared with Figs. 8.15 for Run U. The zonal jet (Fig. 8.26a) appears to have stronger kinks in Run W, which is consistent with Figs. 8.3a and 8.16a; note the point at $y = \pi$. However, because of the larger value of β_0 the potential vorticity gradient barely shows these features, whereas in Run U they were quite evident. The Reynolds stress (Fig. 8.26b) has the same general character as in Run U, but magnified by a factor of about 1.7; this is naturally consistent with the 70% increase in the stationary-transient conversion seen in Fig. 8.20a. Translated into conversion terms (Fig. 8.26c), one sees the same pattern as in Fig. 8.15c: eddy energy gain from straining in the strong-shear regions; mean energy loss from the easterly jet; and a sharpening of the westerly jet that is even more prevalent here than in Run U.

There are more differences in the eddy velocity variances (Fig. 8.26d). Unlike Run U, there is here a slight zonal anisotropy that was also evident in the spectra (e.g. Fig. 8.16b). On the other hand if the $k = 0$ component is removed, then the situation is fairly isotropic. This matter was discussed somewhat in §8c, where it was decided that neither representation is unambiguously superior to the other. What does seem evident, however, is that a stronger value of β_0 has mitigated much of the meridional anisotropy and encouraged more active transient zonal jets.

Another difference concerns the fact that the variance in the easterly jet has nearly twice the amplitude of that in the westerly jet, whereas in Run U they were approximately equal. With $k = 0$ removed the discrepancy is reduced but still present. It is difficult to say what might account for such an asymmetry, but perhaps the question is rather

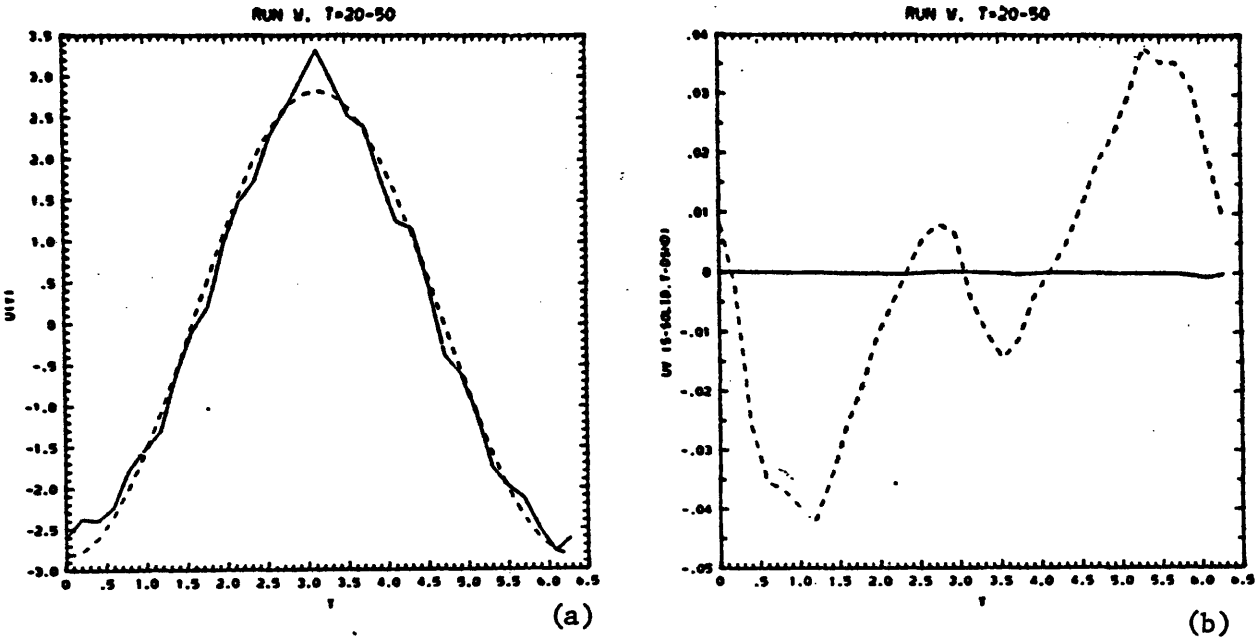


Fig. 8.26: Spatial diagnostics, Run W, t = 20-50. (a) Time-averaged zonal flow $\overline{U}(y)$ (——), basic-state flow (– –); (b) Stationary (——) and transient (– –) Reynolds stress terms $\langle\overline{uv}\rangle(y)$.

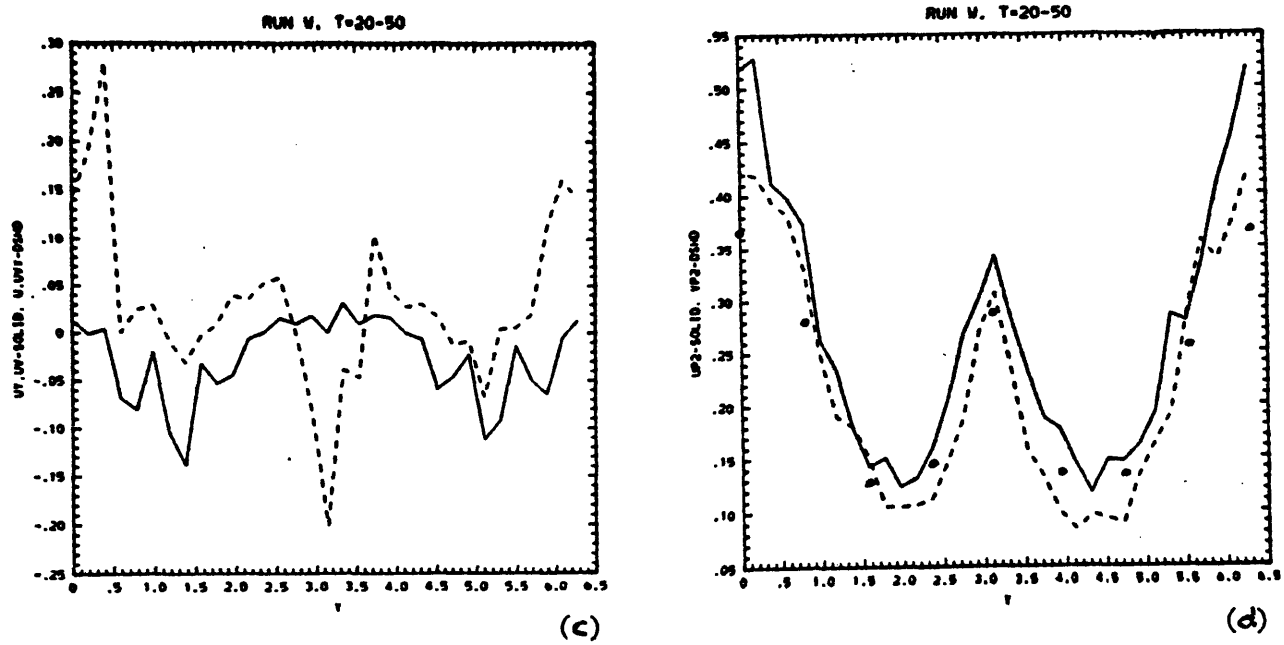


Fig. 8.26: (c) Conversion terms $\overline{U}\,\overline{uv}$ (——) and $\overline{U}(\overline{uv})_y$ (– –); (d) Transient variances $\langle\overline{u'^2}\rangle$(——)$_y$ and $\langle\overline{v'^2}\rangle$(– –), and the dots indicate the former with the k = 0 component removed, at selected y.

why the amplitudes were so similar in Run U; after all, it was seen in the spin-down runs of Chapter VII that the two maxima have quite distinct dynamical origins. In any event I have been unable to come up with a satisfactory answer to either question.

§8e. Run T: Effects of Increased Nonlinearity

The geophysical estimates of the various run parameters being as uncertain as they necessarily are, it is desirable to investigate the possible effects that might arise out of a more turbulent flow regime. Consequently this section considers Run T, which is identical to Run U except that the initial perturbation energy is doubled from 0.5 to 1.0, and the Ekman frictional coefficient is halved to maintain stationarity. The high-order diffusion coefficient could have been multiplied by $\sqrt{2}$ to keep the same grid Reynolds number, but since it appeared to be mopping up the enstrophy cascade quite effectively it was left unaltered. With pure beta-plane turbulence a change in u would only alter the position of n_β, but in the inhomogeneous problem the parameter α of (5.20) is also affected and the change could well be non-trivial.

Fig. 8.27 shows the time evolution of energy amplitudes in Run T, and the first striking surprise is that unlike in Runs U and W, here the (0,1) flow component equilibrates to a strength above its basic-state value. But while Run U appeared in Fig. 8.1 to have equilibrated by about $t = 10$, the behaviour of Run T exhibits a few very strong fluctuations up to $t = 14$, apparently searching out both "sides" (i.e. stronger and weaker) of the basic-state flow in order to find where its attractor lies. Even when it does settle down into a regime with net transient-to-stationary conversion, the (0,1) energy seems to be

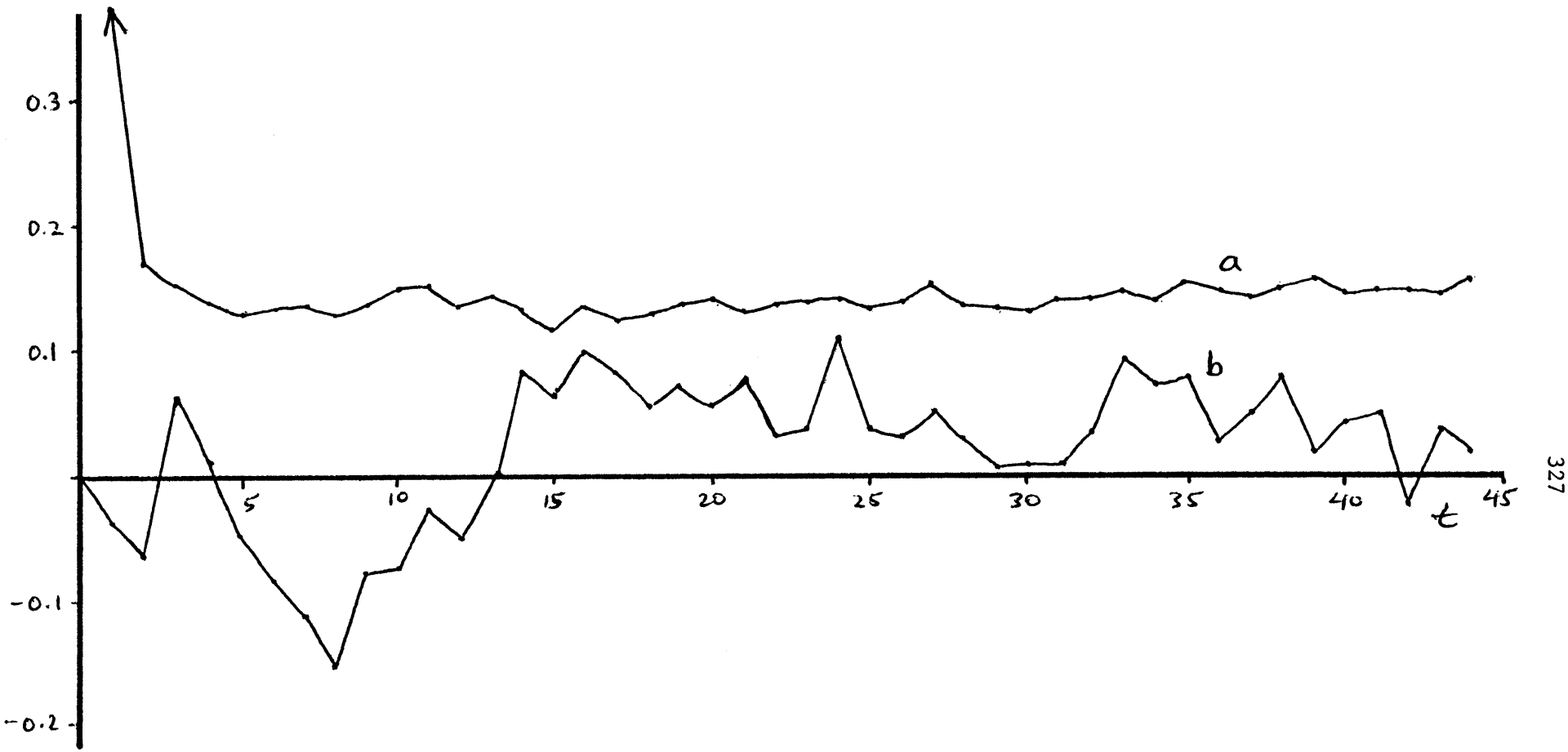


Fig. 8.27: Time evolution of Run T: (a) Energy in forced modes $9 \leq n < 12$; (b) Energy in $(k,\ell) = (0,1)$ mode minus 2.0. Given at integral times, and averaged over every timestep of the preceding model day.

drifting back to its basic-state value on a much slower timescale.

The contrast with the much more stable behaviour of Run U, and indeed of Run W, which fluctuate within an apparently well-defined "attractor basin", is noticeable, and suggests that Run T is close to a borderline between super-equilibrated and sub-equilibrated mean flows. An unfortunate consequence is that a good averaging period is hard to define; for somewhat arbitrary reasons Run T was only extended to t = 44 and so the last 30 days t = 14-44 have been averaged. But note that the eddy turn-around times τ_1 and τ_2 are somewhat shortened, which should produce more independent samples; on the other hand the absence of a clear turbulent equilibrium makes the notion of a statistical ensemble somewhat problematical in this case.

To investigate the dynamics of Run T, consider first the energy spectra shown in Figs. 8.28 and 8.29. The stationary "bulge" that characterizes the forced scales is here much reduced (Fig. 8.28a), presumably because the more energetic turbulence is able to diffuse energy away from those scales more rapidly. The relative anisotropy (Fig. 8.28b) is about the same as in Run U (Fig. 8.3b), but note that the energy of the large scales is more than doubled in Run T; obviously the additional energy is distributed in a way that favours the scales $n < 5$. This increased large-scale trapping is also evident in the 2-D transient energy spectrum (Fig. 8.29b), as is the large-scale meridional and small-scale zonal anisotropy. Interestingly, rather than any higher-mode zonal jets such as are evident in Fig. 8.5a, Fig. 8.29a shows stationary meridional jets at k = 3 and k = 9.

The enhanced accumulation of large-scale transient energy in Run T, beyond the factor of two in the overall perturbation energy, can be

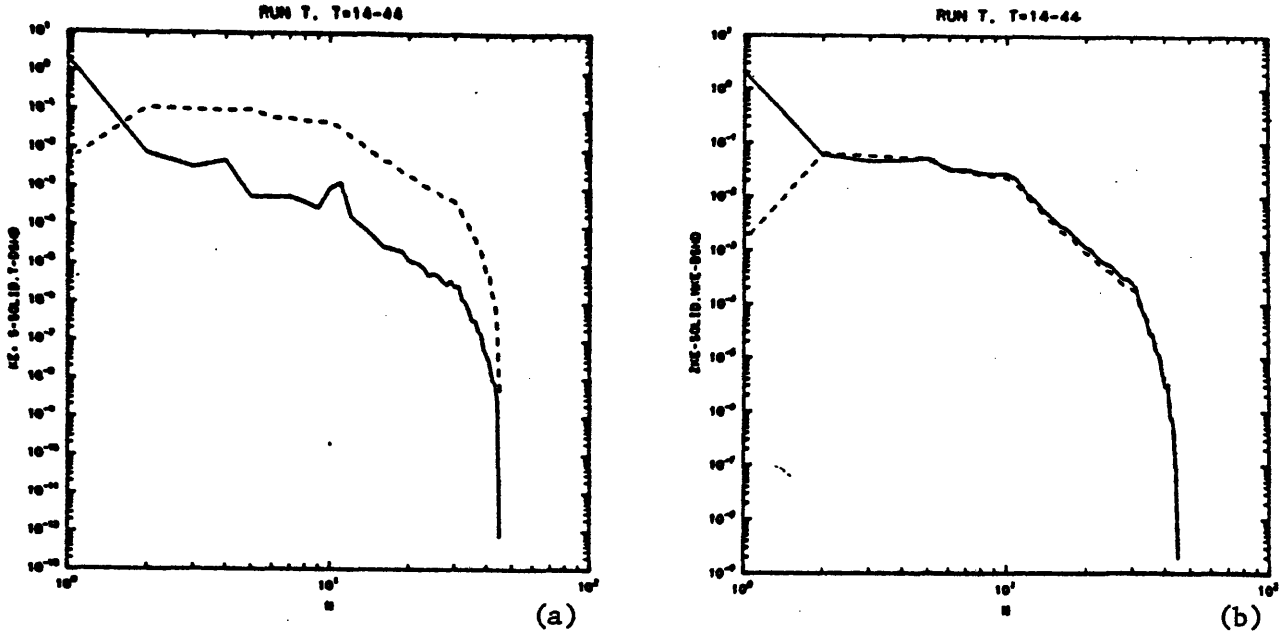


Fig. 8.28: (a) Stationary (——) and transient (– –), and (b) zonal (——) and meridional (– –), energy n-spectra, Run T, t = 14–44.

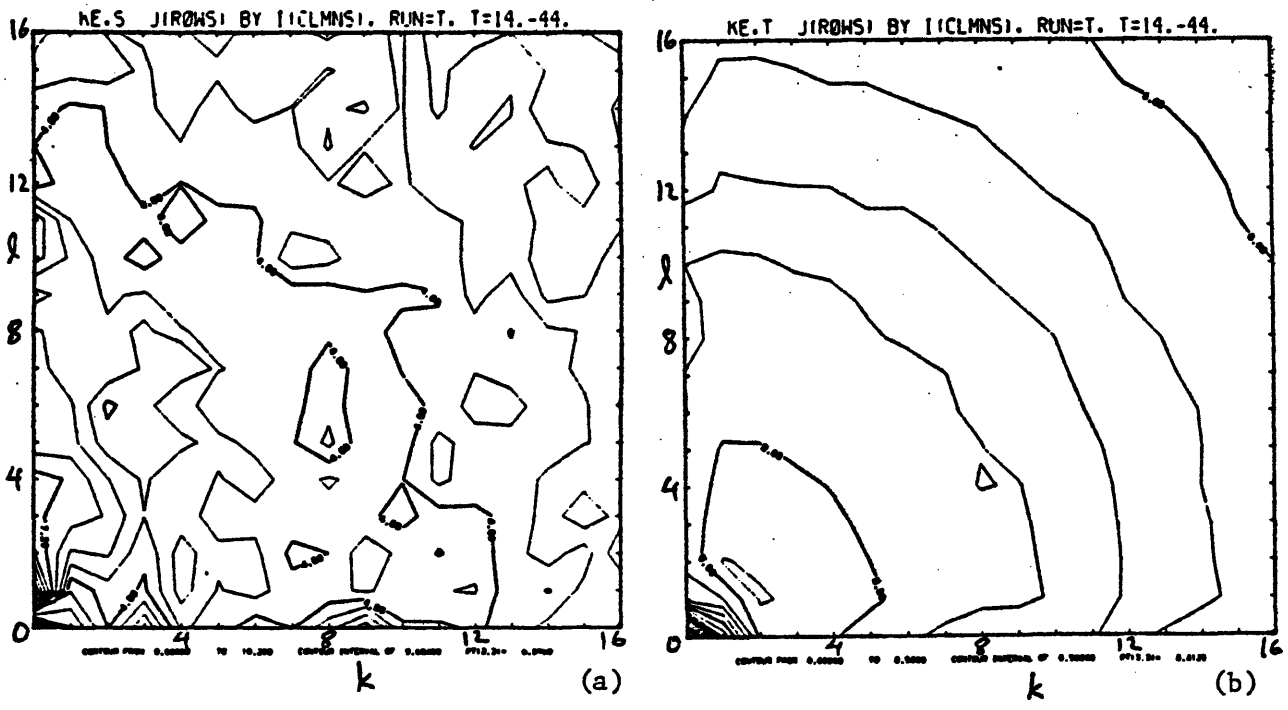


Fig. 8.29: 2-D (k,ℓ)-spectra of (a) stationary and (b) transient energy, Run T, t = 14–44 .

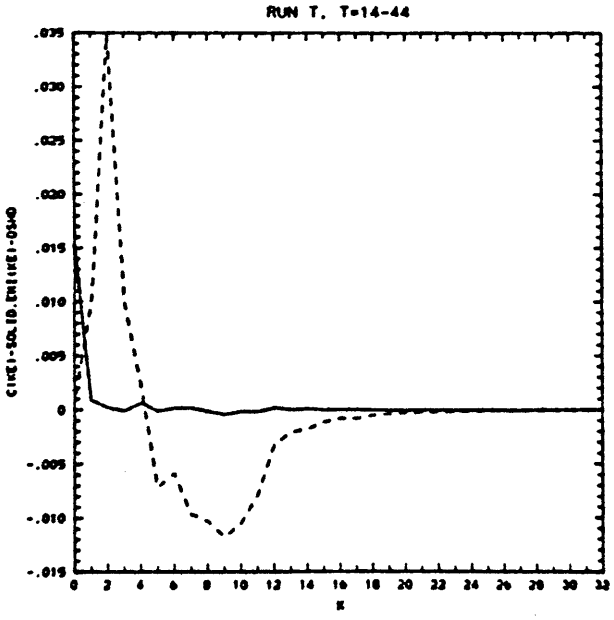


Fig. 8.30: k-space conversion terms C(k) (——) and EMI(k) (– –), Run T, t = 14-44 .

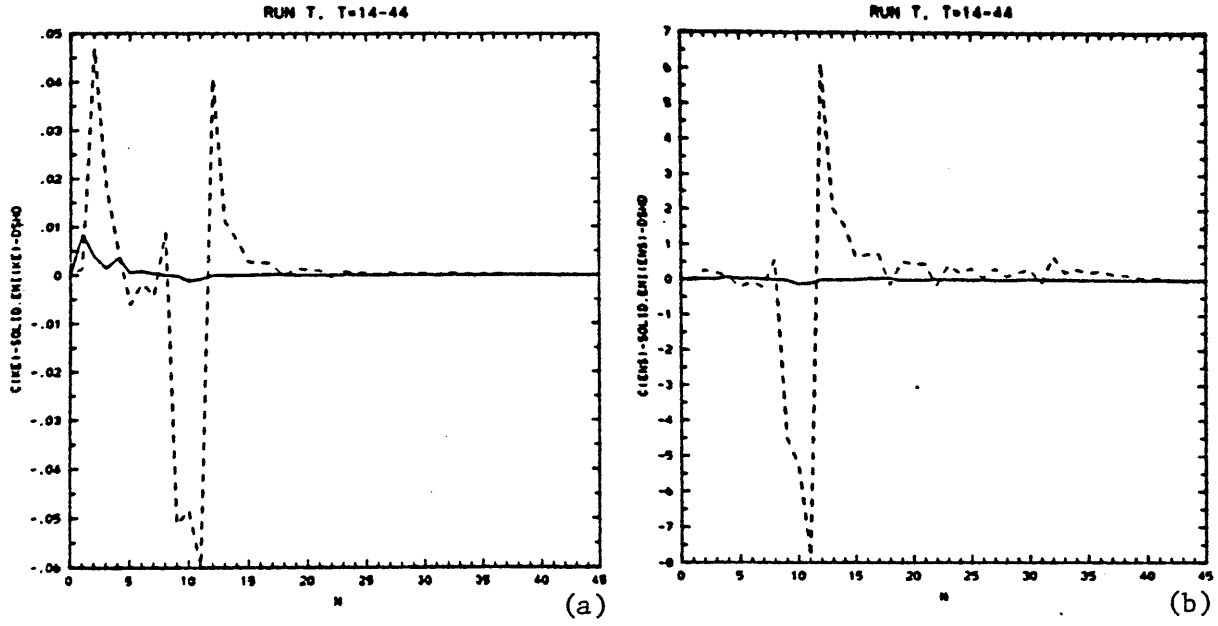


Fig. 8.31: n-space conversion terms: (a) for energy, C(n) (——) and EMI(n) (– –); (b) for enstrophy, $n^2C(n)$ (——) and $n^2EMI(n)$ (– –); both for Run T, t = 14-44 .

plausibly attributed to at least two effects. First, the weaker Ekman drag means that less energy is lost during a disturbance's up-scale cascade, and consequently the forced-dissipative balance is obtained more from the "trapped" large-scale energy. Secondly, it has already been established that turbulent mixing is able to accomplish this trapping, and one would expect more active turbulence to be even more effective.

The explanation for the super-critical equilibration of the (0,1) flow component in Run T must come from the spectral transfer functions, and the k-space energy/enstrophy conversions shown in Fig. 8.30 already tell a large part of the story. It is evident that only $k < 4$ waves show a net gain of energy through the wave, mean-flow interaction, while $k > 4$ waves lose; this contrasts with the $k = 6$ transition seen in Run U (Fig. 8.7a). Such a shift of the gain-loss transition wavenumber is enough to yield a net conversion from the transients to the stationary flow, so that the latter is able to maintain its super-equilibrated (0,1) component against friction.

To explore this issue further, consider the conversion terms as functions of n (Figs. 8.31). The energy term EMI(n) in Run U (Fig. 8.8a) exhibited a minimum at the forced scales $n = 9\text{-}11$, and maxima at $n = 2\text{-}4$, $n = 8$, and $n = 12$; on the other hand the enstrophy term (Fig. 8.8b) showed a damped transfer away from $n = 9\text{-}11$. The interpretation offered in §8c was that the linear dynamics described much of the initial development including transfer by mean-flow straining in the immediate vicinity of the forced scales, but that this was quickly upset by turbulent mixing. However for $n < n_\beta$ the process was again operative, and it acted to bring energy across the wave-turbulence

"boundary". In the case of Run T (Figs. 8.31a,b) the picture for $n > 8$ looks rather similar, but the large-scale side of the forced band is clearly quite different. The former peak at $n = 8$ is now very small, while the broad peak at $n = 2$-4 is sharpened to a very strong one at $n = 2$; scales with $2 < n < 9$ show little net conversion. Taken together, this picture would be consistent with a relatively constant induced energy flux from the forced band all the way up to $n = 2$, however the dynamics of induced transfer suggest this to be unlikely. For an equilibrium run, such diagnostics have their inevitable ambiguity; but the constant-k "slices" to be examined presently may enable the ambiguity to be resolved.

The total nonlinear flux of energy, shown in Fig. 8.32a, is quite similar to that of Run U (Fig. 8.10a) on the small-scale side of the forced band; on the large-scale side the flux between $n = 8$ and $n = 1$ is comparable in magnitude, though the $n = 1$ mode now acts as a source rather than as a sink. The flatness of the "induced" flux MITF (Fig. 8.32a) is apparent, and offers a sharp contrast to MITF in Fig. 8.10a. As far as TF due to turbulent interactions is concerned, its up-scale component is rather stronger in Run T (Fig. 8.32b) than in Run U; it takes up the slack for $n = 3$-8 created by the weakness of EMI.

Figs. 8.30 and 8.31a both show the dominant induced transfers of energy to be into the $(k,\ell) = (2,1)$ mode (hence $n = 1$), and consequently the meridional transfer spectra for $k = 2$ (Figs. 8.33a,b) are of particular interest. Comparing these with Figs. 8.12a,b for Run U, the enormity of the transfer into $\ell = 1$ is indeed the most striking feature. But it comes not so much from the forced scales $n = 9$-11 , as in Run U, but rather from $n = 4$ and $n = 6$ - namely scales just outside n_β. In

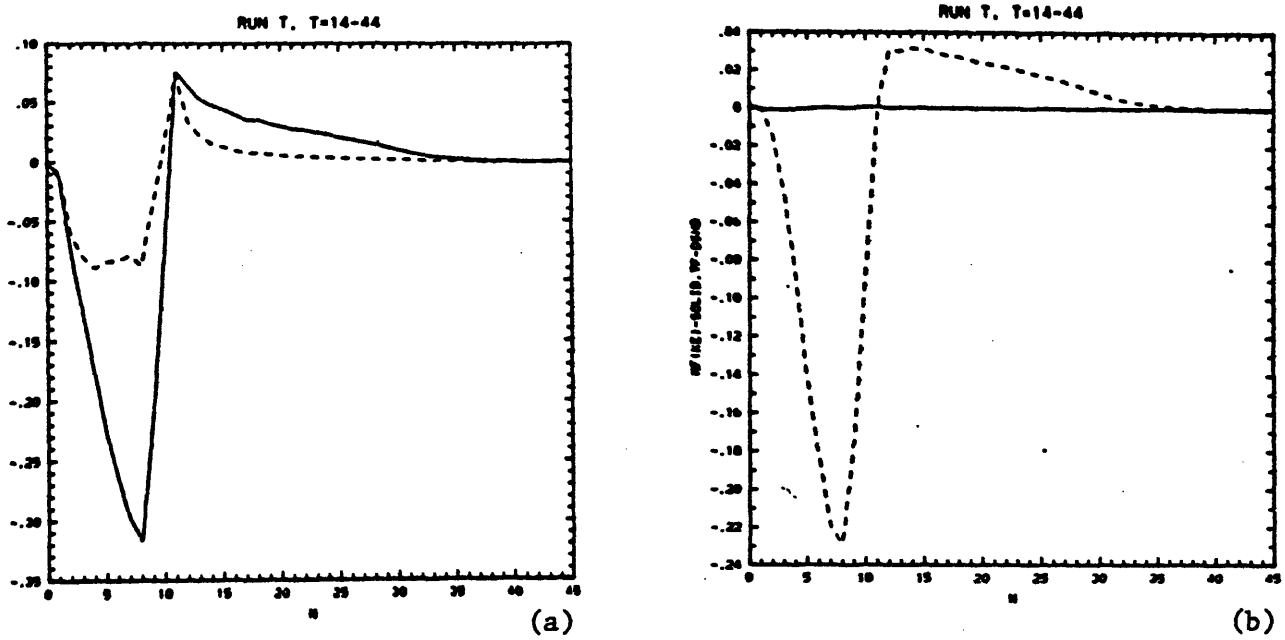


Fig. 8.32: (a) Total flux of energy F(n) (——) and induced flux MITF(n) (– –) ; (b) Stationary flux MF(n) (——) and transient flux TF(n) (– –); Run T, t = 14-44 .

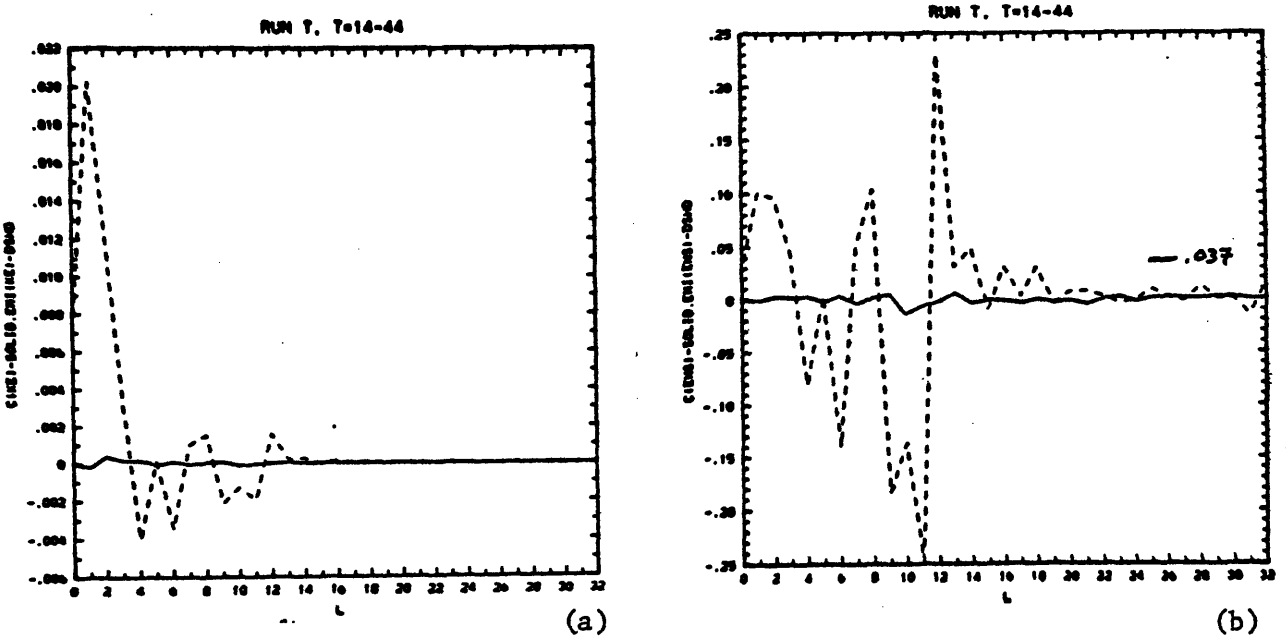


Fig. 8.33: ℓ-space conversion terms for the slice k = 2: (a) for energy, $C(\ell)$ (——) and $EMI(\ell)$ (– –); (b) for enstrophy, $n^2C(\ell)$ (——) and $n^2EMI(\ell)$ (– –); Run T, t = 14-44. Mark on (b) shows the magnitude of the sum.

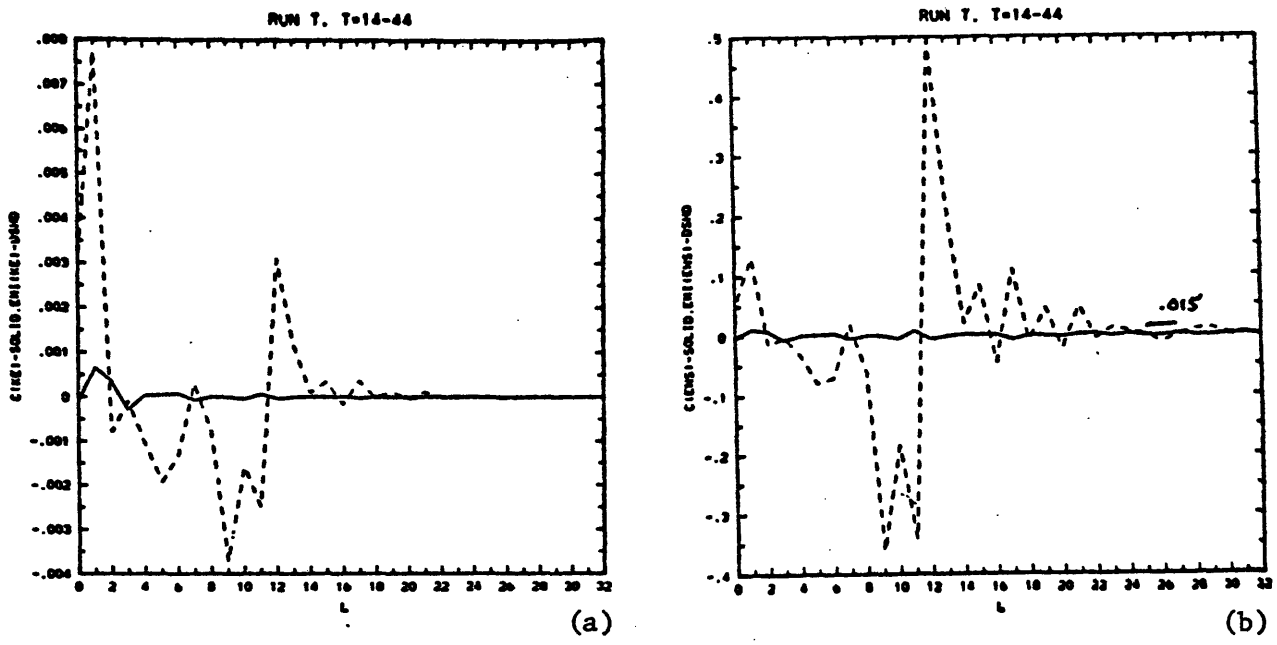


Fig. 8.34: Same as Fig. 8.33, but for k = 4 .

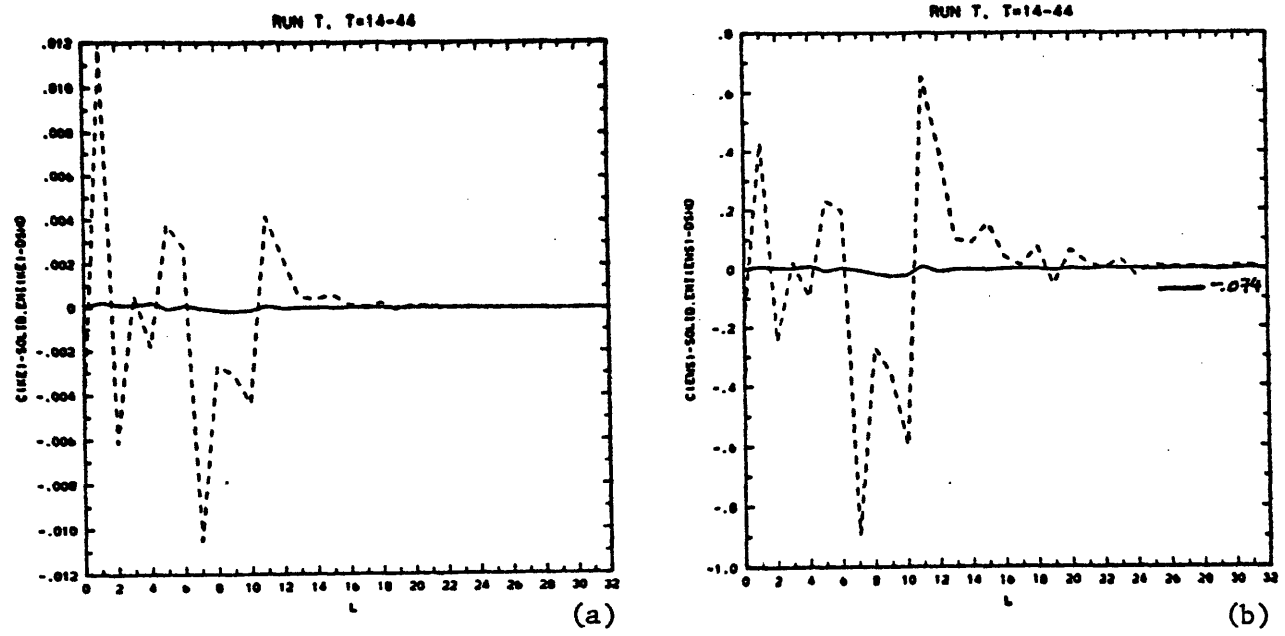


Fig. 8.35: Same as Fig. 8.33, but for k = 6 .

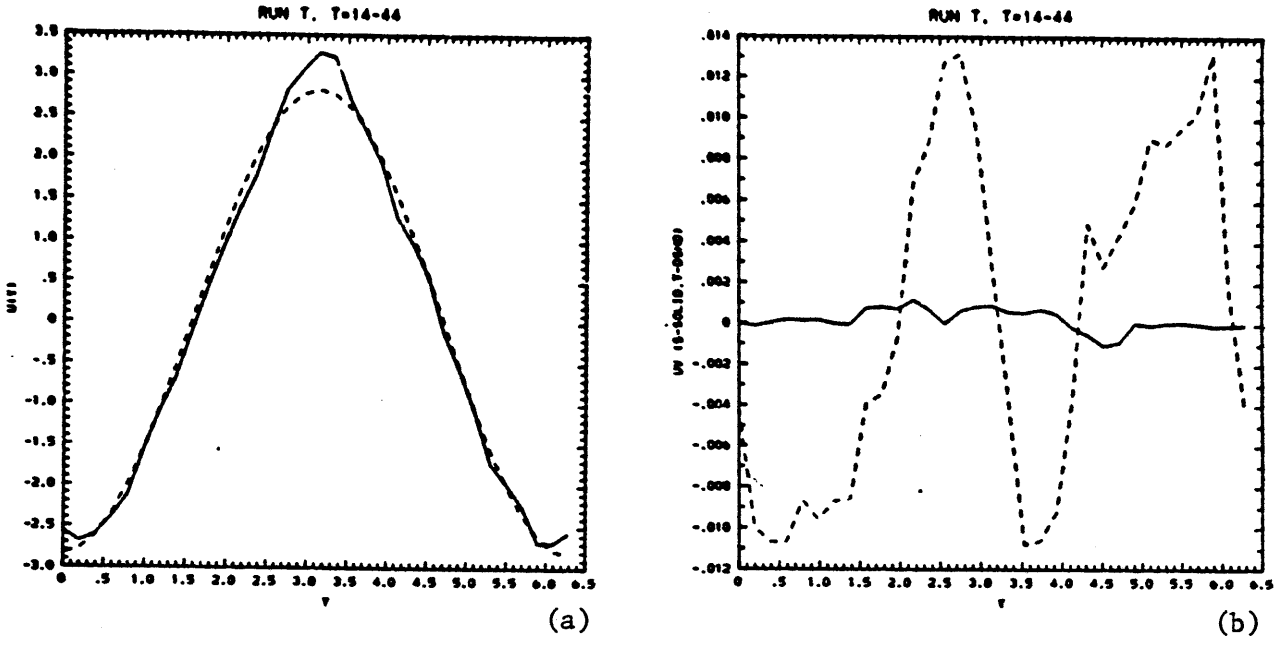


Fig. 8.36: Spatial diagnostics, Run T, t = 14-44. (a) Time-averaged zonal flow $\overline{U}(y)$ (——), basic-state flow (– –); (b) Stationary (——) and transient (– –) Reynolds stress terms $\langle\overline{uv}\rangle(y)$.

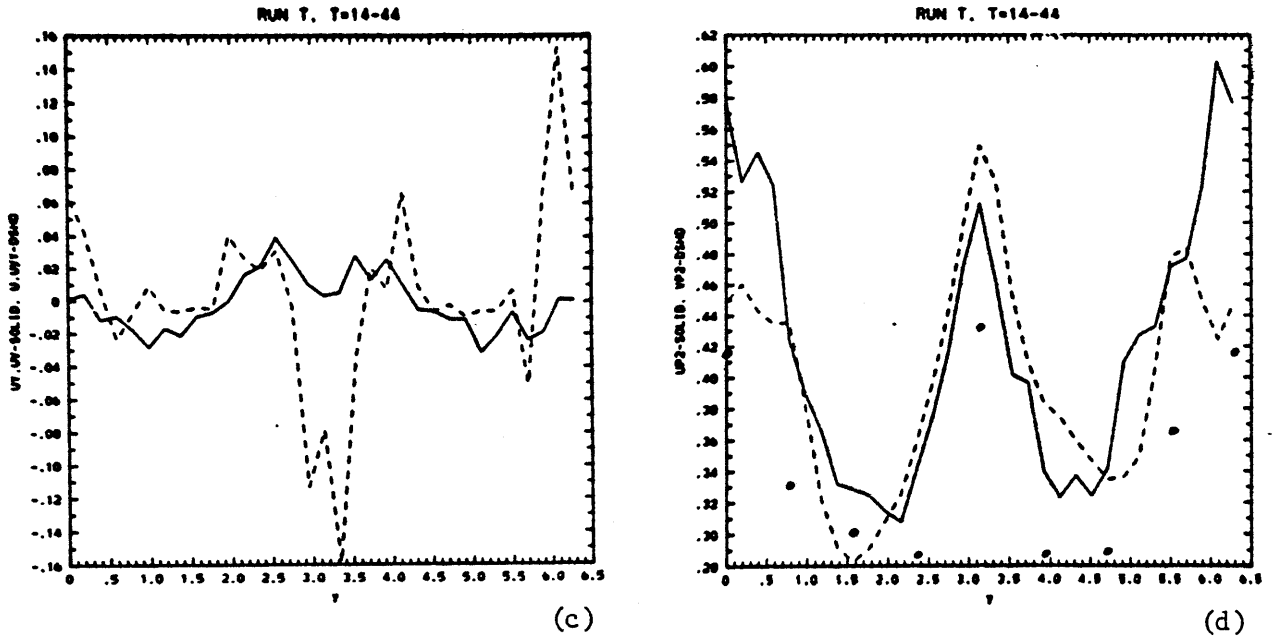


Fig. 8.36: (c) Conversion terms $\overline{U}\,\overline{uv}$ (——) and $\overline{U}(\overline{uv})$ (– –); (d) Transient variances $\langle\overline{u'^2}\rangle_y$ (——) and $\langle\overline{v'^2}\rangle_y$ (– –), and the dots indicate the former with the k = 0 component removed, at selected y.

fact the mean-flow straining around the forced scales is evidently weaker in this more turbulent run, and there appears to be a greater scale separation (though by no means a complete one) between the "linear" and "nonlinear" dynamical regimes. This interpretation is supported by the fact that the error in the approximate conservation of enstrophy is larger than in Run U, as would be expected for the less nonlocal triads involving (0,1) and $n = 5$ rather than $n = 10$. When this error is distributed evenly over all ℓ, however, it remains a negligible effect. The same conclusion holds also for $k = 4$ (Figs. 8.34a,b), and even, though to a lesser extent, for $k = 6$ (Figs. 8.35a, b); both show a negative value of EMI just outside $n = n_\beta$: at $\ell =$ 4-6 for $k = 4$, and at $\ell = 2$-4 for $k = 6$.

Considering finally the physical-space diagnostics for Run T, it is gratifying to find a mean zonal flow (Fig. 8.36a) that is relatively free of the "kinks" that so characterized Runs U and W; based on the spectral diagnostics, this feature can be safely attributed to stronger turbulent mixing at the forced scales which is able to overcome the phase-locking tendency of the forcing mechanism. The converse point is that the spectral dynamics seem insensitive to whether or not there are kinks in the spatial fields, as hypothesized, and this is obviously reassuring. In Run T the acceleration of the westerly jet is clearly evident, while the easterly jet seems relatively unaffected.

Examining the Reynolds stress in Fig. 8.36b, while the extrema occur at the same latitudes their magnitudes are quite altered in comparison with Fig. 8.15b of Run U. The shear $d\langle\overline{uv}\rangle/dy$ is comparable on the westerly-jet side of the mean-shear regions in the two cases, but is quite different in the jet core regions; moreover the two strong extrema

of $\langle\overline{uv}\rangle$ in Run U are here broken up into four roughly equal extrema, and those near the easterly jet are considerably broader than those near the westerly jet.

The effect of these differences on the conversion terms is considerable (Fig. 8.36c): the eddy energy generation is much reduced, while there is a strong eddy loss in the westerly jet. The first point is consistent with the much weaker up-scale induced transfer seen in the spectral diagnostics. While the easterly jet has a loss of mean energy, as in Runs U and W, this loss now goes not so much to the eddies as to the westerly jet; the eddies are evidently playing a major catalytic role of transferring energy spatially, as well as a secondary one of westerly driving. Of course the fluxes are indeterminate in a certain sense, and one should be cautious when inferring specific physical mechanisms to describe their effects.

Transient variances, shown in Fig. 8.36d, exhibit their usual double-peak structure, as well as meridional anisotropy in the westerly and zonal anisotropy in the easterly jet. Moreover the MKE maximum is greater in the westerly than in the easterly jet, unlike either Run U or W. Again the interpretation of these variance features is somewhat uncertain. With the $k = 0$ component removed from the ZKE, one sees meridional anisotropy everywhere and the picture bears more of a resemblance to Run U. This meridional anisotropy was also seen at large scale in the spectra (e.g. Figs. 8.28b,8.29b).

§8f. Run S: Effects of Weaker Friction

While the geophysical estimate of $r = 0.5$ obtained in §8b for the Ekman drag coefficient must be considered realistic for mid-latitude

dynamics, it does seem at face value to be rather strong. If the processes considered in this study were to be investigated with regard to the mesoscale eddy field of the oceans, for example, one would presumably wish to choose a much weaker forced-dissipative balance (whether the model bears any relation to oceanic dynamics is another matter entirely). More to the point, there remains the concern that strong frictional damping in itself renders the linear dynamics irreversible, and it is necessary to separate this effect from the irreversibility provided by turbulent mixing.

It has been argued in §8c that there are indeed ways of verifying the efficacy of the nonlinear dynamics, and the nearly-inviscid spin-down runs of Chapter VII certainly proved that nonlinearity could do the job of trapping large-scale energy. Nevertheless a simulation has been performed with r reduced from 0.5 to 0.03, in order to investigate the dynamics of the weakly-forced regime; because of inexperience (this run being in fact the first performed with the constant-injection mechanism) the perturbation energy was allowed to slide from 0.47 down to 0.35, and the forcing coefficient γ of (8.2) was finally set at 0.000124 after some adjustment. Consequently the reduction in the forced-dissipative intensity is approximately a factor of 20 in comparison with Run U.

From a geophysical standpoint Run S must be considered rather queer, as the spin-down timescale of 17 model days exceeds any other timescale of the problem save the slowest variability in the basic-state flow component; therefore one might anticipate the equilibrium state to be rather close to that of inviscid statistical mechanical equilibrium, hence truncation-dependent and physically suspect. On the other hand when inviscid equilibrium does occur it obtains first at the smallest

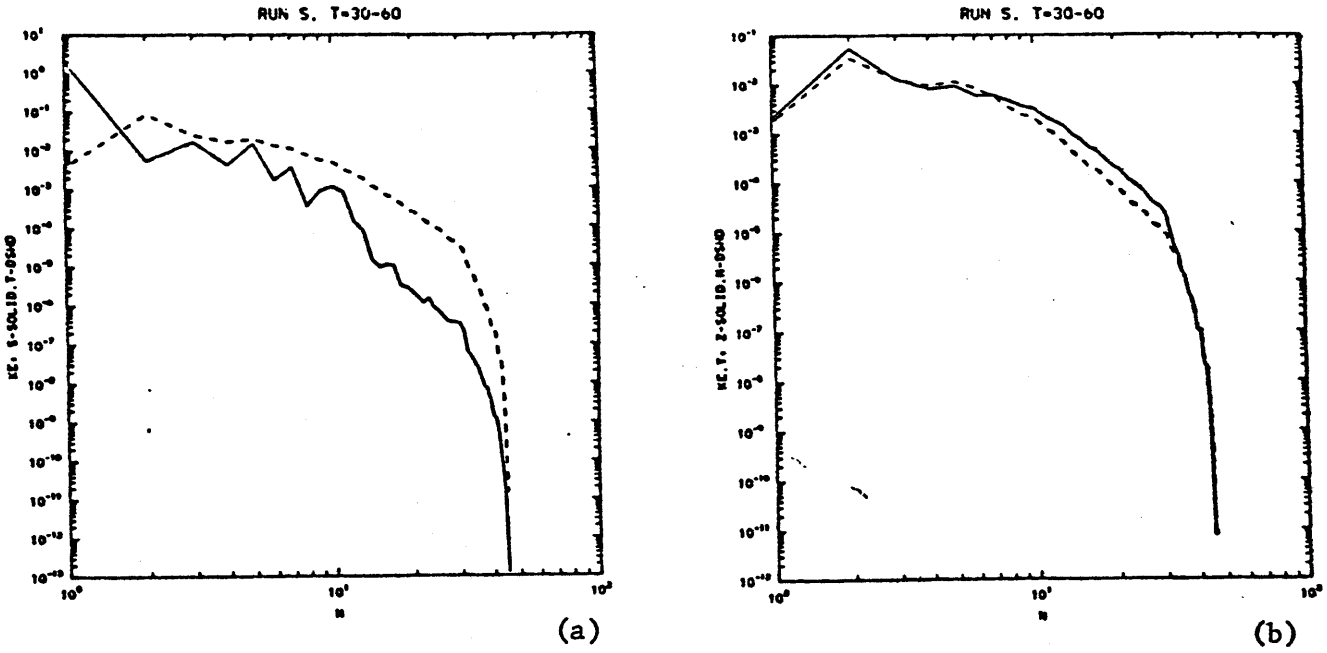


Fig. 8.37: (a) Stationary (——) and transient (– –) energy, and (b) zonal (——) and meridional (– –) transient energy, n-spectra, Run S, t = 30–60.

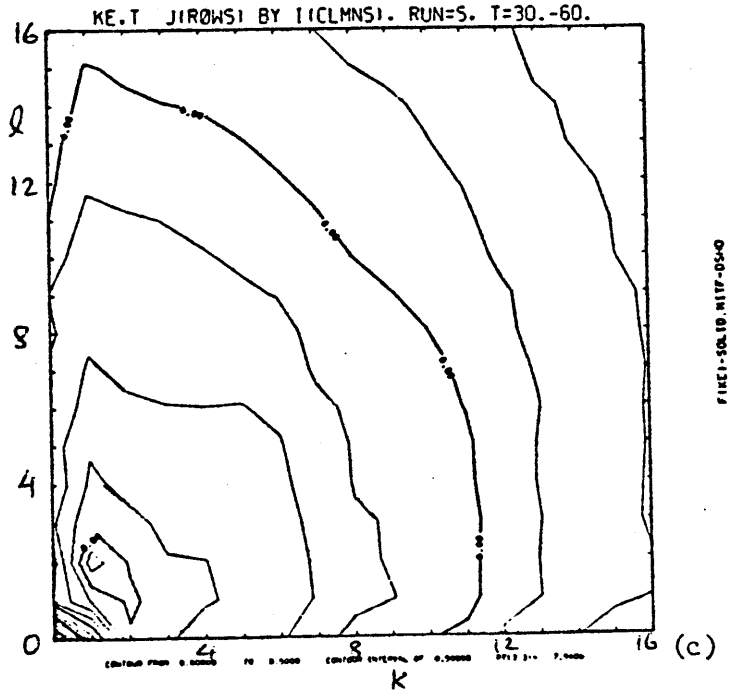


Fig. 8.37: (c) Transient 2-D (k,ℓ) spectrum of energy, Run S, t = 30–60.

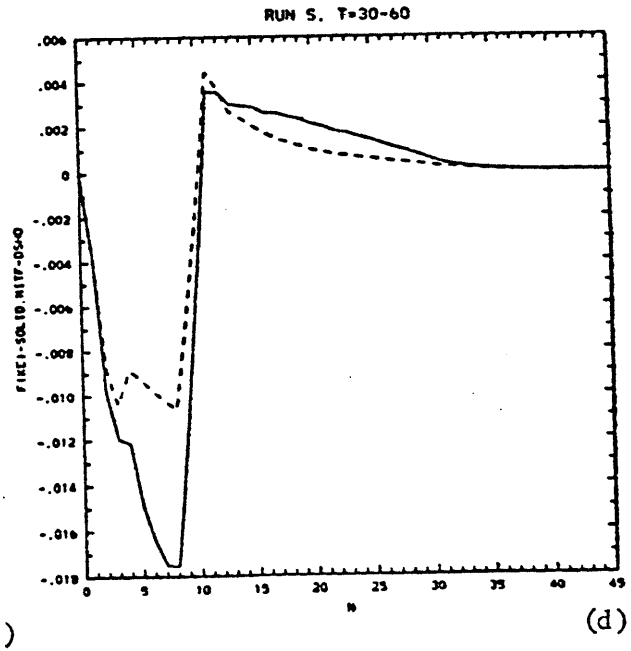


Fig. 8.37: (d) n-space nonlinear energy flux F(n) (——) and induced flux MITF(n) (– –), Run S.

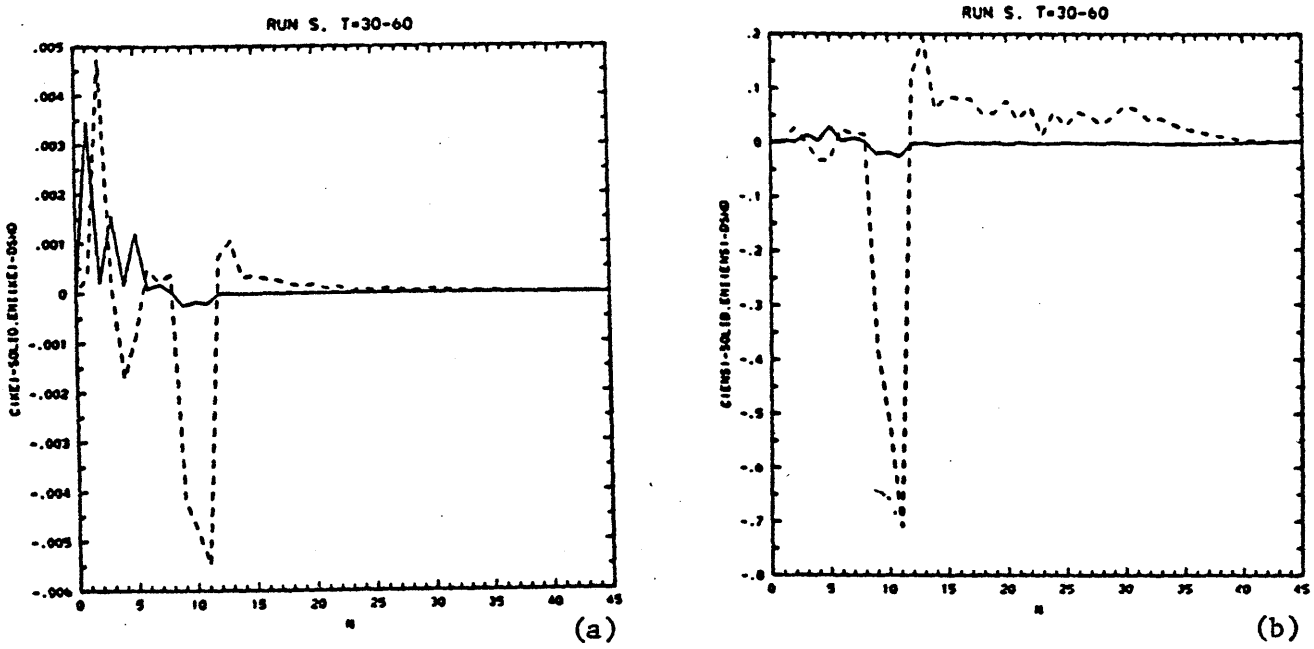


Fig. 8.38: n-space conversion terms: (a) for energy, C(n) (——) and EMI(n) (– –); (b) for enstrophy, $n^2C(n)$ (——) and $n^2EMI(n)$ (– –); both for Run S, t = 30-60 .

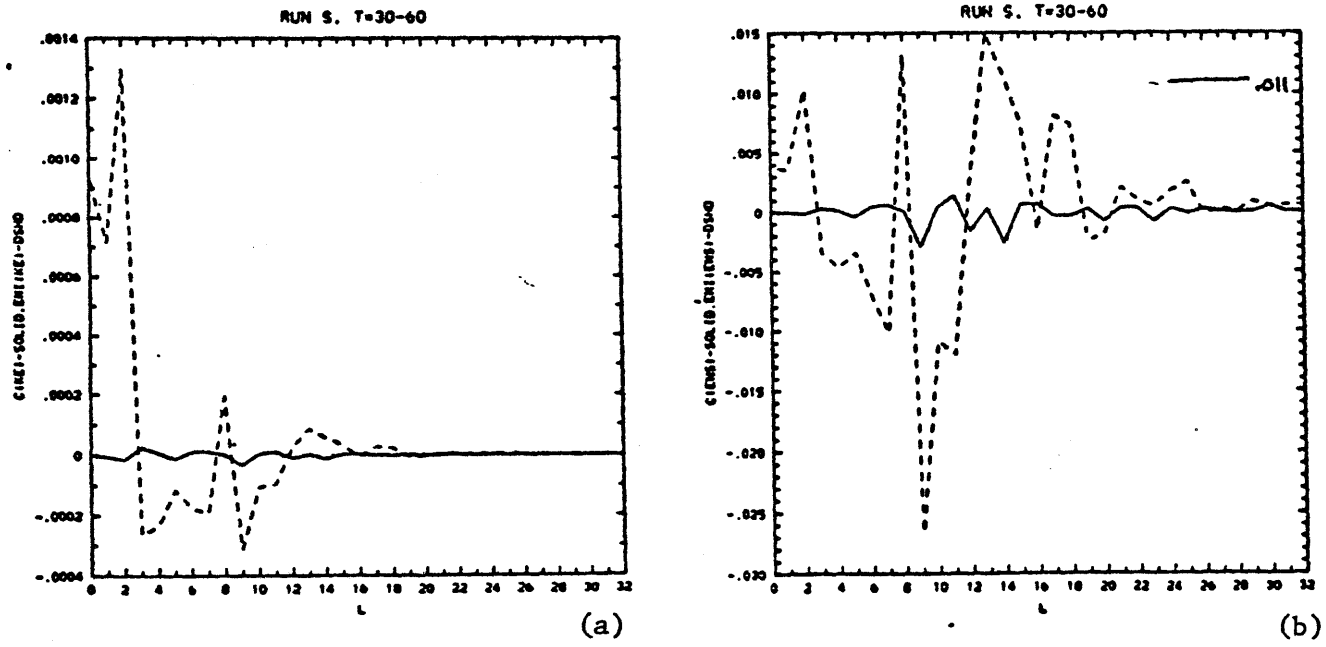


Fig. 8.39: ℓ-space conversion terms for the slice k = 2: (a) for energy, C(ℓ) (——) and EMI(ℓ) (– –); (b) for enstrophy, $n^2C(\ell)$ (——) and $n^2EMI(\ell)$ (– –); Run S, t = 30-60. Mark on (b) shows the magnitude of the sum.

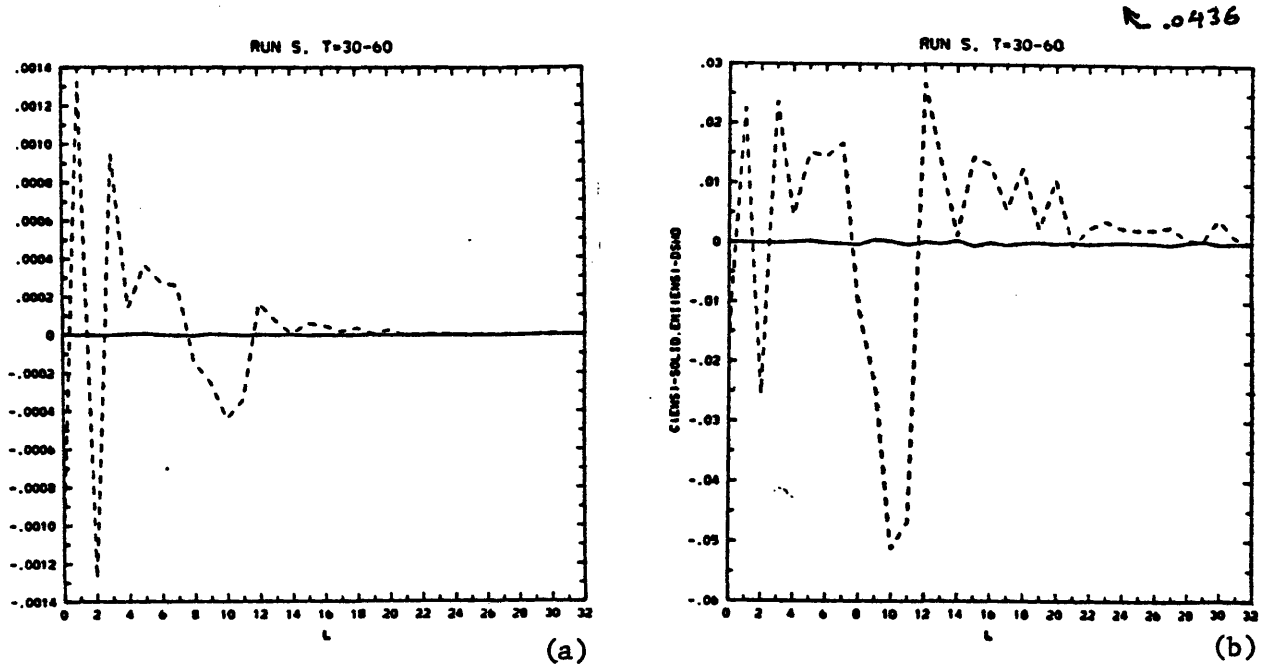


Fig. 8.40: Same as Fig. 8.39, but for k = 4 .

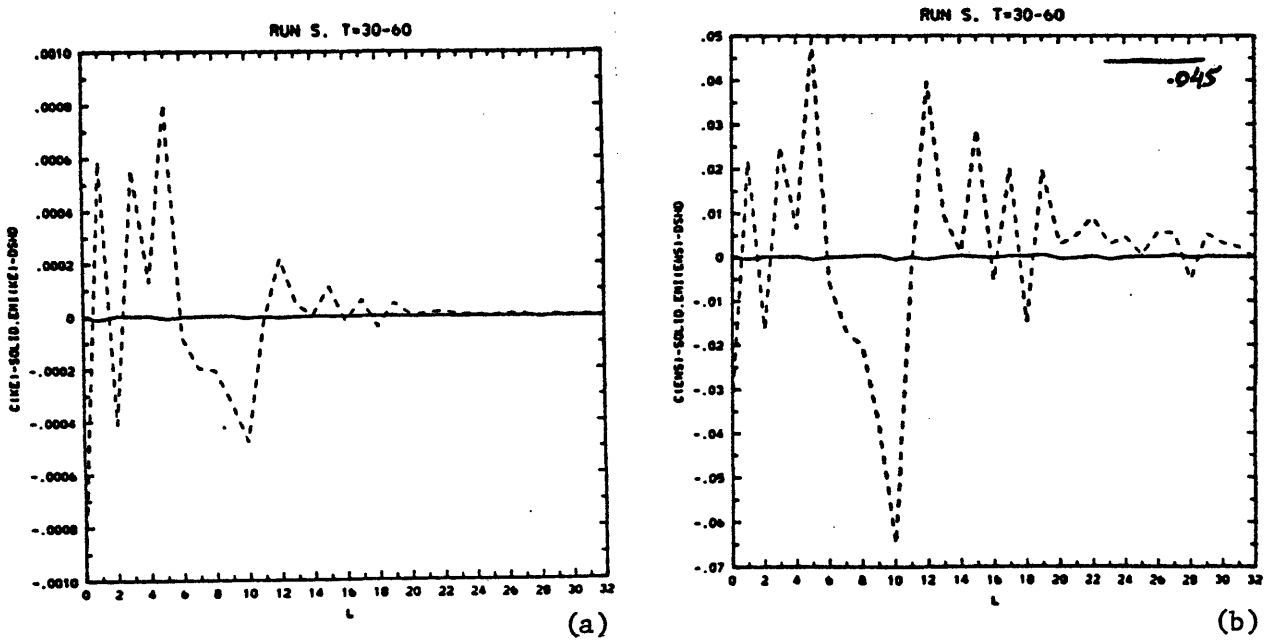


Fig. 8.41: Same as Fig. 8.39, but for k = 6 .

scales, and in this model these support an active enstrophy cascade with high-order diffusion, so the statistical behaviour is uncertain.

To avoid diverging too much by focussing an inordinate amount of attention on Run S, only a few figures will be shown. The point is to establish that even when the friction plays a very weak role, the essential conclusions obtained above still apply. Fig. 8.37a shows the stationary flow component to be far more energetic for $n > 1$ than in the other runs, which is no surprise given the weaker level of turbulent activity. The energy spectrum falls off more rapidly than the $1/k$ relation of inviscid equilibrium (for no mean flow), and reflects a low value of the total enstrophy, as may be seen from the increase of τ_1 and τ_2 in Table 8.1. The enstrophy cascade together with weak Ekman damping is apparently leading to a state of minimal enstrophy, which is quite different from inviscid equilibrium.

Focussing on the transient component itself (Fig. 8.37b), the peak is now strongly at large scale, $n = 2$; meridional anisotropy is present for $n = 4\text{-}6$, which is just inside n_β for Run S; and scales with $n > 8$ are zonally anisotropic. These last two features characterize all the runs to a certain extent, and seem very robust indeed. The 2-D transient spectrum (Fig. 8.37c) also exhibits this anisotropy, but the contours now seem more rough than in other runs, perhaps indicative of the weaker turbulent mixing. The strong peak in the $(k,\ell) = (1,2)$ component, with significant energy in the other $n = 2$ modes (2,2) and (2,1), suggests that the spectrum has filled out at large scale.

Now looking at the nonlinear flux functions in Fig. 8.37d, allowing for the much reduced intensity the picture is not dissimilar from that of Run T (Fig. 8.32a), with the induced flux MITF being roughly

constant for $3 < n < 8$ and providing about half of the total. The n-space stationary-transient interaction terms (Figs. 8.38a,b) definitely show a much stronger C(n) for $n > 1$ than is present in the other runs, but EMI(n) is fairly similar in form to what it is in Figs. 8.31a,b from Run T.

Finally the meridional transfer spectra for fixed k are given in Figs. 8.39 through 8.41. The residuals for EMI(ℓ) of enstrophy are considerably larger than in other runs, which is presumably due to the significant stationary components at scales comparable to the transients themselves (see Fig. 8.37a). Nevertheless this residual, when averaged, is still only a tiny fraction of the interaction at each ℓ, so induced transfer of enstrophy remains a good approximation. For $k = 4$ and $k = 6$, Figs. 8.40 and 8.41 indicate transfer away from the forced wave-number band, in both directions; while the transfer away from $2 < \ell < 8$ occurs for $k = 2$ (Figs. 8.39a,b). Once again these figures show the same essential processes to be operative in Run S as in the others, although the run is perhaps less satisfactory as a turbulence study.

§8g. Summary of Results

The forced-dissipative equilibrium simulations considered in this chapter exhibit a variety of behaviour. It is the object of this section to tie things together by identifying those phenomena which are common and therefore possibly robust, as well as those which seem sensitive to the parameter regime. A second goal is to interpret both classes of phenomena in terms of the linear and nonlinear theory of preceding chapters, guided by insight gleaned from the spin-down simulations of Chapter VII.

Proceeding from the discussion of §7f, the spin-down runs demonstrated the presence of the following spectral characteristics of linear theory in the nonlinear regime: a penetration of disturbance energy and enstrophy past the turbulent cascade-arrest scale n_β; large-scale meridional anisotropy, at least initially; small-scale zonal anisotropy; and significant "induced transfer" of perturbation enstrophy along lines of constant zonal wavenumber k. All of these phenomena are in striking contrast to the behaviour of pure beta-plane turbulence, and are easily understood in terms of the theory presented in Chapter VI.

Examining these four points within the context of the simulations of this chapter, it may be concluded that they are all quite evident, and that they again provide a sharp contrast with comparable beta-plane turbulence equilibrium experiments. Runs U, T, and S exhibit meridional anisotropy for transients with scales $n \lesssim n_\beta$, while Run W with stronger β_0 shifts this to isotropy; but in no case does one see anything approaching the large-scale zonal anisotropy of Runs V and X. The transient enstrophy is approximately conserved in its interaction with the stationary flow, validating the concept of induced spectral transfer along lines of constant k, provided that one compares the interaction at each ℓ with the residual averaged over all ℓ. The success of this description, considering the weakness of the scale separation between the stationary and transient flow components, is in some ways rather remarkable; on the other hand one should perhaps not be too surprised given the reputation of the WKB approximation!

The second set of results described in §7f concerned the nonlinear, turbulent modifications to the linear dynamics. Of these the most obvious was the defeat of the reversibility which characterizes

linear up-scale evolution and amplification; by introducing such irreversibility the nonlinear dynamics were able to trap energy at large scale, making the penetration of the "Rhines radius" $n = n_\beta$ a permanent effect. The specific process which accomplished this was turbulent isotropization, namely the ability of turbulent interactions to diffuse energy and enstrophy very rapidly along arcs of constant total wavenumber n (Herring, 1975).

There is no question that these features apply also in the present simulations, which is no surprise since a forced-dissipative regime with a full spectrum would be expected to be more turbulent than a spin-down one. For $n > n_\beta$ the only significant mean-flow straining seems to occur in the immediate vicinity of the forced wavenumber band, where the input is concentrated, although the small-scale zonal anisotropy attests to some nonlocal straining at all scales. The applicability of linear dynamics to the initial disturbance development, followed by strong turbulent mixing, is reminiscent of similar behaviour seen in fully-nonlinear baroclinic instability studies (e.g. Simmons & Hoskins, 1978; McWilliams & Chow, 1981).

All of the single-jet runs of this chapter exhibit induced down-scale transfer from mean-flow straining for transients in the forced band. While Runs U and W also show approximately symmetric up-scale (enstrophy) transfer, it is however noticeable that Runs T and S both have little up-scale transfer from those scales. The forcing is of course symmetric: an equal amount of energy and enstrophy is injected into modes with $k\ell > 0$ as with $k\ell < 0$, and linear dynamics alone would translate this into an <u>initially</u> symmetric transfer of enstrophy. The observed transfers <u>in equilibrium</u> are nevertheless a different story.

For example, disturbances in the forced band with $k \approx 10$ and small ℓ can rapidly reflect off turning lines at $\ell = 0$ and thus end up as net down-scale transfers, so one might not expect <u>any</u> up-scale transfer from them; indeed, all the runs show that waves with k larger than a certain transition scale (varying from $k = 4$ in Runs T and S to $k = 7$ in Run W) experience a net loss of energy in their wave, mean-flow interaction.

The robust result is that there is a definite zonal-wavenumber transition scale k_0, for which modes with $k > k_0$ show a net loss of energy and hence a largely down-scale enstrophy transfer, while modes with $k < k_0$ exhibit a net gain of energy and thus a substantial up-scale enstrophy transfer. However the value of k_0 is apparently parameter-dependent, and a small change in k_0 can easily lead to a significant alteration in the transfer pattern as a function of n. The picture is furthermore complicated by the fact that turbulent interactions can conceivably create a transfer "source" by mixing phases randomly; in fact this is evidently the case at the wave-turbulence transition scale n_β, particularly in Runs T and S which show transfer from both $n \approx n_\beta$ and $n = 9\text{-}11$.

It is readily apparent that by shifting k_0 and altering the pattern of induced transfer in n-space, the net sense of the wave, mean-flow interaction can be significantly altered: it is therefore no coincidence that Runs U and W, which have a relatively large k_0 and strong induced up-scale transfer from $n = 9\text{-}11$, maintain a weakened basic-state flow with net stationary-to-transient conversion (essentially the mean energy extracted by amplifying eddies is not returned); while Runs T and S, which have a smaller k_0 and weak induced up-scale tranfer from $n = 9\text{-}11$, maintain a strengthened basic-state flow with net transient-to-stationary conversion.

The weakness of the net wave, mean-flow interaction, and its sensitivity to the run parameters, may be at first sight surprising, but it is in fact easily understandable. First, the familiar geophysical examples of barotropic rectification that spring to mind are often baroclinically-driven processes: examples are momentum convergence in baroclinic instability (e.g. McIntyre, 1970), and the driving of deep barotropic currents by eddy form drag (e.g. Holland & Rhines, 1980). Secondly, the interaction constraints imposed by turbulent isotropization of the transient eddy field preclude a strong barotropic response (Pedlosky, 1962). If this constraint is removed, for instance by localizing the disturbance forcing, then the net interaction can be significant (Lorenz, 1953); an example of such barotropic driving by inhomogeneous forcing is given by Rhines (1977, §8C). Of course the generation of zonal jets within beta-plane turbulence theory itself (see Chapter III) provides a counter-example, but the mechanism is relatively weak and easily defeated by competitive processes such as those of mean-flow interaction considered in this thesis.

There are two other points concerning the spectral dynamics which ought to be raised. The first is that the linear dynamics, as expressed through stationary-transient interaction, are largely confined to $n < n_\beta$ and to $n = 9\text{-}11$; this was also seen in the spin-down runs. Nevertheless the presence of the mean flow is evidently felt at all scales to some extent, as attested to by the zonal anisotropy. The second point, which is connected with the first, is that in both Runs U and W the nonlinear energy flux from transient self-interactions, which is the embodiment of the classical turbulent energy cascade, is very similar to its form in the equivalent beta-plane turbulence Runs V and X; the most

notable consequence of this being an arrest of the flux at $n \approx n_\beta$. This suggests that the strong nonlinear dynamics still cut off at n_β, so that it is properly regarded as a wave-turbulence transition scale in the present problem, but with the difference that rapid scale changes can still occur inside this radius owing to interaction with the mean flow: the "induced cascade" takes over from the turbulent one.

With regard to the physical-space diagnostics, it can be safely said that, unlike the case with the spin-down runs, here the large-scale inhomogeneity asserts itself unambiguously. The robust results are that the eddies gain energy from the regions of strongest mean shear; the easterly jet is weakened; and the westerly jet is sharpened. All of these points may be understood in terms of the linear theory of mean-flow straining in Chapter VI, as has been discussed. What is <u>not</u> robust is however the relative importance of these effects, and such parameter dependence of the net mean-eddy interaction is of course intimately linked to the parallel sensitivity of the net stationary-transient interaction mentioned above.

Similarly, while the eddy variances always exhibit maxima in the jet cores and minima in the strongly-sheared regions, the relative anisotropy of the eddies is run-dependent. Generally speaking zonal anisotropy is favoured for the total fields, and meridional anisotropy if the $k = 0$ component is removed, especially in the westerly jet, but there are certainly exceptions.

As a footnote, it should be said that the roughness of the physical-space fields on a scale of $\ell \approx 10$, attributable to the phase-locking tendency of the forcing and in no way connected with the essential large-scale inhomogeneity, is apparently not a cause for concern.

The hypothesis made in §8b was that strong turbulent mixing would quickly confuse the phase structure for scales immediately adjacent to the forced band, thus isolating the memory of the initial conditions from the rest of the flow; this has been tested directly by comparing Runs U and UA, as well as through several indirect means. The issue of robustness of individual run realizations has also been addressed through a variety of techniques, with satisfactory results. Consequently the numerical simulations of this chapter can be approached with confidence.

CHAPTER IX - ATMOSPHERIC OBSERVATIONS, RE-VISITED

§9a. Introduction

The theoretical and numerical work of the last few chapters has provided insight into the nature of barotropic turbulence in the presence of a large-scale inhomogeneous flow. Insofar as the latter represents a component of the atmospheric circulation, a point argued in Chapter IV, it is desirable to return to the observations to see whether the lessons of the present research may aid in the interpretation of those observations, and in particular whether the questions raised in §4d can be answered.

Of course, the simplicity of the model precludes any straightforward comparison of the simulation diagnostics with those from observations; this limitation was recognized at the outset. The point is rather to employ the diagnostic techniques that were so crucial to an understanding of the numerical simulations, to determine the extent to which the same dynamical processes are operative in the atmosphere. The potential importance of such analysis is considerable: for example, it might suggest the dynamics and range of scales that must be considered (either explicitly or through a parameterization) in order for a tropospheric wave, mean-flow interaction study to be well-posed.

It has been argued, I trust successfully, that the problem of inhomogeneous turbulence is best viewed through a decomposition of the flow into stationary and transient components. Then the transient dynamics are a combination of two processes: turbulent interaction involving the transient waves themselves, and stationary-transient interaction. To the extent that there is a scale separation between the

two flow components, the first process is largely describable by 2-D homogeneous turbulence theory, and is operative outside of the "Rhines radius", i.e. for $n > n_\beta$; while the second is understandable as a process of "induced transfer" of transient enstrophy along lines of constant zonal wavenumber. The transfer process itself is determined initially by ray-tracing theory, and later on by irreversible turbulent mixing, with "quasi-linear" dynamics apparently of small importance. However this description is perhaps somewhat facile, as the point at which the turbulent dynamics take over from the linear dynamics is of prime concern to the net sense of the stationary-transient interaction, and seems not to be determinable from the theory; indeed, it turns out to be a rather sensitive feature. The value of the theory with regard to the atmosphere is thus not so much prognostic as diagnostic.

§9b. Stationary-Transient Interaction

The spectral energy and enstrophy equations describing stationary and transient budgets were derived in §7c for Cartesian geometry, and will not be explicitly re-written for the spherical harmonic analysis appropriate to the atmospheric diagnostics. A discussion of the necessary changes can be found in §2h, but there is another matter: the computed nonlinear interactions involve only interactions with the other modes resolved in the analysis, while the atmosphere's true evolution (unlike that of a numerical model) depends on unresolved scales. Consequently the frictional terms shown in §7c must be interpreted in the observational context as general source-sink terms involving interactions with unresolved scales of motion, friction, and other non-conservative effects, and cannot be calculated explicitly.

The key formulae to be considered in this section are (7.16), (7.17), (7.19), and (7.20), with k^2 replaced by $n(n+1)/\rho^2$. To recapitulate, C represents the transient-to-stationary (kinetic) energy conversion "seen by the stationary flow", and EMI the stationary-to-transient energy conversion "seen by the transient flow" (the subscript T is here dropped). The two do not cancel at each wavenumber, but they do when integrated over all wavenumbers; therefore they may be combined into an "induced interaction" term MITI as in (7.23), which together with its enstrophy version are true interaction terms in the sense of (7.24).

Returning first to Figs. 4.6, the breakdown of the energy and enstrophy fluxes presented there can now be interpreted in light of §7c. The "pure stationary" flux is the flux formed from MSI of (7.20b), the "pure transient" that formed from TSI of (7.17b), and the "mixed stationary-transient" that formed from MITI $\equiv$ C + EMI . Based on the results of Chapters VII and VIII, the second of these can safely be interpreted in terms of classical 2-D turbulence theory since the transient energy spectrum is roughly homogeneous and isotropic. The strong transient energy peak at n = 8 (Fig. 4.3a) represents the point at which the transient up-scale energy flux begins to fall off; of course the coincidence of these features is to be expected if the transient self-interactions are indeed spectrally local.

In the single-jet runs examined in Chapters VII and VIII, the transient cascade was arrested at n_β but the energy spectrum failed to peak there. However with the higher-mode jets considered in the Appendix the transient energy was seen to fall off for scales larger than that of the smallest significant stationary component. Interestingly the same feature seems to occur with the atmospheric spectra.

With regard to the "induced flux" which comprises most of the total energy flux for small n (Fig. 4.6a), the experience of this thesis suggests that one must consider its physical interpretation very carefully. In order to facilitate such examination, the conversion terms C and EMI will be shown in three different ways: as functions of n, of the zonal wavenumber m, and (for EMI) of the meridional wavenumber (n-m).

Fig. 9.1 shows the n-space representations of C and EMI for both energy and enstrophy. The stationary flow gains energy principally at $n = 3$, and also over the intermediate-scale range $6 < n < 13$, while losing some at $n = 5$ and 6; on the other hand the transient flow loses energy primarily from the range $6 < n < 13$. In terms of enstrophy, the net conversion is fairly small and the stationary-transient interaction thus seems to be well characterized as a down-scale transfer of enstrophy from a broad source region $6 < n < 24$. What is particularly interesting is that this transfer comes principally from two distinct scales: one around $n = 8$, and one around $n = 15$. The first corresponds to the transient energy peak, the second roughly to the primary energy input (presumably from baroclinic instability) as inferred from Fig. 4.1a. In fact the distribution of EMI is reminiscent of that seen in the spin-down Run 0 (Figs. 7.26d,7.27d).

The energy conversion terms are shown in Fig. 9.2 as functions of the zonal wavenumber m, and the pattern is very similar indeed to that found in the numerical simulations: disturbances with small but non-zero m gain energy through the stationary-transient interaction, while those with larger m experience a loss. Here the transition scale is $m_0 = 2.5$, considerably smaller than any seen in the equilibrium simulations; the strength of the mean-flow rectification is correspondingly greater. The

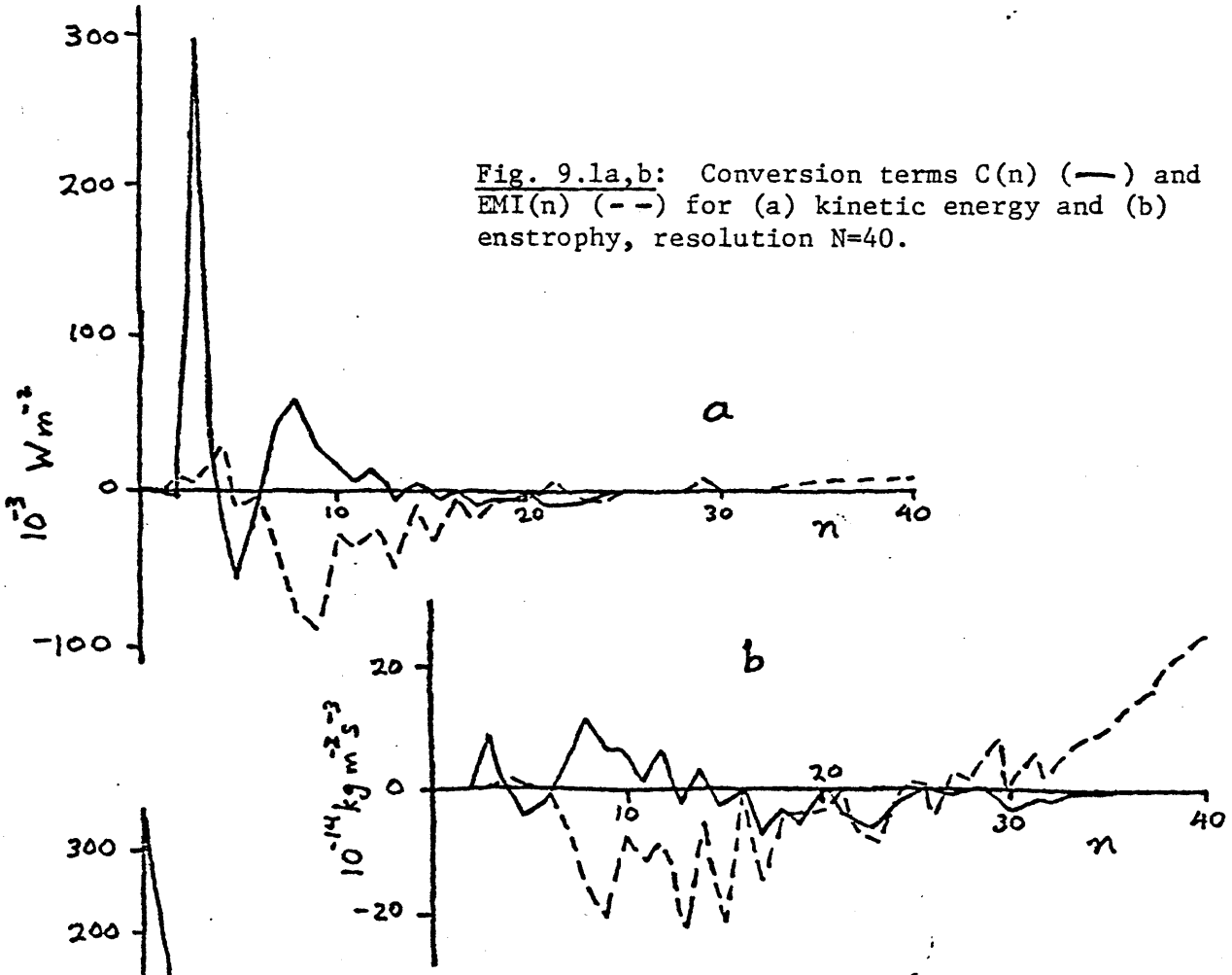


Fig. 9.1a,b: Conversion terms C(n) (——) and EMI(n) (- -) for (a) kinetic energy and (b) enstrophy, resolution N=40.

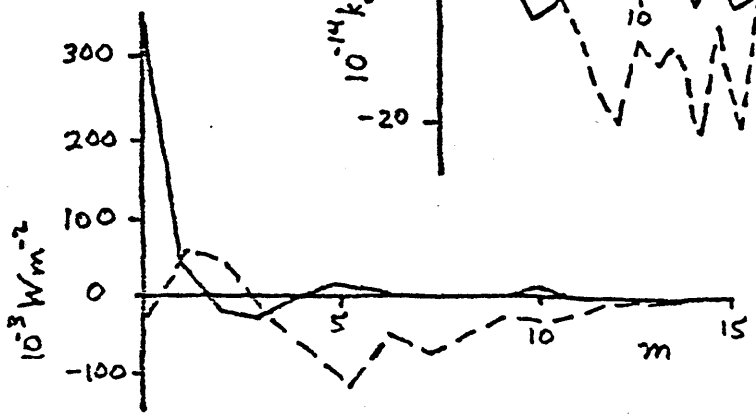


Fig. 9.2: k-space energy conversion terms C(k) (——) and EMI(k) (- -), shown only up to k=15.

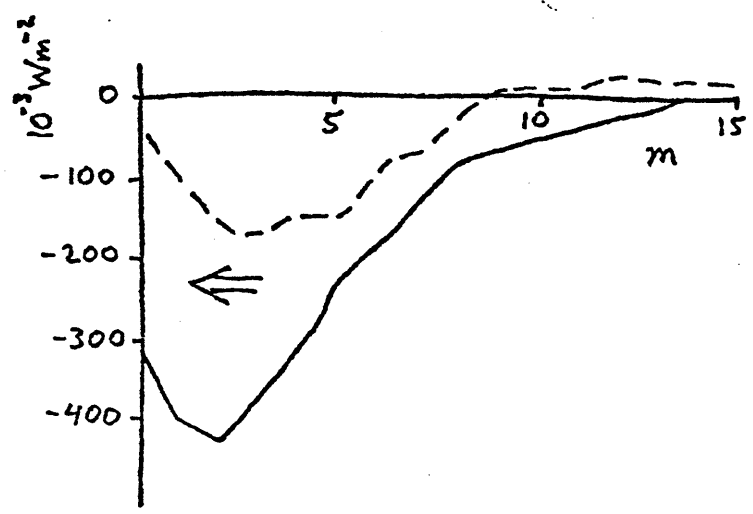


Fig. 9.3: k-space nonlinear energy fluxes: induced flux (——) and transient flux (- -). Only shown to k=15, but actual resolution is to k=40, which is why the fluxes do not close.

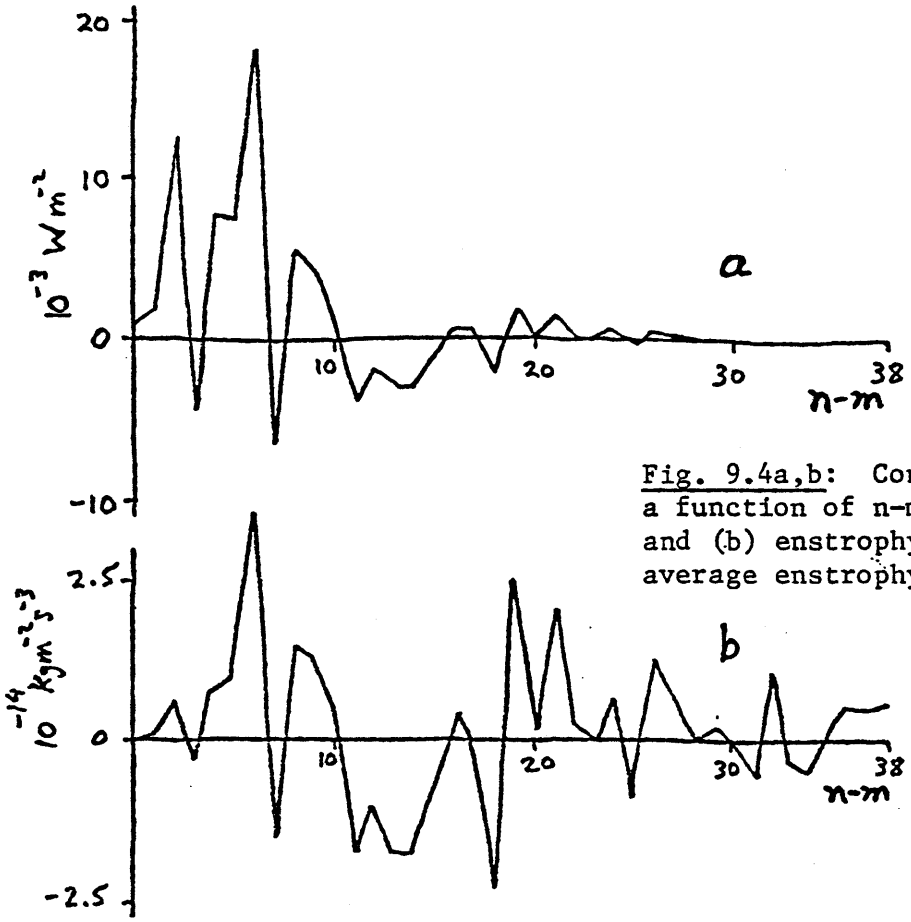


Fig. 9.4a,b: Conversion term EMI for m=2, as a function of n-m , for (a) kinetic energy and (b) enstrophy. Sum for (b) is 6.8, average enstrophy conversion per mode is .18.

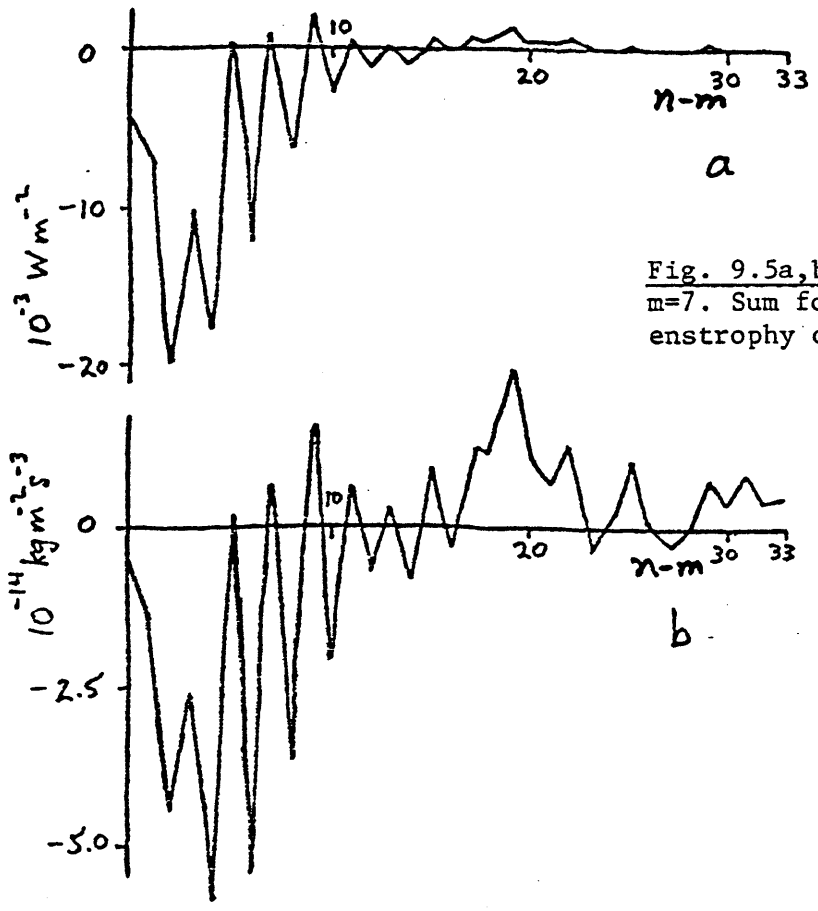


Fig. 9.5a,b: Same as Fig. 9.4, but for m=7. Sum for (b) is -12.0, average enstrophy conversion per mode is -0.35.

overall pattern can be understood in terms of "linear" evolution made irreversible by turbulent mixing, as discussed extensively in Chapters VII and VIII. Unfortunately the transition scale m_0, which in many ways determines the net sense of the conversion, cannot be predicted with the theory as it now stands. This however in no way detracts from the validity of the interpretation.

When the "induced flux" of energy formed from these conversion terms is compared with the transient flux (Fig. 9.3), an interesting fact emerges. Apparently the greatest part, almost 75%, of the observed up-scale energy flux (the stationary part being negligible in k-space) is attributable to the stationary-transient interactions, and is therefore not really a "flux" at all. The last comment describes the fact that while energy may be moving between different m's, it is doing so through highly nonlocal triads involving the mainly zonal stationary flow: different non-zero m's are coupled only indirectly. There is indeed a turbulent flux which is presumably local, but its role is clearly secondary when viewed in this representation.

The last five words which qualify the above sentence are worth emphasizing, for the contrast with the n-space picture (Fig. 4.6a) is considerable. There the transient flux is the dominant process for $n > 8$; moreover the induced flux is more properly called a flux, certainly for enstrophy which is transferred between neighbouring waves, and even to a certain extent for energy. This provides yet another argument against examining only the zonal-wavenumber spectral diagnostics, though it is fundamentally different from those raised previously; now the criticism is that, due to the fact that the stationary flow is largely zonal, what appears to be a local flux or cascade of energy is

in fact primarily a highly nonlocal wave, mean-flow interaction.

As a final diagnostic, it is interesting to consider the conversion terms as functions of the meridional wavenumber (n-m) for fixed zonal wavenumber m; this approach proved most illuminating in identifying the induced transfer of enstrophy in the numerical simulations. Nonlinear interactions in spherical geometry are no longer confined to single triads, a matter discussed in §2h, but it is nonetheless true that an interaction between a zonal ($m = 0$) and a non-zonal ($m \neq 0$) mode involves only modes with the same m (and a range of n). Consequently the same process of induced transfer is at least in principle applicable to the atmosphere, because the latter's stationary flow component is primarily zonal (e.g. Fig. 4.4a); however unlike the case for plane geometry, there is no possible extension of the theory to special non-zonal flows in a spherical geometry.

Only two such "cuts" are chosen: Figs. 9.4 show energy and enstrophy conversions for $m = 2$, while Figs. 9.5 do so for $m = 7$; the first corresponds to the low-m, transient amplification regime, the second to the higher-m, transient decay regime (Fig. 9.2). To avoid cluttering the figures, only the EMI conversion "seen by the transients" is shown; C is certainly significantly non-zero for $m = 2$, but quite negligible for $m = 7$. The data are evidently quite noisy, which is perhaps to be expected from the low information content (i.e., small number of degrees of freedom) of these diagnostics when compared with the integrated conversions of Figs. 9.1 and 9.2. Moreover the averaging period of one month is only about a fifth as long, dynamically speaking, as those used in analysing the simulations of Chapter VIII; if the eddy turn-around times of the model are at all representative of the atmos-

phere, then one month of data is perhaps the minimum required to obtain a significant signal in unintegrated spectral transfers.

Nevertheless Figs. 9.4 and 9.5 do show rather clear patterns. In the first case of $m = 2$, the enstrophy exhibits approximately symmetric transfer out of the range $12 < n < 21$; the net conversion, if spread out over all $n > m$, would be barely visible. When translated into energy, this distribution becomes a one-sided up-scale transfer with net extraction from the stationary flow (Fig. 9.4a), as reflected in Fig. 9.2. While there is certainly a strong transfer into $n = 8$, there is also significant penetration past that scale up to $n = 4$. On the other hand, for $m = 7$ (Figs. 9.5a,b) the phenomenology is essentially that of down-scale transfer of enstrophy from $6 < n < 20$; this naturally implies a net loss of transient energy, in accordance with Fig. 9.2, and in fact there is loss from all scales with almost no energy transfer.

It is therefore evident that the dynamical processes examined in the thesis are indeed most relevant to the atmosphere: the stationary-transient interaction may be characterized as a process of induced spectral transfer of enstrophy along lines of constant zonal wavenumber m, with the transfer being roughly symmetric in n for low m, and entirely down-scale for intermediate m. The first pattern implies a net extraction of stationary energy by the transients, the second a net absorption and rectification; the dominance of the latter process thus gives a net energy conversion from the transient to the stationary flow. It may be recalled from §4b that Shutts (1983b) claimed mean-flow straining, or induced down-scale enstrophy transfer, to be of prime importance to the maintenance of a certain class of blocking configurations; the present analysis suggests the effect to be far more ubiquitous. Moreover it is

apparent that a small change in the transition scale m_0 between the low-m "extraction" regime and the intermediate-m "rectification" regime can have a large effect on the overall strength and direction of energy and enstrophy fluxes, and on the extent of dynamical irreversibility.

§9c. Some Answers?

Over the course of §9b, answers to the questions a through f raised in §4d have emerged. Addressing them in order:

a. The transformation from isotropic, transient KE (a result of baroclinic instability followed by secondary instability or turbulent isotropization, your choice) to zonally anisotropic, stationary KE, occurs principally via mean-flow straining of the transient eddies; spectrally the process is well characterized by down-scale induced transfer of enstrophy along lines of constant zonal wavenumber m, with a consequent absorption of transient energy into the stationary flow. The sense of this transfer is in accordance with ray-tracing theory, provided one assumes the eddies to be initially orientated with their phase lines lying along the horizontal shear (as most baroclinic instability calculations would predict, e.g. McIntyre, 1970).

b. The portion of the spectral cascades attributable to the stationary waves alone (viz. the "stationary flux") is very small. However that part due to stationary-transient interaction is considerable, in fact it is dominant in a zonal-wavenumber representation (Fig. 9.3), and for small n in a spherical harmonic analysis (Fig. 4.6a). This "mixed" flux describes an induced transfer of transient enstrophy, a spectrally-local process, in either n-space or (n-m)-space, but <u>not</u> in m-space. The KE flux must be interpreted in light of the enstrophy dynamics; in particular, the apparent flux into n = 3-5 (Fig. 4.6a) is in reality a transient-to-stationary conversion involving highly-nonlocal triads.

c. The "arrest" of the up-scale KE cascade at n = 3 (Fig. 4.6a) is not explainable in terms of previous homogeneous geostrophic turbulence

theory; rather, it reflects a rectification of the large-scale stationary zonal flow through highly nonlocal triads, as discussed in b. The peak of the transient KE at n = 8 corresponds to a weak arrest of the purely transient flux, and appears to be effected by the stationary flow inhomogeneity - though this aspect of the problem is not well understood. While the transient flux itself is interpretable according to 2-D homogeneous turbulence theory, its arrest is not.

d. The rough isotropy of the transient long waves may be the result of a tendency to large-scale meridional anisotropy associated with the mean-flow straining, which counteracts the effects of beta, but this conclusion must still be considered rather speculative.

e. The "pure transient" fluxes of Figs. 4.6a,b are governed by 2-D homogeneous turbulence theory, while the "mixed stationary-transient" fluxes are understandable according to induced spectral transfer of transient enstrophy by the stationary flow, as discussed above.

f. The resemblance of the total KE and enstrophy fluxes to the predictions of 2-D and geostrophic homogeneous turbulence theory is due in part to the significant role of the turbulent interactions themselves, but relies fundamentally on the fact that the stationary-transient interaction gives the same superficial pattern. In a sense this may not seem too surprising, as the nonlinear interaction of the total flow is governed by conservation of KE and enstrophy; but recall that 2-D turbulence theory can only predict up-scale KE and down-scale enstrophy transfers under an ergodic assumption akin to "spectral broadening", and this assumption is not self-evident with regard to the stationary flow component. In fact there <u>is</u> spectral broadening, but it results from the relatively deterministic dynamics of the stationary-transient interaction in the form of wave-packet dispersion according to ray-tracing theory.

I am unfortunately not in a position to address the last question of §4d, namely g, with any degree of completeness. Nevertheless it may be said that the observed "reverse energy cascade" appears to be of

great importance to the general circulation; in part it is due to turbulent interactions, though this aspect of the dynamics does not directly affect the very largest scales of motion; and in part it describes a transient-to-stationary conversion via nonlocal triad interactions. The implication of this with respect to the modelling of quasi-stationary features (i.e. seasonal flow patterns and climatic anomalies) is that severely truncated or, even worse, linear models cannot hope to address questions of current interest such as equilibration and transition unless a wide spectrum of transient scales is taken into consideration. Such a conclusion is in fact widely appreciated, but is at the same time rather frightening in view of the prospect that reasonable transient-eddy parameterizations for low-order models may not be obtainable. Such parameterization efforts are indeed in progress (e.g. White & Green, 1982; Shutts, 1983a; Källén, 1984); they provide a challenging area for future research.

CHAPTER X - CONCLUDING REMARKS

This thesis represents an attempt to make at least a small contribution to the understanding of a dynamical regime which may be characterized, according to one's point of view, as either inhomogeneous turbulence or strongly nonlinear wave, mean-flow interaction. Occupying the middle ground between two areas in which theoretical success has been notable - homogeneous turbulence on the one hand, and linear or weakly-nonlinear wave, mean-flow interaction on the other - this intermediate regime has hitherto not presented a particularly fruitful field for fluid dynamical endeavour.

In order to make some progress, attention has been focussed on a particular problem of geophysical significance: namely that of barotropic beta-plane turbulence in the presence of a large-scale zonal jet. Then the inhomogeneity arises only from the mean flow, not from the fluid medium, and is restricted to the meridional coordinate; moreover it is of large scale. These simplifications enable a theoretical approach to be pursued, although it must be said that it remains a patchwork rather than a comprehensive theory, whose value is more diagnostic than prognostic. Because of the nature of the problem, experimental results are essential in order to determine the relative importance of different dynamical processes contained within the theoretical framework; the simplest form of such experimentation in the present case is that of direct numerical simulation.

The results of the numerical experiments are summarized at the end of the relevant chapters, specifically in §§7f and 8g and the Appendix, to which the reader is referred; here the discussion is intentionally

kept brief. With regard to the transient dynamics, the situation can be understood as a combination of two processes: transient self-interaction describable according to 2-D homogeneous turbulence theory, and operative primarily outside of the "Rhines radius" $n = n_\beta$; and stationary-transient interaction well characterized as induced spectral transfer of transient enstrophy from the input scales along lines of constant zonal wavenumber k, operative outside of the smallest significant jet scale ($n = 1$ in Chapters VII and VIII, $n > 1$ in the Appendix).

The transient self-interactions by themselves would of course lead to the familiar end-state of beta-plane turbulence, namely an arrest of the up-scale energy cascade at $n = n_\beta$ and a slow focussing into zonal jets of the same scale. On the other hand the stationary-transient interactions, acting in isolation, would lead to an absorption of transient energy into the stationary flow, though in a forced-dissipative situation quasi-linear (or quasi-nonlinear) effects would inevitably enter. But the two processes combined yield a strikingly different picture. The turbulent regime outside $n = n_\beta$ is made slightly inhomogeneous and zonally anisotropic by the mean-flow straining, but not to the extent that the relevance of the homogeneous theory is threatened. The up-scale energy cascade is continued (to smaller n) past n_β through the process of induced enstrophy transfer, but is made irreversible - unlike in the linear case - by (slow) turbulent isotropization. When the stationary flow has a significant component with $n > 1$, then the Appendix shows the "induced cascade" to be arrested there; in pure beta-plane turbulence, to the extent that stationary jets form, this scale is of course identical with n_β.

While the stationary-transient interaction dynamics are indeed

well characterized by induced transfer of transient enstrophy, even for a weak scale separation, the nonlinear closure of this transfer process presents a significant problem. All of the simulations showed a distinct pattern: for small but non-zero zonal wavenumber k, the induced transfer is spectrally symmetric in ℓ about the input scale, and leads to a net up-scale energy transfer and amplification at the expense of the stationary flow; while for intermediate k the transfer process is essentially down-scale, implying absorption of transient energy into the stationary flow. The difficulty lies in determining the transition scale k_0 between these two regimes, and hence the extent of dynamical irreversibility; k_0 appears to be a sensitive function of the external parameters.

Consequently the net sense of the stationary-transient energetic interaction is also sensitive to external conditions, and as far as the stationary-flow problem is concerned this is the quantity of most interest. The weakness of the net interaction is understandable theoretically, and has been discussed in §8g. Nevertheless it means that the robust results all concern the transient dynamics, in particular their spectral characteristics.

The diagnostic utility of the theoretical ideas has been exhibited in relation to the interpretation of atmospheric observations in Chapter IX. While a quantitative comparison of the model diagnostics with those of the atmosphere is impossible, the qualitative correspondence is in many ways quite striking. Most importantly, the insight obtained from application of the new ideas enables some crucial questions raised in Chapter IV to be answered. It would seem that the conceptual picture of a turbulent transient flow interacting in the presence of and with a

large-scale, largely zonal stationary flow, studied in this thesis, is indeed of great relevance to the mid-latitude atmosphere.

However the model problem considered in this research is clearly inadequate for an investigation of the net stationary-transient interaction in the atmosphere, and of the maintenance of and transition between different quasi-stationary flow regimes. To address such questions seriously, at the very least one would need to take account of the spherical geometry which affects the largest scales of motion; of the thermal and orographic external forcing which "creates" the basic-state flow; and of the feedback between the stationary flow and the intermediate-scale forcing arising out of baroclinic instabilty. These are non-trivial complications. At the same time the present work suggests strongly that interactions with a wide range of transient scales cannot be ignored, insofar as the net stationary-transient conversion seems to be rather sensitive to the dynamics and spectral distribution of the transient eddy field. Whether this interaction could be adequately parameterized in a low-order model is a matter of current interest and great concern.

A fundamental obstacle to a sensible investigation of atmospheric behaviour involves the identification of "quasi-stationary" flow configurations, which is quite an ambiguous matter. In the observational analysis of this thesis the difficulty was finessed by examining a monthly mean. But whereas the forced-dissipative model simulations can be made temporally homogeneous by considering a sufficiently long sampling period, the atmosphere does not allow such a possibility. It would seem that the appropriateness of a stationary-transient decomposition in that case can only be determined <u>a posteriori</u>.

REFERENCES

Andrews, D.G., 1983a: A conservation law for small-amplitude quasi-geostrophic disturbances on a zonally-asymmetric basic flow. J.Atmos.Sci., 40, 85-90. [V]

Andrews, D.G., 1983b: A finite-amplitude Eliassen-Palm theorem in isentropic coordinates. J.Atmos.Sci., 40, 1877-1883. [V]

Andrews, D.G., & M.E. McIntyre, 1976: Planetary waves in horizontal and vertical shear: The generalized Eliassen-Palm relation and the mean zonal acceleration. J.Atmos.Sci., 33, 2031-2048. [I,V]

Andrews, D.G., & M.E. McIntyre, 1978a: An exact theory of nonlinear waves on a Lagrangian-mean flow. J.Fluid Mech., 89, 609-646. [I,V]

Andrews, D.G., & M.E. McIntyre, 1978b: On wave-action and its relatives. J.Fluid Mech., 89, 647-664. [V]

Arnol'd, V.I., 1965: Conditions for nonlinear stability of stationary plane curvilinear flows of an ideal fluid. Soviet Math., 6, 773-777. (Dokl.Akad.Nauk.SSSR, 162, 975-978) [V]

Baer, F., 1972: An alternate scale representation of atmospheric energy spectra. J.Atmos.Sci., 29, 649-664. [II]

Baer, F., 1981: Three-dimensional scaling and structure of atmospheric energetics. J.Atmos.Sci., 38, 52-68. [III,IV]

Basdevant, C., & R. Sadourny, 1983: Modélisation des échelles virtuelles dans la simulation numérique des écoulements turbulents bidimensionnels. J.Méch.Théor.Appl., Numéro spécial, 243-269. [II,VII]

Basdevant, C., B. Legras, R. Sadourny & M. Béland, 1981: A study of barotropic model flows: Intermittency, waves and predictability. J.Atmos.Sci., 38, 2305-2326. [II,III,VIII]

Batchelor, G.K., 1953: The Theory of Homogeneous Turbulence. Cambridge University Press, 197 pp. [I,II,V]

Batchelor, G.K., 1959: Small-scale variation of convected quantities like temperature in a turbulent fluid. Part 1. General discussion and the case of small conductivity. J.Fluid Mech., 5, 113-133. [II]

Batchelor, G.K., 1969: Computation of the energy spectrum in homogeneous two-dimensional turbulence. Phys.Fluids, Suppl.II, 12, 233-239. [II]

Blackmon, M.L., J.M. Wallace, N.-C. Lau & S.L. Mullen, 1977: An observational study of the Northern Hemisphere wintertime circulation. J.Atmos.Sci., 34, 1040-1053. [IV]

Blumen, W., 1968: On the stability of quasi-geostrophic flow. J.Atmos.Sci., 25, 929-931. [V]

Blumen, W., 1978: Uniform potential vorticity flow: Parts I and II. J.Atmos.Sci., 35, 774-789. [III]

Boer, G.J., 1983: Homogeneous and isotropic turbulence on the sphere. J.Atmos.Sci., 40, 154-163. [II]

Boer, G.J., & T.G. Shepherd, 1983: Large-scale two-dimensional turbulence in the atmosphere. J.Atmos.Sci., 40, 164-184. [I,II,III,IV,VII,VIII]

Boyd, J.P., 1983: The continuous spectrum of linear Couette flow with the beta effect. J.Atmos.Sci., 40, 2304-2308. [VI]

Bretherton, F.P., 1970: A note on Hamilton's principle for perfect fluids. J.Fluid Mech., 44, 19-31. [V]

Bretherton, F.P., 1971: The general linearised theory of wave propagation. Lectures in Applied Math., 13, 61-102. Providence, R.I.: Amer.Math.Soc. [V]

Bretherton, F.P., & C.J.R. Garrett, 1968: Wavetrains in inhomogeneous moving media. Proc.Roy.Soc.Lond.A, 302, 529-554. [V,VI]

Buckley, R., 1982: On the calculation of intensity in dispersive inhomogeneous media in the ray approximation. Proc.Roy.Soc.Lond.A, 380, 201-209. [VI]

Busse, F.H., 1983: A model of mean zonal flows in the major planets. Geophys.Astrophys.Fluid Dynamics, 23, 153-174. [III]

Charney, J.G., 1947: The dynamics of long waves in a baroclinic westerly current. J.Meteor., 4, 135-162. [IV]

Charney, J.G., 1971: Geostrophic turbulence. J.Atmos.Sci., 28, 1087-1095. [III,IV]

Charney, J.G., & P.G. Drazin, 1961: Propagation of planetary-scale disturbances from the lower into the upper atmosphere. J.Geophys.Res., 66, 83-109. [I,IV,V]

Charney, J.G., R. Fjørtoft & J. von Neumann, 1950: Numerical integration of the barotropic vorticity equation. Tellus, 2, 237-254. [IV]

Cocke, W.J., 1969: Turbulent hydrodynamic line stretching: Consequences of isotropy. Phys.Fluids, 12, 2488-2492. [II]

Craik, A.D.D., 1981: The development of wavepackets in unstable flows. Proc.Roy.Soc.Lond.A, 373, 457-476. [VI]

Craik, A.D.D., 1982: The generalized Lagrangian-mean equations and hydrodynamic stability. J.Fluid Mech., 125, 27-35. [V]

Drazin, P.G., D.N. Beaumont & S.A. Coaker, 1982: On Rossby waves modified by basic shear, and barotropic instability. J.Fluid Mech., 124, 439-456. [VI]

Dunkerton, T.J., 1980: A Lagrangian mean theory of wave, mean-flow interaction with applications to nonacceleration and its breakdown. Rev.Geophys.Space Phys., 18, 387-400. [I,V]

Dunkerton, T.J., 1983: The conservation of pseudoenergy in Lagrangian time-mean flow. J.Atmos.Sci., 40, 2623-2629. [V]

Eady, E.T., 1949: Long waves and cyclone waves. Tellus, 1, 33-52. [III,IV]

Eckart, C., 1963: Some transformations of the hydrodynamic equations. Phys.Fluids, 6, 1037-1041. [V]

Edmon, H.J., B.J. Hoskins & M.E. McIntyre, 1980: Eliassen-Palm cross sections for the troposphere. J.Atmos.Sci., 37, 2600-2616. (See also Corrigendum, J.Atmos.Sci., 38, 1115 (1981), especially second last item.) [IV,V]

Eliassen, A., & E. Palm, 1961: On the transfer of energy in stationary mountain waves. Geofys.Publ., 22, No.3, 1-23. [V]

Farrell, B.F., 1982: The initial growth of disturbances in a baroclinic flow. J.Atmos.Sci., 39, 1663-1686. [III,IV,VI]

Fjørtoft, R., 1950: Application of integral theorems in deriving criteria of stability for laminar flows and for the baroclinic circular vortex. Geofys.Publ., 17, No.6, 1-52. [V]

Fjørtoft, R., 1953: On the changes in the spectral distribution of kinetic energy for two-dimensional, non-divergent flow. Tellus, 5, 225-230. [I,II,III,V,VI]

Fox, D.G., & S.A. Orszag, 1973: Inviscid dynamics of two-dimensional turbulence. Phys.Fluids, 16, 169-171. [II]

Frederiksen, J.S., & B.L. Sawford, 1980: Statistical dynamics of two-dimensional inviscid flow on a sphere. J.Atmos.Sci., 37, 717-732. [II]

Fu, L.-L., & G.R. Flierl, 1980: Nonlinear energy and enstrophy transfer in a realistically stratified ocean. Dyn.Atmos.Oceans, 4, 219-246. [III]

Gall, R., 1976: A comparison of linear baroclinic instability theory with the eddy statistics of a General Circulation Model. J.Atmos.Sci., 33, 349-373. [IV]

Gall, R., R. Blakeslee & R.C.J. Somerville, 1979a: Cyclone-scale forcing of ultralong waves. J.Atmos.Sci., 36, 1692-1698. [IV]

Gall, R., R. Blakeslee & R.C.J. Somerville, 1979b: Baroclinic instability and the selection of the zonal scale of the transient eddies of middle latitudes. J.Atmos.Sci., 36, 767-784. [IV]

Gambo, K., 1982: Vorticity equation of transient ultra-long waves in middle latitudes in winter regarded as Langevin's equation in Brownian motion. J.Met.Soc.Japan, 60, 206-214. [IV]

Gill, A.E., 1974: The stability of planetary waves on an infinite beta-plane. Geophys.Fluid Dynamics, 6, 29-47. [III,V,A]

Green, J.S.A., 1970: Transfer properties of the large-scale eddies and the general circulation of the atmosphere. Quart.J.Roy.Met.Soc., 96, 157-185. [I,IV]

Green, J.S.A., 1977: The weather during July 1976: Some dynamical considerations of the drought. Weather, 32, 120-126. [IV]

Grimshaw, R., 1984: Wave action and wave-mean flow interaction, with application to stratified shear flows. Ann.Rev.Fluid Mech., 16, 11-44. Annual Reviews, Inc. [V]

Haidvogel, D.B., 1983: Periodic and regional models. Eddies in Marine Science, ed. A.R. Robinson, pp. 404-437. Berlin and Heidelberg: Springer-Verlag. [II,VII,VIII]

Haidvogel, D.B., & I.M. Held, 1980: Homogeneous quasi-geostrophic turbulence driven by a uniform temperature gradient. J.Atmos.Sci., 37, 2644-2660. [III]

Hansen, A.R., & T.-C. Chen, 1982: A spectral energetics analysis of atmospheric blocking. Mon.Wea.Rev., 110, 1146-1165. [IV]

Hansen, A.R., & A. Sutera, 1984: A comparison of the spectral energy and enstrophy budgets of blocking versus nonblocking periods. Tellus, 36A, 52-63. [IV]

Hart, J.E., 1979: Finite amplitude baroclinic instability. Ann.Rev.Fluid Mech., 11, 147-172. Annual Reviews, Inc. [IV]

Hartman, R.J., 1975: Wave propagation in a stratified shear flow. J.Fluid Mech., 71, 89-104. [VI]

Hasselmann, K., 1967: Nonlinear interactions treated by the methods of theoretical physics (with application to the generation of waves by wind). Proc.Roy.Soc.Lond.A, 299, 77-100. [VI]

Hayashi, Y., & D.G. Golder, 1983: Transient planetary waves simulated by GFDL spectral General Circulation Models. Part II: Effects of nonlinear energy transfer. J.Atmos.Sci., 40, 951-957. [IV]

Hayes, W.D., 1970: Conservation of action and modal wave action. Proc.Roy.Soc.Lond.A, 320, 187-208. [V]

Held, I.M., 1983: Stationary and quasi-stationary eddies in the extra-tropical troposphere: Theory. Large-Scale Dynamical Processes in the Atmosphere, eds. B.J. Hoskins & R.E. Pearce, pp. 127-168. London: Academic Press. [I,IV,V,VI,VIII]

Herring, J.R., 1975: Theory of two-dimensional anisotropic turbulence. J.Atmos.Sci., 32, 2254-2271. [III,VIII]

Herring, J.R., 1980: Statistical theory of quasi-geostrophic turbulence. J.Atmos.Sci., 37, 969-977. [III]

Herring, J.R., S.A. Orszag, R.H. Kraichnan & D.G. Fox, 1974: Decay of two-dimensional homogeneous turbulence. J.Fluid Mech., 66, 417-444. [II]

Holland, W.R., & P.B. Rhines, 1980: An example of eddy-induced ocean circulation. J.Phys.Ocean., 10, 1010-1031. [VIII]

Holloway, G., 1980: Oceanic internal waves are not weak waves. J.Phys.Ocean., 10, 906-914. [VI]

Holloway, G., & M.C. Hendershott, 1977: Stochastic closure for nonlinear Rossby waves. J.Fluid Mech., 82, 747-765. [III]

Holopainen, E.O., 1978: On the dynamic forcing of the long-term mean flow by the large-scale Reynolds' stresses in the atmosphere. J.Atmos.Sci., 35, 1596-1604. [IV]

Holopainen, E.O., 1983: Transient eddies in mid-latitudes: Observations and interpretation. Large-Scale Dynamical Processes in the Atmosphere, eds. B.J. Hoskins & R.E. Pearce, pp. 201-233. London: Academic Press. [IV,VIII]

Holopainen, E.O., & A.H. Oort, 1981: On the role of large-scale transient eddies in the maintenance of the vorticity and enstrophy of the time-mean atmospheric flow. J.Atmos.Sci., 38, 270-280. [IV]

Holopainen, E.O., L. Rontu & N.-C. Lau, 1982: The effect of large-scale transient eddies on the time-mean flow in the atmosphere. J.Atmos.Sci., 39, 1972-1984. [IV]

Hoskins, B.J, 1983: Modelling of the transient eddies and their feedback on the mean flow. Large-Scale Dynamical Processes in the Atmosphere, eds. B.J. Hoskins & R.E. Pearce, pp. 169-199. London: Academic Press. [I,IV]

Hoskins, B.J., & D.J. Karoly, 1981: The steady linear response of a spherical atmosphere to thermal and orographic forcing. J.Atmos.Sci., 38, 1179-1196. [VI]

Hoskins, B.J., I.N. James & G.H. White, 1983: The shape, propagation and mean-flow interaction of large-scale weather systems. J.Atmos.Sci., 40, 1595-1612. [IV,VIII]

Hoyer, J.-M., & R. Sadourny, 1982: Closure modeling of fully developed baroclinic instability. J.Atmos.Sci., 39, 707-721. [III]

Illari, L., & J.C. Marshall, 1983: On the interpretation of eddy fluxes during a blocking episode. J.Atmos.Sci., 40, 2232-2242. [IV]

Ingersoll, A.P., R.F. Beebe, J.L. Mitchell, G.W. Garneau, G.M. Yagi & J.-P. Müller, 1981: Interaction of eddies and mean zonal flow on Jupiter as inferred from Voyager 1 and 2 images. J.Geophys.Res., 86 (A10), 8733-8743. [III]

Itoh, H., 1983: An observational study on the amplification of planetary waves in the troposphere. J.Met.Soc.Japan, 61, 568-589. [IV]

Jeffreys, H., 1926: On the dynamics of geostrophic winds. Quart.J.Roy.Met.Soc., 52, 85-104. [I,IV]

Källén, E., 1984: Bifurcation mechanisms and atmospheric blocking. Problems and Prospects in Long and Medium Range Weather Forecating, eds. D.M. Burridge & E. Källén, pp. 229-263. Berlin and Heidelberg: Springer-Verlag. [IV,IX]

Kanzawa, H., 1984: Quasi-geostrophic energetics based on a transformed Eulerian equation with application to wave-zonal flow interaction problems. J.Met.Soc.Japan, 62, 36-51. [IV]

Kao, S.K., & C.N. Chi, 1978: Mechanism for the growth and decay of long- and synoptic-scale waves in the mid-troposphere. J.Atmos.Sci., 35, 1375-1387. [IV]

Kenyon, K., 1967: Discussion (of a paper by Longuet-Higgins & Gill). Proc.Roy.Soc.Lond.A, 299, 141-144. [III,A]

Kolmogorov, A.N., 1941: The local structure of turbulence in incompressible viscous fluid for very large Reynolds numbers. C.R.Acad.Sci.URSS, 30, 301-305. (Dokl.Akad.Nauk.SSSR, 30, 299-303). [II]

Kraichnan, R.H., 1967: Inertial ranges in two-dimensional turbulence. Phys.Fluids, 10, 1417-1423. [II,III]

Kraichnan, R.H., 1971: Inertial-range transfer in two- and three-dimensional turbulence. J.Fluid Mech., 47, 525-535. [II]

Kraichnan, R.H., 1975: Statistical dynamics of two-dimensional flow. J.Fluid Mech., 67, 155-175. [II]

Kuo, H.L., 1949: Dynamic instability of two-dimensional non-divergent flow in a barotropic atmosphere. J.Meteor., 6, 105-122. [VI]

Landau, L.D., & E.M. Lifshitz, 1971: The Classical Theory of Fields. 3rd Revised English Edition, Pergamon Press, 374 pp. [V]

Lau, N.-C., 1978: On the three-dimensional structure of the observed transient eddy statistics of the Northern Hemisphere wintertime circulation. J.Atmos.Sci., 35, 1900-1923. [IV]

Lau, N.-C., 1979: The observed structure of tropospheric stationary waves and the local balances of vorticity and heat. J.Atmos.Sci., 36, 996-1016. [IV]

Lau, N.-C., & J.M. Wallace, 1979: On the distribution of horizontal transports by transient eddies in the Northern Hemisphere wintertime circulation. J.Atmos.Sci., 36, 1844-1861. [IV]

Lau, N.-C., & E.O. Holopainen, 1984: Transient eddy forcing of the time-mean flow as identified by geopotential tendencies. J.Atmos.Sci., 41, 313-328. [IV]

Lee, T.D., 1951: Difference between turbulence in a two-dimensional and in a three-dimensional fluid. J.Appl.Phys., 22, 524. [I,II]

Leith, C.E., 1968: Diffusion approximation for two-dimensional turbulence. Phys.Fluids, 11, 671-673. [II]

Leith, C.E., 1971: Atmospheric predictability and two-dimensional turbulence. J.Atmos.Sci., 28, 145-161. [II]

Lighthill, M.J., 1978: Waves in Fluids. Cambridge University Press, 504 pp. [V,VI]

Lilly, D.K., 1969: Numerical simulation of two-dimensional turbulence. Phys.Fluids, Suppl.II, 12, 240-249. [II]

Lilly, D.K., 1972: Numerical simulation studies of two-dimensional turbulence. Geophys.Fluid Dynamics, 3, 289-319; 4, 1-28. [II,VIII]

Lin, C.A., 1980: Eddy heat fluxes and stability of planetary waves. Parts I and II. J.Atmos.Sci., 37, 2353-2380. [IV]

Lin, H., 1982: Weakly inhomogeneous turbulence theory with applications to geophysical flows. Ph.D. Thesis, Department of Meteorology and Physical Oceanography, M.I.T., 146 pp. Published as NCAR Cooperative Thesis NCAR/CT-69. [II,VII]

Loesch, A.Z., 1977: On generation of zonal flows by interacting Rossby waves. Tellus, 29, 306-316. [A]

Longuet-Higgins, M.S., & A.E. Gill, 1967: Resonant interactions between planetary waves. Proc.Roy.Soc.Lond.A, 299, 120-140. [A]

Lorenz, E.N., 1953: The interaction between a mean flow and random disturbances. Tellus, 5, 238-250. [VIII]

Lorenz, E.N., 1960: Maximum simplification of the dynamic equations. Tellus, 12, 243-254. [II,VI]

Lorenz, E.N., 1967: The Nature and Theory of the General Circulation of the Atmosphere. Geneva: World Met. Org., 161 pp. [I,IV]

Lorenz, E.N., 1969: The predictability of a flow which possesses many scales of motion. Tellus, 21, 289-307. [V]

Lorenz, E.N., 1972: Barotropic instability of Rossby wave motion. J.Atmos.Sci., 29, 258-264. [V]

Lorenz, E.N., 1979: Forced and free variations of weather and climate. J.Atmos.Sci., 36, 1367-1376. [IV]

Madden, R.A., 1983: The effect of the interference of traveling and stationary waves on time variations of the large-scale circulation. J.Atmos.Sci., 40, 1110-1125. [IV]

Marshall, H.G., & T.-C. Chen, 1982: Baroclinic nonlinear exchanges of energy and potential enstrophy in the quasi-geostrophic two-layer model. Geophys.Astrophys.Fluid Dynamics, 22, 71-84. [III]

McIntyre, M.E., 1970: On the non-separable baroclinic parallel flow instability problem. J.Fluid Mech., 40, 273-306. [VIII,IX]

McIntyre, M.E., 1981: On the 'wave momentum' myth. J.Fluid Mech., 106, 331-347. [V]

McIntyre, M.E., 1982: How well do we understand the dynamics of stratospheric warmings? J.Met.Soc.Japan, 60, 37-65. [IV]

McIntyre, M.E., & T.N. Palmer, 1983: Breaking planetary waves in the stratosphere. Nature, 305, 593-600. [IV]

McIntyre, M.E., & T.N. Palmer, 1984: The 'surf zone' in the stratosphere. To appear in J.Atmos.Terres.Phys., Hamburg Symposium Issue. [IV]

McWilliams, J.C., 1976: Large scale inhomogeneities and mesoscale ocean waves: A single, stable wave field. J.Mar.Res., 34, 423-456. [V]

McWilliams, J.C., 1983: On the relevance of two-dimensional turbulence to geophysical fluid motions. J.Méch.Théor.Appl., Numéro spécial, 83-97. [IV]

McWilliams, J.C., 1984: The emergence of isolated, coherent vortices in turbulent flow. Preprint, submitted to J.Fluid Mech. [III]

McWilliams, J.C., & J.H.S. Chow, 1981: Equilibrium geostrophic turbulence I: A reference solution in a β-plane channel. J.Phys.Ocean., 11, 921-949. [III,VIII]

Merilees, P.E., & T. Warn, 1972: The resolution implications of geostrophic turbulence. J.Atmos.Sci., 29, 990-991. [III]

Merilees, P.E., & H. Warn, 1975: On energy and enstrophy exchanges in two-dimensional non-divergent flow. J.Fluid Mech., 69, 625-630. [II,III,VI]

Merkine, L.-O., 1977: Convective and absolute instability of baroclinic eddies. Geophys.Astrophys.Fluid Dynamics, 9, 129-157. [VI]

Mobbs, S.D., 1982: Variational principles for perfect and dissipative fluid flows. Proc.Roy.Soc.Lond.A, 381, 457-468. [V]

Müller, P., 1978: On the parameterization of eddy-mean flow interaction in the ocean. Dyn.Atmos.Oceans, 2, 383-408. [VI]

Newell, A.C., 1969: Rossby wave packet interactions. J.Fluid Mech., 35, 255-271. [A]

Ogura, Y., 1963: A consequence of the zero-fourth-cumulant approximation in the decay of isotropic turbulence. J.Fluid Mech., 16, 33-40. [II]

Onsager, L., 1949: Statistical hydrodynamics. Nuovo Cimento, Suppl., 6, 279-287. [I,II]

Opsteegh, J.D., & A.D. Vernekar, 1982: A simulation of the January standing wave pattern including the effects of transient eddies. J.Atmos.Sci., 39, 734-744. [IV]

Orr, W.McF., 1907: Stability or instability of the steady motions of a perfect liquid. Proc.Roy.Irish Acad., 27, 9-69. [VI]

Orszag, S.A., 1970: Analytical theories of turbulence. J.Fluid Mech., 41, 363-386. [II]

Palmer, T.N., 1981: Diagnostic study of a wavenumber 2 stratospheric sudden warming in the transformed Eulerian-mean formalism. J.Atmos.Sci., 38, 844-855. [V]

Pedlosky, J., 1962: Spectral considerations in two-dimensional incompressible flow. Tellus, 14, 125-132. [II,VI,VIII]

Pedlosky, J., 1970: Finite-amplitude baroclinic waves. J.Atmos.Sci., 27, 15-30. [IV,V,VI,VII]

Pedlosky, J., 1975: On secondary baroclinic instability and the meridional scale of motion in the ocean. J.Phys.Ocean., 5, 603-607. [III]

Pedlosky, J., 1979: Geophysical Fluid Dynamics. New York: Springer-Verlag, 624 pp. [III,IV,V,VI,VIII]

Peierls, R., 1979: Surprises in Theoretical Physics. Princeton University Press, 166 pp. [V]

Phillips, N.A., 1954: Energy transformations and meridional circulations associated with simple baroclinic waves in a two-level, quasi-geostrophic model. Tellus, 6, 273-286. [III]

Phillips, O.M., 1966, 1977: The Dynamics of the Upper Ocean. 1st and 2nd editions, Cambridge University Press, 261 and 336 pp. [V,VI]

Pierrehumbert, R.T., 1983: Bounds on the growth of perturbations to non-parallel steady flow on the barotropic beta-plane. J.Atmos.Sci., 40, 1207-1217. [V]

Plumb, R.A., 1983: A new look at the energy cycle. J.Atmos.Sci., 40, 1669-1688. [IV]

Plumb, R.A., 1984a: Transient quasigeostrophic eddies on a zonally nonuniform flow: Conservation theorems for small-amplitude waves. Preprint, submitted to J.Atmos.Sci. [V]

Plumb, R.A., 1984b: On the three-dimensional propagation of stationary waves. Preprint, submitted to J.Atmos.Sci. [V]

Redekopp, L.G., 1977: On the theory of solitary Rossby waves. J.Fluid Mech., 82, 725-745. [V]

Reinhold, B.B., & R.T. Pierrehumbert, 1982: Dynamics of weather regimes: Quasi-stationary waves and blocking. Mon.Wea.Rev., 110, 1105-1145. [IV,V]

Rhines, P.B., 1975: Waves and turbulence on a beta-plane. J.Fluid Mech., 69, 417-443. [I,III,VII,A]

Rhines, P.B., 1977: The dynamics of unsteady currents. The Sea, Volume 6, 189-318. New York: Wiley. [I,II,III,IV,VII,VIII]

Rhines, P.B., 1979: Geostrophic turbulence. Ann.Rev.Fluid Mech., 11, 401-441. Annual Reviews, Inc. [II,III]

Rhines, P.B., & W.R. Holland, 1979: A theoretical discussion of eddy-driven mean flows. Dyn.Atmos.Oceans, 3, 289-325. [I]

Rhines, P.B., & W.R. Young, 1983: How rapidly is a passive scalar mixed within closed streamlines? J.Fluid Mech., 133, 133-145. [V]

Ripa, P., 1983: General stability conditions for zonal flows in a one-layer model on the β-plane or the sphere. J.Fluid Mech., 126, 463-489. [V]

Rossby, C.-G., & Collaborators, 1939: Relation between variations in the intensity of the zonal circulation of the atmosphere and the displacements of the semi-permanent centers of action. J.Mar.Res., 2, 38-55. [III]

Sadourny, R., & C. Basdevant, 1981: Une classe d'opérateurs adaptés à la modélisation de la diffusion turbulente en dimension deux. C.R.Acad.Sc.Paris, Série II, 292, 1061-1064. [II]

Salmon, R., 1978: Two-layer quasi-geostrophic turbulence in a simple special case. Geophys.Astrophys.Fluid Dynamics, 10, 25-52. [III]

Salmon, R., 1980: Baroclinic instability and geostrophic turbulence. Geophys.Astrophys.Fluid Dynamics, 15, 167-211. [III,IV]

Salmon, R., 1982: Geostrophic turbulence. Topics in Ocean Physics, Corso LXXX, 30-78. Soc. Italiana di Fisica, Bologna: North-Holland. [II,VIII]

Salmon, R., 1983: Practical use of Hamilton's principle. J.Fluid Mech., 132, 431-444. [V]

Salmon, R., G. Holloway & M.C. Hendershott, 1976: The equilibrium statistical mechanics of simple quasi-geostrophic models. J.Fluid Mech., 75, 691-703. [II,III]

Sasamori, T., & J.-H. Chen, 1982: The interaction of zonal mean temperature, forced stationary waves and transient waves in the high-latitude troposphere. J.Met.Soc.Japan, 60, 197-205. [IV]

Savijärvi, H., 1978: The interaction of the monthly mean flow and large-scale transient eddies in two different circulation types. Part III: Potential vorticity balance. Geophysica, 15(1), 1-16. [IV]

Schneider, E.K., 1977: Axially symmetric steady-state models of the basic state for instability and climate studies. Part II. Nonlinear calculations. J.Atmos.Sci., 34, 280-296. [IV]

Shutts, G.J., 1983a: Parameterization of traveling weather systems in a simple model of large-scale atmospheric flow. Adv.Geophysics, 25, 117-172. Academic Press. [I,IX]

Shutts, G.J., 1983b: The propagation of eddies in diffluent jetstreams: Eddy vorticity forcing of 'blocking' flow fields. Quart.J.Roy.Met.Soc., 109, 737-761. [IV,IX]

Simmons, A.J., & B.J. Hoskins, 1978: The life cycles of some nonlinear baroclinic waves. J.Atmos.Sci., 35, 414-432. [IV,VIII]

Simmons, W., & The MODE Group, 1978: The mid-ocean dynamics experiment. Deep-Sea Res., 25, 859-910. [III]

Starr, V.P., 1953: A note concerning the nature of the large-scale eddies in the atmosphere. Tellus, 5, 494-498. [I,IV]

Starr, V.P., 1968: Physics of Negative Viscosity Phenomena. New York: McGraw-Hill, 256 pp. [I,IV]

Starr, V.P., J.P. Peixoto & N.E. Gaut, 1970: Momentum and zonal kinetic energy balance of the atmosphere from five years of hemispheric data. Tellus, 22, 251-274. [IV]

Tang, C.-M., & S.A. Orszag, 1978: Two-dimensional turbulence on the surface of a sphere. J.Fluid Mech., 87, 305-319. [II]

Taylor, G.I., 1915: Eddy motion in the atmosphere. Phil.Trans.Roy. Soc.Lond.A, 215, 1-26. (Also in Scientific Papers, 2, 1-23, Cambridge University Press.) [V]

Tennekes, H., 1978: Turbulent flow in two and three dimensions. Bull.Amer.Met.Soc., 59, 22-28. [II]

Tolman, R.C., 1938: Statistical Mechanics. Oxford University Press, 660 pp. [II]

Tomatsu, K., 1979: Spectral energetics of the troposphere and lower stratosphere. Adv.Geophysics, 21, 289-405. Academic Press. [IV]

Tsay, C.-Y., & S.K. Kao, 1978: Linear and nonlinear contributions to the growth and decay of the large-scale atmospheric waves and jet stream. Tellus, 30, 1-14. [IV]

Tung, K.K., 1981: Barotropic instability of zonal flows. J.Atmos.Sci., 38, 308-321. [V]

Tung, K.K., 1983: Initial-value problems for Rossby waves in a shear flow with critical level. J.Fluid Mech., 133, 443-469. [VI,VIII]

White, A.A., & J.S.A. Green, 1982: A non-linear atmospheric long wave model incorporating parametrizations of transient baroclinic eddies. Quart.J.Roy.Met.Soc., 108, 55-85. [IX]

Williams, G.P., 1978: Planetary circulations: 1. Barotropic representation of Jovian and terrestrial turbulence. J.Atmos.Sci., 35, 1399-1425. [III,IV]

Williams, G.P., 1979: Planetary circulations: 3. The terrestrial quasi-geostrophic regime. J.Atmos.Sci., 36, 1409-1435. [III]

Yamagata, T., 1976: On the propagation of Rossby waves in a weak shear flow. J.Met.Soc.Japan, 54, 126-128. [V,VI]

Yamagata, T., & J. Kono, 1976: On energy and enstrophy transfer in two-dimensional non-divergent waves on a beta-plane. J.Met.Soc.Japan, 54, 454-456. [III]

Young, W.R., & P.B. Rhines, 1980: Rossby wave action, enstrophy and energy in forced mean flows. Geophys.Astrophys.Fluid Dynamics, 15, 39-52. [V,VI]

Youngblut, C., & T. Sasamori, 1980: The nonlinear effects of transient and stationary eddies on the winter mean circulation. Part I: Diagnostic analysis. J.Atmos.Sci., 37, 1944-1957. [IV]

Zeng, Q.-C., 1982: On the evolution and interaction of disturbances and zonal flow in rotating barotropic atmosphere. J.Met.Soc.Japan, 60, 24-31. [V,VI]

APPENDIX - SIMULATIONS WITH HIGHER-MODE JETS

There is a very natural question which arises with regard to the present work, and which bears addressing. It is the following: How does the scenario of inhomogeneous turbulence studied here differ fundamentally from fully-developed beta-plane turbulence, in which inhomogeneities in the form of beta-jets arise internally? Given the evidence of the numerical simulations that the two dynamical regimes are indeed quite distinct, perhaps one should rather ask: Why do the zonal jets of beta-plane turbulence not induce large-scale meridional anisotropy and a penetration of transient energy past the "Rhines radius", as the large-scale forced jets do?

To respond to these questions, it is necessary to establish immediately that the absence of the two cited effects in beta-plane turbulence does not provide a counter-example to the theory as developed in this thesis. In the first place, the theory relies formally on a separation in scale between the stationary and transient flow components; and while in practice it seems to work even when the "small parameter" δ of (6.12), judged in terms of the <u>total</u> wavenumber, is $O(\frac{1}{2})$ - not the first time that the WKB approximation proved successful at the limit of its validity! - nevertheless it can scarcely be expected to hold for $\delta > 1$. Furthermore, the jets arising in beta-plane turbulence are relatively weak compared to the overall transient energy level, and thus meander around and pulsate to an extent that one cannot consider them primarily as stationary features.

However these comments do not directly answer the questions, so to investigate this matter further some numerical simulations with higher-

mode basic-state jets have been performed; the results will be discussed in this Appendix. Obviously the possibility then exists for transient energy to reside in scales of motion larger than the stationary flow, and this places the problem in a rather different phenomenological regime than that considered throughout this thesis. Consequently the present section can only hope to scratch the surface of the subject.

The first simulation to be discussed is of the spin-down type treated in Chapter VII; it is entitled Run Q, and has identical external parameters to Run O with the exception of β_0, which is 65 rather than 25, and of course the basic-state flow: rather than (7.2), it takes the form of a quadruple jet,

$$\Psi(y) = \frac{U_0}{4} \sin(4y) \quad ; \quad U(y) = - U_0 \cos(4y) \quad [0 \leq y < 2\pi] \; . \quad (A.1)$$

$U_0 = 2\sqrt{2}$ as before, and F_0 in (7.3) is adjusted accordingly. The reason for the higher value of β_0 is to prevent barotropic instability of the basic-state jet.

Rather than examining the evolution of Run Q from its initial conditions, attention will be focussed for the sake of brevity on the total run period $t = 0\text{-}15$. Figs. A.1 and A.2 show the energy spectra in n-space and in the 2-D (k,ℓ)-space representation. The basic-state jet at $(k = 0 \; , \; \ell = 4)$ and $n = 4$ is evident, as is the rather sharp cut-off of transient energy for $n < 3$; in fact energy never penetrates this scale to a significant extent, even temporarily. It is interesting that between n_β and the jet scale $n = 4$, the pattern of transient-eddy isotropy seen before is preserved; of course one should expect the previous theory to be applicable in this range. Another striking feature is the strong small-scale zonal anisotropy, which may be

attributed to the greater mean-flow straining that results from the stronger shear.

To investigate the spectral dynamics of Run Q, the zonal wavenumber stationary-transient conversion terms are given in Fig. A.3. The same pattern of small-k transient gain and intermediate-k transient loss that appears in all the simulations is again apparent here, but now the former represents a fairly small effect. Presumably this reflects the fact that the small-k disturbances cannot amplify nearly as much since their progress is blocked at $n = 3$, while the development of $k > 4$ modes is unaffected. The net rectification of the zonal flow is however a consistent feature of the spin-down runs.

The spectral energy fluxes in n-space (Fig. A.4) indicate the strong arrest at $n = 3,4$; they also demonstrate that the "induced flux" plays the dominant role at all scales, in contrast to Run 0 where its effects are spectrally localized (Fig. 7.28a). Apparently the combined increase of β_0 and the mean-flow shear has significantly reduced the role of the turbulent interactions. Nevertheless the latter are evidently operative, though on a slower timescale, as reflected in the smoothness of the 2-D transient energy spectral distribution (Fig.A.2a).

Finally examining the stationary-transient interaction in terms of n, there is a large loss of energy from the initial scales with significant net transfer up to $n = 3,4$ (Fig. A.5a). This represents a compressed version of its equivalent for Run 0, Fig. 7.26d, with the two minima around n_β and the initial scales now combined into one; even the net conversion is of a similar strength. With regard to enstrophy (Fig. A.5b) there is now a noticeable net conversion, but the overall pattern is still well characterized as spectral transfer of enstrophy -

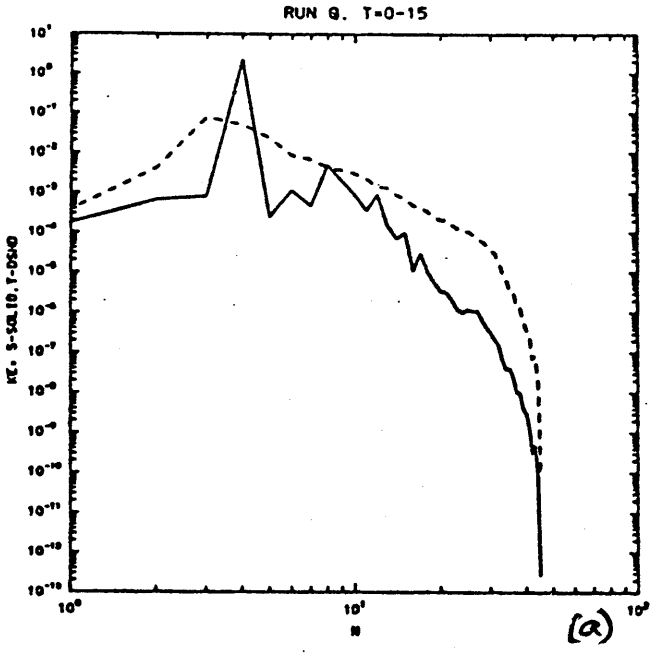


Fig.A.1a: Stationary (——) and transient (- -) energy n-spectra, Run Q, t=0-15.

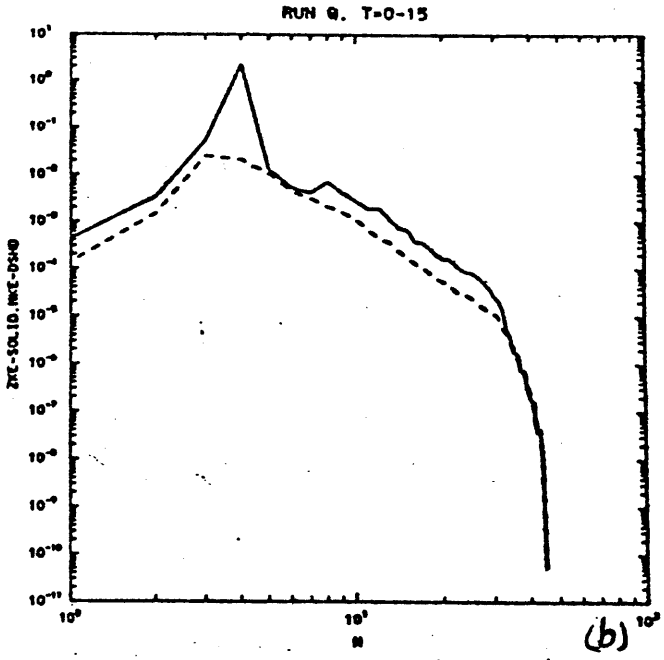


Fig.A.1b: Zonal (——) and meridional (- -) energy n-spectra, Run Q, t=0-15.



Fig. A.2a: Transient 2-D (k,ℓ) energy spectrum, Run Q.

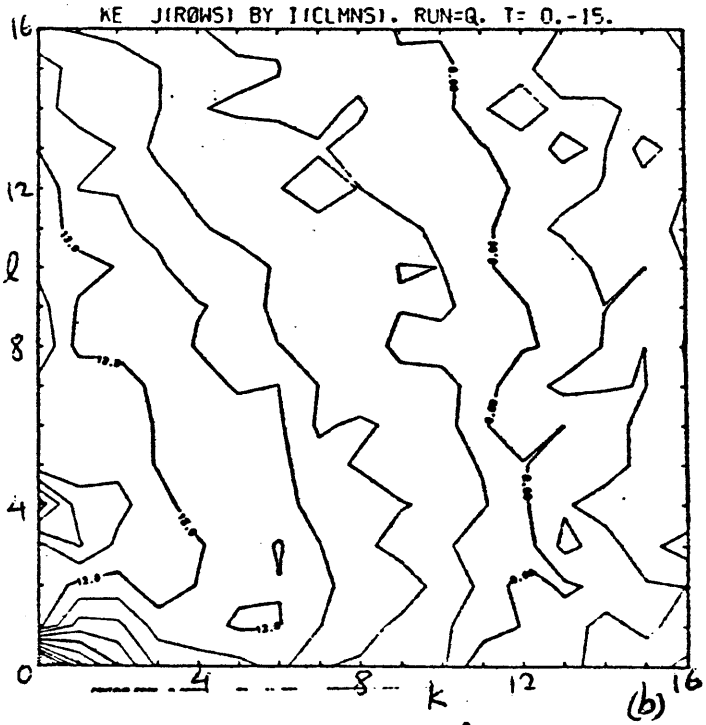


Fig. A.2b: Total 2-D (k,ℓ) energy spectrum, Run Q.

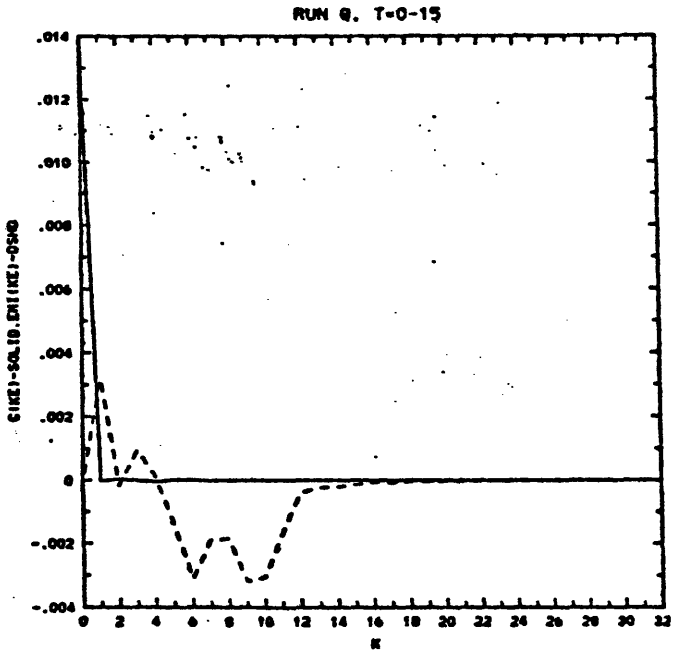


Fig. A.3: k-space energy conversion terms C(k) (——) and EMI(k) (– –), Run Q, t=0-15.

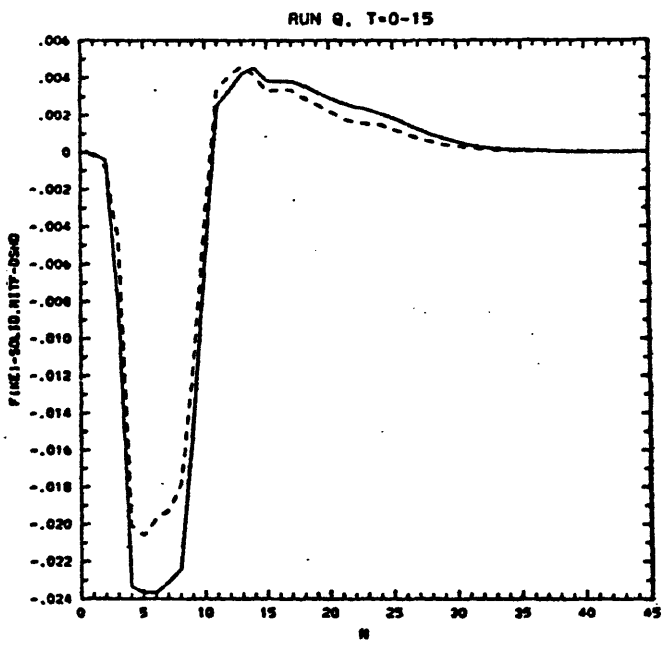
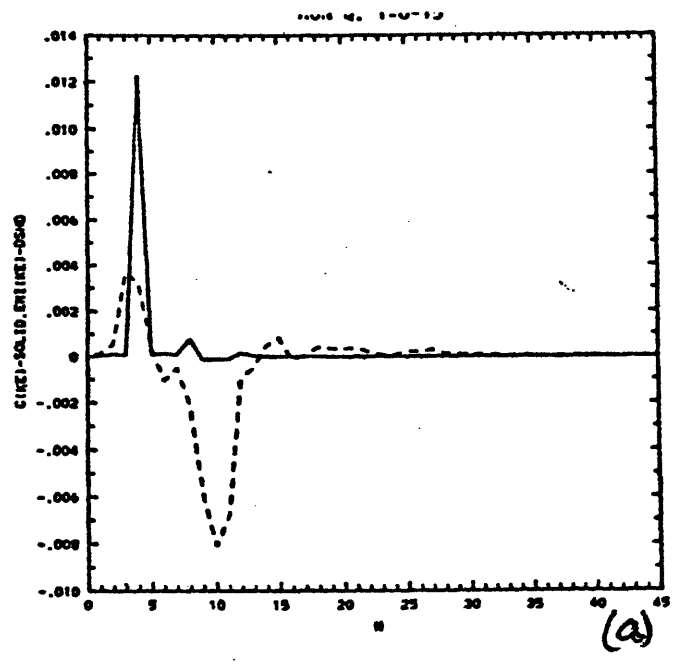


Fig. A.4: n-space nonlinear energy flux F(n) (——) and induced flux MITF(n) (– –), Run Q, t=0-15.



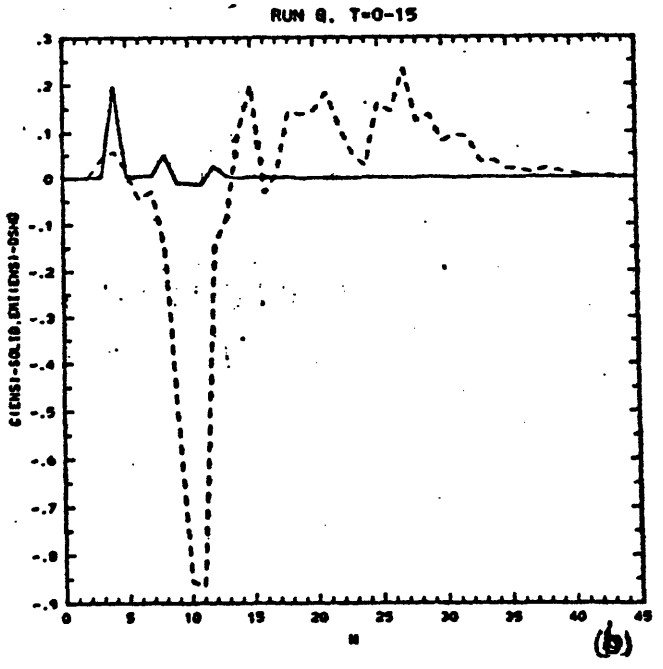


Fig. A.5a,b: n-space conversion terms C(n) (——) and EMI(n) (– –) for (a) energy and (b) enstrophy, Run Q.

mainly down-scale, where the turbulent "truncation" effect seen in Run 0 (Fig. 7.27d) is now absent, and to a limited extent up-scale.

These results suggest that the ideas developed for the large-scale jet are also applicable to an intermediate-scale jet, but that there is a dynamical barrier preventing energy from moving significantly into larger total scales (as judged by n). Another spin-down run was performed with the basic-state jet having equal components at $\ell = 1$ and $\ell = 4$, and the results were essentially identical though the mean-flow rectification was shared (approximately evenly) between the two components; evidently a larger-scale stationary component is not able to succeed in "pulling" energy past the smaller-scale one.

Before discussing the possible theoretical interpretations of these findings, a forced-dissipative equilibrium simulation will be considered. The one presented is Run ZA, which is identical to Run W (the higher-beta run) except that the basic-state flow is now given by

$$\begin{aligned} \Psi(y) &= 2 \sin y + \frac{\sqrt{2}}{3} \sin(3y) + \frac{\sqrt{2}}{5} \sin(5y) \; ; \\ U(y) &= -2 \cos y - \sqrt{2} \left(\cos(3y) + \cos(5y)\right) \; ; \end{aligned} \tag{A.2}$$

the mean energy of this jet is still 2, as in all the simulations. The motivation behind this somewhat peculiar choice is that the atmosphere's stationary wave spectrum has strong zonal peaks in modes n = 1, 3, and 5 (Figs. 4.3a,b), an admittedly questionable rationale given the idealized nature of the model and the obviously unrealistic phase structure of (A.2), yet provocative nonetheless.

Instantaneous spatial maps of the total streamfunction and vorticity fields from Run ZA are given in Figs. A.6; the vorticity is clearly absent from the latitudes of the principal jets $y = 0$ and $y = \pi$, and mean-flow straining is not easy to detect. The time-averaged zonal

flow (Fig. A.7a) is close to its basic-state value, and the potential vorticity gradient (Fig. A.7b) seems safely positive. Oddly enough, the transient eddy variances (Fig. A.7c) exhibit maxima in the weak-jet regions, and minima in the strong-jet ones; however they seem roughly isotropic. The almost total absence of transient eddy activity in the principal easterly jet at $y = 0$ is likely related to the strong peaks of transient energy loss on the easterly-jet side of the source regions (Fig. A.7d); this absorption as disturbances propagate into the easterly jet is what one would expect from ray-tracing theory, but seems to be masked in the single-jet runs by "waveguide" effects involving trapping of energy by turning lines.

Energy spectra are shown in Figs. A.8 in terms of the total wavenumber n. The transient energy falls off noticeably for scales larger than the smallest significant stationary scale, $n = 5$, suggesting the dynamical "barrier" to transient development seen in Run Q above (Fig. A.8a). The transient energy itself is roughly isotropic between the forced scales and $n = 5$, but exhibits zonal anisotropy outside of this range (Fig. A.8d). As in Run Q, a partial suppression of the turbulent cascades is apparently effected by stronger mean-flow shear and higher β_0. The large-scale transient zonal anisotropy does not contradict the theory developed in this thesis, as it occurs at larger scales than the stationary flow where the theory cannot be applied. It is striking that the spectra are now beginning to show some resemblance to those of the atmosphere, but there are many reasons why one should not press this correspondence too far.

The zonal-wavenumber energy conversion terms, shown in Fig. A.9, depict mean-flow rectification in what is now a familiar pattern. The

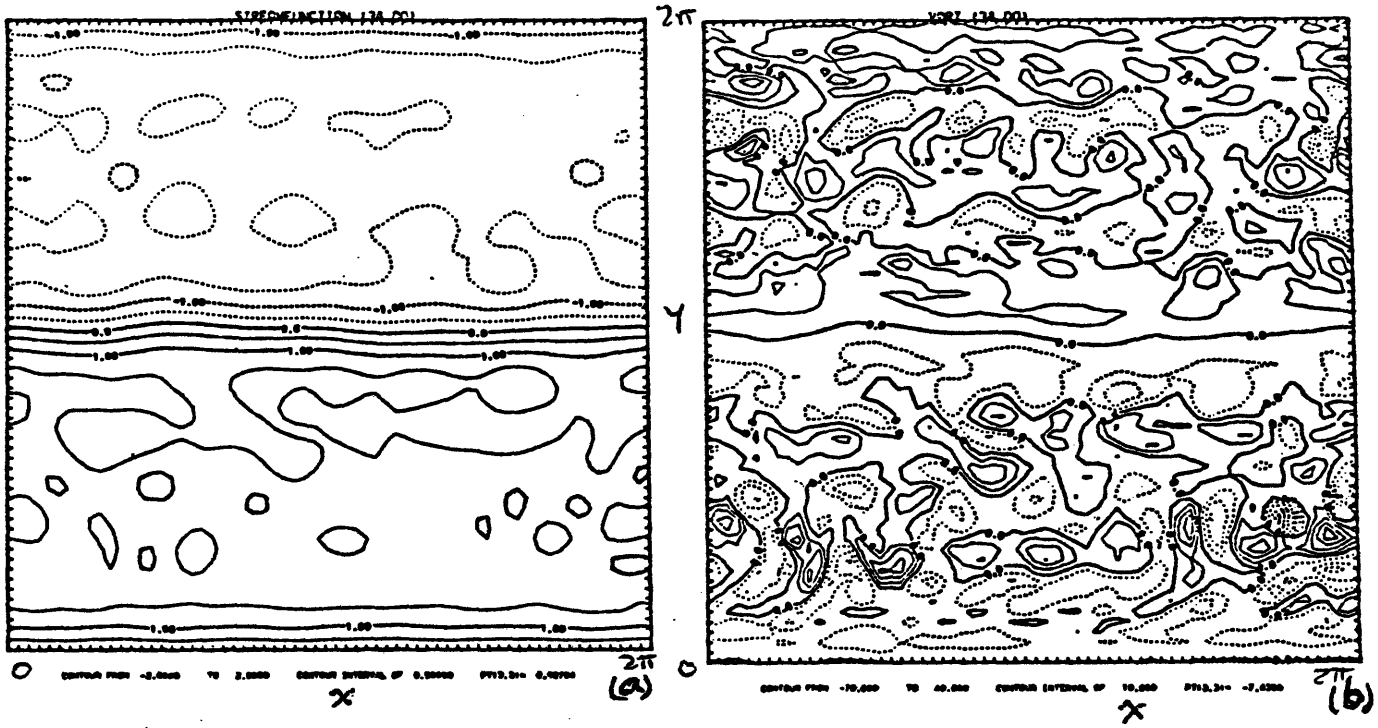


Fig. A.6a,b: Instantaneous spatial maps of total (a) streamfunction and (b) vorticity, Run ZA.

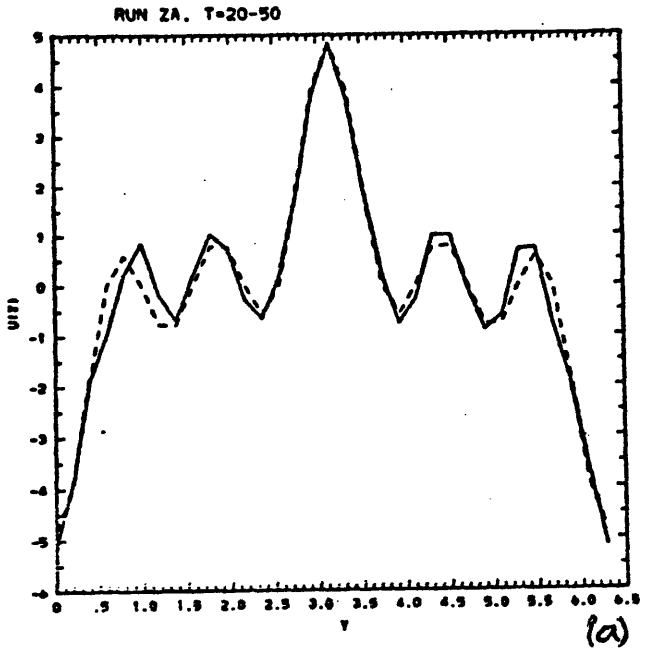


Fig. A.7a: Time-averaged zonal flow $\bar{U}(y)$ (——) and basic-state zonal flow (– –), Run ZA, t=20-50.

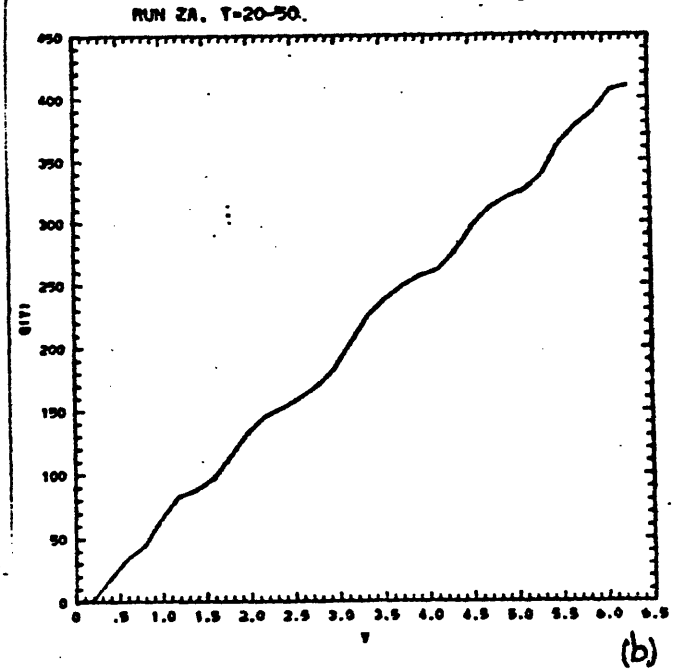


Fig. A.7b: Time-averaged potential vorticity $Q(y) = \beta_0 - U_{yy}$, Run ZA.

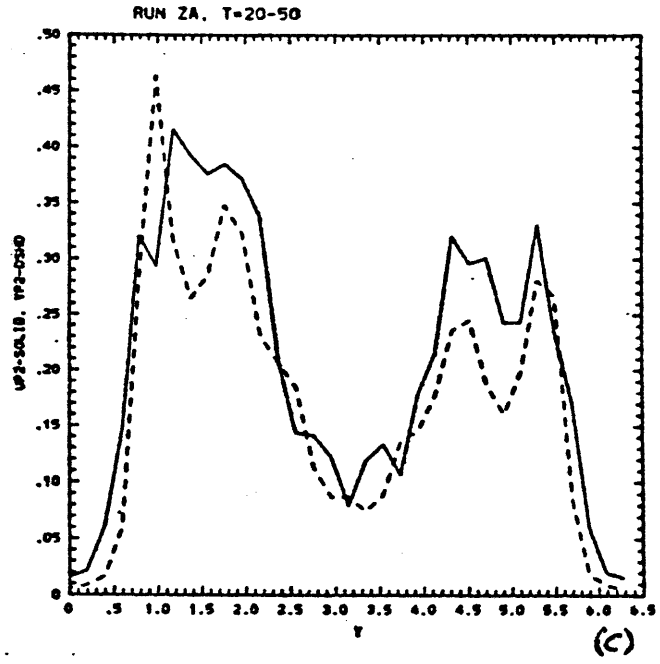


Fig. A.7c: Transient variances $\langle\overline{u'^2}\rangle$(——) and $\langle\overline{v'^2}\rangle$(– –), Run ZA.

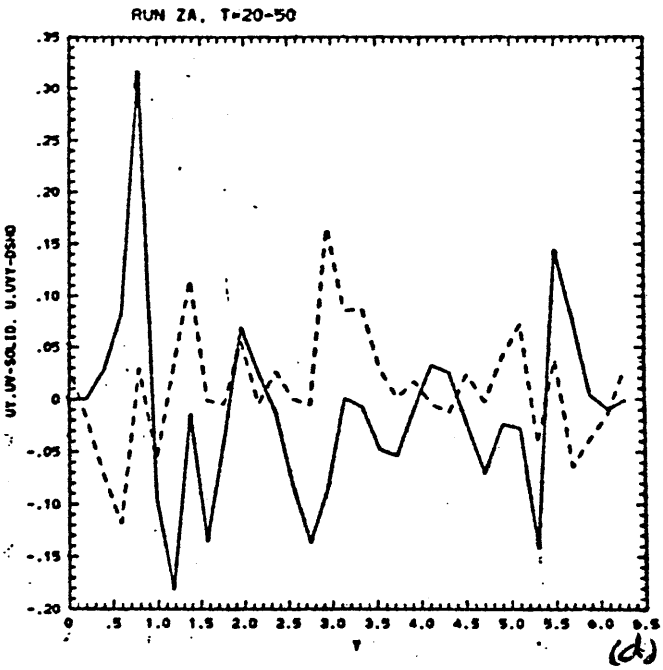


Fig. A.7d: Conversion terms $U\,\overline{uv}$ (——) and $U(\overline{uv})_y$ (– –), Run ZA.

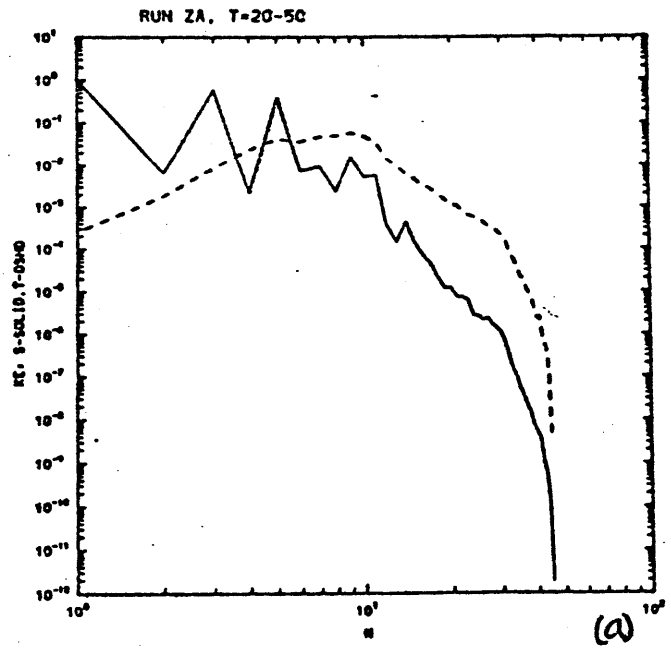


Fig. A.8a: Stationary (——) and transient (– –) energy n-spectra, Run ZA.

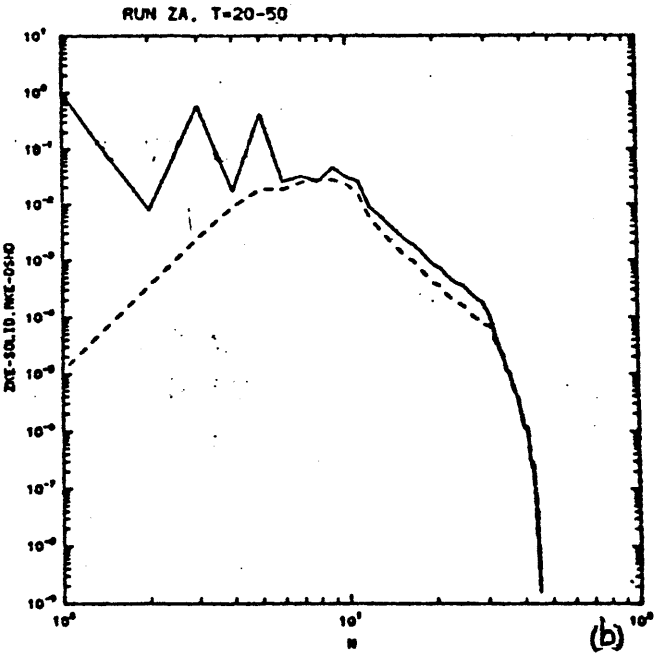


Fig. A.8b: Zonal (——) and meridional (– –) energy n-spectra, Run ZA.

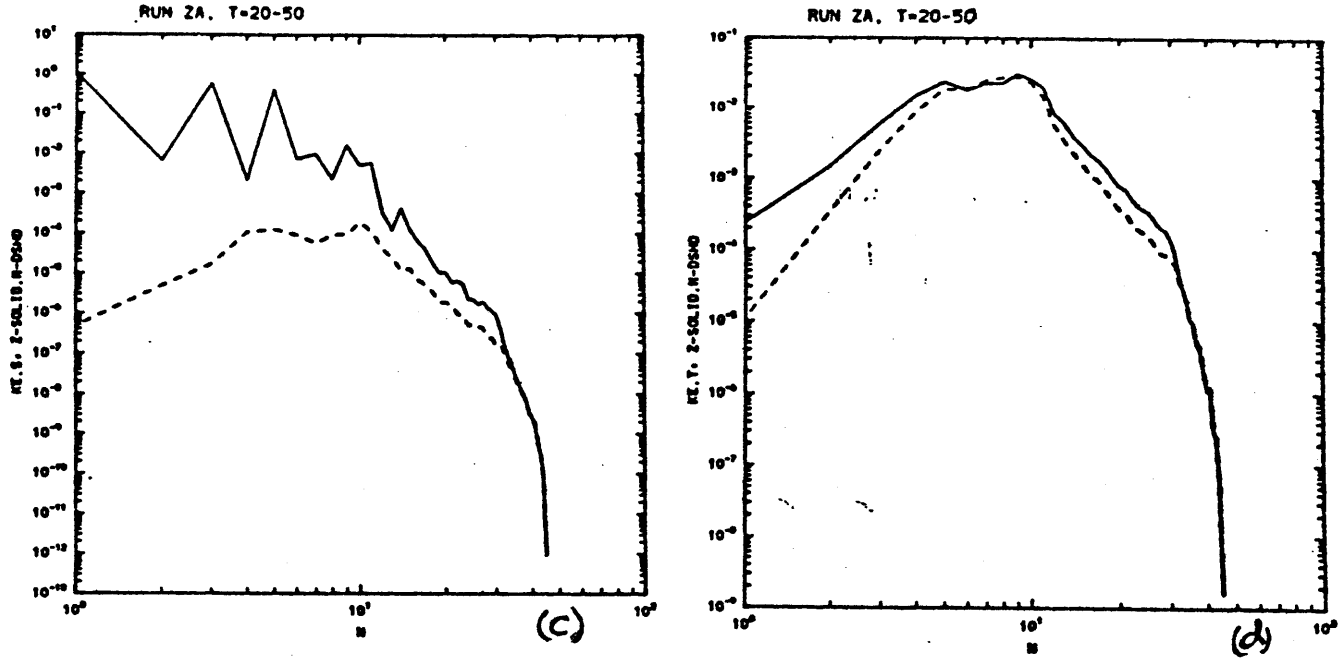


Fig. A.8c,d: Zonal (——) and meridional (– –) components of (c) stationary and (d) transient energy, Run ZA.

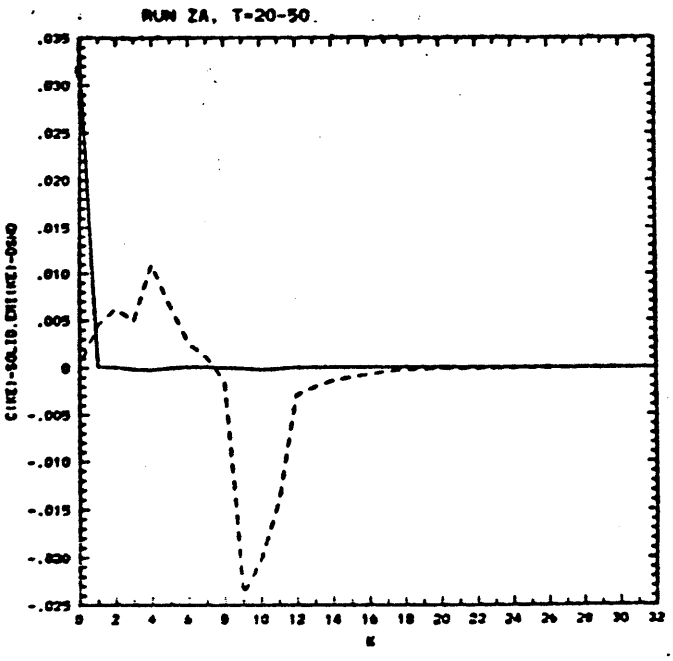


Fig. A.9: k-space energy conversion terms C(k) (——) and EMI(k) (– –), Run ZA, t=20-50.

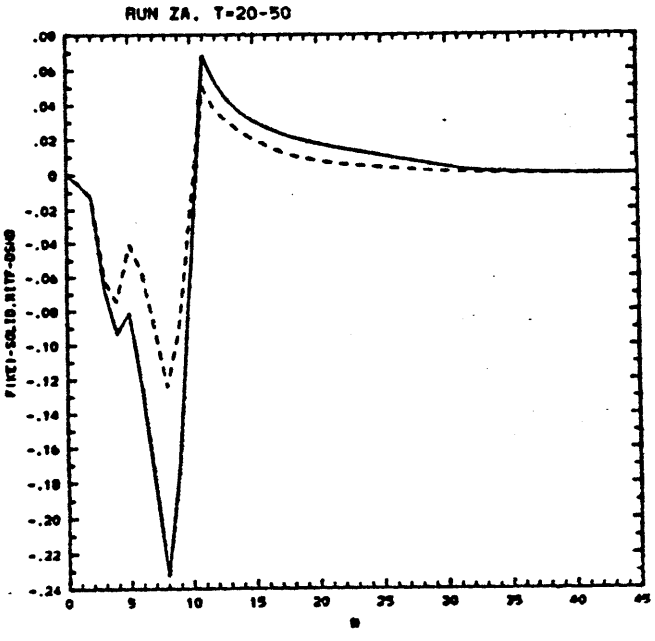


Fig. A.10: n-space nonlinear energy flux F(n) (——) and induced flux MITF(n) (– –), Run ZA.

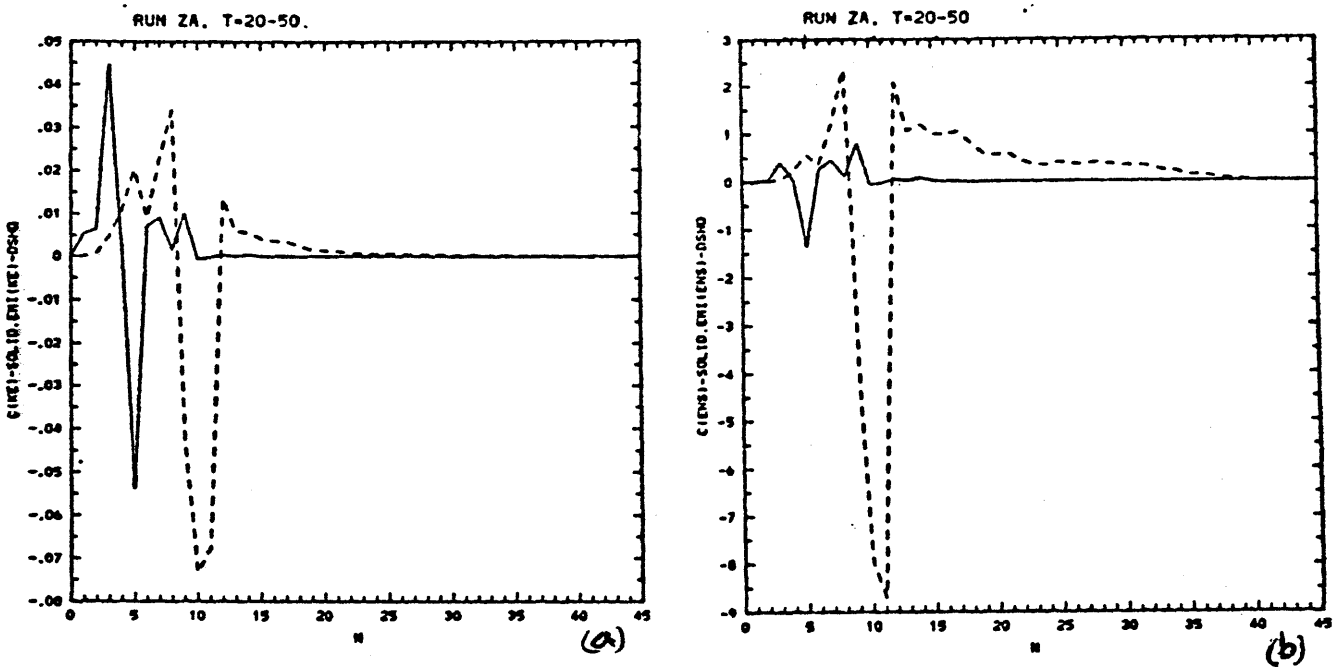


Fig. A.11a,b: n-space conversion terms C(n) (——) and EMI(n) (– –) for (a) energy and (b) enstrophy, Run ZA.

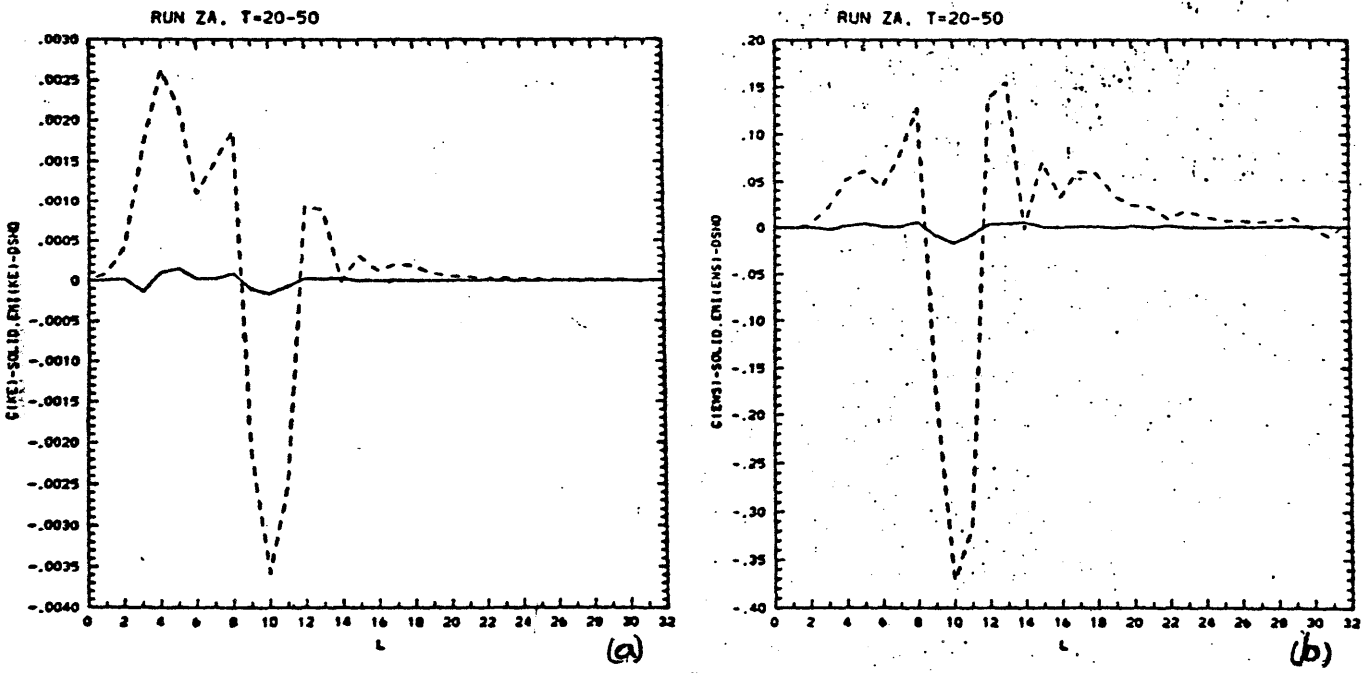


Fig. A.12a,b: ℓ-space conversion terms C(ℓ) (——) and EMI(ℓ) (– –) for k=2, for (a) energy and (b) enstrophy, Run ZA.

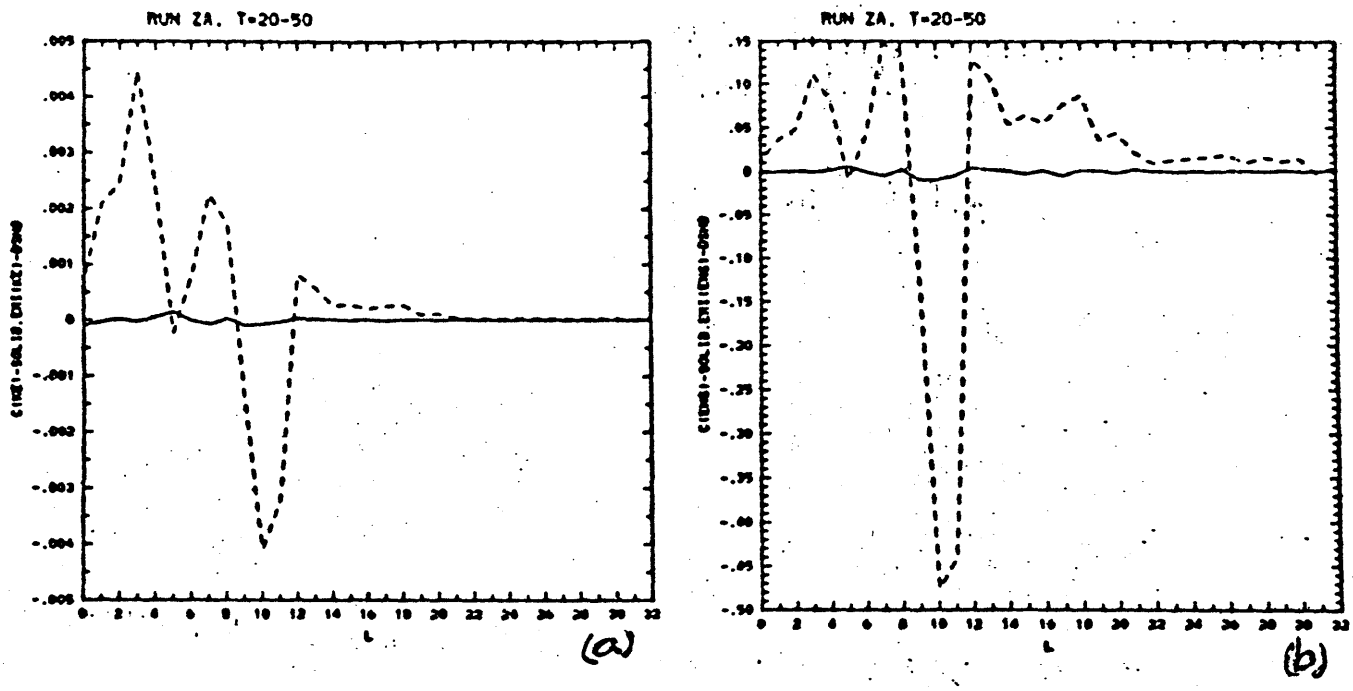


Fig. A.13a,b: Same as Fig. A.12a,b, but for k=4.

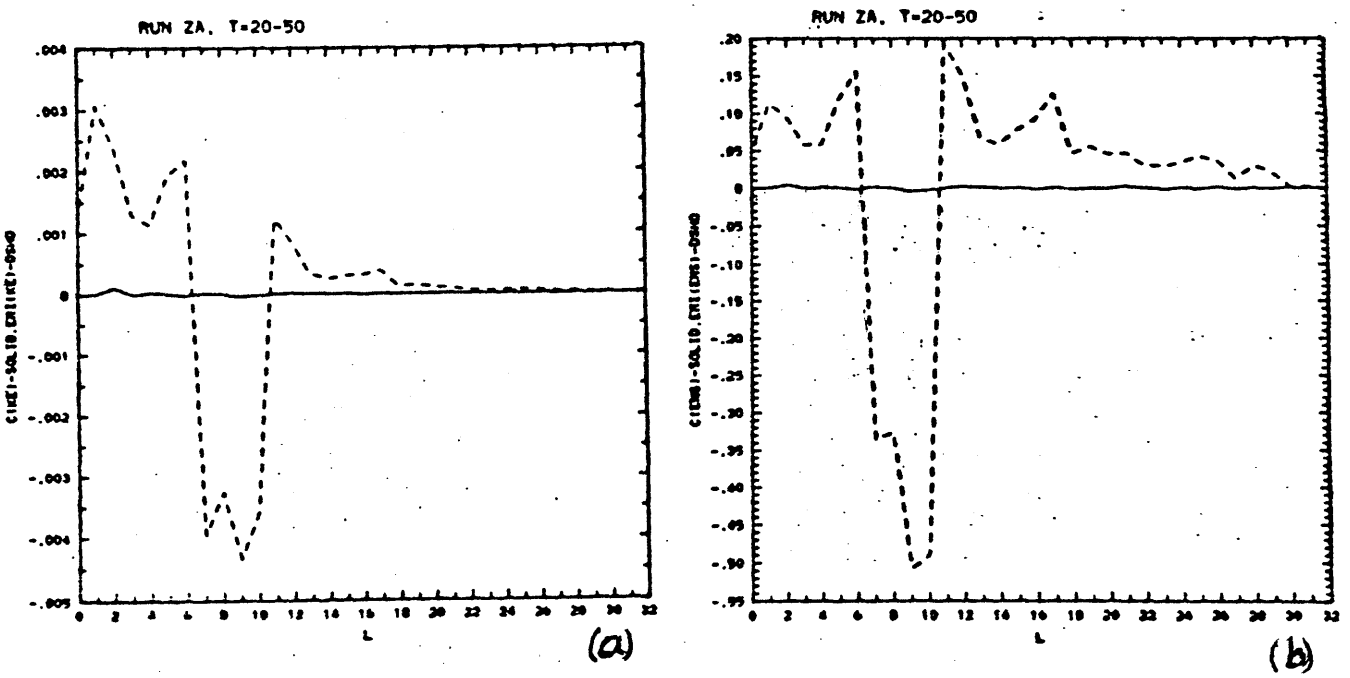


Fig. A.14a,b: Same as Fig. A.12a,b, but for k=6.

differences concern a somewhat higher transition wavenumber k_0 and a far more sharply peaked loss from $8 < k < 12$; this may be attributed to a weaker turbulent cascade, which fails to spread the loss out over smaller k. In fact this interpretation is quite correct: the spectral fluxes are clearly dominated by the "induced" component (Fig. A.10), with the transient flux playing a minor role.

When one examines the n-space stationary-transient interaction terms, it is evident that EMI has the character of induced transfer for both energy and enstrophy (Figs. A.11a,b); while there is a net rectification of stationary energy, there is strong cancellation in the conversion terms, with the strengthening of $n = 3$ approximately matching the weakening of $n = 5$. The enstrophy transfer is mainly down-scale, but it has a sufficiently strong up-scale component to give a considerable up-scale energy transfer.

At the risk of presenting too many figures, the conversion terms in ℓ-space for fixed k are worth showing because they convincingly verify the efficacy of the spectral transfer process. $k = 2$, 4, and 6 all show roughly symmetric transfer of enstrophy away from the forced scales (Figs. A.12b, A.13b, A.14b), with the consequent up-scale transfer and amplification of energy (Figs. A.12a, A.13a, A.14a); notably the transfer process is arrested in each instance at $n = 5$. Ray-tracing theory alone would predict net down-scale transfer in every case, which clearly does not obtain here; consequently dynamical irreversibility is again entering.

Another forced-dissipative equilibrium simulation, Run Z, was performed with a quadruple-jet basic-state flow. In that case the net conversion was from the stationary to the transient flow. The pattern

of EMI was essentially similar to that of Run ZA, however, with the induced up-scale transfer being blocked at n = 4. As in the single-jet runs, the robust features concern the transient spectral dynamics, with the net stationary-transient conversion depending in a sensitive way on the external parameters.

It is fairly evident from the numerical results that the WKB "induced transfer" approach does not describe the behaviour of disturbance scales with a total wavenumber which is smaller than that of the smallest-scale significant component of the stationary flow. The question then becomes, What theory does so describe it? Since the non-dimensional parameter β is greater than unity for both the basic-state flow and the large-scale perturbations, a logical candidate would seem to be some sort of finite-amplitude resonant interaction formalism, expanding about Rossby-wave solutions in powers of β^{-1}.

Unfortunately there is not a great deal written in this rather technical field, and this is not the place to rectify that situation (were it possible to do so!). But it seems to me that there are a few possible explanations for the observed behaviour. Beginning with resonant interaction theory itself, it has been known at least since the work of Longuet-Higgins & Gill (1967) that zonal flows on an infinite beta-plane cannot gain or lose energy through discrete resonant triads; at best they can act as a catalyst, enabling an exchange between two non-zonal modes. When the zonal flow consists of a single meridional wavenumber ℓ_0, then these other modes must lie on the line $\ell = \ell_0/2$.

There are at least three ways in which this negative result can be overcome while still retaining the context of the resonant interaction formalism. Newell (1969) discusses two of them: the first being through

a "sideband resonance" involving Rossby wave packets, the second arising out of resonant quartets. With regard to the former possibility, it is interesting to note that when one considers slightly non-zonal flows (i.e. a wavenumber $(\varepsilon k_0, \ell_0)$ with ε small), the locus of resonantly interacting discrete triads takes the form of a double-lobed "hourglass" which in the vicinity of ℓ_0 is approximated by a cross centred at $(\varepsilon k_0/2, \ell_0/2)$ (Longuet-Higgins & Gill, 1967); moreover the vertical axis of the cross (small k) represents unstable waves with respect to the nearly-zonal flow, the horizontal axis ($\ell \approx \ell_0/2$) stable waves (Gill, 1974). This suggests that the sideband resonance mechanism provides a "sponge" along $\ell \approx \ell_0/2$, in the sense that disturbances reaching that scale will be absorbed by the zonal flow. Kenyon's (1967) numerical tendency calculations involving a continuous spectrum indeed demonstrate that rectification of the $(\varepsilon k_0, \ell_0)$ mode comes largely from waves with $\ell \approx \ell_0/2$.

The weakness of this argument in relation to the present simulations is that the resolved spectrum is in fact discrete; on the other hand a wave packet can be approximated by a discrete spectrum to a certain extent, as evidenced by the success of the ray-tracing theory in the case of a scale separation, so this possibility cannot be ruled out.

An alternative mechanism for zonal-flow interaction was proposed by Loesch (1977), who showed that discrete finite-amplitude resonant triads on a beta-plane channel could generate zonal flows on the time-scale of the resonant interaction. The applicability of Loesch's result to the present situation is also problematical insofar as the domain is periodic rather than confined in the meridional direction. But the essential dynamics of Loesch's analysis seem as though they could arise

out of periodic quantization conditions just as much as from the boundary conditions appropriate to a channel: a discrete spectrum of normal modes is supported in both geometries. However it must be emphasized that this speculation has not been verified. In any event it is not at all clear from Loesch's paper which non-zonal waves would be most likely to feed energy to the zonal flow, so there is no direct way to test the theory.

A final candidate, discussed by both Newell and Loesch, is that of resonant quartets. While the timescale of this interaction is (asymptotically) slow it must be said that a faster timescale is not necessarily required, especially at finite amplitude. But it is not easy to see how one might identify the role of this mechanism in the simulations.

The difficulty of the present situation arises largely out of the fact that while β does exceed unity, it does not do so by a great degree, and this intermediate regime is the one which is most difficult to treat. Gill (1974), for example, considers small perturbations from the asymptotic limits $\beta \to 0$ and $\beta \to \infty$, but this nevertheless leaves a gap in the most crucial range. It may be that more qualitative non-resonant arguments such as those of Rhines (1975) provide the only trustworthy approach.